

**NMR-Spectroscopic Investigations in Asymmetric
Brønsted Acid Catalysis – Structural Space,
Hydrogen Bonding and Non-Covalent
Interactions**

Dissertation

zur Erlangung des Doktorgrades der Naturwissenschaften

(Dr. rer. nat.)

Der Fakultät für Chemie und Pharmazie

Der Universität Regensburg



vorgelegt von

Johannes Gramüller

aus Landshut

im Jahr 2022

Die vorliegende Dissertation beruht auf Arbeiten, die zwischen Dezember 2018 und September 2022 am Arbeitskreis von Professor Dr. Ruth M. Gschwind am Institut für Organische Chemie der Universität Regensburg durchgeführt wurden.

Promotionsgesuch eingereicht am: 18. Oktober 2022

Die Arbeit wurde angeleitet von: Prof. Dr. Ruth M. Gschwind

Promotionsausschuss:

Vorsitzender: Apl. Prof. Dr. Rainer Müller

1. Gutachterin: Prof. Dr. Ruth M. Gschwind

2. Gutachter: Prof. Dr. Werner Kremer

3. Prüferin: Prof. Dr. Julia Rehbein

Meiner Familie

Table of contents

1. Introduction and Outline.....	1
1.1. Brønsted acid catalysis	1
1.2. Outline	3
1.3. References.....	7
2. General remarks	8
2.1. Structure of this work.....	8
2.2. List of publications.....	8
3. Brønsted Acid Catalysis – The Effect of 3,3'-Substituents on the Structural Space and the Stabilization of Imine/Phosphoric Acid Complexes	12
3.1. Abstract	13
3.2. Introduction.....	14
3.3. Results and Discussion	16
3.3.1. Investigated complexes and their NMR properties	16
3.3.2. Structural space of TIPSY/imine complexes	19
3.3.3. Structural space of TRIM/imine complexes and dimerization trends of CPAs.....	23
3.3.4. Effect of substituents on enantioselectivity in the transfer hydrogenation of ketimines ..	25
3.3.5. Theoretical model structures and structure comparison	26
3.3.6. Computational Details.....	29
3.4. Conclusion	30
3.5. References.....	31
3.6. Supporting Information.....	33
3.6.1. General information.....	33
3.6.2. Dilution experiments for dimer identification	35
3.6.3. Chemical shift assignment of TRIM/imine complexes	37
3.6.4. Structure identification of all TRIM/imine complexes	41
3.6.5. Exchange pathways in binary TRIM/imine complexes.....	51
3.6.6. DOSY measurements for TRIM dimer	51

3.6.7. Determination of <i>ee</i> values	53
3.6.8. Correlation of <i>ee</i> with CPA parameters.....	54
3.6.9. HPLC analysis	56
3.6.10. References.....	60
4. Relaxation Dispersion NMR to reveal fast Dynamics in Brønsted Acid Catalysis: Influence of Sterics and H-bond strength on conformations and substrate hopping	61
4.1. Abstract	62
4.2. Introduction.....	63
4.3. Results and Discussion	66
4.3.1. System selection.....	66
4.3.2. Possible exchange pathways.....	67
4.3.3. Probe selection (proton site selection)	68
4.3.4. $R_{1\rho}$ measurements.....	69
4.3.5. TRIP/1-3 <i>E</i> imine complexes: H-bond dependent exchange pathway A.....	71
4.3.6. TRIM/1-3 <i>E</i> imine complexes: Reduced sterics allow for rotations	72
4.3.7. TRIM/4 <i>E</i> imine complex: Disabling of rotation by steric hindrance.....	76
4.3.8. TiPSY/1 <i>E</i> imine complex: Influence of 3,3'-substituents on the H-Bond switching rate.....	77
4.4. Conclusion	78
4.5. References.....	79
4.6. Supporting Information.....	82
4.6.1. Experimental data	82
4.6.2. Synthesis of Imine Substrates	83
4.6.3. Sample preparation.....	83
4.6.4. Spectrometer data	84
4.6.5. 1D ^1H off-resonance $R_{1\rho}$	85
4.6.6. Results of the $R_{1\rho}$ measurements.....	88
4.6.7. NMR-Structural analysis of CPA/imine complexes.....	91
4.6.8. References.....	99

4.7. Additional Findings	100
4.7.1. Introduction.....	100
4.7.2. Extension of model systems.....	101
4.7.3. R _{1p} measurements and detailed structural analysis.....	103
4.7.4. Conclusion	109
4.7.5. References.....	110
5. What is the Role of Acid-Acid Interactions in Asymmetric Phosphoric Acid Organocatalysis? A Detailed Mechanistic Study using Interlocked and Non-Interlocked Catalysts	111
5.1. Abstract	112
5.2. Introduction.....	113
5.3. Results and Discussion	115
5.3.1. General approach.....	115
5.3.2. Influence of the catenane ring sizes.....	115
5.3.3. First reduction step: Kinetic analysis.....	116
5.3.4. NMR-spectroscopic investigation of catalyst dimerization.....	124
5.3.5. Overall mechanistic picture for catalyst 3.....	127
5.4. Conclusion	128
5.5. References.....	129
5.6. Supporting Information.....	131
5.6.1. General information.....	131
5.6.2. Temperature screening.....	132
5.6.3. Solvent screening	132
5.6.4. Chemical shift assignments	134
5.6.5. Hydrogen bond investigation	135
5.6.6. Structural investigations of 3•4b	136
5.6.7. Diffusion Ordered Spectroscopy	138
5.6.8. Structural investigation in 2:1 complexes	141
5.6.9. References.....	141

5.7. Additional findings.....	142
5.7.1. Selection of model systems.....	142
5.7.2. NMR spectroscopic studies on 3b•3b•9a.....	142
5.7.3. Computational studies on 3b•3b•9a.....	145
5.7.4. Overview of CPA•CPA•imine systems.....	147
5.7.5. Conclusion.....	149
5.7.6. References.....	150
6. Bidentate Substrate Binding in Brønsted Acid Catalysis: Structural Space, Hydrogen Bonding and Dimerization.....	151
6.1. Abstract.....	152
6.2. Introduction.....	153
6.3. Results and Discussion.....	154
6.3.1. Initial System Screening and dimer formation.....	154
6.3.2. Molecular dynamic simulations of [1a/2a] ₂ dimers.....	157
6.3.3. Accessing CPA/imine monomers.....	159
6.4. Conclusion.....	163
6.5. References.....	164
6.6. Supporting Information.....	165
6.6.1. General information.....	165
6.6.2. Imine synthesis.....	167
6.6.3. Diffusion ordered spectroscopy (DOSY).....	180
6.6.4. Chemical Shift assignments.....	184
6.6.5. Initial system screening.....	186
6.6.6. Accessing CPA/imine monomers.....	191
6.6.7. Hydrogen bond analysis.....	195
6.6.8. NOE studies.....	197
6.6.9. References.....	198
7. A Thioxanthone Sensitizer with a Chiral Phosphoric Acid Binding Site: Properties and Applications in Visible Light-Mediated Cycloadditions.....	199

7.1. Abstract	200
7.2. Introduction.....	201
7.3. Results and Discussion	202
7.4. Conclusion	208
7.5. References.....	208
7.6. Supporting Information.....	210
8. Enantioselective [2+2] Photocycloaddition <i>via</i> Iminium Ions: Catalysis by a Sensitizing Chiral Brønsted Acid.....	218
8.1. Abstract	219
8.2. Introduction.....	220
8.3. Results and Discussion	221
8.4. Conclusion	226
8.5. References.....	226
8.6. Supporting Information.....	229
8.6.1. General information.....	229
8.6.2. Sample preparation.....	230
8.6.3. Variable temperature NMR.....	230
8.6.4. Chemical shift assignment and structural analysis of 6c/7e	232
8.6.5 Hydrogen bonding analysis in 6c/7e	234
8.6.6. Diffusion ordered spectroscopy (DOSY).....	236
8.6.7. Low temperature NMR studies with catalyst 6f.....	237
8.6.8. References.....	240
8.7. Additional Findings.....	241
8.7.1. Structural studies at 298 K	241
8.7.2. Illumination experiments	242
8.7.3. References.....	246
9. Tilting the Balance: London Dispersion Systematically Enhances Enantioselectivities in Brønsted Acid Catalyzed Transfer Hydrogenation of Imines.....	247
9.1. Abstract	248

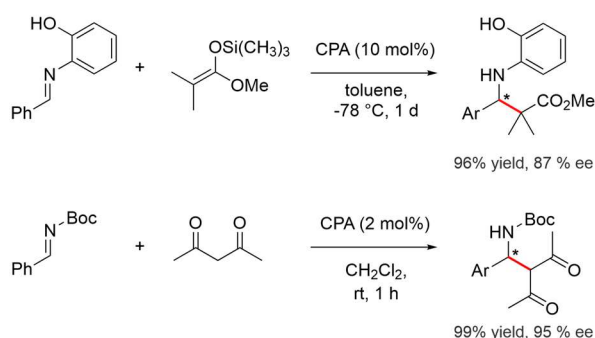
9.2. Introduction.....	249
9.3. Results and Discussion	252
9.3.1. Accessing Z-imine populations via CEST.....	252
9.3.2. London dispersion in CPA/N-aryl imine complexes	255
9.3.3. London dispersion in CPA/imine/nucleophile complexes.....	258
9.3.4. Impact of London dispersion on enantioselectivity	261
9.4. Conclusions.....	265
9.5. References.....	266
9.6. Supporting Information	269
9.6.1. General information	269
9.6.2. Imine synthesis and transfer hydrogenations.....	273
9.6.3. Chemical exchange saturation transfer (CEST) experiments	295
9.6.4. Additional measurements on CPA/N-aryl complexes	299
9.6.5. Additional measurements on CPA/N-benzyl complexes.....	300
9.6.3. Overview and spectra for Z/E ratios.....	302
9.6.7. Ternary complex formation.....	304
9.6.8. Competing transition states	306
9.6.9. Control experiments.....	308
9.6.10. Additional enantioselectivities	310
9.6.11. HPLC chromatograms	311
9.6.12. References.....	332
9.7. Additional Findings	333
10. Conclusion	353
11. Curriculum Vitae.....	356
12. Danksagung	359
13. Eidesstattliche Versicherung	361

1. Introduction and Outline

1.1. Brønsted acid catalysis

„Catalysis is probably one of the most important cultural achievements of humankind, similarly to the development of agriculture” as stated by Nobel laureate Benjamin List summarizes the tremendous, but typically overlooked influence of catalysis in our daily lives.^[1] Catalysis takes a key role in many processes and thus is involved in the processing of a majority of manufactured goods^[2] and without catalysis as a crucial part of nitrogen fixation in the “Haber-Bosch” process the current world population would be halved.^[3] Catalysis as one of the “12 principles of green chemistry” paves the pathway for more atom economic and selective transformations^[4] and lays the foundation for asymmetric synthesis of compounds especially targeted in pharmaceutical industry. Besides bio- and metal catalysis, organocatalysis has become the third pillar of asymmetric catalysis^[5] and features “small organic molecules, where an inorganic element is not part of the active principle”.^[6] Over the last 25 years, organocatalysis has become an integral part of synthetic chemistry, as highlighted by dedicating the Nobel prize in chemistry 2021 “for the development of asymmetric organocatalysis” to Benjamin List and David McMillan, two pioneers of the field. The long-lasting success story of using acids to promote reactivity was incorporated in the field by combining acidic motifs with organic frameworks to induce chirality. First examples for Brønsted acid catalysts were given by Jacobsen^[7] and Rawal^[8] in 1998 and 2003, but the breakthrough was achieved in 2004 by Akiyama^[9] and Terada^[10] with the development of chiral phosphoric acids (CPA) on the example of asymmetric Mannich reactions (see Figure 1A).

A) Mannich reactions by Akiyama and Terada



B) chiral phosphoric acids (CPA)

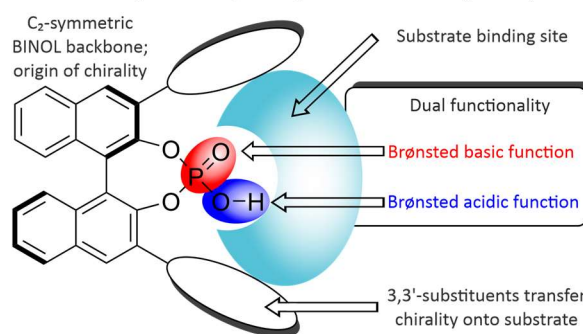


Figure 1: A) Mannich reactions performed by Akiyama (top) and Terada (bottom). B) Design principle of a chiral phosphoric acid catalysts. The C₂-symmetric backbone is the origin of chirality, which is transferred onto the substrate inside the binding site by the 3,3'-substituents. A Brønsted acidic and basic function allow for dual activation of substrates.

Featuring a phosphoric acid motif (see Figure 1B), typically substrates with C=X double bonds are activated via protonation, resulting in increased electrophilicity by an energetically lowered lowest unoccupied molecular orbital (LUMO). The substrate is fixated in the binding site mainly via Coulomb

1. Introduction and Outline

and/or hydrogen bonding interactions, and the stereoinductive environment for subsequent transformations is created by the combination of the C₂-symmetric backbone and 3,3'-substituents.^[11–13] Further development of the catalysts led to a variety of different backbone frameworks, a plethora of 3,3'-substituents featuring almost exclusively (substituted) aromatic building blocks and various acidic motifs.^[13] Additionally, current research features catalysts with two linked acids to further confine the reaction space^[14] or combines Brønsted acid catalysis with metal- or photocatalysis.^[15–18]

The combination of backbone, 3,3'-substituent and acidic motif as modular entities allows to highly adapt the Brønsted acid catalyst to each individual synthetic challenge, but makes a sophisticated and rational catalyst design indispensable. Exemplarily, Goodman *et al.* developed a model based on steric parametrization of CPAs and reactants to predict and favor the major product stereoisomer (see Figure 2A).^[19–21] Additionally, Sigman *et al.* demonstrated that a data-driven multivariate linear regression approach involving steric and electronic descriptors allows to obtain a general understanding of how to optimize the catalyst and reaction conditions (see Figure 2B).^[22]

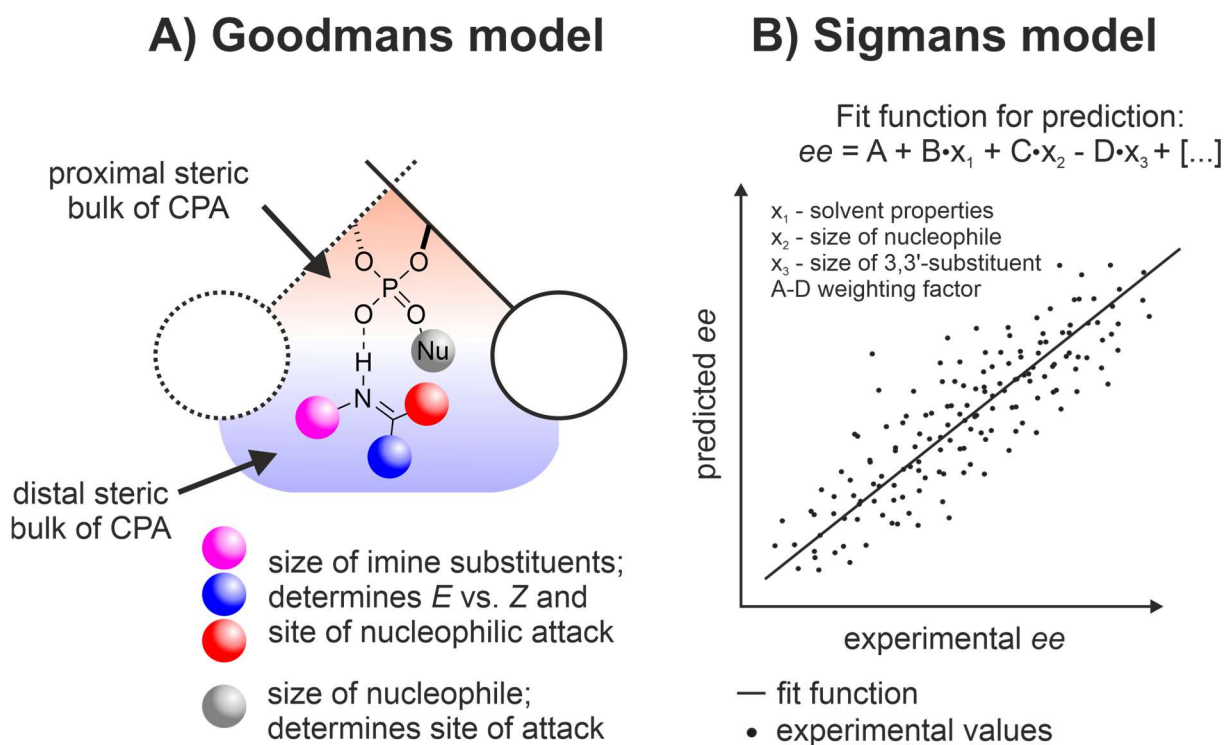


Figure 2: A) Goodman's model for predicting the stereoselective outcome of CPA catalyzed transformations based on steric parametrization of the imine residues, the nucleophile and the 3,3'-substituent (proximal and distal bulk). B) Sigman's multivariate linear regression model for CPA catalyzed nucleophilic additions to imines. The resulting fit function features various molecular parameters x , reflecting amongst others the solvent properties, size of nucleophile and size of 3,3'-substituents.

However, both approaches rely exclusively on computations and do not necessarily capture unprecedented changes of reaction mechanisms. Hence, mechanistic studies to obtain a better and broader understanding of Brønsted acid catalyzed transformations, especially regarding mode and degree of

activation, structural space and confinement, secondary non-covalent interactions decisive for stereoselectivity, association and aggregation of catalyst and reactants and different general reaction pathways are indispensable to achieve a holistic approach for rational reaction design.

1.2. Outline

In the pursue of establishing a holistic understanding of Brønsted acid catalysis, this thesis presents a series of detailed experimental studies focusing on NMR-spectroscopy as central analytical tool to shed light onto different mechanistic pathways, aggregation, hydrogen bonding and origin of stereoselectivity in the field of asymmetric Brønsted acid catalysis.

In the third chapter of this thesis, the CPA catalyzed transfer hydrogenation of imines was selected as a model system to exemplarily elucidate the structural space of binary CPA/imine reaction intermediates by low temperature 2D NMR spectroscopy. Building up on previous research regarding one specific CPA catalyst, 5 more CPAs were selected to cover the whole range of steric properties of the catalysts 3,3'-substituent and binary complexes with 7 different imine substrates with varying electrostatic properties were studied. In total, 16 CPA/imine combinations were screened and 8 combinations were investigated in detail. Analogous to previous studies, four core structures Type I *E*, Type II *E*, Type I *Z* and Type II *Z* were observed, featuring either the *E*- or *Z*- imine in two conformations (Type I and II), which differ in the orientation of the imine inside the CPA binding pocket (rotated by $\sim 180^\circ$). While at low temperature (-93°C), the CPA/*E*-imine and CPA/*Z*-imine complexes give separated NMR signal sets, only one averaged set of signals is observed for the respective Type I and Type II conformations, as they are fast exchanging on the NMR time scale even at low temperatures. An astonishing invariance of these four CPA/imine core structures independent of the 3,3'-substituents properties was found in the NOESY NMR studies and corroborated by computations. Additionally, for the first time [CPA/imine]₂ dimers were observed and analyzed in solution, which feature two stacked imine molecules in a shifted face-to-face arrangement in between two catalyst molecules. These [CPA/imine]₂ dimers are extending the structural space of catalytic intermediates and are expected to resemble an off-cycle equilibrium with the monomeric CPA/imine complexes. This chapter was published in Chemical Science.

In the fourth chapter of this thesis, the fast exchange process between the Type I *E* and Type II *E* conformation of binary CPA/imine intermediates could be accessed by Relaxation Dispersion NMR, allowing to extend the time-frame of observable dynamic processes from the millisecond to the microsecond (nanosecond with additional low temperature) time scale. ¹H off-resonance R_{1ρ} NMR allowed not only to determine exchange rates (2500 – 19 000 s⁻¹) between the Type I *E* and Type II *E* conformation,

1. Introduction and Outline

but with measurements at different temperatures it was even possible to quantify the populations of these intermediates. Analysis of the exchange rates for various systems allowed to obtain detailed insights into the exchange mechanisms and their dependency on the steric properties and acidity of the CPA catalyst. This chapter was published in the Journal of the American Chemical Society. Further investigations explored, if the equilibrium between the fast exchanging Type I *E* and Type II *E* conformation can serve as a molecular balance system to quantify interaction energies between catalyst and imine.

The fifth chapter shed light onto the dimerization of CPAs and its impact as alternative dimeric reaction channel. On the example of the CPA catalyzed two-fold transfer hydrogenation of quinolines, the catalyst concentration depending competition between monomeric and dimeric reaction channel was studied. Kinetic measurements showed that interlocking two CPAs by a catenane scaffold forced the system into the dimeric reaction channel, while employing a macrocyclic catalyst suppressed it. For acyclic standard CPA catalysts, a non-linear dependency of reaction rate and catalyst loading was found and a catalyst order of 1.25 to 1.75 was derived by kinetic measurements depending on the catalyst loading. Additionally, a strong dependence of the enantioselectivity on the catalyst loading was observed for acyclic CPAs, demonstrating the competition of monomeric and dimeric channel. Low temperature NMR measurements at a 2:1 ratio of catalyst and quinoline substrate revealed the presence of monomeric CPA/quinoline and dimeric CPA/CPA/quinoline intermediates and were corroborated by Diffusion Ordered Spectroscopy (DOSY) measurements. This chapter was published in Chemical Science. Further investigations translated the findings on respective CPA/imine system, showing the presence of CPA/CPA/*E*-imine and CPA/CPA/*Z*-imine dimers at a 2:1 ratio of catalyst and imine.

The sixth chapter of this thesis elucidates the structural space, hydrogen bonding and dimerization of CPA/imine complexes with a bidentate binding motif enabled by an additional hydrogen bond donor. 19 binary complex samples of 8 *N*-(*ortho*)-hydroxy aryl imines and 8 CPAs were investigated by low temperature NMR and revealed an astonishingly broad structural space, although a bidentate binding motif was surmised to result in a rigid and well-defined preorganization of catalyst and substrate. DOSY NMR measurements characterized the observable species as various [CPA/imine]₂ dimers and molecular dynamic (MD) simulations identified different dimeric motifs, all in which two imine molecules form each one hydrogen bond to two CPA molecules, effectively bridging two catalysts. Fine-tuning of steric and electrostatic properties of the imine and CPA allowed to suppress the dimer formation and to access the CPA/imine monomer. The bidentate binding by two hydrogen bonds could be unambiguously determined by detection of trans-hydrogen bond scalar coupling. NOESY NMR elucidated the CPA/imine monomer structure, in which the imine is placed in between the 3,3'-substituents of the catalyst, revealing the origin of stereoselectivity for related transformations: one 3,3'-substituent is

1. Introduction and Outline

shielding one site of the imine, thus enforcing an asymmetric nucleophilic attack. This work is under revision in Chemical Science.

The seventh and eighth chapter of this thesis were done in collaboration with Franziska Pecho from the group of Prof. Dr. Thorsten Bach and focused on merging Brønsted acid catalysis with photocatalysis. Employing a photosensitizing thioxanthone unit as 3,3'-substituent allows to activate substrates via protonation, to bind them in a stereoinductive environment by hydrogen bonding and facilitates a selective energy transfer onto the substrate by the light harvesting thioxanthone antenna upon illumination with visible light. As a proof of principle, in the seventh chapter this new CPA catalyst was used for the asymmetric [2+2] photocycloaddition of β -carboxyl-substituted cyclic enones, yielding enantiomeric ratios up to 93:7. Binding of the carboxylic acid to the CPA catalyst was proven by low temperature NMR studies via NOESY and DOSY NMR experiments. Variable temperature NMR experiments allowed to derive temperature coefficients for the chemical shift of the hydrogen bonded proton signals and revealed the presence of monomeric and dimeric/oligomeric CPA/substrate species. This chapter was published in *Chemistry – A European Journal*. Following up on this proof-of-principle study, the thioxanthone substituted CPA was employed in the asymmetric [2+2] photocycloaddition of cyclic N,O-acetals as described in the eighth chapter of this thesis. Upon protonation by the catalyst, the open iminium ion form is generated and the now unprotected hydroxy-group forms an additional hydrogen bond to the catalyst. Cycloaddition products with various olefins were received in yields up to 96% and enantiomeric ratios up to 99:1 and even higher diastereoselectivities were obtained. Low temperature NMR measurements confirmed the cyclic N,O-acetal opening and bidentate binding of catalyst and imine substrate via hydrogen bonding. The CPA/imine intermediate was characterized as hydrogen bond assisted ion pair and two different substrate conformations were identified, differing in the arrangement of the substrate backbone. This chapter was published in the *Journal of the American Chemical Society*. Further investigations explored the reaction mechanism under visible light illumination with the thioxanthone CPA and standard CPAs in combination with transition metal photocatalysts.

The ninth chapter of this thesis focuses on secondary non-covalent interactions which are decisive for the enantioselectivities in CPA catalyzed transformations, resulting in a conceptual approach on exploiting London dispersion interactions to systematically enhance stereoselectivities. The CPA catalyzed transfer hydrogenation of (*E*)- or (*Z*)-*N*-phenyl ketimines was selected as suitable model reaction. The equilibrium between the low populated *Z*-imine (~1%) and major populated *E*-imine (~99%) could be accessed by Chemical Exchange Saturation Transfer (CEST) NMR experiments. Implementing *tert*-butyl groups as dispersion energy donor (DED) residues in the imine framework resulted in a stabilization of the *Z*-imine by London dispersion up to 4.5 kJ/mol. NMR studies revealed that this additional

1. Introduction and Outline

stabilization is transferred onto the structurally confined reaction intermediates (binary CPA/imine and ternary CPA/imine/nucleophile complex), while the steric bulk of the DED residues has no significant effect on the structures of the intermediates. It was even possible to read out the effect of the dispersion stabilization in the obtained stereoselectivities, resulting in a clear correlation between London dispersion stabilization and enantioselectivity. This approach allowed to convert moderate-good to good-excellent enantioselectivities under dispersion control, exceeding the typical enantiomeric ratios for standard imine substrates. This work is accepted for publication in the Journal of the American Chemical Society. Additional studies explored the applicability of the approach for a different nucleophile.

In summary, this thesis presents a series of NMR-spectroscopic studies corroborated by synthetic and computational investigations to shed light onto various mechanistic aspects of catalysis with chiral phosphoric acid catalysts bearing a 1,1'-bi-2-naphthol (BINOL) backbone. Central research aims were i) elucidation of substrate activation by protonation and binding by hydrogen bonding, especially regarding bidentate binding with additional hydrogen bond donors, ii) extension of the structural space of CPA/substrate complexes resembling mechanistic intermediates, especially focusing on the formation of higher aggregates such as CPA/CPA/substrate and bridged/non-bridged [CPA/imine]₂ dimers, iii) revelation of dynamic behavior and exchange processes within catalytic intermediates as well as iv) conceptualization of new approaches to increase stereoselectivities, especially by implementation of London dispersion interactions. The presented work significantly extends the previous mechanistic knowledge about asymmetric catalysis with Brønsted acid organocatalysts and contributes to establish a holistic understanding of this catalysis, allowing for a better, more rational and more sophisticated reaction design in the future.

1.3. References

- [1] Benjamin List, 71st Lindau Nobel Laureate Meeting, Lindau, 30.06.2022. See <https://www.mediatheque.lindau-nobel.org/recordings/39774>
- [2] C. R. A. Catlow, M. G. Davidson, C. Hardacre, G. J. Hutchings, *Philos. Trans. R. Soc. London A* **2016**, *374*, 1–2.
- [3] J. W. Erisman, M. A. Sutton, J. Galloway, Z. Klimont, W. Winiwarter, *Nat. Geosci.* **2008**, *1*, 636–639.
- [4] P. Anastas, N. Eghbali, *Chem. Soc. Rev.* **2010**, *39*, 301–312.
- [5] P. I. Dalko, Ed. , *Comprehensive Enantioselective Organocatalysis*, Wiley-VCH Verlag GmbH & Co. KGaA, Weinheim, Germany, **2013**.
- [6] B. List, *Chem. Rev.* **2007**, *107*, 5413–5415.
- [7] M. S. Sigman, E. N. Jacobsen, *J. Am. Chem. Soc.* **1998**, *120*, 4901–4902.
- [8] Y. Huang, A. K. Unni, A. N. Thadani, V. H. Rawal, *Nature* **2003**, *424*, 146.
- [9] T. Akiyama, J. Itoh, K. Yokota, K. Fuchibe, *Angew. Chem. Int. Ed.* **2004**, *43*, 1566–1568.
- [10] D. Uraguchi, M. Terada, *J. Am. Chem. Soc.* **2004**, *126*, 5356–5357.
- [11] T. Akiyama, *Chem. Rev.* **2007**, *107*, 5744–5758.
- [12] M. Terada, *Synthesis* **2010**, 1929–1982.
- [13] D. Parmar, E. Sugiono, S. Raja, M. Rueping, *Chem. Rev.* **2014**, *114*, 9047–9153.
- [14] L. Schreyer, R. Properzi, B. List, *Angew. Chem. Int. Ed.* **2019**, *58*, 12761–12777.
- [15] Z. P. Yang, W. Zhang, S. L. You, *J. Org. Chem.* **2014**, *79*, 7785–7798.
- [16] M. Rueping, R. M. Koenigs, I. Atodiresei, *Chem. Eur. J.* **2010**, *16*, 9350–9365.
- [17] F. Pecho, Y. Q. Zou, J. Gramüller, T. Mori, S. M. Huber, A. Bauer, R. M. Gschwind, T. Bach, *Chem. Eur. J.* **2020**, *26*, 5190–5194.
- [18] L. J. Rono, H. G. Yayla, D. Y. Wang, M. F. Armstrong, R. R. Knowles, *J. Am. Chem. Soc.* **2013**, *135*, 17735–17738.
- [19] L. Simón, J. M. Goodman, *J. Org. Chem.* **2011**, *76*, 1775–1788.
- [20] J. P. Reid, L. Simón, J. M. Goodman, *Acc. Chem. Res.* **2016**, *49*, 1029–1041.
- [21] J. P. Reid, J. M. Goodman, *Chem. Eur. J.* **2017**, *23*, 14248–14260.
- [22] J. P. Reid, M. S. Sigman, *Nature* **2019**, *571*, 343–348.

2. General remarks

2.1. Structure of this work

The main part of this thesis is divided into seven chapters, six of them are published or accepted for publication in a scientific journal and one is currently under revision for publication. At the beginning of each chapter the contributions of each author are listed in detail. Each chapter is organized into abstract, introduction, results and discussion, conclusion, references, supporting information and (if applicable) additional findings. In the subchapters supporting information, only parts of the published versions are given. This includes additional discussions and experimental details of the contribution of Johannes Gramüller. Experimental details of the work of co-authors are not given unless necessary and computational results are omitted. For each chapter, the full version of the supporting information is available online free of charge. Each chapter has an individual numbering of molecules, figures, schemes and tables, starting at 1 for each chapter. If in the supporting information only parts of the published version are given, the numbering of figures and schemes is not changed and therefore can start not at 1. References are numbered individually for each chapter and within each chapter individually for abstract to conclusion, supporting information and additional findings, starting at 1 for each chapter.

2.2. List of publications

The following publications are integrated in this work (chapters 3-9). The individual contributions of each author are given in the beginning of the respective chapter. Chapter 6 is currently under revision for publication.

Chapter 3: M. Melikian, J. Gramüller, J. Hioe, J. Greindl, R.M. Gschwind, Brønsted acid catalysis – the effect of 3,3'-substituents on the structural space and the stabilization of imine/phosphoric acid complexes. *Chemical Science* **2019**, *10*, 5226-5234. (shared first author)

Chapter 4: N. Lokesh, J. Hioe, J. Gramüller, R.M. Gschwind, Relaxation Dispersion NMR to Reveal Fast Dynamics in Brønsted Acid Catalysis: Influence of Sterics and H-Bond Strength on Conformations and Substrate Hopping. *Journal of the American Chemical Society* **2019**, *141*, 16398-16407.

Chapter 5: D. Jansen, J. Gramüller, F. Niemeyer, T. Schaller, M.C. Letzel, S. Grimme, H. Zhu, R.M. Gschwind, J. Niemeyer, What is the role of acid–acid interactions in asymmetric phosphoric acid organocatalysis? A detailed mechanistic study using interlocked and non-interlocked catalysts. *Chemical Science* **2020**, *11*, 4381-4390.

2. General remarks

Chapter 6: J. Gramüller, P. Dullinger, D. Horinek, R. M. Gschwind, Bidentate Substrate Binding in Brønsted Acid Catalysis: Structural Space, Hydrogen Bonding and Dimerization. *Chemical Science* **2022**, *13*, 14366-14372.

Chapter 7: F. Pecho, Y. Zou, J. Gramüller, T. Mori, S.M. Huber, A. Bauer, R.M. Gschwind, T. Bach, A Thioxanthone Sensitizer with a Chiral Phosphoric Acid Binding Site: Properties and Applications in Visible Light-Mediated Cycloadditions. *Chemistry – A European Journal* **2020**, *26*, 5190-5194.

Chapter 8: F. Pecho, Y. Sempere, J. Gramüller, F.M. Hörmann, R.M. Gschwind, T. Bach, Enantioselective [2 + 2] Photocycloaddition via Iminium Ions: Catalysis by a Sensitizing Chiral Brønsted Acid. *Journal of the American Chemical Society* **2021**, *143*, 9350-9354.

Chapter 9: J. Gramüller, M. Franta, R. M. Gschwind, Tilting the Balance: London Dispersion Systematically Enhances Enantioselectivities in Brønsted Acid Catalyzed Transfer Hydrogenation of Imines. *Journal of the American Chemical Society* **2022**, *144*, 19861-19871.

In addition to these, during the PhD studies leading to this work contributions to several other publications were made. These are not included as chapters in the presented PhD thesis to keep the general topic of this thesis concise and because the own work was not a major part of the final project/publication. Hence, only an overview is given and the contribution to the work is noted.

1) K. Rothermel, M. Melikian, J. Hioe, J. Greindl, J. Gramüller, M. Žabka, N. Sorgenfrei, T. Hausler, F. Morana, R.M. Gschwind, Internal acidity scale and reactivity evaluation of chiral phosphoric acids with different 3,3'-substituents in Brønsted acid catalysis. *Chemical Science* **2019**, *10*, 10025-10034.

In this work, the hydrogen bonding of binary CPA/imine complexes was studied by low temperature NMR spectroscopy. The hydrogen bond strength was characterized by ^1H and ^{15}N chemical shifts and $^1\text{h}_{\text{HN}}$ coupling constants. Comparison of these values for different CPAs and imines allowed to qualitatively assess the internal acidity of different catalysts. In combination with NMR isomerization kinetics, it was suggested that the rate determining step of the reaction is a balance between the ternary CPA/imine/Hantzsch ester formation and the imine isomerization.

All NMR measurements with the TRIM catalyst **1d** (with 3 imines; *E* and *Z* complexes) were performed by Johannes Gramüller. This includes acquisition of the ^1H and ^{15}N chemical shifts, $^1\text{J}_{\text{NH}}$ coupling constants, experiments to validate fast formation of the binary CPA/imine complex and reactivity experiments with TRIM/imine complex and Hantzsch Ester at 180 K and 220 K. Johannes Gramüller assisted in interpretation of experimental data and the writing of the manuscript.

2. General remarks

2) R. R. Annapureddy, F. Burg, J. Gramüller, T. P. Golub, C. Merten, S. M. Huber, T. Bach, Silver-Catalyzed Enantioselective Sulfimidation Mediated by Hydrogen Bonding Interactions. *Angew. Chem. Int. Ed.* **2021**, 60, 7920-7926.

In this work, 3-thiosubstituted 2-quinolines and 2-pyridones were subjected to enantioselective sulfimidation using a nitrene source and Ag^+ as catalyst. 1,10-phenanthroline and a chiral phenanthroline derivative bearing a lactam hydrogen bonding site for substrate recognition were used as ligands. Mechanistic investigations featuring DFT calculations, ESI mass spectrometry and a Hammett analysis revealed that the active catalyst is a heteroleptic silver complex featuring one chiral and one achiral phenanthroline ligand.

The Diffusion Ordered Spectroscopy (DOSY) NMR measurements on homo- and heteroleptic silver complexes with achiral and chiral phenanthroline ligands were performed by Johannes Gramüller. All results are discussed in chapter 4 of the supporting information.

3) R. Yadav, M. Weber, A. K. Singh, L. Münzfeld, J. Gramüller, R. M. Gschwind, M. Scheer, P. W. Roesky, A Structural Diversity of Molecular Alkaline-Earth-Metal Polyphosphides: From Supramolecular Wheel to Zintl Ion. *Chemistry – A European Journal*, **2021**, 27, 14128-14137.

In this work, a series of polyphosphides was synthesized by activating polyphosphorus sources with group 2 reagents such as organo-magnesium. The formation of a tetrameric supramolecular wheel was observed by X-ray crystallography and in solution with NMR spectroscopy (spin system and diffusion coefficients).

The Diffusion Ordered Spectroscopy (DOSY) NMR measurements and interpretation of the results were performed by Johannes Gramüller. All results are discussed in chapter 4 of the supporting information.

4) J. Kelly, J. Gramüller, R. M. Gschwind, R. Wolf, Low-oxidation state cobalt–magnesium complexes: ion-pairing and reactivity. *Dalton Transactions*, **2021**, 50, 13985-13992.

In this work, a series of magnesium cobaltates ($\text{Ligand}^1\text{MgCo}(\text{Ligand}^2)_2$) was synthesized. Diffusion Ordered Spectroscopy (DOSY) NMR measurements, X-ray crystallography and DFT calculations showed that these magnesium cobaltates form contact ion-pairs in toluene and solvent separated ion-pairs in THF. The effect of ion-pairing on the reactivity was studied with a phosphorus nucleophile, yielding either heteroleptic or homoleptic product complexes.

The Diffusion Ordered Spectroscopy (DOSY) NMR measurements and interpretation of the results were performed by Johannes Gramüller. All results are discussed in chapter 3 of the supporting information (starting from Figure S35).

2. General remarks

5) P. Degot, V. Huber, A. E. Maangar, J. Gramüller, L. Rohr, D. Tourad, T. Zemb, R. M. Gschwind, W. Kunz, Triple role of sodium salicylate in solubilization, extraction, and stabilization of curcumin from *Curcuma longa*. *Journal of Molecular Liquids* **2021**, 329, 115538.

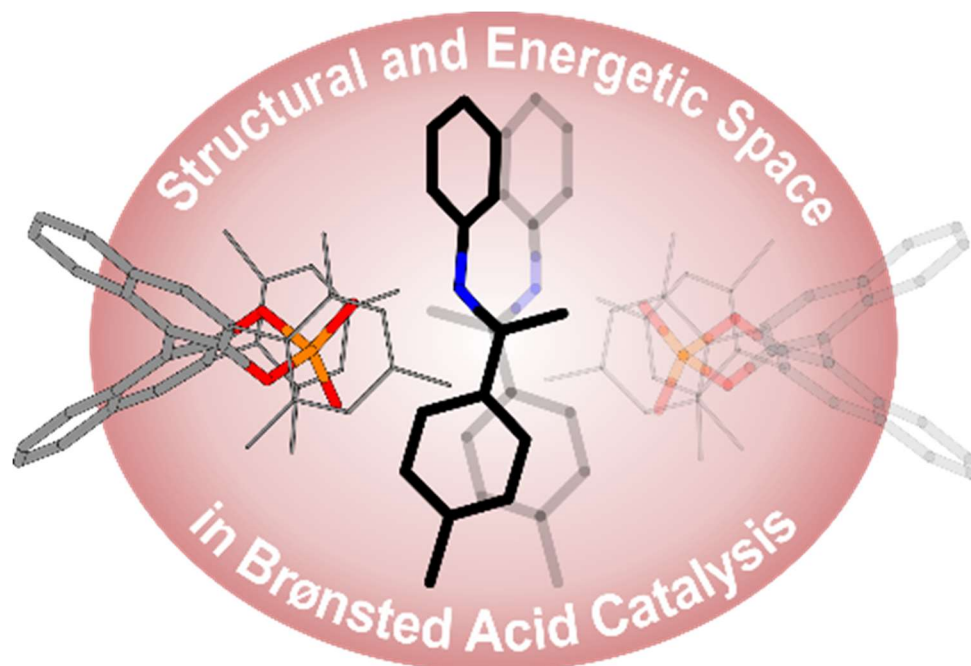
For summary of the publication and contribution see 6).

6) Asmae El Maangar, Johannes Gramüller, Verena Huber, Pierre Degot, Didier Touraud, Ruth M. Gschwind, Werner Kunz, Thomas Zemb, Solubilisation-microstructure relationship of trivalent salts in hydrotropic ternary systems, *to be submitted*.

In publications 5 and 6, a ternary phase system consisting of water, ethyl acetate and sodium salicylate was used for the extraction of curcumin from *Curcuma longa* and its potential for the solubilization/extraction of rare earth metals such as lanthanum was investigated. The ternary phase system was studied and characterized by a variety of different techniques, including Diffusion Ordered Spectroscopy (DOSY) NMR measurements and Small- and Wide-Angle X-Ray Scattering (SWAXS) experiments.

All Diffusion Ordered Spectroscopy (DOSY) NMR measurements were performed by Johannes Gramüller, including additional reference measurements not included in the publications. Overall, more than 200 DOSY NMR measurements on over 60 samples were performed.

3. Brønsted Acid Catalysis – The Effect of 3,3'-Substituents on the Structural Space and the Stabilization of Imine/Phosphoric Acid Complexes



Maxime Melikian,[†] Johannes Gramüller,[†] Johnny Hioe, Julian Greindl and Ruth M. Gschwind

Chem. Sci., 2019, **10**, 5226-5234 ([†] authors contributed equally to this work).

DOI: 10.1039/C9SC01044K

A) NMR measurements for the structure determination and chemical shift assignments for catalysts TIPSU and TRIFP were performed by Maxime Melikian. M. M. assisted in writing the manuscript. B) NMR measurements for the structure determination and chemical shift assignments for catalysts TRIM, 1-naph and 9-phen were performed by Johannes Gramüller. All *ee* values were determined by Johannes Gramüller. Johannes Gramüller assisted in writing the manuscript (mainly writing the chapter on TRIM/imine complexes and substituent effect on enantioselectivity). C) All theoretical calculations were performed by Johnny Hioe. D) The manuscript was mainly written by Julian Greindl and Johnny Hioe. E) R. M. Gschwind contributed to conceptualization of the project, design of experiments, interpretation of data, writing and proof-reading of the manuscript and provided funding.

Source of this chapter: RSC Publications, <https://pubs.rsc.org/en/content/articlelanding/2019/sc/c9sc01044k#fn1>

Reproduced with permission from the Royal Society of Chemistry. Text and figures may differ from the published version. The complete corresponding Supporting Information is provided free of charge at <https://doi.org/10.1039/C9SC01044K>.

3.1. Abstract

BINOL derived chiral phosphoric acids (CPAs) are widely known for their high selectivity. Numerous 3,3' substituents are used for a variety of stereoselective reactions and theoretical models of their effects are provided. However, experimental data about the structural space of CPA complexes in solution is extremely rare and so far restricted to NMR investigations of binary TRIP/imine complexes featuring two *E*- and two *Z*-imine conformations. Therefore, in this paper the structural space of 16 CPA/imine binary complexes is screened and 8 of them are investigated in detail by NMR. For the first time dimers of CPA/imine complexes in solution were experimentally identified, which show an imine position similar to the transition state in transfer hydrogenations. Furthermore, our experimental and computational data revealed an astonishing invariance of the four core structures regardless of the different steric and electronic properties of the 3,3'-substituent. However, a significant variation of *E/Z*-ratios is observed, demonstrating a strong influence of the 3,3'-substituents on the stabilization of the imine in the complexes. These experimental *E/Z*-ratios cannot be reproduced by calculations commonly applied for mechanistic studies, despite extensive conformational scans and treatment of the electronic structure at a high level of theory with various implicit solvent corrections. Thus, these first detailed experimental data about the structural space and influence of the 3,3' substituent on the energetics of CPA/imine complexes can serve as basis to validate and improve theoretical predictive models.

3.2. Introduction

In the field of Brønsted acid catalysis^{1,2} a variety of different catalyst classes have emerged in recent years, one of the most famous being BINOL (1,1'-bi-2-naphthol) derived chiral phosphoric acids (CPAs).^{3,4} CPAs have been successfully applied in various enantioselective syntheses such as transfer hydrogenations (see Figure 1a),^{5,6} reductive aminations,^{7,8} Mannich type reactions,⁹⁻¹¹ Strecker reactions,¹² and enantioselective additions.^{13,14} The main difference between these BINOL derived CPAs are the 3,3' substituents, which significantly influence not only yields, but especially the stereoselectivity of these reactions. Typical 3,3' substituents successfully employed are e.g. 2,4,6-triisopropylphenyl groups in the Brønsted acid catalyst TRIP, 3,5-bis(trifluoromethyl) groups in TRIFP, or triphenylsilyl groups in TiPSY (see Figure 1b).^{5,6,15} When the bulkiness of the 3,3' substituents is increased, the cited transfer hydrogenations and the reductive amination generally show an increase in enantiomeric excess, but also a sudden drop in yield and enantioselectivity when using extended aromatic systems such as naphthyl, or 4-biphenyl groups.⁵⁻⁷ The reason for these differences is for most of these reactions largely unexplored and vary from reaction to reaction.¹⁶ As a result many synthetic methods using BINOL derived CPAs had to be developed via trial and error or screening methods.^{17,18}

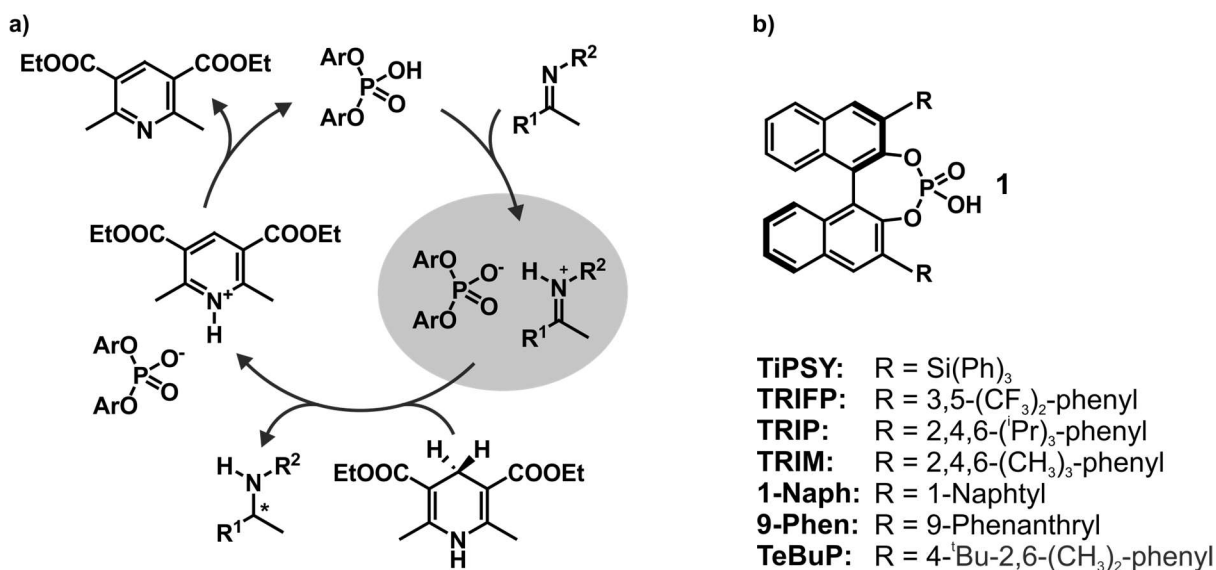


Figure 1. a) Catalytic cycle of the transfer hydrogenation of imines with a chiral phosphoric acid catalyst and a Hantzsch ester as reducing agent. The binary complexed highlighted in grey is the focus of this work; b) Brønsted acid catalysts with different 3,3' groups.

To shed light on the involved structures and to reveal the key interactions of reactivity and stereoselectivity so far mainly theoretical calculations and multivariant linear regression models have been applied.^{19,20} Thus, Goodman *et al.* linked the enantioselectivity to structural parameters of CPAs, such as the rotational barrier of the 3,3'-substituent describing the steric bulk close to the hydrogen bond and the cone angle AREA(Θ) of the substrate binding pocket, reflecting remote steric bulk.²¹ Furthermore, combining that with a steric classification of electrophiles and nucleophiles Goodman *et al.* developed

3. Brønsted Acid Catalysis – The Effect of 3,3'-Substituents on the Structural Space and the Stabilization of Imine/Phosphoric Acid Complexes

a webtool for predicting suitable CPA catalysts based on reactant structures.^{22–24} Parallel to that, Sigman *et al.* demonstrated how a data-driven approach can be capable of revealing nonintuitive insights about interactions involved in stereoselectivity determination by analysing the dependence of *ee* on steric and electronic molecular descriptors.^{20,25–27}

In contrast to the theoretical studies the information about the structures of CPAs/imine complexes based on experimental data is rather limited so far. To our knowledge, only two crystal structures were provided from the groups of MacMillan⁷ and Schneider²⁸ with strongly deviating structural features (see Figure 2 for structures and Figure 1 for substituents). While a TiPSY/imine complex adopts core structure *Type II E* proposed by theoretical calculations (see Figure 2a and c)²⁹ the second crystal structure of a TeBuP/imine complex exhibits an intermediate position of structures *Type I E* and *Type II E* (see Figure 2b and c).

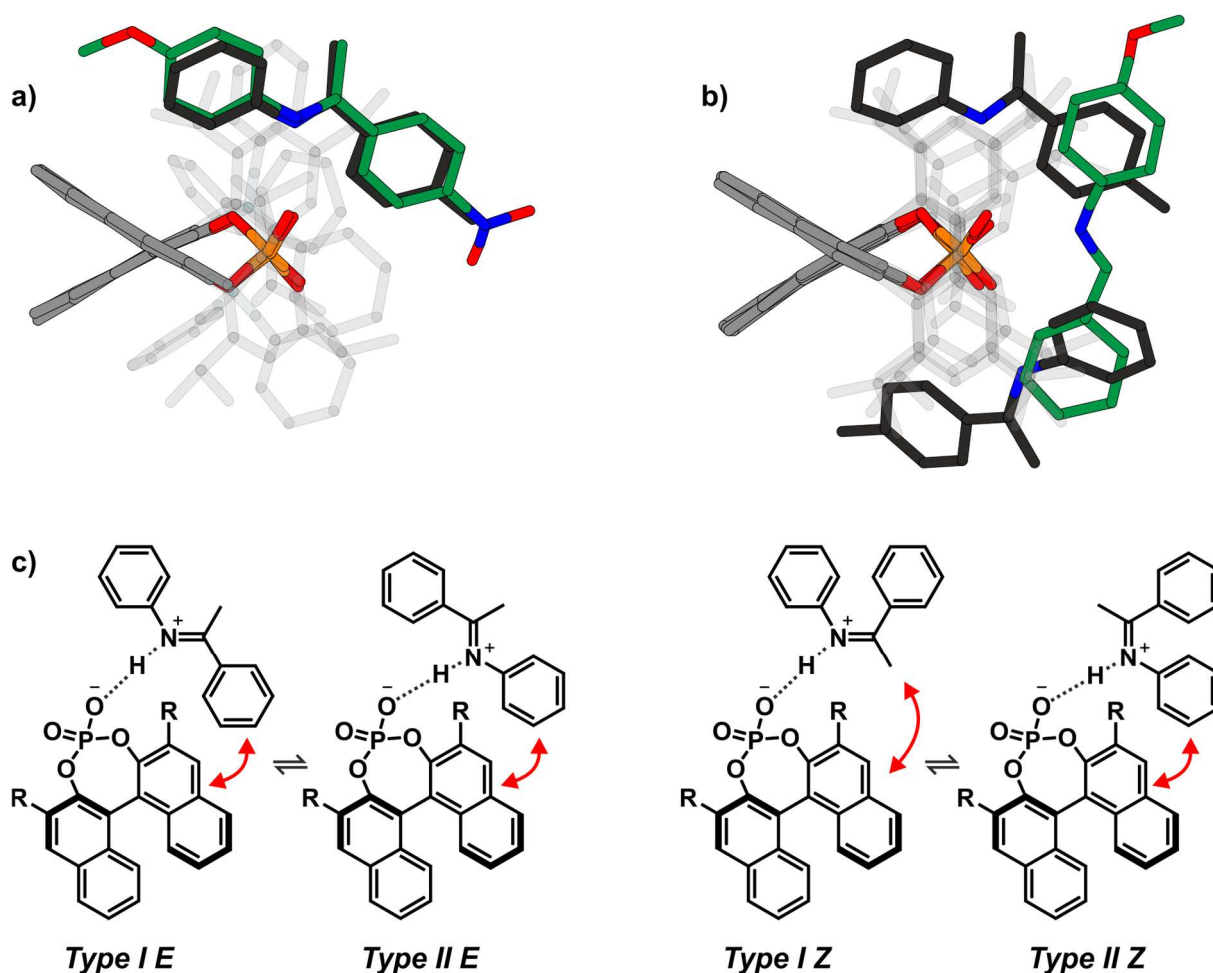


Figure 2. a) Structure similarity of a crystal structure of a TiPSY/imine complex⁷ (green) and structure *Type II E* of a TRIP/imine complex identified in our previous work²⁹ (black). b) structure deviation of the crystal structure of a TeBuP/imine complex²⁸ (green) vs both *Type I E* (black above) and *Type II E* (black below) of a TRIP/imine complex. The imine shows an intermediate position of *Type I E* and *Type II E*. c) The four core structures of the binary complex identified in our previous work.²⁹ The red arrows mark some of the identified NOE interactions.

3. Brønsted Acid Catalysis – The Effect of 3,3'-Substituents on the Structural Space and the Stabilization of Imine/Phosphoric Acid Complexes

In solution the experimental data base is similarly sparse. While two remarkable studies provided some NMR data about a ternary CPA complex³⁰ and a CPA reaction intermediate³¹ the first comprehensive insight about the structural space of CPA imine complexes and their hydrogen bond properties in solution was provided by our group on the example of TRIP/imine complexes.^{29,32} In depth NMR investigations revealed ionic complexes with extremely strong and highly covalent hydrogen bonds³² and a structural space covering the four core structures (*Type I/II E/Z*, shown in Figure 2c),²⁹ which were previously already predicted for ternary CPA/imine/nucleophile complexes by theoretical calculations.³³ However, the effect of varying 3,3'-substituents on the structure of CPA/imine complexes as well as on their population has so far remained elusive.

Therefore, in this report we present the first experimental data about the influence of different 3,3'-substituents on the structures and *E/Z* populations of complexes between chiral phosphoric acids and imines. A screening covering 16 binary complexes with 5 different chiral phosphoric acids and 7 imines and in depths structural investigations on selected examples reveal an astonishing invariance of the four main structures *Type I E*, *Type II E*, *Type I Z* and *Type II Z*. Moreover, for the first time dimeric CPA/imine complexes in solution were characterised, hence extending the structural space of those complexes in solution and forming a bridge to the dimeric crystal structure. In addition, comprehensive data about the *E/Z* population of these complexes are provided, which deviate significantly from the calculated values (e.g. for TRIP/5: experimental $\Delta G_{\text{rel } E/Z} = 2.0$ kJ/mol; theoretical $\Delta G_{\text{rel } E/Z} = 9.3$ kJ/mol).²⁹ This indicates a strong influence of refined dispersion interactions and/or solvent interactions not reflected by the commonly applied solvent models and offers the possibility to validate energetic results for theoretical prediction models in ion pairing catalysis.

3.3. Results and Discussion

3.3.1. Investigated complexes and their NMR properties

In order to investigate the influence of different 3,3'- substituents of CPAs as well as different substituents of the imines on the structures of CPA/imine complexes and their *E/Z* populations, we selected several CPA catalysts and imines (see Figure 3) used in synthesis³⁴ and screened their NMR properties. Dichloromethane was used as solvent, since it gave small signal linewidths and the highest achievable signal dispersion at low temperatures.²⁹ Furthermore, temperatures between 170 K and 200 K were needed to sufficiently slow down exchange processes in solution and most of the structural investigations were performed at 180 K unless otherwise noted.

3. Brønsted Acid Catalysis – The Effect of 3,3'-Substituents on the Structural Space and the Stabilization of Imine/Phosphoric Acid Complexes

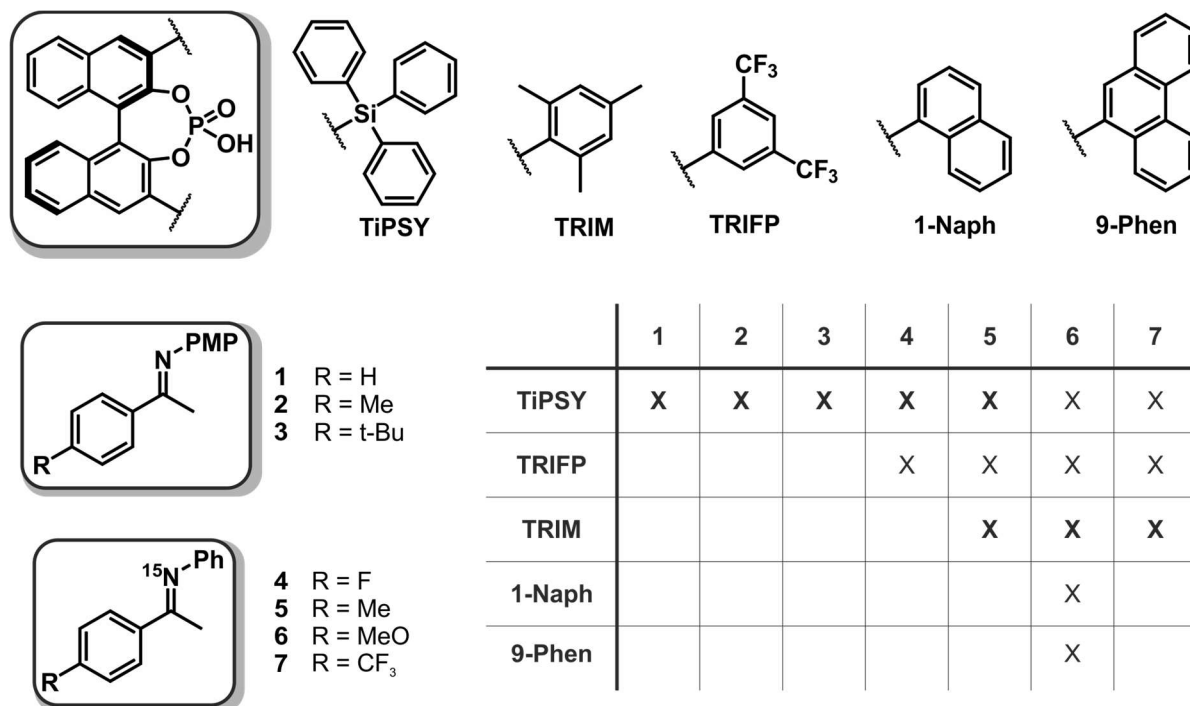


Figure 3. Chiral phosphoric acids and imines with different functional groups that were used for the NMR-spectroscopic investigations of CPA/imine complexes (PMP = *p*-methoxyphenyl). All screened CPA/imine combinations are shown in the table. A bold X marks complexes, which could be investigated in detail. For all systems, a 1:1 ratio of CPA and imine was used.

In principle, CPA/imine complexes with TiPSY and TRIFP produced basic signal pattern very similar to TRIP (see Figure 4). The spectra showed highly overcrowded aromatic regions and two well separated hydrogen bond signals for the *E* and *Z* complexes. Thus, quantification of *E* and *Z* complexes is straightforward by integration of the H-bond protons. The access to a detailed structural analysis however depended individually on the overlap of key signals and their linewidths. For TiPSY complexes a structural analysis could be completed despite the significantly higher signal overlap in the aromatic region compared to TRIP. For TRIFP complexes line width factors and chemical shift overlap of key signals prevented any further structural analysis.

3. Brønsted Acid Catalysis – The Effect of 3,3'-Substituents on the Structural Space and the Stabilization of Imine/Phosphoric Acid Complexes

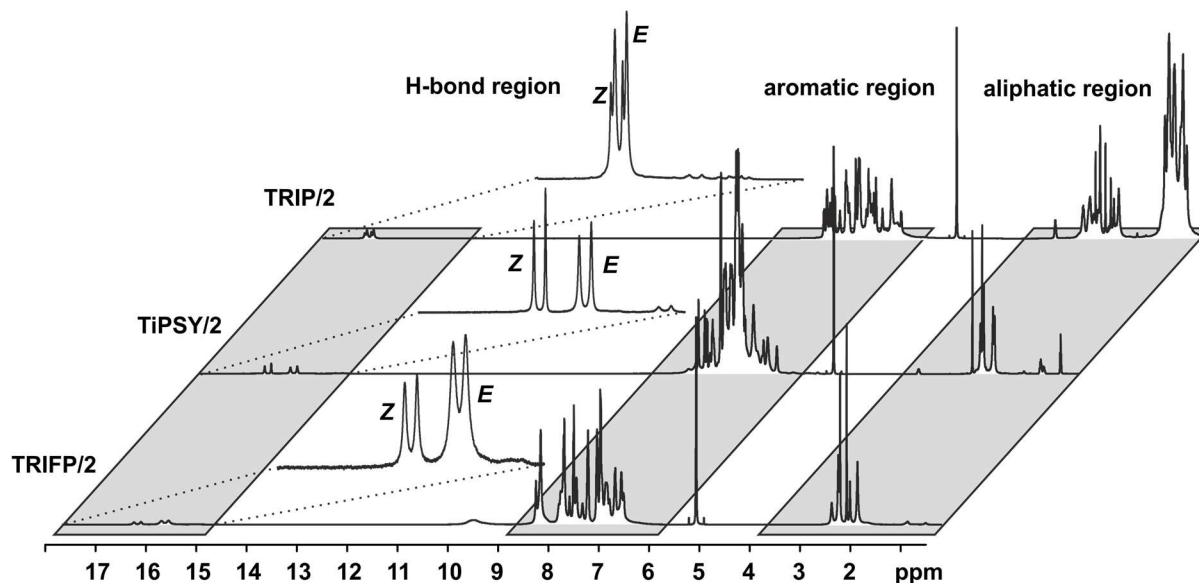


Figure 4. Spectral resolution of the ^1H spectra of complexes between catalysts TRIP, TiPSY and TRIFP and imine **2** at 180 K in CD_2Cl_2 ; in all cases well separated signals of the hydrogen bonds indicate the E/Z populations, while deviations in linewidths and chemical shift overlap of key signals allow the structural investigations via NOE analysis only for complexes with TiPSY.

For complexes with TRIM, 9-Phen, and 1-Naph as catalyst additional signals in the hydrogen bond region appeared at slightly lower chemical shifts (12.0 - 14.0 ppm) indicating an extended structural space for these complexes (see Figure 5). The detailed structural investigations of TRIM complexes (see below,) and dilution experiments for TRIM, 9-phen and 1-naph (see Supplementary S1-3) identified these species as dimers, most probably enabled by attractive interactions between the 3,3'- substituents of TRIM, 9-Phen, and 1-Naph and the imines. For 9-Phen and even more pronounced for 1-Naph, a plethora of additional signals appeared in the hydrogen bond region of the ^1H spectrum at 180 K. Given the asymmetry of the 3,3'-substituents of these catalysts and a rotational barrier of ≈ 14 kcal/mol,²¹ at least two slow exchanging rotational isomers of these catalyst are expected at 180 K, causing a signal splitting of the E and Z complexes, hence revealing the whole conformational space of these binary complexes.

3. Brønsted Acid Catalysis – The Effect of 3,3'-Substituents on the Structural Space and the Stabilization of Imine/Phosphoric Acid Complexes

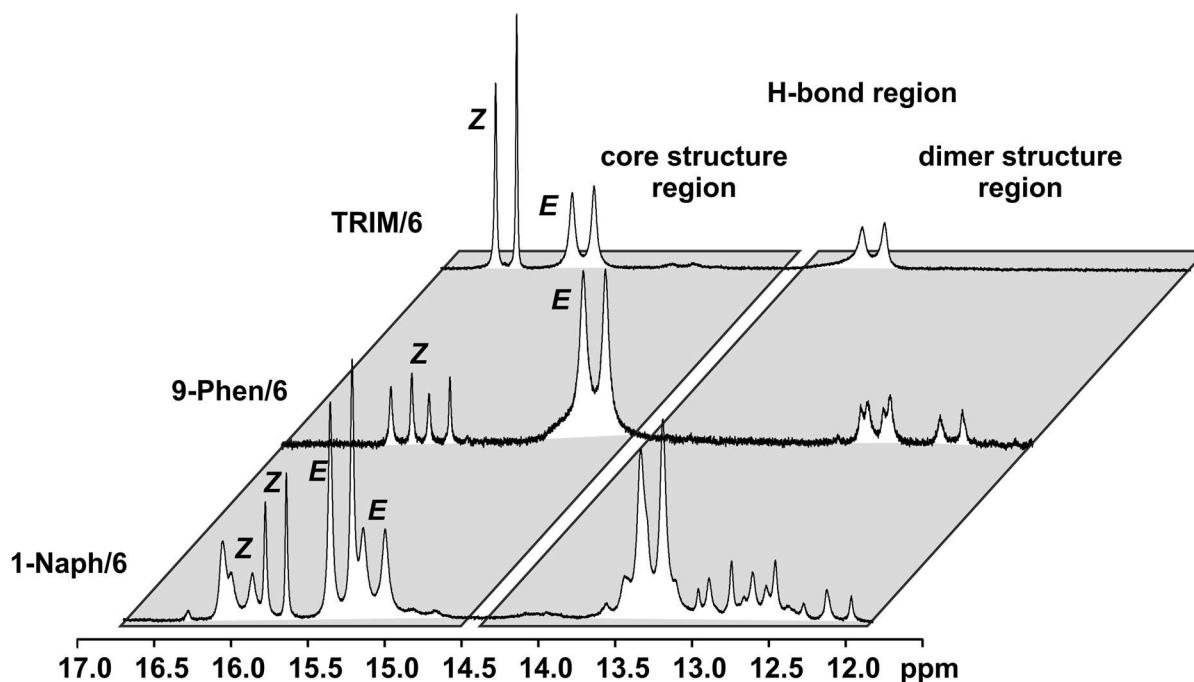


Figure 5 ^1H spectra of the H-bond region of catalysts TRIM, 9-Phen and 1-Naph at 180 K in CD_2Cl_2 reveal the extended structural space of these catalysts including dimeric complexes and additional conformations due to asymmetric 3,3' substituents in 9-Phen and 1-Naph.

Based on this NMR screening and initial 2D assignments, binary complexes with TIPSY and imines **1**, **2**, **3**, **4** and **5** as well as TRIM and imines **5**, **6**, **7** were selected for the in detail structural investigations described in the following.

3.3.2. Structural space of TiPSY/imine complexes

For complexes providing such degree of signal overlap as shown in the aromatic region in Figure 4, there are quite a few NMR spectroscopic techniques that are typically used to improve signal dispersion. These are mainly 3D experiments such as 3D- ^{15}N NOESY HSQC³⁵ or 3D ^{13}C NOESY HSQC³⁶ or pure shift techniques.^{37–39} Especially the multidimensional approach^{40–42} is broadly applied in biochemistry and requires the use of specific labelling strategies.^{43–45} Due to the limited possibilities to include isotope labelling via different synthetic strategies into the catalyst or the imine, the chemical exchange even at low temperatures²⁹ and the lowered solubility at the required temperatures, all of these more advanced techniques proved to be too insensitive to provide structural information in our case. Instead we focused mainly on the most sensitive one- and two-dimensional NMR methods ($^1\text{H}, ^1\text{H}$ / $^1\text{H}, ^{13}\text{C}$ 2D spectra for assignments and selective 1D NOESY^{46–48} / 2D NOESY / $^1\text{H}, ^{19}\text{F}$ HOESY^{49,50} spectra for structural investigations).

3. Brønsted Acid Catalysis – The Effect of 3,3'-Substituents on the Structural Space and the Stabilization of Imine/Phosphoric Acid Complexes

Table 1. Experimental *E/Z* ratios of the investigated CPA/imine complexes in CD₂Cl₂ at 180 K. Due to linewidth and signal overlap, a general error of 5% is expected.

	1	2	3	4	5	6	7
TRIP	n.d.	62:38	n.d.	n.d.	67:33	77:23	86:14
TiPSY	45:55	53:47	51:49	68:32	56:44	70:30	71:29
TRIFP	n.d.	n.d.	n.d.	83:17	70:30	81:19	69:30
TRIM	n.d.	n.d.	n.d.	n.d.	47:53	49:51	55:45

In TiPSY/imine mixtures (1:1) at 180 K varying *E/Z* complex ratios were found with a trend to higher *Z* amounts compared to TRIP/imine and TRIFP/imine complexes (see Table 1). A similar trend can be observed for TRIM/imine complexes. In TiPSY/**4**, the *E/Z* ratio reached 68:32, in TiPSY/**2** 53:47 and in TiPSY/**3** 51:49. For TiPSY/**1** even a 45:55 *E/Z* ratio was found, a rare example with higher *Z*-imine concentration (see Supplementary S4-5 for spectra). A complete assignment of the TiPSY/imine complexes was done for imines **1**, **2**, **3** and **4** at 180 K (for spectra see Supplementary S6-S28). Despite a severe signal overlap in the crowded aromatic region, most of the signals were unambiguously assigned. The assignment of the *E Type* core structures of the TiPSY/imine complexes (*Type I E*, *Type II E*) is shown exemplarily on imine **4**. With the help of ¹⁹F spectroscopy the spectral resolution can be vastly improved by reducing the complexity of the obtained spectra.⁵¹⁻⁵³ Orientation *Type I E* was identified in a 2D ¹H ¹⁹F HOESY experiment. A total of four HOE cross-peaks were found between the fluorine atom of imine **4** and the BINOL backbone of the catalyst (Figure 6).

3. Brønsted Acid Catalysis – The Effect of 3,3'-Substituents on the Structural Space and the Stabilization of Imine/Phosphoric Acid Complexes

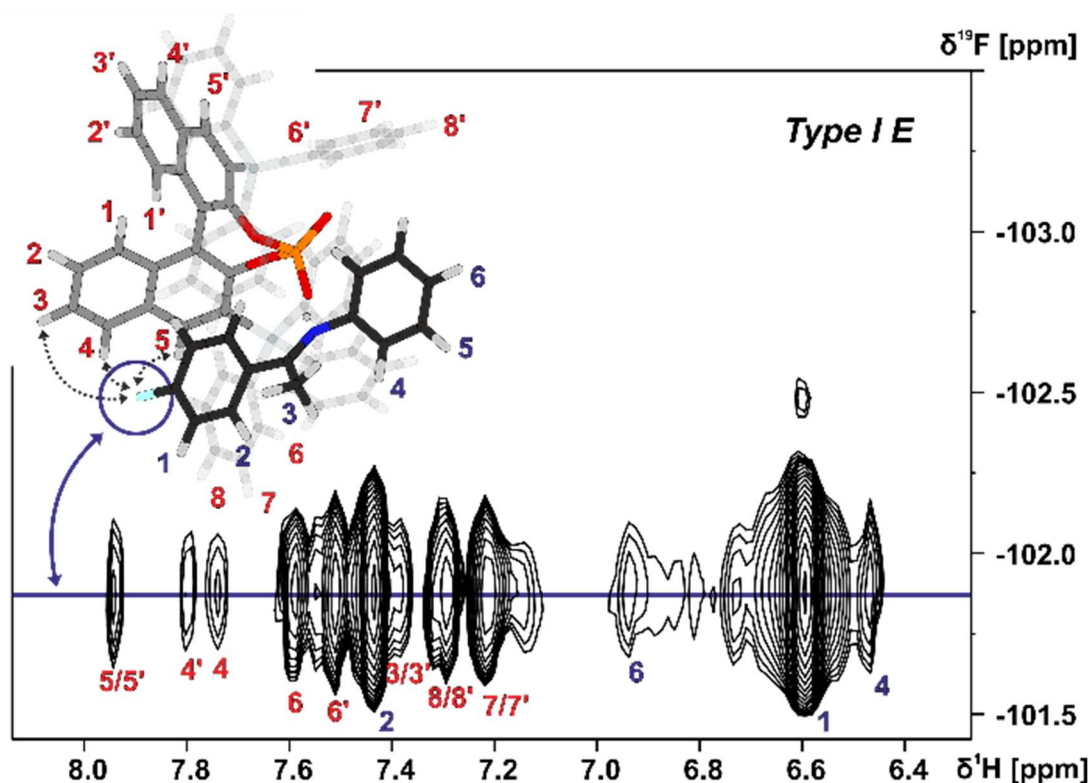


Figure 6. Section of a $^1\text{H},^{19}\text{F}$ 2D HOESY spectrum of TiPSY/4 at 180 K in CD_2Cl_2 at 600 MHz; Red dashed lines correspond to the intermolecular HOEs identifying complex structure *Type I E* (for detailed NMR parameters see Supplementary S19).

The presence of these HOE cross-peaks between imine **4** and the protons 3, 4 and 5 of the TiPSY backbone in combination with the hydrogen bond confirm the existence of the *Type I E* structure. Due to a dissociation, rotation and re-association of the TiPSY/imine complexes (Figure 7), HOEs are also observed between the fluorine atom of **4** and the opposite naphthyl moiety of the catalyst (Figure 6, HOE to proton 4'). This exchange is slow on the NMR timescale compared to the tilting mechanism that leads to an exchange between structures *Type I E* and *Type II E* (Figure 7). A rotation of the *E*-imine inside the complex can be excluded, since the rotational barrier for this process would be by far too high due to the steric hindrance of imine inside the complex. Orientation *Type II E* in the TiPSY/4 complex was similarly identified by using selective 1D NOESY experiments with saturation on proton 6 (see Supplementary S20) Similar NOE patterns for conformations *Type I E* and *Type II E* were observed for TiPSY complexes with the imines **1**, **2** and **3** (Supplementary S14-S18).

In contrast to the TiPSY/*E*-imine structures, only one set of signals is observed for the BINOL backbone of the catalyst in the TiPSY *Z*-imine complexes. This can be explained by the reduced steric hindrance of the *Z*-imine enabling an exchange between orientation *Type I Z* and *Type II Z* via rotation of the imine around the hydrogen bond (Figure 7). This exchange pathway in addition to the exchange via tilting of the imine (see TiPSY/*E*-imine), results in only one average set of ^1H signals for the BINOL backbone of the catalyst.²⁹

3. Brønsted Acid Catalysis – The Effect of 3,3'-Substituents on the Structural Space and the Stabilization of Imine/Phosphoric Acid Complexes

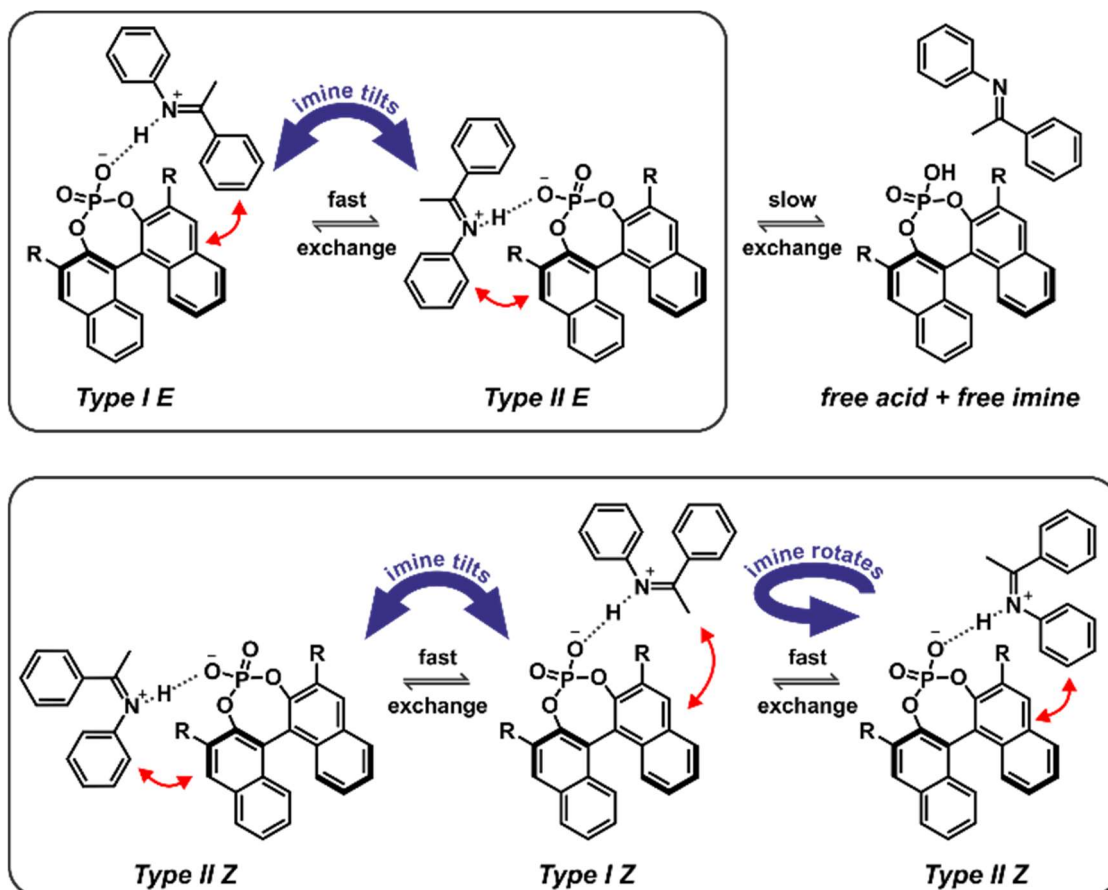


Figure 7. Complex exchange processes in TiPSY/imine complexes; an exchange via tilting of the imine is observed between structures *Type I E* and *Type II E* as well as a disassociation and association process of the TiPSY/*E*-imine complexes; the exchange via tilting is fast on the NMR time-scale and leads to a different interaction pattern for each half of the catalyst; the dissociation and association process is slow on the NMR time-scale and leads to exchange peaks between the catalyst halves; in addition to an exchange via tilting of the imine, the reduced steric hindrance of the *Z*-imine enables an additional fast exchange between structures *Type I Z* and *Type II Z* via rotation, leading to a different signal pattern.

Both orientations *Type I Z* and *Type II Z* were detected for the TiPSY/*Z*-imine complexes. Complex TiPSY/**3** is used exemplarily for the assignment of *Type I Z* (Figure 8). In the ^1H NOESY spectrum, two specific intermolecular NOEs between the α -methyl group of the imine and the BINOL backbone of the catalyst were found. This interaction, in combination with the strong hydrogen bond between catalyst and imine shows the existence of orientation *Type I Z* in solution. Similarly, orientation *Type II Z* could be confirmed in selective 1D NOESY spectra (Supplementary S26) and the same NOE pattern were observed for all investigated complexes TiPSY/**1,2,3,4** (Supplementary S21-S28).

Thus, despite significantly deviating 3,3' substituent/imine interactions causing different *E/Z* ratios in TiPSY/imine complexes (see Table 1), for all TiPSY/imine complexes studied in detail the structures *Type I E* and *Type II E* as well as *Type I Z* and *Type II Z* could be elucidated by NMR.

3. Brønsted Acid Catalysis – The Effect of 3,3'-Substituents on the Structural Space and the Stabilization of Imine/Phosphoric Acid Complexes

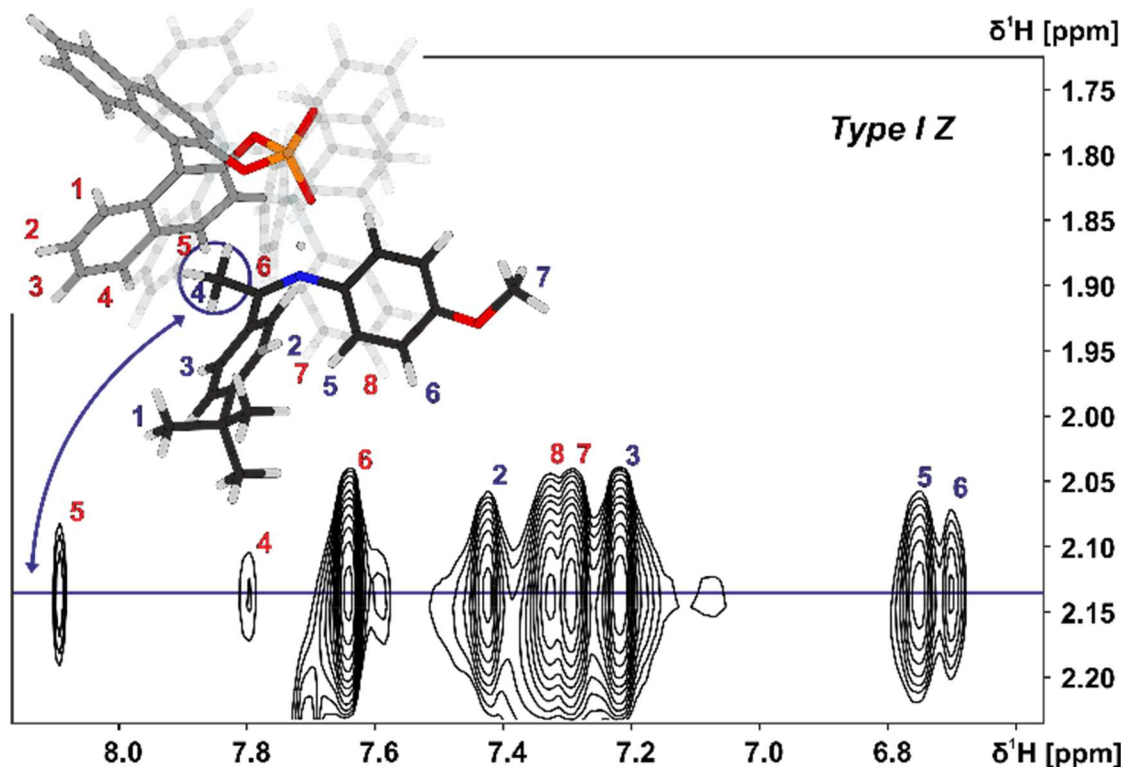


Figure 8. Excerpt of the 2D NOESY spectrum of TIPSU/3 at 180 K in CD_2Cl_2 at 600 MHz; intermolecular cross-peaks (red numbers) detail the interaction between α -methyl group of **3** (blue spin 4) and BINOL backbone of the catalyst (for detailed parameters see Supplementary S25).

3.3.3. Structural space of TRIM/imine complexes and dimerization trends of CPAs

For TRIM complexes with imines **5**, **6**, and **7** the same four core structures *Type I/II E/Z* were experimentally identified by NOE analysis (for assignment and spectra see Supplementary S33-42). In contrast to TRIP and TIPSU only one set of catalyst signals for both *Type I/II E* structures even at 180 K is observed, which can be explained by an additional exchange pathway. This pathway is potentially enabled via facilitated rotation like it is the case for *Type I/II Z* and/or an enhanced dissociation-association process of the complex. (for detailed explanation see Supplementary S43).²¹

Furthermore, the additional hydrogen bonded signals as discussed above (see Figure 5) were identified as $[\text{TRIM}/E\text{-imine}]_2$ dimers and were in detail investigated on complex TRIM/**7**.¹¹ Chemical exchange between TRIM/**7E** and $[\text{TRIM}/\mathbf{7E}]_2$ was identified by EXSY signals and dilution of the sample lead to a complete shift of the monomer-dimer equilibrium towards the monomers (see Supplementary S1-3). In addition, DOSY measurements corroborated the assignment as a dimer (see Supplementary S44). Theoretical calculations supported by distinct changes of the measured chemical shifts (see Figure 9) confirm the observed dimer structures to be similar to the reported crystal structure of Schneider²⁸ (see Figure 11 below).

3. Brønsted Acid Catalysis – The Effect of 3,3'-Substituents on the Structural Space and the Stabilization of Imine/Phosphoric Acid Complexes

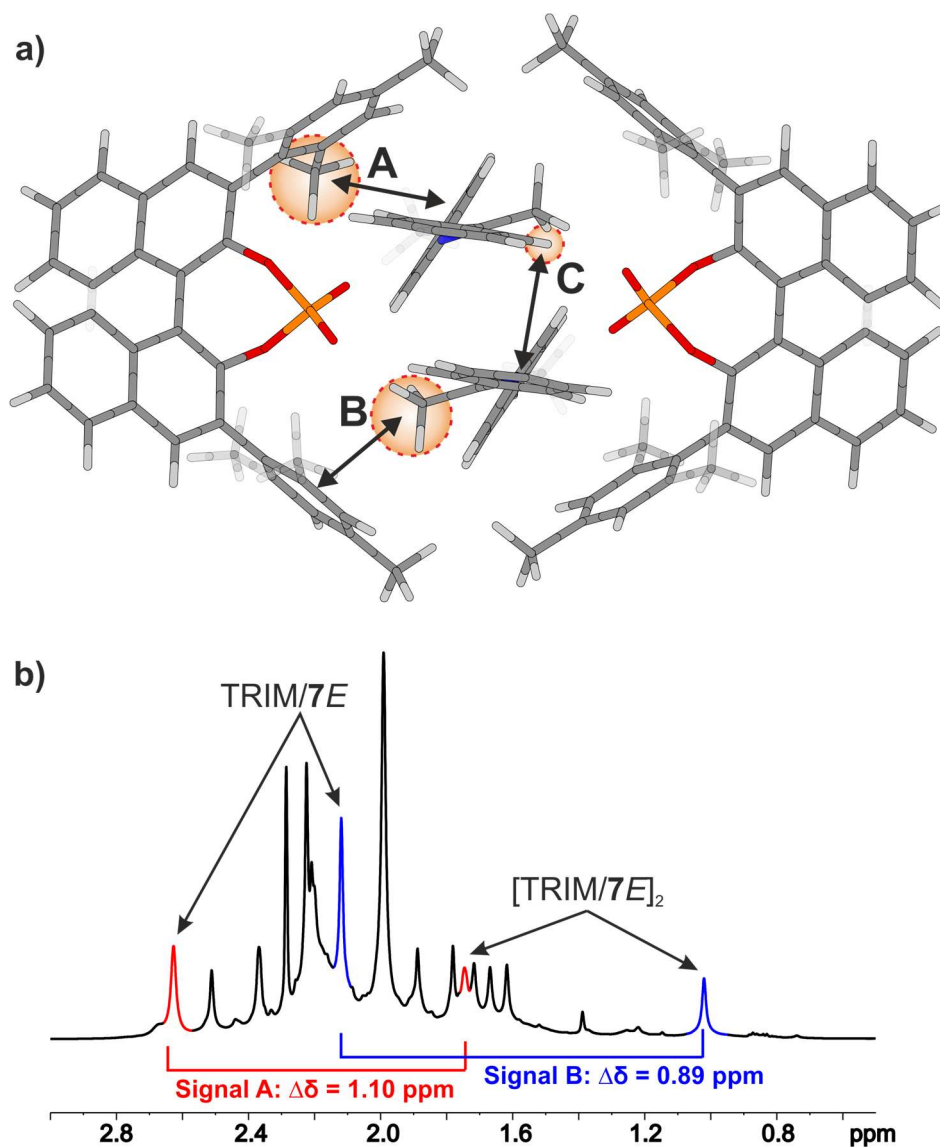


Figure 9. a) Theoretically calculated dimer structure model on the example of the $[\text{TRIM}/5E]_2$ complex reveals the steric proximity of the protons A-C to phenyl entities which causes paratropic shielding effects and induces severe highfield shifts. b) Excerpt of the ^1H spectrum of TRIM/7 at 180 K in CD_2Cl_2 at 600 MHz highlighting the highfield shift of proton A (red) and B (blue) of the dimer compared to the monomer. The significant highfield shifts of A-C compared to the monomeric structure (A: 1.10 ppm, B: 0.89 ppm, C: 1.56 ppm) experimentally corroborate the computed structure and indicate CH- π and π - π interactions

The 3,3'-substituent dependent formation of CPA/imine dimers gave rise to the question, which 3,3'-substituent properties enable or restrict dimer formation. Remarkably, all catalysts forming dimers possess medium rotational barriers of the 3,3'-substituent (13.63-21.58 kcal/mol) as described by Goodman.²¹ This hints at the influence of putative van der Waals interactions between the catalyst 3,3'-substituent and the imine on the energetic interaction profile supporting dimer formation. The presence of such interactions is indicated for $[\text{TRIM}/7E]_2$ by a strong highfield shift of proton A (Figure 9), caused by steric proximity to a phenyl entity of the imine. For TRIFP and TiPSY a low rotational barrier (2.02 and 1.35 kcal/mol respectively)²¹ points out the lack of moieties capable of such interactions, while the high rotational barrier of TRIP (28.40 kcal/mol)²¹ potentially indicates steric repulsion

3. Brønsted Acid Catalysis – The Effect of 3,3'-Substituents on the Structural Space and the Stabilization of Imine/Phosphoric Acid Complexes

overwriting attractive interactions. Furthermore, putative CH- π interactions between the α -Methyl group of the imine and the phenyl entities of the 3,3'-substituent (Interaction B in Figure 9 a) as well as π - π interactions between the two imines (Interaction C in Figure 9 a) might compensate the loss of interactions between the imine and BINOL-backbone present in the monomeric structures.²⁹ Moreover, other 3,3'-substituent properties such as electrostatic repulsion, e.g. due to the CF₃-groups in a hypothetical TRIFP dimer, or severe entropic penalties upon dimerization for catalysts with a high degree of conformational freedom of the 3,3'-substituents such as TIPSU and TRIP³² might also affect dimerization trends.

It was reported that interlocked CPA catalysts can form P=O...-(HO)P hydrogen bonded pseudo-dimers which provide significantly higher stereoselectivity as their non-interlocked analogues.⁵⁴ However, for synthetic applications CPA/imine dimers are not expected to have any influence as their population diminishes when approaching catalyst concentrations used in synthesis.^{6,7,55}

Hence, the existence of a dimer in the crystal structure of TeBuP and in the NMR spectra of TRIM, 9-Phen, and 1-Naph corroborates our previous assumption²⁹ that attractive interactions between 3,3'-substituent and imine play a key role in the energetics of CPA complexes. Thus, the dimerization trend might be tentatively proposed as a qualitative measure for steric properties and polarizability of the 3,3'-substituent.

3.3.4. Effect of substituents on enantioselectivity in the transfer hydrogenation of ketimines

After ensuring the analogy of all catalytic relevant and NMR accessible structures, the influence of the 3,3'-substituents on the enantioselectivity was investigated. Therefore, the *ee* values for the transfer hydrogenation of imines **5**, **6** and **7** with ethyl Hantzsch ester catalyzed by TRIP, TIPSU, TRIFP, TRIM, 1-naph and 9-phen were determined (see Supplementary S45). As anticipated based on earlier work of Rueping,⁵ List⁶ and MacMillan⁷ and on the webtool BINOPTimal developed by Goodman,²⁴ TIPSU (90-95 % *ee*) gave the highest enantiomeric excess, followed by TRIP (83-86 % *ee*) and TRIFP (74-91 % *ee*), while TRIM (56-70%), 1-naph (46-56%) and 9-phen (47-59%) gave lower enantioselectivities. While imine **5** and **6** gave almost identical *ee* values for all investigated catalysts, the CF₃ substituted imine **7** deviated up to ± 15 % for TRIFP, TRIM, 1-naph, and 9-phen. Since imines **5**, **6** and **7** have a similar steric bulk this deviation suggests that steric interactions are not the only key factor, but that also electrostatic interactions can significantly modulate the enantioselective outcome. Next, linear correlations between the observed enantioselectivities and steric descriptors (AREA(θ) or rotational barrier) of the 3,3' substituents as previously postulated by Goodman²¹ were tested. However, neither with area θ

3. Brønsted Acid Catalysis – The Effect of 3,3'-Substituents on the Structural Space and the Stabilization of Imine/Phosphoric Acid Complexes

nor with the rotational barrier a linear correlation was found for our data. (see Supplementary S46). Moreover, the enantioselectivities also showed no correlation with the *E/Z* ratios of the binary complexes (see Supplementary S46). This shows that a single parameter derived from catalyst alone or binary complex is not sufficient to adequately predict the stereoselective outcome at least of the investigated reaction. Rather multiple factors seem to affect the energetics of the reaction pathway, which will be subject of further investigations.

3.3.5. Theoretical model structures and structure comparison

The above mentioned experimentally identified dimeric structures seem to be stabilized by attractive interactions, often associated with London dispersion forces. The presence of such interaction modes was already investigated and proven for TRIP/imine complexes in the previous theoretical structural studies utilizing NCI analysis and NOE analysis.^{29,32} The binary complex is mainly anchored by a strong hydrogen bond,³² however equally important, it is also bolstered by numerous weak attractive interactions between the imine and the catalyst's backbone as well as the bulky 3,3'-substituents.²⁹ These interactions are also pervasive in other catalysts with different 3,3' motives.

Our theoretical calculations of TRIP, TiPSY, TRIFP, TRIM/**5-7** confirm the general existence of the four core structures (*Type I/II E/Z*) (for computational details and data on additional CPAs, see Supplementary S49) in accordance with previous results for similar complexes.²⁹ Each of the *E*- and *Z*-imine complexes features two different orientations of the imine (Figure 10). In the *Type I* orientation, the ketone moiety is located in close proximity to the BINOL backbone of the catalyst. In the *Type II* orientation, the imine is rotated around the hydrogen bond by $\sim 180^\circ$ and the aniline moiety is located close to the BINOL backbone.

3. Brønsted Acid Catalysis – The Effect of 3,3'-Substituents on the Structural Space and the Stabilization of Imine/Phosphoric Acid Complexes

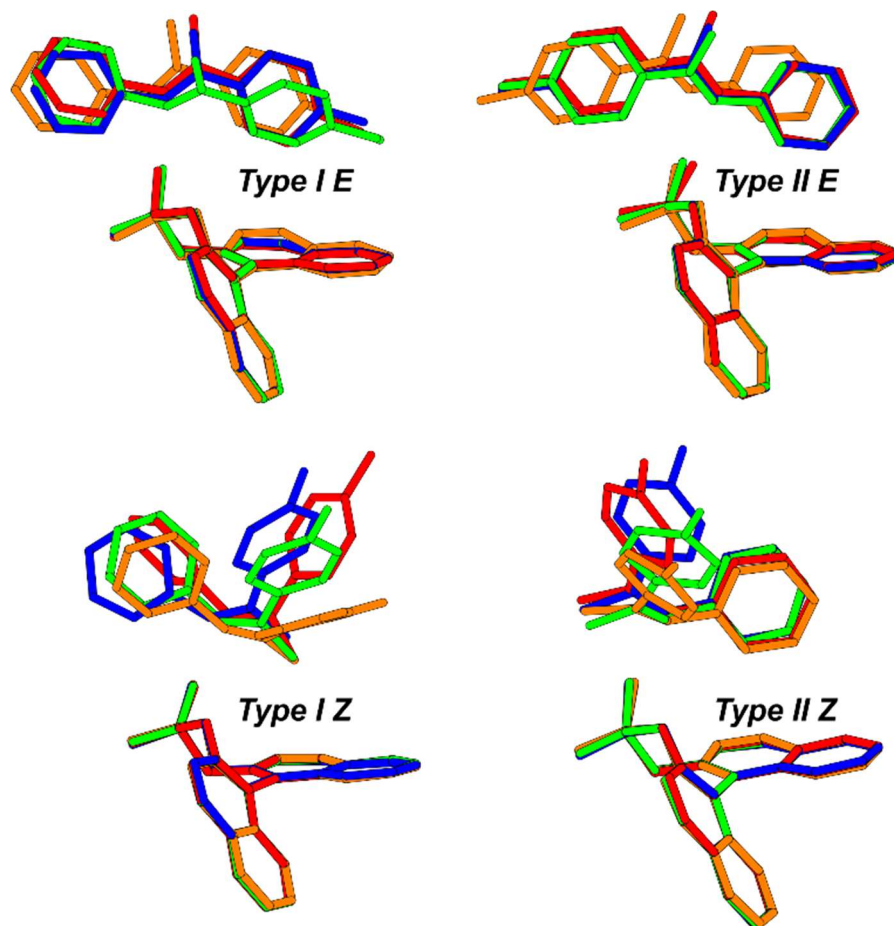


Figure 10. Theoretical calculations of the TiPSY, TRIP, TRIFP, TRIM/5 complex show the invariance of four core structures. Despite that, the *E/Z* ratios and the tendency towards dimerization vary strongly within the CPA/imine complexes. Moreover, quantum chemical calculations of *E/Z*-ratio showed a significant offset to the experimental values. Colour code: TiPSY red, TRIP blue, TRIFP orange, TRIM green.

Geometrical comparison of the four core structures from the calculation revealed a high degree of invariance in the CPA/imine complexes, which is, to our surprise, retained despite significant variation of 3,3'-substituent of the catalyst (Figure 10). As in TRIP/imine complexes²⁹ the two orientations of the *E*- and *Z*-imine are obtained in TiPSY, TRIFP, TRIM/5-7 binary complexes. Furthermore, similar van der Waals interaction types (π - π , CH- π) are clearly recognizable from the structural analysis. In accordance with the previous studies,³² the acidic proton is located closer to the imine in TiPSY and TRIFP binary complexes, which indicates a strong predominant zwitter ionic, but also partly covalent character (POH angle $\approx 110^\circ - 120^\circ$). Due to the high degree of invariance of the core structures, the *E/Z*-ratio in the binary complexes is altered due to the difference in stabilization of *E*- and *Z*-imine by the 3,3'-substituent. It is noteworthy to mention that despite a good agreement between experimentally and theoretically determined structures, the theoretical *E/Z*-ratio deviates significantly from the measured *E/Z*-ratio (Table 2).

Mostly, only the qualitative trend could be predicted correctly with exception of TRIM-complexes, i.e. experimentally the *E*-complex is less stable than the *Z*-complex. Despite extensive conformational

3. Brønsted Acid Catalysis – The Effect of 3,3'-Substituents on the Structural Space and the Stabilization of Imine/Phosphoric Acid Complexes

search (for computational details see below), application of various dispersion corrected density functionals (GGA, hybrid GGA, meta-hybrid GGA), post-HF methods (MP2, SCS-MP2, DLPNO-CCSD(T)) and implicit solvation models (SMD, COSMO-RS), the thermodynamic stability of the considered CPA/Z-isomers is gravely underestimated. One of the most common encountered error sources in the theoretical calculation during the simulation of large flexible molecules is the initial sampling using molecular mechanics not being able to find the initial structure near to global minimum. This problem is augmented, especially in our case, by the poor parameterization of strongly hydrogen-bridged and zwitter-ionic complexes. Nevertheless, given the number of sampling conformations, experimental NOE contacts and the remarkable agreement of calculated coupling constants with the experimental values,³² the possibility of not finding the global minimum of the Z-complex is reduced significantly.

Since the weak interactions, e.g. dispersion effect in the complex, were already accounted in the post-HF methods, the underlying cause for the deviation might be either the missing explicit solvent-solute interaction favouring the Z-isomers due to its compactness, and hence a larger available solvent-solute interaction space, or the inaccurate implicit solvation of such zwitter-ionic species. For the former, tremendous increase of computational cost is expected making full ab initio calculations very restricted. An initial calculation of solvated complexes in a solvent box consisting of 300 solvent molecules has been performed and accurate calculations are planned for the future. For the latter, recent thorough investigation of solvent effect on the attenuation of inter- and intramolecular dispersive interaction showed that the current frequently employed implicit solvent models fail to describe dispersive solvent-solute interaction.⁵⁶ In summary, several underlying reasons for the failure to predict the E/Z-ratio are multiple. First, considering the huge conformational space of the complex, accurate initial sampling is necessary to catch the nearest minimum for DFT refined optimization. In this case, accurate semi-empirical methods, such as tight-binding method⁵⁷ and sampling using meta-dynamics may resolve the sampling issue in large electronic structures. Second, accurate description for solvation might be still underdeveloped for strongly bound zwitter-ionic species with large aromatic surfaces causing the solvent attenuation of dispersive interaction. Therefore, further improvement for implicit solvent correction is necessary.

Table 2: E/Z ratios of different catalysts with imine 5.

	Experimental E:Z	Theoretical E:Z
TRIP/5	79 : 21	99.80 : 0.20
TRIFP/5	70 : 30	96.80 : 3.20
TiPSY/5	56 : 44	99.97 : 0.03
TRIM/5	47 : 53	80.41 : 19.59

3. Brønsted Acid Catalysis – The Effect of 3,3'-Substituents on the Structural Space and the Stabilization of Imine/Phosphoric Acid Complexes

In addition, a structure model for dimeric CPA/imine complexes was computed on the example of TRIM/5 (see figure 9 and 11). This dimeric structure features two imines, nested between two catalysts. An extended dispersion force between the 3,3'-substituents of the two catalysts and the two extended aromatic imines is observed. The additional imine in the dimeric complex seems to be positioned at the nucleophilic attack site, when comparing the structure to the hydride transfer transition state with Hantzsch ester as the reducing agent. An overlap of the imine substrates and the Hantzsch ester is observed which suggests similar interaction modes (Figure 11c).

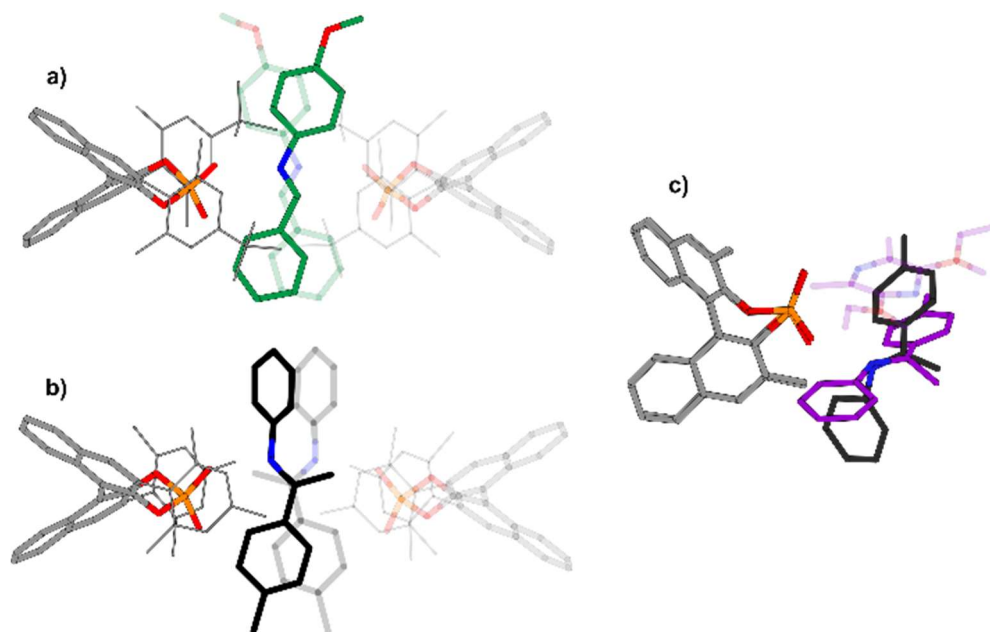


Figure 11. Reported crystal structure of a TeBuP/imine dimer (a) and calculated structure of a TRIM/imine dimer (b). The structures are similar despite comparing an aldimine (a) to a ketamine structure (b). c) Comparison of the dimeric structure of a TRIM complex (black imine) with the calculated transition state consisting of a CPA (the 3,3' substituents of the catalysts have been omitted to improve the visibility), an imine (purple) and a Hantzsch ester (purple, transparent). The steric influence of the second imine in the dimeric structure (b) is similar to the additional bulk of the Hantzsch ester in the transition state.

3.3.6. Computational Details

All binary complexes were optimized at DFT level of theory using TPSS functional with D3 correction in continuum of DCM. To mimic experimental low temperature condition the dielectric constant of DCM was increased to 16.20. Preconformational sampling was performed using force-field with MMFF parameter. Overall 1137 conformations of TRIP/imine were generated in the force-field procedure and subjected to ab initio geometry optimization. Low lying conformations were selected according to experimental constrains (NOE contacts). For other catalyst/imine conformations, core structures based on TRIP/imine complexes were taken and adapted. Post-HF single point calculations at SCS-MP2/CBS level of theory were performed on the optimized geometry (see Supplementary 46 for extrapolation procedure).

3.4. Conclusion

A combination of detailed NMR spectroscopic studies and theoretical calculations was used to investigate the structural space of CPA/imine complexes with varying 3,3'-substituents. Our experimental data revealed the coexistence of four core structures (*Type I/II E* and *Type I/II Z*) in solution, similar to those described for binary complexes of TRIP. These core structures show a high invariance, independent of the used CPA, which is corroborated by theoretical calculations of TiPSY/imine, TRIFP/imine and TRIM/imine complexes. For the first time dimeric CPA/imine complexes were identified in solution for TRIM, 9-Phen and 1-Naph with an imine occupying the space analogous to the transition state in the transfer hydrogenation. Surprisingly, this dimer consisting of two binary complexes is stabilized exclusively by attractive non covalent interactions. Hence, not only the steric repulsion term but also the attractive term of the large 3,3'-substituents has to be considered for the energetics of CPA complexes. Despite the good agreement of experiment and theory for the identified structures, a significant disparity was found for the *E/Z* ratios of the complexes. All binary complexes exhibit an increased population of the *Z*-structures, which cannot be reproduced in the calculations. A possible reason is an insufficient description of solvent-complex interactions. This study may allow to validate and improve theoretical predictive models by providing for the first time detailed experimental data about the structural space and influence of the 3,3'-substituent on the energetics of CPA/imine complexes.

3. Brønsted Acid Catalysis – The Effect of 3,3'-Substituents on the Structural Space and the Stabilization of Imine/Phosphoric Acid Complexes

3.5. References

#1 Due to chemical exchange between TRIM/imine, [TRIM/imine]₂ and free imine and the resulting line broadening as well as signal overlap, only the complex TRIM/7 could be analysed in detail, as it gave adequate line widths.

#2 Significant line broadening for distinct proton signals of TRIPs isopropyl and TIPSYSs phenyl-moieties at 180 K caused by medium chemical exchange between different substituent conformations demonstrated a high degree of conformational freedom for these catalysts.

- 1 D. Parmar, E. Sugiono, S. Raja and M. Rueping, *Chem. Rev.*, 2014, **114**, 9047–9153.
- 2 D. Parmar, E. Sugiono, S. Raja and M. Rueping, *Chem. Rev.*, 2017, **117**, 10608–10620.
- 3 T. Akiyama, J. Itoh, K. Yokota and K. Fuchibe, *Angew. Chem. Int. Ed.*, 2004, **43**, 1566–1568.
- 4 D. Uruguchi and M. Terada, *J. Am. Chem. Soc.*, 2004, **126**, 5356–5357.
- 5 M. Rueping, E. Sugiono, C. Azap, T. Theissmann and M. Bolte, *Org. Lett.*, 2005, **7**, 3781–3783.
- 6 S. Hoffmann, A. M. Seayad and B. List, *Angew. Chem. Int. Ed.*, 2005, **44**, 7424–7427.
- 7 R. I. Storer, D. E. Carrera, Y. Ni and D. W. C. MacMillan, *J. Am. Chem. Soc.*, 2006, **128**, 84–86.
- 8 K. Saito and T. Akiyama, *Chem. Commun.*, 2012, **48**, 4573–4575.
- 9 M. Yamanaka, J. Itoh, K. Fuchibe and T. Akiyama, *J. Am. Chem. Soc.*, 2007, **129**, 6756–64.
- 10 X. Xu, Y. Qian, L. Yang and W. Hu, *Chem. Commun.*, 2010, **47**, 797–799.
- 11 E. P. Ávila, R. M. S. Justo, V. P. Gonçalves, A. A. Pereira, R. Diniz and G. W. Amarante, *J. Org. Chem.*, 2015, **80**, 590–594.
- 12 K. Shen, X. Liu, Y. Cai, L. Lin and X. Feng, *Chem. – A Eur. J.*, 2009, **15**, 6008–6014.
- 13 C. Gharui, S. Singh and S. C. Pan, *Org. Biomol. Chem.*, 2017, **15**, 7272–7276.
- 14 S. Saha and C. Schneider, *Chem. Eur. J.*, 2015, **21**, 2348–2352.
- 15 S. G. Ouellet, A. M. Walji and D. W. C. Macmillan, *Acc. Chem. Res.*, 2007, **40**, 1327–1339.
- 16 C. Min and D. Seidel, *Chem. Soc. Rev.*, 2017, **46**, 5889–5902.
- 17 Q. Kang, Z.-A. Zhao and S.-L. You, *Org. Lett.*, 2008, **10**, 2031–2034.
- 18 K. Saito, K. Horiguchi, Y. Shibata, M. Yamanaka and T. Akiyama, *Chem. Eur. J.*, 2014, **20**, 7616–7620.
- 19 R. Maji, S. C. Mallojjala and S. E. Wheeler, *Chem. Soc. Rev.*, 2018, **47**, 1142–1158.
- 20 A. Milo, A. J. Neel, F. D. Toste and M. S. Sigman, *Science*, 2015, **347**, 737–743.
- 21 J. P. Reid and J. M. Goodman, *J. Am. Chem. Soc.*, 2016, **138**, 7910–7917.
- 22 J. P. Reid, L. Simón and J. M. Goodman, *Acc. Chem. Res.*, 2016, **49**, 1029–1041.
- 23 L. Simón and J. M. Goodman, *J. Org. Chem.*, 2011, **76**, 1775–1788.
- 24 J. P. Reid and J. M. Goodman, *Chem. Commun.*, 2019, **55**, 1778–1781.
- 25 C. B. Santiago, J. Y. Guo and M. S. Sigman, *Chem. Sci.*, 2018, **9**, 2398–2412.
- 26 A. J. Neel, A. Milo, M. S. Sigman and F. D. Toste, *J. Am. Chem. Soc.*, 2016, **138**, 3863–3875.
- 27 M. Orlandi, J. A. S. Coelho, M. J. Hilton, F. D. Toste and M. S. Sigman, *J. Am. Chem. Soc.*, 2017, **139**, 6803–6806.
- 28 M. Sickert, F. Abels, M. Lang, J. Sieler, C. Birkemeyer and C. Schneider, *Chem. Eur. J.*, 2010, **16**, 2806–2818.
- 29 J. Greindl, J. Hioe, N. Sorgenfrei, F. D. Morana and R. M. Gschwind, *J. Am. Chem. Soc.*, 2016, **49**, 15965–15971.
- 30 W. Tang, S. Johnston, J. A. Iggo, N. G. Berry, M. Phelan, L. Lian, J. Bacsá and J. Xiao, *Angew. Chem. Int. Ed.*, 2013, **52**, 1668–1672.
- 31 L. Liu, M. Leutzsch, Y. Zheng, M. W. Alachraf, W. Thiel and B. List, *J. Am. Chem. Soc.*, 2015, **137**, 13268–13271.
- 32 N. Sorgenfrei, J. Hioe, J. Greindl, K. Rothermel, F. Morana, N. Lokesh and R. M. Gschwind, *J. Am. Chem. Soc.*, 2016, **138**, 16345–16354.
- 33 L. Simón and J. M. Goodman, *J. Am. Chem. Soc.*, 2008, **130**, 8741–8747.
- 34 T. Akiyama, *Chem. Rev.*, 2007, **107**, 5744–5758.
- 35 E. R. P. Zuiderweg and S. W. Fesik, *Biochemistry*, 1989, **28**, 2387–2391.
- 36 J. Schleucher, M. Schwendinger, M. Sattler, P. Schmidt, O. Schedletzky, S. J. Glaser, O. W. Sørensen and C. Griesinger, *J. Biomol. NMR*, 1994, **4**, 301–306.

3. Brønsted Acid Catalysis – The Effect of 3,3'-Substituents on the Structural Space and the Stabilization of Imine/Phosphoric Acid Complexes

- 37 M. Foroozandeh, R. W. Adams, M. Nilsson and G. A. Morris, *J. Am. Chem. Soc.*, 2014, **136**, 11867–11869.
- 38 J. Mauhart, S. Glanzer, P. Sakhaei, W. Bermel and K. Zangger, *J. Magn. Reson.*, 2015, **259**, 207–215.
- 39 K. Zangger, *Prog. Nucl. Magn. Reson. Spectrosc.*, 2015, **86–87**, 1–20.
- 40 D. Uhrin, J. Bramham, S. J. Winder and P. N. Barlow, *J. Biomol. NMR*, 2000, **18**, 253–259.
- 41 A. Verma and B. Baishya, *J. Magn. Reson.*, 2016, **266**, 51–58.
- 42 S. Akoka and P. Giraudeau, *Magn. Reson. Chem.*, 2015, **53**, 986–994.
- 43 R. J. Lichtenecker, N. Coudeville, R. Konrat and W. Schmid, *ChemBioChem*, 2013, **14**, 818–821.
- 44 C. Prasanna, A. Dubey and H. S. Atreya, in *Methods in Enzymology*, Academic Press, 2015, vol. 565, pp. 167–189.
- 45 D. P. Frueh, A. C. Goodrich, S. H. Mishra and S. R. Nichols, *Curr. Opin. Struct. Biol.*, 2013, **23**, 734–739.
- 46 H. Kessler, H. Oschkinat, C. Griesinger and W. Bermel, *J. Magn. Reson.*, 1986, **70**, 106–133.
- 47 K. Stott, J. Stonehouse, J. Keeler, T.-L. Hwang and A. J. Shaka, *J. Am. Chem. Soc.*, 1995, **117**, 4199–4200.
- 48 D. Jeannerat and J. Furrer, *Comb. Chem. High Throughput Screen.*, 2012, **15**, 15–35.
- 49 C. Yu and G. C. Levy, *J. Am. Chem. Soc.*, 1984, **106**, 6533–6537.
- 50 P. S. Pregosin, P. G. Anil Kumar and I. Fernández, *Chem. Rev.*, 2005, **105**, 2977–2998.
- 51 K. Shikii, S. Sakurai, H. Utsumi, H. Seki and M. Tashiro, *Anal. Sci.*, 2004, **20**, 1475–1477.
- 52 D. P. Cistola and K. B. Hall, *J. Biomol. NMR*, 1995, **5**, 415–419.
- 53 L. Fusaro, E. Locci, A. Lai and M. Luhmer, *J. Phys. Chem. B*, 2010, **114**, 3398–3403.
- 54 R. Mitra, H. Zhu, S. Grimme and J. Niemeyer, *Angew. Chem. Int. Ed.*, 2017, **56**, 11456–11459.
- 55 M. Sickert and C. Schneider, *Angew. Chem. Int. Ed.*, 2008, **47**, 3631–3634.
- 56 R. Pollice, M. Bot, I. J. Kobylanski, I. Shenderovich and P. Chen, *J. Am. Chem. Soc.*, 2017, **139**, 13126–13140.
- 57 S. Grimme, C. Bannwarth and P. Shushkov, *J. Chem. Theory Comput.*, 2017, **13**, 1989–2009.

3.6. Supporting Information

3.6.1. General information

Experimental data

Deuterated solvents were purchased from Deutero or Sigma Aldrich where dry solvents were essential, CD₂Cl₂ was freshly distilled over CaH₂ and Toluene-d₈ was refluxed over Na/Benzophenone under argon atmosphere. Freon mixtures were prepared from CDCl₃ and SbCl₅/SbF₃ according to literature procedures and stored in small lecture bottles.^[1,2] The catalysts were purchased from Sigma Aldrich or synthesized from the bisphenols according the procedure of Klusmann et al.^[3]

Synthesis of Imine Substrates

The imines were prepared as described in literature.^[4-7] The toluene was used either in p.A. quality or was dried by refluxing over sodium. The ¹⁵N-enriched aniline for the presented syntheses below, was purchased from Euriso-top GmbH and Sigmar Aldrich.

Preparation of binary complexes in CD₂Cl₂

The catalyst was dried for 30 min at 150°C under reduced pressure. Ketimine and catalyst were directly weighed into a 5 mm NMR tube under an inert argon atmosphere. CD₂Cl₂ (0.6 ml) and 1.0 ml of tetramethylsilane atmosphere were added to the tube. The sample was stored in an -80°C freezer. A 1:1 ratio of catalyst/ketimine was used for all samples. A concentration of 25 mmol, 50 mmol/L or 100 mM was used for all samples, depending on solubility at low temperatures.

Spectrometer data

NMR experiments were performed on Bruker Avance III HD 400 MHz spectrometer, equipped with 5 mm BBO BB-1H/D probe head with Z-Gradients and a Bruker Avance III HD 600 MHz spectrometer, equipped with a 5 mm TBI 1H/31P and a 5 mm CPPBBO BB-1H/19F. Triple resonance experiments were performed on the TBI probe head.. Temperature was controlled in the VT-experiments by BVT 3000 and BVTE 3900. For NMR measurements employing standard NMR solvents 5 mm NMR tubes were used, if not otherwise noted. For samples in freonic mixtures as solvents, 5 mm heavy wall (1.4 mm wall thickness) NMR tubes equipped with J. Young valves from Wilmad were used. NMR Data were processed, evaluated and plotted with TopSpin 3.2 software. Further plotting of the spectra was performed with Corel Draw X14 – X17 software. ¹H, ¹³C chemical shifts were referenced to TMS or the respective solvent signals. The heteronuclei ¹⁵N, ¹⁹F and were referenced, employing $\nu(X) = \nu(\text{TMS}) \times \frac{\epsilon_{\text{reference}}}{100 \%}$ according to Harris et al.^[8] The following frequency ratios and reference compounds were used: $\epsilon(^{15}\text{N}) = 10.132912$ (lq. NH₃) and $\epsilon(^{19}\text{F}) = 94.094011$ (CCl₃F)

3. Brønsted Acid Catalysis – The Effect of 3,3'-Substituents on the Structural Space and the Stabilization of Imine/Phosphoric Acid Complexes

Pulse programs

All pulse programs used are standard Bruker NMR pulse programs.

Acquisition Parameters

^1H NMR: Pulse program: zg; Relaxation delay = 2 – 3 s, Acquisition time = 2.48 s, SW = 22.0 ppm, TD = 64k, NS = 8 – 64; zg30; Relaxation delay = 2 s, Acquisition time = 2.48 s, SW = 22.0 ppm, TD = 64k, NS = 8 – 64;

2D- ^1H , ^1H NOESY: Pulse program: noesygpqh/noesygpqh; Relaxation delay = 5 - 8 s, NS = 8-32, mixing time (D8) = 300.00 ms; TD = 4096; increments = 512 - 1k;

2D- ^1H , ^1H COSY: Pulse program: cosygpqh; Relaxation delay = 5 - 8 s, NS = 8-32, TD = 4096; increments = 512 - 1k;

^{13}C NMR: Pulse program: zgpg30; Relaxation delay = 2.00 s, Acquisition time = 0.80 s, SW = 270.0 ppm, TD = 64k, NS = 1k – 2k;

2D- ^1H , ^{13}C HSQC: Pulse program: hsqcedetgpsisp2.3; Relaxation delay = 4 - 8 s, NS = 8-32, $^1J_{\text{XH}} = 145$ Hz; TD = 4096; increments = 512 - 1k;

2D- ^1H , ^{13}C HMBC: Pulse program: hmbcgpqh; Relaxation delay = 4 - 8 s, NS = 8-32, $^1J_{\text{XH}} = 145$ Hz, J_{XH} (long range) = 10 Hz; TD = 4096; increments = 512 - 1k;

2D- ^1H , ^{31}P HMBC: Pulse program: inv4gpqh; Relaxation delay = 4 - 8 s, NS = 8-32, TD = 4096; increments = 256 - 1k;

^{15}N NMR: Pulse program: zg; Relaxation delay = 10.00 s, Acquisition time = 0.54 s, SW = 502.8 ppm, TD = 32k, NS = 256 – 2048;

2D- ^1H , ^{15}N HMBC: Pulse program: inv4gpqh; Relaxation delay = 5 - 8 s, NS = 16-32, delay for evolution of long range couplings (D6) = 20.00 ms; TD = 4096; increments = 128 - 512;

^{19}F -NMR: Pulse program: zg30; Relaxation delay = 2 – 3 s, Acquisition time = 11.60 s, SW = 10.0 ppm, TD = 128k, NS = 8 – 64;

2D- ^1H , ^{19}F HOESY: Pulse program: hoesyph; Relaxation delay = 5 - 8 s, NS = 16-32, mixing time (D8) = 500.00 ms; TD = 4096; increments = 1k;

Selective 1D- ^1H , ^1H NOESY: Pulse program: selnogp; Relaxation delay = 5 - 8 s, NS = 128-2k, mixing time (D8) = 25 – 1000 ms (150 – 200 ms and NS = 1k-2k for structure identification); TD = 64k; 180° shaped pulse = 50 – 150 ms, shape = Gauss 180.

3.6.2. Dilution experiments for dimer identification

S1. Diluted spectra of TRIM/7

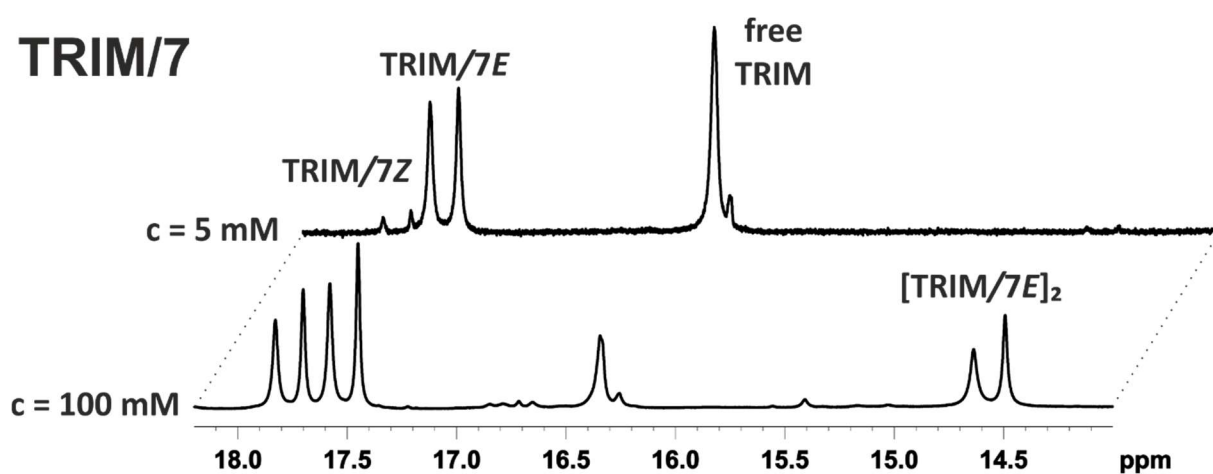


Figure S34: ^1H -spectra of TRIM/7 at 180 K in CD_2Cl_2 at 600 MHz with a concentration of 5 mM or 100 mM. The signal of $[\text{TRIM}/7\text{E}]_2$ disappears at lower concentration, corroborating the assignment as a dimeric species. The changing E/Z ratio of TRIM/7E and TRIM/7Z at 5 mM and 100 mM is caused by insufficient equilibration at room temperature before measuring.

S2. Diluted spectra of 1-naph/6

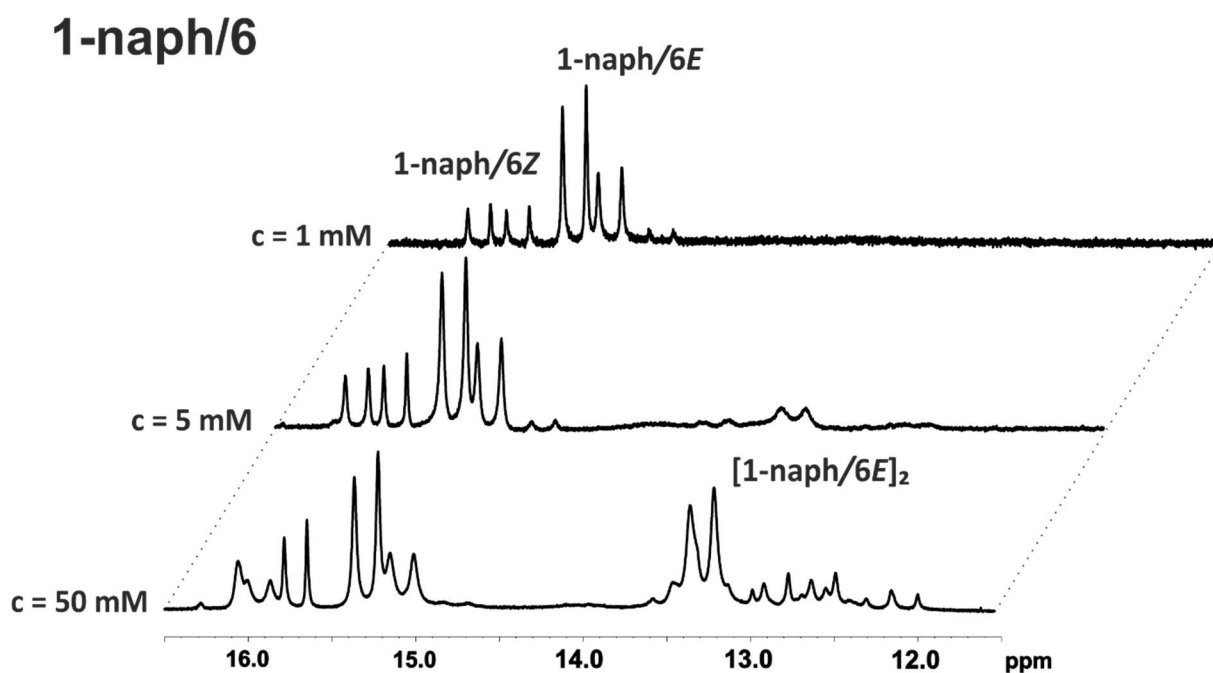


Figure S35: ^1H -spectra of 1-naph/6 at 180 K in CD_2Cl_2 at 600 MHz with a concentration of 1 mM, 5 mM or 50 mM. The signal of $[\text{1-naph}/6\text{E}]_2$ disappears at lower concentration, corroborating the assignment as a dimeric species.

3. Brønsted Acid Catalysis – The Effect of 3,3'-Substituents on the Structural Space and the Stabilization of Imine/Phosphoric Acid Complexes

S3. Diluted spectra of 9-phen/6

9-phen/6

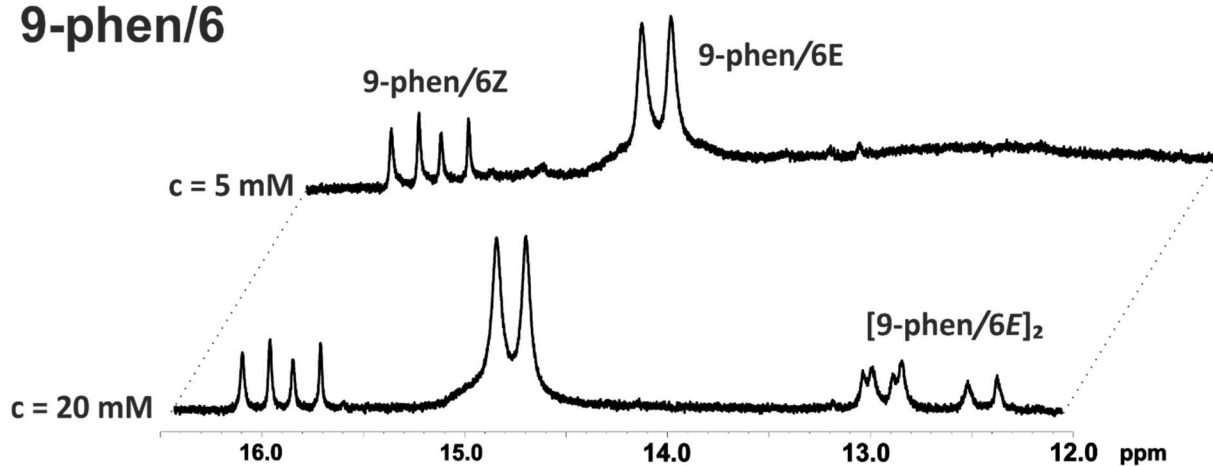


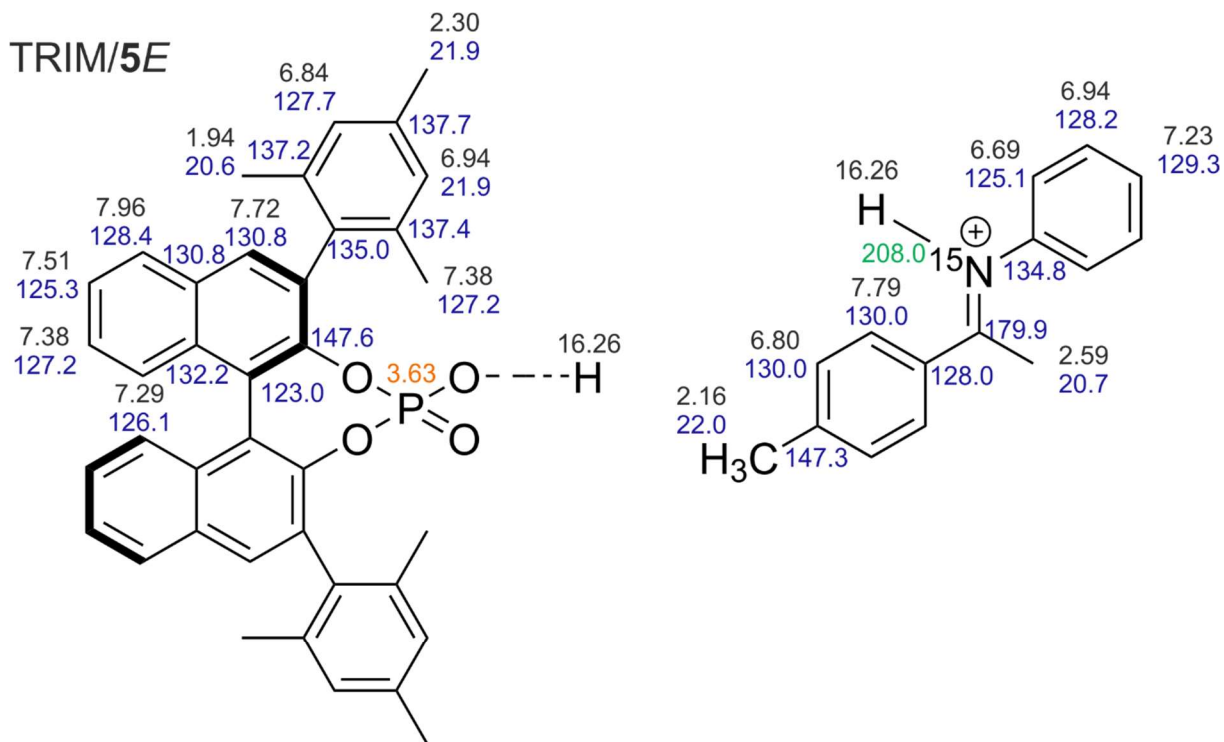
Figure S36: ¹H-spectra of 9-phen/6 at 180 K in CD₂Cl₂ at 600 MHz with a concentration of 5 mM or 20 mM. The signal of [9-phen/6E]₂ disappears at lower concentration, corroborating the assignment as a dimeric species.

3.6.3. Chemical shift assignment of TRIM/imine complexes

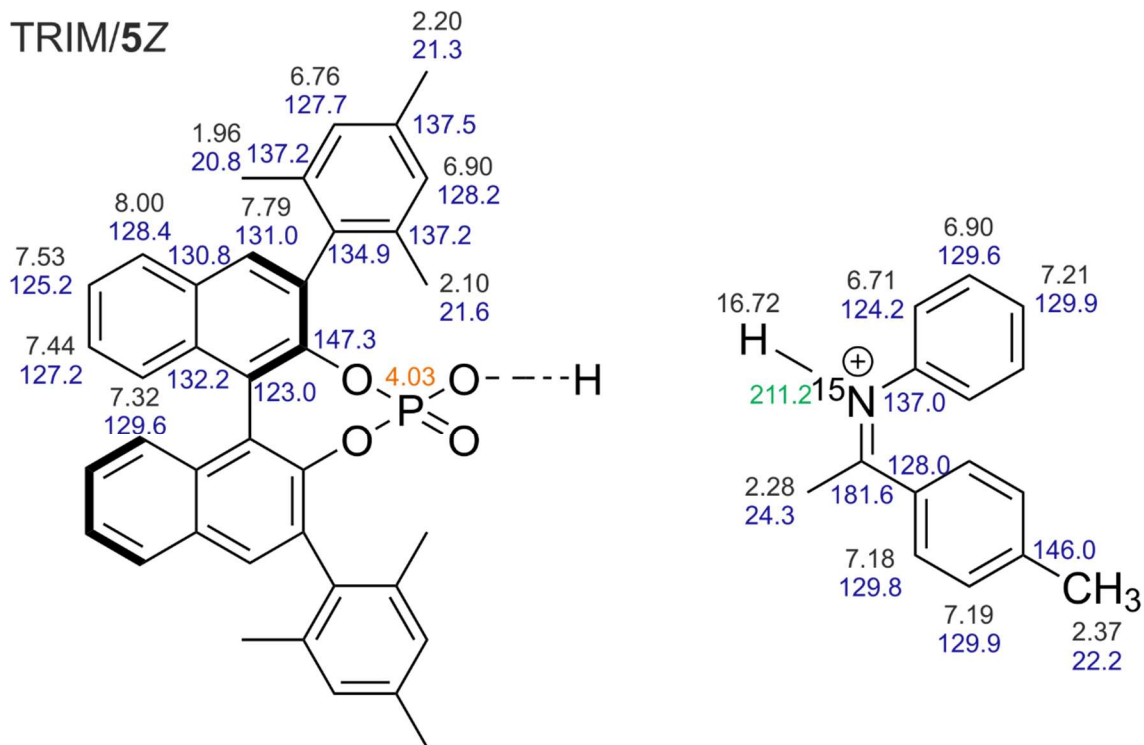
S29. Complexes (TRIM/5)

Colour code: blue – ^1H / black – ^{13}C / green – ^{15}N / orange – ^{31}P

TRIM/5E



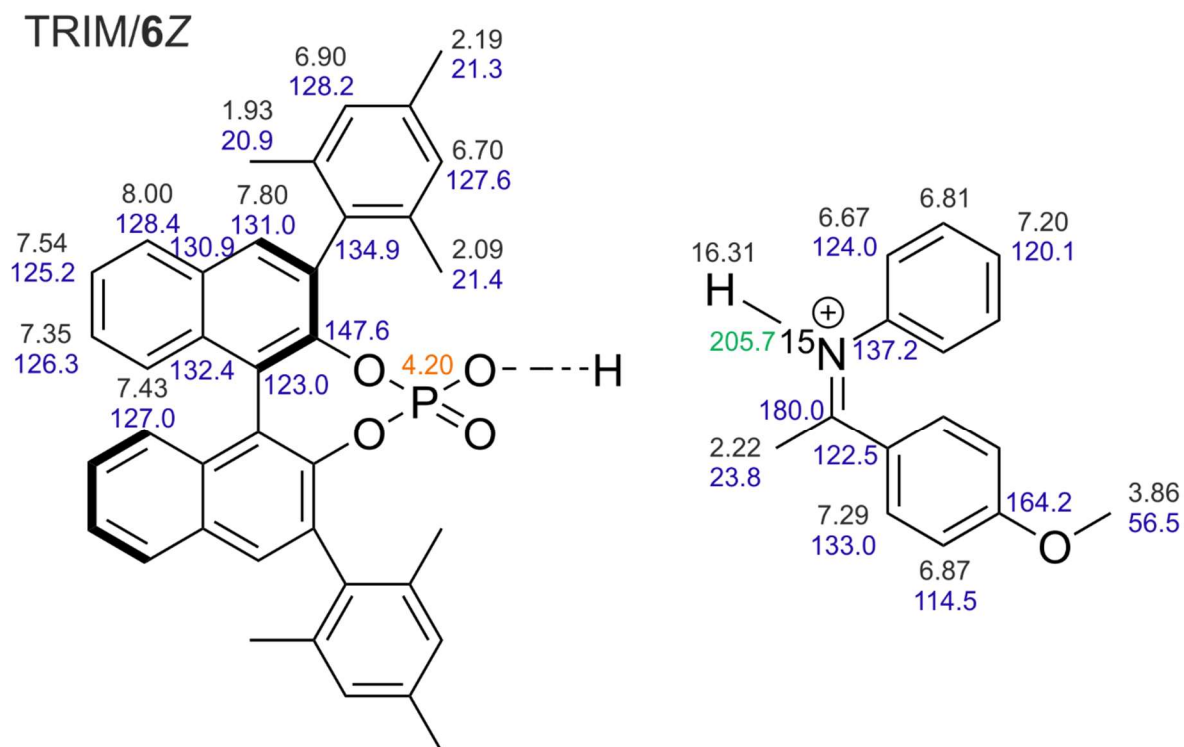
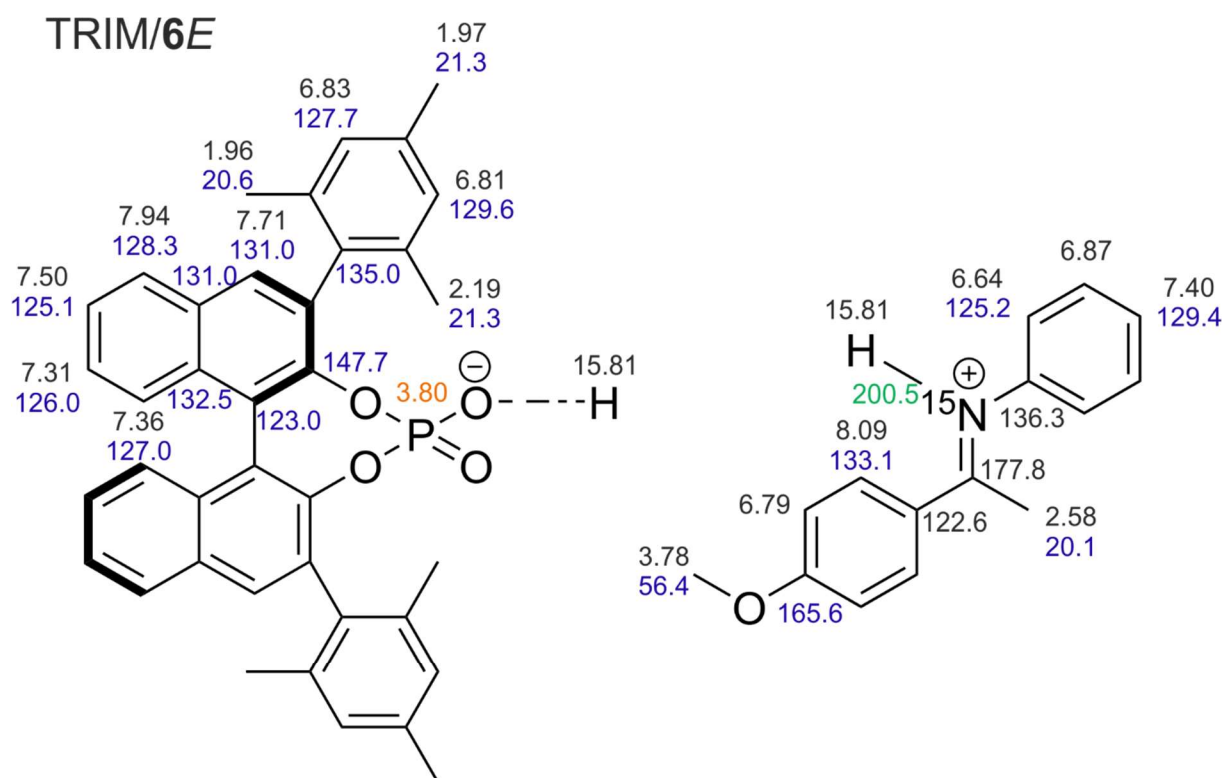
TRIM/5Z



3. Brønsted Acid Catalysis – The Effect of 3,3'-Substituents on the Structural Space and the Stabilization of Imine/Phosphoric Acid Complexes

S30. Complexes (TRIM/6)

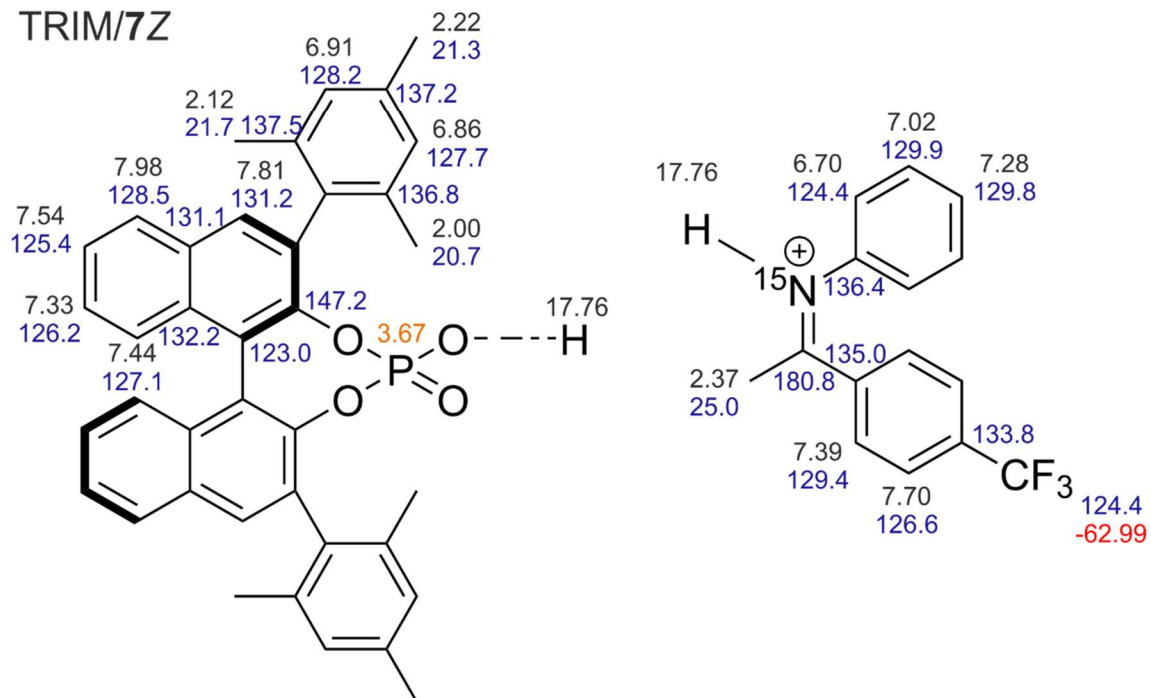
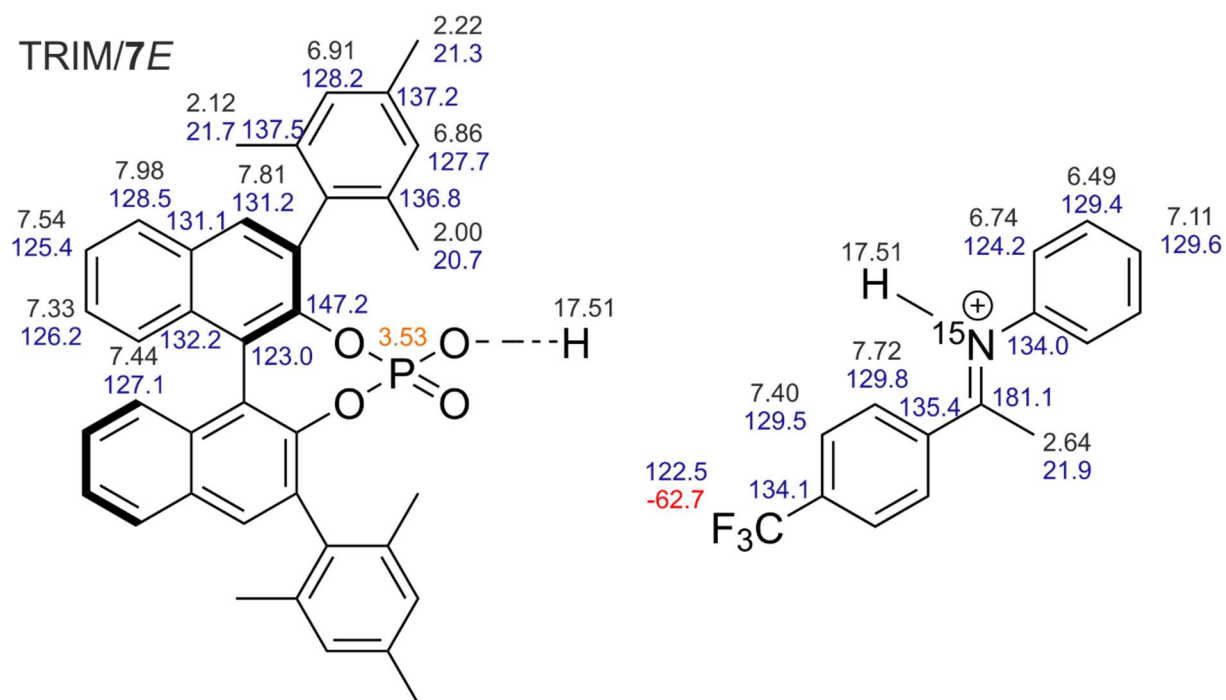
Colour code: blue – ^1H / black – ^{13}C / green – ^{15}N / orange – ^{31}P



3. Brønsted Acid Catalysis – The Effect of 3,3'-Substituents on the Structural Space and the Stabilization of Imine/Phosphoric Acid Complexes

S31. Complexes (TRIM/7)

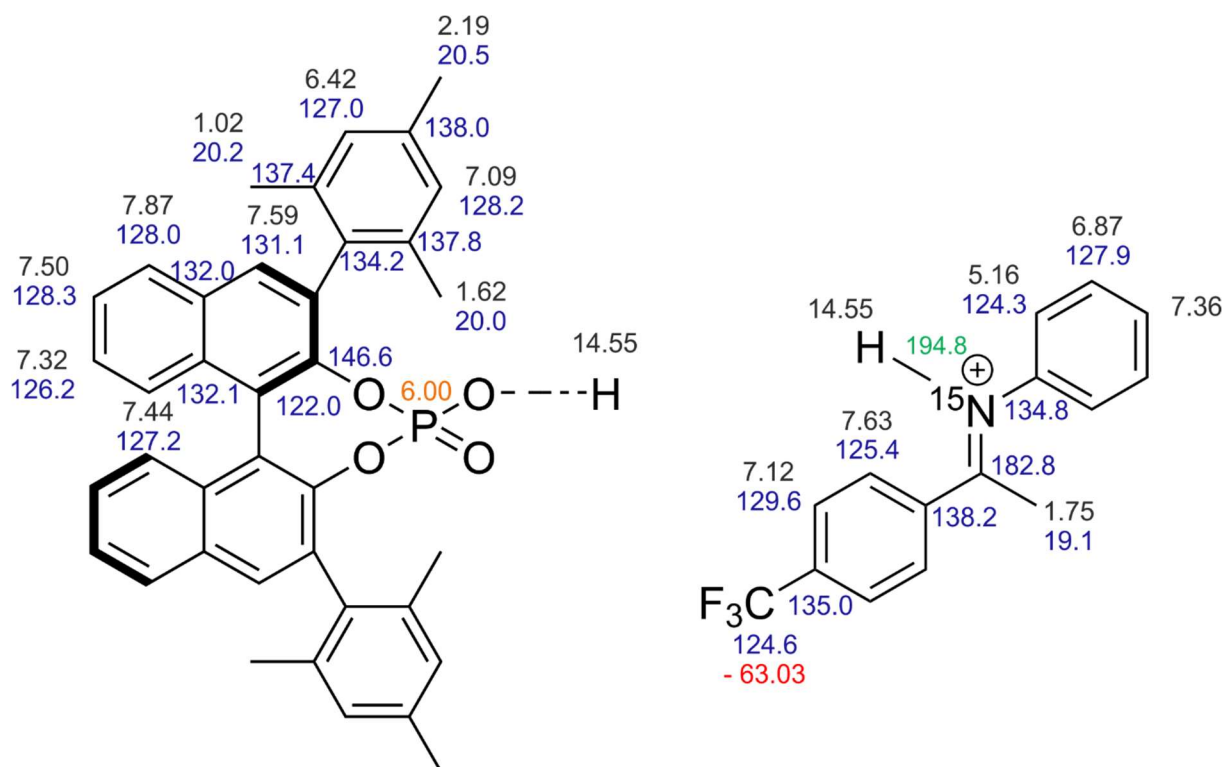
Colour code: blue – ^1H / black – ^{13}C / green – ^{15}N / orange – ^{31}P / red – ^{19}F



3. Brønsted Acid Catalysis – The Effect of 3,3'-Substituents on the Structural Space and the Stabilization of Imine/Phosphoric Acid Complexes

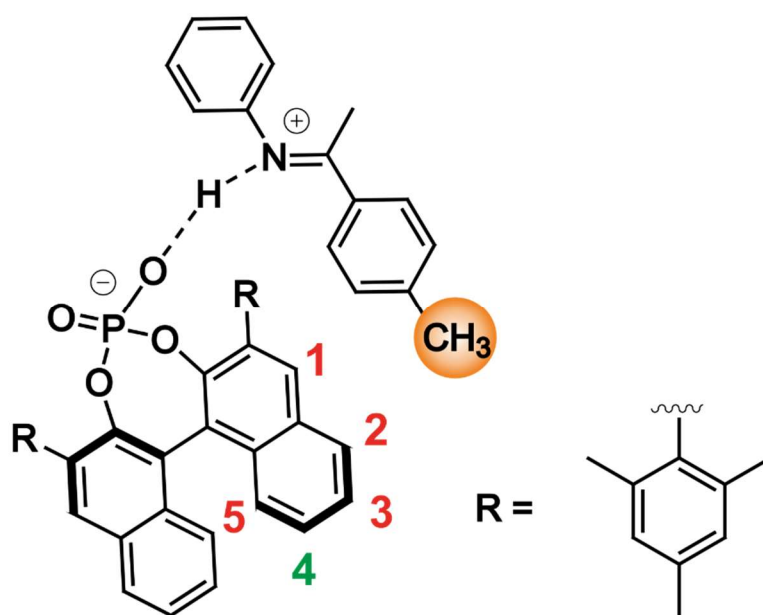
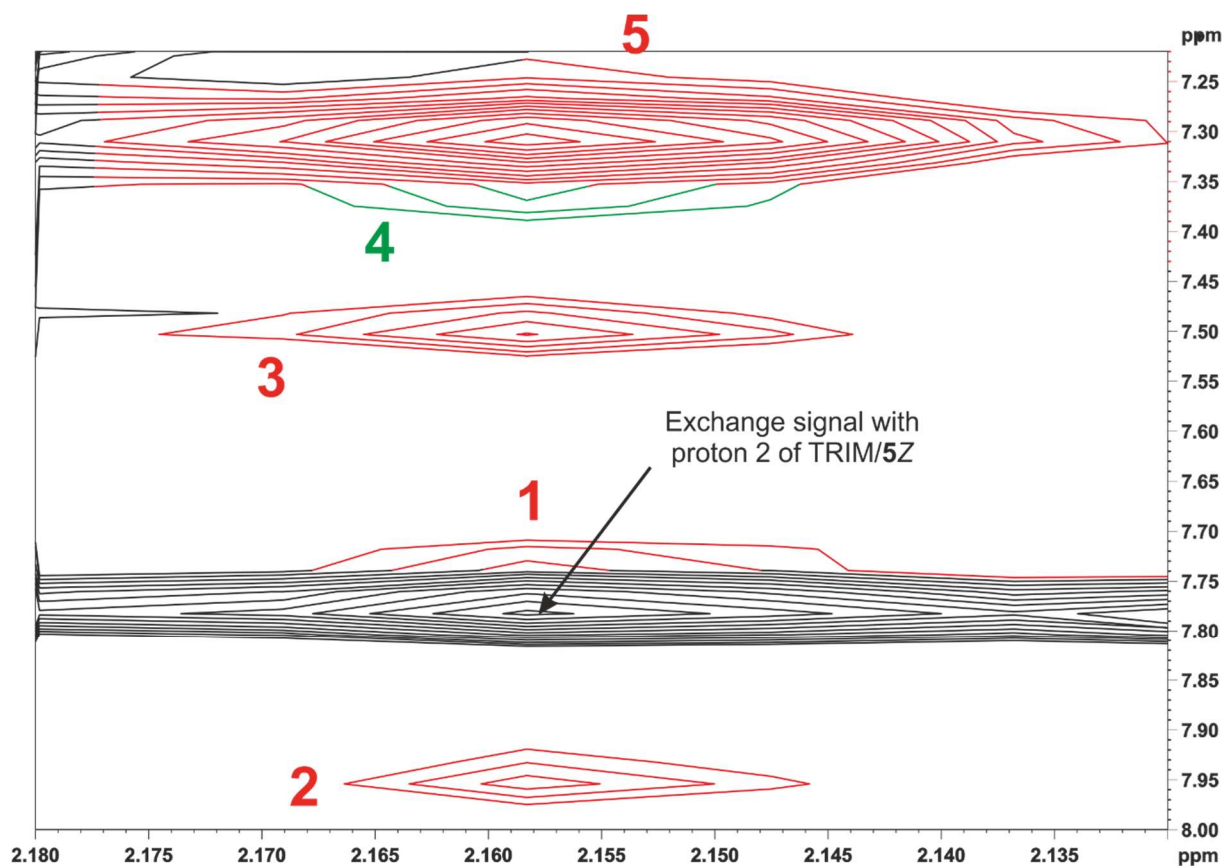
S32. Complexes [TRIM/7E]₂

Colour code: blue – ¹H / black – ¹³C / green – ¹⁵N / orange – ³¹P / red – ¹⁹F



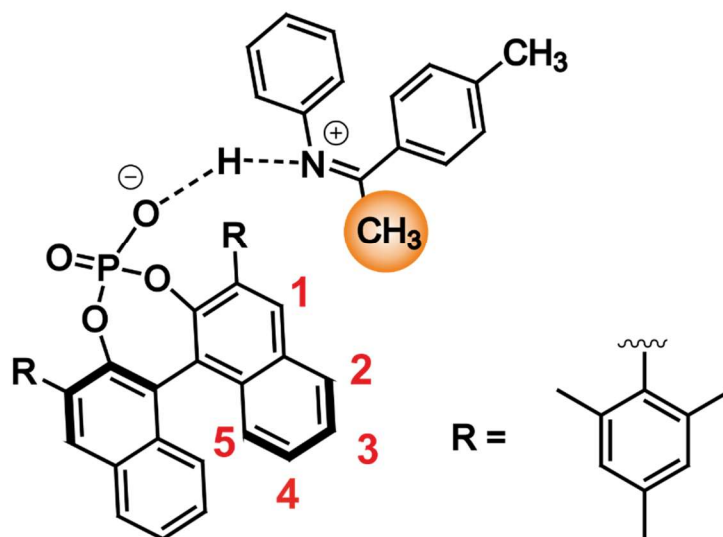
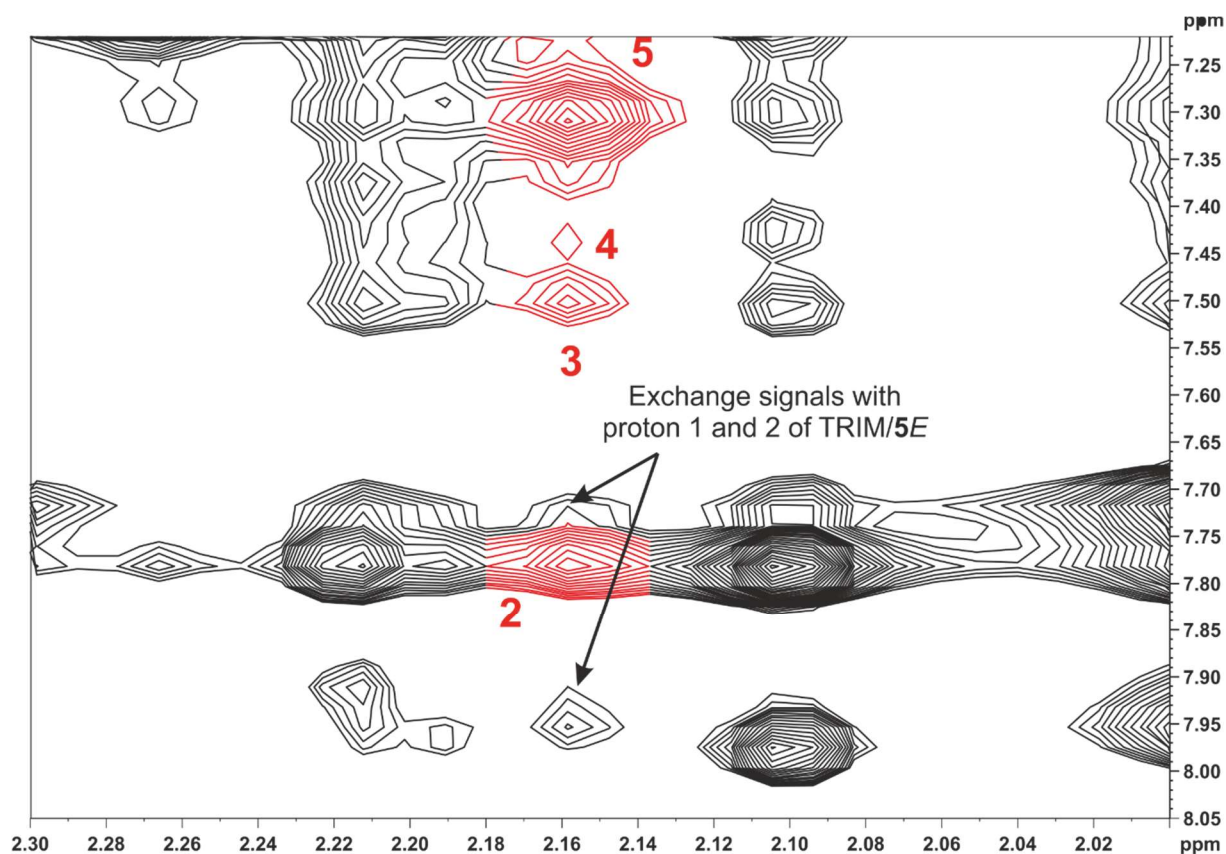
3.6.4. Structure identification of all TRIM/imine complexes

S33. Type I TRIM/5E Complex



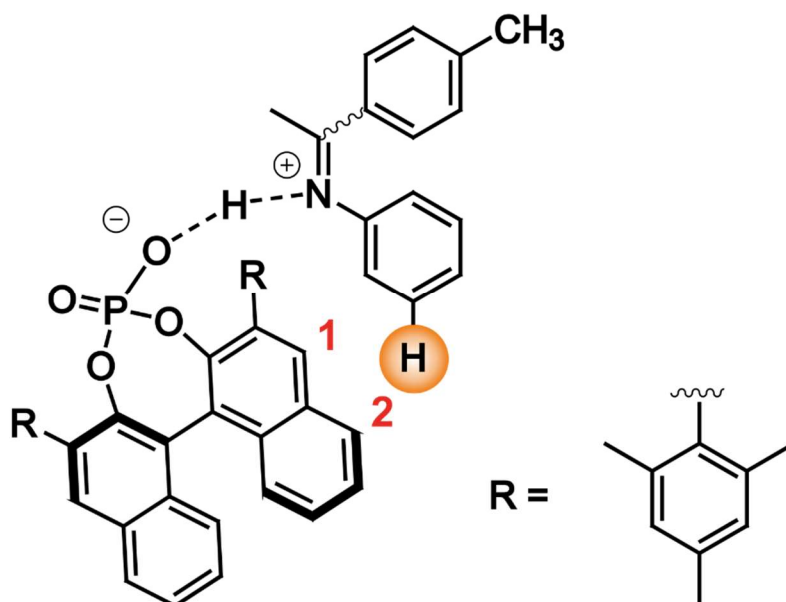
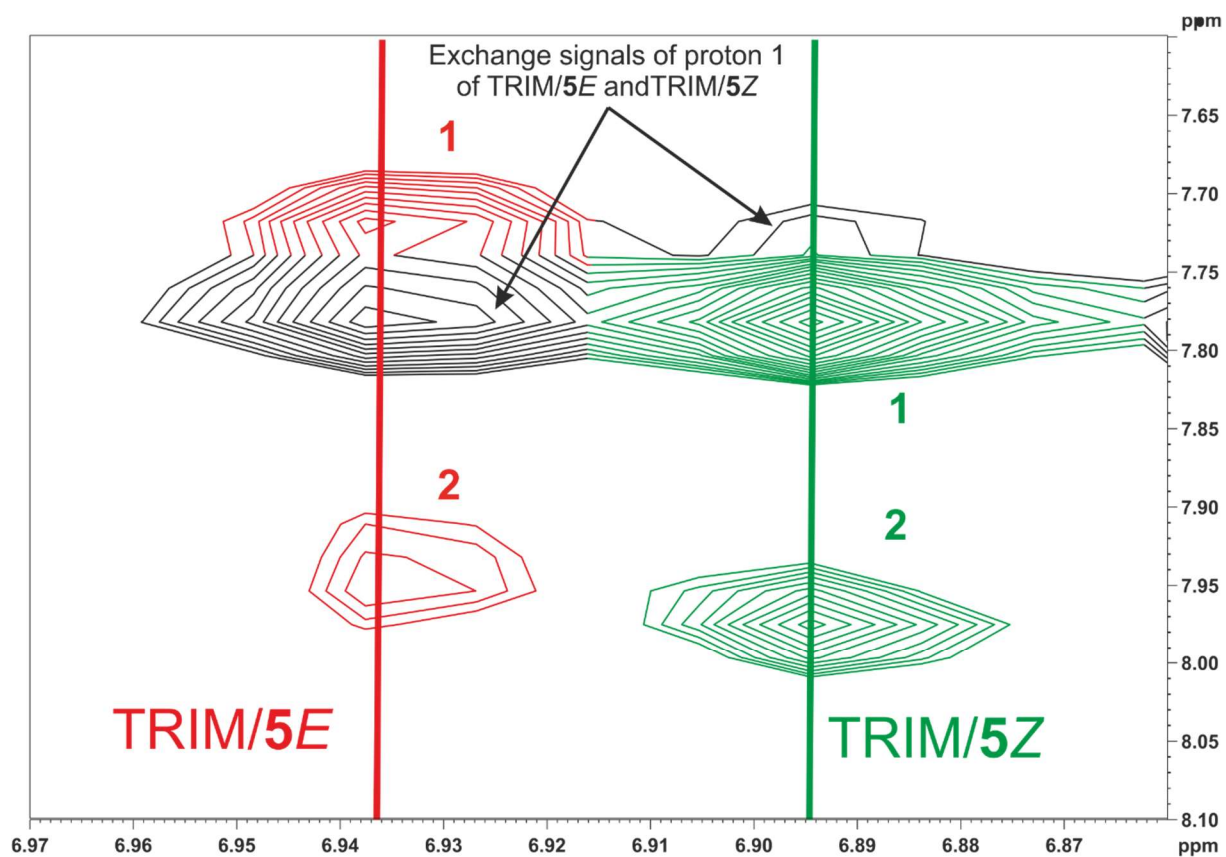
3. Brønsted Acid Catalysis – The Effect of 3,3'-Substituents on the Structural Space and the Stabilization of Imine/Phosphoric Acid Complexes

S34. Type I TRIM/5Z Complex



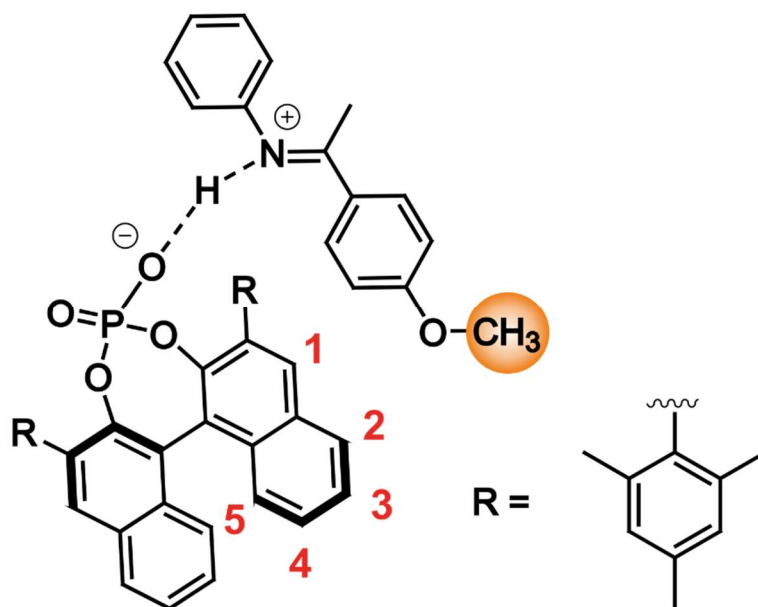
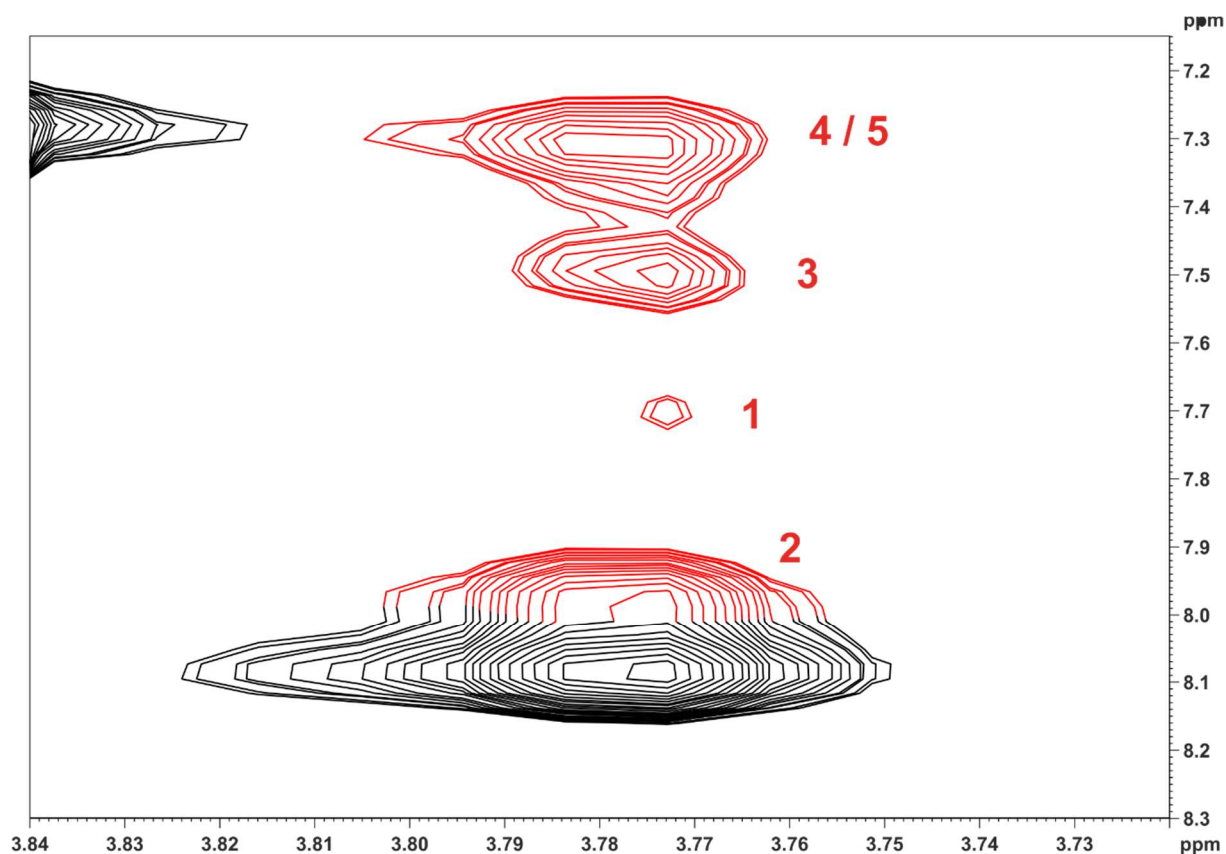
3. Brønsted Acid Catalysis – The Effect of 3,3'-Substituents on the Structural Space and the Stabilization of Imine/Phosphoric Acid Complexes

S35. Type II TRIM/5EZ Complexes



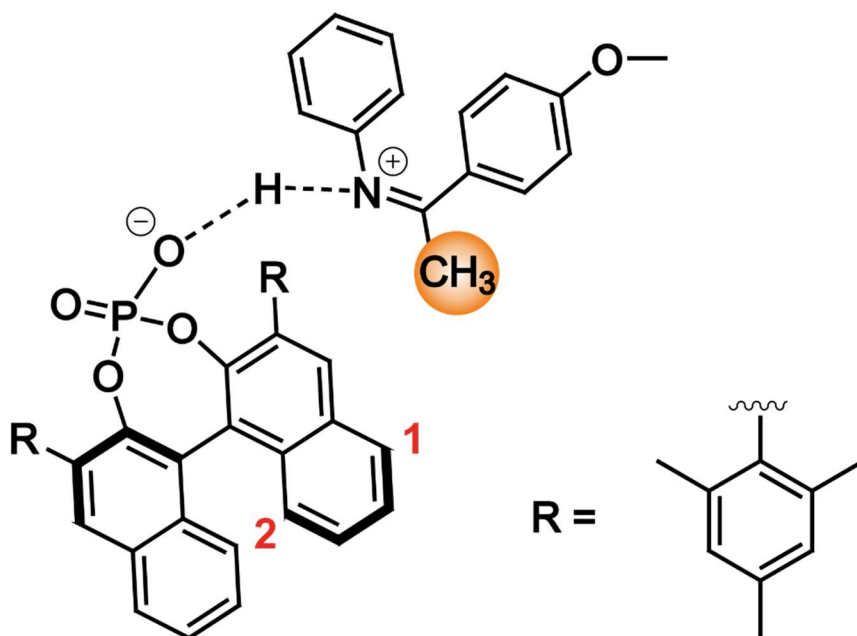
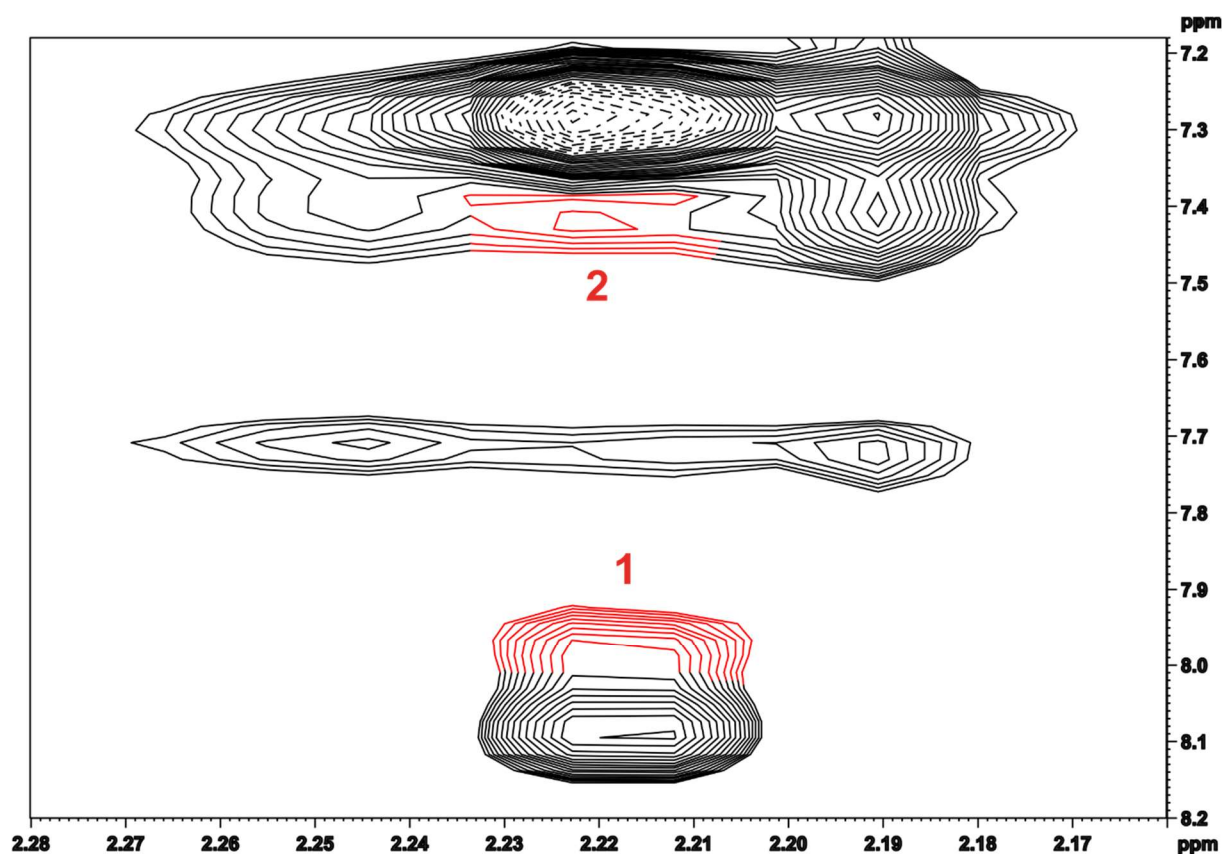
3. Brønsted Acid Catalysis – The Effect of 3,3'-Substituents on the Structural Space and the Stabilization of Imine/Phosphoric Acid Complexes

S36. Type I TRIM/6E Complexes



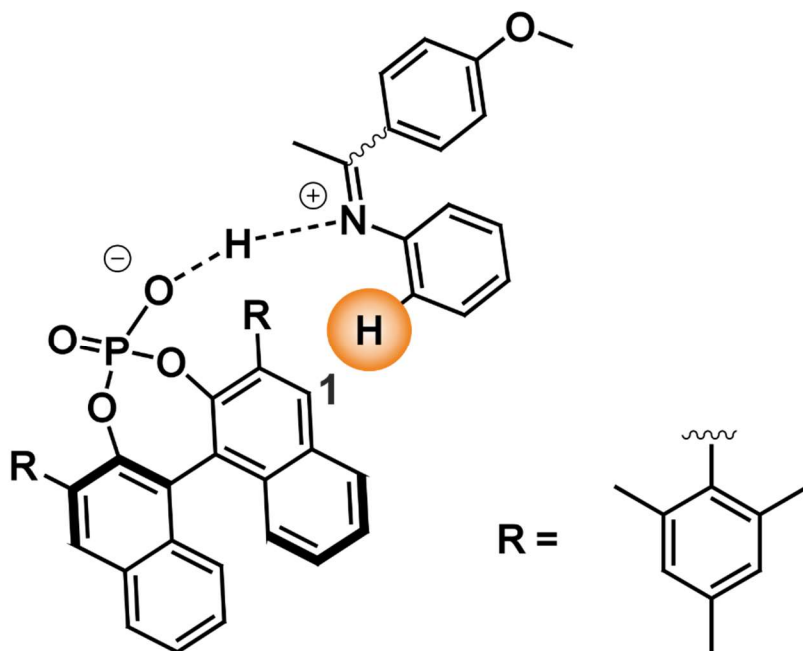
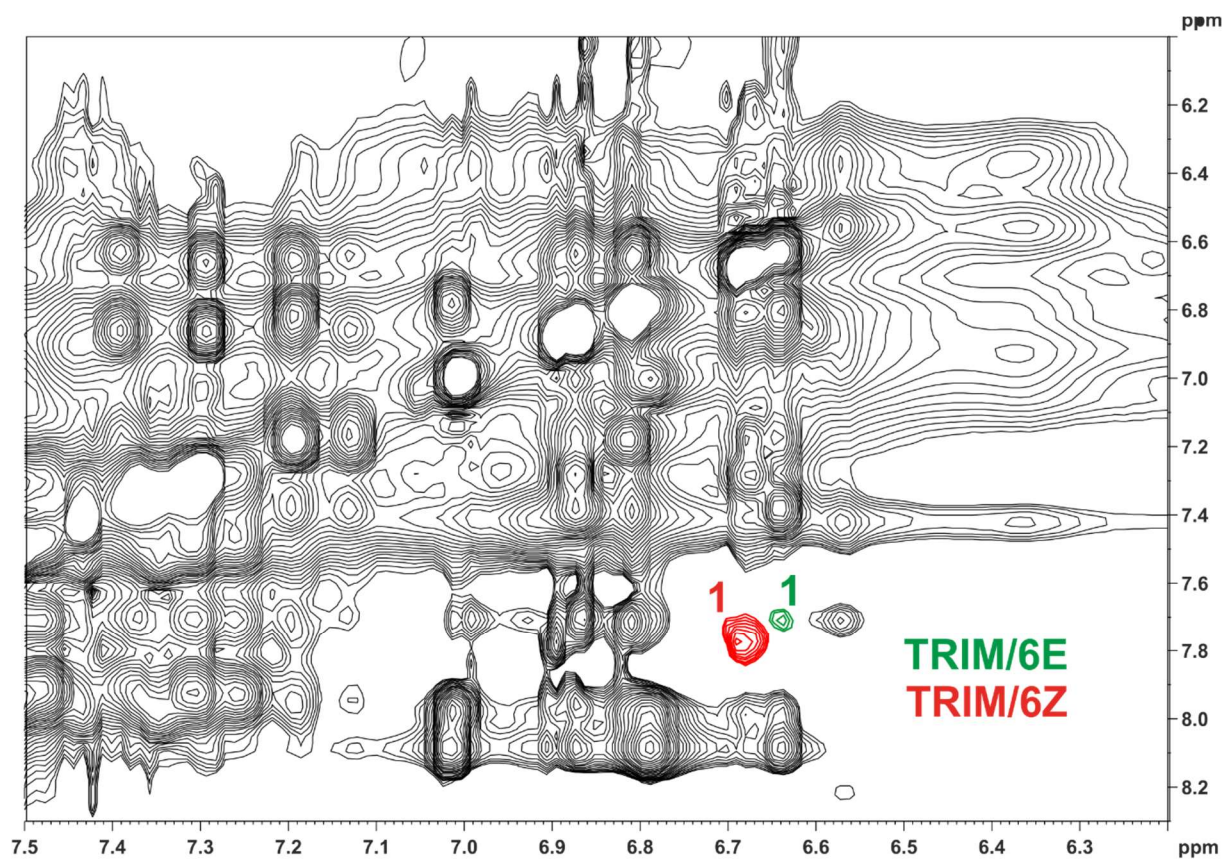
3. Brønsted Acid Catalysis – The Effect of 3,3'-Substituents on the Structural Space and the Stabilization of Imine/Phosphoric Acid Complexes

S37. Type I TRIM/6Z Complexes



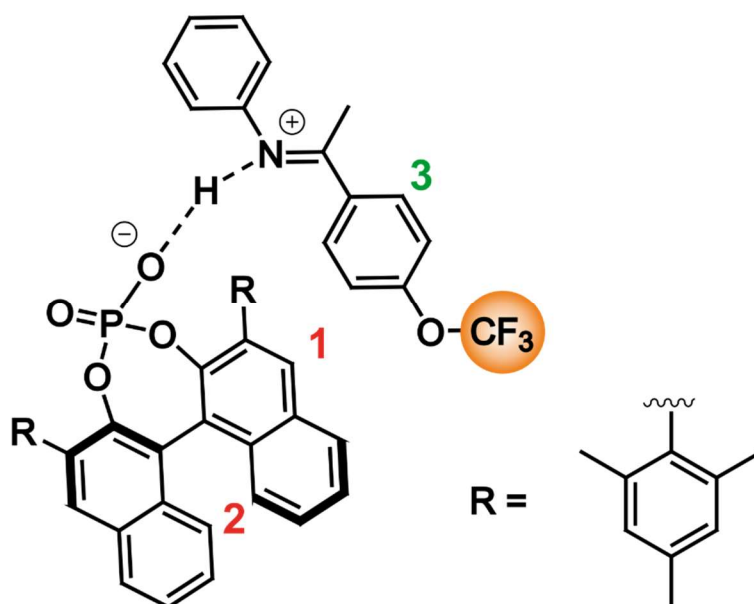
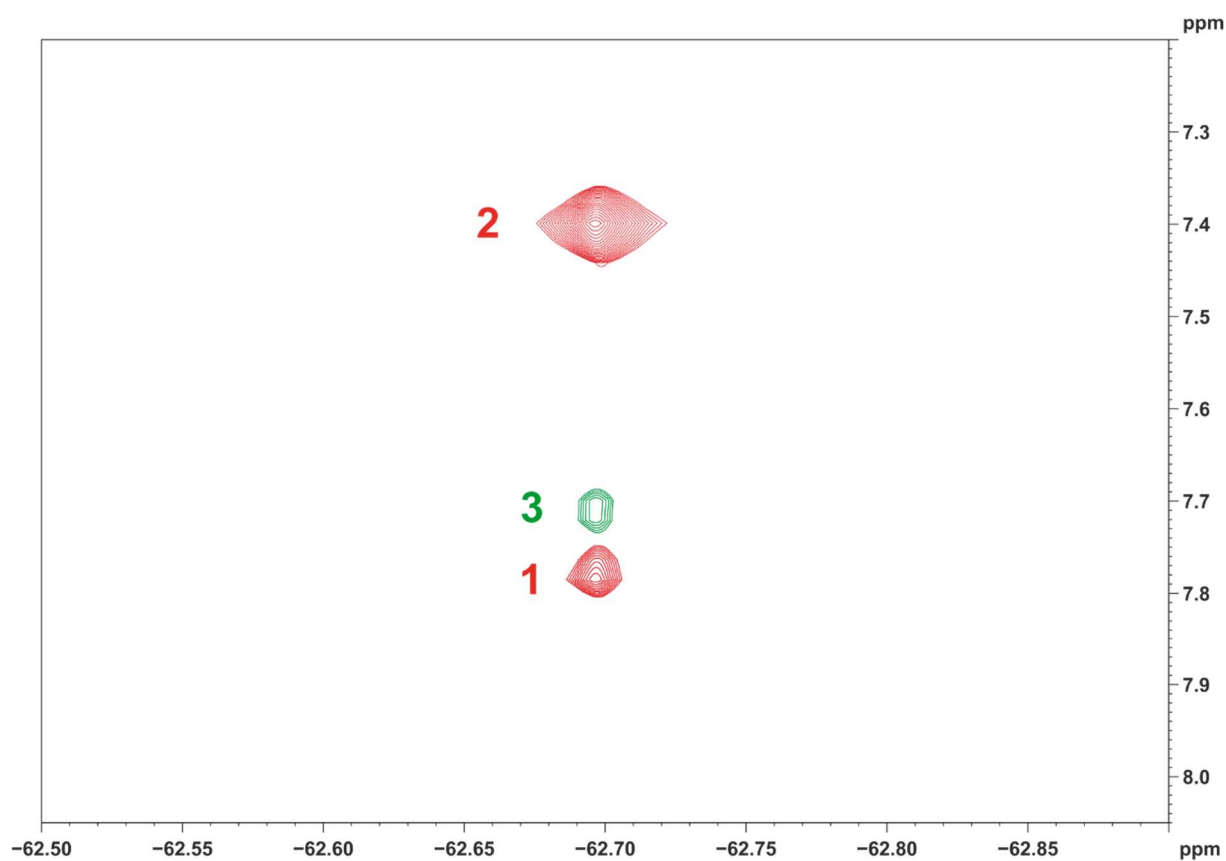
3. Brønsted Acid Catalysis – The Effect of 3,3'-Substituents on the Structural Space and the Stabilization of Imine/Phosphoric Acid Complexes

S38. Type II TRIM/6EZ Complexes



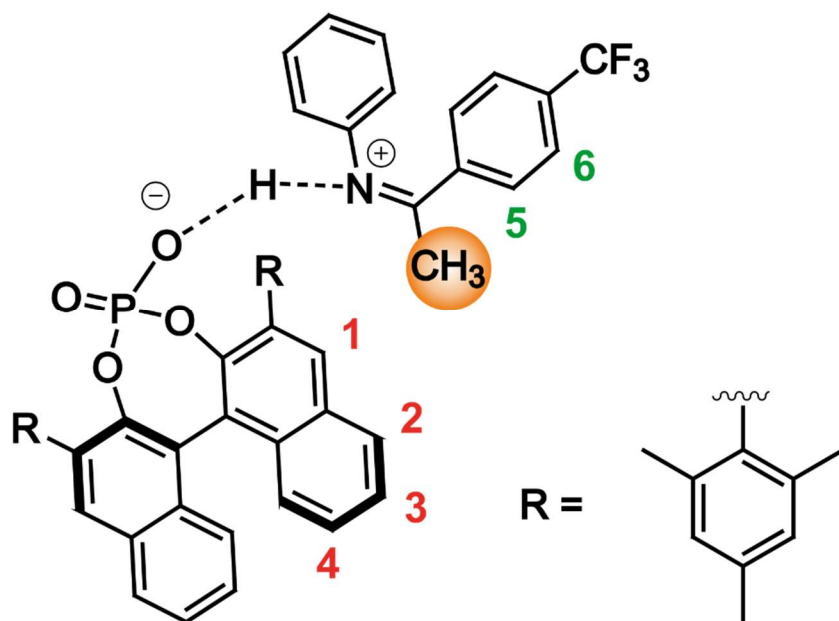
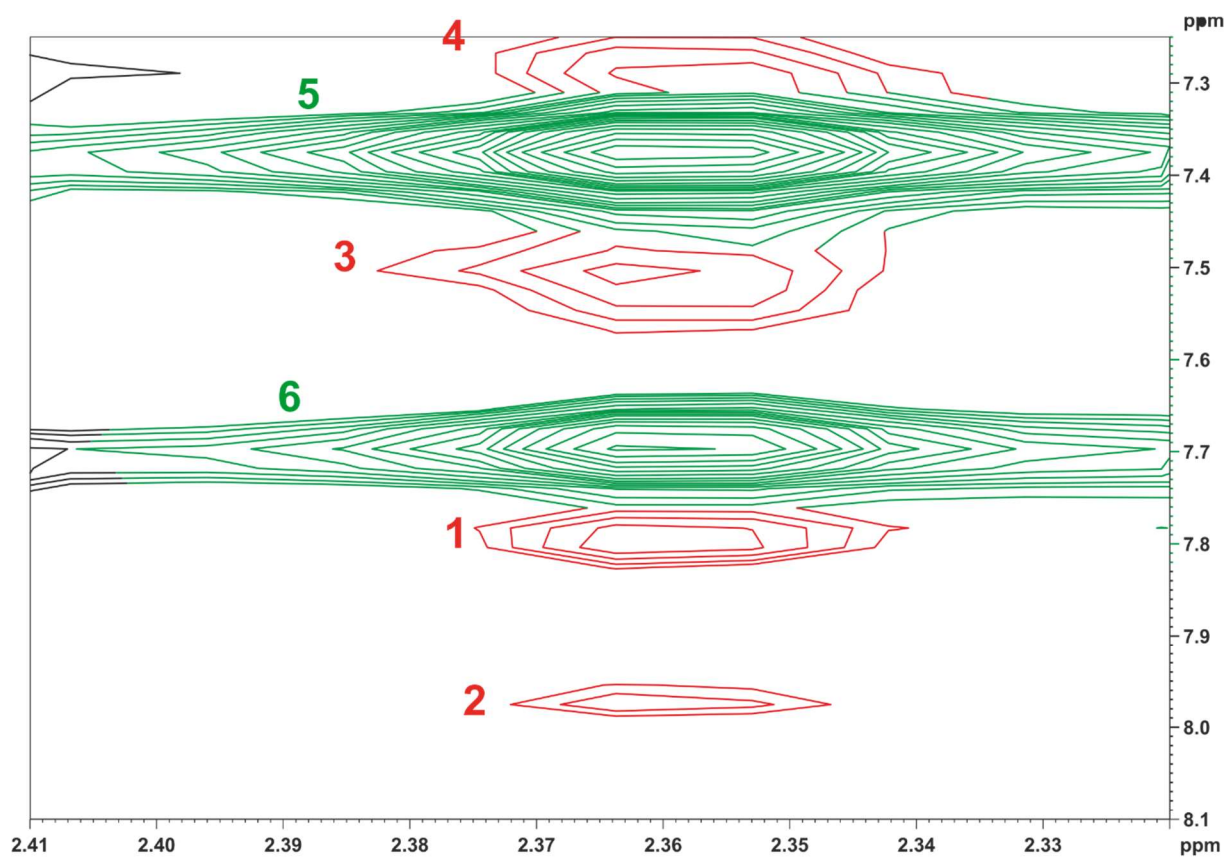
3. Brønsted Acid Catalysis – The Effect of 3,3'-Substituents on the Structural Space and the Stabilization of Imine/Phosphoric Acid Complexes

S39. Type I TRIM/7E Complex



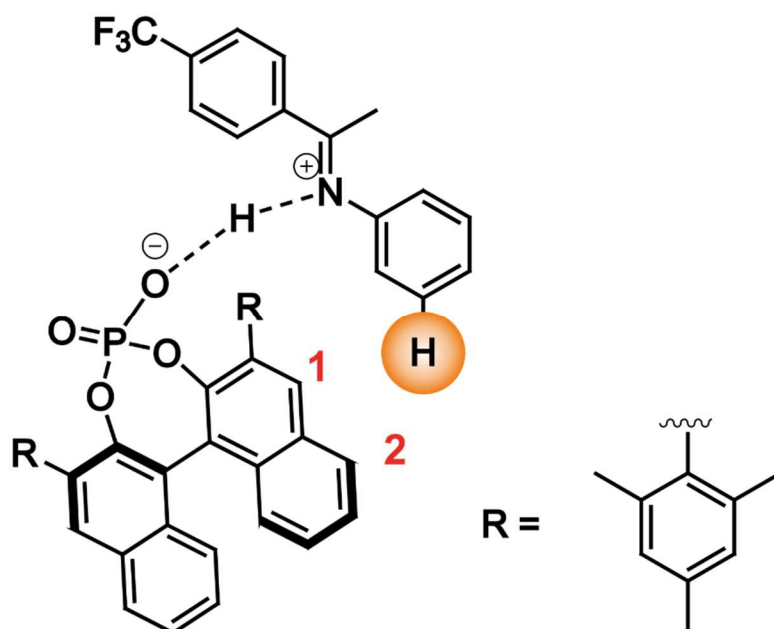
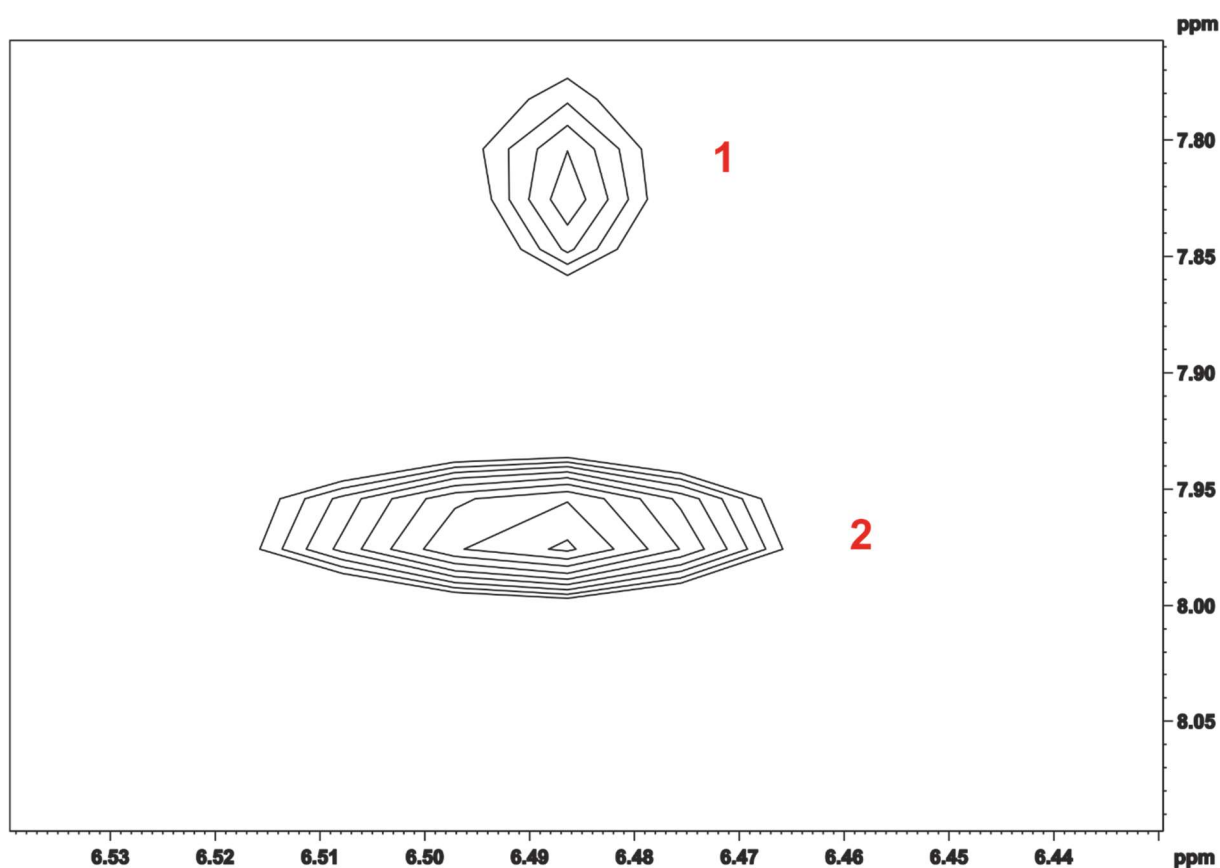
3. Brønsted Acid Catalysis – The Effect of 3,3'-Substituents on the Structural Space and the Stabilization of Imine/Phosphoric Acid Complexes

S40. Type I TRIM/7Z Complex



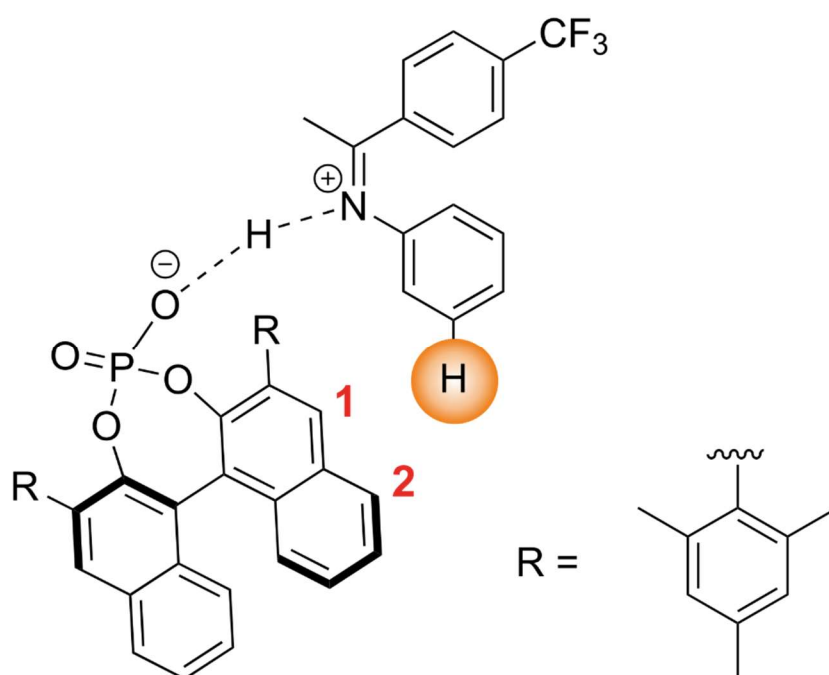
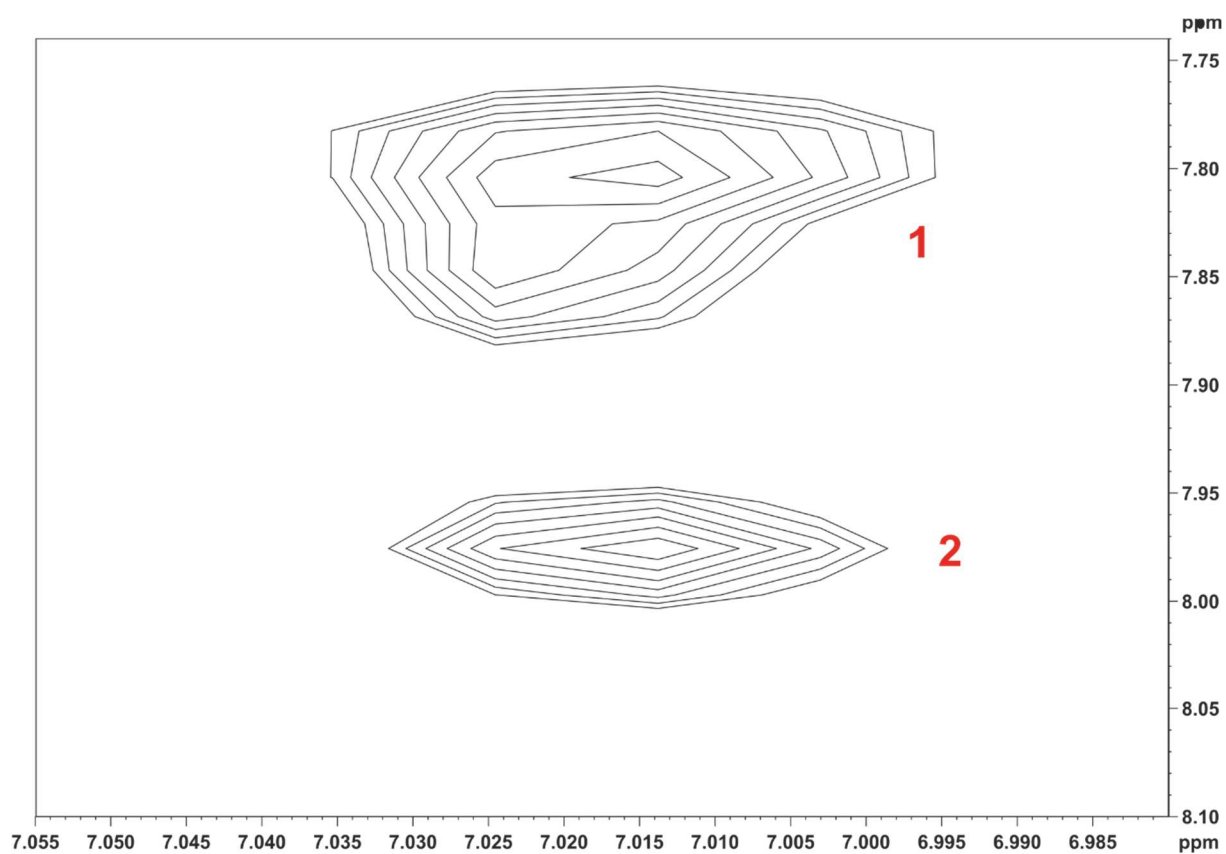
3. Brønsted Acid Catalysis – The Effect of 3,3'-Substituents on the Structural Space and the Stabilization of Imine/Phosphoric Acid Complexes

S41. Type II TRIM/7E Complex



3. Brønsted Acid Catalysis – The Effect of 3,3'-Substituents on the Structural Space and the Stabilization of Imine/Phosphoric Acid Complexes

S42. Type II TRIM/7Z Complex



3.6.5. Exchange pathways in binary TRIM/imine complexes

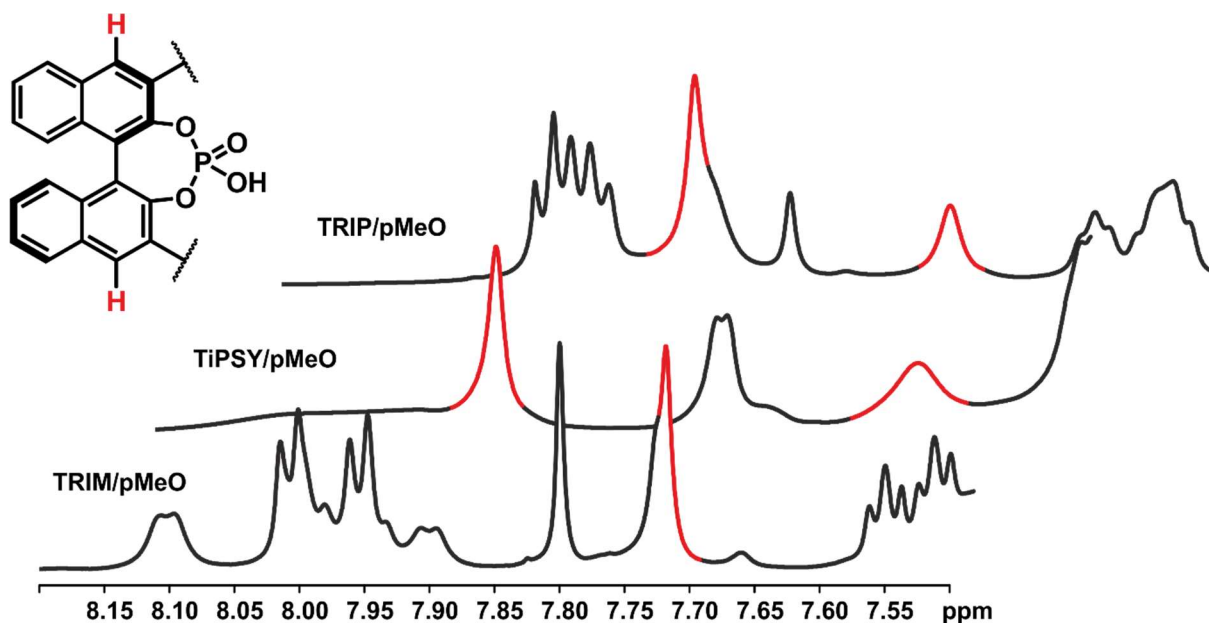


Figure S43: 1D ^1H spectra of catalysts TRIP, TiPSY and TRIM/6 at 180 K in CD_2Cl_2 at 600 MHz; for TRIP and TiPSY, a splitting of the signal sets of the BINOL backbone is seen, as exemplarily shown for one proton labelled in red; TRIM/imine complexes only show one averaged set of signals for both halves of the backbone.

A possible reason for this averaging in the TRIM/imine complexes might be a faster exchange between the free imine and the imine inside the complex or an additional exchange pathway between structures *Type I E* and *Type II E* via rotation of the imine similar to the Z-structures. The latter might be enabled due to the reduced Area(Θ) value of TRIM.^[9]

3.6.6. DOSY measurements for TRIM dimer

The DOSY measurements were performed with the convection suppressing DSTE (double stimulated echo) pulse sequence developed by Jerschow and Müller in a pseudo 2D mode at 180 K.^[10] TMS was used to reference the viscosity of the solvent. The diffusion time delay was set to 45 ms. The gradient pulse lengths (p16, SMSQ10.100 pulse shape) were optimized for each species to give a sigmoidal signal decay for varying gradient strengths. Optimal pulse lengths of 2.9 – 3.1 ms, 6.0 ms and 7.0 ms were found for TMS, TRIM/7 and $[\text{TRIM}/7\text{E}]_2$, respectively. For each species, twenty spectra with linear varying gradient strength of 5% - 95% or 10% - 95% have been measured. Either the H-bond proton signals or the methyl-groups of the 3,3'-substituents have been used as probes. The signal intensities of the respective groups were analyzed as a function of the gradient strength by Bruker TopSpin 3.2 software T1/T2 relaxation package by employing the Stejskal-Tanner equation.^[11] The sigmoidal fit provided the translational self-diffusion coefficients D_i listed in Table S33. The molecular radii were derived by the Stokes-Einstein equation.^[12]

3. Brønsted Acid Catalysis – The Effect of 3,3'-Substituents on the Structural Space and the Stabilization of Imine/Phosphoric Acid Complexes

$$D_i = \frac{k_B T}{\pi \eta r_H}$$

D_i is the self-diffusion coefficient derived by the measurement, η is the viscosity of the solvent and r_H is the hydrodynamic radius of the observed molecule. Due to the three-side exchange between $[\text{TRIM}/\mathbf{7E}]_2$, $\text{TRIM}/\mathbf{7E}$ and free, not complexated TRIM and $\mathbf{7}$, the absolute obtained self-diffusion coefficients are not meaningful. If two molecules A and B with different diffusion constants are in slow exchange with each other, the observed diffusion coefficients are a combination of the intrinsic diffusion coefficients of A and B without exchange, weighed with the respective lifetimes of A and B.^[13,14] Hence, only a qualitative interpretation of the DOSY spectra was possible. Molecular radii of 9.54 and 12.57 Å were found for $\text{TRIM}/\mathbf{7E}$ and $[\text{TRIM}/\mathbf{7E}]_2$, respectively. The derived larger molecular size clearly corroborates the assignment as a dimer.

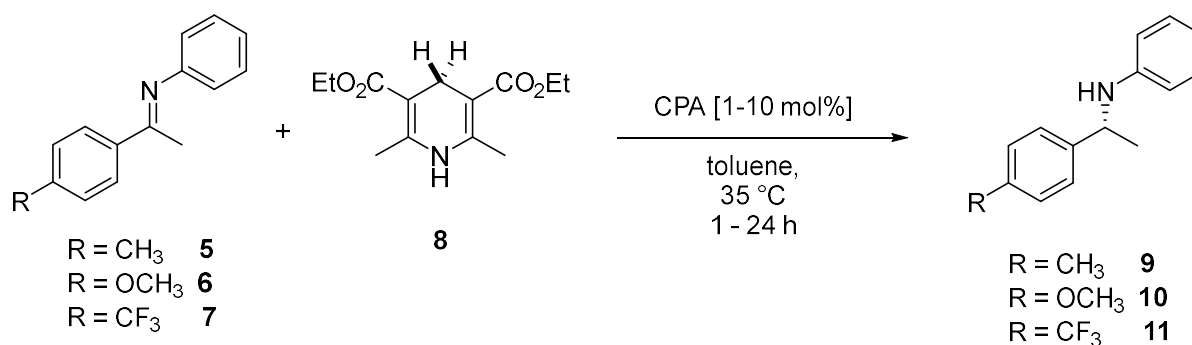
S44. Self-diffusion coefficients

Table S44: Measured self-diffusion coefficients and derived molecular radii. Entry 1-6: SW = 22 Hz, O1P = 2.00 ppm, gradient strength 5-95% linear; entry 7-11: SW = 22 Hz, O1P = 9.00 ppm, gradient strength 10-95% linear. No diffusion coefficients based on the H-Bond proton signals of $[\text{TRIM}/\mathbf{7E}]_2$ could be derived due to low signal intensities. Diffusion coefficients of different signals of the same species were averaged.

Entry	Species	p16 [ms]	probe signal [ppm]	D_i [m^2/s] · 10 ⁻¹²	Averaged	r_H [Å]
1	TMS	3.10	0.00	16.81		
2	TRIM/ 7EZ	6.00	2.22	3.645		
3	TRIM/ 7EZ	6.00	2.12	3.732	3.693	9.54
4	TRIM/ 7EZ	6.00	2.00	3.702		
5	$[\text{TRIM}/\mathbf{7E}]_2$	7.00	1.62	2.774	2.761	12.57
6	$[\text{TRIM}/\mathbf{7E}]_2$	7.00	1.02	2.748		
7	TMS	3.00	0.00	19.35		
8	TRIM/ 7Z	6.00	17.83	4.334	4.393	9.25
9	TRIM/ 7Z	6.00	17.70	4.419		
10	TRIM/ 7E	6.00	17.58	4.361		
11	TRIM/ 7E	6.00	17.45	4.457		

3. Brønsted Acid Catalysis – The Effect of 3,3'-Substituents on the Structural Space and the Stabilization of Imine/Phosphoric Acid Complexes

3.6.7. Determination of ee values



A Schlenk tube was dried at 350 °C under reduced pressure for several minutes. Imine **5-7** (0.1 mmol, 1.0 eq.), the CPA catalyst (0.01 eq. or 0.1 eq. for TiPSY) and Hantzsch Ester **8** (36.5 mg, 0.14 mmol, 1.4 eq.) were weighed into the tube. The tube was evacuated and flushed with Argon three times. Under Argon flow, anhydrous toluene (1.0 mL) was added. The reaction was stirred at 35 °C for 1 – 24 h. 0.1 – 0.2 mL of the crude reaction mixture was taken and quenched by addition to a vial filled with hexane (2.0 mL) and NEt_3 (10 μL , 7.3 μg , 0.072 mmol, 7.2 – 72 eq. based on the catalyst). The mixture was filtered and analysed by chiral HPLC (see S47 for further details).

Table S45: ee values of the transfer hydrogenation of imines **5-7** with Hantzsch Ester catalysed by various CPAs.

Catalyst	Imine 5		
	major [Area%]	minor [Area%]	ee [%]
TRIP	92.2	7.8	84
TRIFP	87.2	12.7	75
TiPSY	95.1	4.9	90
1-naph	79.4	20.6	59
9-phen	78.0	21.9	56
TRIM	85.6	14.3	71
Catalyst	Imine 6		
	major [Area%]	minor [Area%]	ee [%]
TRIP	93.0	7.0	86
TRIFP	87.0	13.0	74
TiPSY	95.5	4.5	92
1-naph	78.1	21.9	56
9-phen	77.8	22.2	56
TRIM	85.0	15.0	70
Catalyst	Imine 7		
	major [Area%]	minor [Area%]	ee [%]
TRIP	91.7	8.3	83
TRIFP	95.6	4.3	91
TiPSY	97.7	2.3	95
1-naph	73.4	26.6	47
9-phen	73.0	27.0	46
TRIM	78.2	21.8	56

3. Brønsted Acid Catalysis – The Effect of 3,3'-Substituents on the Structural Space and the Stabilization of Imine/Phosphoric Acid Complexes

3.6.8. Correlation of *ee* with CPA parameters

Table S46: List of experimental *ee* values, E- and Z-imine populations in the binary CPA/imine complexes and steric descriptors as used by Goodman.^[15]

Catalyst	Imine									Steric Descriptors	
	5			6			7			AREA(Θ) [°]	Rot. Barrier [kcal/mol]
	<i>ee</i>	% E	% Z	<i>ee</i>	% E	% Z	<i>ee</i>	% E	% Z		
TRIP	84	67	33	86	77	23	83	86	14	51	28.4
TRIFP	75	70	30	74	81	19	91	69	31	62	2.02
TiPSY	90	56	44	92	70	30	95	71	29	29	1.13
TRIM	71	47	53	70	49	51	56	55	45	61	21.58
1-naph	56	-	-	56	-	-	46	-	-	62	13.63
Phen	59	-	-	56	-	-	47	-	-	48	14.45

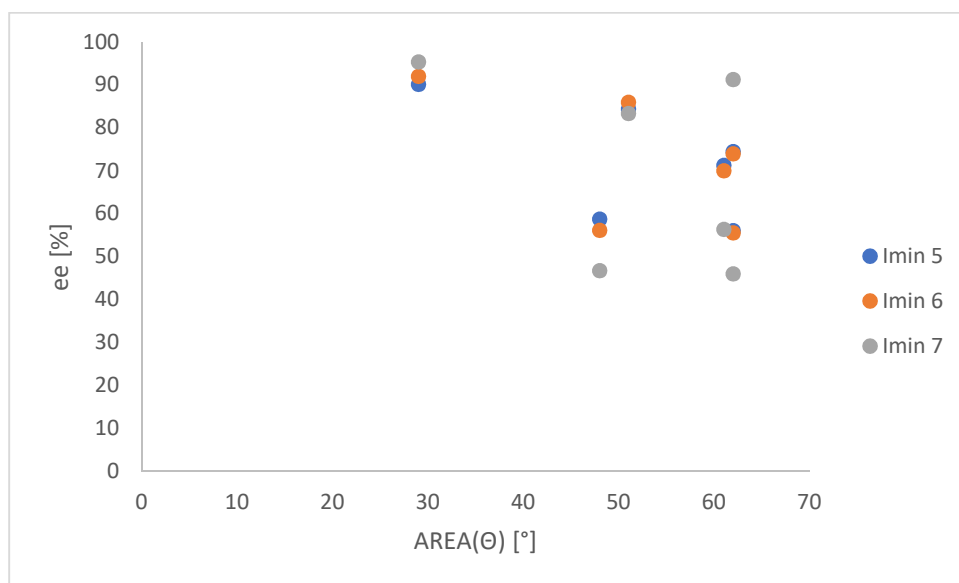


Figure S46.1: Plot of the *ee* values of the transfer hydrogenation of imines 5-7 catalyzed by TRIP, TRIFP, TiPSY, TRIM, 1-naph and 9-phen against the AREA(Θ) value computed by Goodman.^[15] No correlation is observed.

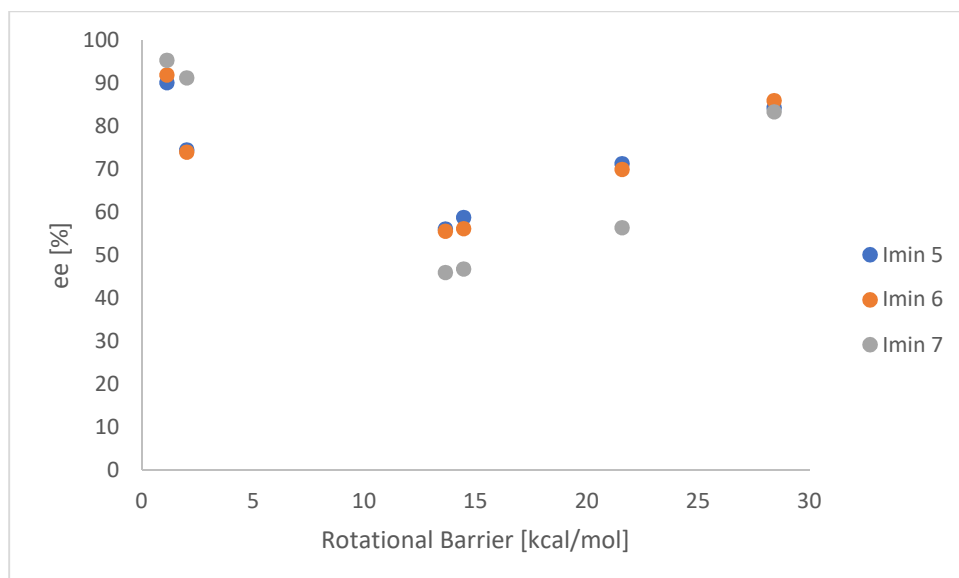


Figure S46.2: Plot of the *ee* values of the transfer hydrogenation of imines 5-7 catalyzed by TRIP, TRIFP, TiPSY, TRIM, 1-naph and 9-phen against the Rotational Barrier value computed by Goodman.^[15] No linear correlation is observed.

3. Brønsted Acid Catalysis – The Effect of 3,3'-Substituents on the Structural Space and the Stabilization of Imine/Phosphoric Acid Complexes

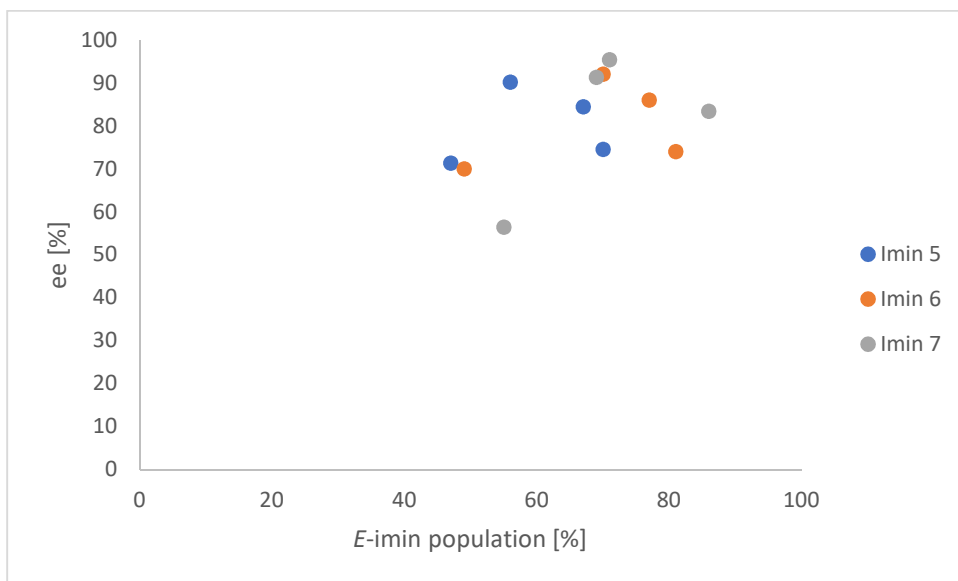


Figure S46.3: Plot of the ee values of the transfer hydrogenation of imines 5-7 catalyzed by TRIP, TRIFP, TiPSY, TRIM, 1-naph and 9-phen against the experimentally observed population of the E-imine in the binary complex. No correlation is observed.

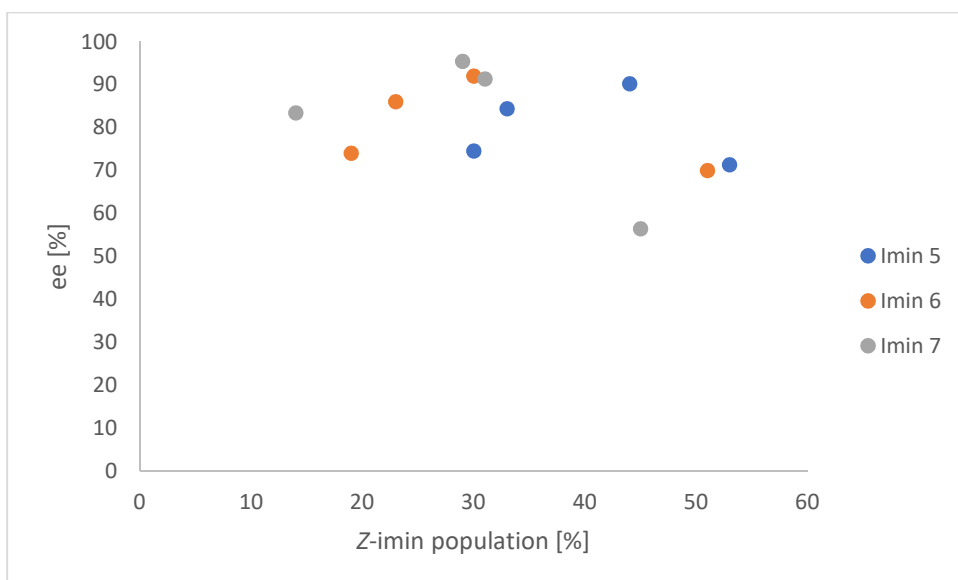


Figure S46.4: Plot of the ee values of the transfer hydrogenation of imines 5-7 catalyzed by TRIP, TRIFP, TiPSY, TRIM, 1-naph and 9-phen against the experimentally observed population of the Z-imine in the binary complex. No correlation is observed.

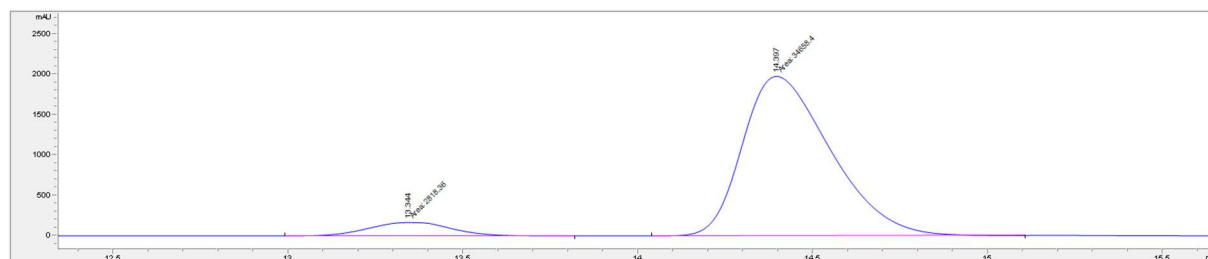
3. Brønsted Acid Catalysis – The Effect of 3,3'-Substituents on the Structural Space and the Stabilization of Imine/Phosphoric Acid Complexes

3.6.9. HPLC analysis

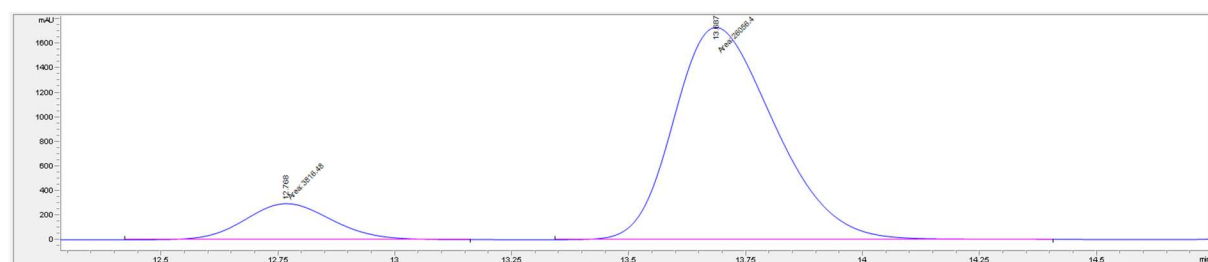
To determine the *ee* values of imines **5-7**, identical HPLC equipment and conditions have been used as previously employed by our group.^[16] For further details, especially preparation and separation of the racemic amines **9-11** see the supporting information of the cited literature. Enantiomeric excess values (*ee*) of products were determined by HPLC on chiral stationary phase employing an Agilent 1290 Infinity LC system equipped with a binary pump, autosampler and a photodiode array detector and using CHIRALCEL OD-H and CHIRALPAK IA and IC columns. Amine **9**: The *ee* was determined by CSP-HPLC, CHIRALCEL OD-H column, eluent *n*-hexane/*i*-propanol 98/2, flow 0.6 mL/min, retention times: $\tau_1=13.34$ min, $\tau_2=14.40$ min, column compartment temperature 20 °C, $\lambda=220$ nm. Amine **10**: The *ee* was determined by CSP-HPLC, CHIRAPACK IC column, eluent *n*-hexane/*i*-propanol 99/1, flow 0.9 mL/min, retention times: $\tau_1=8.22$ min, $\tau_2=8.59$ min, column compartment temperature 20 °C, $\lambda=220$ nm. Amine **11**: The *ee* was determined by CSP-HPLC, CHIRALPAK IA column, eluent *n*-hexane/*i*-propanol 98/2, flow 0.9 mL/min, retention times: $\tau_1=12.84$ min, $\tau_2=13.89$ min, column compartment temperature 20 °C, $\lambda=220$ nm

Amine **9**, catalyzed by

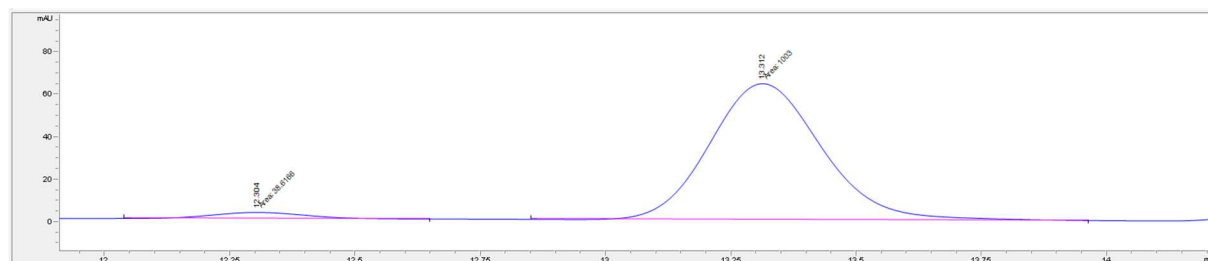
TRIP



TRIFP

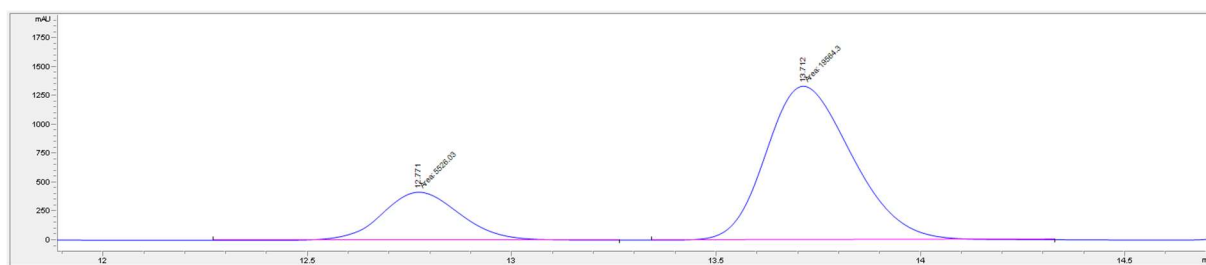


TIPSY

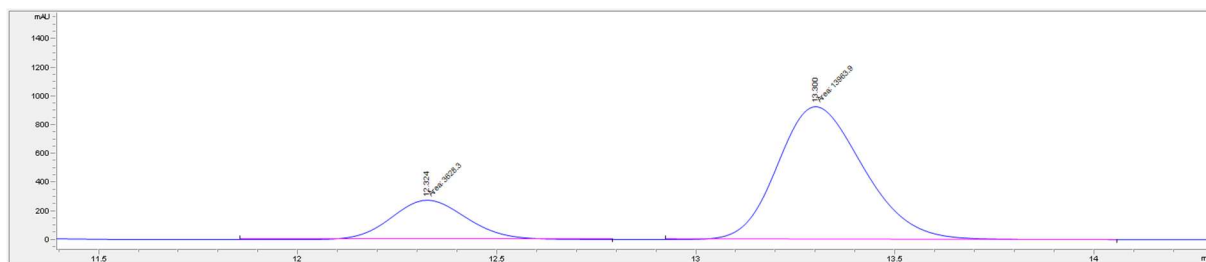


3. Brønsted Acid Catalysis – The Effect of 3,3'-Substituents on the Structural Space and the Stabilization of Imine/Phosphoric Acid Complexes

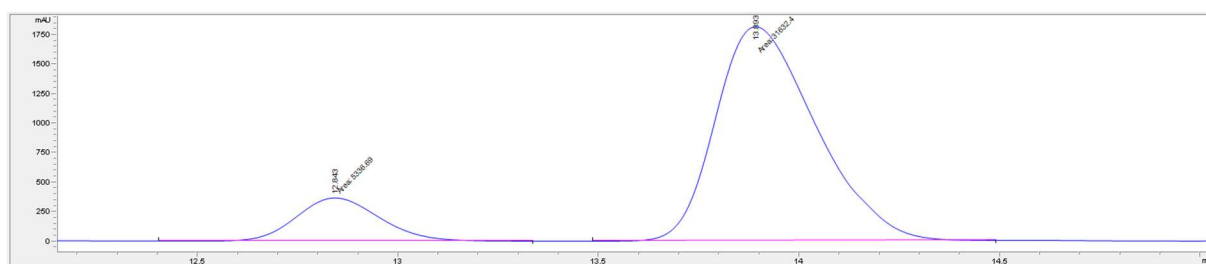
1-naph



9-phen

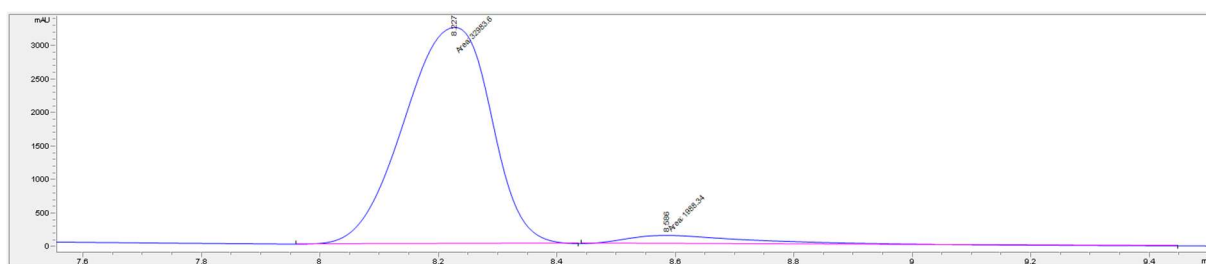


TRIM

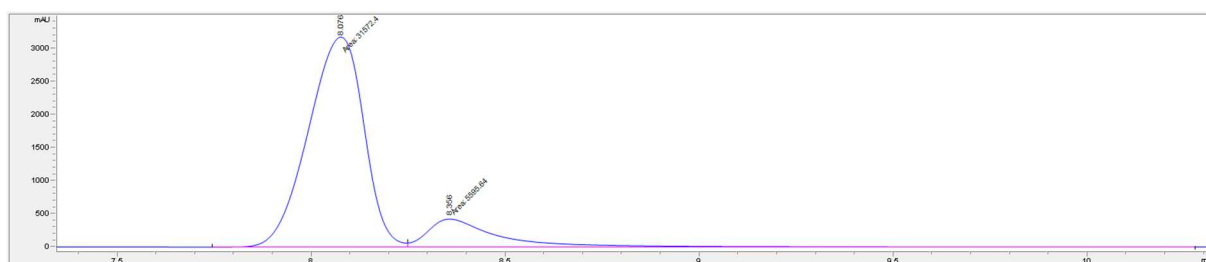


Amine **10**, catalyzed by

TRIP

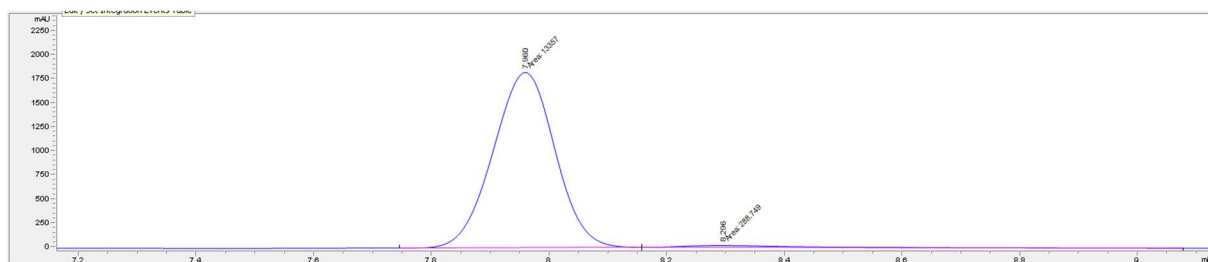


TRIFP

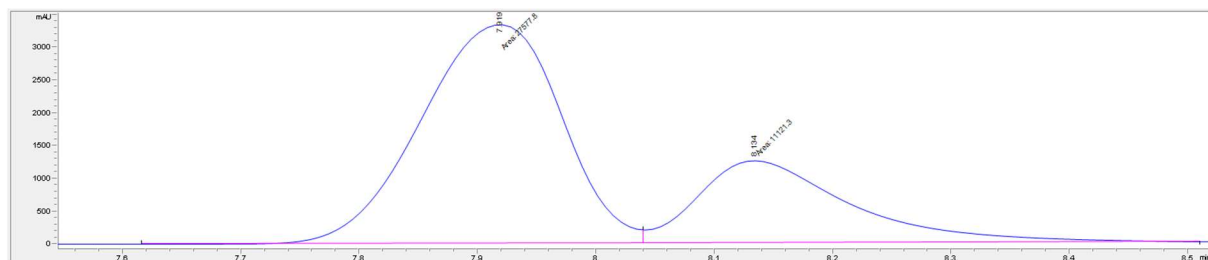


3. Brønsted Acid Catalysis – The Effect of 3,3'-Substituents on the Structural Space and the Stabilization of Imine/Phosphoric Acid Complexes

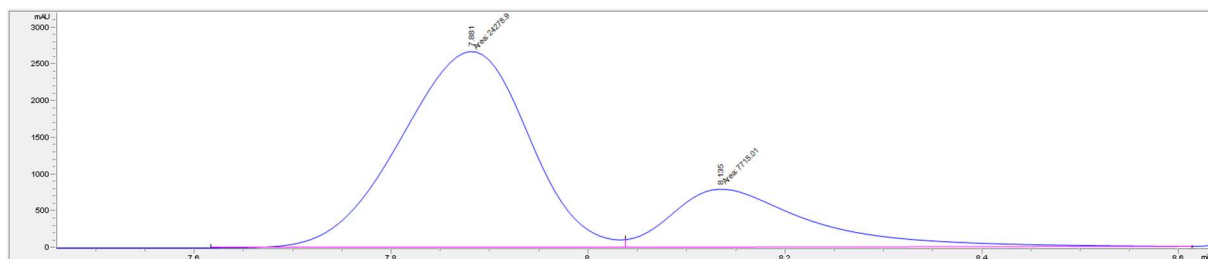
TIPSY



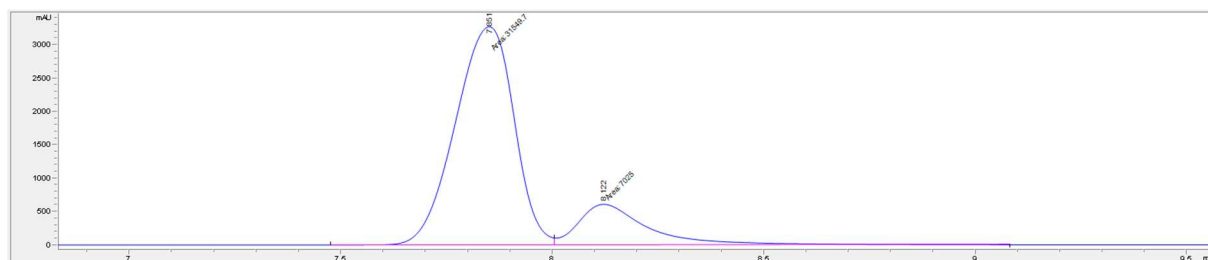
1-naph



9-phen

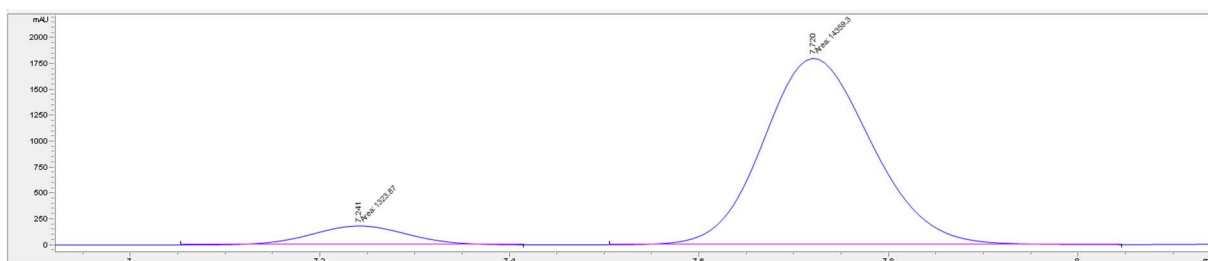


TRIM



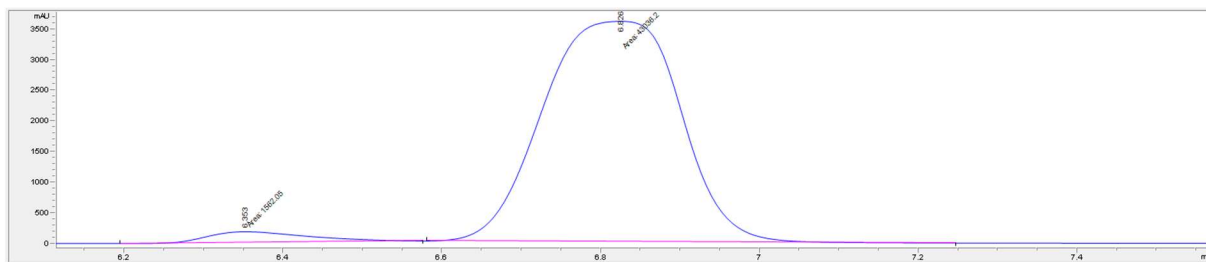
Amine **11**, catalyzed by

TRIP

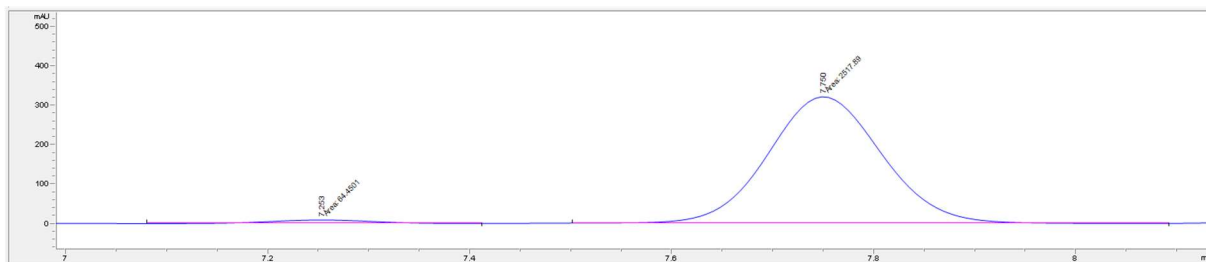


3. Brønsted Acid Catalysis – The Effect of 3,3'-Substituents on the Structural Space and the Stabilization of Imine/Phosphoric Acid Complexes

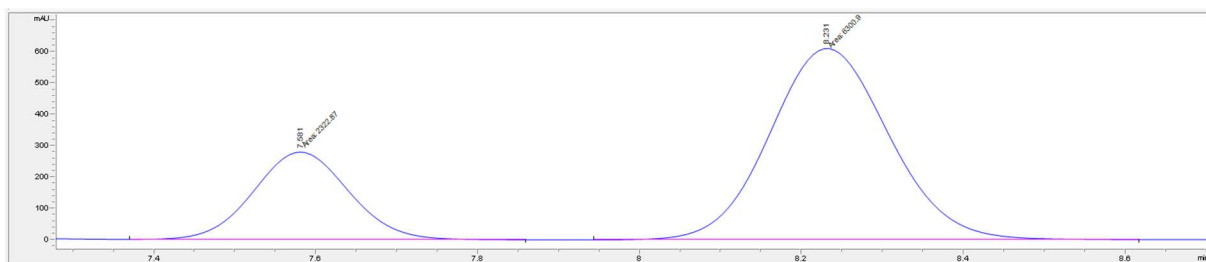
TRIFP



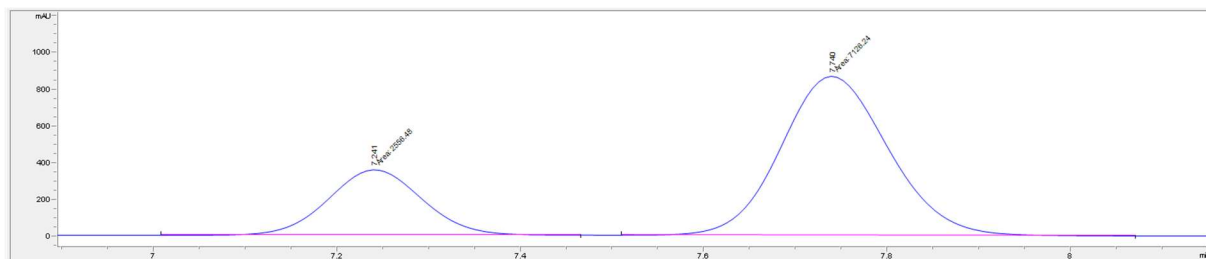
TIPSY



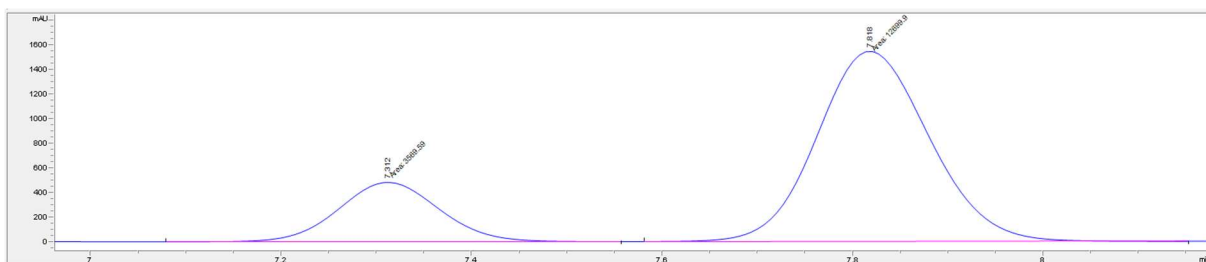
1-naph



9-phen



TRIM

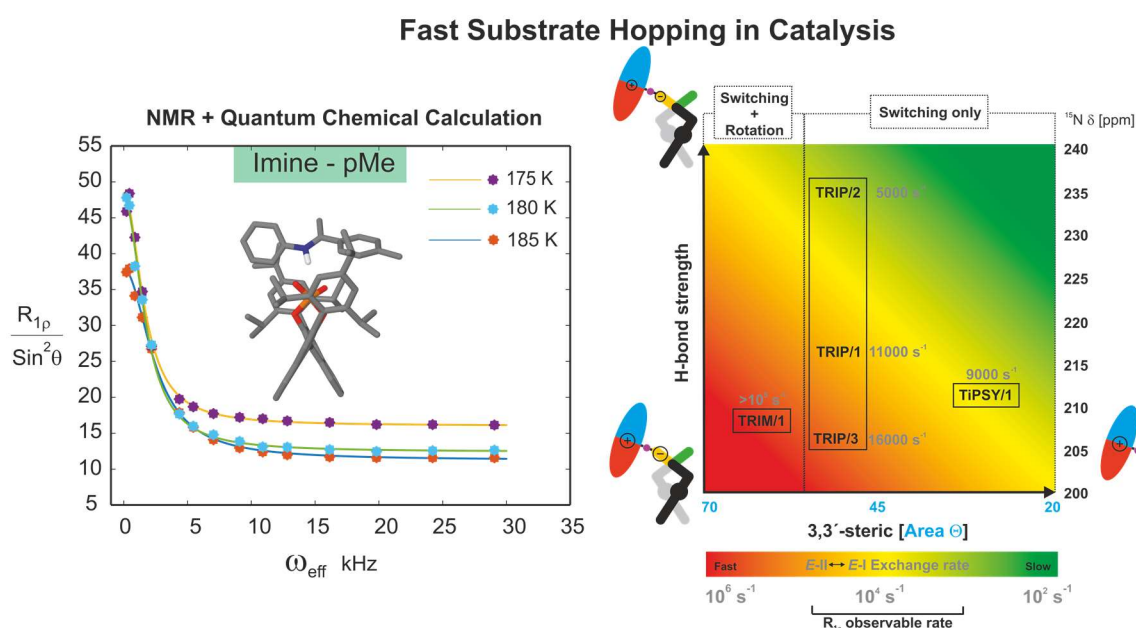


3. Brønsted Acid Catalysis – The Effect of 3,3'-Substituents on the Structural Space and the Stabilization of Imine/Phosphoric Acid Complexes

3.6.10. References

- [1] J. Siegel, F. Anet, *J. Org. Chem.* **1988**, *9*, 2629–2630.
- [2] I. G. Shenderovich, A. P. Burtsev, G. S. Denisov, N. S. Golubev, H.-H. Limbach, *Magn. Reson. Chem.* **2001**, *39*, S91–S99.
- [3] M. Klusmann, L. Ratjen, S. Hoffmann, V. Wakchaure, R. Goddard, B. List, *Synlett* **2010**, *2010*, 2189–2192.
- [4] N. Sorgenfrei, J. Hioe, J. Greindl, K. Rothermel, F. Morana, N. Lokesh, R. M. Gschwind, *J. Am. Chem. Soc.* **2016**, *138*, 16345–16354.
- [5] J. Greindl, J. Hioe, N. Sorgenfrei, F. D. Morana, R. M. Gschwind, *J. Am. Chem. Soc.* **2016**, *49*, 15965–15971.
- [6] F. Aznar, C. Valde, *J. Am. Chem. Soc.* **2009**, *131*, 4031–4041.
- [7] Y. Schramm, F. Barrios-Landeros, A. Pfaltz, *Chem. Sci.* **2013**, *4*, 2760–2766.
- [8] R. K. Harris, E. D. Becker, S. M. Cabral de Menezes, R. Goodfellow, P. Granger, *Magn. Reson. Chem.* **2002**, *40*, 489–505.
- [9] J. P. Reid, J. M. Goodman, *Chem. Eur. J.* **2017**, *23*, 14248–14260.
- [10] A. Jerschow, N. Müller, *J. Magn. Reson.* **1997**, *125*, 372–375.
- [11] E. O. Stejskal, J. E. Tanner, *J. Chem. Phys.* **1965**, *42*, 288–292.
- [12] A. MacChioni, G. Ciancaleoni, C. Zuccaccia, D. Zuccaccia, *Chem. Soc. Rev.* **2008**, *37*, 479–489.
- [13] E. J. Cabrita, S. Berger, *Magn. Reson. Chem.* **2002**, *40*, 122–127.
- [14] P. C. M. V. Z. C. T. W. Moonen, P. Van Gelderen, W. Geerten, Vuister, *J. Magn. Reson.* **1992**, *97*, 419–425.
- [15] J. P. Reid, J. M. Goodman, *J. Am. Chem. Soc.* **2016**, *138*, 7910–7917.
- [16] P. Renzi, J. Hioe, R. M. Gschwind, *J. Am. Chem. Soc.* **2017**, *139*, 6752–6760.
- [17] J. M. Tao, J. P. Perdew, V. N. Staroverov, G. E. Scuseria, *Phys. Rev. Lett.* **2003**, *91*, 146401.
- [18] S. Grimme, J. Antony, S. Ehrlich, H. Krieg, S. Grimme, J. Antony, S. Ehrlich, H. Krieg, *J. Chem. Phys.* **2010**, *132*, 154104.
- [19] S. Grimme, *J. Chem. Phys.* **2003**, *118*, 9095.
- [20] Gaussian 09, Revision D.01, M. J. Frisch, G. W. Trucks, H. B. Schlegel, G. E. Scuseria, M. A. Robb, J. R. Cheeseman, G. Scalmani, V. Barone, G. A. Petersson, H. Nakatsuji, X. Li, M. Caricato, A. Marenich, J. Bloino, B. G. Janesko, R. Gomperts, B. Mennucci, H. P. Hratchian, J. V. Ortiz, A. F. Izmaylov, J. L. Sonnenberg, D. WilliamsYoung, F. Ding, F. Lipparini, F. Egidi, J. Goings, B. Peng, A. Petrone, T. Henderson, D. Ranasinghe, V. G. Zakrzewski, J. Gao, N. Rega, G. Zheng, W. Liang, M. Hada, M. Ehara, K. Toyota, R. Fukuda, J. Hasegawa, M. Ishida, T. Nakajima, Y. Honda, O. Kitao, H. Nakai, T. Vreven, K. Throssell, J. A. Montgomery, Jr., J. E. Peralta, F. Ogliaro, M. Bearpark, J. J. Heyd, E. Brothers, K. N. Kudin, V. N. Staroverov, T. Keith, R. Kobayashi, J. Normand, K. Raghavachari, A. Rendell, J. C. Burant, S. S. Iyengar, J. Tomasi, M. Cossi, J. M. Millam, M. Klene, C. Adamo, R. Cammi, J. W. Ochterski, R. L. Martin, K. Morokuma, O. Farkas, J. B. Foresman, and D. J. Fox, Gaussian, Inc., Wallingford CT, 2016.
- [21] Neese, F.; "Software update: the ORCA program system, version 4.0" *WIREs Comput Mol Sci* **2018**, *8*:e1327. doi: 10.1002/wcms.1327

4. Relaxation Dispersion NMR to reveal fast Dynamics in Brønsted Acid Catalysis: Influence of Sterics and H-bond strength on conformations and substrate hopping



Nanjundappa Lokesh, Johnny Hioe, Johannes Gramüller and Ruth M. Gschwind

J. Am. Chem. Soc. **2019**, *141*, 41, 16398–16407. DOI: 10.1021/jacs.9b07841

A) Nanjundappa Lokesh performed, analyzed and interpreted the majority of NMR measurements, especially setting up and optimizing the $R_{1\rho}$ method. B) All theoretical calculations were performed by Johnny Hioe. C) Johannes Gramüller performed parts of the NMR measurements, especially all regarding TRIM/4, TiPSY/1, DOSY measurements and estimation of rotational correlation time, exchange with free imines as well as all measurements of the additional findings. D) Data interpretation and writing of the manuscript was done by all authors, with Nanjundappa Lokesh doing the major part. E) R. M. Gschwind contributed to conceptualization of the project, design of experiments, interpretation of data, writing and proof-reading of the manuscript and provided funding.

Source of this chapter: ACS Publications, <https://pubs.acs.org/doi/10.1021/jacs.9b07841>.

Reproduced with permission. Text and figures may differ from the published version. The complete corresponding Supporting Information is provided free of charge at <https://pubs.acs.org/doi/10.1021/jacs.9b07841>.

4.1. Abstract

NMR provides both structural and dynamic information, which are key to connect intermediates and to understand reaction pathways. However, fast exchanging catalytic intermediates are often inaccessible by conventional NMR due its limited time resolution. Here we show the combined application of ^1H off-resonance $R_{1\rho}$ NMR method and low temperature (185-175 K) to resolve intermediates exchanging on a μs time scale (ns at room temperature). The potential of the approach is demonstrated on chiral phosphoric acid (CPA) catalysts in their complexes with imines. The otherwise inaccessible exchange kinetics of the $E\text{-I}\rightleftharpoons E\text{-II}$ imine conformations and thermodynamic $E\text{-I}:E\text{-II}$ imine ratios inside the catalyst pocket are experimentally determined and corroborated by calculations. The $E\text{-I}\rightleftharpoons E\text{-II}$ exchange rate constants ($k_{\text{ex}}^{185\text{K}}$) for different catalyst-substrate binary complexes varied between 2500-19000 s^{-1} ($\tau_{\text{ex}} = 500\text{-}50 \mu\text{s}$). Theoretical analysis of these exchange rate constants revealed the involvement of an intermediary tilted conformation $E\text{-III}$, which structurally resembles the hydride transfer transition state. The main $E\text{-I}$ and $E\text{-II}$ exchange pathway is a hydrogen bond strength dependent tilting-switching-tilting mechanism via a bifurcated hydrogen bond as transition state. The reduction in the sterics of the catalyst showed an accelerated switching process by at least an order of magnitude and enabled an additional rotational pathway. Hence, the exchange process is mainly a function of the intrinsic properties of the 3,3'-substituents of the catalyst. Overall, we believe that the present study opens a new dimension in catalysis via experimental access to structures, populations and kinetics of catalyst-substrate complexes on the μs time scale by ^1H off-resonance $R_{1\rho}$ method.

4.2. Introduction

In the past decade, ion pair catalysis has witnessed an enormous growth in synthetic applications.¹ Especially, Brønsted acid catalysis is a well explored class for various enantioselective syntheses.²⁻⁷ However, experiment based structural and mechanistic studies are very rare and often the mechanistic insights are obtained by theoretical calculations.⁸⁻¹¹ As a result, the absence of experimental constraints may lead to an underdetermination of the assumed theoretical models. Therefore, experimental detection and characterization of key intermediates and their interactions are pivotal in the elucidation of the plausible pathways of a catalytic reaction and to validate the theoretical models. Often, structural insights of intermediates and their spatial arrangement are obtained from X-ray crystal structures, which provides highly valuable structural information at atomic level. However, these crystal structures reveal often only a single point of the whole conformational space and thus can conceal the existing dynamics of substrate catalyst complexes (e.g. in the case of chiral phosphoric acids in their binary complexes with imines only one⁵ out of four¹² main conformations was found with X-ray). In addition, solid state effects may induce thermodynamic preferences differing from those in solution (e.g. dimers versus monomers in ion pair catalysts¹³) and thus complicate the interpretation. In addition, the obtained intermediate structures are generally disconnected points on the reaction profile, which have to be interpolated to connect the points and later extrapolated to interpret the reaction outcome.

In solution the formed substrate-catalyst complexes exist as Boltzmann distributed conformers. These intermediates differ in their interaction patterns, e.g. hydrogen bonds, Coulombic interactions, covalent and non-covalent interactions,^{12,14,15} which are vital and might be deterministic for the reaction outcome.¹⁶⁻¹⁹ In this regard, solution NMR spectroscopy provides both structural and dynamic information about multiple Boltzmann distributed intermediate states of a catalytic reaction. Especially the dynamic information allows connections between the intermediates on the reaction profile and thus reveal rich insights into the reaction mechanism.²⁰ Indeed, NMR e.g. has been successfully applied to detect intermediates and elucidate reaction mechanisms in photo-,²¹ organo-^{18,22} and transition metal catalysis,²³⁻²⁸ to study weak intermolecular interactions,^{29,30} to reveal aggregations of organic,^{15,31} inorganic and organometallic molecules^{32,33} and to extract kinetic isotope effects.^{34,35} Despite this great success, the inherent low sensitivity and low time resolution of NMR makes the detection of exchanging and low populated intermediates challenging. In terms of detection of transient low populated key intermediates in the slow exchange regime (~ms time scale), we successfully demonstrated the application of chemical exchange saturation transfer (CEST)³⁶ in organocatalysis,³⁷ photocatalysis,³⁸ and Silicide Zintl ions chemistry.³⁹ However, for investigating fast exchanging intermediates, not only the sensitivity but also the time resolution has to be extended. In this context, NMR relaxation dispersion

4. Relaxation Dispersion NMR to reveal fast Dynamics in Brønsted Acid Catalysis: Influence of Sterics and H-bond strength on conformations and substrate hopping

experiments can play a significant role to quantify the populations and dynamics in the fast exchange regime (ms- μ s time scale).⁴⁰⁻⁴² This approach works based on a systematic deciphering of chemical exchange contribution to the relaxation via systematic incrementation of the RF field (B_1), which reveals chemical exchange rates, populations and chemical shift information. In the past decades, the relaxation dispersion NMR experiments CPMG and $R_{1\rho}$ methods were successfully applied to study fast dynamics and structures of low populated⁴³ biomolecular conformations (proteins and RNA), which are key to enzymatic functions.^{40,41} Both CPMG and $R_{1\rho}$ reveal the same information.⁴⁴ However, to access faster dynamics the CPMG method is restricted by the number of repeatable π -pulses in a given time period and further requires experimental data at multiple magnetic fields.^{40,45} In contrast, the $R_{1\rho}$ methods apply a continuous RF pulse (spin-lock) and its field (B_1) is systematically varied to access dynamics and hence it is not limited by number of repeatable pulses and suitable for measurement of faster dynamics in terms of NMR.⁴² The 2D analogous CPMG and $R_{1\rho}$ relaxation dispersion experiments with ^{15}N and ^{13}C nuclei as probes were preferred in Biomolecular NMR due to their well resolved chemical shifts in the spectra and the reduced dipolar and scalar interactions.^{40-42,44} However, this approach can only disclose dynamics down to ≈ 40 μ s time scale.⁴⁶ Additionally, selective labelling of catalyst and substrates in organic reactions is challenging. On the other hand, protons are more sensitive both towards the magnetic field and towards changes in the chemical environment. Thus, it reveals better structural information and relatively faster exchange processes.^{45,47} Furthermore, due to the natural abundance of protons in organic molecules, protons are the preferred choice for studying catalytic reactions. However, protons as relaxation dispersion probes suffer from extensive scalar and dipolar interactions, which complicate the analysis and hence limit the applications of proton based $R_{1\rho}$ methods. The recent advancement in selective labelling techniques and NMR pulse sequences have partially addressed these problems. One significant advancement was the development of an off-resonance $R_{1\rho}$ method, in which the spin lock field (B_1) and its offset were simultaneously varied to modulate the effective field, while still maintaining the constant angle (35.30°) of the spin locked magnetization.^{48,49} This enables higher effective fields than the on-resonance $R_{1\rho}$ method and also improves the accuracy by reducing the coherent evolution due to scalar couplings and minimizing the cross-relaxation contributions to the measured rates. Currently, with the recently reported high-power spin locking field facilitated by cryogenically cooled probes, it is possible to push the off-resonance $R_{1\rho}$ method to access < 40 μ s time scale dynamics as well.^{46,47} These improvements have also enabled the application of relaxation dispersion NMR methods in recent ligand binding studies.^{45,47} Despite these recent developments and extended applications of relaxation dispersion NMR experiments, so far to the best of our knowledge the relaxation dispersion NMR methods were not applied in mechanistic or structural studies in chemical catalysis.

4. Relaxation Dispersion NMR to reveal fast Dynamics in Brønsted Acid Catalysis: Influence of Sterics and H-bond strength on conformations and substrate hopping

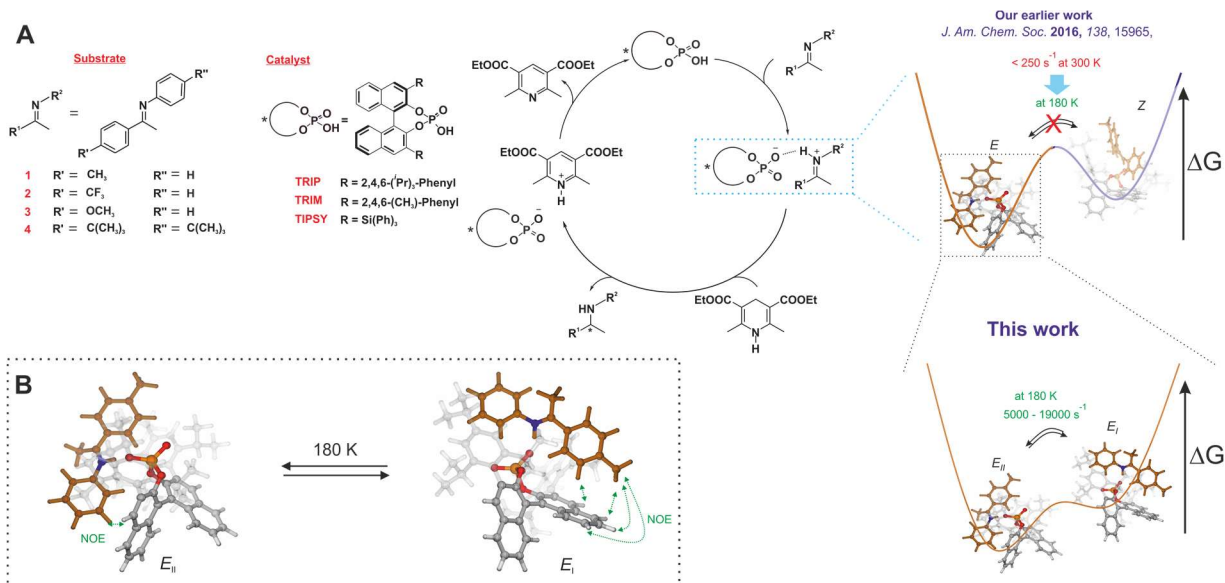


Figure 1. A) Investigated systems and catalytic cycle of the transfer hydrogenation of ketimines with chiral phosphoric acids: Our earlier work showed the existence of *E*- and *Z*-imine/catalyst binary complex and two fast exchanging conformations for each configuration based on NOE analysis.^{12,15} In the present work, we resolved the fast exchanging *E*-conformations and quantified the rate by $R_{1\rho}$ experiments and corroborated by calculations for the given catalyst/substrate combinations. **B)** Structures of the two *E*-conformations of TRIP/imine complexes (Type I and Type II), which are in fast exchange even at 180 K.

Recently in the field of chiral phosphoric acid (CPA) catalysis, we achieved significant progress in structural investigations¹² and H-bond characterization¹⁴ of catalyst-imine binary complexes by application of NMR spectroscopy and computational chemistry. For the first time, we showed the coexistence of *E*- and *Z*-imine binary complexes by NMR (Figure 1A). In-depth NOE analysis and computational results revealed four major core structures, two correspond to the *E*-imine (*E*-I and *E*-II, Figure 1B) and the other two correspond to the *Z*-imine (*Z*-I and *Z*-II). These four core structures (*E*-I/II and *Z*-I/II) possess zwitterionic character and are anchored by a strong hydrogen bond with a highly covalent character. Surprisingly, despite the strong hydrogen bond, we observed a fast exchange (on the NMR time scale) between the substructures (*E*-I \rightleftharpoons *E*-II; *Z*-I \rightleftharpoons *Z*-II) even at very low temperature (130 K). Additionally, for binary complexes of various CPAs and imines, we established an internal acidity scale,⁵⁰ and confirmed the *E*-I/II and *Z*-I/II complexes as four core structures in all of these systems.⁵¹ As demonstrated later in this work, the internal acidity (H-bond strength) and the steric properties of the CPA and/or imine play a significant role in the exchange of *E*-I and *E*-II.

Despite this enormous progress, due to the fast exchange between *E*-I \rightleftharpoons *E*-II and *Z*-I \rightleftharpoons *Z*-II conformers (Figure 1), the quantification of their population and dynamics in the catalyst pocket have remained inaccessible so far and could only be accessed by theoretical calculations. However, the theoretical calculations can have a significant offset to the experimental values, i.e. *E*/*Z*-ratio in the CPA/imine complexes.¹⁵ Thus, the validation of theoretical methods applied is highly desirable if possible. The experimental and theoretical determination of the kinetic and thermodynamic properties of these

4. Relaxation Dispersion NMR to reveal fast Dynamics in Brønsted Acid Catalysis: Influence of Sterics and H-bond strength on conformations and substrate hopping

conformers can reveal delicate information such as non-covalent interactions (H-bond, dispersion, electrostatic), active pathways or possible structures of the transition states. This in turn provides in-depth understanding of the behavior of the catalyst-substrate complex at molecular level, i.e. flexibility of the system,⁵² and serves as a basis for further rational development. Additionally, it enables validation and refinement of theoretical models.

Despite our best efforts, i.e. NMR measurements down to 130 K in freonic solvent mixtures, so far it has not been possible to access experimentally the populations and exchange rates of *E-I/E-II* or *Z-I/Z-II*. One approach to solve this problem is further reduction of the temperature to slow down the exchange rate. However, the practicability is limited due to the freezing of the solvent. Moreover, it is also difficult to achieve very low temperatures in standard NMR spectrometers.

To access fast dynamics on a molecular level in chemical catalysis, in this work for the first time the combination of low temperature (185-175 K) and ¹H off-resonance R_{1ρ} was successfully applied to a real catalytic system. Furthermore, fast conformational exchanges (on the NMR time scale and in absence of the reductant) in CPA/*E*-imine complexes were experimentally resolved. The rate constants or free energy barriers for the exchange processes were quantified and corroborated by theoretical calculations. Furthermore, by merging NMR-spectroscopic and theoretical results we identified the exact exchange mechanism between *E-I* and *E-II*. We could elucidate the influence of the hydrogen bond strength and 3,3'-substituents on the exchange rates and the operative exchange pathways. This was the first time to the best of our knowledge that microsecond dynamics ($\tau_{\text{ex}} = 500\text{-}50 \mu\text{s}$) in a catalytic complex were observed in such depths that even a fast hydrogen bond switching/substrate hopping in catalysis was quantified by NMR spectroscopy.

4.3. Results and Discussion

4.3.1. System selection

For establishing the method, initially we selected the binary TRIP/**1**-imine complex due to our detailed knowledge about structures and behavior at low temperature condition. The presence of the binary complex is proven by the large trans hydrogen bond scalar coupling (2-3 Hz) traversing between ³¹P and ¹⁵N nuclei.¹⁴ In 1:1 CPA/imine mixtures, the binary complex is formed in a sufficient amount (typically >70% in 1:1 mixtures) which is adequate for the current investigation.⁵⁰ At 180 K, based on our previous solvent screening, we found that dichloromethane (CD₂Cl₂) provides best chemical shift dispersion and narrow linewidths. The low temperature condition is crucial to freeze the exchange be-

4. Relaxation Dispersion NMR to reveal fast Dynamics in Brønsted Acid Catalysis: Influence of Sterics and H-bond strength on conformations and substrate hopping

tween *E*- and *Z*-complex, which allows individual analysis of the two configurational complexes by simplifying the exchange matrix. From our previous structural investigation, the presence of *E*-I and *E*-II as well as *Z*-I and *Z*-II are predicted by DFT-calculations and experimentally proven by NOE contacts and hydrogen bond analysis.^{12,14} In the *E*-I conformation, NOE contacts between the ketone moiety of the imine and the BINOL backbone of the catalyst were observed, while the *E*-II conformation was confirmed by NOE contacts between the aniline moiety and the BINOL backbone (Figure 1B). For TRIP/*E*-imine complexes, we observed different signal sets for the two naphthyl fragments of the BINOL backbone in the proton spectrum. In contrast, only one set of signals for the backbone of the *Z*-imine was assigned, which indicates a different fast exchange process between Type I and Type II, leading to backbone averaging.

4.3.2. Possible exchange pathways

In principal, the fast exchange between Type I and II can be realized by three different pathways (Figure 2). In all pathways, first the imine tilts to an intermediate position denoted as Type III.1/2 (see SI for structure). These structures adopt a similar hydrogen bond geometry as in the ground state *E*-I/II. However, the *E*-imine in Type III.1/2 is found in the middle of the catalyst's binding pocket, similar to its position in the hydride transfer step or in dimers of the binary complex.¹⁵ Thus, the interaction between the imine and BINOL-backbone is lost in the intermediate *E*-III.1/2. Subsequently after the tilting, the imine either switches the hydrogen bond donor atom (pathway **A**) or rotates inside the binding pocket without switching the H-bond (pathway **B**). Afterwards, additional tilting leads to the Type I structures. For both pathways (**A** and **B**), the two different naphthyl-fragments B1 and B2 of the BINOL backbone experience a different chemical environment and thus show different signals in the proton spectra. According to our previous NOE and chemical shifts analysis, the exchange between *E*-I and *E*-II via rotation only (pathway **B**: $n = 0$) is excluded in TRIP, TRIM and TiPSY binary complexes.^{12,15}

The pathway **C** is an intervention of pathway **A** by the rotation or pathway **B** by the switching of the imine. This process can lead to the same conformation (Figure 2 pathway **C**: $n = \text{odd}$; Type *E*-II \rightarrow *E*-II) or to different conformation (Figure 2 pathway **C**: $n = \text{even}$; Type *E*-II \rightarrow *E*-I). In the first scenario with n is an odd number, the aniline part of the imine (red colored half ellipsoid) at the beginning of this process is placed above the naphthyl-moiety B1 (black naphthyl-fragment), and at the end the aniline part is located above B2 (grey naphthyl-fragment). As both structures are C_2 related, the two naphthyl-fragments B1 and B2 experience the identical chemical environment. In a similar way, for the second scenario ($n = \text{even}$), exchange between Type I and Type II occurs. Both scenarios can occur with equal probability. Thus, for the system in equilibrium, pathway **C** will lead to an exchange between Type I

4. Relaxation Dispersion NMR to reveal fast Dynamics in Brønsted Acid Catalysis: Influence of Sterics and H-bond strength on conformations and substrate hopping

and II as well as to one averaged set of backbone signals with the combined information of Type I and Type II.

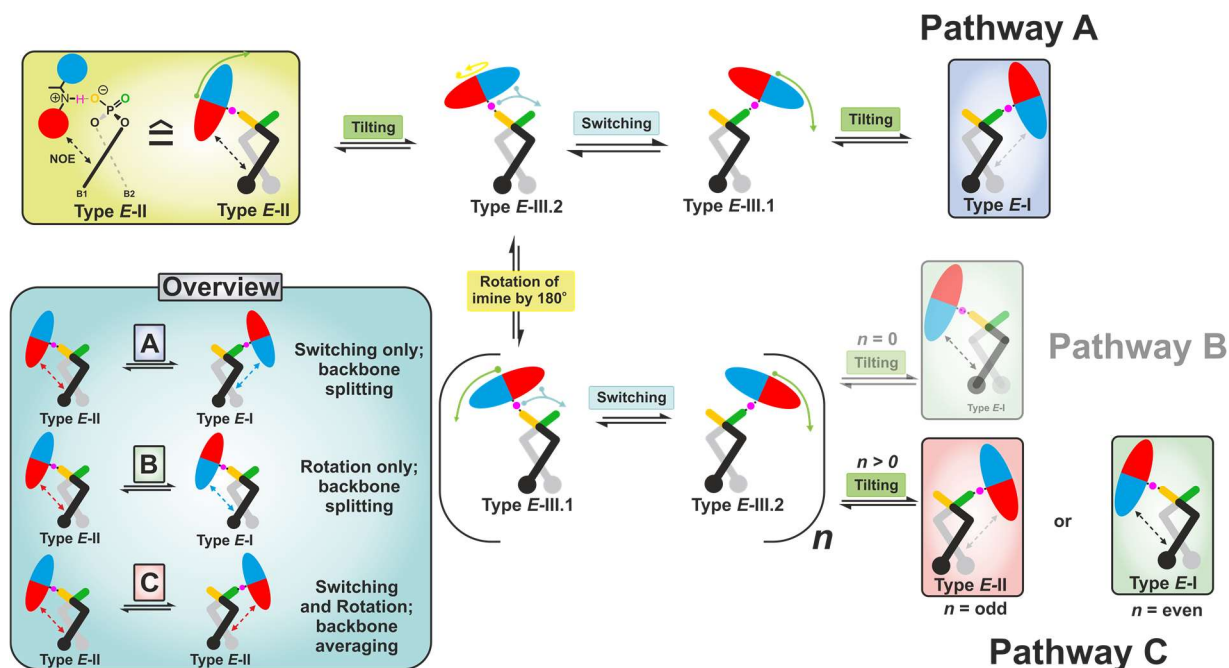


Figure 2. Possible fast exchange pathways between E-I and E-II. In pathway A, the interconversion between E-II and E-I occurs inside the complex by tilting, switching and tilting via the intermediate E-III.2/E-III.1. In contrast, in pathway B ($n = 0$; H-bond switching off), the exchange occurs via rotation only. In pathway C ($n > 0$; H-bond switching on), rotation and switching are coupled yielding either the same conformation ($n = \text{odd}$) or different conformation ($n = \text{even}$). n is the number of occurring switching events prior to tilting.

In our previous work,¹² pathway A was assumed to be operative for binary TRIP/E-imine complexes based on steric considerations, i.e. the E-imine cannot rotate inside the binding pocket, and in accordance with that backbone splitting was observed.⁵³ However, so far these dynamic exchange pathways were only deduced from NOE contacts and backbone splitting.

To analyze and quantify these fast exchange processes, we applied the recently reported 1D ¹H off-resonance R_{1ρ} method.⁴⁷ The application of the method mainly involves two parts, selection of proton sites and optimization of the method. The complete details of the method optimization are given in SI. The selection of proton sites is discussed below.

4.3.3. Probe selection (proton site selection)

In order to maximize the accuracy of the method, the selected proton or protons must satisfy the following conditions: it should (i) exhibit a significant change in chemical environment (chemical shift) during the E-I ⇌ E-II exchange, (ii) be free from ¹H-¹H scalar couplings (iii) and the selected proton peak should be free from signal overlap. Based on these criteria, we selected two probes for the TRIP/1 complex, i.e. the protons of the para methyl group of the imine (Figure 3, green shaded, imine-pMe)

4. Relaxation Dispersion NMR to reveal fast Dynamics in Brønsted Acid Catalysis: Influence of Sterics and H-bond strength on conformations and substrate hopping

and the H₁ proton (Figure 3, red shaded) from the catalyst backbone. Both undergo significant chemical shift changes during the $E-I \rightleftharpoons E-II$ process and are free from significant ^1H - ^1H scalar couplings. The respective singlet peaks from these two probes of TRIP/**1** are depicted in 1D ^1H spectrum (Figure 3). If both probes are sensing the same chemical exchange process, then both should show similar exchange rates.

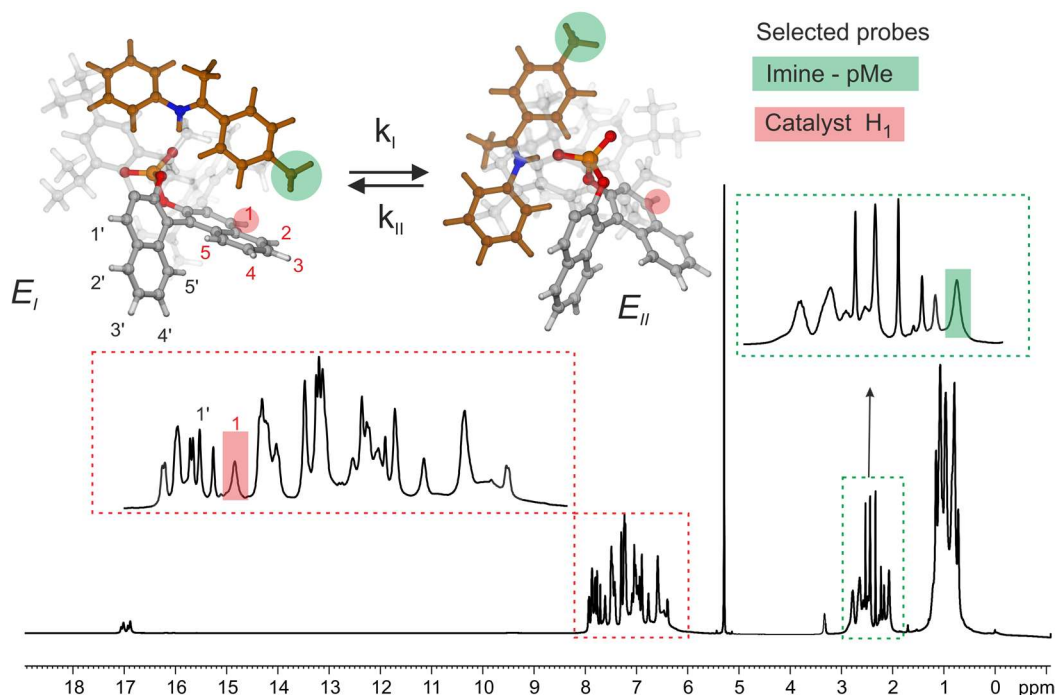


Figure 3. Selection criteria of probes (proton sites) for $R_{1\rho}$: 1) significant change in the chemical environment; 2) free from significant scalar coupling; 3) free from signal overlap. The selected protons and the corresponding peaks in the 1D ^1H spectrum at 600 MHz and 180 K in CD_2Cl_2 are marked in red (catalyst site) and green (imine site).

4.3.4. $R_{1\rho}$ measurements

Initially, the $R_{1\rho}$ relaxation was measured for both the proton sites at 180 K by using optimized constant spinlock duration and varying the effective field (B_{eff} , see SI). The experimental results for both protons showed an offset-Lorentzian decay of $R_{1\rho}$ (obtained as $R_{1\rho}/\sin^2\theta$, θ is 35°) with increasing effective field (Figure 4), which indicates that the proton sites experience a fast chemical exchange process. The exchange rate (k_{ex}) of this fast chemical exchange process was extracted by curve fitting (for fit equation see SI Eq. 1).⁵⁴ Similar k_{ex} for both probes were observed (at 180 K, for imine-*p*Me $k_{\text{ex}} \approx 12000 \text{ s}^{-1}$ and for H₁ of catalyst $k_{\text{ex}} \approx 11000 \text{ s}^{-1}$), which reveals that both the proton sites are experiencing the same fast $E-I \rightleftharpoons E-II$ process.

After this initial establishment of the protocol, we extended the measurement of $R_{1\rho}$ for both probes at two other temperatures (185 K and 175 K, Figure 4) to extract the population ratio $E-II:E-I$, which

4. Relaxation Dispersion NMR to reveal fast Dynamics in Brønsted Acid Catalysis: Influence of Sterics and H-bond strength on conformations and substrate hopping

facilitates the determination of the free energy barrier ΔG^\ddagger . At all three temperatures we observed comparable exchange rates for both probes, which again confirms that both experience the same process. Further analysis (see SI) revealed a population ratio of E -II: E -I of 75:25 on average and an activation barrier for E -I \rightarrow E -II of 30 kJ/mol at 180 K (Figure 4). The theoretically predicted ratio at 180 K between E -II and E -I of 61:39 corroborates further the experimental results. This good agreement is at the first glance surprising, since the offset of the predicted E : Z ratio to the experiment was shown in the previous work to be significantly large (calc. E : Z = 99.9 : 0.1 vs. exp. E : Z = 80:20).¹⁵ This can be explained by the similarity in their interactions and geometries between the Type E I and Type E II. The better agreement between theory and experiment validates the theoretical model at least within E -conformations. Furthermore, due to this agreement between theory and experiment a reliable analysis of the exchange process in terms of interactions (H-bonds and steric) is possible by theory.

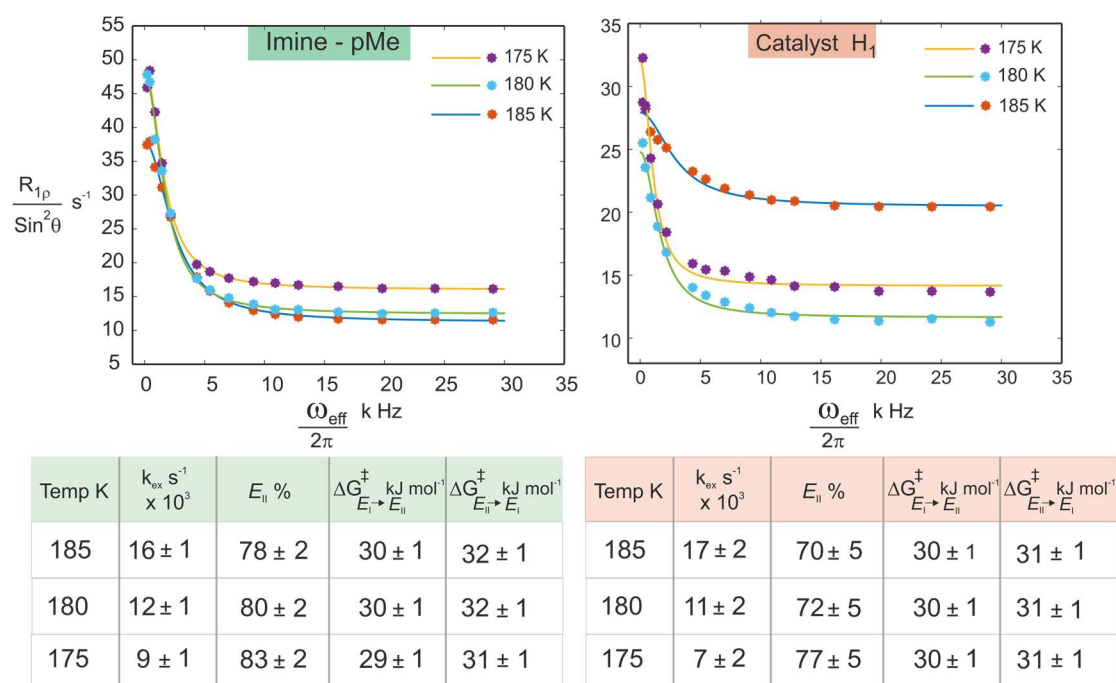


Figure 4. The offset-Lorentzian decay curves from the $R_{1\rho}$ measurements for both probes (p Me-proton from imine and H_1 from the catalyst) indicate the presence of a fast E -I \rightleftharpoons E -II process. The k_{ex} values of both probes (extracted by curve fitting) show similar values, which confirms that both probes experience the same exchange process. $R_{1\rho}$ measurements at three different temperatures (175 K to 185 K) allows the extraction of population and the individual exchange rates of both directions.⁵⁵

In conclusion, we successfully applied the $R_{1\rho}$ method to measure exchange rates on the μ s time scale in a real catalytic system, which is the prerequisite to systematically address the influence of steric and H-bond strength on the exchange process.

4.3.5. TRIP/1-3E imine complexes: H-bond dependent exchange pathway A

Next, we attempted to assign the measured exchange rate in TRIP/1E to the possible pathways. In our systems, exchange proceeding via dissociation-reassociation is slow on the NMR time scale ($< 50 \text{ s}^{-1}$, see SI for details) and does not match with the measured experimental rates ($10^3\text{-}10^4 \text{ s}^{-1}$). Hence, dissociation can be excluded. The steric bulk of the 3,3'- and imine-substituents hinder the rotation inside the binding pocket, which excludes pathway B (see Figure 2 for exchange pathways). This is validated further in the presented work by the semiempirical molecular dynamic (xtb-MD⁵⁶) showing that rotation does not occur in TRIP/1E even at highly elevated temperatures (300 K - 370 K; see SI).⁵⁷ In pathway A (tilting, switching, tilting), the imine relocates from E-I/II towards E-III.1/2 and subsequently the hydrogen bond switches from one oxygen atom to the other (Figure 2). For the tilting step, theoretical calculations predicted complex multi-events involving torsions of the aromatic moieties of the imine and simultaneous translation towards E-III.1/2. Due to the complexity of the tilting process and the number of involved transition states between E-I/II and E-III.1/2, no barrier could be estimated. Structural analysis showed that the hydrogen bond in the tilting step and the resulting intermediates E-III.1/2 is only slightly modulated. Hence, we can assume in a first approximation that the barrier for the tilting is affected by the interaction loss between the BINOL backbone and imine as well as the slight weakening of the hydrogen bond. For the switching step, the corresponding transition state revealed a bifurcated hydrogen bond type and an elongation of the hydrogen bond as well as a drastic change in the POH angle compared to E-I/II and E-III.1/2 (see Figure 5B). Therefore, a significant weakening of the hydrogen bond in the transition state is anticipated.⁵⁸ Together with the interaction loss with the BINOL backbone, a large enthalpic penalty is expected for this switching step. Thus, compared to the tilting step, the H-bond switching is postulated to be rate determining and be largely dependent on the hydrogen bond strength. Indeed, the calculated free energy barrier relative to E-II for the switching ($\Delta G_{\text{calc}}^{\ddagger}(\text{II} \rightarrow \text{I})$) equals +31.4 kJ/mol, which adequately fits to the experimental value ($\Delta G_{\text{exp}}^{\ddagger}(\text{II} \rightarrow \text{I}) = +31.3 \text{ kJ/mol}$) and suggests that the $R_{1\rho}$ determined k_{ex} corresponds to the rate determining switching process.

To further confirm this experimentally, we selected a series of imines with similar steric bulk but varying basicity to modulate the hydrogen bond strength (Figure 5). The highest exchange rate is determined for the TRIP complex with imine **3**, followed by **1** and **2**. Next the order of hydrogen bond strengths was established according to our previous investigations^{14,50} and according to this the least basic imine **2** possesses the strongest hydrogen bond and the most basic imine **3** the weakest, while **1** is in between.¹⁴ This shows an inverse correlation between the hydrogen bond strength and the exchange rate or a direct correlation to the free energy barrier. The increased barrier due to the stronger H-bond was also computed for imines **1** and **2** (for the process $\text{II} \rightarrow \text{I}$: $\Delta\Delta G_{\text{exp}}^{\ddagger}(\mathbf{2-1}) = +1.4$

4. Relaxation Dispersion NMR to reveal fast Dynamics in Brønsted Acid Catalysis: Influence of Sterics and H-bond strength on conformations and substrate hopping

kJ/mol; $\Delta\Delta G_{\text{calc}}^{\ddagger}(\mathbf{2-1}) = +3.1$ kJ/mol), which corroborates the experimental results. Thus, within the investigated TRIP/imine complexes, i.e. similar steric environment, the exchange between *E*-I and *E*-II is strongly dependent on the H-bond strength. This is congruent with our previous assumption that hydrogen bond switching (pathway **A**) is the operative exchange pathway. In summary, both experimental and theoretical results clearly proved that the H-bond switching step is the measured process and rate determining in pathway **A**.

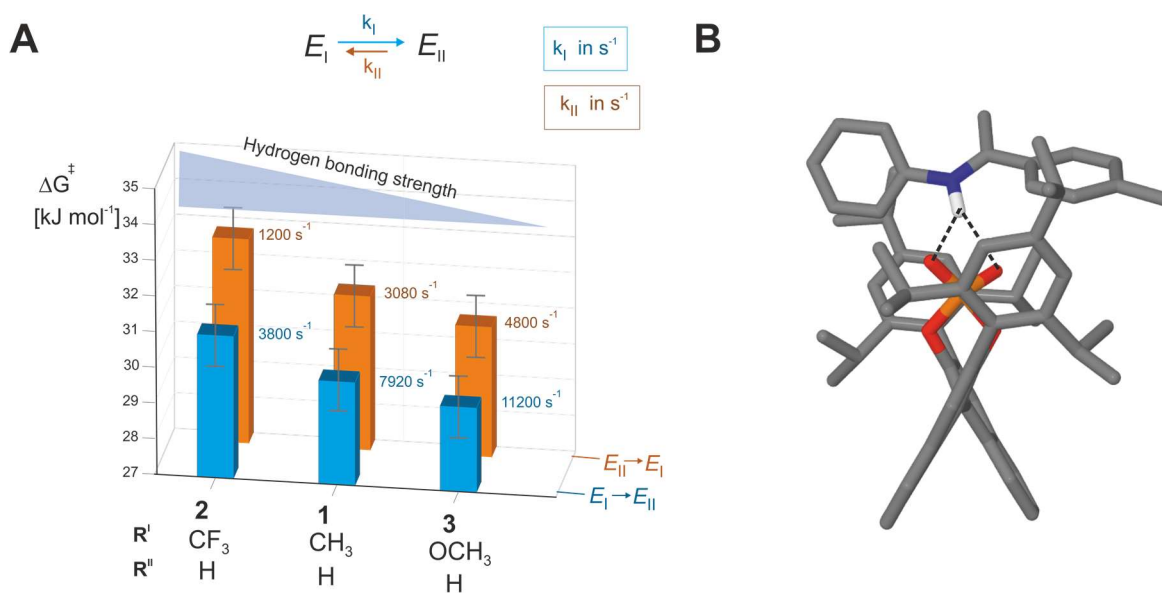
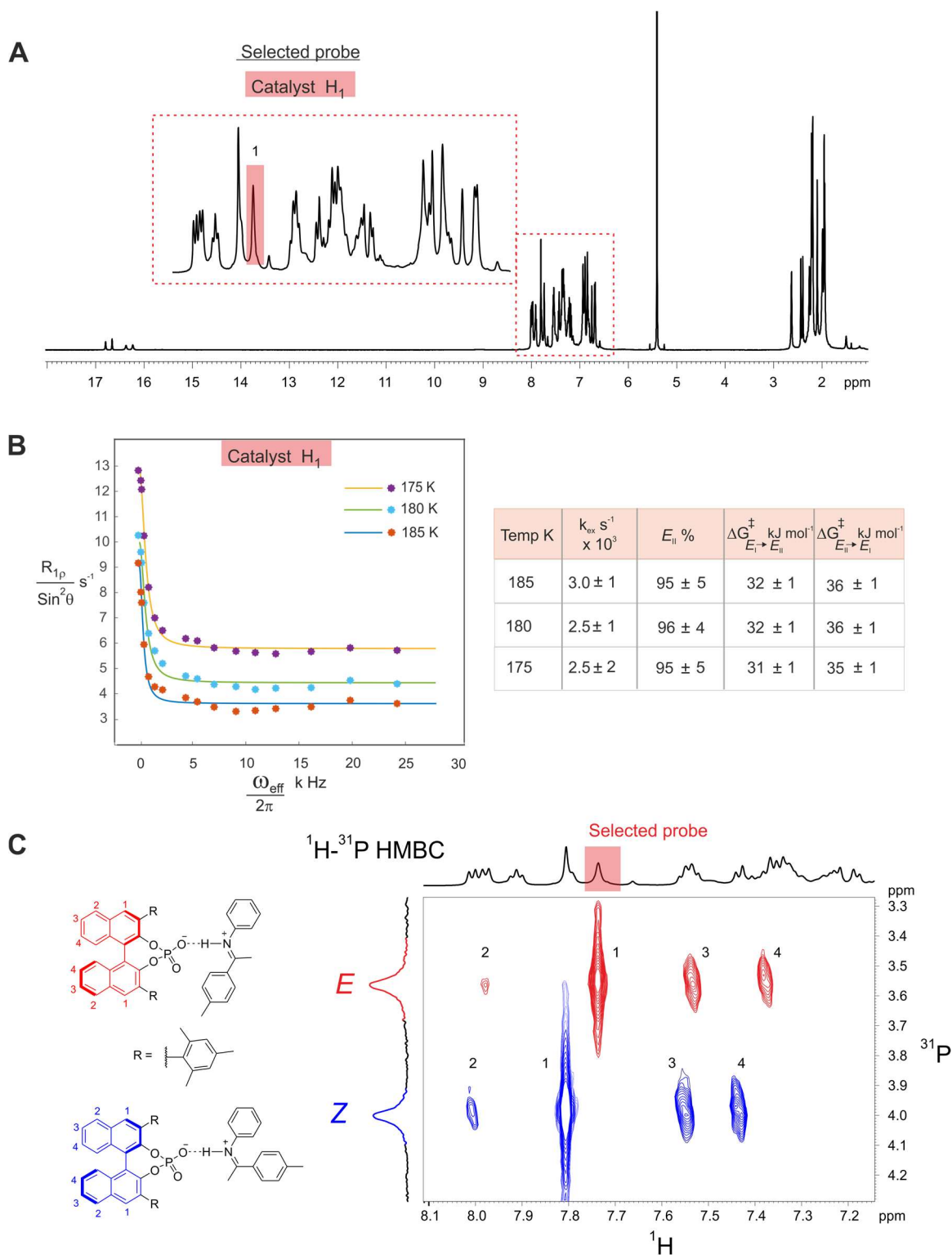


Figure 5. TRIP/imine complexes show a H-bond strength dependent exchange rate (measured at 180 K) **A**) Upon decrease of the H-bond strength (via different substituents at the *para*-position of the ketimine) the free activation barrier of the *E*-I \rightleftharpoons *E*-II process for pathway **A** (H-bond switching) is reduced. **B**) Theoretical calculations of the transition state of the H-bond switching show a bifurcated H-bond corroborating the experimental observation of a H-bond strength dependent process.

4.3.6. TRIM/1-3*E* imine complexes: Reduced sterics allow for rotations

To understand the effect of the 3,3'-substituents on the exchange process, which are key to reactivities and selectivities in these catalytic reactions,^{59,60} we selected TRIM (see figure 1A for structure) as CPA due to its structural similarity to TRIP. In our previous investigations on binary TRIM/imine complexes, we could identify the same four core structures *E*-I, *E*-II, *Z*-I and *Z*-II but also observed several alterations compared to the TRIP systems.¹⁵ With identical imines TRIM forms weaker hydrogen bonds compared to TRIP, which should result in a faster hydrogen bond switching process. Furthermore, in TRIM, neither *E*- nor *Z*-imine complexes showed a signal splitting of the BINOL-backbone (Figure 6C: averaged BINOL backbone), which suggests pathway **C** as an exchange pathway between *E*-I and *E*-II. Moreover, dimers of the binary complex [TRIM/*E*-imine]₂ were also identified, which are in slow exchange with the respective monomeric *E* complexes and the free imine.

4. Relaxation Dispersion NMR to reveal fast Dynamics in Brønsted Acid Catalysis: Influence of Sterics and H-bond strength on conformations and substrate hopping



4. Relaxation Dispersion NMR to reveal fast Dynamics in Brønsted Acid Catalysis: Influence of Sterics and H-bond strength on conformations and substrate hopping

Similar to the investigated TRIP systems, the catalyst signal H₁ was used as probe, because the corresponding peak is well separated (Figure 6A). In addition, a significant chemical shift difference between *E*-I and *E*-II was expected for the H₁-proton. Unlike in TRIP/**1**, the imine signal of the *para*-CH₃ substituent of **1** (Figure 6A) was not suitable, as it partially overlapped with the CH₃-signals of the 3,3'-substituent. The same optimized parameters as for TRIP were used in the TRIM systems (for details see SI). Surprisingly, the determined exchange rate of $3 \cdot 10^3 \text{ s}^{-1}$ for TRIM/**1** was significantly lower than that for TRIP ($11 \cdot 10^3 \text{ s}^{-1}$ see Figure 6B), although a faster exchange was expected due to the weaker hydrogen bond. Hence, we further modulated the hydrogen bond strength in TRIM/imine complexes by varying the imine. However, the TRIM complexes with *E*-imines **1**, **2** and **3** gave similar exchange rates of $2\text{-}3 \cdot 10^3 \text{ s}^{-1}$ despite the alteration in H-bond strength (see SI for details on TRIM/**2** and TRIM/**3**). This lack of dependency for TRIM/*E*-complexes demonstrates that either a different exchange pathway is operative compared to the respective TRIP systems or a shift of the rate determining step occurs, which is then independent of the H-bond strength. Furthermore, the observed averaging of the BINOL-backbone indicates also an alteration in the exchange mechanism. This is validated by theoretical calculations, which predicted a much lower switching barrier for TRIM/**1** than the experimentally observed ($\Delta G_{\text{calc}}^{\ddagger}(\text{II} \rightarrow \text{I}) = +26.4 \text{ kJ/mol}$; $\Delta G_{\text{exp}}^{\ddagger}(\text{II} \rightarrow \text{I}) = +36.0 \text{ kJ/mol}$).

As in TRIP systems, the exchange between TRIM/**1E** and free imine as well as with the dimer [TRIM/**1E**]₂ is slow on the NMR timescale and separated sets of signals were identified for these species. Hence, exchange pathway via association/dissociation or any process including the dimer do not contribute significantly to the measured exchange rates. For pathway **A**, we expected a backbone splitting as in TRIP, which is not in agreement with the observed signal averaging.⁶¹ On the other hand, the reduced steric bulk of TRIM compared to TRIP⁹ could potentially enable rotation of the *E*-imine in the binding pocket. Thus, pathway **C** could be operative, and the two naphthyl-fragments of the BINOL-backbone will be symmetrized by the exchange. To corroborate the participation of rotation in the exchange pathway, VT-MD simulations from 300 K to 350 K were performed. Indeed, the trajectory analysis of the MD at 340 K (Figure 7) revealed that in contrast to TRIP, rotation of the *E*-imine in the binary TRIM/**1** complex is possible. From the MD-simulation of TRIM/**1**, the fast switching and tilting of the imine (pathway **A**) occur over the defined time frame of 4000 ps (Figure 7: red and green shaded binary complexes), which allows the exchange between Type I and Type II. The intervention of tilting and switching by the imine rotation event takes place after ca. 3000 ps (dotted line) and converts the red shaded binary complex to the green shaded binary complex. This leads to an averaging of BINOL backbone peaks observed in NMR.

4. Relaxation Dispersion NMR to reveal fast Dynamics in Brønsted Acid Catalysis: Influence of Sterics and H-bond strength on conformations and substrate hopping

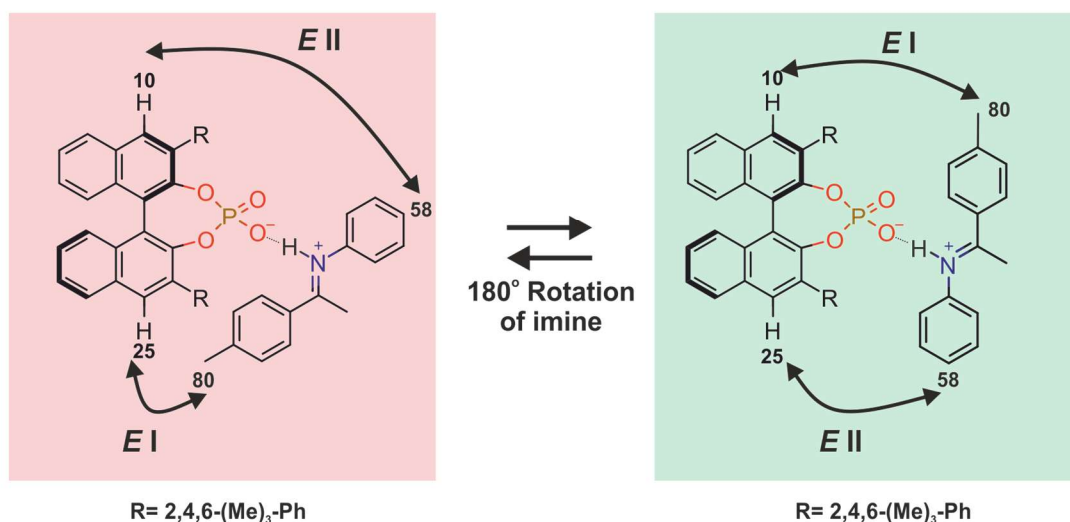
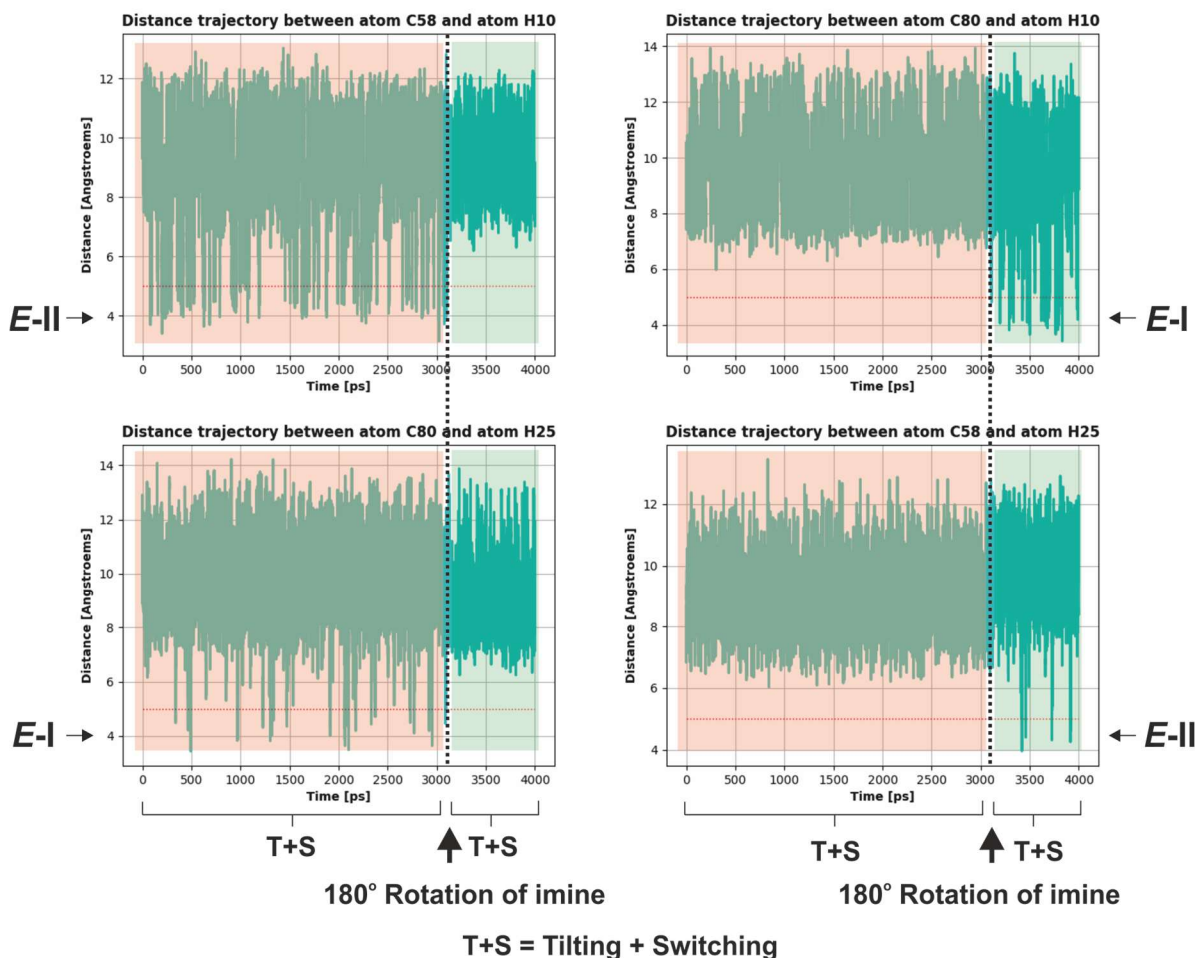


Figure 7. xtb-MD simulations corroborate a rotational exchange process in TRIM/1E. Distance trajectory between selected atoms from semi-empirical MD at 340 K for a TRIM/1E complex in CD₂Cl₂. From 0 – 3000 ps (red shaded box), tilting and switching of imine inside the complex occurs (similar to the exchange between Type E-I and E-II in TRIP). Then a rotation occurs after 3000 ps (dotted line) with continued switching and tilting (green shaded box) leading to an averaged BINOL-backbone signal observed in NMR. The red shaded binary complex is related to the green shaded binary complex by a 180° rotation of the imine. In the red shaded binary complex E-II conformation is marked by a short distance between C58 and H10, while in the E-I conformation C80 is in proximity with H25. The green shaded binary complex showed the alternation of the contact matrix after the rotation of the imine.

4.3.7. TRIM/4E imine complex: Disabling of rotation by steric hindrance

To hinder the rotation of the *E*-imine inside the complex and thus to validate indirectly the previous results, we increased the steric bulk of the imine by introducing two *t*-butyl groups, one on each side (see Figure 8 for imine **4**). The structural analysis of TRIM/4 (see SI for details) revealed the presence of the four core structures by NOE analysis. As in all other investigated TRIP and TRIM systems, two sets of signals were obtained, one featuring an *E*-imine and the other a *Z*-imine. This implies that the exchange between Type I and Type II is present and fast on the NMR time scale. Interestingly, in contrast to all other investigated TRIM/imine complexes, no dimers [TRIM/4]₂ were detected, which indicates that the steric repulsion overrides the attractive interactions in the dimer. Additionally, signal splitting of the BINOL-backbone is now observed indicating that the rotation process is now disabled as intended (Figure 8C). In terms of H-bond strength, TRIM/4E is positioned between TRIM/1E and TRIM/3E (for details SI).

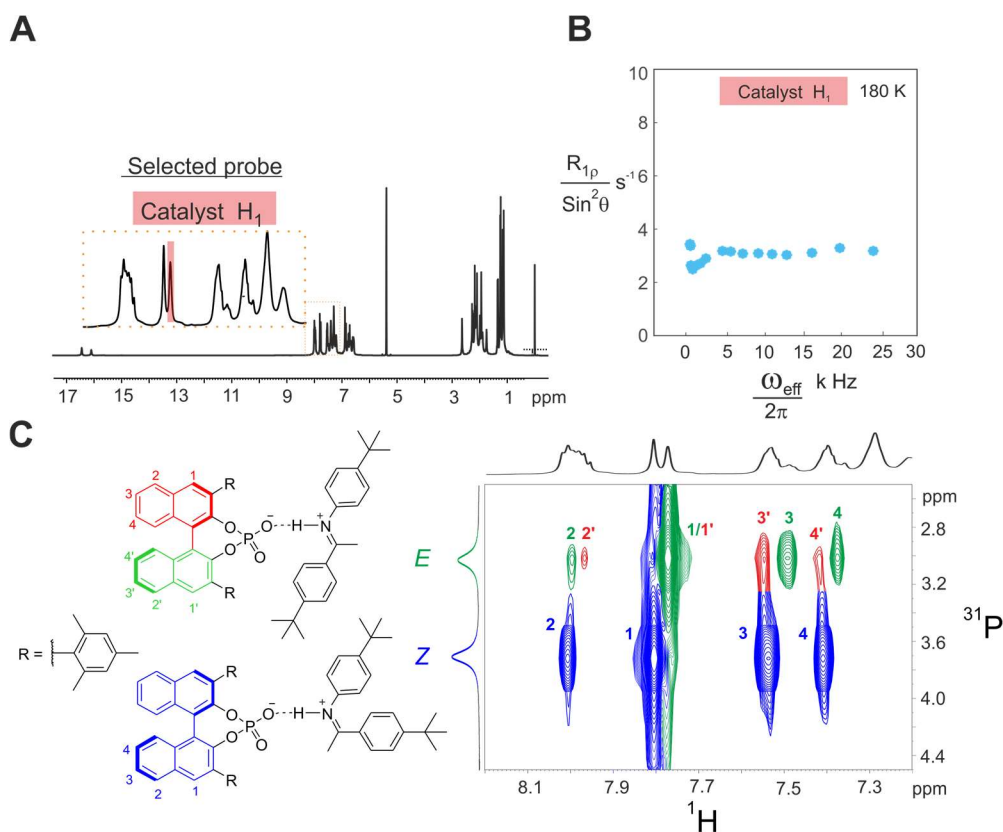


Figure 8. R_{1p} measurements for TRIM/4E complex showing disabled rotation by the increased steric of the imine **4**. **A**) Selected peak in the spectra to observe and quantify the *E*-II/*E*-I exchange process. **B**) No offset-Lorentzian decay was detected by R_{1p} experiment indicating both no rotation and a too fast switching. **C**) The backbone splitting is restored in the ¹H-³¹P HMBC spectrum due to disabled rotation.

The application of the R_{1p} method with the identical pulse program parameters as before on the catalyst backbone signal H₁ shows no signal decay on increased ω_{eff} (Figure 8B). This means, the fast exchange process between *E*-I and *E*-II (see above) is not in the time scale accessible by R_{1p} ($10^3 - 10^5$ s⁻¹). The computationally estimated exchange rate of TRIM/1E for the switching step is in the order of

4. Relaxation Dispersion NMR to reveal fast Dynamics in Brønsted Acid Catalysis: Influence of Sterics and H-bond strength on conformations and substrate hopping

10^6 s^{-1} . For TRIM/**4E** an even higher exchange rate is expected due to the weaker hydrogen bond assuming that the increased steric of imine **4E** does not interfere with the switching process. Hence, the absence of decay in the $R_{1\rho}$ for TRIM/**4E** is due to the absence of the rotation. In other words, the decay we observed in TRIM/**1-3E** is the rotation in pathway **C**. Thus, we demonstrated that the modification of 3,3'-substituents can alter the operative exchange pathways, i.e. enabling rotation due to reduced steric hindrance. In addition, acceleration of the H-bond switching rate is possible due to the modulations of H-bond strength and catalyst's steric properties.

4.3.8. TiPSY/**1E** imine complex: Influence of 3,3'-substituents on the H-Bond switching rate

To qualitatively determine the influence of the catalyst's sterics on the rate of the switching process, we selected TiPSY/**1E**. Due to the increased steric property of TiPSY,⁹ the rotation of the *E*-imine (pathway **B** and **C**) inside the catalyst pocket is disabled similar to the situation in TRIP and was confirmed by the backbone splitting in ¹H spectra (see SI). NOE analysis showed a fast exchange between Type *E-I* and *E-II* as in other binary complexes, leaving the exchange pathway **A** being the only operative mechanism.¹⁵ According to the ¹⁵N chemical shift^{14,15} (see Figure 9), TiPSY/**1E** possesses a H-bond strength between TRIP/**1E** and TRIP/**3E**. Thus, if the switching process is solely dependent on the H-bond strength, we expect an exchange rate between the ones of TRIP/**1E** and TRIP/**3E**. However, if also the steric requirement of the 3,3'-substituent of the catalyst has an influence, then a deviating exchange rate is expected. The obtained plot from the $R_{1\rho}$ measurement showed a decay and an exchange rate of 9000 s^{-1} at 180 K (see SI and Figure 9). Hence, the operative tilting-switching process is detectable, and its rate is lower than expected from its H-bond strengths. This result confirms the trend already indicated by the switching rates of the TRIP and TRIM/imine complexes:⁶² the switching process is a function of two variables: H-bond strength and steric properties of the 3,3'-substituents (Figure 9).

4. Relaxation Dispersion NMR to reveal fast Dynamics in Brønsted Acid Catalysis: Influence of Sterics and H-bond strength on conformations and substrate hopping

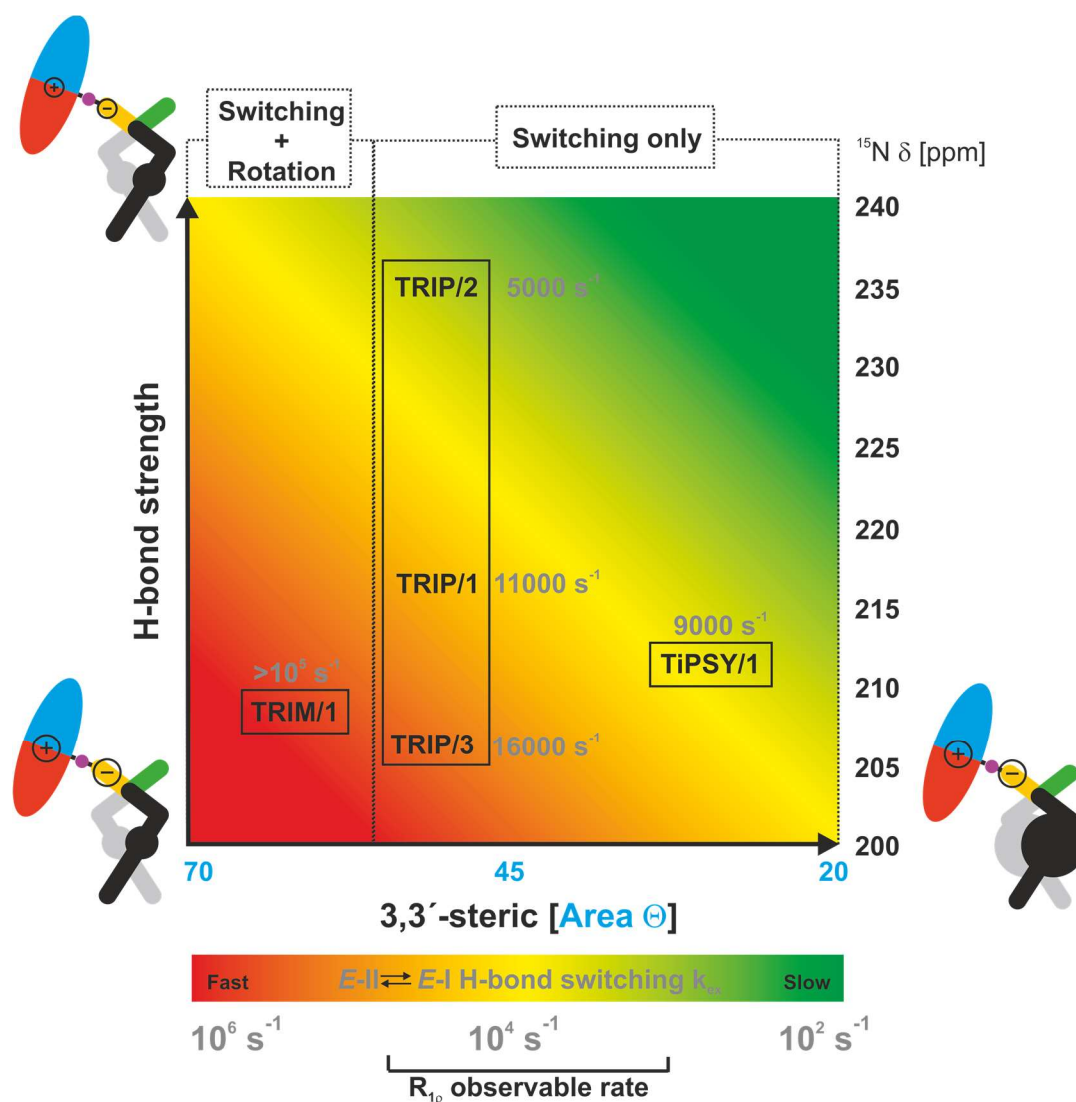


Figure 9. Overview of the present work showing the influence of the size of the 3,3'-substituents (according to the cone size of the binding pocket)⁹ and the H-bond strength (expressed by $\delta(^{15}\text{N})$ ^{50,63,64} on the exchange pathway and rate. Variation of the imine basicity in TRIP complexes modulates the switching rate proving an H-bond strength dependent process. Reduced sterics and weakening of the H-bond as in TRIM/imine complexes accelerate the H-bond switching process beyond detection in R_{1p} measurements and allow for the rotation of the imine. An increase of 3,3'-steric bulk in a TiPSY imine complex disables the rotation and decelerates the switching process significantly. The newly applied R_{1p} method in catalysis extends the measurable exchange rate from 10^3 to 10^5 s^{-1} .

4.4. Conclusion

This study illustrates the potential of relaxation dispersion NMR in chemical catalysis. In contrast to biomolecules, in our system low temperature applications are possible, which extend the time resolution again by three orders of magnitude (e.g. 300 K to 180 K results in a factor of 5000). As a result, processes on the ns time scale at room temperature can be resolved with NMR at low temperature.

As a result, the application of R_{1p} measurements at low temperatures even allowed to analyze the kinetics of a single hydrogen bond switch, which to our knowledge is so far unprecedented in chemical

4. Relaxation Dispersion NMR to reveal fast Dynamics in Brønsted Acid Catalysis: Influence of Sterics and H-bond strength on conformations and substrate hopping

catalysis. By combining these $R_{1\rho}$ measurements and theoretical calculations we succeeded to quantify the dynamics and visualize different possible pathways (switching, switching-rotation combined) for $E-I \rightleftharpoons E-II$ imine exchange inside the CPA catalyst cavity in ion pair catalysis. These observed mechanistic pathways at molecular level were dependent on both sterics and H-bond strengths (Figure 9). Alteration at either catalyst or substrate affected the dynamics in terms of both magnitude and mechanism. The rate of the tilting-switching process increased with the decrease of H-bond strength under comparable sterics, indicating H-bond switching as the rate determining step, which was corroborated by theoretical calculations. On the other hand, reduced sterics significantly accelerated (at least by an order of magnitude) the switching process and in addition enabled a rotational pathway.

We believe that this conformational resolution of catalyst-substrate complex structures and their dynamics (in absence of the reductant) by experiment opens a new era in mechanistic investigations of catalytic reactions, towards designing and understanding the catalytic reactions in terms of conformational space (flexibility) and weak interactions (H-bond strength and sterics).

4.5. References

- (1) Mahlau, M.; List, B. Asymmetric Counteranion-Directed Catalysis: Concept, Definition, and Applications. *Angew. Chem. Int. Ed.* **2013**, *52* (2), 518–533.
- (2) Akiyama, T.; Itoh, J.; Yokota, K.; Fuchibe, K. Enantioselective Mannich-Type Reaction Catalyzed by a Chiral Brønsted Acid. *Angew. Chem. Int. Ed.* **2004**, *43* (12), 1566–1568.
- (3) Uraguchi, D.; Terada, M. Chiral Brønsted Acid-Catalyzed Direct Mannich Reactions via Electrophilic Activation. *J. Am. Chem. Soc.* **2004**, *126* (17), 5356–5357.
- (4) Parmar, D.; Sugiono, E.; Raja, S.; Rueping, M. Complete Field Guide to Asymmetric BINOL-Phosphate Derived Brønsted Acid and Metal Catalysis: History and Classification by Mode of Activation; Brønsted Acidity, Hydrogen Bonding, Ion Pairing, and Metal Phosphates. *Chem. Rev.* **2014**, *114* (18), 9047–9153.
- (5) Storer, R. I.; Carrera, D. E.; Ni, Y.; MacMillan, D. W. C. Enantioselective Organocatalytic Reductive Amination. *J. Am. Chem. Soc.* **2006**, *128* (1), 84–86.
- (6) Rueping, M.; Sugiono, E.; Azap, C.; Theissmann, T.; Bolte, M. Enantioselective Brønsted Acid Catalyzed Transfer Hydrogenation: Organocatalytic Reduction of Imines. *Org. Lett.* **2005**, *7* (17), 3781–3783.
- (7) Hoffmann, S.; Seayad, A. M.; List, B. A Powerful Brønsted Acid Catalyst for the Organocatalytic Asymmetric Transfer Hydrogenation of Imines. *Angew. Chem. Int. Ed.* **2005**, *44* (45), 7424–7427.
- (8) Marcelli, T.; Hammar, P.; Himó, F. Phosphoric Acid Catalyzed Enantioselective Transfer Hydrogenation of Imines: A Density Functional Theory Study of Reaction Mechanism and the Origins of Enantioselectivity. *Chem. Eur. J.* **2008**, *14* (28), 8562–8571.
- (9) Reid, J. P.; Goodman, J. M. Goldilocks Catalysts: Computational Insights into the Role of the 3,3' Substituents on the Selectivity of BINOL-Derived Phosphoric Acid Catalysts. *J. Am. Chem. Soc.* **2016**, *138* (25), 7910–7917.
- (10) Simón, L.; Goodman, J. M. A Model for the Enantioselectivity of Imine Reactions Catalyzed by BINOL-Phosphoric Acid Catalysts. *J. Org. Chem.* **2011**, *76* (6), 1775–1788.

4. Relaxation Dispersion NMR to reveal fast Dynamics in Brønsted Acid Catalysis: Influence of Sterics and H-bond strength on conformations and substrate hopping

- (11) Reid, J. P.; Goodman, J. M. Selecting Chiral BINOL-Derived Phosphoric Acid Catalysts: General Model To Identify Steric Features Essential for Enantioselectivity. *Chem. Eur. J.* **2017**, *23*, 14248–14260.
- (12) Greindl, J.; Hioe, J.; Sorgenfrei, N.; Morana, F.; Gschwind, R. M. Brønsted Acid Catalysis-Structural Preferences and Mobility in Imine/Phosphoric Acid Complexes. *J. Am. Chem. Soc.* **2016**, *138* (49), 15965–15971.
- (13) Saha, S.; Schneider, C. Brønsted Acid-Catalyzed, Highly Enantioselective Addition of Enamides to in Situ-Generated Ortho-Quinone Methides: A Domino Approach to Complex Acetamidotetrahydroxanthenes. *Chem. Eur. J.* **2015**, *21* (6), 2348–2352.
- (14) Sorgenfrei, N.; Hioe, J.; Greindl, J.; Rothermel, K.; Morana, F.; Lokesh, N.; Gschwind, R. M. NMR Spectroscopic Characterization of Charge Assisted Strong Hydrogen Bonds in Brønsted Acid Catalysis. *J. Am. Chem. Soc.* **2016**, *138* (50), 16345–16354.
- (15) Melikian, M.; Gramüller, J.; Hioe, J.; Greindl, J.; Gschwind, R. M. Brønsted Acid Catalysis – the Effect of 3,3'-Substituents on the Structural Space and the Stabilization of Imine/Phosphoric Acid Complexes. *Chem. Sci.* **2019**, *10*, 5226–5234.
- (16) Seegerer, A.; Hioe, J.; Hammer, M. M.; Morana, F.; Fuchs, P. J. W.; Gschwind, R. M. Remote-Stereocontrol in Dienamine Catalysis: Z-Dienamine Preferences and Electrophile-Catalyst Interaction Revealed by NMR and Computational Studies. *J. Am. Chem. Soc.* **2016**, *138* (31), 9864–9873.
- (17) Renzi, P.; Hioe, J.; Gschwind, R. M. Decrypting Transition States by Light: Photoisomerization as a Mechanistic Tool in Brønsted Acid Catalysis. *J. Am. Chem. Soc.* **2017**, *139* (19), 6752–6760.
- (18) Burés, J.; Armstrong, A.; Blackmond, D. G. Explaining Anomalies in Enamine Catalysis: “Downstream Species” as a New Paradigm for Stereocontrol. *Acc. Chem. Res.* **2016**, *49* (2), 214–222.
- (19) Neel, A. J.; Hilton, M. J.; Sigman, M. S.; Toste, F. D. Exploiting Non-Covalent π Interactions for Catalyst Design. *Nature* **2017**, *543* (7647), 637–646.
- (20) Nikitin, K.; O’Gara, R. Mechanisms and Beyond: Elucidation of Fluxional Dynamics by Exchange NMR Spectroscopy. *Chem. Eur. J.* **2019**, *25* (18), 4551–4589.
- (21) Nitschke, P.; Lokesh, N.; Gschwind, R. M. Combination of Illumination and High Resolution NMR Spectroscopy: Key Features and Practical Aspects, Photochemical Applications, and New Concepts. *Prog. Nucl. Magn. Reson. Spectrosc.* **2019**, *114–115*, 86–134.
- (22) Renzi, P.; Hioe, J.; Gschwind, R. M. Enamine/Dienamine and Brønsted Acid Catalysis: Elusive Intermediates, Reaction Mechanisms, and Stereoinduction Modes Based on in Situ NMR Spectroscopy and Computational Studies. *Acc. Chem. Res.* **2017**, *50* (12), 2936–2948.
- (23) Pichota, A.; Pregosin, P. S.; Valentini, M.; Wörle, M.; Seebach, D. NMR Studies of Chiral, Tetranuclear Cu I Catalysts Based on Monodentate Thiol Analogues of TADDOL. *Angew. Chem. Int. Ed.* **2000**, *39* (1), 153–156.
- (24) Böttcher, B.; Schmidts, V.; Raskatov, J. A.; Thiele, C. M. Determination of the Conformation of the Key Intermediate in an Enantioselective Palladium-Catalyzed Allylic Substitution from Residual Dipolar Couplings. *Angew. Chem. Int. Ed.* **2010**, *49* (1), 205–209.
- (25) Butts, C. P.; Filali, E.; Lloyd-Jones, G. C.; Norrby, P. O.; Sale, D. A.; Schramm, Y. Structure-Based Rationale for Selectivity in the Asymmetric Allylic Alkylation of Cycloalkenyl Esters Employing the Trost “Standard Ligand” (TSL): Isolation, Analysis and Alkylation of the Monomeric Form of the Cationic H₃-Cyclohexenyl Complex [(H₃-c-C₆H). *J. Am. Chem. Soc.* **2009**, *131* (29), 9945–9957.
- (26) Keske, E. C.; West, T. H.; Lloyd-Jones, G. C. Analysis of Autoinduction, Inhibition, and Autoinhibition in a Rh-Catalyzed C-C Cleavage: Mechanism of Decyanative Aryl Silylation. *ACS Catal.* **2018**, *8* (9), 8932–8940.
- (27) Bertz, S. H.; Cope, S.; Dorton, D.; Murphy, M.; Ogle, C. A. Organocuprate Cross-Coupling: The Central Role of the Copper(III) Intermediate and the Importance of the Copper(I) Precursor. *Angew. Chem. Int. Ed.* **2007**, *46* (37), 7082–7085.
- (28) Corbucci, I.; Petronilho, A.; Müller-Bunz, H.; Rocchigiani, L.; Albrecht, M.; Macchioni, A. Substantial Improvement of Pyridine-Carbene Iridium Water Oxidation Catalysts by a Simple Methyl-to-Octyl Substitution. *ACS Catal.* **2015**, *5* (5), 2714–2718.
- (29) Brand, T.; Cabrita, E. J.; Berger, S. Intermolecular Interaction as Investigated by NOE and Diffusion Studies. *Prog. Nucl. Magn. Reson. Spectrosc.* **2005**, *46* (4), 159–196.
- (30) Ciancaleoni, G.; Bertani, R.; Rocchigiani, L.; Sgarbossa, P.; Zuccaccia, C.; Macchioni, A. Discriminating Halogen-Bonding from Other Noncovalent Interactions by a Combined NOE NMR/DFT Approach. *Chem. Eur. J.* **2015**, *21* (1), 440–447.

4. Relaxation Dispersion NMR to reveal fast Dynamics in Brønsted Acid Catalysis: Influence of Sterics and H-bond strength on conformations and substrate hopping

- (31) Dale, H. J. A.; Hodges, G. R.; Lloyd-Jones, G. C. Taming Ambident Triazole Anions: Regioselective Ion Pairing Catalyzes Direct N-Alkylation with Atypical Regioselectivity. *J. Am. Chem. Soc.* **2019**, *141* (17), 7181–7193.
- (32) Pregosin, P. S.; Anil Kumar, P. G.; Fernández, I. Pulsed Gradient Spin-Echo (PGSE) Diffusion and ¹H,¹⁹F Heteronuclear Overhauser Spectroscopy (HOESY) NMR Methods in Inorganic and Organometallic Chemistry: Something Old and Something New. *Chem. Rev.* **2005**, *105* (8), 2977–2998.
- (33) McGarrity, J. F.; Ogle, C. A. High-Field ¹H NMR Study of the Aggregation and Complexation of n-Butyllithium in Tetrahydrofuran. *J. Am. Chem. Soc.* **1985**, *107* (7), 1805–1810.
- (34) Singleton, D. A.; Thomas, A. A. High-Precision Simultaneous Determination of Multiple Small Kinetic Isotope Effects at Natural Abundance. *J. Am. Chem. Soc.* **1995**, *117* (36), 9357–9358.
- (35) Kurouchi, H.; Singleton, D. A. Labelling and Determination of the Energy in Reactive Intermediates in Solution Enabled by Energy-Dependent Reaction Selectivity. *Nat. Chem.* **2018**, *10* (2), 237–241.
- (36) Guivel-Scharen, V.; Sinnwell, T.; Wolff, S. D.; Balaban, R. S. Detection of Proton Chemical Exchange between Metabolites and Water in Biological Tissues. *J. Magn. Reson.* **1998**, *133* (1), 36–45.
- (37) Lokesh, N.; Seegerer, A.; Hioe, J.; Gschwind, R. M. Chemical Exchange Saturation Transfer in Chemical Reactions: A Mechanistic Tool for NMR Detection and Characterization of Transient Intermediates. *J. Am. Chem. Soc.* **2018**, *140* (5), 1855–1862.
- (38) Wang, S.; Lokesh, N.; Hioe, J.; Gschwind, R. M.; König, B. Photoinitiated Carbonyl-Metathesis: Deoxygenative Reductive Olefination of Aromatic Aldehydes: Via Photoredox Catalysis. *Chem. Sci.* **2019**, *10* (17), 4580–4587.
- (39) Lorenz, C.; Hastreiter, F.; Hioe, J.; Lokesh, N.; Gärtner, S.; Korber, N.; Gschwind, R. M. The Structure of [HSi9]3⁻ in the Solid State and Its Unexpected Highly Dynamic Behavior in Solution. *Angew. Chem. Int. Ed.* **2018**, *57* (39), 12956–12960.
- (40) Korzhnev, D. M.; Kay, L. E. Probing Invisible, Low-Populated States of Protein Molecules by Relaxation Dispersion NMR Spectroscopy: An Application to Protein Folding. *Acc. Chem. Res.* **2008**, *41* (3), 442–451.
- (41) Xue, Y.; Kellogg, D.; Kimsey, I. J.; Sathyamoorthy, B.; Stein, Z. W.; McBairty, M.; Al-hashimi, H. M. *Characterizing RNA Excited States Using NMR Relaxation Dispersion*, 1st ed.; Elsevier Inc., 2015; Vol. 558.
- (42) Palmer, A. G.; Massi, F. Characterization of the Dynamics of Biomacromolecules Using Rotating-Frame Spin Relaxation NMR Spectroscopy. *Chem. Rev.* **2006**, *106* (5), 1700–1719.
- (43) Down to 0.5% of the major exchange partner.
- (44) Walinda, E.; Morimoto, D.; Sugase, K. Resolving Biomolecular Motion and Interactions by R2 and R1ρ Relaxation Dispersion NMR. *Methods* **2018**, *148*, 28–38.
- (45) Moschen, T.; Grutsch, S.; Juen, M. A.; Wunderlich, C. H.; Kreutz, C.; Tollinger, M. Measurement of Ligand-Target Residence Times by ¹H Relaxation Dispersion NMR Spectroscopy. *J. Med. Chem.* **2016**, *59* (23), 10788–10793.
- (46) Ban, D.; Gossert, A. D.; Giller, K.; Becker, S.; Griesinger, C.; Lee, D. Exceeding the Limit of Dynamics Studies on Biomolecules Using High Spin-Lock Field Strengths with a Cryogenically Cooled Probehead. *J. Magn. Reson.* **2012**, *221*, 1–4.
- (47) Trigo-Mouriño, P.; Griesinger, C.; Lee, D. Label-Free NMR-Based Dissociation Kinetics Determination. *J. Biomol. NMR* **2017**, *69* (4), 229–235.
- (48) Desvaux, H.; Wary, C.; Birlirakis, N.; Berthault, P. Study of Slow Molecular Motions in Solution Using Off-Resonance Irradiation in Homonuclear NMR I. Long Dipolar Correlation Times. *Mol. Phys.* **1995**, *86* (5), 1049–1058.
- (49) Desvaux, H.; Berthault, P.; Birlirakis, N.; Goldman, M. Off-Resonance ROESY for the Study of Dynamic Processes. *Journal of Magnetic Resonance, Series A*. 1994, pp 219–229.
- (50) Rothermel, K.; Melikian, M.; Hioe, J.; Greindl, J.; Gramüller, J.; Matej Žabka; Sorgenfrei, N.; Hausler, T.; Morana, F.; Gschwind, R. M. Internal Acidity Scale and Reactivity Evaluation of Chiral Phosphoric Acids with Different 3,3'-Substituents in Brønsted Acid Catalysis. *Chem. Sci.* **2019**, DOI: 10.1039/C9SC02342A.
- (51) In addition, we were able to detect dimer structures of CPA/imine complexes in solution along with the four core structures. The aggregate was stabilized solely by weak non-covalent interaction and its amount is very much dependent on the motif of the 3, 3'-substituents.

4. Relaxation Dispersion NMR to reveal fast Dynamics in Brønsted Acid Catalysis: Influence of Sterics and H-bond strength on conformations and substrate hopping

- (52) Crawford, J. M.; Sigman, M. S. Conformational Dynamics in Asymmetric Catalysis: Is Catalyst Flexibility a Design Element? *Synth.* **2019**, *51* (5), 1021–1036.
- (53) For binary TRIP/Z-imine complexes the lack of BINOL-splitting was interpreted in terms of pathway C, as the Z-imine has a sterically more compact structure, which allows rotation within the complex.
- (54) Akke, M.; Palmer, A. G. Monitoring Macromolecular Motions on Microsecond to Millisecond Time Scales by R 1 ρ –R 1 Constant Relaxation Time NMR Spectroscopy. *J. Am. Chem. Soc.* **1996**, *118* (4), 911–912.
- (55) The Significantly Higher Limiting $R_{1\rho}$ value at high ω_{eff} of the catalyst at 185 K may be due to very fast additional conformational exchange processes of the isopropyl groups or rotation of the aryl rings of the imine.
- (56) Bannwarth, C.; Ehlert, S.; Grimme, S. GFN2-XTB - An Accurate and Broadly Parametrized Self-Consistent Tight-Binding Quantum Chemical Method with Multipole Electrostatics and Density-Dependent Dispersion Contributions. *J. Chem. Theory Comput.* **2019**, *15* (3), 1652–1671.
- (57) In addition, the NOESY pattern of TRIP in complex with an imine derived from *para*-methoxy aniline excludes pathway B.
- (58) Steiner, T. The Hydrogen Bond in the Solid State. *Angew. Chem. Int. Ed.* **2002**, *41* (1), 49–76.
- (59) Kang, Q.; Zhao, Z.-A.; You, S.-L. Asymmetric Transfer Hydrogenation of Beta,Gamma-Alkynyl Alpha-Imino Esters by a Brønsted Acid. *Org. Lett.* **2008**, *10* (10), 2031–2034.
- (60) You, S.; Gu, Q.; Rong, Z.; Zheng, C. Desymmetrization of Cyclohexadienones via Brønsted Acid-Catalyzed Enantioselective Oxo-Michael Reaction. *J. Am. Chem. Soc.* **2010**, *132* (12), 4056–4057.
- (61) Due to the reduced spectral resolution at 180 K and signal overlapping, the existence of backbone splitting which is not sufficiently resolved cannot be absolutely excluded.
- (62) TRIM/4E has a slightly weaker H-bond strength than TRIP/1-3E; However, based on the H-Bond strengths and switching rates in TRIP/1-3E, a switching rate in the same order of magnitude would be anticipated for TRIM/4E.
- (63) Benedict, H.; Shenderovich, I. G.; Malkina, O. L.; Malkin, V. G.; Denisov, G. S.; Golubev, N. S.; Limbach, H. H. Nuclear Scalar Spin-Spin Couplings and Geometries of Hydrogen Bonds. *J. Am. Chem. Soc.* **2000**, *122* (9), 1979–1988.
- (64) Sharif, S.; Denisov, G. S.; Toney, M. D.; Limbach, H.-H. NMR Studies of Coupled Low-and High-Barrier Hydrogen Bonds in Pyridoxal-5'-Phosphate-Enzyme Model Systems in Polar Solution Supporting Information. *J. Am. Chem. Soc.* **2007**, *129* (11), 6313–6327.

4.6. Supporting Information

4.6.1. Experimental data

Deuterated solvents were purchased from Deutero or Sigma Aldrich. Where dry solvents were essential, CD₂Cl₂ was freshly distilled over CaH₂ and Toluene was refluxed over Na/Benzophenone under argon atmosphere. The catalysts were purchased from Sigma Aldrich or STREM chemicals.

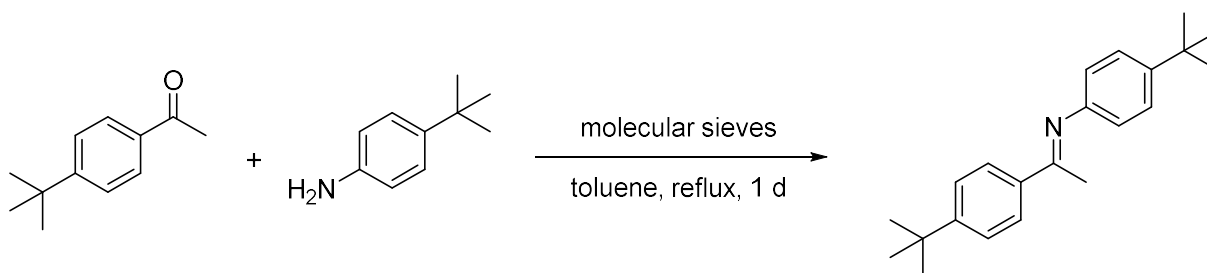
High-resolution mass spectra were measured by the central analytics division in the Institute of Organic Chemistry. Gas chromatography coupled with a mass selective detector was performed on an Agilent 6890N Network GC-System.

4. Relaxation Dispersion NMR to reveal fast Dynamics in Brønsted Acid Catalysis: Influence of Sterics and H-bond strength on conformations and substrate hopping

4.6.2. Synthesis of Imine Substrates

The imines were prepared as described in the literature.¹⁻⁴ The toluene was used either in p.A. quality or was dried by refluxing over sodium. The ¹⁵N-enriched aniline (if used) was purchased from Eurisotop GmbH and Sigma Aldrich.

(E)-N,1-bis(4-(tert-butyl)phenyl)ethan-1-imine [5]



Molecular sieves 4 Å (4 g) was weighed into a 50 mL Schlenk flask and dried with a heat gun at 350 °C for 30 min under reduced pressure. Under Argon flow, 4-(tert-butyl)aniline (10.0 mmol, 1.49 g, 1.60 mL, 1.0 eq) and 1-(4-(tert-butyl)phenyl)ethan-1-one (10.0 mmol, 1.76 g, 1.83 mL, 1.0 eq.) were added and dissolved in 20 mL anhydrous toluene. Under Argon flow, a reflux condenser was added to the setup and flushed with argon for 3 min. A drying tube filled with CaCl₂ was added to the setup. The solution was refluxed for 24 h. Afterward, the heating bath was removed, and the reaction mixture allowed to cool down. The orange mixture was filtrated, and the solvent was removed under reduced pressure to give an orange-yellow solid. The crude product was washed with methanol to give the product (4.76 mmol, 1.46 g, 48%) as yellow needles predominantly as its *E*-isomer (>99% determined by ¹H NMR).

¹H-NMR (400.1 MHz, CD₂Cl₂) δ_H = 7.91 (m, 2H), 7.48 (m, 2H), 7.37 (m, 2H), 6.71 (m, 2H), 2.21 (s, 3H), 1.36 (s, 9H), 1.34 ppm (s, 9H).

¹³C-NMR {¹H} (100.6 MHz): δ_C = 164.8, 153.7, 149.2, 145.8, 137.0, 126.8, 125.7, 125.2, 119.0, 34.7, 34.1, 31.2, 31.0, 16.9 ppm.

HR-MS (ESI, *m/z*): found 307.2289 (M)⁺ (calculated for 307.2300 for C₂₂H₂₉N); Diff(ppm) = -1.92 ppm.

4.6.3. Sample preparation

The catalyst was dried for 30 min at 150°C under reduced pressure. Ketimine and catalyst were directly weighed into a 5 mm NMR tube under an inert argon atmosphere. CD₂Cl₂ (0.6 ml; freshly distilled over CaH₂) and 1.0 ml of tetramethylsilane atmosphere were added to the tube. The sample was stored in

4. Relaxation Dispersion NMR to reveal fast Dynamics in Brønsted Acid Catalysis: Influence of Sterics and H-bond strength on conformations and substrate hopping

an -80°C freezer. A 1:1 ratio of catalyst/ketimine was used for all samples unless stated otherwise. A concentration of 0.25 – 100 mM was used, as indicated specifically.

4.6.4. Spectrometer data

NMR experiments were performed on Bruker Avance III HD 400 MHz spectrometer, equipped with 5 mm BBO BB-1H/D probe head with Z-Gradients and a Bruker Avance III HD 600 MHz spectrometer, equipped with a 5 mm CPPBBO BB-1H/19F. The temperature was controlled in the VT-experiments by BVT 3000 and BVTE 3900. For NMR measurements employing standard NMR solvents 5 mm NMR tubes were used, if not otherwise noted. NMR Data were processed, evaluated and plotted with TopSpin 3.2 software. Further plotting of the spectra was performed with Corel Draw X14 – X17 software. ^1H , ^{13}C chemical shifts were referenced to TMS or the respective solvent signals. The heteronuclei ^{19}F and ^{31}P were referenced, employing $\nu(X) = \nu(\text{TMS}) \times \Xi_{\text{reference}} / 100 \%$ according to Harris et al.⁵ The following frequency ratios and reference compounds were used: $\Xi(^{19}\text{F}) = 94.094011$ (CCl_3F), $\Xi(^{31}\text{P}) = 40.480742$ (H_3PO_4).

Pulse programs

All pulse programs used are standard Bruker NMR pulseprograms except for the $R_{1\rho}$ measurements.

Acquisition Parameters

^1H NMR: Pulse program: zg; Relaxation delay = 2 – 3 s, Acquisition time = 2.48 s, SW = 22.0 ppm, TD = 64k, NS = 8 – 64; zg30; Relaxation delay = 2 s, Acquisition time = 2.48 s, SW = 22.0 ppm, TD = 64k, NS = 8 – 64; $2\text{D-}^1\text{H}, ^1\text{H}$ NOESY: Pulse program: noesygpph/noesygpphpp; Relaxation delay = 5 - 8 s, NS = 8-32, mixing time (D8) = 300.00 ms; TD = 4096; increments = 512 - 1k; $2\text{D-}^1\text{H}, ^1\text{H}$ COSY: Pulse program: cosygppqf; Relaxation delay = 5 - 8 s, NS = 8-32, TD = 4096; increments = 512 - 1k; ^{13}C NMR: Pulse program: zgpg30; Relaxation delay = 2.00 s, Acquisition time = 0.80 s, SW = 270.0 ppm, TD = 64k, NS = 1k – 2k; $2\text{D-}^1\text{H}, ^{13}\text{C}$ HSQC: Pulse program: hsqcedetgpsisp2.3; Relaxation delay = 4 - 8 s, NS = 8-32, $^1J_{\text{XH}} = 145$ Hz; TD = 4096; increments = 512 - 1k; $2\text{D-}^1\text{H}, ^{13}\text{C}$ HMBC: Pulse program: hmbcgpplndqf; Relaxation delay = 4 - 8 s, NS = 8-32, $^1J_{\text{XH}} = 145$ Hz, $J_{\text{XH}}(\text{long range}) = 10$ Hz; TD = 4096; increments = 512 - 1k; $2\text{D-}^1\text{H}, ^{31}\text{P}$ HMBC: Pulse program: inv4gplrndqf; Relaxation delay = 4 - 8 s, NS = 8-32, TD = 4096; increments = 256 - 1k; ^{15}N NMR: Pulse program: zg; Relaxation delay = 10.00 s, Acquisition time = 0.54 s, SW = 502.8 ppm, TD = 32k, NS = 256 – 2048; $2\text{D-}^1\text{H}, ^{15}\text{N}$ HMBC: Pulse program: inv4gplrndqf; Relaxation delay = 5 - 8 s, NS = 16-32, delay for evolution of long range couplings (D6) = 20.00 ms; TD = 4096; increments = 128 - 512; ^{19}F -NMR: Pulse program: zg30; Relaxation delay = 2 – 3 s, Acquisition time =

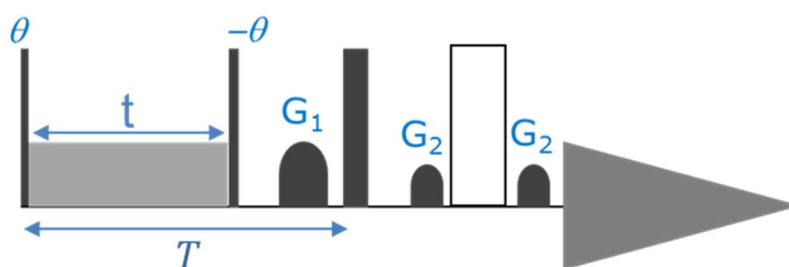
4. Relaxation Dispersion NMR to reveal fast Dynamics in Brønsted Acid Catalysis: Influence of Sterics and H-bond strength on conformations and substrate hopping

11.60 s, SW = 10.0 ppm, TD = 128k, NS = 8 – 64; $2D\text{-}^1\text{H}, ^{19}\text{F}$ HOESY: Pulse program: hoesyph; Relaxation delay = 5 - 8 s, NS = 16-32, mixing time (D8) = 500.00 ms; TD = 4096; increments = 1k;

4.6.5. 1D ^1H off-resonance $R_{1\rho}$

Pulse sequence

The recent reported 1D ^1H off-resonance $R_{1\rho}$ pulse sequence is adopted with slight modification for our measurement.^{6,7}



$$R_{1\rho} = -\frac{1}{T} \ln \frac{I}{I_0}$$

Figure S1: Applied pulse sequence and mathematical relation to measure $R_{1\rho}$ experimentally. The applied angle (θ) is 35° . A spinlock period (t) of 100 ms is applied. The filled (black) and unfilled rectangular pulses respectively indicate 90° and 180° hard pulses. The gradient pulses of $G_1 = 70\%$ and $G_2 = 40\%$ of the maximum were applied. I_0 is the intensity without any spinlock period and I is the intensity with spinlock period measured over a multiple effective magnetic field.

Parameter Optimization

The spinlock period (t) was incremented in 10 ms steps with maximum spinlock power (≈ 20 kHz). At each step, the temperature was monitored (sample heating can occur due to application of high intensity spinlock field over an extended time). Around 120 ms, temperature oscillation was observed. To avoid any influence of temperature changes on the measurement, the spinlock period of 100 ms was applied in all our measurements. The normal relaxation period ($T-t$) in the absence of the spinlock is tested for 3 delays (50 ms, 100 ms and 150 ms). For all three different relaxation periods ($T-t$), we found similar exchange rates within the experimental errors. To minimize signal loss due to relaxation, ($T-t$) of 50 ms was used in all our measurements.

4. Relaxation Dispersion NMR to reveal fast Dynamics in Brønsted Acid Catalysis: Influence of Sterics and H-bond strength on conformations and substrate hopping

Method testing

To test the applicability of the $R_{1\rho}$ method, we applied the above described pulse sequence with optimized parameters on the known peak in the spectrum (*para*-methyl protons of the hydrolyzed imine ketone part), which does not experience any chemical exchange process (on a ms- μ s timescale) and on the same proton for the CPA/imine complex which experiences chemical exchange. The measured rate for the hydrolyzed ketone showed a nearly straight line (no offset-Lorentzian decay with increasing effective field ω_{eff}), which was expected for non exchanging protons. For the same proton in the binary CPA/imine complex, an offset-Lorentzian decay was observed, which demonstrates the presence of chemical exchange on a ms- μ s timescale.

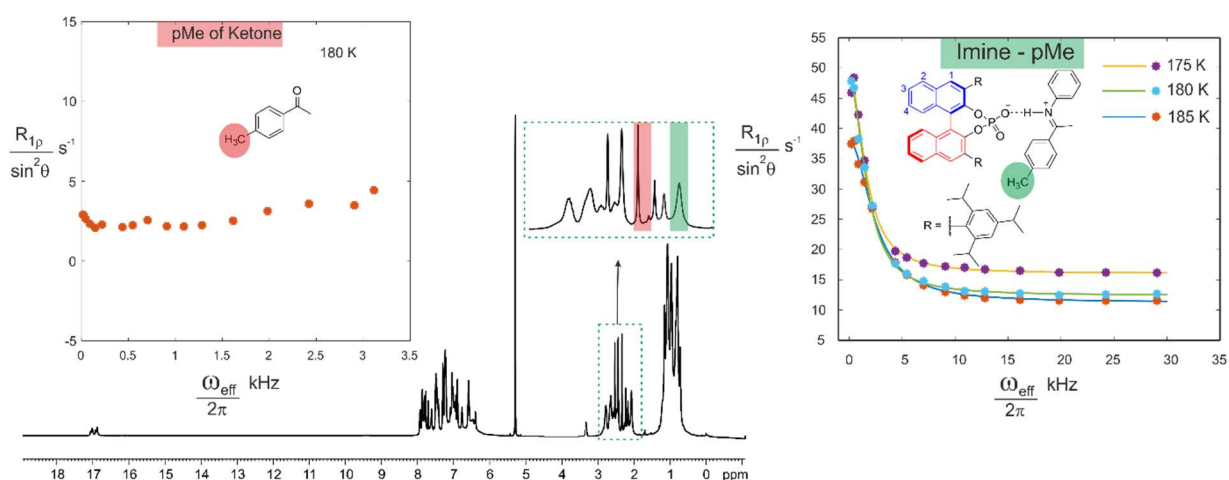


Figure S2: To test the method, we selected the proton peak of the *p*-methyl group in the hydrolyzed ketone moiety (red shaded) and the proton peak of the *p*-methyl imine in the TRIP/imine binary complex (green shaded) within the same sample (to maintain identical conditions). The hydrolyzed ketone does not undergo any chemical exchange on a ms- μ s time scale. The corresponding measured $R_{1\rho}$ data at 180 K with incremental effective field showed a near horizontal line, proving the absence of chemical exchange (left side). On the other hand, the imine inside the catalyst undergoes $E_i \rightleftharpoons E_{ii}$ exchange and thus the corresponding $R_{1\rho}$ data at 185, 180 and 175 K with incremental effective field showed offset-Lorentzian decays for the *p*-methyl protons in the TRIP/imine complex. This confirms the presence of chemical exchange process and hence validates our method for chemical exchange detection in ms- μ s range.

Curve fitting

In order to analyze the $R_{1\rho}$ measurements, the signal intensities (integrals) are determined for every effective field strength ω_{eff} (i.e. every different spinlock power) and normalized to the reference integral (spinlock power = 0 W). Initially, to extract k_{ex} , the measured experimental points are curve fitted to the following theoretically described equation by using MATLAB (see literature for further details⁸).

$$\frac{R_{\text{eff}}}{\sin^2\theta} = R_2 - R_1 + \frac{(\Delta\omega)^2 P_A P_B \tau_{\text{ex}}}{(1 + \tau_{\text{ex}}^2 \omega_{\text{eff}}^2)} \quad (\text{Eq. 1})$$

4. Relaxation Dispersion NMR to reveal fast Dynamics in Brønsted Acid Catalysis: Influence of Sterics and H-bond strength on conformations and substrate hopping

Here R_2 is the tranverse relaxation rate constant

R_1 is the longitudinal relaxation rate constant

$\Phi = (\Delta\omega)^2 P_A P_B \tau_{ex}$ encodes both chemical shift difference and population of the minor (P_B) and major (P_A) exchange species

Φ and the average isotropic chemical shift Ω (in ppm) are related by

$$\Phi = -\Omega^2 + a\Omega + b \quad (\text{Eq. 2})$$

Here,

$$a = 2\Omega_A - \Delta\omega$$

$$b = \Omega_A(\Delta\omega - \Omega_A)$$

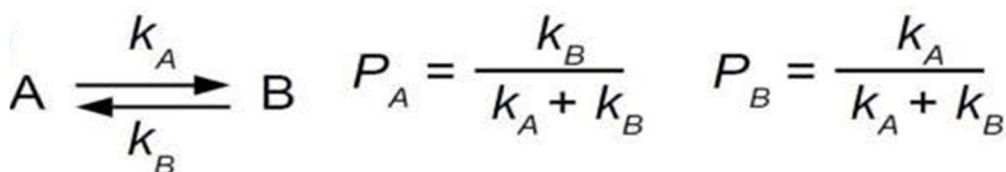
These can be rearranged as

$$\Delta\omega = (a^2 + 4b)^{1/2}, \text{ and } \Omega_{A,B} = [a \pm (a^2 + 4b)^{1/2}]/2 \quad (\text{Eq. 3})$$

Φ and Ω can be obtained experimentally at different temperatures. Assuming the chemical shift difference $\Delta\omega$ between major (A) and minor (B) species is constant, one can calculate $\Delta\omega$. From $\Delta\omega$ value and Φ values, populations can be extractable.

Directionality

For the chemical exchange between A and B, the exchange rate constant k is: $k_{ex} = k_A + k_B$. By using populations and k_{ex} one can extract rate constants k_A and k_B on both sides.



If a temperature independence within the varied range of 10 K is assumed, then the coefficients a and b can be determined by least squares optimization. Subsequently, $\Delta\omega$ is calculated by $\Delta\omega = (a^2 + 4b)^{1/2}$, and $\Omega_{A,B} = [a \pm (a^2 + 4b)^{1/2}]/2$. Once $\Delta\omega$ is known, P_A , P_B , k_A and k_B are obtained from

4. Relaxation Dispersion NMR to reveal fast Dynamics in Brønsted Acid Catalysis: Influence of Sterics and H-bond strength on conformations and substrate hopping

Φ_{ex} and k_{ex} at each temperature. Hence, in order to separate the populations and chemical shift difference from the term ϕ , it requires additional experimental $R_{1\rho}$ measurements at more than one temperature. Therefore, we measured $R_{1\rho}$ experiments for each sample at two or three temperatures (185 K, 180 K and 175 K).

4.6.6. Results of the $R_{1\rho}$ measurements

TRIP/3

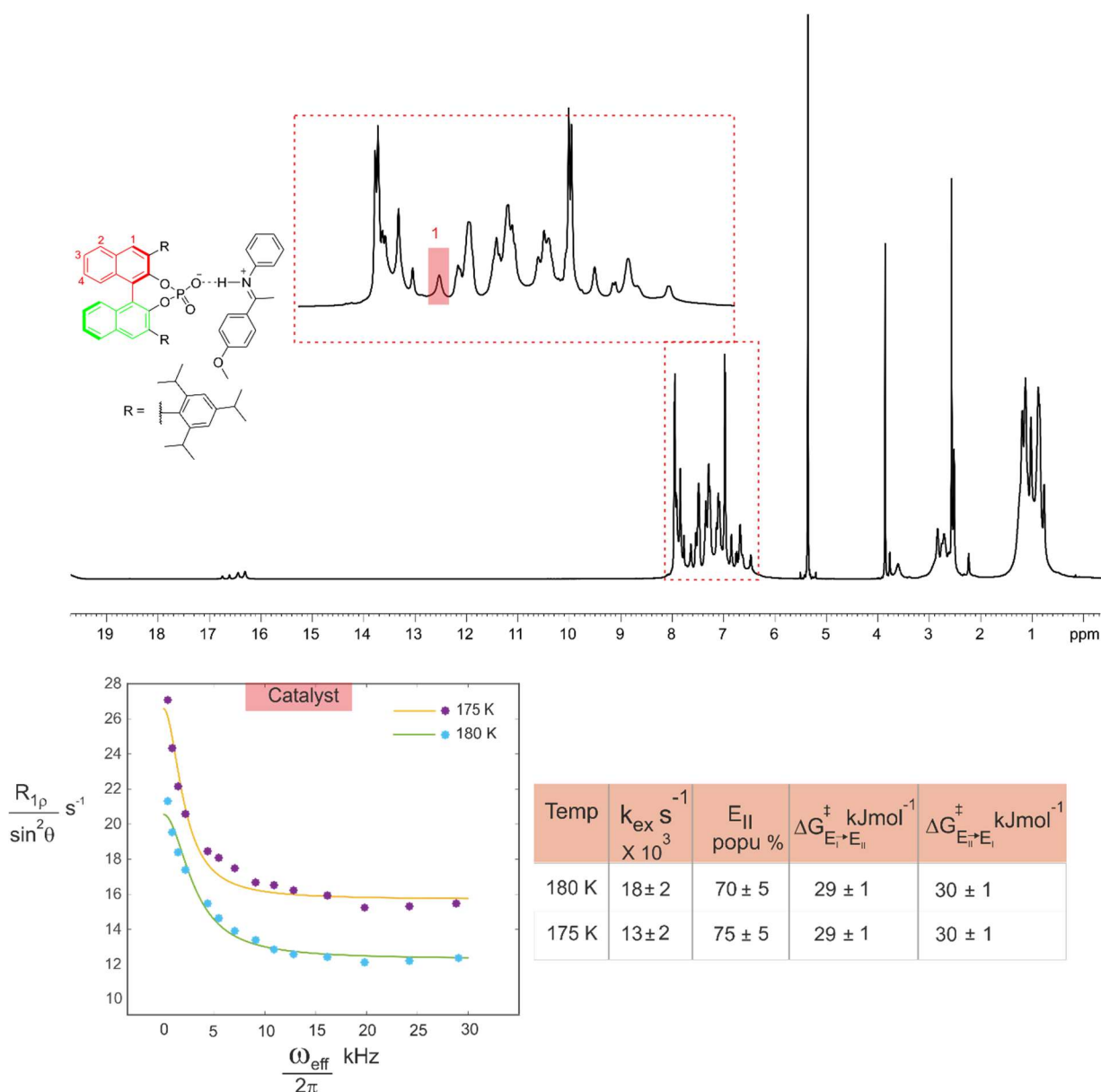


Figure S3: $R_{1\rho}$ measurement for the TRIP/3 complex. The proton H_1 of the catalyst (marked in the spectrum, red shaded) was selected as probe. The offset-Lorentzian decay indicates the presence of chemical exchange ($k_{\text{ex}} \approx 18000 \text{ s}^{-1}$ at 180 K). With experimental data obtained at two different temperatures, the populations and directionality were extracted.

4. Relaxation Dispersion NMR to reveal fast Dynamics in Brønsted Acid Catalysis: Influence of Sterics and H-bond strength on conformations and substrate hopping

TRIP/2

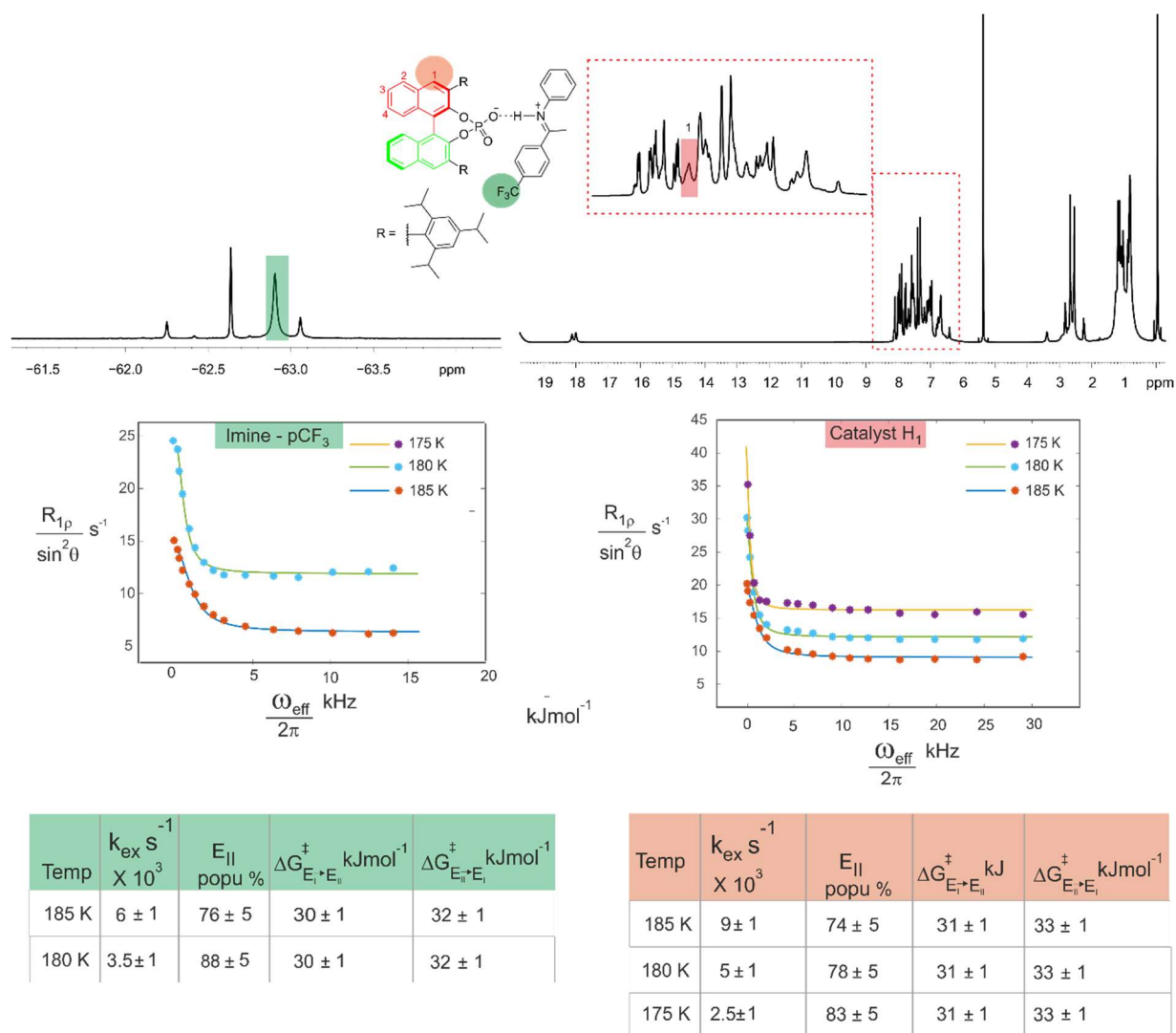


Figure S4: $R_{1\rho}$ measurement for TRIP/2 complex. The proton H_1 of the catalyst (shaded in red) and the fluorine signals of the imine- CF_3 group (shaded in green) were selected as probes. The offset-Lorentzian decay indicates presence of chemical exchange ($k_{\text{ex}} \approx 3\text{-}5 \cdot 10^3 \text{ s}^{-1}$ at 180 K). With experimental data obtained at three different temperatures, the populations and directionality were extracted.

4. Relaxation Dispersion NMR to reveal fast Dynamics in Brønsted Acid Catalysis: Influence of Sterics and H-bond strength on conformations and substrate hopping

TiPSY/1

Temp K	$k_{\text{ex}} \text{ s}^{-1} \times 10^3$	$E_{\text{II}} \%$	$\Delta G_{E_i \rightarrow E_i}^{\ddagger} \text{ kJ mol}^{-1}$	$\Delta G_{E_{ii} \rightarrow E_i}^{\ddagger} \text{ kJ mol}^{-1}$
185	3.0 ± 1	95 ± 5	32 ± 1	36 ± 1
180	2.5 ± 1	96 ± 4	32 ± 1	36 ± 1
175	2.5 ± 2	95 ± 5	31 ± 1	35 ± 1

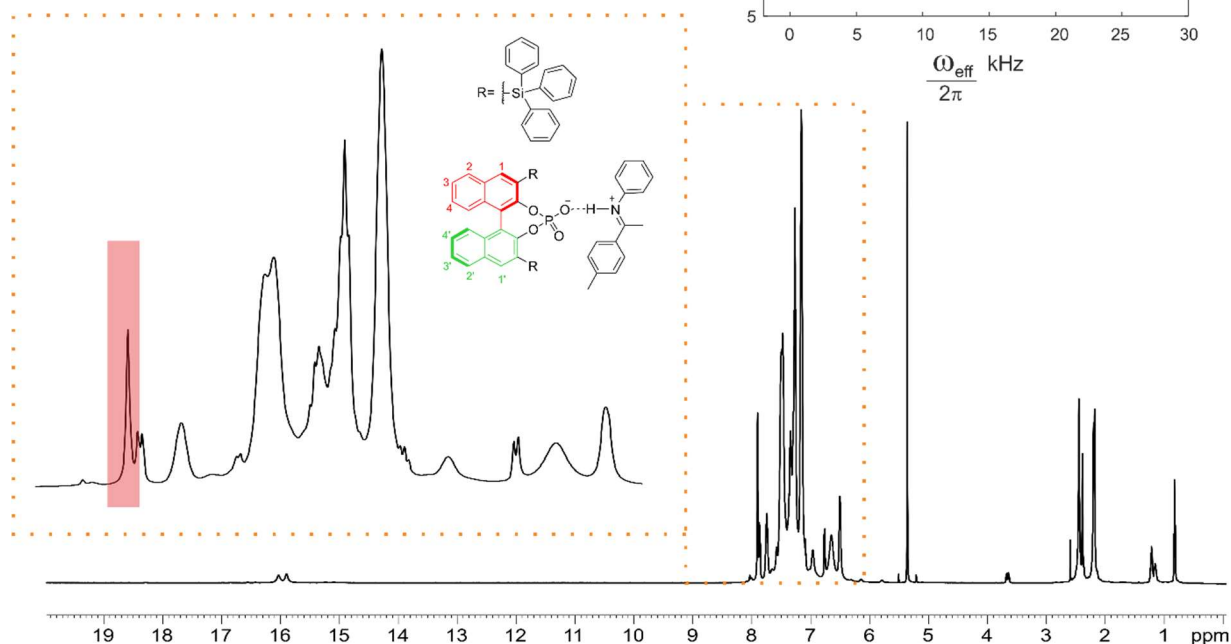
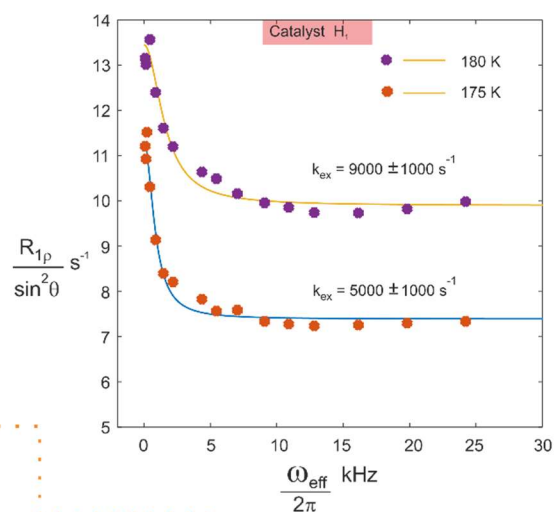


Figure S5: R_{1p} measurement for TiPSY/1 complex, (to avoid signal overlap, the sample was prepared with nearly exclusive population of the *E*-complex; see above for sample preparation). The proton H₁ of the catalyst (shaded in red) was selected as probe. The offset-Lorentzian decay indicates presence of chemical exchange ($k_{\text{ex}} \approx 9 \text{ ks}^{-1}$ at 180 K).

4. Relaxation Dispersion NMR to reveal fast Dynamics in Brønsted Acid Catalysis: Influence of Sterics and H-bond strength on conformations and substrate hopping

TRIM/2 and TRIM/3

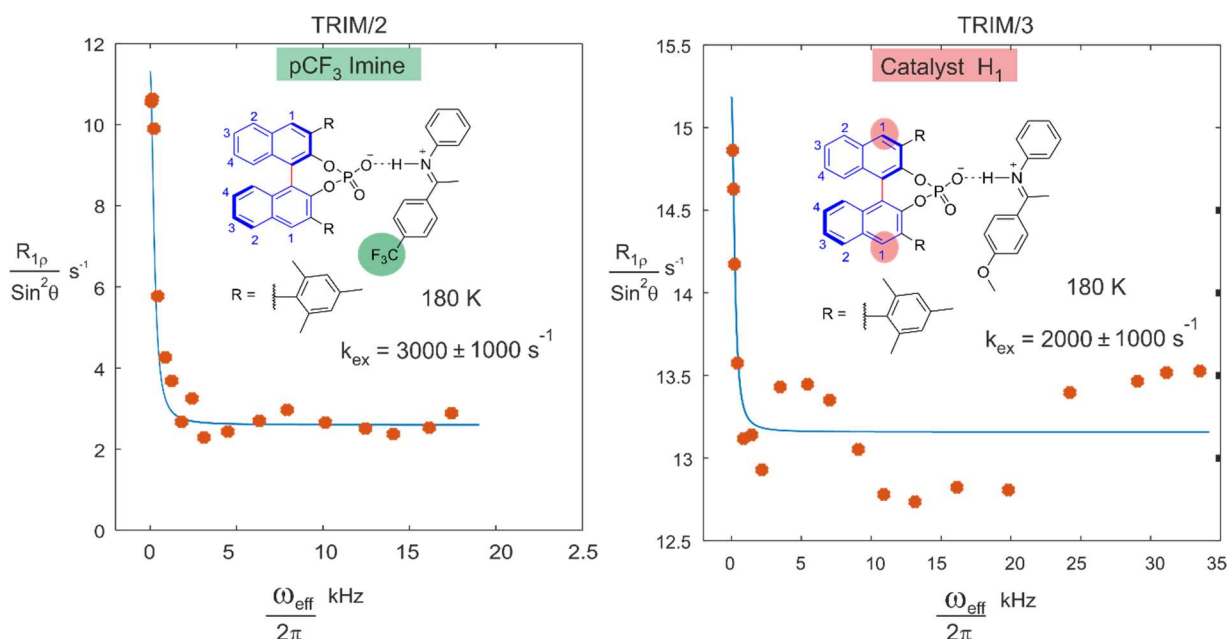


Figure S6: $R_{1\rho}$ measurements for TRIM/2 and TRIM/3 complexes. For TRIM/2, the CF₃ group of the imine was used as a probe (shaded in green) and for TRIM/3 the proton H₁ of the catalyst (shaded in red) was selected as probe. The offset-Lorentzian decay in both system indicates the presence of chemical exchange ($k_{\text{ex}} \approx 2000\text{-}3000$ s⁻¹ at 180 K).

For TRIM/2 and TRIM/3, the offset-Lorentzian decay fit does not match the experimental decay as precisely as for the other systems. Hence, a larger experimental error is expected. However, the $R_{1\rho}$ measurements for TRIM/2 and TRIM/3 complexes indicate that similar exchange rates ($k_{\text{ex}} \approx 2000\text{-}3000$ s⁻¹ at 180 K) are obtained for TRIM/1-3 regardless of the hydrogen bond strength.

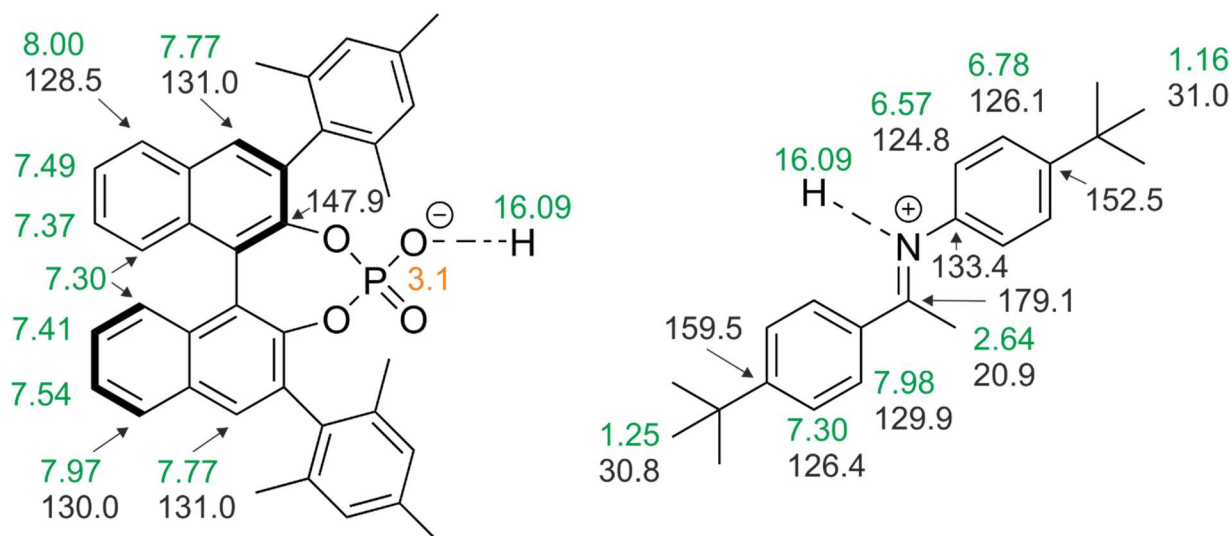
4.6.7. NMR-Structural analysis of CPA/imine complexes

The investigated complexes TRIP/1-3, TiPSY/1 and TRIM/1-3 were already described in the previous work.^{2,9} The NMR-structural analysis of TRIM/4 is described below. In addition, the backbone splitting of TiPSY/1 is discussed in detail below.

Chemical Shift assignment of TRIM/4

The ¹H (black) and ¹³C (green) chemical shifts (in ppm) of all investigated complexes were assigned with standard 2D NMR experiments (¹H,¹H COSY, ¹H,¹H TOCSY, ¹H,¹H NOESY, ¹H,¹³C HSQC, ¹H,¹³C HMBC) at 180 K. The ³¹P (orange) chemical shift (in ppm) was assigned by ¹H,³¹P HMBC. Due to signal overlap and lacking resolution and intensity of 2D correlations, not all signals could be assigned.

4. Relaxation Dispersion NMR to reveal fast Dynamics in Brønsted Acid Catalysis: Influence of Sterics and H-bond strength on conformations and substrate hopping



In accordance with our previous analysis of hydrogen bond strengths,¹ the ^1H chemical shift of the hydrogen bond strength reflects the H-bond strength (in our system, higher chemical shifts correlate with stronger H-bonds). Hence, the H-bond strength of TRIM/**4E** (16.09 ppm) is in between TRIM/**1E** (16.26 ppm) and TRIM/**3E** (15.80 ppm).⁹

Identification of Type I E and Type II E

Analogous to our previous work,^{2,9} for the *Type I E* structure, the *tert*-butyl group of the ketone part of the imine (marked in blue) is placed above the BINOL backbone. The blue NOE cross signals A and B to the Naphthyl backbone reveal the presence of the *Type I E* structure (Figure 7) for TRIM/**4E**. The NOE cross signal D (black) is a result of overlapping NOE signals between the *tert*-butyl group and the naphthyl backbone and the *tert*-butyl group and the attached phenyl ring (backbone: 8.00 ppm, phenyl ring of imine: 7.98 ppm). For the *Type II E* structure, the *tert*-butyl group of the aniline part of the imine is placed above the BINOL backbone and thus the red NOE cross signals A-D reveal the presence of the *Type II E* structure.

4. Relaxation Dispersion NMR to reveal fast Dynamics in Brønsted Acid Catalysis: Influence of Sterics and H-bond strength on conformations and substrate hopping

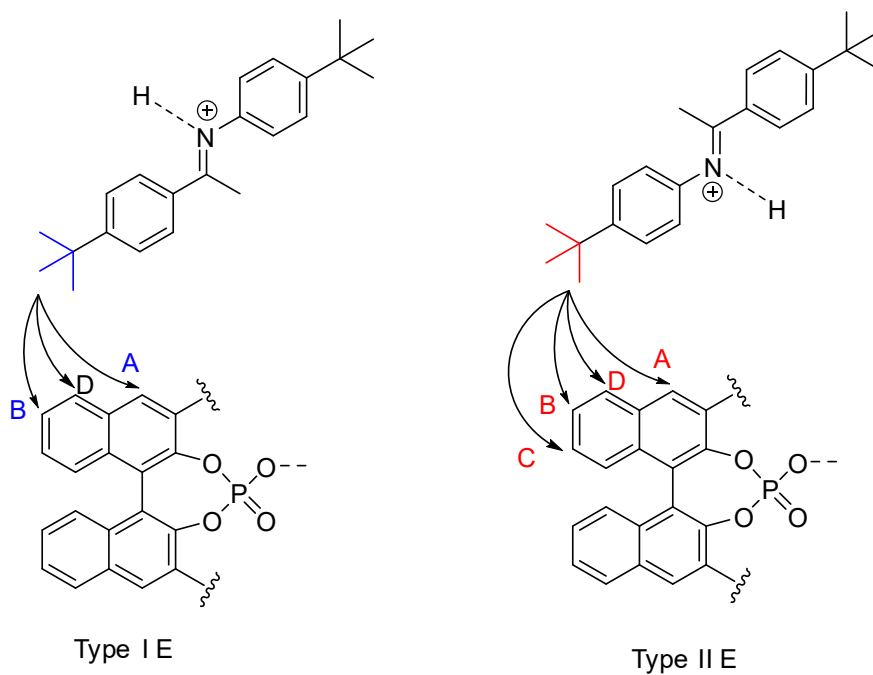
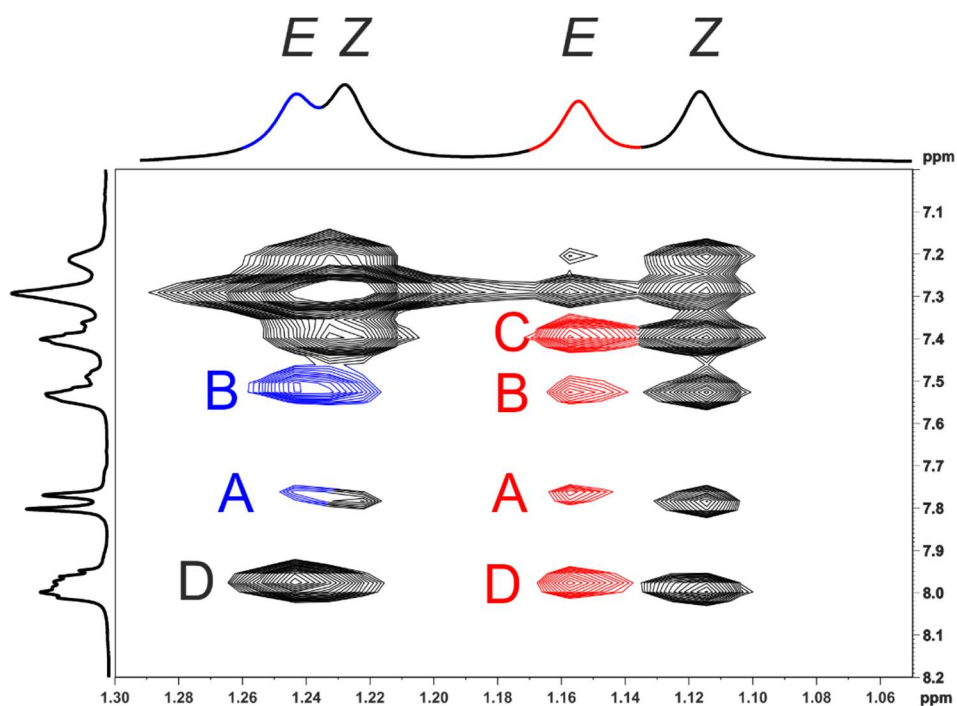


Figure S7: Excerpt of the $^1\text{H},^1\text{H}$ NOESY spectrum of TRIM/4 at 180 K and 600 MHz (100 mM sample) in CD_2Cl_2 . The blue NOE cross signals indicate the presence of the *Type I E* structure, while the red NOE signals indicate the presence of the *Type II E* structure.

4. Relaxation Dispersion NMR to reveal fast Dynamics in Brønsted Acid Catalysis: Influence of Sterics and H-bond strength on conformations and substrate hopping

DOSY measurements of TRIM/4

To prove that the observed species in TRIM/4 are monomers of the binary complexes, DOSY measurements (Diffusion ordered spectroscopy) were performed to derive the molecular radii of the present species.

The DOSY measurements were performed with the convection suppressing DSTE (double stimulated echo) pulse sequence developed by Jerschow and Müller in a pseudo 2D mode.¹⁰ TMS was used to reference the viscosity of the solvent at 180 K. The diffusion time delay was set to 45 ms. The gradient pulse lengths (p16, SMSQ10.100 pulse shape) were optimized for each species to give a sigmoidal signal decay for varying gradient strengths. Optimal pulse lengths of 3.0 ms and 6.0 ms were found for TMS and TRIM/4, respectively. For each species, twenty spectra with linear varying gradient strength of 5% - 95% have been measured. The used probe signals for the analysis are listed in table S1. The signal intensities of the respective groups were analyzed as a function of the gradient strength by Bruker TopSpin 3.2 software T1/T2 relaxation package by employing the Stejskal-Tanner equation.¹¹ No line broadening occurred for increasing gradient strength. The sigmoidal fit provided the translational self-diffusion coefficients D_i listed in Table S1. The molecular radii were derived by the Stokes-Einstein equation¹² using Chens correction.¹³

$$D_i = \frac{k_B T}{6\pi\eta r_H} * (1 + 0.695 * (\frac{r_{solv}}{r_H})^{2.234}) \quad (Eq. 4)$$

D_i is the self-diffusion coefficient derived by the measurement, η is the viscosity of the solvent, r_H is the hydrodynamic radius of the observed molecule and r_{solv} the radius of the solvent. No form factor correction was applied. The viscosity was determined by measuring the diffusion coefficient of the reference tetramethylsilane (TMS) and solving the equation for η with the literature value¹⁴ of the radius of 2.96 Å. The solvent radius of CD_2Cl_2 (2.46 Å) was taken from the reference.¹⁵

Table S1: Probe signals, measured diffusion coefficients and derived molecular radii for TRIM/5.

Entry	Species	p16 [ms]	Observed signal [ppm]	D_i [m^2/s] · 10 ⁻¹²	Averaged	r_H [Å]
1	TMS	3.10	0.00	21.32		
2	TRIM/4E	6.00	1.16	4.76		
3	TRIM/4E	6.00	2.64	4.80	4.69	9.54
4	TRIM/4E	6.00	7.77	4.50		

The derived molecular radius (9.54 Å) is similar to the one reported previously for TRIM monomers.⁹ Thus, the DOSY measurements showed that the species investigated by the $R_{1\rho}$ measurement is the binary TRIM/4E complex.

4. Relaxation Dispersion NMR to reveal fast Dynamics in Brønsted Acid Catalysis: Influence of Sterics and H-bond strength on conformations and substrate hopping

Estimation of the rotational correlation time of binary CPA/imine complexes

A general rotational correlation time of 10-50 ns was estimated for the investigated binary complexes of chiral phosphoric acids and imines with their hydration shell. Stokes Law (Eq. 5) was used to calculate the rotational correlation time based on the results of the DOSY measurements of TRIM/**4E**.

$$\tau_c = \frac{4\pi\eta r^3}{3kT} \quad (\text{Eq. 5})$$

The radius of the binary complex of TRIM/**4** with its hydration shell was determined by DOSY measurements (see respective chapter) and a radius of 9.54 Å was determined for the complex with its hydration shell. The viscosity ($3.05 \cdot 10^{-2} \text{ kg m}^{-1} \text{ s}^{-1}$) of the solution at 180 K was determined by Equation 4 based on the DOSY measurement on TMS. A rotational correlation time of 44.6 ns was calculated for TRIM/**4E** with its hydration shell. Given the bulkiness of the two tert-butyl substituents of imine **4**, it is expected that the other investigated complexes have smaller radii, resulting in smaller rotational correlation times. Hence, a general rotational correlation time around 10 – 50 ns was estimated.

TiPSY/**1**

In the TiPSY/**1** complex, the backbone splitting could not be resolved at 180 K and 600 MHz in CD₂Cl₂ (see figure). However, in our previous investigations we observed that the backbone splitting in TiPSY complexes is very small and could often not be resolved sufficiently (see SI of literature).⁹ Goodman *et al.* demonstrated that the binding pocket for TiPSY is significantly smaller than for TRIP (no rotation possible).¹⁶ The biggest binding pocket for the investigated CPAs was determined for TRIM (rotation possible). Hence, a rotation of the imine inside the binding pocket of TiPSY can be excluded, even if the backbone splitting can not be resolved sufficiently.

The sample was prepared with an exclusive population of the *E*-imine. To achieve that, the sample was prepared according to the general procedure described above. However, before adding the solvent, the NMR-tube with TiPSY and **1** was cooled to -90 °C in acetone/liquid N₂ and the precooled solvent was added to the tube. The low temperature suppressed *E*→*Z* isomerization of the imine.

4. Relaxation Dispersion NMR to reveal fast Dynamics in Brønsted Acid Catalysis: Influence of Sterics and H-bond strength on conformations and substrate hopping

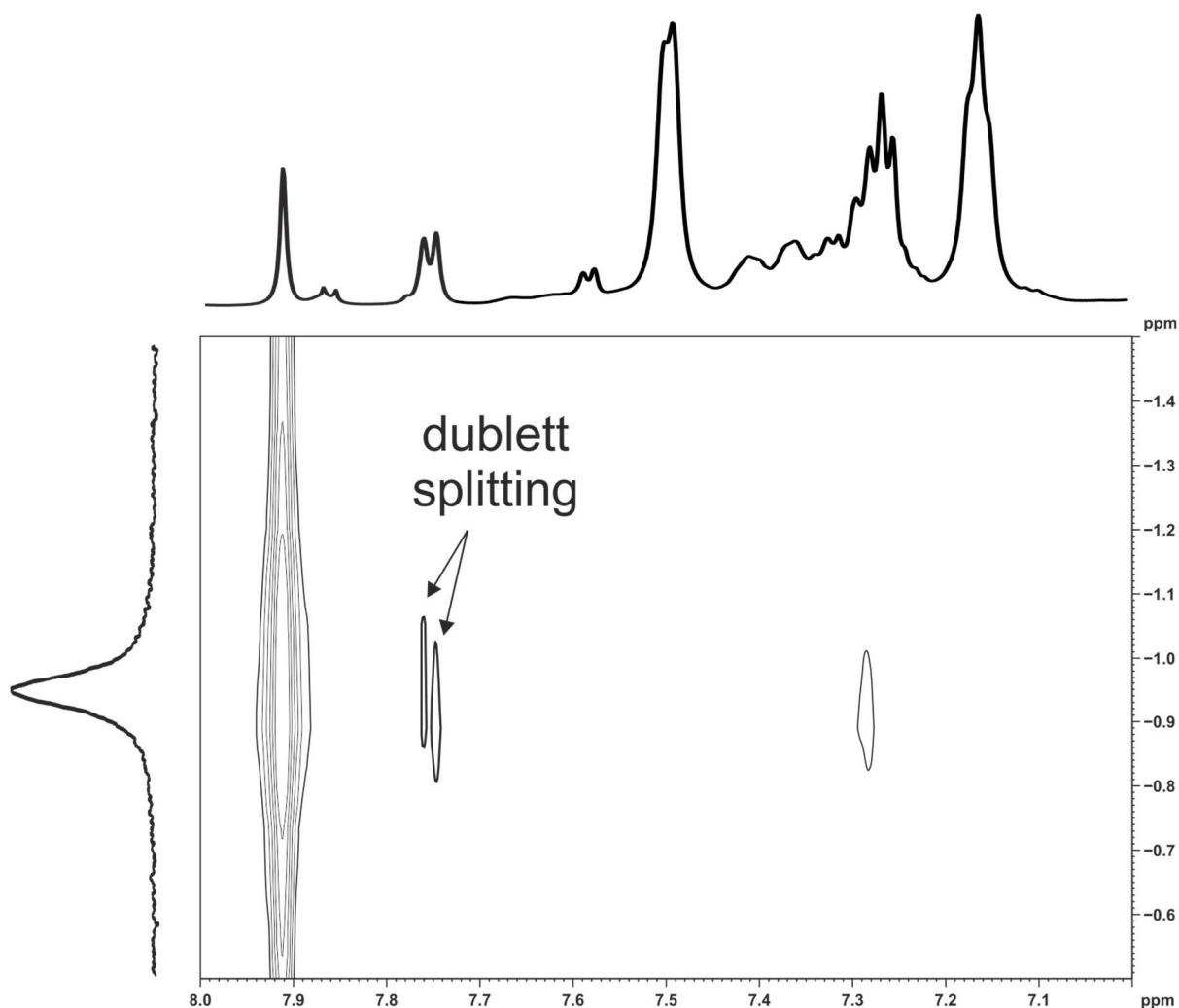


Figure S8: Excerpt of the $^1\text{H},^{31}\text{P}$ HMBC spectrum of TiPSY/1 (E-only, 25 mM, TiPSY:1 = 1:1) at 180 K and 600 MHz in CD_2Cl_2 . The sample was prepared with an exclusive population of E-imine species.

Exchange with free imines

Typically, in 1:1 complexes of TRIP, TRIM and TiPSY, the complexation of the imine was incomplete ($\approx 25\%$ free imine present). Thus, for complexes with imines **1-3**, the assignment of the free imines was done for the CPA/imine samples. For imine **4**, a NMR sample with the imine only (50 mM, CD_2Cl_2 , 180 K and 600 MHz) was measured and compared to the chemical shifts in the CPA/**4** sample. For TRIM/**4**, no free imine was observed in the binary complex sample.

As the free imines **1-4** gave chemical shifts well separated from the respective CPA/E-imine complexes (see figure 9 for free imines and assignments of the binary complex in literature^{2,9}), the exchange between free and complexed imine is slow on the NMR time scale. Thus, the exchange pathway via dissociation and re-association causing averaging of the BINOL backbone can be excluded to significantly contribute to the measured exchange rates in the R_{10} measurements.

4. Relaxation Dispersion NMR to reveal fast Dynamics in Brønsted Acid Catalysis: Influence of Sterics and H-bond strength on conformations and substrate hopping

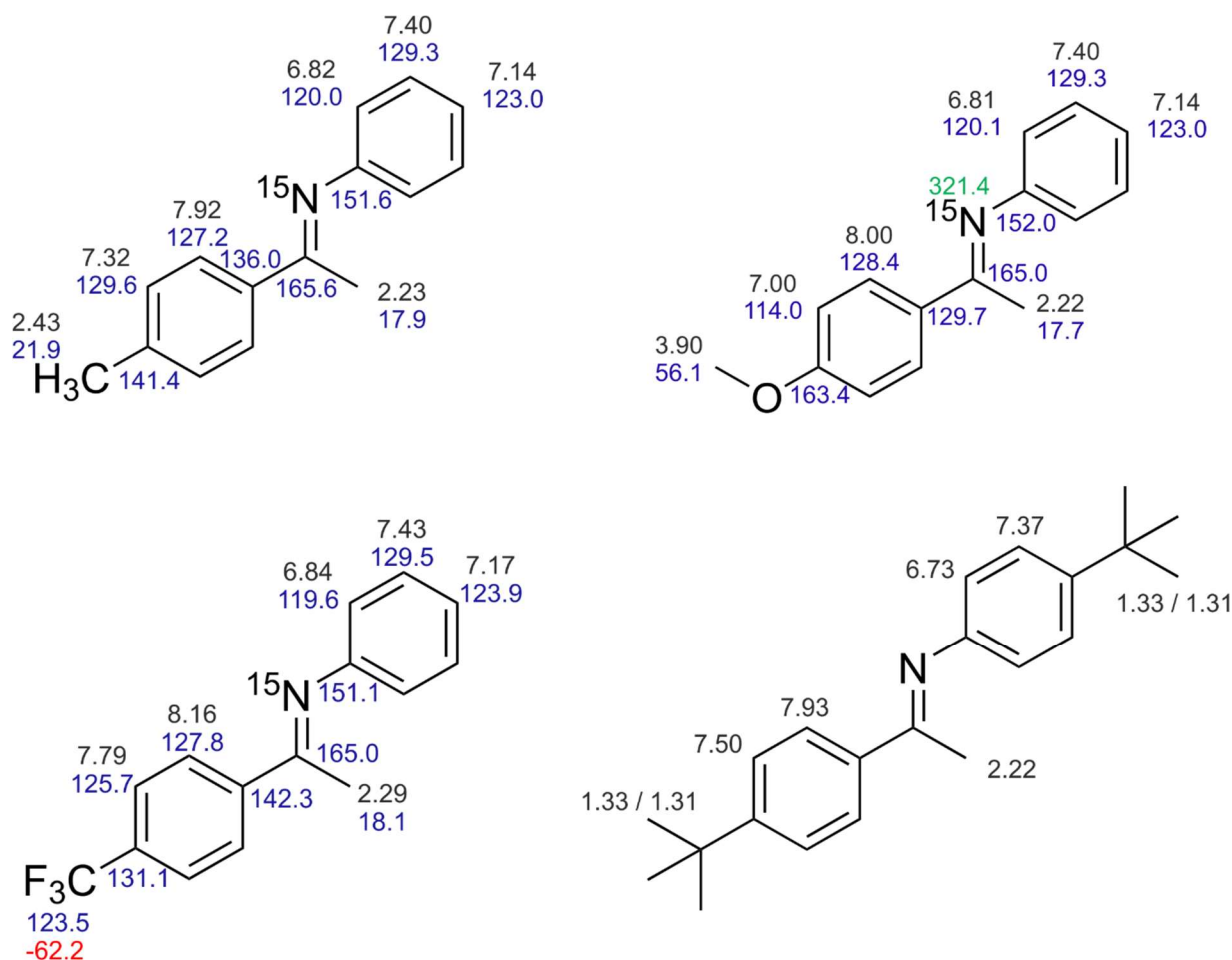


Figure S9: Chemical shift assignment of the free imines **1-4** at 180 K in CD_2Cl_2 .

Additional fitting of TRIM/**1E**

Due to the strong signal decay within the first few percent of the horizontal axis for TRIM/**1E** (Figure 6B in the manuscript), fewer data points are in the decay region relevant for the fit, which could affect the quality of the fit and thus the precision of the extracted rate. However, the fit curves for lower (500 s^{-1}) and higher ($10\,000 \text{ s}^{-1}$) exchange rates as the optimized one (2500 s^{-1}) significantly deviate from the data set (Figure 10). In addition, a TRIM/**1E** sample at different concentration (0.25 mM) was measured with more ω_{eff} increments. The extracted exchange rate of 2500 s^{-1} is identical to the previous one and the fit for lower or higher exchange rates does not match the data set (Figure 11).

Hence, the quality of the fit for TRIM/**1E** is adequately precise to reveal that the exchange rate for TRIM/**1E** is significantly lower than for TRIP/**1E** ($\approx 10\,000 \text{ s}^{-1}$).

4. Relaxation Dispersion NMR to reveal fast Dynamics in Brønsted Acid Catalysis: Influence of Sterics and H-bond strength on conformations and substrate hopping

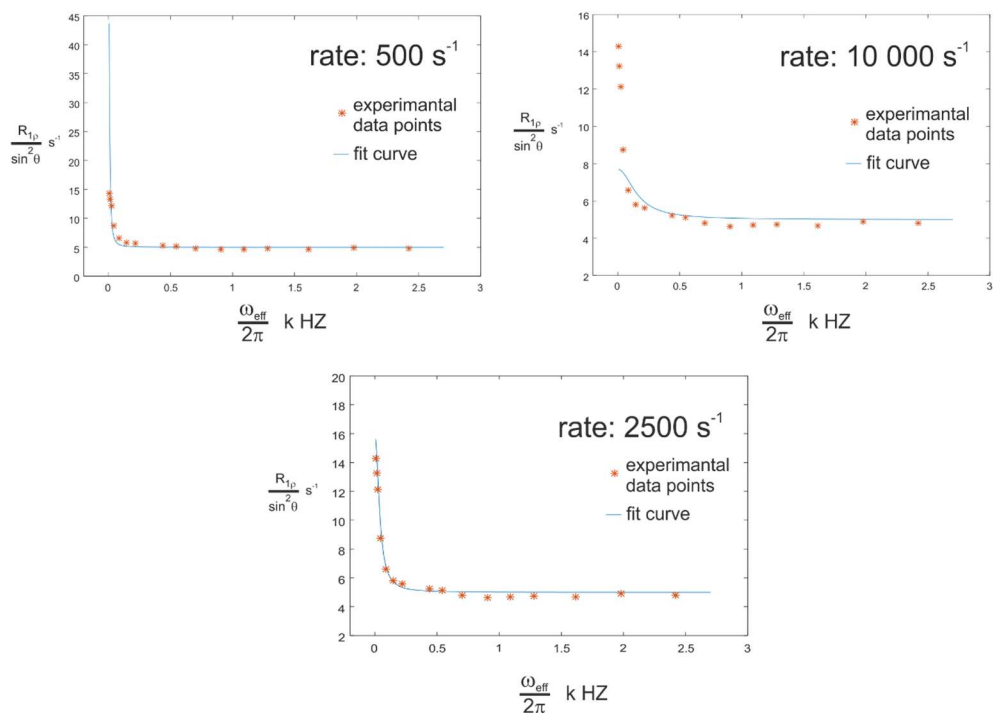


Figure S10: Additional curve fitting for the signal decay of TRIM/1E with different exchange rates at a concentration of 5 mM. The determined exchange rate of 2500 s^{-1} fits the data set best, while lower or higher exchange rates result in a significant offset. Other parameters, e.g. the population of E-I and E-II were not changed.

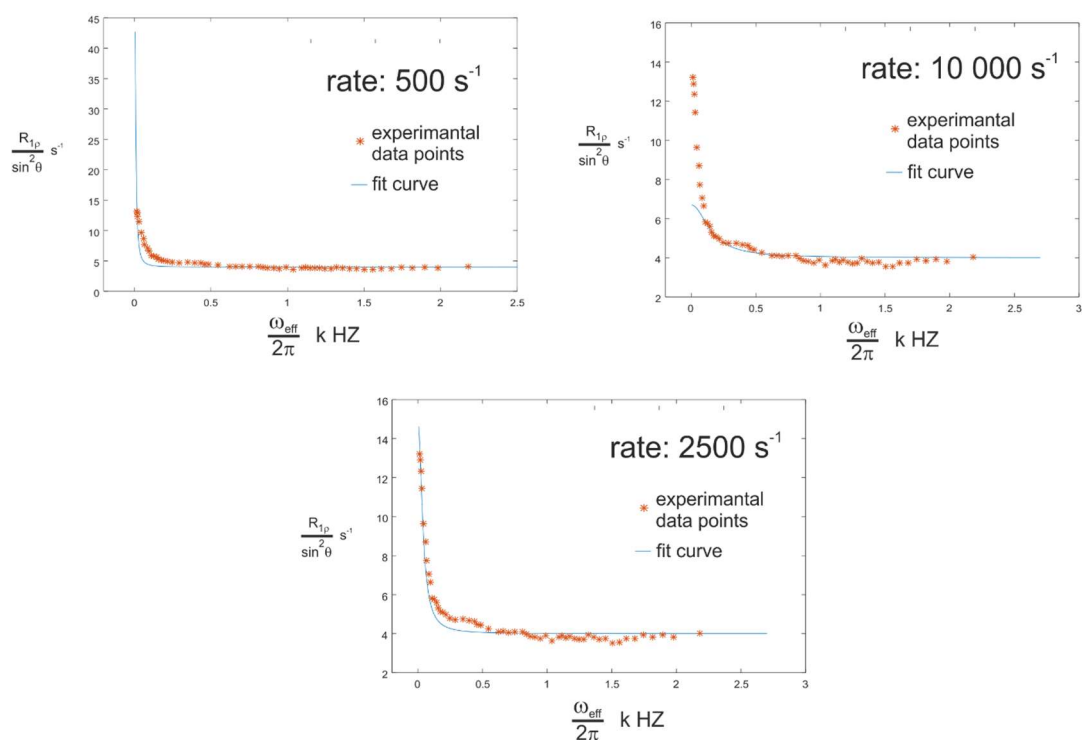


Figure S10: Additional curve fitting for the signal decay of TRIM/1E with different exchange rates at a concentration of 0.25 mM and additional ω_{eff} increments. The determined exchange rate of 2500 s^{-1} fits the data set best, while lower or higher exchange rates result in a significant offset. Other parameters, e.g. the population of E-I and E-II were not changed.

4. Relaxation Dispersion NMR to reveal fast Dynamics in Brønsted Acid Catalysis: Influence of Sterics and H-bond strength on conformations and substrate hopping

4.6.8. References

- (1) Sorgenfrei, N.; Hioe, J.; Greindl, J.; Rothermel, K.; Morana, F.; Lokesh, N.; Gschwind, R. M. NMR Spectroscopic Characterization of Charge Assisted Strong Hydrogen Bonds in Brønsted Acid Catalysis. *J. Am. Chem. Soc.* **2016**, *138* (50), 16345–16354.
- (2) Greindl, J.; Hioe, J.; Sorgenfrei, N.; Morana, F.; Gschwind, R. M. Brønsted Acid Catalysis-Structural Preferences and Mobility in Imine/Phosphoric Acid Complexes. *J. Am. Chem. Soc.* **2016**, *138* (49), 15965–15971.
- (3) Aznar, F.; Valde, C. Modular Synthesis of Indoles from Imines and o-Dihaloarenes or o-Chlorosulfonates by a Pd-Catalyzed Cascade Process. *J. Am. Chem. Soc.* **2009**, *131* (8), 4031–4041.
- (4) Schramm, Y.; Barrios-Landeros, F.; Pfaltz, A. Discovery of an Iridacycle Catalyst with Improved Reactivity and Enantioselectivity in the Hydrogenation of Dialkyl Ketimines. *Chem. Sci.* **2013**, *4*, 2760–2766.
- (5) Harris, R. K.; Becker, E. D.; Cabral de Menezes, S. M.; Goodfellow, R.; Granger, P. NMR Nomenclature: Nuclear Spin Properties and Conventions for Chemical Shifts. IUPAC Recommendations 2001. International Union of Pure and Applied Chemistry. Physical Chemistry Division. Commission on Molecular Structure and Spectroscopy. *Magn. Reson. Chem.* **2002**, *40* (7), 489–505.
- (6) Trigo-Mouriño, P.; Griesinger, C.; Lee, D. Label-Free NMR-Based Dissociation Kinetics Determination. *J. Biomol. NMR* **2017**, *69* (4), 229–235.
- (7) Akke, M.; Palmer, A. G. Monitoring Macromolecular Motions on Microsecond to Millisecond Time Scales by R 1 ρ -R 1 Constant Relaxation Time NMR Spectroscopy. *J. Am. Chem. Soc.* **1996**, *118* (4), 911–912.
- (8) Palmer, A. G.; Kroenke, C. D.; Loria, J. P. *Nuclear Magnetic Resonance Methods for Quantifying Microsecond-to-Millisecond Motions in Biological Macromolecules*; Elsevier Masson SAS, 2001; Vol. 339.
- (9) Melikian, M.; Gramüller, J.; Hioe, J.; Greindl, J.; Gschwind, R. M. Brønsted Acid Catalysis – the Effect of 3,3'-Substituents on the Structural Space and the Stabilization of Imine/Phosphoric Acid Complexes. *Chem. Sci.* **2019**, *10*, 5226–5234.
- (10) Jerschow, A.; Müller, N. Suppression of Convection Artifacts in Stimulated-Echo Diffusion Experiments. Double-Stimulated-Echo Experiments. *J. Magn. Reson.* **1997**, *125* (2), 372–375.
- (11) Stejskal, E. O.; Tanner, J. E. Spin Diffusion Measurements: Spin Echoes in the Presence of a Time-Dependent Field Gradient. *J. Chem. Phys.* **1965**, *42* (1), 288–292.
- (12) MacChioni, A.; Ciancaleoni, G.; Zuccaccia, C.; Zuccaccia, D. Determining Accurate Molecular Sizes in Solution through NMR Diffusion Spectroscopy. *Chem. Soc. Rev.* **2008**, *37* (3), 479–489.
- (13) Chen, H. C.; Chen, S. H. Diffusion of Crown Ethers in Alcohols. *J. Phys. Chem.* **1984**, *88* (21), 5118–5121.
- (14) Ben-Amotz, D.; Willis, K. G. Molecular Hard-Sphere Volume Increments. *J. Phys. Chem.* **1993**, *97* (29), 7736–7742.
- (15) Zuccaccia, D.; Macchioni, A. An Accurate Methodology to Identify the Level of Aggregation in Solution by PGSE NMR Measurements: The Case of Half-Sandwich Diamino Ruthenium(II) Salts. *Organometallics* **2005**, *24* (14), 3476–3486.
- (16) Reid, J. P.; Goodman, J. M. Goldilocks Catalysts: Computational Insights into the Role of the 3,3' Substituents on the Selectivity of BINOL-Derived Phosphoric Acid Catalysts. *J. Am. Chem. Soc.* **2016**, *138* (25), 7910–7917.

4.7. Additional Findings

4.7.1. Introduction

London dispersion, the attractive part of the Van der Waals potential is ubiquitously present and pairwise additive, but nevertheless frequently neglected and underestimated, especially in the field of asymmetric catalysis.^[1] Especially organocatalysts such as chiral phosphoric acids feature extended aromatic systems and/or bulky alkyl systems, which can form π - π , σ - π and σ - σ interactions. In the binary CPA/imine complexes resembling catalytic intermediates, non-covalent interaction analysis and computations showed that London dispersion interactions strongly contribute to the structure and stabilization of these intermediates.^[2,3] However, no general concept on how to beneficially exploit London dispersion in catalysis has emerged yet.^[1]

In order to do so, it is crucial to study and quantify the effect of dispersion energy donor (DED) substituents in real catalytic systems as well as read out their effect in the corresponding stereoselectivities. The combination of low temperature NMR and the relaxation dispersion $R_{1\rho}$ method allows to drastically enhance the time resolution of NMR and access exchange rates as well as populations of fast exchanging conformers. This offers the unique opportunity to use the equilibrium between the Type I E and Type II E CPA/imine conformers (see chapter 4.2 figure 1B, chapter 4.3 figure 2) as a molecular balance system to quantify the interaction energy between imine substituents and the BINOL backbone of the CPA catalyst (see Figure 10 blue arrow).

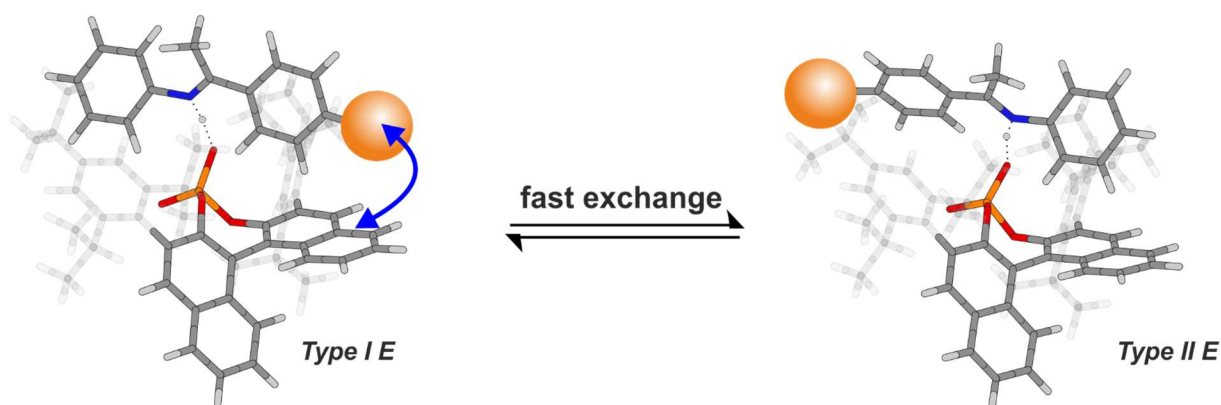


Figure 10: Molecular balance system based on the fast exchanging Type I E and Type II E conformers of CPA/imine complexes. In the Type I E structure, the imine substituent in *para* position interacts with the BINOL backbone of the catalyst, while in the Type II E structure it is directed away and can interact with the 3,3'-substituent (shown in transparent).

While in the Type I E structure the *para*-substituent of the imine is placed on top of the BINOL backbone, it is directed away in the Type II E structure, where only an interaction to the 3,3'-substituent of the catalyst is possible. For catalysts with small 3,3'-substituents the latter interaction might be negligible and thus the energetic difference ΔG between Type I E and Type II E derived from the population difference is modulated by the interaction between imine substituent and BINOL backbone. It was

4. Relaxation Dispersion NMR to reveal fast Dynamics in Brønsted Acid Catalysis: Influence of Sterics and H-bond strength on conformations and substrate hopping

shown that the structure of CPA/imine complexes is highly conserved regarding changes of the imine and 3,3'-substituent.^[4] Thus, similar to a double mutant cycle^[5] a reference system e.g. with a hydrogen atom as imine substituent can be used to obtain the $\Delta\Delta G = \Delta G_{\text{DED}} - \Delta G_{\text{reference}}$ value which reflects the interaction energy between imine substituent and BINOL backbone as a measure of the dispersion energy donor capability of different residues.

Hence, to validate the applicability of this conformational molecular balance, CPA/imine systems were studied to control, if the interaction between imine substituent and 3,3'-substituent can be neglected and if the exchange rates and populations of the Type I *E* and Type II *E* conformers in these systems can be accessed by $R_{1\rho}$ measurements.

4.7.2. Extension of model systems

In the previous work, binary CPA/imine complexes of TRIP and TRIM with imines **1-4** were studied (see chapter 4.3). For the conformational balance system, catalysts TRIM and Ph-CPA were selected to reduce the size of the 3,3'-substituent in order to prevent an interaction between 3,3'-substituent and imine substituent (see figure 11). Imines **5** and **6** bearing a ^tBu or ⁱPr group were selected to increase the size and dispersion energy donor capability (in comparison to imine **1**), while imine **7** was selected to account for different substituent effects on the electrostatic properties of the phenyl ring and their subsequent impact on the interaction profile between the phenyl ring and the BINOL backbone.

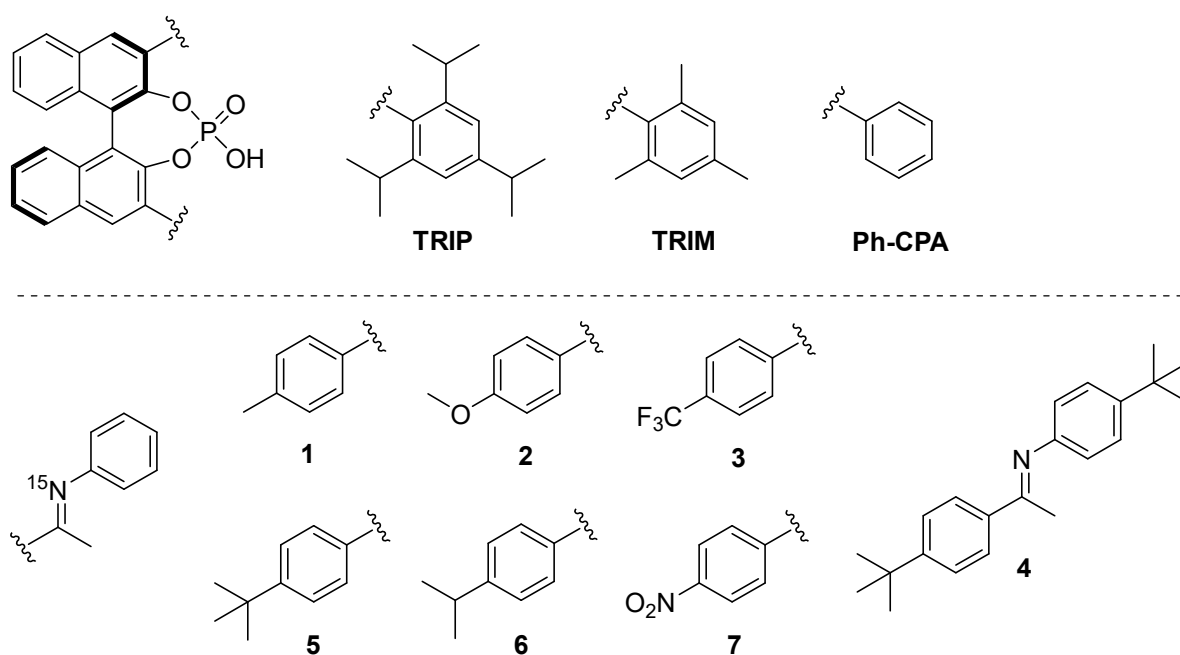


Figure 11: Extension of model systems for the conformational molecular balance. TRIM and Ph-CPA were selected to reduce the size of the 3,3'-substituent, while imine **5-7** were selected to modulate the dispersion energy donors and electrostatic properties of the imine.

4. Relaxation Dispersion NMR to reveal fast Dynamics in Brønsted Acid Catalysis: Influence of Sterics and H-bond strength on conformations and substrate hopping

First, binary TRIM/5-7 samples were investigated to ensure the presence of the Type I *E* and Type II *E* conformation as well as conservation of the structure. Analogous to previous studies, all NMR measurements were performed at 180 K in CD₂Cl₂ to obtain an optimally resolved spectrum. In the hydrogen bond region of the spectra, the signals of the binary TRIM/imine complexes featuring either the *E*- or *Z*-imine could be clearly identified (see figure 12 red signals; due to the ¹⁵N labelling, the signals show doublet splitting). Additionally, similar to previous studies on TRIM/imine systems, an additional high-field shifted hydrogen bond signal is monitored, reflecting [TRIM/imine]₂ dimers (figure 12, blue signal).^[4] For TRIM/7, additional signals were observed which likely correspond to TRIM/TRIM/7 complexes and potentially the free acid (figure 12, purple signal).^[6]

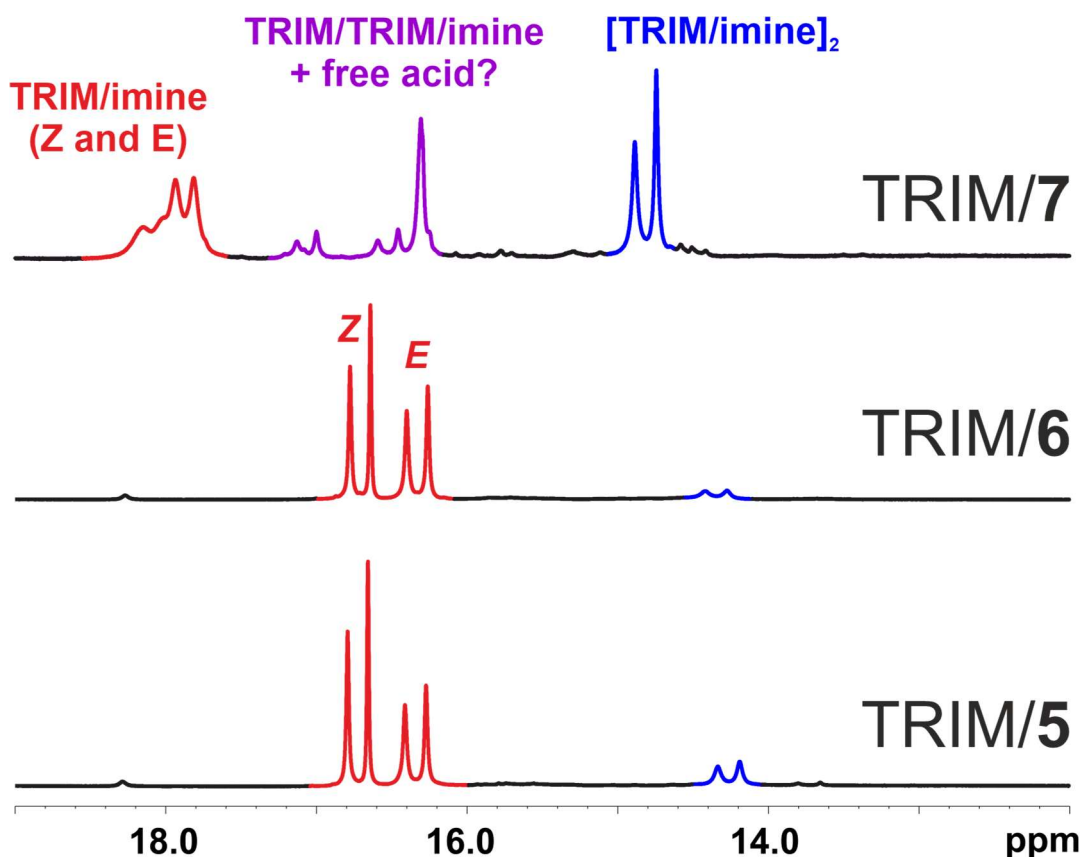


Figure 12: Hydrogen bond region of TRIM/5-7 at a ratio of 1:1 and a concentration of 100 mM at 180 K and 600 MHz in CD₂Cl₂. The binary TRIM/imine complexes are marked in red (*Z* and *E*), the dimeric [TRIM/imine]₂ complexes are marked in blue and the signals likely corresponding to TRIM/TRIM/7 and free TRIM are marked in purple. Only the binary TRIM/imine complexes (red) were analysed in detail.

Based on a series of homo- and heteronuclear 1D and 2D NMR spectra, a chemical shift assignment for TRIM/5 and TRIM/6 could be achieved. This allowed to identify the chemical shifts of the BINOL backbone for TRIM/5*E* and TRIM/6*E*, which are the necessary probe signals for the R_{1ρ} measurements. Analysis of the NOESY spectrum revealed the presence of the Type I *E* and Type II *E* structure and confirmed the fast exchange process between them (they appear as one averaged set of signals at 180 K). This furthermore validated the conservation of the Type I *E* and Type II *E* structure and ensured comparability with the previous measurements.

4.7.3. $R_{1\rho}$ measurements and detailed structural analysis

In order to validate if the exchange rate and population difference between Type I *E* and Type II *E* in TRIM/5 and TRIM/6 can be accessed, relaxation dispersion $R_{1\rho}$ NMR measurements at three different temperatures were performed. In the previous work, for TRIM/1-3*E* the rotation of the imine inside the binding pocket was the monitored process. For TRIM/4*E*, the additional steric bulk of the imine hindered this rotation and thus the switching process would be monitored, but was not accessible as it was too fast. Thus, in order to access the conformational equilibrium between Type I *E* and Type II *E*, fast rotation of the imine inside the binding pocket must be possible. For TRIM/6*E*, the standard temperatures 175, 180 and 185 K were selected in analogy to the previous measurements. For TRIM/5*E* signal splitting of the BINOL backbone was observed at 175 K and coalescence at 180 K (see figure 13), which clearly indicates that fast rotation of the imine inside the binding pocket is not possible anymore (see chapter 4.3 figure 2). However, increasing the temperature to 195 – 205 K lead to averaging and narrowing of the BINOL backbone signals (see figure 13), indicating that at these temperatures rotation of the imine is fast on the NMR time scale. These findings precisely pin down the conditions for TRIM when the rotation is slow or fast on the NMR timescale at the given conditions. For one *iso*-propyl residue, fast rotation is still possible at 180 K. For one *tert*-butyl group, the rotation is slow below 180 K and fast at slightly higher temperatures. For two *tert*-butyl groups, the rotation is slow or completely switched off. Thus, the $R_{1\rho}$ measurements for TRIM/5*E* were performed at 195, 200 and 205 K to enable fast rotation of the imine. Analogous to the previous measurements, the H_1 proton of the BINOL backbone was selected as probe (see figure 13).

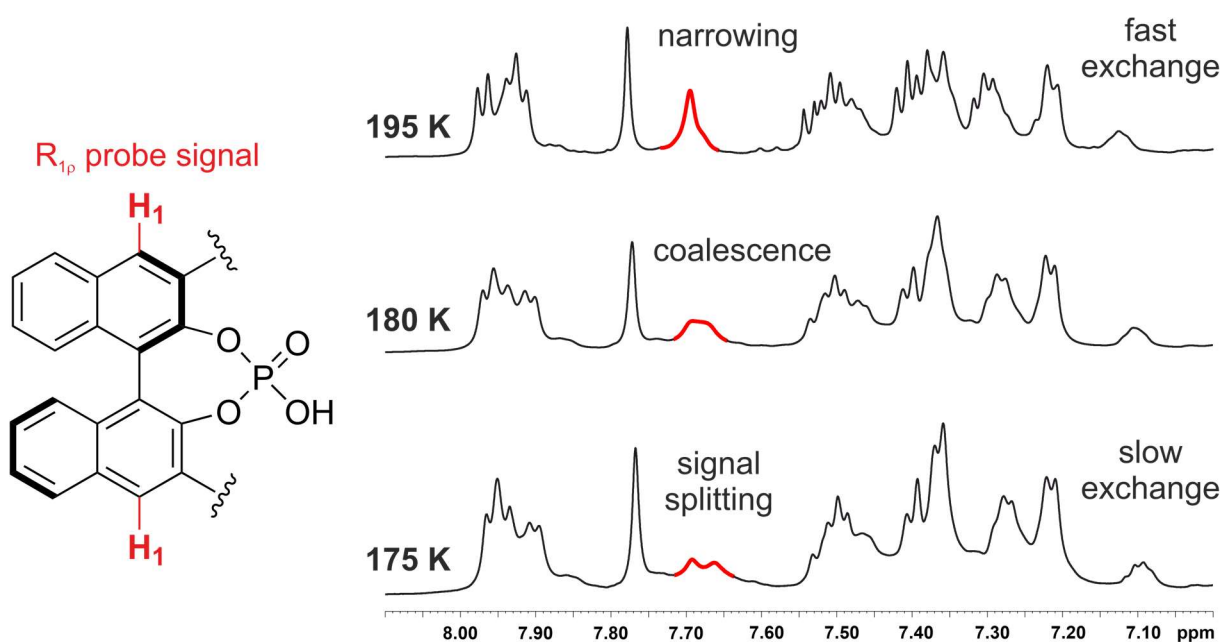
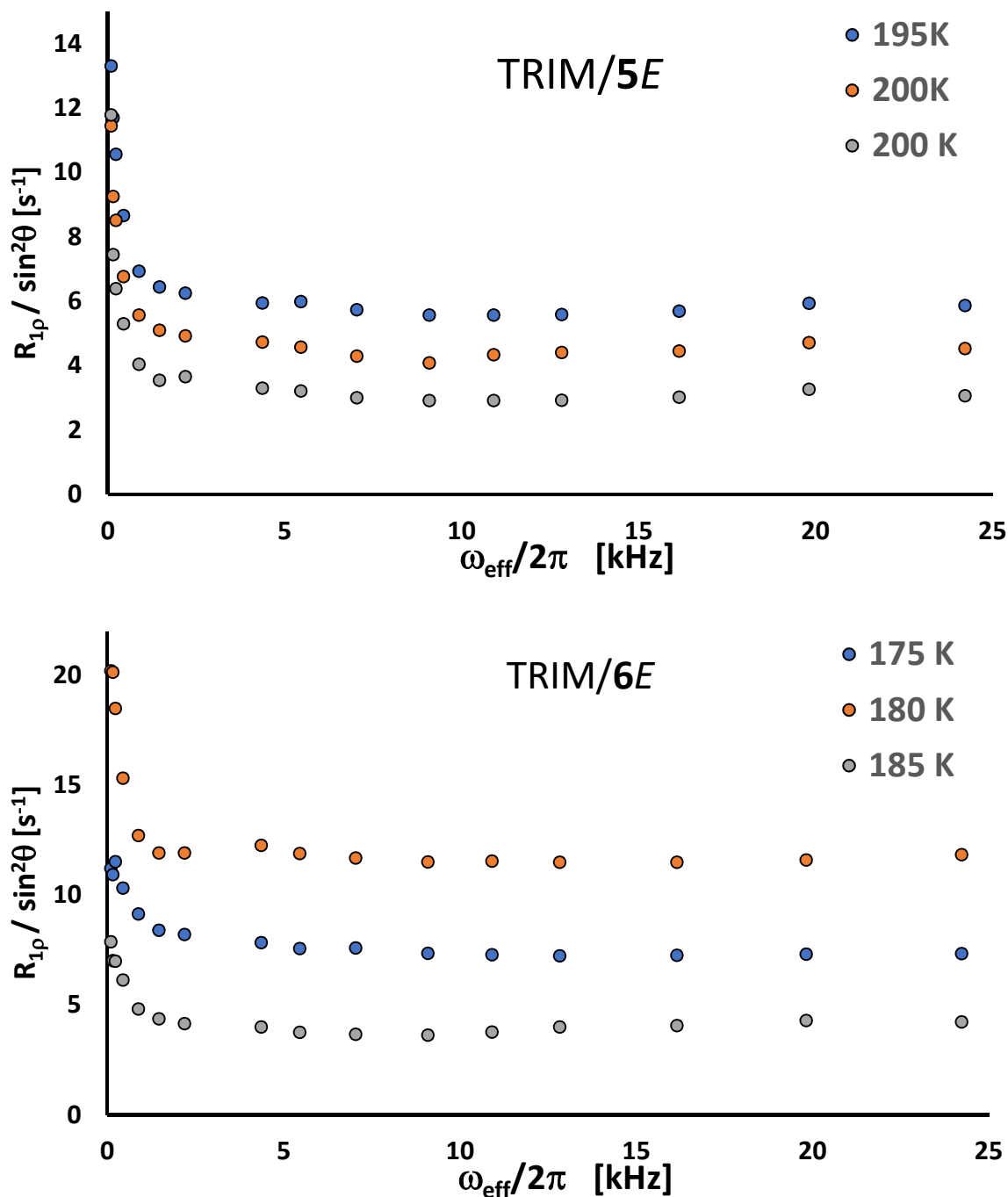


Figure 13: Selected probe signal for the $R_{1\rho}$ measurements and signals of proton H_1 at 175, 180 and 195 K for TRIM/5 at a ratio of 1:1 and a concentration of 100 mM at 600 MHz in CD_2Cl_2 . While at 175 K, signal splitting is observed, the signals coalesce at 180 K and line narrowing is observed at 195 K, demonstrating the transition from slow to fast exchange process of the imine rotation.

4. Relaxation Dispersion NMR to reveal fast Dynamics in Brønsted Acid Catalysis: Influence of Sterics and H-bond strength on conformations and substrate hopping



TRIM/5E		TRIM/6E	
Temperature [K]	Exchange rate [$\times 10^3 \text{ s}^{-1}$]	Temperature [K]	Exchange rate [$\times 10^3 \text{ s}^{-1}$]
195	1.9	175	5.4
200	1.6	180	2.2
205	0.7	185	3.1

Figure 14: Plot of the offset-Lorentzian decay curves from the R_{1p} measurements for TRIM/5E and TRIM/6E at different temperatures at a 1:1 ratio at 600 MHz in CD_2Cl_2 and the derived exchange rates. Due to an expected broad experimental error range (error range $1\text{-}2 \times 10^3 \text{ s}^{-1}$ in previous measurements), smaller differences in exchange rates are not reflected adequately and thus, higher exchange rates are observed for lower temperatures.

4. Relaxation Dispersion NMR to reveal fast Dynamics in Brønsted Acid Catalysis: Influence of Sterics and H-bond strength on conformations and substrate hopping

For TRIM/5E, exchange rates of 1.9, 1.6 and $0.7 \times 10^3 \text{ s}^{-1}$ were determined at 195, 200 and 205 K, while for TRIM/6E, values of 5.4, 2.2 and $3.1 \times 10^3 \text{ s}^{-1}$ were derived at 175, 180 and 185 K (see figure 14). In the previous measurements, an experimental error range of $1\text{-}2 \times 10^3 \text{ s}^{-1}$ was found (see chapter 4.3. figure 4 and chapter 4.6 figure S6). The measured differences in exchange rates fall within this error range and thus the resulting changes in exchange rates when changing the temperatures are not captured adequately. This is reflected in the qualitative trends of the data, giving in general higher exchange rates for lower temperatures, although the opposite should apply. Hence, the performed $R_{1\rho}$ measurements only give an estimation of the exchange rates. The resulting exchange rate for TRIM/6E is similar to the results obtained for TRIM/1-3E ($k_{\text{ex}} \approx 2\text{-}3 \times 10^3 \text{ s}^{-1}$) at the same temperature (see chapter 4.3 figure 6 and 4.6 figure S6). It is assumed that the precision of the measurement can be enhanced if more spectra, especially during the initial decay (low spinlock power) are measured. Due to the insufficient precision in the measurements of TRIM/5 and TRIM/6, no populations of the Type I E and Type II E were determined. Nevertheless, the $R_{1\rho}$ measurements clearly showed that the exchange process between Type I E and Type II E includes rotation of the imine as rate-determining step and is still accessible if bulkier dispersion energy donor substituents such as *iso*-propyl and *tert*-butyl are used. This shows that also for DED substituted imines, the populations of the Type I E and Type II E conformations can be accessed.

In order to correctly interpret these populations in terms of interaction energy, it is necessary that the interaction between the imine substituent and the 3,3'-substituent of the CPA is negligible. London dispersion interactions as well as NOE contacts both are short-ranged and scale with a distance factor of r^{-6} . The detection of intermolecular NOEs is thus a good indication for the potential presence of non-covalent interactions.

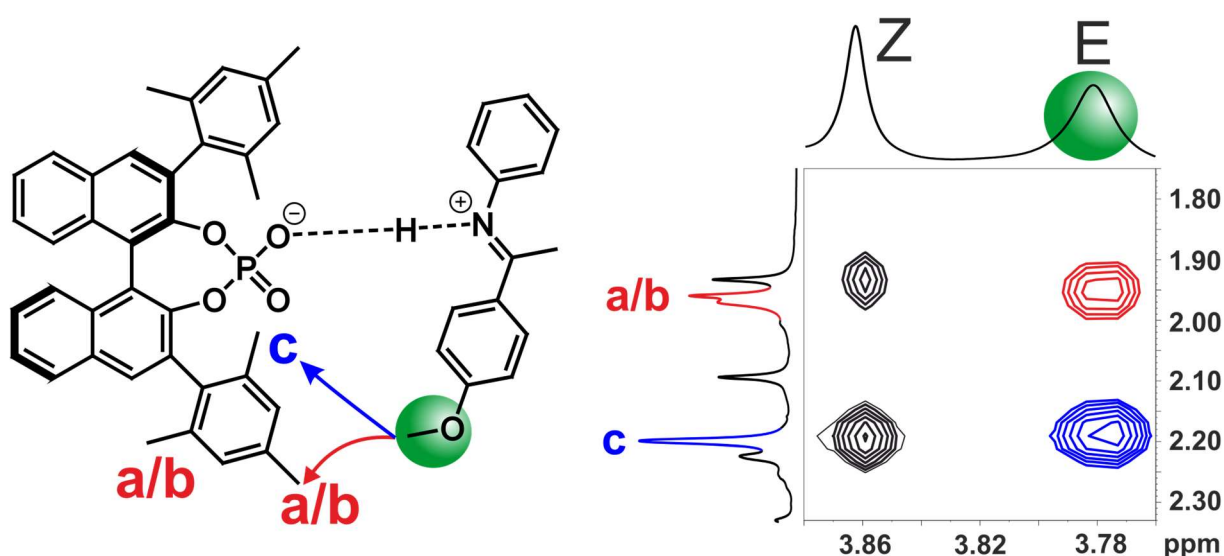


Figure 15: Excerpt of the NOESY spectrum of TRIM/2 at a 1:1 ratio at 180 K and 600 MHz in CD_2Cl_2 showing NOE contacts between the methoxy group (green) and the methyl groups of the 3,3'-substituent (a/b in red, c in blue).

4. Relaxation Dispersion NMR to reveal fast Dynamics in Brønsted Acid Catalysis: Influence of Sterics and H-bond strength on conformations and substrate hopping

Exemplarily, the NOESY spectrum of TRIM/2 was analysed in detail regarding contacts between the methoxy group of the imine and the 3,3'-substituent of the CPA (see figure 15), as its chemical shift assignment and structural elucidation was performed in detail previously^[4] and the methoxy group is a well resolved and baseline separated probe. NOE contacts between the methoxy group and the methyl groups of the 3,3'-substituent (figure 15, blue and red cross signal) could be clearly identified, which strongly indicates that also London dispersion interactions between these groups can be present. This was further corroborated by preliminary non-covalent interaction analysis,^[7] which showed an attractive interaction between these groups for the Type II *E* conformation and more importantly stacking of the respective phenyl rings. Thus, the interaction between the imine substituent and the 3,3'-substituent of the catalyst is not negligible for TRIM/imine systems, which prevents a correct interpretation of the populations of the Type I *E* and Type II *E* conformations in terms of interaction energy.

Hence, the size of the 3,3'-substituent was further reduced to only a phenyl ring and the binary complex samples of Ph-CPA/1 and Ph-CPA/2 were studied in detail regarding the structure and presence of the Type I *E* and Type II *E* conformations, accessibility of the fast exchange process by $R_{1\rho}$ and interaction profile between the imine substituent and the 3,3'-substituent. Both systems showed the typical hydrogen bond pattern, featuring two doublets reflecting the binary *Z*- and *E*-imine complex.

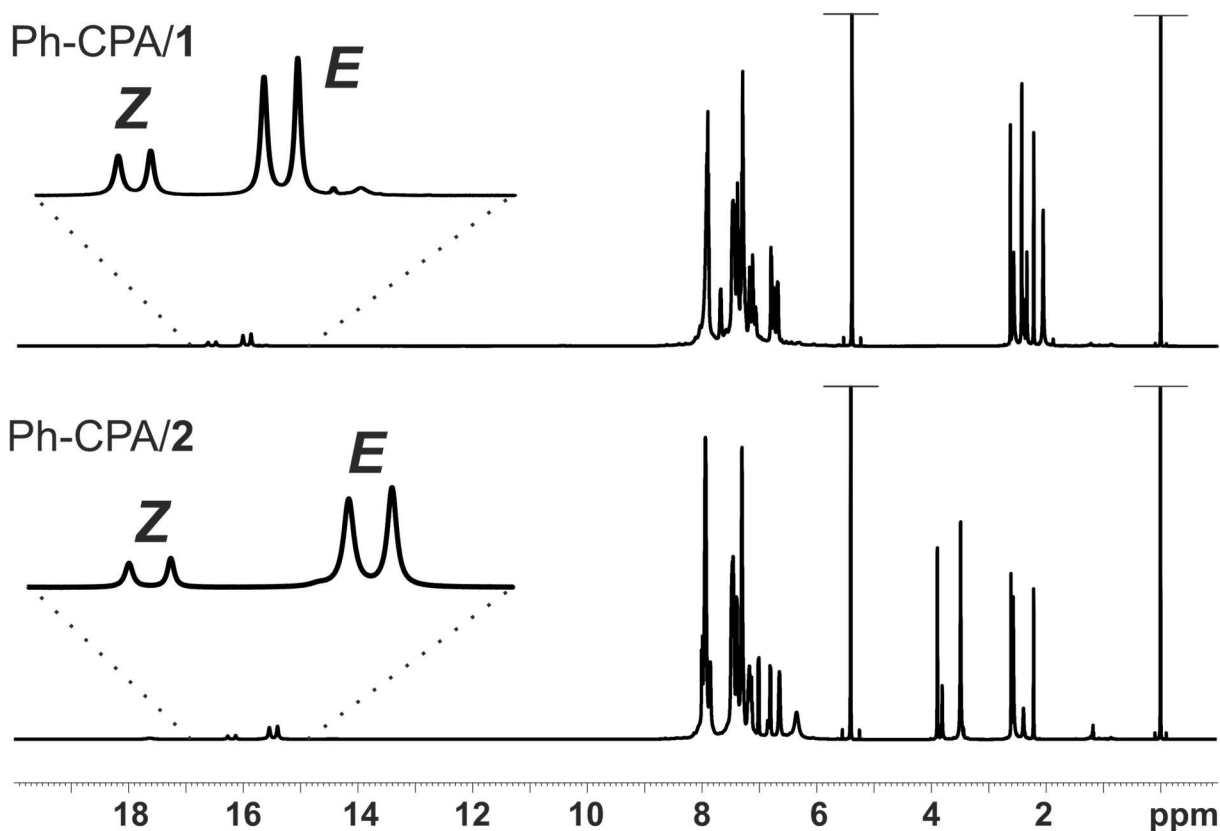


Figure 16: ^1H NMR spectra of Ph-CPA/1 and Ph-CPA/2 at a concentration of 50 mM and a 1:1 ratio in CD_2Cl_2 at 180 K and 600 MHz. Both spectra show two doublets in the hydrogen bond region, corresponding to the respective *Z* and *E*-imine complexes.

4. Relaxation Dispersion NMR to reveal fast Dynamics in Brønsted Acid Catalysis: Influence of Sterics and H-bond strength on conformations and substrate hopping

Based on a series of homo- and heteronuclear NMR spectra, a chemical shift assignment for both systems could be achieved. However, the aromatic signals of the Ph-CPA showed severe line broadening and signal overlap, which made an assignment especially for the 3,3'-substituents not possible. In comparison to the corresponding systems with TRIP and TRIM, the ^1H and ^{15}N chemical shifts of the hydrogen bond are highfield shifted and the $^1J_{\text{NH}}$ coupling constant is increased (see table 1 for values for the *E*-complexes. The same trends are present for the *Z*-complexes). This clearly demonstrates a stronger proton transfer onto the substrate, which reflects a higher internal acidity of the Ph-CPA and a weaker hydrogen bond.^[8]

Table 1: Hydrogen bond parameters ($\delta(^1\text{H})$, $\delta(^{15}\text{N})$ and $^1J_{\text{NH}}$) of Ph-CPA/*1E* and Ph-CPA/*2E* in comparison to the respective values for TRIP and TRIM found in previous studies.^[8] The values were recorded at 180 K in CD_2Cl_2 .

System	$\delta(^1\text{H})$ [ppm]	$\delta(^{15}\text{N})$ [ppm]	$^1J_{\text{NH}}$ [Hz]
TRIP/ <i>1E</i>	17.07	216.0	79.2
TRIM/ <i>1E</i>	16.26	208.0	83.9
Ph-CPA/ <i>1E</i>	15.98	205.7	84.6
TRIP/ <i>2E</i>	16.47	206.6	82.2
TRIM/ <i>2E</i>	15.80	200.5	85.4
Ph-CPA/ <i>2E</i>	15.47	198.6	85.9

Based on the previous studies on the influence of the hydrogen bond strength on the switching process (see chapter 4.3 figure 5), the switching process for Ph-CPA/*1E* and Ph-CPA/*2E* will be faster as for the respective TRIM systems. As the switching process for TRIM/*1E* and TRIM/*2E* was already too fast to be captured by the $R_{1\rho}$ measurements, it will not be accessible for Ph-CPA. However, given the reduced steric bulk of the 3,3'-substituent, rotation of the imine inside the binding pocket should be possible and thus potentially be monitored, allowing access to the populations of the Type I *E* and Type II *E* conformations. An initial test measurement was performed for Ph-CPA/*1E*, using the *para*-methyl group of the imine as probe signal in analogy to the measurements on TRIP/*1E* and TRIM/*1E* (see figure 17). The experiment yielded a decay curve, demonstrating the presence of an accessible fast exchange process and an exchange rate of $\approx 5.0 \times 10^3 \text{ s}^{-1}$ was derived. This rate is similar, but higher than for TRIM/*1E* and clearly shows that for Ph-CPA/*1E* the rotation process is possible and monitored by the measurements. The higher exchange rate, corresponding to a faster rotation of the imine inside the binding pocket originates in the reduced steric bulk of the 3,3'-substituent of the CPA. Hence, for Ph-CPA the conformational equilibrium between the Type I *E* and Type II *E* conformations is in principal accessible by the $R_{1\rho}$ measurements, capturing the rotation of the imine.

4. Relaxation Dispersion NMR to reveal fast Dynamics in Brønsted Acid Catalysis: Influence of Sterics and H-bond strength on conformations and substrate hopping

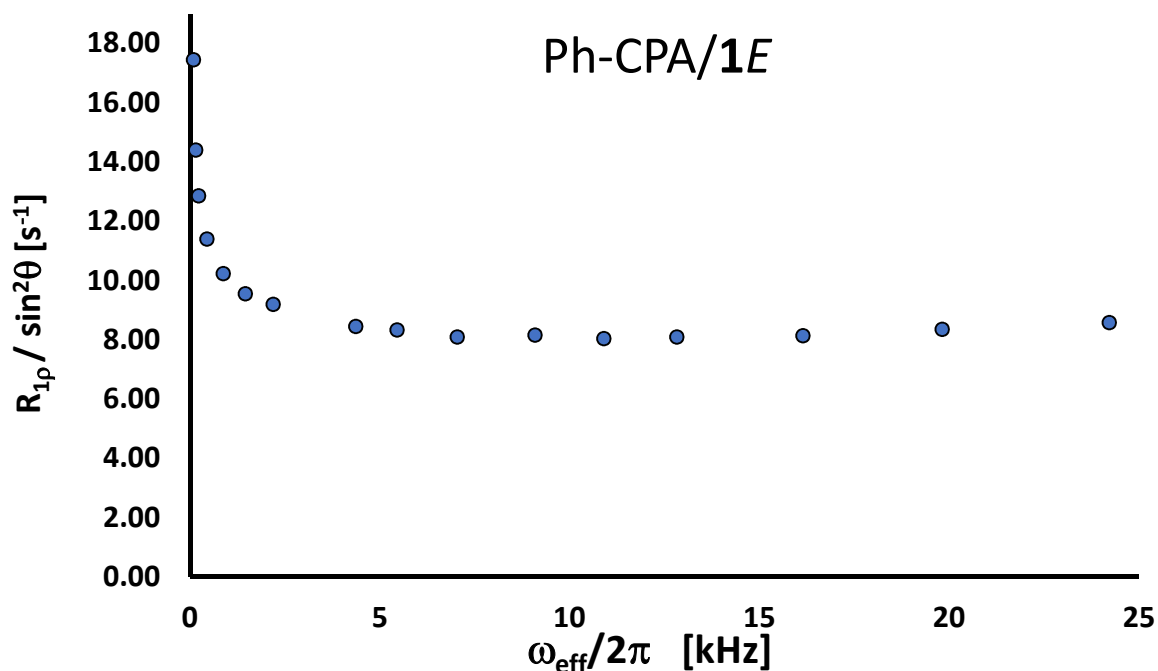


Figure 17: Plot of the offset-Lorentzian decay curve from the R_{1p} measurements for Ph-CPA/1E at 180 K, a 1:1 ratio and 600 MHz in CD_2Cl_2 . An exchange rate $k_{\text{ex}} \approx 5.0 \times 10^3 s^{-1}$ was derived.

However, as for TRIM/5 and TRIM/6 the populations of Type I *E* and Type II *E* can only be correctly interpreted in terms of energy if the interaction between the imine substituent and the 3,3'-substituents are negligible. For Ph-CPA/1 and Ph-CPA/2 it was not possible to perform an analysis of the NOESY spectra, as the chemical shifts for the 3,3'-phenyl substituents could not be assigned due to line broadening and signal overlap. Preliminary non-covalent interaction analysis^[7] on Ph-CPA/2E (Type II conformation) indicated that albeit the interaction between the imine substituent and the 3,3'-substituent might not be present, stacking of the phenyl ring of the imine (*para*-substituted ketone part) and the phenyl ring of the 3,3'-substituent definitely is. This stacking interaction is modulated by the electrostatic properties of the imine substituent. Albeit a direct interaction between imine substituent and 3,3'-substituent might be prevented, the substituent effect on the phenyl ring cannot be neglected. Hence, the imine substituent interacts with the BINOL backbone in the Type I *E* conformation and at least has a substituent effect on the interaction pattern in the Type II *E* conformation. Therefore, the contribution of the imine substituent cannot be clearly dissected based on this conformational equilibrium and it is not ideal as a molecular balance system.

4.7.4. Conclusion

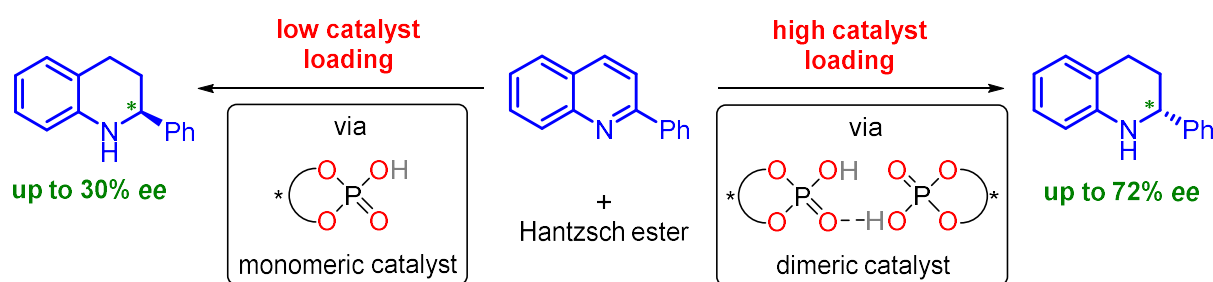
Building up on the previous studies on the fast exchange processes in binary CPA/imine complexes, it was tested if the conformational equilibrium between the Type I *E* and Type II *E* conformation, now accessible by $R_{1\rho}$ measurements can be used as a molecular balance system. In the Type I *E* conformation, the *para*-substituent of the imine interacts with the BINOL backbone and in the Type II *E* conformation potentially with the 3,3'-substituent. For an adequate interpretation of the populations in terms of interaction energy, it is necessary that the latter interaction is negligible and therefore CPAs with small 3,3'-substituents were studied. Measurements with TRIM and imines **5** and **6**, bearing a *tert*-butyl or *iso*-propyl group as dispersion energy donors were performed. A detailed structural analysis by NMR spectroscopy ensured the presence of the Type I *E* and Type II *E* conformation and conservation of these structures when increasing the bulk of the imine substituent. $R_{1\rho}$ measurements elucidated the presence and accessibility of a fast exchange process, which corresponds to the rotation of the imine inside the binding pocket. Analysis of the NOESY data however revealed that the interaction between the imine substituent and the 3,3'-substituent of TRIM is not negligible. Therefore, the even smaller Ph-CPA was selected as additional model system in combination with imines **1** and **2**. Analysis of the hydrogen bond parameters revealed that Ph-CPA is more acidic than TRIM and TRIP, resulting in a weaker hydrogen bond anchoring the binary complexes. Initial $R_{1\rho}$ measurements revealed the presence and accessibility of a fast exchange process, which reflects the rotation of the imine inside the binding pocket. Due to the reduced steric bulk of the 3,3'-substituent, this process is faster than for the respective TRIM complexes. The interaction pattern between imine substituents and 3,3'-substituent could not be accessed by NOESY NMR due to line broadening and signal overlap. However, initial non-covalent interaction analysis on the Type II *E* conformation indicate that the imine substituent will affect the stability and population of the Type II *E* conformation by its substituent effect on the phenyl ring, which is engaged in a stacking π -interaction with the 3,3'-substituent. Therefore, the interaction energy between imine substituent and BINOL backbone cannot be determined precisely, as the contribution of the imine substituent on the stabilization of the Type I *E* conformation cannot be clearly dissected by analysis of the populations. Hence, the conformational equilibrium between Type I *E* and Type II *E* is not sufficiently precise for determining London dispersion interactions.

4. Relaxation Dispersion NMR to reveal fast Dynamics in Brønsted Acid Catalysis: Influence of Sterics and H-bond strength on conformations and substrate hopping

4.7.5. References

- [1] J. P. Wagner, P. R. Schreiner, *Angew. Chem. Int. Ed.* **2015**, *54*, 12274–12296.
- [2] J. Greindl, J. Hioe, N. Sorgenfrei, F. Morana, R. M. Gschwind, *J. Am. Chem. Soc.* **2016**, *138*, 15965–15971.
- [3] M. Žabka, R. M. Gschwind, *Chem. Sci.* **2021**, 15263–15272.
- [4] M. Melikian, J. Gramüller, J. Hioe, J. Greindl, R. M. Gschwind, *Chem. Sci.* **2019**, *10*, 5226–5234.
- [5] S. L. Cockroft, C. A. Hunter, *Chem. Soc. Rev.* **2007**, *36*, 172–188.
- [6] D. Jansen, J. Gramüller, F. Niemeyer, T. Schaller, M. C. Letzel, S. Grimme, H. Zhu, R. M. Gschwind, J. Niemeyer, *Chem. Sci.* **2020**, *11*, 4381–4390.
- [7] P. Dullinger, M. Žabka, *unpublished results*.
- [8] K. Rothermel, M. Melikian, J. Hioe, J. Greindl, J. Gramüller, M. Žabka, N. Sorgenfrei, T. Hausler, F. Morana, R. M. Gschwind, *Chem. Sci.* **2019**, *10*, 10025–10034.

5. What is the Role of Acid-Acid Interactions in Asymmetric Phosphoric Acid Organocatalysis? A Detailed Mechanistic Study using Interlocked and Non-Interlocked Catalysts



Dennis Jansen, Johannes Gramüller, Felix Niemeyer, Torsten Schaller, Matthias C. Letzel, Stefan Grimme, Hui Zhu, Ruth Gschwind, and Jochen Niemeyer

Chem. Sci., 2020, **11**, 4381-4390. DOI: 10.1039/D0SC01026J

A) Dennis Jansen, Felix Niemeyer, Torsten Schaller, Matthias C. Letzel and Jochen Niemeyer designed, performed and interpreted all experiments except theoretical calculations and detailed NMR studies (they performed the NMR kinetic measurements). They wrote the manuscript excluding the parts on computations and NMR-spectroscopic investigation of catalyst dimerization. B) Hui Zhu and Stefan Grimme performed the theoretical calculations. C) Johannes Gramüller performed and interpreted all NMR measurements regarding the subchapter NMR-spectroscopic investigation of catalyst dimerization. He did not perform the NMR kinetic measurements. He wrote the corresponding part of the manuscript. Everything regarding the additional findings was done by Johannes Gramüller except the DFT structure optimization, which was performed by Philipp Dullinger. D) For the NMR-part, Ruth M. Gschwind contributed to design of experiments, interpretation of data, writing and proof-reading of the manuscript part and provided funding.

Source of this chapter: RSC Publications, <https://pubs.rsc.org/en/content/articlelanding/2020/sc/d0sc01026j>

Reproduced with permission from the Royal Society of Chemistry. Text and figures may differ from the published version. The complete corresponding Supporting Information is provided free of charge at <https://pubs.rsc.org/en/content/articlelanding/2020/sc/d0sc01026j>

5.1. Abstract

Organocatalysis has revolutionized asymmetric synthesis. However, the supramolecular interactions of organocatalysts in solution are often neglected, although the formation of catalyst aggregates can have a strong impact on the catalytic reaction. For phosphoric acid based organocatalysts, we have now established that catalyst-catalyst interactions can be suppressed by using macrocyclic catalysts, which react predominantly in a monomeric fashion, while they can be favored by integration into a bifunctional catenane, which react mainly as phosphoric acid dimers. For acyclic phosphoric acids, we found a strongly concentration dependent behavior, involving both monomeric and dimeric catalytic channels. Based on a detailed experimental analysis, DFT-calculations and a direct NMR-based observation of the catalyst aggregates, we could demonstrate that intermolecular acid-acid interactions have a drastic influence on the reaction rate and stereoselectivity of the asymmetric transfer-hydrogenation catalyzed by chiral phosphoric acids.

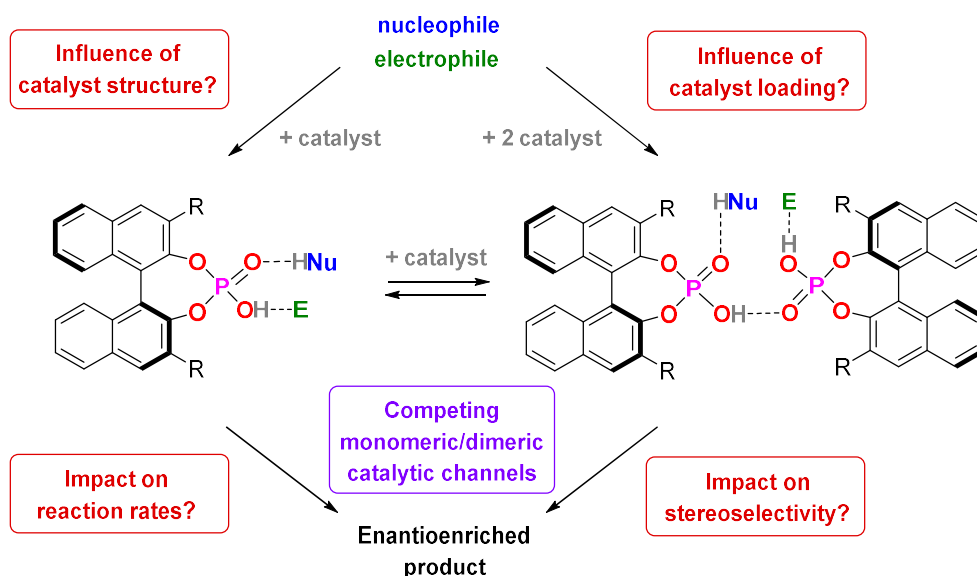
5.2. Introduction

Many organocatalysts, such as amines, diols, amino-acid derivatives, (thio)ureas or phosphoric acids are highly functionalized organic molecules, oftentimes featuring hydrogen-bond donor and acceptor moieties or even Brønsted-acidic and Brønsted-basic functional groups within the same molecule.^[1] Also, many organocatalytic reactions rely on the use of high catalyst loadings and are performed in aprotic organic solvents.^[2,3,4] This makes the formation of aggregates highly likely, be it catalyst•catalyst aggregates or higher-order catalyst•catalyst•substrate aggregates. The comprehension and control of such aggregation processes would not only enable a better understanding of organocatalytic processes, but also open up new possibilities in catalysis, when such catalyst aggregates can be designed and applied in a controlled fashion.

In previous works, aggregation of organocatalysts was observed in a few cases: In urea-catalysis, Jacobsen has shown that catalyst-catalyst interactions can both be detrimental or beneficial.^[5] The identification of a cooperative substrate activation in a catalyst•catalyst•substrate complex led to the development of tethered^[6] and macrocyclic^[7] bis-urea catalysts. Supramolecular catalyst aggregation has also been observed for chincona-alkaloid based organocatalysts, in this case leading to catalyst deactivation and decreased enantioselectivities.^[8] In case of BINOL-based phosphoric acids,^[9] Gong showed that acid-acid interactions lead to a different solubility of the racemic and the homochiral catalyst species, resulting in strong nonlinear effects.^[10] Phosphoric acid aggregation has also been proven by spectroscopic means: Dimers and trimers of dimethylphosphoric acid were identified by NMR^[11] and Hunger could show the presence of multimers for complexes of diphenyl phosphoric acid and a quinoline.^[12] For chiral phosphoric acids (CPA) with a BINOL-backbone, extended aromatic surfaces allow additional weak non-covalent interactions, which further stabilize hydrogen-bonded catalyst•substrate complexes,^{[13],[14]} and can also enable the formation of higher aggregates, such as dimers of CPA•imine complexes.^[15]

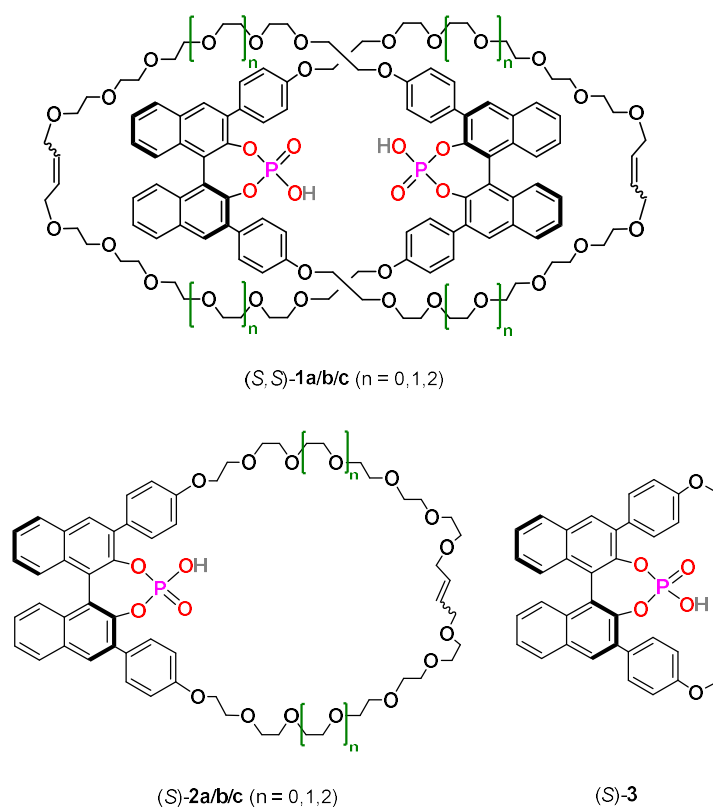
We recently found that integration of two BINOL-phosphoric acids in a catenane structure^[16] leads to drastic changes both in reaction rates and stereoselectivities for the transfer hydrogenation of quinolines. DFT-calculations suggested that a hydrogen-bond mediated acid-acid interaction^{[17],[18]} leads to a more stereoselective dimeric catalyst channel (featuring two acids and both substrates), as opposed to a less stereoselective monomeric channel (involving one acid and both substrates). We thus concluded that the mechanical interlocking of two phosphoric acids is an effective mean to channel the reaction through the dimeric channel, but of course other factors that lead to increased acid-acid interactions (such as higher catalyst loadings) might have a similar effect (Scheme 1). This could impact the outcome of a large range of asymmetric transformations that are mediated by chiral Brønsted-acids.

5. What is the Role of Acid-Acid Interactions in Asymmetric Phosphoric Acid Organocatalysis? A Detailed Mechanistic Study using Interlocked and Non-Interlocked Catalysts



Scheme 1: Key questions for this investigation.

For this reason, we have now performed a detailed mechanistic study, trying to shed light on these effects. We investigated the influence of catalyst structure and loading, using catenated, macrocyclic and acyclic phosphoric acids as catalysts (catalysts **1/2/3**, scheme 2). This enabled us to understand how the competing catalytic pathways impact the catalytic reaction in terms of reaction rates and stereoselectivities, thus demonstrating the importance of acid-acid interactions in Brønsted-acid organocatalysis.



Scheme 2: Catenated catalysts (*S,S*)-**1a/b/c**, macrocyclic catalysts (*S*)-**2a/b/c** and acyclic catalyst (*S*)-**3** used in this study.

5.3. Results and Discussion

5.3.1. General approach

The reactivity and stereoselectivity of the three different catalysts was investigated using the reduction of 2-phenylquinoline (**4**) with dihydropyridine **7** (Hantzsch-ester) to give tetrahydroquinoline **6** and pyridine **8** (Table 1). The reaction was carried out in toluene at 25 °C, as established previously.^[17] Time-resolved data was obtained by NMR-spectroscopy. Rate constants were determined both by nonlinear fitting^[19] and linear fitting of the conversion plots, which gave almost identical results (SI table S4-S7 and chapter 9). We also performed progress kinetic analysis (RPKA) based on different and same excess measurements.^[20] Mechanistic information was obtained by variable time normalization analysis (VTNA, see SI chapter 4.4).^{[21],[22]}

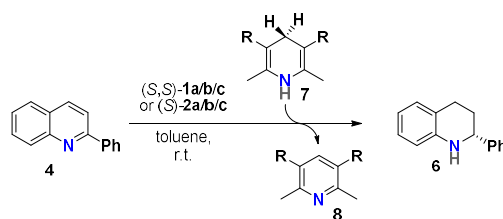
5.3.2. Influence of the catenane ring sizes

As a starting point, we employed catenanes **1a/b/c** with varying ring-sizes, assuming that the ring-size will influence the (mechano)intramolecular acid-acid interactions, thus effecting reaction rates and stereoselectivities. In addition to the previously reported hexaethyleneglycol-based species **1b/2b**,^[16] we generated the smaller, pentaethyleneglycol-based systems **1a/2a** and the larger, heptaethyleneglycol-based systems **1c/2c** (SI chapter 2). Interestingly, there is a clear increase in yields of both catenanes and macrocycles with increasing ring size (5%/7%/10% for **1a/b/c** and 8%/11%/15% for **2a/b/c**),^[23] suggesting that the longer linkers have a sufficient length for the intramolecular ring-closing metathesis, while the shorter linkers lead to increased formation of oligomeric byproducts.

In catalysis, the catenanes **1a/b/c** show drastically enhanced stereoselectivities in comparison to the macrocycles **2a/b/c** (as earlier reported for the **1b/2b** pair).^[17] However, there was no impact of the ring-sizes on the stereoselectivity: Enantiomeric excesses were in the range of 81-84% in favor of the (*R*)-product for catenanes (*S,S*)-**1a/b/c**, while the macrocycles (*S*)-**2a/b/c** consistently favored the (*S*)-product with 12-17% *ee*. However, the reaction rates of **1a/b/c** clearly depend on the ring-size, with the smaller catenanes showing higher rates ($v_0 = 3.7 \cdot 10^{-7} / 3.1 \cdot 10^{-7} / 2.0 \cdot 10^{-7} \text{ M s}^{-1}$ for **1a/b/c** at 10% catalyst loading). This suggests that the geometry of the stereodetermining transition-states is not influenced by the ring-sizes, but the association/dissociation of starting materials/products is slightly slowed down in the presence of larger, more flexible macrocycles.

5. What is the Role of Acid-Acid Interactions in Asymmetric Phosphoric Acid Organocatalysis? A Detailed Mechanistic Study using Interlocked and Non-Interlocked Catalysts

Table 1. Results of the transfer hydrogenation of 2-phenylquinoline with catalysts **1a/b/c** and **2a/b/c**.

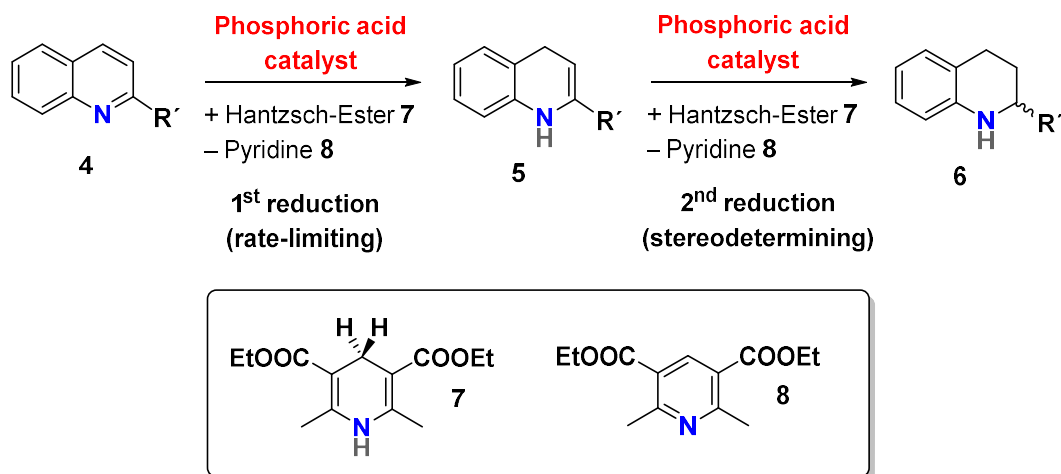


Catalyst ^[a]	ee [%] ^[b]	v_0 [10^{-7} M s^{-1}]	Catalyst ^[a]	ee [%] ^[b]
(<i>S,S</i>)- 1a	81	3.7	(<i>S</i>)- 2a	-17
(<i>S,S</i>)- 1b	84	3.1	(<i>S</i>)- 2b	-12
(<i>S,S</i>)- 1c	82	2.0	(<i>S</i>)- 2c	-17

[a] 2.5 mol% catalyst, 5 mM quinoline. [b] Determined by chiral HPLC. Values given for the excess of (*R*)-**6**.

5.3.3. First reduction step: Kinetic analysis

The mechanism for the phosphoric acid catalyzed transfer-hydrogenation of quinolines involves two steps (Scheme 3): First, quinoline **4** is reduced to the corresponding 1,4-dihydroquinoline **5**, followed by reduction to the chiral 1,2,3,4-tetrahydroquinoline **6**. Both steps involve activation of the substrate by protonation, followed by Hantzsch-Ester coordination, hydride-transfer and product-dissociation. Like other phosphoric acid-catalyzed reactions, the stereoselectivity of such transfer-hydrogenations strongly depends on the nature of the phosphoric acid, with bulky 3,3'-substituents allowing for high stereoselectivities.^[9] Thus, excellent selectivities were achieved even at low catalyst loadings for 2-arylquinolines^[4a] or benzoxazines^[4b] using a phosphoric acid with phenanthryl-groups in the 3,3'-positions.



Scheme 3: Two-step transfer-hydrogenation of quinolines **4** to tetrahydroquinolines **5**.

5. What is the Role of Acid-Acid Interactions in Asymmetric Phosphoric Acid Organocatalysis? A Detailed Mechanistic Study using Interlocked and Non-Interlocked Catalysts

This catalytic mechanism^{[3],[24]} closely resembles the related transfer-hydrogenation of imines.^[25] Our recent DFT results support this mechanism and suggest that the rate-limiting transition state occurs in the first reduction of **4** to **5**, namely in the protonation of the 1,4-dihydroquinoline-species. In comparison, the subsequent stereoselective second reduction towards **6** has a lower barrier. Moreover, our DFT-results suggest an additional mechanistic pathway involving two phosphoric acids, which we assume in case of the catenane-catalysts **1**.^[17] However, to the best of our knowledge, an experimental elucidation of these mechanisms has not been reported. To probe the suggested mechanism, we firstly determined the reaction orders for substrates **4** and **7** (reaction orders *m*, *n*) and the role of product inhibition. Secondly, the order in catalyst (reaction order *p*) was determined for the catalysts **1c/2c/3**.

$$v = -\frac{d[Q]}{dt} = k_{obs} \cdot [Q]^m \cdot [HE]^n = k \cdot [Cat]^p \cdot [Q]^m \cdot [HE]^n \text{ (eq. 1)}$$

A first analysis of the time-resolved NMR-data (SI fig. S2/S3) shows that the reduction of **4** to **6** occurs selectively with no side products. The intermediate 1,4-dihydroquinoline was not observed in any of our experiments, mainly due to its high free energy (low concentration) as suggested by our recent DFT calculations.^[17] Since the reduction of **4** into **5** is rate-limiting, the reaction orders *p*, *m*, *n* describe the first reduction step from **4** to **5**.

Substrate orders and product inhibition

For the catenated catalyst **1c**, rate measurements at different concentrations of quinoline **4** and Hantzsch-ester **7** indicated a linear dependence of reaction rate on the substrate concentrations. In the resulting $\ln v_0 / \ln [\text{substrate}]$ plots (fig. 1a/b), we could determine reaction orders of 0.8 (for **4**) and 0.7 (for **7**), respectively. This is in good agreement with the VTNA-plots (fig. 1c/d, see fig. S7 for other values of *m/n*), which show excellent overlap of all curves for substrate orders of 1 for both the quinoline and the Hantzsch-ester. Accordingly, the substrate orders for the macrocyclic catalyst and acyclic catalysts **2c/3** were determined based on VTNA only. It was found that both substrates have a reaction order of close to 1 for both catalysts (SI fig. S11/S15). Thus, there is no difference with regard to the substrate orders for the different catalysts **1c/2c/3**. In addition, we performed some excess experiments in order to investigate potential catalyst deactivation or product inhibition (SI fig. S10/S14/S19). In all cases, we observed only minor differences, so that there seems to be neither catalyst deactivation nor product inhibition for all three catalysts **1c/2c/3**.

5. What is the Role of Acid-Acid Interactions in Asymmetric Phosphoric Acid Organocatalysis? A Detailed Mechanistic Study using Interlocked and Non-Interlocked Catalysts

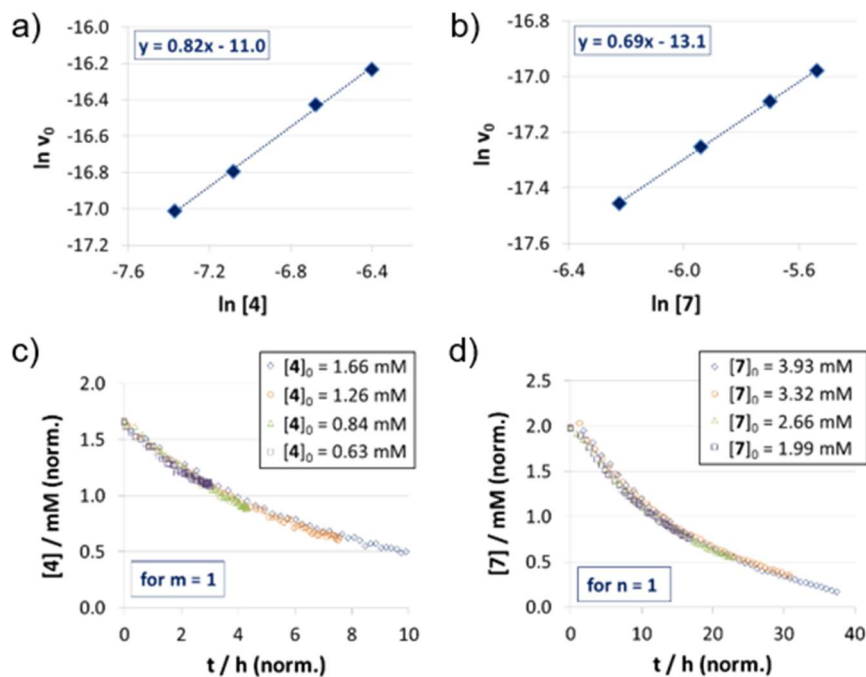


Figure 1: Substrate order determination by different excess experiments for quinoline **4** (a, c) and Hantzsch-ester **7** (b, d) in case of catenane **1c**: $\ln v_0 / \ln [\text{Substrate}]$ plots (v_0 in $\text{M}^{-1} \text{s}^{-1}$, substrate concentrations in M) (a, b) and VTNA-plots (c, d).

Catalyst orders and aggregation

The reaction orders of the catalysts were determined in a series of experiments with different concentrations of catalysts **1c/2c/3**. For the catenated and macrocyclic catalysts **1c/2c**, the v_0 vs. [Catalyst] plots (fig. 2a/d) clearly show a linear increase of rate upon increasing the catalyst loading in a range of 5–50 mol%. Thus, we could determine the order in catalyst based on the respective double logarithmic plots (fig. 2b/e), resulting in catalyst orders of 0.82 (for the bifunctional catenane **1c**) and 0.91 (for the monofunctional macrocycle **2c**). Once again, the first order dependence is also found by VTNA, which shows excellent overlap for $p = 1$ in both cases (fig. 2c/f, for other values for p see SI fig. S9/S13). For the macrocyclic catalyst **2c**, the linear rate vs. loading behaviour and the catalyst order of $p = 1$ show that this system reacts mostly via the monomeric channel, independent of catalyst concentration. As for the catenane **1c**, the linear rate vs. loading relationship also indicates that this system consistently follows one catalytic mechanism only, although the catalyst order ($p = 1$) alone does not allow a conclusion if the monomeric or dimeric catalyst channel is dominating. However, the initial rate of the catenated catalyst **1c** is significantly lower than that of the macrocyclic catalyst **2c** (e.g. $v_0 = 0.88 \cdot 10^{-7} \text{ M s}^{-1}$ for **1c**, $v_0 = 1.5 \cdot 10^{-7} \text{ M s}^{-1}$ for **2c**, each at 0.07 mM catalyst loading), despite the fact that the catenated catalyst features two phosphoric acids units. This is in line with the DFT-calculated lower rate for a dimeric catalyst channel, so that we assume the dimeric catalysis channel to be dominating for the catenated catalyst **1c** in the first, rate-determining reaction step.

5. What is the Role of Acid-Acid Interactions in Asymmetric Phosphoric Acid Organocatalysis? A Detailed Mechanistic Study using Interlocked and Non-Interlocked Catalysts

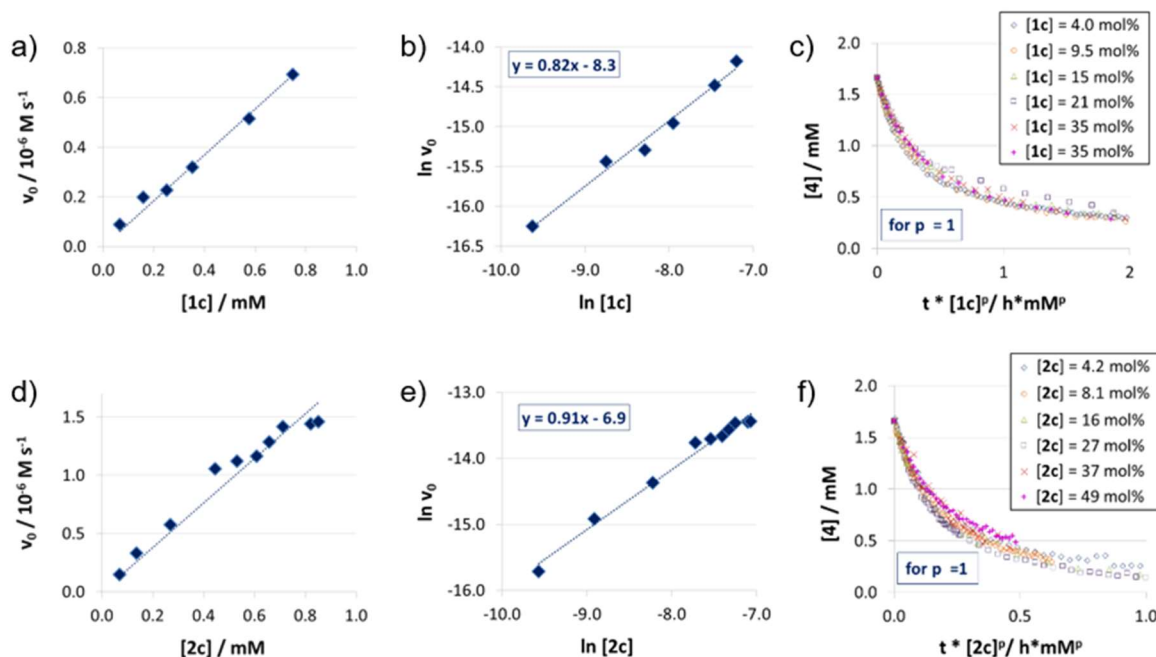


Figure 2: Catalyst order determination for catalysts **1c** (a, b, c) and **2c** (d, e, f): Initial rates (all at 1.66 mM quinoline **4** and 3.93 mM Hantzsch-ester **7**) (a, d), $\ln v_0 / \ln [\text{catalyst}]$ plots (v_0 in $\text{M}^{-1} \text{s}^{-1}$, catalyst concentrations in M) (b, d) and VTNA-plots (selected catalyst concentrations only) (c, f).

In contrast to catalysts **1c/2c**, the acyclic phosphoric acid **3** shows a nonlinear behavior: In the v_0 vs. $[\mathbf{3}]$ plot (fig. 3a), increase of catalyst loading leads to a much stronger rate increase at lower loadings than it does at higher loadings.

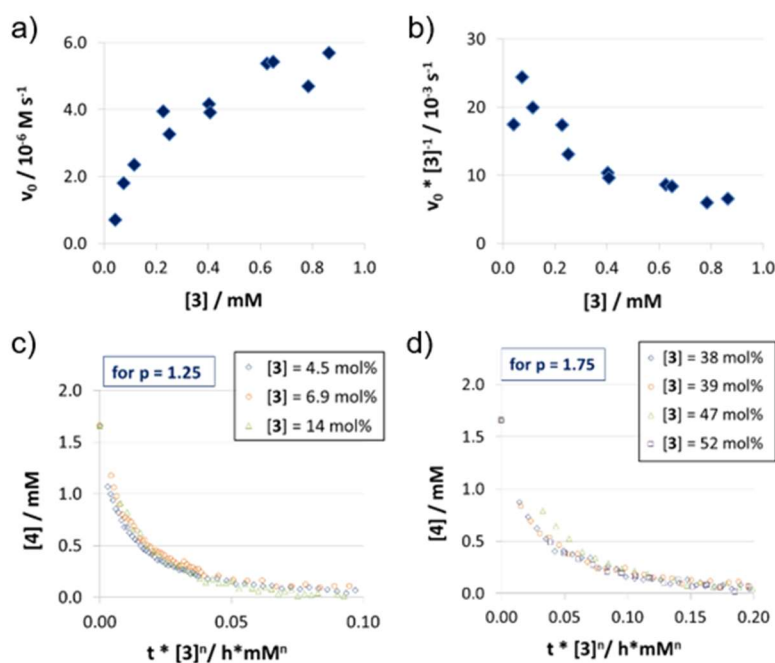


Figure 3: Catalyst order determination for catalyst **3**: Initial rates (a) and normalized initial rates (b) (all at 1.66 mM quinoline **4** and 3.93 mM Hantzsch-ester **7**) and VTNA-plots at low (c) and high (d) catalyst concentrations (selected catalyst concentrations only).

5. What is the Role of Acid-Acid Interactions in Asymmetric Phosphoric Acid Organocatalysis? A Detailed Mechanistic Study using Interlocked and Non-Interlocked Catalysts

Looking at the normalized initial rates $v_0 / [\mathbf{3}]$ (fig. 3b), we found that the normalized rate decreases initially, before it reaches a plateau at higher loadings. In order to see if the nonlinear behavior in rate is due to a change in catalyst order, we performed VTNA. While we find an order of $p = 1.25$ at low catalyst loading, the VTNA clearly shows a larger order of $p = 1.75$ at high catalyst loadings (fig. 3c/d, for other values of p see SI fig. S17/S18). Thus, we believe that the nonlinear behavior of $\mathbf{3}$ can be interpreted based on competing reaction mechanisms: At low catalyst concentrations, the monomeric channel is dominating, although the dimeric channel still contributes. Vice versa, the dimeric channel, which involves two phosphoric acids in the rate-determining transition state, dominates at higher catalyst loading.

In order to relate these orders in catalyst to the overall observed reaction rates (as shown in fig. 3a), it must be noted that the rate not only depends on the relative concentrations of the competing rate-determining intermediates (involving one or two catalyst molecules), but also on the corresponding activation energies (or reaction rates) of the monomeric and the dimeric channels.

Activation energies and influence of dimerization

For the catenane $\mathbf{1c}$, the activation energy was determined experimentally as 17.3 kcal/mol by Lineweaver-Burke analysis (SI fig. S20). Based on this, we could also determine all other activation energies (Table 2) by comparing the normalized initial rates $v_{\text{Norm}} = v_0 / [\text{Cat}]$ (also see SI fig. S21). These are almost constant for different catalyst loadings in case of $\mathbf{1c}/\mathbf{2c}$ ($v_{\text{Norm}}(\mathbf{1c}) = 1.04 \cdot 10^{-3} \text{ s}^{-1}$, $v_{\text{Norm}}(\mathbf{2c}) = 2.06 \cdot 10^{-3} \text{ s}^{-1}$), as would be expected based on the linear rate vs. loading relationship. In the nonlinear case of catalyst $\mathbf{3}$, the maximum initial rate, equivalent to the rate constant for the purely monomeric channel, can be obtained as the y-intercept in a linear extrapolation for low catalyst loadings ($v_{\text{Max}} = v_{\text{Norm}}(\mathbf{3}_{\text{Mono}}) = 22.7 \cdot 10^{-3} \text{ s}^{-1}$). In turn, the maximum rate for the dimeric channel can be estimated from the plateau for high catalyst loadings ($v_{\text{Norm}}(\mathbf{3}_{\text{Di}}) < 6.29 \cdot 10^{-3} \text{ s}^{-1}$).

This shows that there is a smaller difference in activation energies for the macrocycle/catenane pair ($\Delta E_{\text{A}}(\mathbf{1c}/\mathbf{2c}) = 0.4 \text{ kcal/mol}$) than for the monomeric/dimeric channel for catalyst $\mathbf{3}$ ($\Delta E_{\text{A}}(\mathbf{3}_{\text{Di}}/\mathbf{3}_{\text{Mono}}) = 0.8 \text{ kcal/mol}$). The difference between the macrocyclic and acyclic catalysts is even more pronounced (1.0-1.4 kcal/mol), showing that the ethylene-glycol chains significantly reduce the reaction rate (as already seen for the differently sized catenanes $\mathbf{1a/b/c}$). This could be due to steric interactions with the substrates or due to intramolecular hydrogen-bonding of the P(O)OH-unit to the polyether chains, as found in our earlier DFT-work.^[17]

5. What is the Role of Acid-Acid Interactions in Asymmetric Phosphoric Acid Organocatalysis? A Detailed Mechanistic Study using Interlocked and Non-Interlocked Catalysts

Table 2. Normalized initial rate constants and activation energies for **1c/2c/3**.

Catalyst	$v_0 / [\text{Cat}] [10^{-3} \text{ s}^{-1}]$	$E_A [\text{kcal mol}^{-1}]$
1c	1.04 ^[a]	17.3 ^[d]
2c	2.06 ^[a]	16.9 ^[e]
3_{Di} (>0.6 mM)	<6.29 ^[b]	>16.3 ^[e]
3_{Mono} (<0.25 mM)	22.7 ^[c]	15.5 ^[e]

[a] Mean value for all catalyst concentrations, [b] Mean value for catalyst concentrations >0.6 mM, [c] Determined as y-intercept in the $v_0 / [\text{Cat}]$ plot for loading <0.25 mM, [d] Determined by Lineweaver-Burke analysis, [e] Calculated from E_A (**1c**) based on the relative rates.

Detailed analysis for the acyclic phosphoric acid **3**

As detailed above, the nonlinear rate-behavior for the acyclic catalyst **3** can be attributed to both concentration effects and a change in rate constant. At higher concentrations, a smaller number of active species is present (since two molecules of **3** are needed in the dimeric channel), together with a smaller rate constant for this channel ($v_{\text{norm}}(\mathbf{3}_{\text{Mono}})/v_{\text{norm}}(\mathbf{3}_{\text{Di}}) = 4.2$, vide supra). Thus, the total rate data (fig. 3) was analyzed in order to determine the mole fractions of catalyst that act via the monomeric and the dimeric channel, respectively (SI chapter 5). The resulting speciation plot^[26] (fig. 4a) reveals that under the conditions employed (1.66 mM quinoline, 3.93 mM Hantzsch-ester, toluene solvent), the crossing point of both curves lies at ca. 0.25 mM catalyst (15 mol%). However, taking into account the lower relative rate for the dimeric channel, the impact of catalyst-dimerization on total rate is less significant (fig. 4b), and only above 0.4 mM, the contribution of the dimeric channel exceeds that of the monomeric channel.

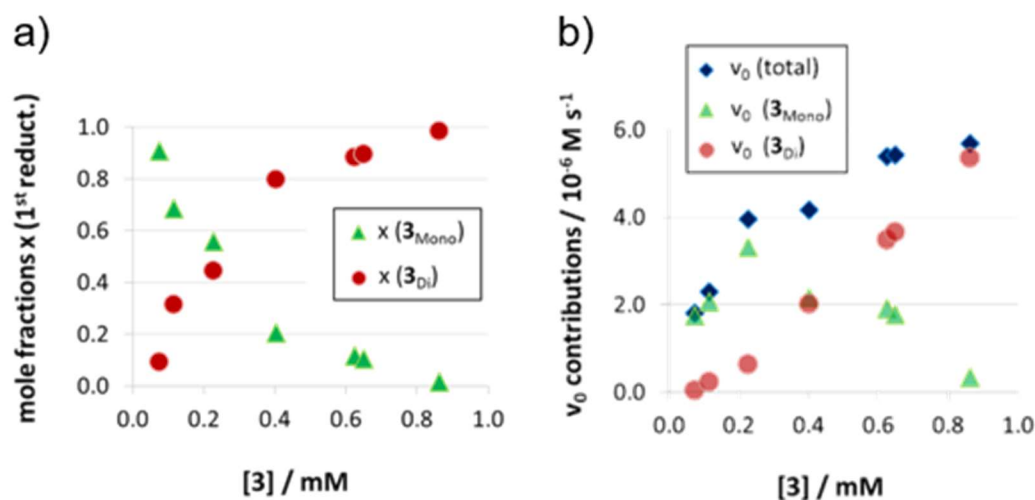


Figure 4: Mole fractions (a) and v_0 contributions (b) for the monomeric and dimeric channel for different concentrations of catalyst **3** for the first reduction step [$x(\mathbf{3}_{\text{Mono}})$: mole fraction of monomeric catalyst, $x(\mathbf{3}_{\text{Di}})$: mole fraction of phosphoric acid **3** bound in dimeric catalyst].

5. What is the Role of Acid-Acid Interactions in Asymmetric Phosphoric Acid Organocatalysis? A Detailed Mechanistic Study using Interlocked and Non-Interlocked Catalysts

Second reduction step: Influence of aggregation on stereoselectivity

The rate analysis does not give any insight into the second, stereodetermining reduction step. Thus, we investigated the influence of the overall concentration and of catalyst loading on the enantiomeric excess of the tetrahydroquinoline product **6**, since this gives direct information about the second reduction. Firstly, we found that at higher overall concentrations (5.0 mM instead of 1.66 mM quinoline), but identical absolute catalyst concentrations, stereoselectivities are shifted towards (*R*)-**6** (e.g. +20%/–22% *ee* at 25 μ M catalyst, meaning 1.5/0.5 mol% loading at 1.66/5.0 mM quinoline concentration, fig.S22b). However, for identical relative catalyst loadings, we find almost identical stereoselectivities (e.g. +72%/+71% *ee* at 50 mol%, meaning 0.83/2.5 mM catalyst concentration at 1.66/5.0 mM quinoline concentration, fig. S22c). Thus, the stereoselectivity depends mostly on the substrate/catalyst ratio, which would be in line with competing monomeric and dimeric catalyst channels: High substrate concentrations favour the formation catalyst•dihydroquinoline•Hantzsch-Ester complexes at the expense of higher-order catalyst•catalyst•dihydroquinoline•Hantzsch-Ester complexes, thus shifting the reaction towards the less stereoselective, monomeric channel. Based on the fact that the substrate concentrations influence the stereoselectivity, we also checked whether there is a dependence of the conversion on the stereoselectivity. This might be possible because of changing concentrations of substrates **4/7** and products **6/8** might influence the distribution between monomeric and dimeric channels based on different association constants. However, no change in stereoselectivity was found between 15-95% conversion at 1 mol% catalyst loading (SI table S11 and fig. S26). Secondly, we investigated the influence of catalyst loading over a broad concentration range (0.0017 mM to 0.83 mM catalyst concentration, meaning 0.1 to 50 mol% at 1.66 mM quinoline). We observed there there is a drastic change in enantioselectivity (fig. 5): At low catalyst concentrations, the (*S*)-product enantiomer is favored (–29% *ee*), while at high catalyst concentrations the selectivity reaches up to 72% *ee* in favor of the (*R*)-isomer.

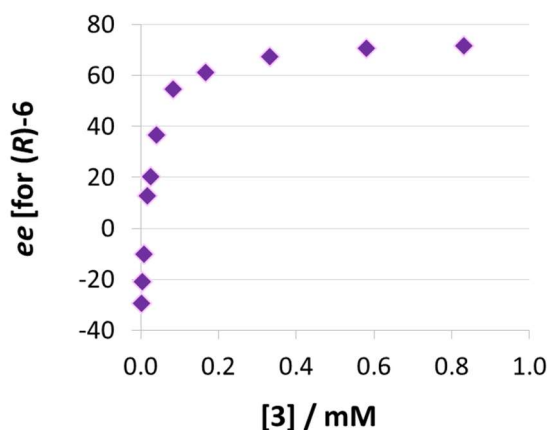


Figure 5: Influence of catalysts loading on enantioselectivities for catalyst **3** (given as enantiomeric excess for (*R*)-**6**).

5. What is the Role of Acid-Acid Interactions in Asymmetric Phosphoric Acid Organocatalysis? A Detailed Mechanistic Study using Interlocked and Non-Interlocked Catalysts

This means that the monomeric catalyst and the dimeric channel not only have different, but actually inverted stereoselectivities. This reflects the enantioselectivities of the macrocyclic and catenated catalysts **2c/1c** (-17% *ee*/+84% *ee*), which underpins their predominant reactivity via monomeric (for **2c**) and dimeric (for **1c**) catalytic channels. A control experiment using 1 mol% phosphoric acid **3** plus 49 mol% benzoic acid (+10% *ee*, c.f. +13% *ee* for 1 mol% **3** only) showed that the dimeric channel requires high concentrations of the phosphoric acid and the same effect cannot easily be achieved when using carboxylic acids as assisting Brønsted-acids (SI table S59).

The strong curvature of the *ee* vs. **[3]** curve suggests that the dimeric (more stereoselective) channel has a stronger contribution in the second reduction step than in the first reduction step. This is in line with our previous DFT-results, which indicate that for the stereodetermining step, the dimeric channel actually possesses a lower barrier than its monomeric counterpart (6.8 kcal/mol vs. 8.5 kcal/mol).^[17] To generate the corresponding speciation plot, we estimated the relative rates of the monomeric and dimeric channel based on the DFT-data ($k(\mathbf{3}_{\text{Di}})/k(\mathbf{3}_{\text{Mono}}) = 17.7$, according to $\Delta E_{\text{A}} = 1.7$ kcal/mol)^[17], since this data is not directly available experimentally. The resulting plot shows a different distribution of monomeric and dimeric channels in comparison to the first reduction step (fig. 6a). The mole fraction of catalyst acting via the dimeric channel is lower, and the crossing of both curves is observed at ca. 0.5 mM catalyst loading (30 mol%). However, the impact of the dimeric channel on the second reduction (and thus on the stereoselectivity) is significantly enhanced by its higher relative rate (fig. 6b). Only below a catalyst concentration of 0.012 mM (0.7 mol%), the enantioselectivity is dominated by the monomeric channel, leading to overall preference for the (*S*)-product. At 0.17 mM (10 mol%) loading, the stereoselectivity already reaches 61% *ee* for the (*R*)-isomer, which is close to the highest stereoselectivity of 72% observed at 0.83 mM (50 mol%) loading. This demonstrates the relative importance of the dimeric channel in terms of stereoselectivity, even at low catalyst loadings.

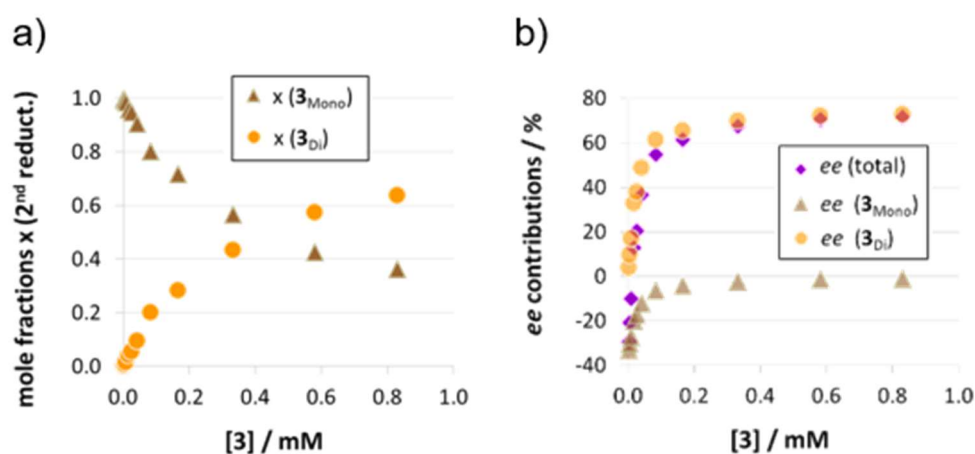


Figure 6: Mole fractions and *ee* contributions for the monomeric and dimeric channel for different concentrations of catalyst **3** for the second reduction step.

5.3.4. NMR-spectroscopic investigation of catalyst dimerization

Model systems and experimental conditions

Next, detailed NMR-spectroscopic studies were performed to elucidate the structural space including the dimeric reaction channel for acyclic catalyst **3**. Temperatures between 180-200 K were used to sufficiently slow down exchange processes and to detect separated hydrogen bonded protons (SI fig. S26). Since in toluene **3** was nearly insoluble at these temperatures, CD₂Cl₂ was used, which provided sufficient solubility and signal dispersion (for spectra and solvents see SI fig. S27).^[27] In addition, DFT-calculations revealed that analogous species should be present in CD₂Cl₂ and toluene (SI chapter 7). Experimentally, we verified that in dichloromethane there is also a strong influence of catalyst loading on enantioselectivities. As expected by DFT, the absolute stereoselectivities in dichloromethane are lower (–33% to –6% ee for 1-50 mol% catalyst loading, SI fig. SXX), nevertheless showing that competing monomeric and dimeric channels are also operating in dichloromethane.

Quinolines **4b-d** (fig. 7a) were selected as model substrates, as they possess suitable probes for ¹H and ¹⁹F NMR spectroscopy. Furthermore, they modulate the basicity of the quinoline and thus allow for an alteration of the hydrogen bond strength. Samples with a 1:1 or 2:1 stoichiometry of **3:4b-d** at NMR suitable concentrations (10-50 mM of **3**) were employed to study the structures of the complex **3•Qu** or the complex **3•3•Qu**, respectively.

1:1 stoichiometries (**3•Qu** complexes)

To shed light on the structures involved in the monomeric catalysis channel, samples of **3** and **4b-d** with a 1:1 stoichiometry were investigated. For **4b**, only one hydrogen bond proton signal was detected at 16.83 ppm (fig. 7b), which is a typical chemical shift for protons in strong hydrogen bonds^[28] and similar to the hydrogen bond signals in CPA•imine complexes.^{[13],[29]} The detection of magnetization transfers between the H-bond proton and both quinoline and CPA further corroborated the assignment of this hydrogen bond signal (SI fig. S29). The presence of the **3•4b** complex was further validated by diffusion ordered spectroscopy (DOSY) measurements. Similar hydrodynamic radii for **3** (9.36±0.05 Å) and **4b** (8.5±0.20 Å) revealed the dominant presence of the complex and are in the same order as the radii of CPA•imine complexes.^[15] Using different homo- and heteronuclear 2D spectra, a chemical shift assignment of **3•4b** could be accomplished (SI fig. S29) as well as an in-depth NOE analysis (SI fig. S31). Two different conformations with a ≈180° rotated orientation of the quinolines were identified, which are on a fast exchange on the NMR time scale^{[14],[15],[30]} (SI fig. S31 for a more detailed description of the structures and exchange pathway).^[15] One of the conformations validated the previously computed structure of the **3•Qu** complex.^[17]

5. What is the Role of Acid-Acid Interactions in Asymmetric Phosphoric Acid Organocatalysis? A Detailed Mechanistic Study using Interlocked and Non-Interlocked Catalysts

Similar ^1H spectra were obtained with quinolines **4c** and **4d**. Decreasing the basicity of the quinoline resulted in low field shifted proton signals (**4b**: 16.83 ppm, **4c**: 17.42 ppm, **4d**: 18.08 ppm; SI fig. S30), which corresponds to an increase in hydrogen bond strength.^[31] Thus, similar to CPA•imine complexes,^{[13],[29]} CPA•Qu complexes are present as hydrogen bond assisted ion pairs anchored by a strong, charge assisted hydrogen bond.^{[13],[29]} At 1:1 ratios, higher aggregates, such as **3•3•Qu** complexes are below the NMR-detection limit. In summary, monomeric **3•Qu** complexes are analogous to the previously investigated CPA•imine systems^{[13],[14],[15],[29],[30]} and are at least for the monomeric channel a representative for catalyst•substrate complexes in CPA catalyzed transformations.

2:1 stoichiometries (**3•3•Qu** complexes)

In order to populate and characterize the **3•3•Qu** complex (fig. 7a), samples with a 2:1 stoichiometry of **3** to **4b-d** were investigated. For quinoline **4b**, three dominant hydrogen bonded protons with a ratio of $\text{H}^1 : \text{H}^2 : \text{H}^3 \approx 1 : 2.4 : 2.4$ were observed (fig. 7b).^[32] Proton H^1 corresponds to the **3•4b** complex, as it has a nearly identical chemical shift as the H-bond proton in the respective sample with a 1:1 stoichiometry ($\Delta\delta(^1\text{H}) = 0.07$ ppm).

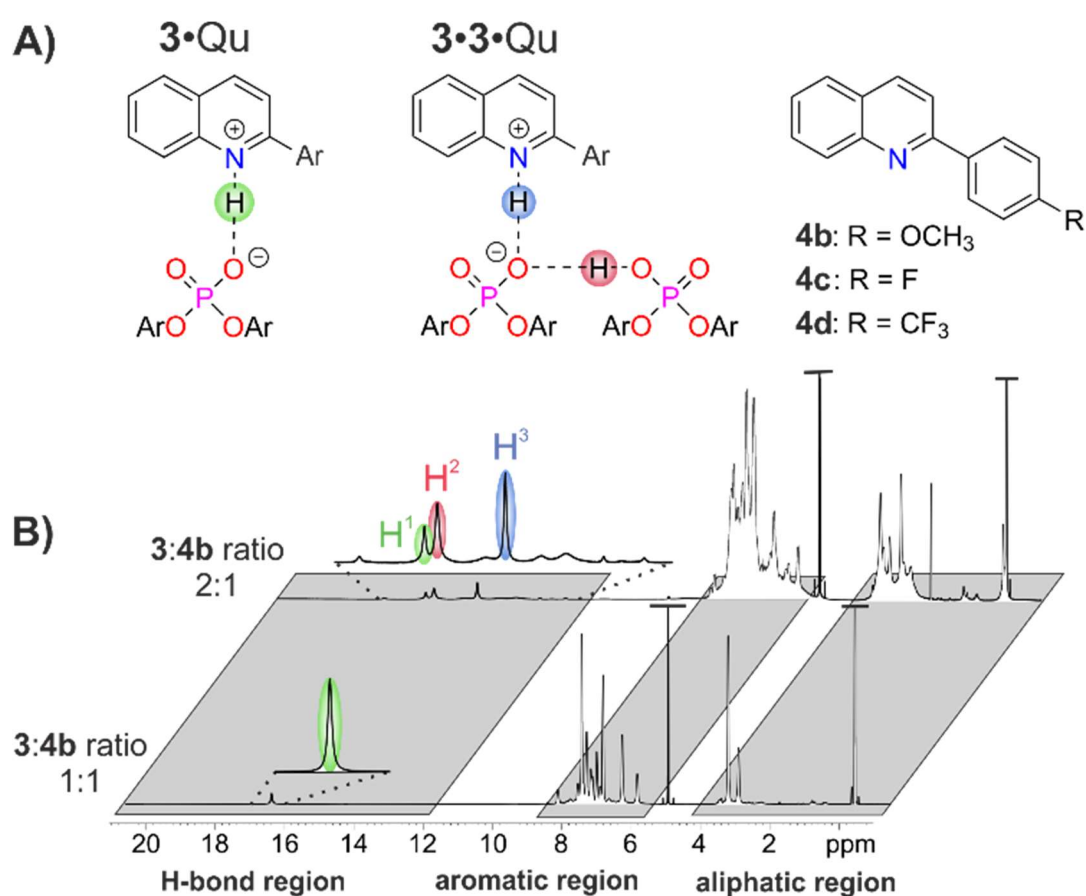


Figure 7: a) Schematic structures of the **3•Qu** and **3•3•Qu** complexes and substituents of quinolines **4b-d**. b) Spectral resolution of the ^1H spectra of complexes of **3** and **4b** at a 1:1 or 2:1 stoichiometry at 200 K and 600 MHz in CD_2Cl_2 . In the 1:1 system, only one H-bond is detected, presumably of the **3•4b** complex. For the 2:1 system, three major H-bonds are observed at 16.76 (H^1), 16.51 (H^2) and 15.27 ppm (H^3), most likely of the **3•4b** (H^1) and **3•3•4b** (H^2 , H^3) complex.

5. *What is the Role of Acid-Acid Interactions in Asymmetric Phosphoric Acid Organocatalysis? A Detailed Mechanistic Study using Interlocked and Non-Interlocked Catalysts*

Protons H² and H³ have similar integrals, which fits the expected hydrogen bonding situation for the **3•3•4b** complex. Proton H¹ and H³ showed exchange signals in the NOE spectrum (SI fig. S32). In addition, both protons show similar low field shifts with quinolines **4c** and **4d**, i.e. a similar modulation of the H-bond strength (SI fig. S30). Thus, proton H³ is assigned to the PO⁻⋯H·N⁺ hydrogen bond (fig. 7b, highlighted in blue) and proton H² to the PO⁻⋯H·OP hydrogen bond (fig. 7b, highlighted in red) of the **3•3•4b** complex. The significant high field shift of proton H³ compared to proton H¹ reveals a weaker PO⁻⋯H·N⁺ hydrogen bond, i.e. a stronger proton transfer on the quinoline in the **3•3•4b** complex compared to the **3•4b** complex.^[31] This weakening is often found in bifurcated hydrogen bonds^[28] and can be rationalized by the compensation of an increasing negative partial charge on the phosphate by the additional PO⁻⋯H·OP hydrogen bond enabled by the second CPA. For CPA•imine systems, a correlation between hydrogen bond strength and reactivity has been observed previously, giving lower reactivities for weaker hydrogen bonds.^[13] This trend is also reflected for the monomeric and dimeric reaction channel in the investigated quinoline systems, as the dimeric reaction channel featuring a weaker PO⁻⋯H·N⁺ hydrogen bond shows lower reaction rates than the monomeric channel (fig. 8). Moreover, additional hydrogen bond signals were observed in the ¹H spectrum at a 2:1 stoichiometry, which are low populated and/or have severe line broadening (fig. 7b, magnified H-bond region). EXSY signals in the NOESY spectrum revealed that these signals are in chemical exchange with the PO⁻⋯H·N⁺ or PO⁻⋯H·OP hydrogen bond protons of the **3•4b** and **3•3•4b** structures, thus suggesting the presence of different/higher aggregates of **3** and **4b**. Additional detailed NMR-structural analysis of the **3•3•4b** complex could not be achieved due to strong line broadening and signal overlaps (see aromatic region in fig. 7b). Similar ¹H spectra were obtained for quinolines **4c** and **4d** (SI fig. S30). Measurements at lower temperatures were not fruitful due to the poor solubility of **3** in the required freonic mixtures^[27] (CDCl₂F, CDCIF₂). However, the spectra at 300 K were significantly simplified and better resolved, as the different species (free **3** and Qu, **3•Qu**, **3•3•Qu** and potential higher aggregates) are in fast exchange on the NMR time scale. DOSY measurements were performed at a 1:1 and 2:1 stoichiometry to further confirm the postulated presence of **3•3•4b** in the 2:1 samples (SI table S12). Due to the chemical exchange of the different species, the measured diffusion coefficients and derived hydrodynamic radii are an average of the values of the different species, weighted by their respective population and lifetime.^[33] Similar hydrodynamic radii were derived for the quinoline and the CPA, demonstrating that also at 300 K the catalyst-quinoline complexes are the dominant species (SI table S12). When comparing the derived hydrodynamic radii for the 1:1 and 2:1 stoichiometries, a size increase of ≈1.8-2.7 Å was observed for the quinolines in the 2:1 samples, which is in agreement with the previously reported offset for CPA•Imine complexes and their dimers (≈ 3 Å).^[15] The increased radii clearly show that higher aggregates, such as the **3•3•Qu** complex are populated when employing a 2:1 ratio of catalyst and quinoline.

5.3.5. Overall mechanistic picture for catalyst 3

In summary, our combined kinetic, stereoselectivity, DFT and NMR analysis of the transfer-hydrogenation of quinolines with the acyclic catalyst **3** has revealed the following key findings (also see fig. 8):

- The catalytic reaction using catalyst **3** involves competing monomeric and dimeric channels, as found by analysis of the kinetics and stereoselectivity and by DFT.
- Both the **3**•Qu and **3**•**3**•Qu complexes, which are relevant for the monomeric and dimeric channel, were directly observed by low-temperature NMR-spectroscopy.
- For the first reduction step (**4** to **5**), kinetics, H-bond analysis and DFT jointly show that the reduction occurs faster for the monomeric catalyst than for the dimeric one (cycles M1 and D1, fig. 8). For this reason, the influence of the dimeric channel on the reaction rate is less pronounced and the dimeric channel only dominates above 0.25 mM / 15 mol% catalyst.
- For the second, stereoselective reduction step, the effect of catalyst concentration on stereoselectivity shows that the monomeric and dimeric channels not only have different, but even inverted stereoselectivities. This reflects the selectivities of the macrocyclic and catenated catalysts **1c/2c**.
- As corroborated by DFT, the stereoselective second reduction (**5** to **6**) occurs faster for the dimeric channel (cycles M2 and D2, fig. 8). Thus, the impact of catalyst dimerization on the stereo-selectivity is much more pronounced, with the dimeric channel dominating even at catalyst loading as low as 0.012 mM (0.7 mol%).

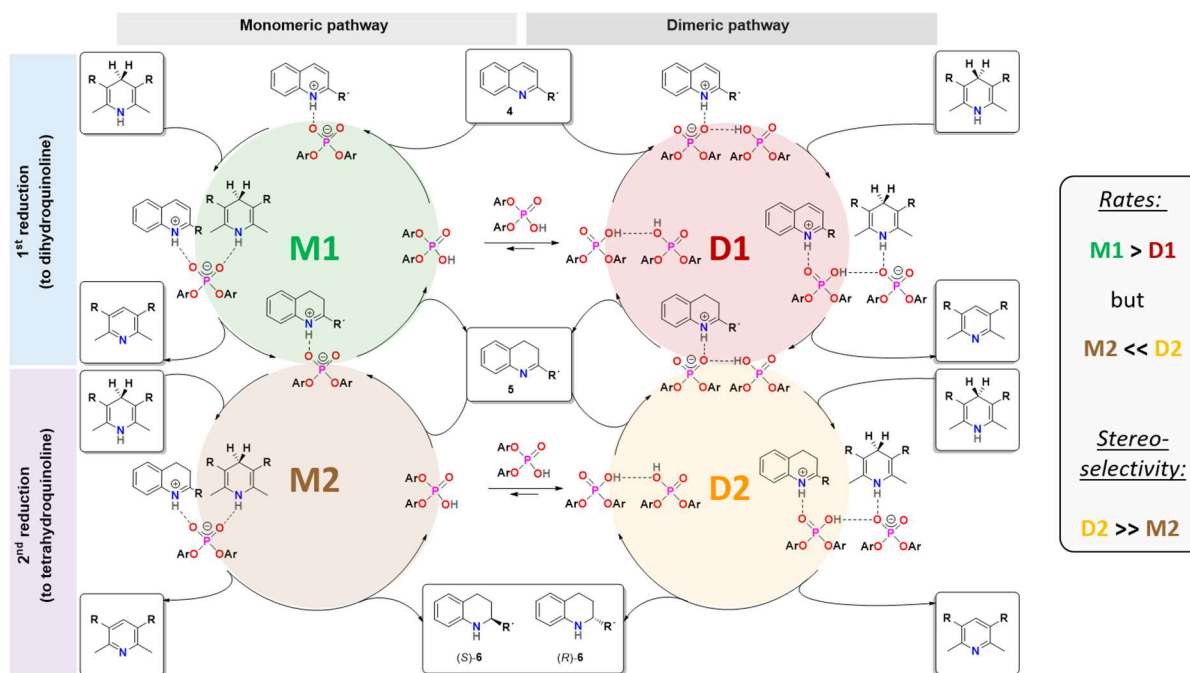


Figure 8: Revised mechanistic picture for the transfer-hydrogenation of quinolines catalyst by chiral phosphoric acids.

5.4. Conclusion

In conclusion, we have elucidated the importance of acid-acid interactions in phosphoric-acid based organocatalysis, using the transfer-hydrogenation of quinolines as an example. Based on a detailed mechanistic analysis of the catenated, macrocyclic and acyclic phosphoric acids **1/2/3**, we established that the catalytic reactions in case of the catenated and macrocyclic catalysts **1/2** are dominated by the dimeric and the monomeric channel, respectively. In stark contrast, but consistent with our recent DFT-work, the acyclic phosphoric acid **3** shows a concentration-dependent change in the reaction mechanism, involving either one or two catalyst molecules in the rate- or and stereodetermining intermediates. The formation of complexes involving two catalyst species and one quinoline molecule by was directly proven by NMR-spectroscopy. While the influence of these intermolecular acid-acid interactions on reaction kinetics is moderate, the impact on stereoselectivity is very pronounced, even leading to opposite enantioselectivities for the monomeric (-30% ee) and the dimeric catalysis channel (+70% ee). Based on these findings, we elaborated a revised mechanism for the phosphoric acid catalyzed transfer hydrogenation of quinolines.

In comparison to other phosphoric-acid catalyzed transfer hydrogenations, it becomes clear that acid-acid interactions may well be relevant in these cases as well.^{[4],[34]} While we find a significant effect on the dimeric channel at concentrations as low as 0.012 mM, commonly employed catalyst concentrations in the literature are significantly higher (ranging from 1 mM^{[4],[34a],[34g]} to 2 mM,^[34d-f] 8 mM^[34c] or even 10 mM^[34b]). Certainly, the extent of intermolecular acid-acid interactions will depend strongly on the catalyst structure and has been shown to be lower for bulky phosphoric acids such as TRIP.^[35] In addition, other factors such as the substrate structures and the solvent may favour or disfavour the formation of higher aggregates. Nevertheless, dimeric catalysis channels may be relevant, if not dominating, in other phosphoric-acid catalyzed transformations as well. We are currently investigating the influence of acid-acid interactions for other catalyst structures and other catalytic reactions in our laboratory, since the better understanding of such supramolecular interactions may have a major impact for the future development of phosphoric-acid catalyzed asymmetric transformations.

5. What is the Role of Acid-Acid Interactions in Asymmetric Phosphoric Acid Organocatalysis? A Detailed Mechanistic Study using Interlocked and Non-Interlocked Catalysts

5.5. References

- [1] A. Berkessel, H. Gröger, *Asymmetric Organocatalysis - From Biomimetic Concepts to Applications in Asymmetric Synthesis*, Wiley-VCH, Weinheim, **2005**.
- [2] List's proline-catalyzed aldol reactions (see ref. [3]) uses 30-40 mM catalyst, while Rueping's phosphoric acid catalyzed hydrogenation of quinolines (see ref. [4a]) uses 1-5 mM catalyst.
- [3] B. List, R. A. Lerner, C. F. Barbas, *J. Am. Chem. Soc.* **2000**, *122*, 2395-2396.
- [4] a) M. Rueping, A. P. Antonchick, T. Theissmann, *Angew. Chem. Int. Ed.* **2006**, *45*, 3683-3686; b) M. Rueping, A. P. Antonchick, T. Theissmann, *Angew. Chem. Int. Ed.* **2006**, *45*, 6751-6755.
- [5] D. D. Ford, D. Lehnerr, C. R. Kennedy, E. N. Jacobsen, *J. Am. Chem. Soc.* **2016**, *138*, 7860-7863.
- [6] C. R. Kennedy, D. Lehnerr, N. S. Rajapaksa, D. D. Ford, Y. Park, E. N. Jacobsen, *J. Am. Chem. Soc.* **2016**, *138*, 13525-13528.
- [7] Y. Park, K. C. Harper, N. Kuhl, E. E. Kwan, R. Y. Liu, E. N. Jacobsen, *Science* **2017**, *355*, 162-166.
- [8] a) S. H. Oh, H. S. Rho, J. W. Lee, J. E. Lee, S. H. Youk, J. Chin, C. E. Song *Angew. Chem. Int. Ed.* **2008**, *47*, 7872-7875; b) H. S. Rho, S. H. Oh, J. W. Lee, J. Y. Lee, J. Chin, C. E. Song, *Chem. Commun.* **2008**, 1208-1210; c) H. B. Jang, H. S. Rho, J. S. Oh, E. H. Nam, S. E. Park, H. Y. Bae, C. E. Song, *Org. Biomol. Chem.* **2010**, *8*, 3918-3922; d) G. Tárkányi, P. Király, T. Soós, S. Varga, *Chem. Eur. J.* **2012**, *18*, 1918-1922; e) R. Salvio, L. Massaro, A. Puglisi, L. Angelini, A. Antenucci, S. Placidi, F. Sciubba, L. Galantini, M. Bella, *Org. Biomol. Chem.* **2018**, *16*, 7041-7049.
- [9] a) D. Parmar, E. Sugiono, S. Raja, M. Rueping, *Chem. Rev.* **2014**, *114*, 9047-9153; b) D. Parmar, E. Sugiono, S. Raja, M. Rueping, *Chem. Rev.* **2017**, *117*, 10608-10620; c) L. Schreyer, R. Properzi, B. List, *Angew. Chem. Int. Ed.* **2019**, *58*, 12761-12777.
- [10] N. Li, X.-H. Chen, S.-M. Zhou, S.-W. Luo, J. Song, L. Ren, L.-Z. Gong, *Angew. Chem. Int. Ed.* **2010**, *49*, 6378-6381.
- [11] C. Detering, P.M. Tolstoy, N.S. Golubev, G.S. Denisov, H.-H. Limbach, *Dokl. Phys. Chem.* **2001**, 353-356.
- [12] C. Malm, H. Kim, M. Wagner, J. Hunger, *Chem. Eur. J.* **2017**, *23*, 10853-10860.
- [13] K. Rothermel, M. Melikian, J. Hioe, J. Greindl, J. Gramüller, M. Žabka, N. Sorgenfrei, T. Hausler, F. Morana, R. M. Gschwind, *Chem. Sci.* **2019**, *114*, 1929.
- [14] J. Greindl, J. Hioe, N. Sorgenfrei, F. Morana, R. M. Gschwind, *J. Am. Chem. Soc.* **2016**, *138*, 15965-15971.
- [15] M. Melikian, J. Gramüller, J. Hioe, J. Greindl, R. M. Gschwind, *Chem. Sci.* **2019**, *10*, 5226-5234.
- [16] R. Mitra, M. Thiele, F. Octa-Smolín, M. C. Letzel, J. Niemeyer, *Chem. Commun.* **2016**, *52*, 5977-5980.
- [17] R. Mitra, H. Zhu, S. Grimme, J. Niemeyer, *Angew. Chem. Int. Ed.* **2017**, *56*, 11456-11459.
- [18] For reviews on acid-acid interactions in organocatalysis see: a) H. Yamamoto, K. Futatsugi, *Angew. Chem. Int. Ed.* **2005**, *44*, 1924-1942; b) C. Min, D. Seidel, *Chem. Soc. Rev.* **2017**, *46*, 5889-5902; c) R. Mitra, J. Niemeyer, *ChemCatChem* **2018**, *10*, 1221-1234.
- [19] C. L. Perrin, *J. Chem. Educ.* **2017**, *94*, 669-672.
- [20] a) D. G. Blackmond, *Angew. Chem. Int. Ed.* **2005**, *44*, 4302-4320; b) J. S. Mathew, M. Klussmann, H. Iwamura, F. Valera, A. Futran, E. A. C. Emanuelsson, D. G. Blackmond, *J. Org. Chem.* **2006**, *71*, 4711-4722.
- [21] a) J. Burés, *Angew. Chem. Int. Ed.* **2016**, *55*, 16084-16087; b) J. Burés, *Angew. Chem. Int. Ed.* **2016**, *55*, 2028-2031; c) C. D.-T. Nielsen, J. Burés, *Chem. Sci.* **2019**, *10*, 348-353.
- [22] The translation of the concentration vs. time profiles into reaction rates adds additional inaccuracy in the data analysis. This is avoided by directly using concentration vs. time profiles in VTNA instead of using rate vs. time profiles in classical RPKA.
- [23] Yields for **1b/2b** are lower than reported earlier (14%/22%) [see ref. 11]. We attribute this to a different chromatography system that was used for this work.
- [24] a) J. P. Reid, J. M. Goodman, *Org. Biomol. Chem.* **2017**, *15*, 6943-6947; b) J. P. Reid, J. M. Goodman, *Chem. Eur. J.* **2017**, *23*, 14248-14260; c) J. P. Reid, L. Simón, J. M. Goodman, *Acc. Chem. Res.* **2016**, *49*, 1029-1041; d) L. Simón, J. M. Goodman, *J. Am. Chem. Soc.* **2008**, *130*, 8741-8747; e) Y. Shibata, M. Yamanaka, *J. Org. Chem.* **2013**, *78*, 3731-3736; f) T. Marcelli, P. Hammar, F. Himo, *Chem. Eur. J.* **2008**, *14*, 8562-8571.
- [25] J. Pastor, E. Rezabal, A. Voituriez, J.-F. Betzer, A. Marinetti, G. Frison, *J. Org. Chem.* **2018**, *83*, 2779-2787.

5. What is the Role of Acid-Acid Interactions in Asymmetric Phosphoric Acid Organocatalysis? A Detailed Mechanistic Study using Interlocked and Non-Interlocked Catalysts

- [26] For the dimeric catalyst, the mole fraction represents the amount of catalyst that is bound in the dimeric catalyst (meaning that the molar amount of dimeric catalyst is half of the molar amount of phosphoric acid as expressed by the mole fraction)
- [27] J. S. Siegel, F. A. L. Anet, *J. Org. Chem.* **1988**, 53, 2629-2630.
- [28] T. Steiner *Angew. Chem. Int. Ed.* **2002**, 41, 48-76.
- [29] N. Sorgenfrei, J. Hioe, J. Greindl, K. Rothermel, F. Morana, N. Lokesh, R. M. Gschwind, *J. Am. Chem. Soc.* **2016**, 138, 16345-16354.
- [30] N. Lokesh, J. Hioe, J. Gramüller, R. M. Gschwind, *J. Am. Chem. Soc.* **2019**, 141, 16398-16407.
- [31] S. Sharif, G. S. Denisov, M. D. Toney, H.-H. Limbach, *J. Am. Chem. Soc.* **2007**, 129, 6313-6327.
- [32] The experimentally observed thermodynamic preference for the complex **3•3•4b** ($\Delta G_{\text{exp}}(\mathbf{3}\cdot\mathbf{3}\cdot\mathbf{4b} - \mathbf{3}\cdot\mathbf{4b}) = -1.5$ kJ) is qualitatively represented in the theoretical calculations, although by far less pronounced ($\Delta G_{\text{theor}}(\mathbf{3}\cdot\mathbf{3}\cdot\mathbf{4b} - \mathbf{3}\cdot\mathbf{4b}) = -12.2$ kJ). Such a significant quantitative offset between experiment and computations was also found for CPA•imine systems and probably originates in dispersion interactions with the solvent (see reference 15).
- [33] a) E. J. Cabrita, S. Berger, *Magn. Reson. Chem.* **2002**, 40, 122-127; b) C. T.W. Moonen, P. van Gelderen, G. W. Vuister, P. C.M. van Zijl, *J. Magn. Res.* **1992**, 97, 419-425.
- [34] a) S. Hoffmann, A. M. Seayad, B. List, *Angew. Chem. Int. Ed.* **2005**, 44, 7424-7427; b) M. Rueping, E. Sugiono, C. Azap, T. Theissmann, M. Bolte, *Org. Lett.* **2005**, 7, 3781-3783; c) R. I. Storer, D. E. Carrera, Y. Ni, D. W. C. MacMillan, *J. Am. Chem. Soc.* **2006**, 128, 84-86; d) G. Li, J. C. Antilla, *Org. Lett.* **2009**, 11, 1075-1078; e) A. Aillerie, V. L. de Talancé, A. Moncomble, T. Bousquet, L. Pélineski, *Org. Lett.* **2014**, 16, 2982-2985; f) X.-F. Cai, R.-N. Guo, G.-S. Feng, B. Wu, Y.-G. Zhou, *Org. Lett.* **2014**, 16, 2680-2683; g) Y. Zhang, R. Zhao, R. L.-Y. Bao, L. Shi, *Eur. J. Org. Chem.* **2015**, 3344-3351.
- [35] a) [1] M. R. Monaco, D. Fazzi, N. Tsuji, M. Leutzsch, S. Liao, W. Thiel, B. List, *J. Am. Chem. Soc.* **2016**, 138, 14740-14749; b) For a review including the crystal structure of the TRIP-dimer see: M. R. Monaco, G. Pupo, B. List, *Synlett* **2016**, 27, 1027-1040.

5.6. Supporting Information

5.6.1. General information

SAMPLE PREPARATION

Samples in CD₂Cl₂: The acyclic chiral phosphoric acid catalyst **3** was weighed into a 5 mm NMR tube and dried at 150 °C for at least 30 min under reduced pressure. After the tube came to room temperature, quinolines **4b-d** were weighed directly into the NMR tube. The tube was evacuated and flushed with Argon three times. Freshly distilled CD₂Cl₂ (0.6 mL) was added under Argon flow and TMS atmosphere (0.5 mL) was added. The tube was closed and sealed with parafilm. The samples were stored in the fridge at -80°C.

Samples in freonic mixtures: Acyclic chiral phosphoric acid catalyst **3** was weighed into a 5 mm heavy wall J-Young valve NMR tube and dried under reduced pressure at 150 °C and 30 min. After the tube came to room temperature, quinoline **4b** was weighed directly into the NMR tube. The tube was evacuated and flushed with Argon three times. The sample was connected to a vacuumline and the NMR tube was frozen in a Dewar filled with liquid nitrogen and a freonic mixture was condensed through a column filled with P₂O₅ and KOH into the NMR tube. The overall concentration was judged by the filling level freonic solution at r.t. (14 cm ~ 512 μL). The samples in the freonic mixtures were stored at ~ 4°C between the measurements.

NMR PULSE PROGRAM PARAMETERS

Standard pulse sequences from the Bruker pulse sequence catalogue (zg, zg30, etc.) with the following parameters have been used.

¹H-NMR: Pulse program zg30, Relaxation delay = 2.00 s, Acquisition time = 2.54 s, SW = 22 ppm, TD = 66 K, ns = 1 – 256; ¹³C NMR: Pulse program: zgpg30, Relaxation delay = 2.00 s, Acquisition time = 0.80 s, TD = 66 K; SW = 270.0 ppm, TD = 64k, NS = 1k – 2k; ¹⁹F-NMR: Pulse program: zg30; Relaxation delay = 2.00 s, Acquisition time = 5.79 s, SW = 20.0 ppm, TD = 131k, NS = 64; ³¹P-NMR: Pulse program: zgpg30; Relaxation delay = 1.00 s, Acquisition time = 2.25 s, SW = 40-60.0 ppm, TD = 65k, NS = 64 - 512; 2D-¹H,¹H NOESY: Pulse program: noesygpph; Relaxation delay = 5.00 s, NS = 8-16, mixing time (D8) = 300.00 ms; TD = 4096; increments = 256 - 1k; 2D-¹H,¹H COSY: Pulse program: cosygppqf; Relaxation delay = 5.00 s, NS = 4-16, TD = 4096; increments = 512; 2D-¹H,¹³C HSQC: Pulse program: hsqc-detgpsisp2.3; Relaxation delay = 6 s, NS = 8-16, ¹J_{XH} = 145 Hz; TD = 4096; increments = 512; 2D-¹H,¹³C HMBC: Pulse program: hmbcgplpndqf; Relaxation delay = 4.00 s, NS = 8-16, ¹J_{XH} = 145 Hz, J_{XH}(long range) = 10 Hz; TD = 4096; increments = 512 - 1k; 2D-¹H,³¹P HMBC: Pulse program: inv4gplrndqf; Relaxation delay = 6.00 s, NS = 4-16, TD = 4096; increments = 256 - 512; ¹H DOSY: Pulse

5. What is the Role of Acid-Acid Interactions in Asymmetric Phosphoric Acid Organocatalysis? A Detailed Mechanistic Study using Interlocked and Non-Interlocked Catalysts

program: see at respective chapter, Relaxation delay = 2.00 s – 6.00 s, NS = 64-512, TD = 58 K, increments = 20, Diffusion time delay = 45.0 ms, gradient strength 5-95% linear, gradient pulse: 0.6 – 2.0 ms.

5.6.2. Temperature screening

By lowering the temperature, exchange process within the system and the hydrogen bonds could be slowed and sharper line widths and a better signal dispersion was obtained. For samples with a 1:1 stoichiometry of CPA and quinoline, 180 K proved to be the optimum temperature for measurements, as it provided best line widths and signal dispersion. For samples with a 2:1 stoichiometry of CPA and quinoline (see Figure S1 for **3/4b**) 180 - 200 K was found as the optimum temperature range. For **4b**, measurements (especially determination of the integrals) were done at 200 K due to the optimum line separation of the two signals at 16.75 and 16.51 ppm. For quinolines **4c** and **4d**, 180 K was selected as measurement temperature.

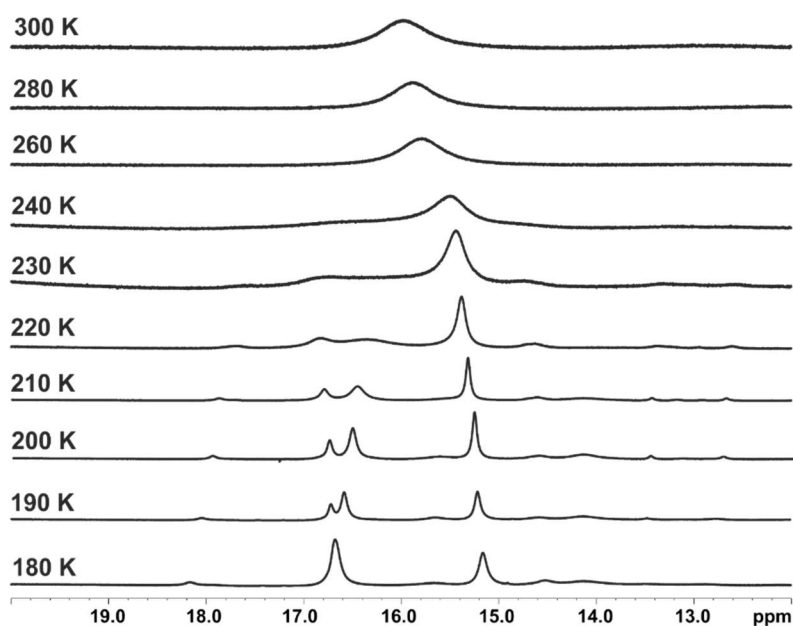


Figure S1: Excerpts of the hydrogen bond region at 600 MHz in CD_2Cl_2 at variable temperatures of a sample containing **3** and **4b** at a 2:1 stoichiometry at a catalyst concentration of 50 mM. Different scaling factors were applied to better visualize the line broadening for increased temperatures, but the spectra were recorded with identical parameters, e.g. identical number of scans (64).

5.6.3. Solvent screening

Deuterated toluene, chlorobenzene, dichloromethane and freonic mixture of CDCl_2F and CDClF_2 were tested as solvents to investigate binary CPA•quinoline complexes. Toluene provided poor solubility of the catalyst at low temperatures (see Figure S2B). Chlorobenzene was not applicable due to its higher freezing point ($\approx -45^\circ\text{C}$), because at that temperature the exchange processes were not sufficiently

5. What is the Role of Acid-Acid Interactions in Asymmetric Phosphoric Acid Organocatalysis? A Detailed Mechanistic Study using Interlocked and Non-Interlocked Catalysts

slowed down to detect hydrogen bond signals with adequate line widths (see Figure S2C). In freonic mixture, the catalyst **3** was insoluble. Hence, CD₂Cl₂ was selected as solvent as it provided good solubility, gave narrow line widths and a good signal dispersion at 180 K.

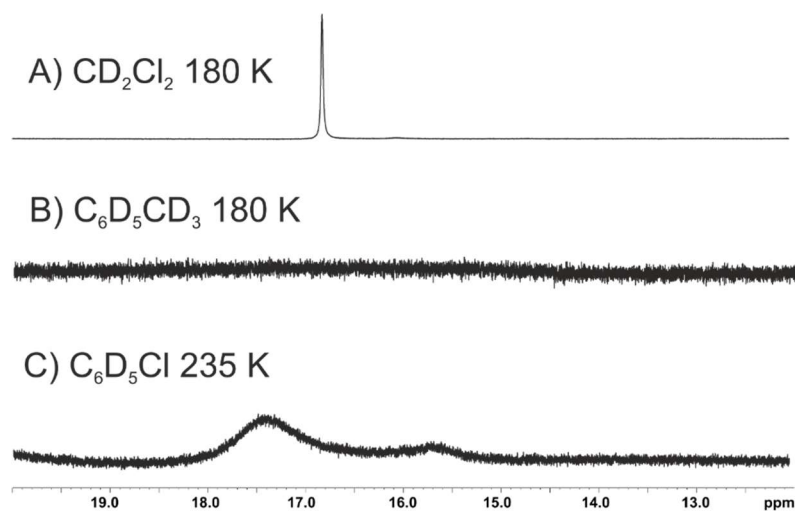


Figure S2: Excerpt of the spectra of **3:4b** at a 1:1 stoichiometry and a concentration of 10 mM in A) CD₂Cl₂ at 180 K, B) in deuterated toluene at 180 K and C) in C₆D₅Cl at 235 K. Only the hydrogen bond region (12-20 ppm) is shown. Different scaling factors were applied, but the spectra were measured with identical parameters, e.g. identical number of scans (64).

In the previous work, the transfer hydrogenation of **4a** with catalyst **3** in CH₂Cl₂ gave a significantly different *ee* value than in toluene^[2], which can indicate a limited comparability of the NMR-structure investigations in CD₂Cl₂ compared to the reaction analysis in toluene. However, theoretical calculations showed that in dichloromethane analogous species should be populated as in toluene.

5. What is the Role of Acid-Acid Interactions in Asymmetric Phosphoric Acid Organocatalysis? A Detailed Mechanistic Study using Interlocked and Non-Interlocked Catalysts

5.6.4. Chemical shift assignments

^1H (black), ^{13}C (blue) and ^{31}P (green) chemical shifts of the **3•4b** complex at a 1:1 stoichiometry were assigned with standard 2D NMR experiments ($^1\text{H}, ^1\text{H}$ COSY, $^1\text{H}, ^1\text{H}$ NOESY, $^1\text{H}, ^{13}\text{C}$ HSQC, $^1\text{H}, ^{13}\text{C}$ HMBC and $^1\text{H}, ^{31}\text{P}$ HMBC) at 180 K. Some ^{13}C chemical shifts could not be assigned.

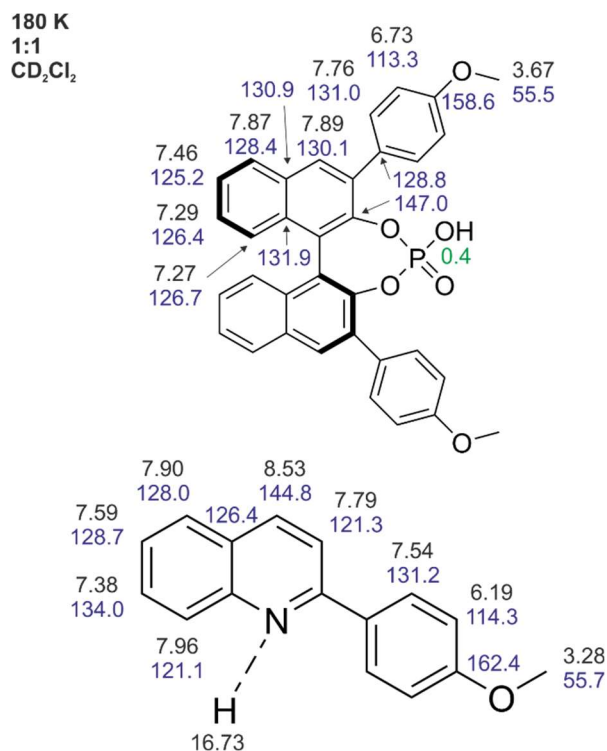


Figure S3: Chemical shift assignment of the binary **3•4b** complex at a 1:1 stoichiometry in CD_2Cl_2 .

5.6.5. Hydrogen bond investigation

The presence of the hydrogen bond was shown by the detection of magnetization transfer between the proton in the hydrogen bond and the phosphorus atom of **3** (see S24, red, $^1\text{H},^{31}\text{P}$ HMBC) and one proton of **4b** (see S24, blue, $^1\text{H},^1\text{H}$ COSY). The detection of magnetization transfer between the hydrogen bonded proton and both CPA and substrate was also shown in the previous investigations in CPA•imine systems.^[9]

In agreement with the previous NMR investigations on CPA•imine complexes,^[9] more basic quinolines (pK_b : **4b** > **4c** > **4d**) feature weaker hydrogen bond protons (lower chemical shift of the H-bond proton) due to a stronger proton transfer onto the quinoline (stronger ion pair character). This trend is observed for the proton in the $\text{PO}^- \cdots \text{H} \cdot \text{N}^+$ hydrogen bond in the binary **3**•Qu complex at a 1:1 and 2:1 stoichiometry (Figure S5, green proton), as well as for the $\text{PO}^- \cdots \text{H} \cdot \text{N}^+$ hydrogen bond in the **3**•**3**•Qu complex (Figure S5, blue proton). For the $\text{PO}^- \cdots \text{H} \cdot \text{OP}$ hydrogen bond in the **3**•**3**•Qu complex (Figure S5, red proton), this trend is not observed because that hydrogen bond is not directly affected by the quinoline substituent.

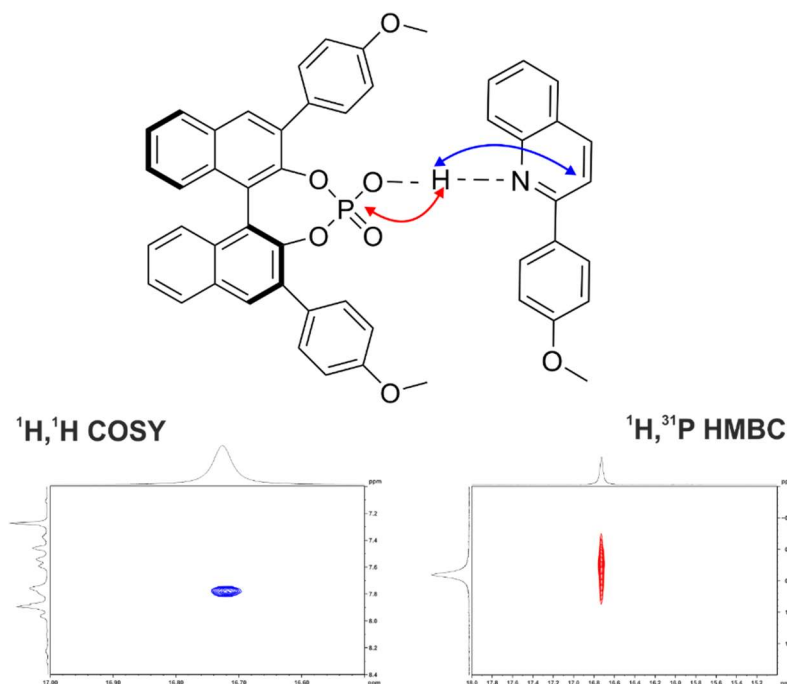


Figure S4: Excerpts of the $^1\text{H},^1\text{H}$ COSY and $^1\text{H},^{31}\text{P}$ HMBC spectra of **3:9a** at a 1:1 stoichiometry and a concentration of 50 mM in CD_2Cl_2 at 600 MHz. The detection of magnetization transfer between the hydrogen bonded proton and the quinoline (left, blue) and the phosphorus atom of **3** (right, red) proves the presence of a hydrogen bond.

5. What is the Role of Acid-Acid Interactions in Asymmetric Phosphoric Acid Organocatalysis? A Detailed Mechanistic Study using Interlocked and Non-Interlocked Catalysts

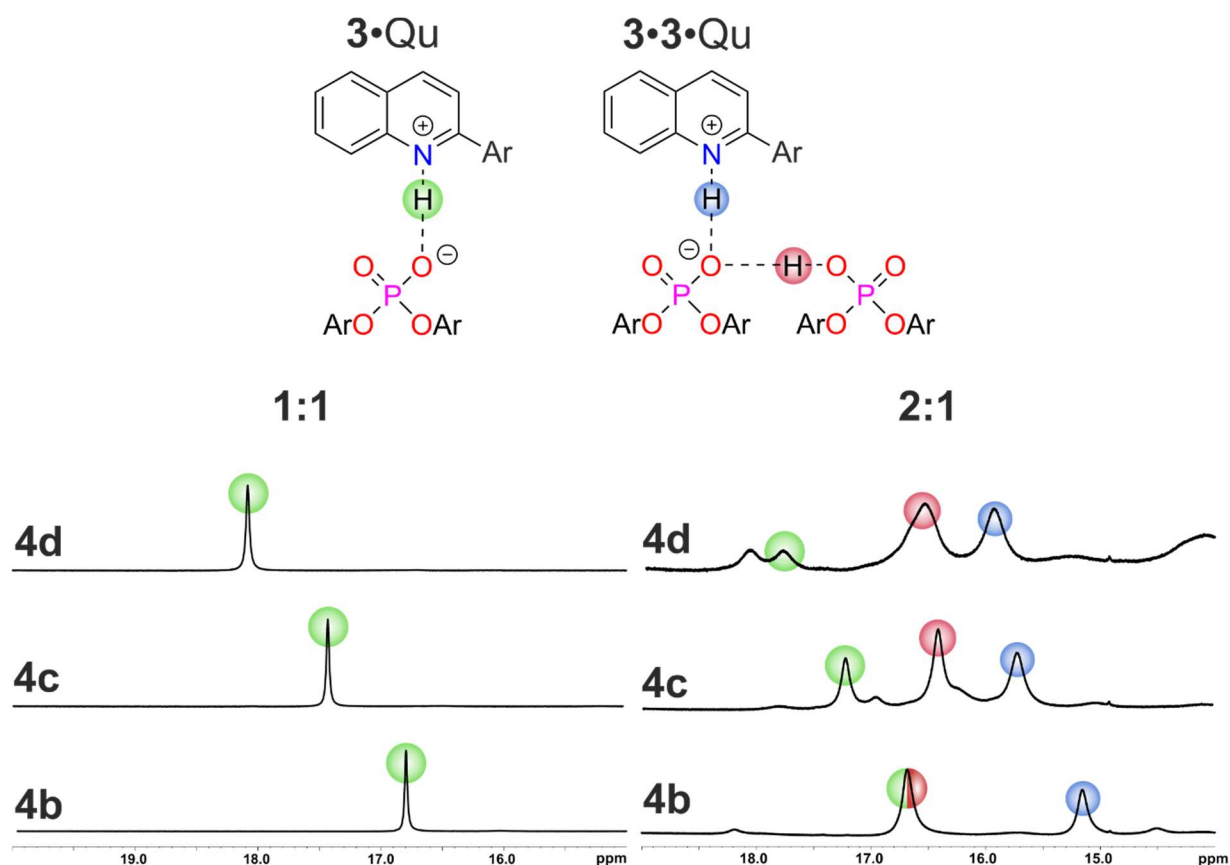


Figure S5: Excerpts of the ^1H spectra of **3** and **4b-d** at a 1:1 (left) or 2:1 (right) stoichiometry at 600 MHz and 180 K in CD_2Cl_2 . Modulation of the basicity of the quinoline gives stronger hydrogen bonds (higher chemical shifts) for less basic quinolines, demonstrating a hydrogen bond assisted ion pair nature of the complexes.

5.6.6. Structural investigations of **3•4b**

Based on the chemical shift assignment, a NOESY analysis was performed to reveal the structure of binary **3•4b** complex. NOE contacts of the MeO group of the catalyst (Figure S6, highlighted in orange) were detected to both sides of the quinoline (blue and red arrows). It should be noted that in the previously computed structures^[2] only one MeO group of the catalyst is in close contact to the quinoline. Hence, the detection of NOE contacts A and B, as well as C and D (Figure S6) reveals the presence of two different conformations of the binary **3•4b** complex which are in a fast exchange with each other and thus give only one set of signals. This observation is analogous to the previous studies on binary CPA•imine complexes, where also two fast exchanging conformers (Type I and Type II) were identified.^[10]

5. What is the Role of Acid-Acid Interactions in Asymmetric Phosphoric Acid Organocatalysis? A Detailed Mechanistic Study using Interlocked and Non-Interlocked Catalysts

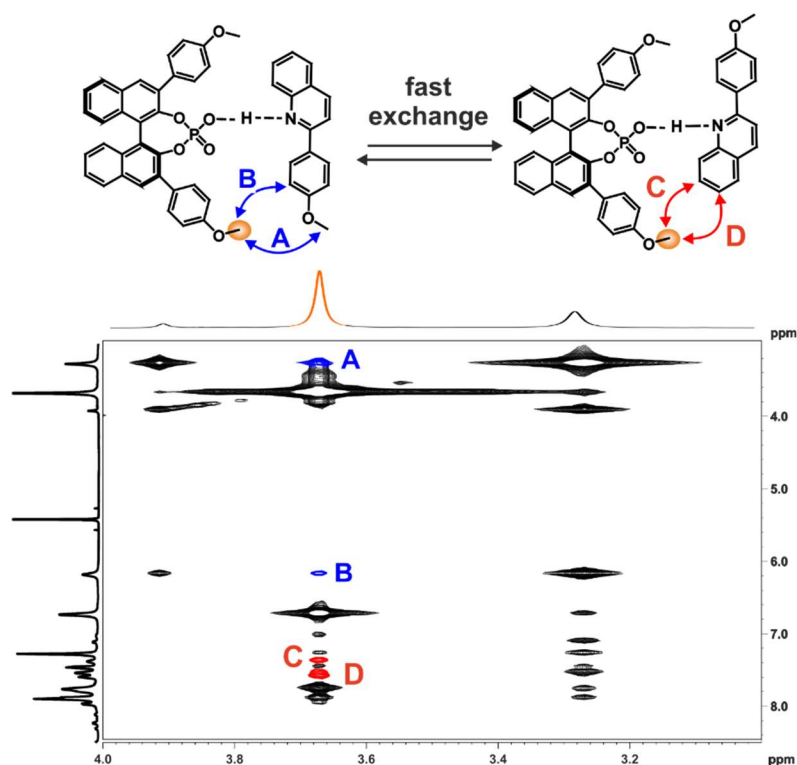


Figure S6: Identified structures and their respective characteristic NOE cross signals at 600 MHz and 180 K for a **3:4b** sample at a 1:1 stoichiometry and a concentration of 50 mM in CD_2Cl_2 .

Both structures are on a fast exchange on the NMR time scale and thus give one averaged set of signals. In analogy with previous investigations in binary CPA•imine complexes,^[11] only one set of signals for both naphthyl-fragments of the CPA BINOL-backbone was observed. This shows in combination with the strong binding of catalyst and substrate that the exchange pathway between the two fast exchanging binary CPA•Qu structures features switching of the hydrogen bond donor oxygen atom, as well as a rotation of the quinoline (see SI figure S31 for a more detailed explanation). The possible rotation of the substrate while bound to the catalyst reveals a bigger binding pocket of 3 compared to other catalysts typically used in synthesis.^[11]

In summary, the NMR structural investigations for binary monomeric **3**•Qu complexes showed that these systems are analogous in terms of structures, their dynamics and hydrogen bonding to binary monomeric CPA•imine complexes. Thus, at least in case of monomeric complexes the investigated system is a typical representative of catalyst•substrate complexes in CPA catalyzed transformations.

5.6.7. Diffusion Ordered Spectroscopy

The DOSY measurements were performed with the convection suppressing DSTE (double stimulated echo) pulse sequence developed by Jerschow and Müller in a pseudo 2D mode.^[12] TMS was used to reference the viscosity of the solvent. The diffusion time delay was set to 45 ms. The gradient pulse lengths (p16, SMSQ10.100 pulse shape) were optimized for each species to give a sigmoidal signal decay for varying gradient strengths and range between 700 to 1500 μs at 300 K. For each species, twenty spectra with linear varying gradient strength of 5% - 95% have been measured. The used probe signals for the analysis are listed in the respective tables. The signal intensities of the respective groups were analyzed as a function of the gradient strength by Bruker TopSpin 3.2 software T1/T2 relaxation package by employing the Stejskal-Tanner equation.^[13] No line broadening occurred for increasing gradient strength. The sigmoidal fit provided the translational self-diffusion coefficients D_i listed in the respective tables. The molecular radii were derived by the Stokes-Einstein equation^[14] using Chens correction.^[15]

$$D_i = \frac{k_B T}{6\pi\eta r_H} * (1 + 0.695 * \left(\frac{r_{\text{solv}}}{r_H}\right)^{2.234})$$

D_i is the self-diffusion coefficient derived by the measurement, η is the viscosity of the solvent, r_H is the hydrodynamic radius of the observed molecule and r_{solv} the radius of the solvent. No form factor correction was applied. The viscosity was determined by measuring the diffusion coefficient of the reference tetramethylsilane (TMS) and solving the equation for η with the literature value^[16] of the radius of 2.96 Å. The solvent radius of CD_2Cl_2 (2.46 Å) was taken from the reference.^[17]

For the error estimation, the separate diffusion coefficients for different probes belonging to the same species (e.g. all probes of the quinoline for the CPA•quinoline complex) were averaged and the standard deviation was determined. The molecular radii were determined based on the averaged diffusion coefficient, the averaged diffusion coefficient plus the standard deviation and the averaged diffusion coefficient minus the standard deviation. The resulting radii are given as the radius derived from the averaged diffusion coefficient and the error range is given by:

$$\text{Error range} = \frac{1}{2} * [(r_i^{\text{aver}} - r_i^{\text{aver}+StDev}) + (r_i^{\text{aver}-StDev} - r_i^{\text{aver}})]$$

Where r_i^{aver} is the radius derived from the averaged diffusion coefficient, $r_i^{\text{aver}+StDev}$ is the minimum radius derived from the averaged diffusion coefficient plus the standard deviation and $r_i^{\text{aver}-StDev}$ is the maximum radius derived from the averaged diffusion coefficient minus the standard deviation.

5. What is the Role of Acid-Acid Interactions in Asymmetric Phosphoric Acid Organocatalysis? A Detailed Mechanistic Study using Interlocked and Non-Interlocked Catalysts

Table S1: Summary of the determined diffusion coefficients and derived molecular radii for samples of **3** and **4b-d** with a 1:1 or 2:1 stoichiometry at 300 K or 180 K and for **3** or **4b** alone.

Temper.	Sample	Species	D _i (averaged)	D _i (StaDev)	D _i (min)	D _i (max)	r _i (averaged)	r _i (min)	r _i (max)	Result	+/-	D _i TMS
[K]			[m ² /s] e-10	[m ² /s] e-10	[m ² /s] e-10	[m ² /s] e-10	[Å]	[Å]	[Å]	[Å]	[Å]	[m ² /s] e-10
300	3/4b 1:1	4b	1.1753	0.0318	1.1435	1.2071	6.1531	6.0164	6.2979	6.15	0.21	3.273
300	3/4b 1:1	3	1.0055	0.0784	0.9271	1.0839	7.0387	6.5934	7.5634	7.04	0.71	3.273
300	3/4b 2:1	4b	0.7404	0.0125	0.7279	0.7529	8.8086	8.674	8.9479	8.81	0.20	3.092
300	3/4b 2:1	3	0.7241	0.0033	0.7208	0.7273	8.9922	8.9548	9.0300	8.99	0.06	3.092
300	3	3	0.8832	0.0024	0.8808	0.8856	7.7630	7.7441	7.782	7.76	0.03	3.210
300	4b	4b	2.0647	0.1009	1.9638	2.1655	3.8388	3.7163	3.9744	3.84	0.19	3.109
180	3/4b 1:1	4b	0.05147	0.000518	0.0510	0.0520	9.359	9.312	9.4058	9.36	0.07	22.95
180	3/4b 1:1	3	0.05698	0.00143	0.0556	0.0584	8.5213	8.3306	8.7222	8.52	0.29	22.95
300	3/4c 1:1	4c	1.3383	0.0704	1.2679	1.4086	5.3604	5.1456	5.6007	5.36	0.33	3.153
300	3/4c 1:1	3	0.955575	0.00480	0.9508	0.9604	7.1233	7.0921	7.1551	7.12	0.05	3.153
300	3/4c 2:1	4c	0.7510	0.0264	0.7246	0.7774	8.0489	7.8018	8.3148	8.05	0.38	2.841
300	3/4c 2:1	3	0.7352	0.00359	0.7316	0.7387	8.2058	8.1696	8.2424	8.21	0.05	2.841
300	3/4d 1:1	4d	0.8562	-	-	-	7.6806	-	-	7.68	-	3.075
300	3/4d 1:1	3	0.7255	0.0168	0.7088	0.7423	8.9296	8.7438	9.1245	8.93	0.28	3.075
300	3/4d 2:1	4d	0.6842	0.0113	0.6730	0.6955	9.4766	9.3339	9.6242	9.48	0.22	3.094
300	3/4d 2:1	3	0.7292	0.0263	0.7029	0.7555	8.9333	8.6469	9.242	8.93	0.44	3.094

In general, an increase of the determined radii of approx. 2 Å was determined for samples with a 2:1 stoichiometry compared to the respective 1:1 samples, demonstrating the population of higher aggregates of the CPA•quinoline complexes.

5. What is the Role of Acid-Acid Interactions in Asymmetric Phosphoric Acid Organocatalysis? A Detailed Mechanistic Study using Interlocked and Non-Interlocked Catalysts

Table S2: Probe signal and their respective diffusion coefficients for all measured samples. The chemical shifts in the DOSY experiments were not referenced and hence the given values can deviate from the chemical shifts in the given assignments.

A) 3:4b; 1:1; 300 K; p16 = 1200 us		
Species	$\delta(^1\text{H})$ [ppm]	D_i [m^2/s] e-10
4b	8.52	1.191
4b	8.18	1.131
3	7.72	0.9569
4b	7.55	1.204
3	6.70	0.9737
3	3.66	1.086

C) CPA 3; 300 K; p16 = 1400 us		
Species	$\delta(^1\text{H})$ [ppm]	D_i [m^2/s] e-10
3	8.10	0.8845
3	8.05	0.8818
3	7.38	0.8801
3	6.92	0.8826
3	3.56	0.8871

E) 3:4b 1:1; 180 K, p16 = 5500 us		
Species	$\delta(^1\text{H})$ [ppm]	D_i [m^2/s] e-12
3	7.46	5.182
3	7.28	5.129
3	7.86	5.165
4b	6.31	5.841
3	3.74	5.113
4b	3.40	5.555
TMS	0.00	23.00

G) 3:4c; 2:1, 300 K; p16 = 1500 us		
Species	$\delta(^1\text{H})$ [ppm]	D_i [m^2/s] e-10
4c	8.45	0.788
4c	7.85	0.7283
3	7.81	0.7318
3	7.52	0.7408
3	6.60	0.7323
4c	6.52	0.7366
3	3.50	0.7357

I) 3:4d; 2:1, 300 K; p16 = 1300 us		
Species	$\delta(^1\text{H})$ [ppm]	D_i [m^2/s] e-10
4d	8.67	0.6953
4d	8.28	0.6688
4d	8.18	0.6886
-	7.92	0.7614
-	7.62	0.7092
-	7.55	0.7070
3	6.74	0.7614
3	3.74	0.7071

B) 3:4b; 2:1; 300 K; p16 = 1500 us		
Species	$\delta(^1\text{H})$ [ppm]	D_i [m^2/s] e-10
4b	8.36	0.7572
3	7.82	0.7204
3	7.53	0.7288
3	6.58	0.7217
4b	6.35	0.7369
3	3.47	0.7253
4b	3.34	0.7272

D) Quinoline 4b; 300 K; p16 = 900 us		
Species	$\delta(^1\text{H})$ [ppm]	D_i [m^2/s] e-10
4b	8.08	2.090
4b	7.88	2.272
4b	7.83	1.953
4b	7.71	2.017
4b	7.51	2.028
4b	7.05	2.028

F) 3:4c; 1:1, 300 K; p16 = 1300 us		
Species	$\delta(^1\text{H})$ [ppm]	D_i [m^2/s] e-10
4c	8.66	1.457
4c	8.23	1.297
3	7.73	0.9635
4c	7.65	1.277
3	7.50	0.9544
4c	6.78	1.3220
3	6.79	0.9538
3	3.81	0.9506

H) 3:4d; 1:1, 300 K; p16 = 1300 us		
Species	$\delta(^1\text{H})$ [ppm]	D_i [m^2/s] e-10
4d	8.66	1.457
4d	8.23	1.297
3	7.73	0.9635
4d	7.65	1.277
3	7.50	0.9544
4d	6.78	1.3220
3	6.79	0.9538
3	3.81	0.9506

5.6.8. Structural investigation in 2:1 complexes

The exchange between **3•4b** and **3•3•4b** can be observed in the NOESY spectrum (see S29). Exchange peaks (marked in red) between the signal at 16.75 ppm (**3•4b**) and 15.27 ppm (**3•3•4b**) show that the PO⁻...H·N⁺ hydrogen bond of the **3•3•4b** complex is the signal at 15.27 ppm, as the PO·H·OP hydrogen bond signal at 16.51 ppm does not show exchange signals.

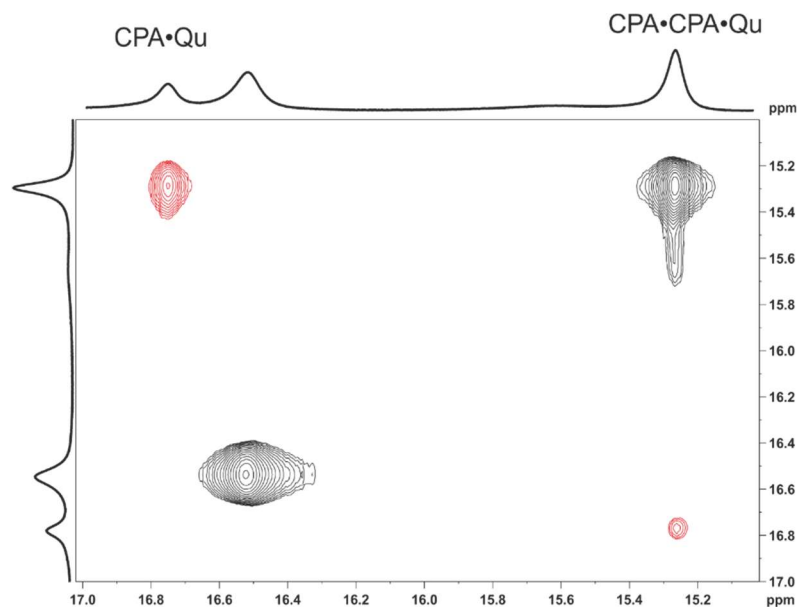


Figure S7: Excerpt of the NOESY spectrum of a 2:1 sample of **3•4b** at 200 K and 600 MHz in CD₂Cl₂. The exchange peaks between the different signals are marked in red.

5.6.9. References

- [9] a) K. Rothermel, M. Melikian, J. Hioe, J. Greindl, J. Gramüller, M. Žabka, N. Sorgenfrei, T. Hausler, F. Morana, R.M. Gschwind, *Chem. Sci.* **2019**, DOI: 10.1039/C9SC02342A; b) N. Sorgenfrei, J. Hioe, J. Greindl, K. Rothermel, F. Morana, N. Lokesh, R.M. Gschwind, *J. Am. Chem. Soc.* **2016**, *138*, 16345-16354.
- [10] a) J. Greindl, J. Hioe, N. Sorgenfrei, F. Morana, R.M. Gschwind, *J. Am. Chem. Soc.* **2016**, *138*, 15965-15971; b) M. Melikian, J. Gramueller, J. Hioe, J. Greindl, R.M. Gschwind, *Chem. Sci.* **2019**, *10*, 5226-5234.
- [11] N. Lokesh, J. Hioe, J. Gramüller, R.M. Gschwind, *J. Am. Chem. Soc.* **2019**, *141*, 16398-16407.
- [12] A. Jerschow, N. Müller, *J. Magn. Reson.* **1997**, *125* (2), 372-375.
- [13] E. O. Stejskal, J. E. Tanner, *J. Chem. Phys.* **1965**, *42* (1), 288-292.
- [14] A. MacChioni, G. Ciancaleoni, C. Zuccaccia, D. Zuccaccia, *Chem. Soc. Rev.* **2008**, *37* (3), 479-489.
- [15] H. C. Chen, S. H. Chen, *J. Phys. Chem.* **1984**, *88* (21), 5118-5121.
- [16] D. Ben-Amotz, K. G. Willis, *J. Phys. Chem.* **1993**, *97* (29), 7736-7742.
- [17] D. Zuccaccia, A. Macchioni, *Organometallics* **2005**, *24* (14), 3476-3486.

5.7. Additional findings

5.7.1. Selection of model systems

After elucidating the role of CPA dimers in the transfer hydrogenation of quinolines we aimed to explore if these findings are transferable onto the transfer hydrogenation of imines, especially as Rueping *et al.* noted a dependence of enantioselectivity and concentration of the reaction mixture for this reaction.^[1] Hence, an initial NMR system screening with catalysts **3b-f** and imines **9a-d** was performed (see figure 9). Catalyst **3b** and imine **9d** were selected, as this was the combination used by Rueping where a concentration effect was noted.^[1] Catalysts **3c-f** were selected for modulation of steric and electrostatic properties while retaining a rather small 3,3'-substituent, as bulky 3,3'-substituents might hinder dimerization. Imines **9a-c** were selected as typical substrates with different electrostatic properties and for comparability with previous studies on monomeric CPA/imine systems.^[2,3] In analogy to the previous measurements on CPA•CPA•Qu systems (see chapter 5.3.4.), all measurements were performed in CD₂Cl₂ at 180 K with a 2 : 1 ratio of catalyst and imine at a concentration range of 40-60 mM of the CPA.

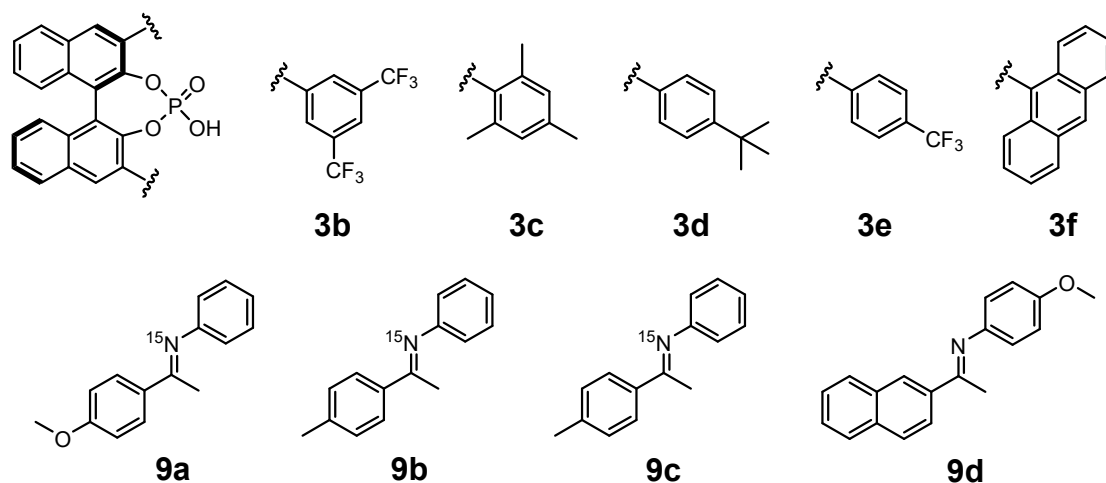


Figure 9: Selected model systems for the investigations of CPA•CPA•imine complexes.

5.7.2. NMR spectroscopic studies on **3b•3b•9a**

For **3b/9a** at a 2:1 ratio, in principle an analogous hydrogen bond pattern (see figure 10) was observed as for the CPA•CPA•Qu systems (see chapter 5.3.4.). Due to the ¹⁵N labelling of the imine, the PO---H-N hydrogen bonded protons show doublet splitting, which allows a clear distinction to the signals reflecting the PO--H--OP hydrogen bond. At a 2:1 ratio, the monomeric **3b•E-9a** (red) and **3b•Z-9a** (blue) complexes are present and were identified by comparison with the spectrum at a 1:1 ratio. In addition, the hydrogen bonded proton signals for the PO---H-N hydrogen bond for **3b•3b•E-9a** (magenta) and

5. What is the Role of Acid-Acid Interactions in Asymmetric Phosphoric Acid Organocatalysis? A Detailed Mechanistic Study using Interlocked and Non-Interlocked Catalysts

3b•3b•Z-9a (purple) as well as their respective PO--H--OP hydrogen bonds (orange) could be clearly identified. A ratio of monomer : dimer of $\approx 1 : 3.6$ was determined, showing that at a 2:1 ratio of catalyst and imine, the **3b•3b•9a** complexes are not exclusively populated.

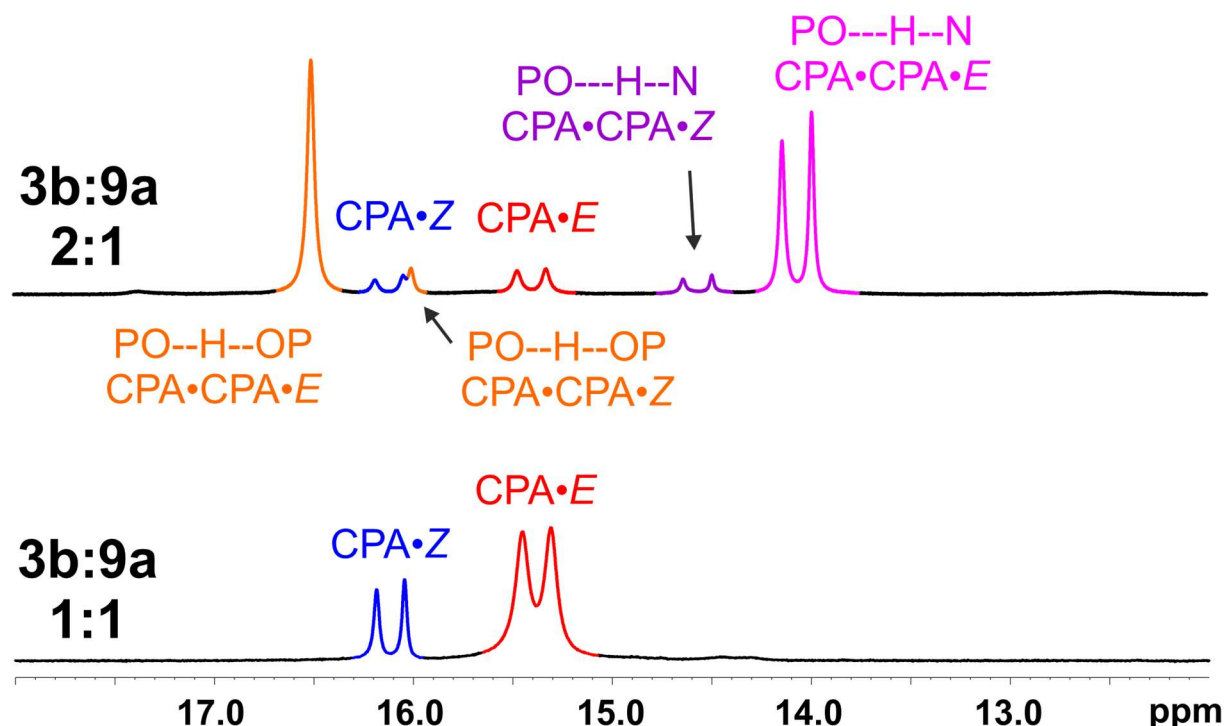


Figure 10: Excerpt of the ^1H NMR spectra of **3b/9a** at a 2:1 (top) or 1:1 (bottom) ratio, showing the hydrogen bonded proton signals. Signals for the monomeric **3b•E-9a** (red) and **3b•Z-9a** (blue) complex are observed and in addition signals for the PO---H-N hydrogen bond for **3b•3b•E-9a** (magenta) and **3b•3b•Z-9a** (purple) as well as their respective PO--H--OP hydrogen bonds (orange).

The assignment of *E*- and *Z*-imine was based on the NOESY spectrum and the typical highfield shift of the PO---H-N hydrogen bonded proton signal for the *E*-complexes.^[2,3] Based on a series of homo- and heteronuclear NMR spectra, a partial chemical shift assignment could be achieved. Based on that, DOSY measurements were performed, using the well-separated *para*-methoxy groups of **3b•E-9a** and **3b•3b•E-9a** as probes. For the monomeric complex, a hydrodynamic volume of 2150 \AA^3 was determined, while for the dimer a value of 3760 \AA^3 was derived. The almost doubled volume clearly validates the assignment of the CPA•CPA•imine dimers. Analysis of the NMR parameters for the hydrogen bonds shows a clear highfield shift of the ^1H and ^{15}N chemical shifts and increase of the $^1J_{\text{NH}}$ coupling constant when comparing the dimeric and monomeric species with the same imine configuration (see table 3). As demonstrated in our previous research,^[4,5] this reflects a stronger proton transfer onto the substrate and a weaker hydrogen bond.

5. What is the Role of Acid-Acid Interactions in Asymmetric Phosphoric Acid Organocatalysis? A Detailed Mechanistic Study using Interlocked and Non-Interlocked Catalysts

Table 3: Hydrogen bond parameters ($\delta(^1\text{H})$, $\delta(^{15}\text{N})$ and $^1J_{\text{NH}}$) of the different **3b/9a** species derived from the 2:1 sample at a concentration of 40/20 mM in CD_2Cl_2 at 180 K.

System	$\delta(^1\text{H})$ [ppm]	$\delta(^{15}\text{N})$ [ppm]	$^1J_{\text{NH}}$ [Hz]
3b•E-9a	15.39	196.0	87.1
3b•3b•E-9a (OHN)	14.06	188.3	88.6
3b•3b•E-9a (OHO)	16.53	-	-
3b•Z-9a	16.10	203.8	84.6
3b•3b•Z-9a (OHN)	14.56	200.0	87.7
3b•3b•Z-9a (OHO)	16.00	-	-

Based on the partial chemical shift assignment, an analysis of the NOESY spectrum was performed to obtain insights into the structure of CPA•CPA•imine dimers. However, given the presence of 4 different complexes (monomer, dimer, *E* and *Z*) and the resulting chemical shift overlap accompanied by line broadening due to exchange processes (e.g. between **3b•E-9a** and **3b•3b•E-9a** as indicated by EXSY peaks for the PO---H-N hydrogen bonded proton signal), detailed insights could not be obtained. Nevertheless, in the ^1H ^{19}F HOESY spectrum, clear contacts between the 3,3'-substituent and the *para*-methoxy and $\alpha\text{-CH}_3$ group of the most populated **3b•3b•E-9a** could be identified.

In the previous work on monomeric CPA•imine^[2,3] and CPA•quinoline (see chapter 5.3.4.) systems, two different conformations were found for each monitored binary complex. These conformations differ in the orientation of the imine/quinoline (rotated by 180°) and are exchanging fast on the NMR time scale. Thus, they appear as one averaged set of signals, but could be identified via the NOESY NMR pattern. Additionally, applying the relaxation dispersion $R_{1\rho}$ NMR method^[6] allowed to access the exchange rate as well as the populations of the two underlying conformations for this fast exchange process. For **3b•3b•9a**, the line broadening and signal overlap prevented a detailed analysis of the NOE pattern. Therefore, qualitative $R_{1\rho}$ NMR measurements were performed to elucidate if a fast exchange process between two different conformations is present. These measurements were only done for **3b•3b•E-9a**, as the respective *Z*-species was too low populated. As suitable probe signals, the *para*-methoxy and $\alpha\text{-CH}_3$ group of **9a** as well as one signal for the CPA were selected, which belongs either to the BINOL backbone or the *ortho*-protons of the 3,3'-substituents. The measurements were performed analogous to the previous $R_{1\rho}$ measurements with the optimized parameters (see chapter 4 and reference^[6]). For all three probe signals, a clear decay curve was found, which validates the presence of a fast exchange process (see figure 11). Hence, for **3b•3b•E-9a** and most likely also for **3b•3b•Z-9a**, at least two different conformations are present, which are exchanging fast on the NMR timescale.

5. What is the Role of Acid-Acid Interactions in Asymmetric Phosphoric Acid Organocatalysis? A Detailed Mechanistic Study using Interlocked and Non-Interlocked Catalysts

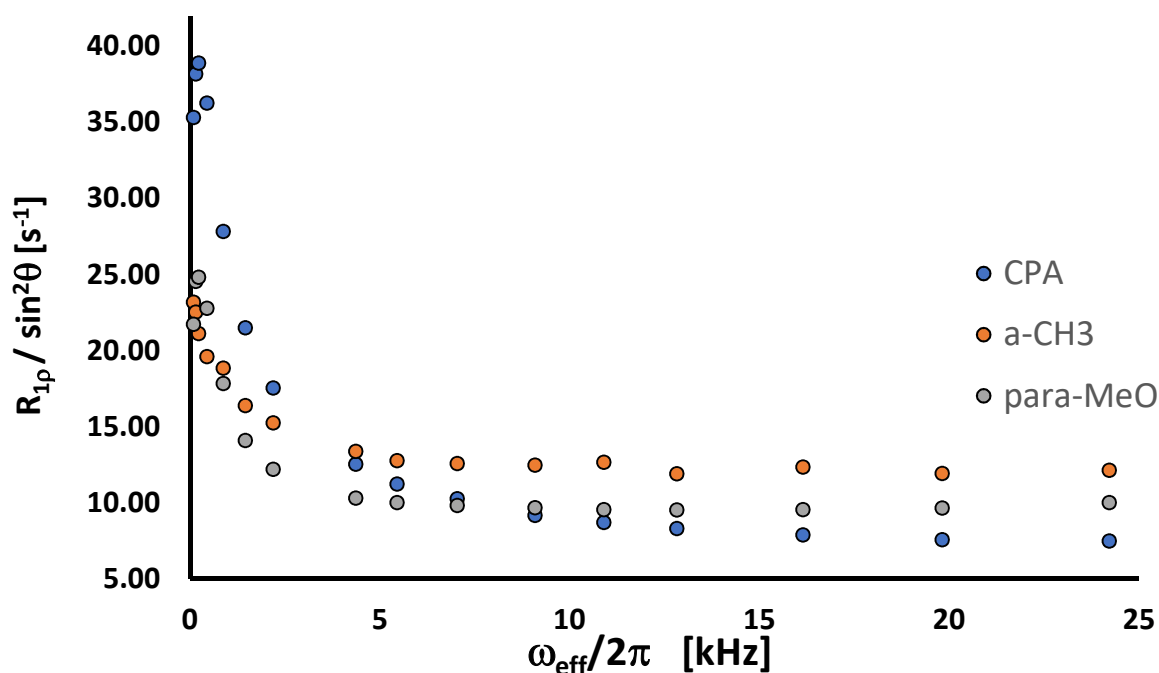


Figure 11: Plot of the offset-Lorentzian decay curve from the R_{1p} measurements for **3b•3b•E-9a**.

5.7.3. Computational studies on **3b•3b•9a**

To obtain more detailed insights into the structure of CPA•CPA•imine dimers, a preliminary DFT structure optimization for **3b•3b•E-9a** was done based on the previously found CPA•CPA•quinoline structure.^[7] **3b•3b•E-9a** was optimized using ORCA 4.1.2^[8] employing the implicit SMD solvent model using an epsilon value of 16.2 for dichloromethane (to account for the NMR measurements performed at 180 K)^[9], the BP functional, the RI approximation and the def2-SVP basis set. In analogy to the previous computations for monomeric CPA•imine complexes and in agreement with the R_{1p} NMR measurements, the structures of two conformers (denoted as Type I and Type II) were optimized for which the imine was rotated by 180°. For both optimized structures, the *para*-methoxy and α -CH₃ substituents of **9a** are in close proximity to one 3,3'-substituent of **3b**, which agrees with the ¹H ¹⁹F HOESY and ¹H NOESY NMR experiments (see figure 12 red arrows). In the previous structure optimization for CPA•CPA•Qu, both PO--H--OP and PO---H-N hydrogen bonds were formed to the same oxygen atom of one CPA molecule (see chapter 5.3.4. figure 7). This motif was also found in the Type I structure (see figure 12 bottom left). However, for the Type II structure the PO--H--OP and PO---H-N hydrogen bond are formed to two different oxygen atoms of the same CPA molecule (see figure 12 bottom right). This results in a different orientation of the phosphoryl oxygen of the second CPA molecule (see figure 12, marked in green). For the Type I conformer, the phosphoryl oxygen is close to the PO---H-N hydrogen bond, while for the Type II conformer it is directed away from the imine. In the previous structure optimization for CPA•CPA•Qu•Hantzsch-ester, the quinoline was bound to one CPA, while the

5. What is the Role of Acid-Acid Interactions in Asymmetric Phosphoric Acid Organocatalysis? A Detailed Mechanistic Study using Interlocked and Non-Interlocked Catalysts

Hantzsch-ester formed a hydrogen bond to the second CPA. This resulted in a stacking of quinoline and Hantzsch-ester in between two catalyst molecules and determined the stereoselective outcome for this step. For **3b•3b•E-9a**, in the Type I conformer the phosphoryl oxygen atom of the second CPA is close to the imine and offers a free, available binding site for the Hantzsch-ester. This would result in a stacked arrangement of imine and Hantzsch-ester without much reorganization. In the Type II conformer however, the phosphoryl oxygen is directed away from the imine and binding of Hantzsch-ester would not result in a close spacial proximity of imine and Hantzsch-ester without significant reorganization.

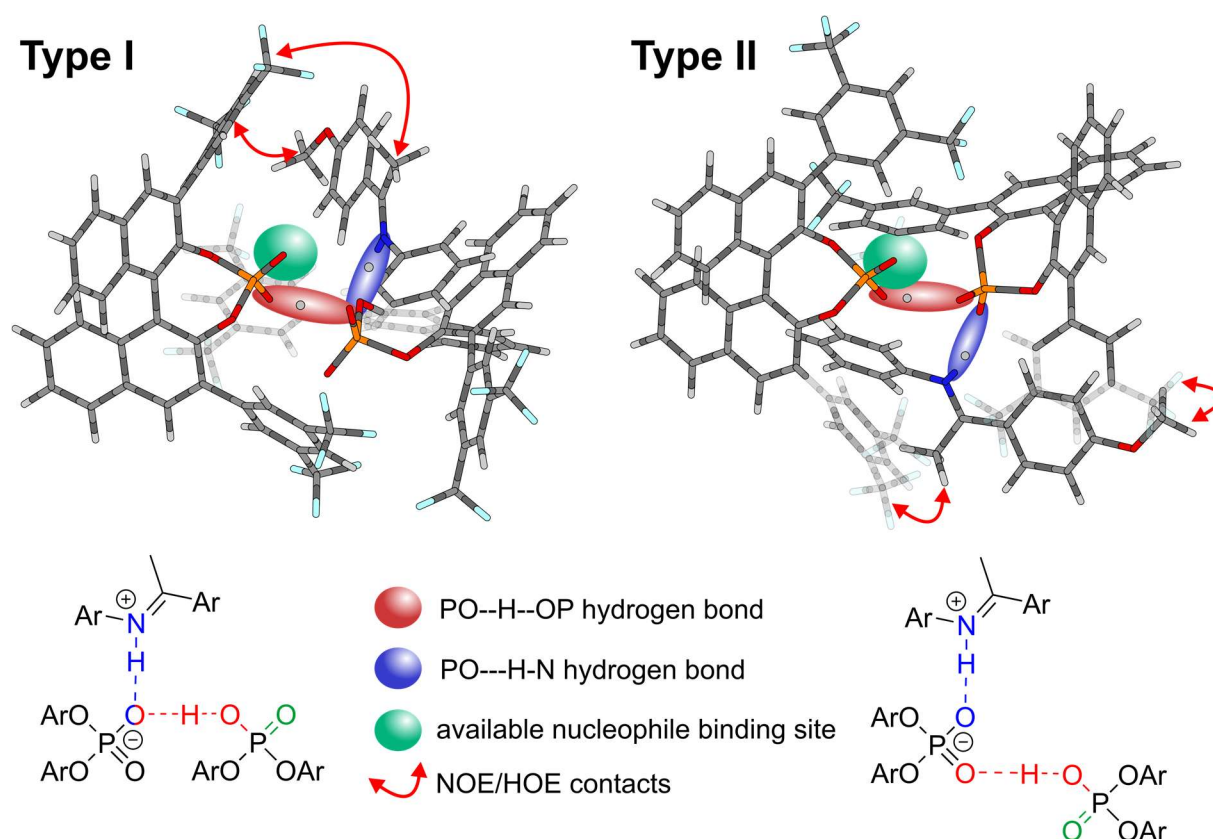


Figure 12: Optimized structure for the Type I and Type II conformer for for **3b•3b•E-9a** (top) and the schematic differences in their hydrogen bond motifs (bottom). Colour code: Black: carbon, grey: hydrogen, red: oxygen, orange: phosphorus, dark blue: nitrogen, light blue: fluorine.

This indicates that for the Type II conformer subsequent binding of the Hantzsch-ester will either not result in an arrangement suitable for the hydride transfer or that major reorganization is needed, which makes it unfavourable. However, these computations were performed on a preliminary level and a thorough conformer screening and optimization would be needed to validate, if these conformers are indeed the most stable ones.

5.7.4. Overview of CPA•CPA•imine systems

Based on the results for **3b/9a**, especially the established hydrogen bonded proton pattern featuring monomeric and dimeric, as well as *E*- and *Z*-complexes, measurements with systems **3b/9b-d** and **3c-f/9a** were performed to shed light onto the influence of catalyst and substrate for populating dimeric CPA•CPA•imine systems. For the spectra with catalyst **3b**, a similar pattern of the hydrogen bonded proton signals was found for imines **9a-d** (see figure 13). For **3b/9b** only the dimeric species were populated and no signals for the monomeric complexes were monitored. Similarly, for **3b/9d** the dimeric species were the major populated ones, although the two signals at 15.9 and 16.4 ppm next to the PO--H--OP signals likely correspond to the monomeric species. For **3b/9c**, the monomeric species are present but the typical dimer pattern was not observed. Likely, the signals between 15.2 and 16.2 ppm reflect the dimeric species and the signals for the PO---H--N and PO--H--OP hydrogen bonds for *E*- and *Z*- complex overlap.

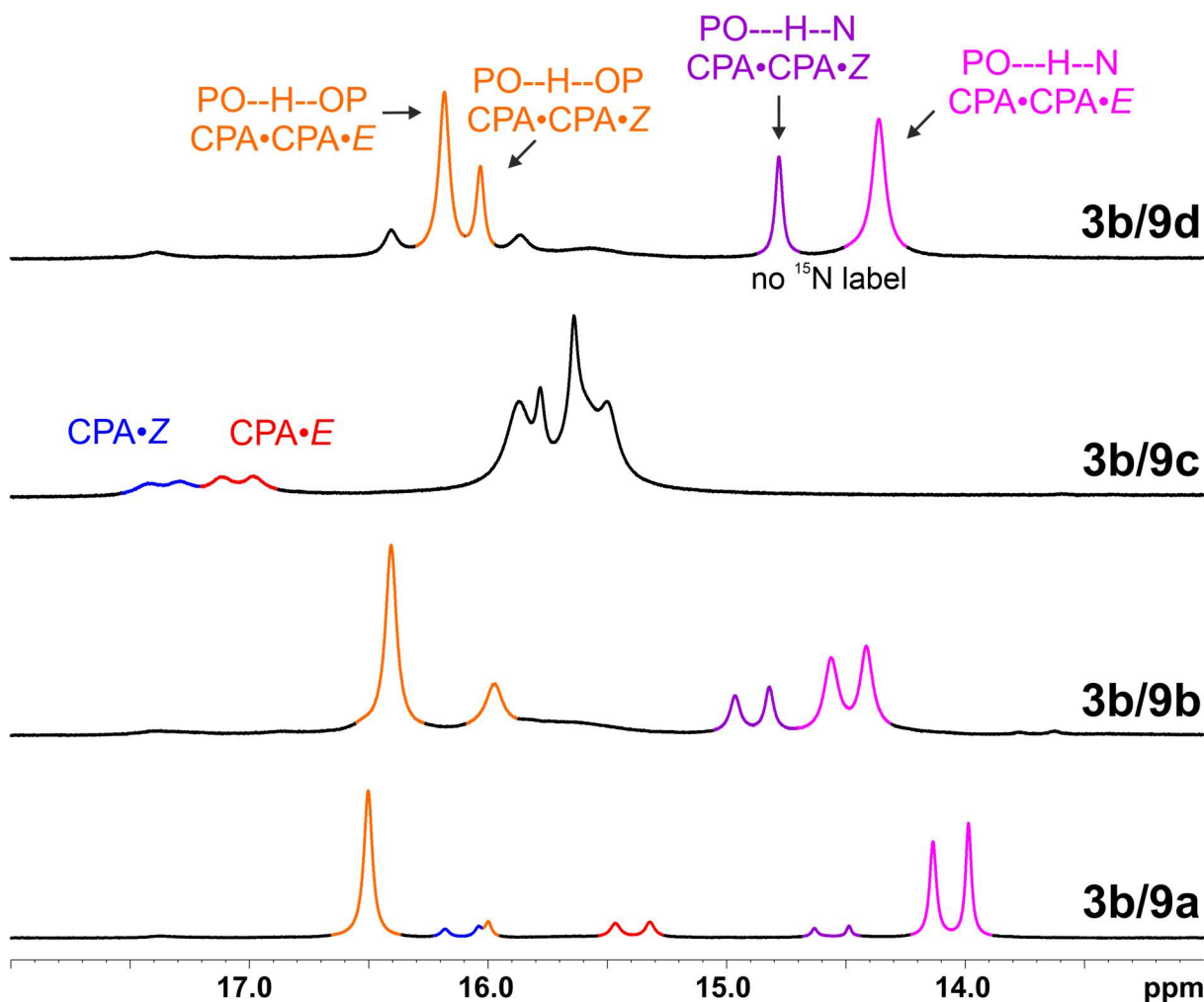


Figure 13: Excerpt of the ^1H NMR spectra of **3b/9a-d** at a 2:1 ratio, showing the hydrogen bonded proton signals. Signals for the monomeric **3b•E-9** (red) and **3b•Z-9** (blue) complexes are observed and in addition signals for the PO---H--N hydrogen bond for **3b•3b•E-9** (magenta) and **3b•3b•Z-9** (purple) as well as their respective PO--H--OP hydrogen bonds (orange).

5. What is the Role of Acid-Acid Interactions in Asymmetric Phosphoric Acid Organocatalysis? A Detailed Mechanistic Study using Interlocked and Non-Interlocked Catalysts

Hence, for catalyst **3b** at a 2:1 ratio of CPA and imine, the dimeric CPA•CPA•imine species were found to be the major populated species. This indicates that for catalyst **3b** the dimeric reaction channel is available for a broad scope of substrates. However, similar as for **3b/9a**, severe signal overlap and line broadening prevented any more detailed insights into the structure of **3b/9b-d**.

When changing the catalyst, a strong effect on the hydrogen bond pattern and the population of the dimeric species was observed (see figure 14). For **3d/9a**, the monomeric complexes and the [CPA•E-imine]₂ dimer of the monomeric complex were observed and assigned by comparison to the spectrum at a 1:1 ratio.^[2] In addition to that, the hydrogen bond signals for the **3c•3c•E-9a** complex could be identified as minor populated species by the ¹J_{NH} coupling constant and EXSY peaks in the NOESY spectrum.

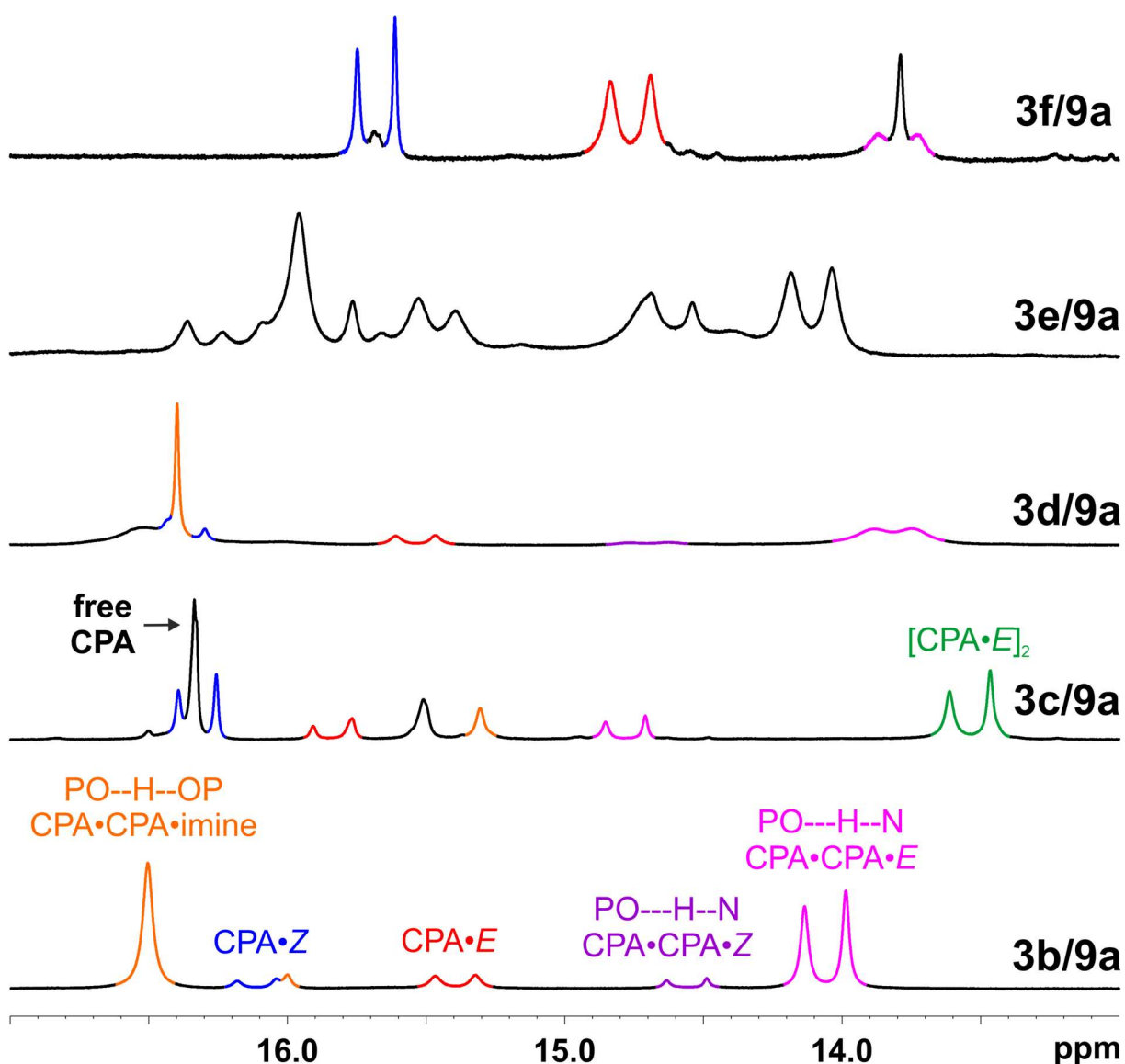


Figure 14: Excerpt of the ¹H NMR spectra of **3b-f/9a** at a 2:1 ratio, showing the hydrogen bonded proton signals. Signals for the monomeric **3•E-9a** (red) and **3•Z-9a** (blue) complexes are observed and in addition signals for the PO---H-N hydrogen bond for **3•3•E-9a** (magenta) and **3•3•Z-9a** (purple) as well as their respective PO--H--OP hydrogen bonds (orange). Furthermore, signals for the free CPA and [CPA•imine]₂ dimers (green) are monitored.

5. What is the Role of Acid-Acid Interactions in Asymmetric Phosphoric Acid Organocatalysis? A Detailed Mechanistic Study using Interlocked and Non-Interlocked Catalysts

For **3d/9a**, the monomeric species were tentatively assigned based on their $^1J_{\text{NH}}$ coupling constants and pattern similarity to the other spectra. The remaining two doublets are suggested to reflect the **3d•3d•E-9a** and **3d•3d•Z-9a** complex based on the EXSY peaks in the NOESY spectrum with the respective monomeric complexes. However, it could also be that these signals correspond to **[3d•9a]₂** dimers of the monomeric complex and the signal assigned for the PO--H--OP hydrogen bond corresponds to the free CPA. For **3e/9a**, no clear assignment was possible due to the presence of multiple species and signal overlap. For **3f/9a**, the monomeric species were assigned by comparison to the spectrum at a 1:1 ratio. The signal for **3d•3d•E-9a** was tentatively assigned based on the $^1J_{\text{NH}}$ coupling constant but was not further corroborated and the respective PO--H--OP hydrogen bond signal could not be clearly assigned. Hence, in summary the formation of CPA•CPA•imine species depends strongly on the selection of the catalyst.

In conclusion, within the investigated set of systems the formation and preference for CPA•CPA•imine complexes depended strongly on the selection of the catalyst but not significantly on the selection of the imine. These findings were derived for a CPA:imine ratio of 2:1, while under catalytic conditions usually a catalyst loading below 10-20% is used. However, the previous studies for quinoline systems showed that the dimeric reaction channel can be dominant at such conditions due to its thermodynamic preference over the monomeric channel. Although there is no direct correlation between the population of CPA•CPA•imine complexes at the NMR sample conditions and the activation barrier for the hydride transfer in the dimeric/monomeric reaction channel, the observed trends suggest that the competition between dimeric and monomeric channel is more strongly affected by the catalyst and less by the imine.

5.7.5. Conclusion

Based on the findings on CPA•CPA•quinoline systems, the role of CPA•CPA dimers in the transfer hydrogenation of imines was explored. Low temperature NMR measurements revealed that at a 2:1 ratio of catalyst and imine, both monomeric CPA•imine and dimeric CPA•CPA•imine complexes are present, which is in analogy to the findings for quinoline systems. In addition, the imine can be present as *E*- or *Z*-isomer. In the CPA•CPA•imine dimers, the imine is stronger protonated than in the monomeric complex due to the cooperativity effect introduced by the additional PO--H--OP hydrogen bond which results in a weaker hydrogen bond. Relaxation dispersion $R_{1\rho}$ NMR measurements revealed the presence of at least two conformers for these dimers, which are exchanging fast on the NMR time scale and appear as one averaged set of signals. A preliminary DFT study shed light onto the differences of these conformers. In the Type I conformer, both PO--H--OP and PO---H-N hydrogen bonds are directed to

5. What is the Role of Acid-Acid Interactions in Asymmetric Phosphoric Acid Organocatalysis? A Detailed Mechanistic Study using Interlocked and Non-Interlocked Catalysts

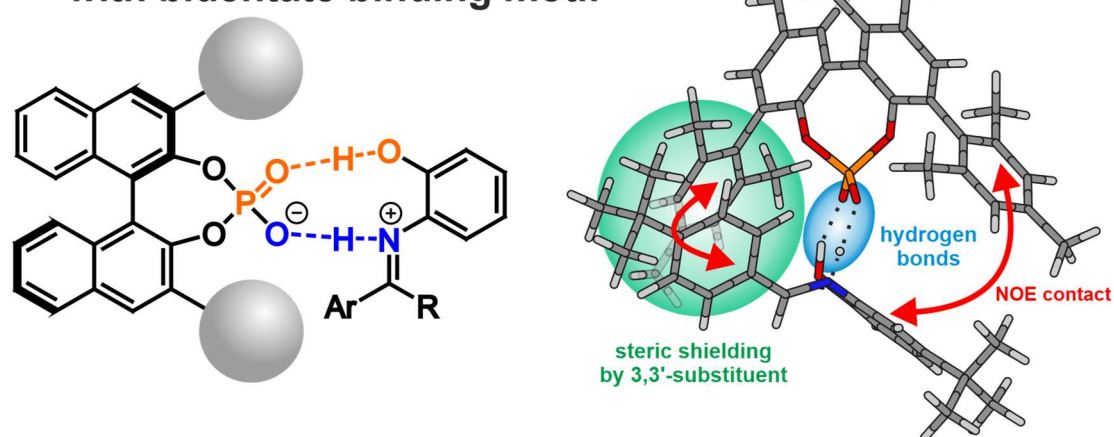
the same oxygen atom of one CPA molecule, while in the Type II conformer they are directed to two different oxygen atoms of the same CPA molecule. Due to this difference in the hydrogen bond motif, in the Type I conformer the binding site for the Hantzsch-ester nucleophile is available, while in the Type II conformer major reorganization would be necessary to result in a suitable arrangement for the hydride transfer step. Additionally, the preference for the formation of CPA•CPA•imine dimers was found to be strongly dependent on the selected CPA and mostly unaffected by the selection of the imine, which suggests that the impact of the dimeric reaction channel is mainly dominated by the selected catalyst.

5.7.6. References

- [1] M. Rueping, E. Sugiono, C. Azap, T. Theissmann, M. Bolte, *Org. Lett.* **2005**, *7*, 3781–3783.
- [2] M. Melikian, J. Gramüller, J. Hioe, J. Greindl, R. M. Gschwind, *Chem. Sci.* **2019**, *10*, 5226–5234.
- [3] J. Greindl, J. Hioe, N. Sorgenfrei, F. D. Morana, R. M. Gschwind, *J. Am. Chem. Soc.* **2016**, *49*, 15965–15971.
- [4] N. Sorgenfrei, J. Hioe, J. Greindl, K. Rothermel, F. Morana, N. Lokesh, R. M. Gschwind, *J. Am. Chem. Soc.* **2016**, *138*, 16345–16354.
- [5] K. Rothermel, M. Melikian, J. Hioe, J. Greindl, J. Gramüller, M. Žabka, N. Sorgenfrei, T. Hausler, F. Morana, R. M. Gschwind, *Chem. Sci.* **2019**, *10*, 10025–10034.
- [6] N. Lokesh, J. Hioe, J. Gramüller, R. M. Gschwind, *J. Am. Chem. Soc.* **2019**, *141*, 16398–16407.
- [7] P. Dullinger, M. Žabka, *unpublished results*.
- [8] F. Neese, *Comput. Mol. Sci.* **2012**, *2*, 73–78.
- [9] J. Greindl, J. Hioe, N. Sorgenfrei, F. Morana, R. M. Gschwind, *J. Am. Chem. Soc.* **2016**, *138*, 15965–15971.

6. Bidentate Substrate Binding in Brønsted Acid Catalysis: Structural Space, Hydrogen Bonding and Dimerization

Brønsted acid/substrate complexes with bidentate binding motif



Johannes Gramüller, Philipp Dullinger, Dominik Horinek and Ruth M. Gschwind,

Chem. Sci. **2022**, *13*, 14366-14372. DOI: 10.1039/D2SC05076E

A) Johannes Gramüller planned, performed and analyzed all experiments, especially synthesis of all imines and all NMR experiments. He wrote the manuscript with input from all authors. B) All computations were planned, performed and analyzed by Philipp Dullinger. He contributed in writing the manuscript parts about the computational studies. C) Dominik Horinek assisted in the computations and writing of the manuscript. D) Ruth M. Gschwind contributed to design of experiments, interpretation of data, writing and proof-reading of the manuscript part and provided funding.

6.1. Abstract

BINOL derived chiral phosphoric acids (CPAs) are a prominent class of catalysts in the field of asymmetric organocatalysis, capable of transforming a wide selection of substrates with high stereoselectivities. Exploiting the Brønsted acidic and basic dual functionality of CPAs, substrates with both a hydrogen bond acceptor and donor functionality are frequently used as the resulting bidentate binding via two hydrogen bonds is expected to strongly confine the possible structural space and thus yield high stereoselectivities. Despite the huge success of CPAs and the popularity of a bidentate binding motif, experimental insights into their organization and origin of stereoselection are scarce. Therefore, in this work the structural space and hydrogen bonding of CPAs and N-(*ortho*-hydroxyaryl) imines (19 CPA/imine combinations) was elucidated by low temperature NMR studies and corroborated by computations. The postulated bidentate binding of catalyst and substrate by two hydrogen bonds was experimentally validated by detection of trans-hydrogen bond scalar couplings. Counterintuitively, the resulting CPA/imine complexes showed a broad potential structural space and a strong preference towards the formation of [CPA/imine]₂ dimers. Molecular dynamics simulations showed that in these dimers, the imines form each one hydrogen bond to two CPA molecules, effectively bridging them. By finetuning steric repulsion and noncovalent interactions, rigid and well-defined CPA/imine monomers could be obtained. NOESY studies corroborated by theoretical calculations revealed the structure of that complex, in which the imine is located in between the 3,3'-substituents of the catalyst and one site of the substrate is shielded by the catalyst, pinpointing the origin of stereoselectivity for downstream transformations.

6.2. Introduction

Brønsted Acids have emerged as a powerful type of catalyst, adaptable to a myriad of asymmetric transformations.³⁻⁵ The general concept is to lower the LUMO (Lowest Unoccupied Molecular Orbital) energy of the substrate via protonation by the Brønsted acidic catalyst functionality, thus facilitating a reaction with a nucleophile. By creating a stereoinductive environment around the substrate due to Coulomb-, hydrogen bonding- and other non-covalent interactions, the catalyst paves an asymmetric pathway for the reaction. The versatility of chiral Brønsted acids is augmented by a Brønsted basic site, which enables additional modes of activation and organization of the reactants (see Figure 1 top).⁵ Exemplarily, the phosphoryl functionality of BINOL derived chiral phosphoric acids (CPA) can act as a hydrogen bond acceptor towards nucleophiles bearing a hydrogen bond donor, thus organizing both electro- and nucleophile in a defined way.⁶⁻¹⁰ This “three-point-interaction model” was recognized to be crucial for delivering high stereoselectivities.¹¹⁻¹³ Moreover, by implementing both a hydrogen bond acceptor and donor functionality into the substrate,¹⁴⁻²⁰ bidentate binding of the catalyst and substrate results in a presumably rigid preorganization of the substrate, in which one side of the substrate is shielded by the catalyst residues. In their seminal report on CPA catalysed Mannich-type reactions, Akiyama *et al.* employed such a bidentate binding motif with the intention to furnish a highly confined structural space (see Figure 1, right part) and noted a significant change in enantioselectivity, if the *ortho*-hydroxy group was omitted or placed in *para*-position.¹⁴ Their computational study revealed a transition state, in which the substrate is anchored by two hydrogen bonds and is located in between the 3,3'-substituents.¹⁴ This orientation is similar to the transition states which were found *e.g.* for the transfer hydrogenation of imines with Hantzsch Ester^{11,21} reflecting the “three-point-interaction model” and to dimers of complexes featuring CPAs and imines without additional hydrogen bond donors.²² However, to the best of our knowledge experimental insights into the structural space of bidentate CPA/substrate complexes are limited to one recent example in asymmetric photocatalysis provided by our group, in which no detailed structural analysis could be derived.¹⁹ Therefore, in this report we present a detailed NMR spectroscopic study corroborated by molecular dynamics (MD) simulations on the structural space and hydrogen bonding of complexes featuring 8 CPAs and 8 N-(*ortho*-hydroxy-aryl) imines (19 CPA/imine combinations). Low temperature NMR measurements revealed a broad structural space with a strong preference for the formation of [CPA/imine]₂ dimers, demonstrating that the principal idea of using a bidentate binding motif to restrict the structural space is not applying. MD simulations revealed that different dimer motifs are thermally accessible, in which each imine molecule bridges two different CPA molecules via hydrogen bonding. Breaking these dimers by fine-tuning steric repulsion and non-covalent interactions gave access to a rigid and well-defined monomeric CPA/imine complex. Combined NOESY NMR studies and computations revealed the structure of

6. Bidentate Substrate Binding in Brønsted Acid Catalysis: Structural Space, Hydrogen Bonding and Dimerization

this monomeric complex and confirmed the assumed origin of stereoselectivity for downstream transformations.

Previous work:

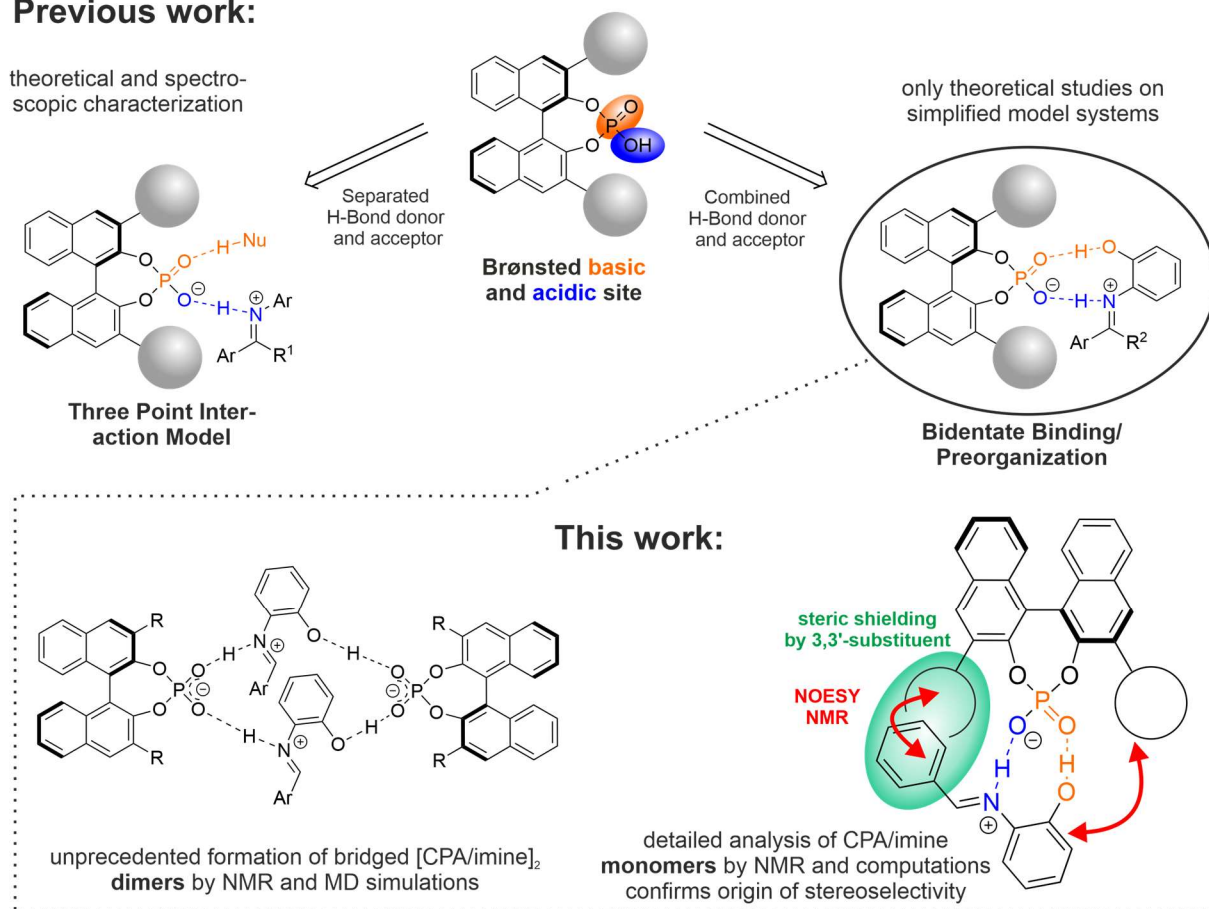


Figure 1: Top) Dual functionality of Brønsted acids enabling either parallel binding of electro- and nucleophile or bidentate binding of the substrate in a presumably rigid, defined way by hydrogen bonding. While the parallel binding motif is well explored experimentally and *in silico*, no detailed experimental insights exist for the bidentate binding motif. Bottom) Key questions and results of the presented work feature spectroscopic and computational studies on the monomeric CPA/imine complex, confirming the surmised origin of stereoselectivity and unprecedented detection of [CPA/imine]₂ bridged dimers.

6.3. Results and Discussion

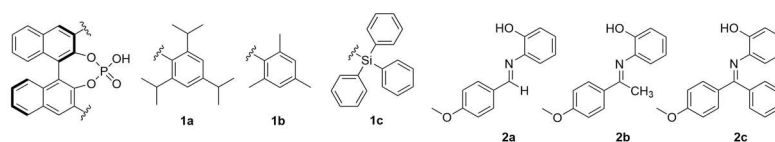
6.3.1. Initial System Screening and dimer formation

To obtain an access to the structural space of bidentate CPA/imine complexes, an initial system screening with catalysts **1a-c** and imines **2a-c** was carried out (see Figure 2A). Catalysts **1a-c** were selected due to their wide application in synthesis, their symmetry, solubility and different steric properties. For imines **2a-c**, a *para*-methoxy residue was selected as potential probe for structural investigations via NOESY NMR and the α -imine substituent was varied to modulate steric effects and subsequently the ratio between *E* and *Z* imine (*Z* population increasing for $\alpha\text{-H} < \alpha\text{-CH}_3 < \alpha\text{-Ph}$). All NMR measurements were carried out at a temperature of 180 K to slow down potential exchange processes and thus

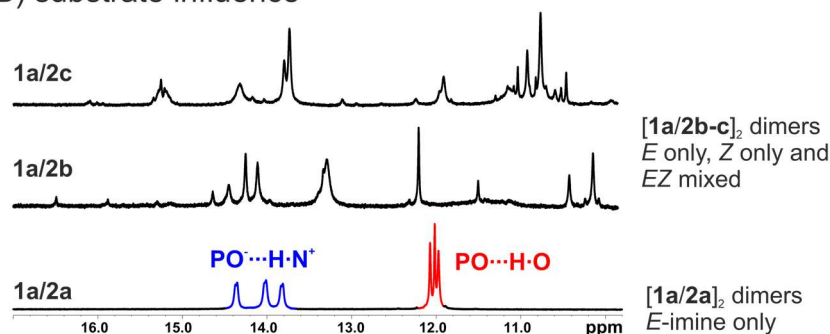
6. Bidentate Substrate Binding in Brønsted Acid Catalysis: Structural Space, Hydrogen Bonding and Dimerization

to obtain an optimally resolved hydrogen bond pattern. In the previous work by Akiyama,^{1,14} toluene was used as solvent as it yielded the best stereoselectivity in the initial reaction optimization. However, similar to our previous studies,²³ the low temperature ¹H-NMR spectra in toluene gave very broad signals and were not suitable for further investigations (see SI Figure S4). Hence dichloromethane (CD₂Cl₂) was selected as solvent for the NMR investigations, providing superior signal dispersion, linewidths and solubility. In addition, previous studies of CPA/imine complexes were successfully conducted in CD₂Cl₂ in our working group.^{22–25} For the system **1a/2a**, 6 proton signals were monitored in the H-bond region of the spectrum, corresponding to 3 distinct CPA/imine complexes with a ratio of ~ 1 : 1.7 : 1.1. The signals at ~14 ppm (Figure 2B, blue signals) were assigned to the PO⁻...H-N⁺ hydrogen bonds based on the scalar coupling to the α-H protons of **2a** (²*h*J_{HH} = 13.6 Hz), which was confirmed by ¹H ¹H COSY spectrum. The signals at ~12 ppm (Figure 2B, red signals) reflect the PO⁻...H-O hydrogen bonds and were assigned based on cross signals in the ¹H ³¹P HMBC spectrum and cross peaks with the protons of the N-aryl group in the ¹H ¹H COSY spectrum.

A) model systems



B) substrate influence



C) catalyst influence

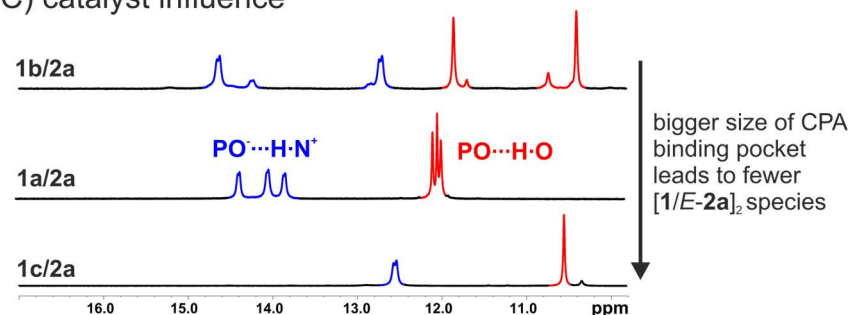


Figure 2: A) Selected catalysts and substrates for the initial system screening. B) Section of the ¹H NMR spectra of **1a/2a** (bottom), **1a/2b** (middle) and **1a/2c** (top) at a 1:1 ratio and a concentration of 50, 10 and 10 mM respectively in CD₂Cl₂ at 600 MHz and 180 K. For **1a/2a**, three distinct species were observed, while for **1a/2b-c**, a multitude of different signals was monitored. C) Section of the ¹H NMR spectra of **1a/2a** (middle), **1b/2a** (top) and **1c/2a** (bottom) at a 1:1 ratio and a concentration of 50, 10 and 10 mM respectively in CD₂Cl₂ at 600 MHz and 180 K.

6. Bidentate Substrate Binding in Brønsted Acid Catalysis: Structural Space, Hydrogen Bonding and Dimerization

In contrast, for **1a/2b-c** (see Figure 2B) a multitude of hydrogen bonded proton signals is detected, reflecting an unexpected broad structural space (similar spectra were obtained for **1b/2b-c**; see SI S6). For **1a/2a**, the three observed species could be assigned as different [**1a/E-2a**]₂ dimers, featuring exclusively the *E*-imine (see below). For **1a-b/2b-c**, we strongly assume that analogous [CPA/imine]₂ dimers are present, featuring either the *E*- or *Z*-imine or a mixture of both which increases the number of observed species. This variety of dimeric structures in combination with the potential presence of additional monomeric [CPA/imine] species causes the observed broad structural space reflected in the multitude of different H-bonded proton signals.

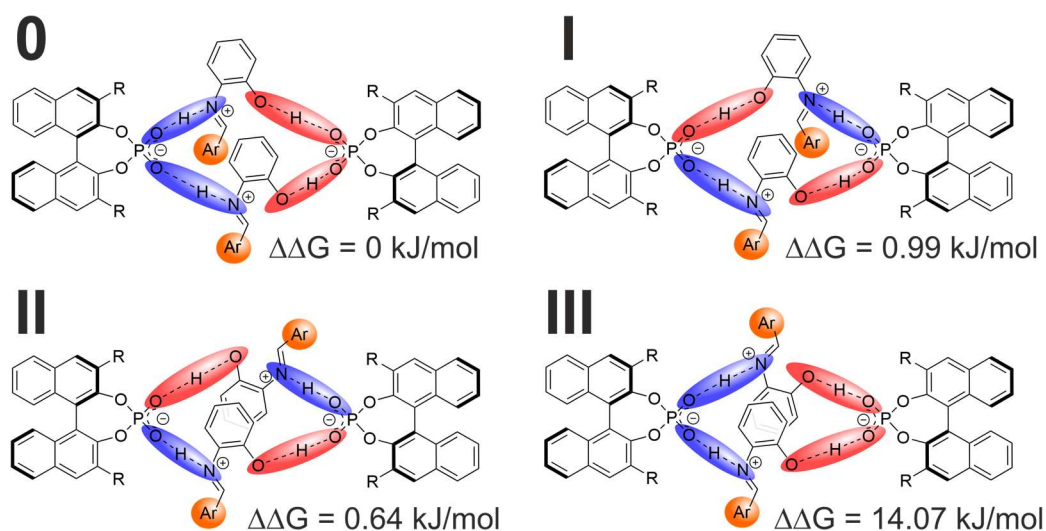
To obtain more detailed structural insights, in the following the system **1a/2a** was investigated. Low temperature sample preparation and photo-isomerization experiments (see SI Figure S7 and S8 for detailed discussion) validated that all 3 species exclusively feature *E*-imines. This is in agreement with previous findings that the size of the α -substituent is one major driving force towards the *Z*-imine besides reduced steric hinderance within the CPA binding pocket.^{22,23} Based on a series of two-dimensional NMR spectra, a partial chemical shift analysis could be achieved for the three **1a/2a** species (see SI Figure S1), however detailed structural insights via analysis of the NOESY spectrum could not be obtained due to line broadening and severe signal overlap. To shed light onto the nature of the **1a/2a** complexes, Diffusion Ordered Spectroscopy (DOSY) NMR measurements were carried out. For all three species, similar self-diffusion coefficients were found and an average hydrodynamic radius of $11.8 \pm 0.87 \text{ \AA}$ was derived, which is similar to the previously reported radius of [**1b/imine**]₂ dimers.²² A control experiment with catalyst **1a** and a reference imine without *ortho*-hydroxy group (see SI Tables S1-2 for further details) gave a hydrodynamic radius of $8.8 \pm 0.15 \text{ \AA}$, which matches the previously reported radii for monomeric CPA/imine complexes.²² Hence, for **1a/2a**, three [CPA/*E*-imine]₂ dimers with different hydrogen bonding situations are formed (see below for further discussion). For substrate **2a**, the selected CPA had a strong effect on the number of observed hydrogen bonded proton signals and thus number of species present (see Figure 2C). While for catalyst **1a** three different species were monitored, four species were observed for **1b** and only one species for catalyst **1c**. For **1c/2a**, no further detailed NMR-spectroscopic studies were performed due to strong signal overlap in the aromatic region. However, DOSY measurements revealed a hydrodynamic radius of $\sim 12.4 \text{ \AA}$, clearly indicating it as a dimeric species (see SI Table S5). Based on the similar signal pattern and chemical shift range, we assume that the 4 different species observed for **1b/2a** are also dimers. Noteworthy, for the selected set of catalysts **1a-c/2a**, the size of the 3,3'-substituents (**1c** > **1a** > **1b**)²⁶ correlates with the number of observed species (**1c** < **1a** < **1b**), hinting that bulkier catalyst residues can restrict the structural space of the dimeric [CPA/imine]₂ species.

6.3.2. Molecular dynamic simulations of [1a/2a]₂ dimers

As a detailed structural analysis by NMR spectroscopy for **1a/2a** was not fruitful due to signal overlap and line broadening, simulations were performed to shed light onto the general differences between the at least three observed dimeric species. Hence, force field MD simulations at conditions similar to the NMR experiments (1 bar, 200 K, c = 50 mM in CH₂Cl₂ – details see SI) were performed. Force field MD is the method of choice for investigating dynamic, aggregation and H-bonding behaviour of the molecules **1a/2a** in solution at finite temperature with reasonable computational cost. Since the NMR experiments show that the molecules are hydrogen bond assisted ion pairs (see SI chapter 7 for further discussion) exclusively the ion pair protonation state (phosphate and iminium) were simulated. Thus, dissociation is unfavourable and was not observed in the simulations. In our previous research on imine substrates without an *ortho*-hydroxy substituent, we detected and characterized dimeric [CPA/imine]₂ complexes, in which the two imines were stacked in a shifted face-to-face arrangement between two CPA molecules.²² However, for the *ortho*-hydroxy substituted imines, in principle two general hydrogen bonding arrangements can be envisioned: Either one imine is bound to one CPA via a bidentate binding motif (as shown in Figure 1 top right) and two of these units aggregate (non-bridging H-bond motif) or each imine molecule bridges two different CPA molecules via hydrogen bonding (bridging H-bond motif; see Figure 3).

A cluster analysis for an initial simulation with individual CPA and iminium molecules of **1a/2a** showed no significant number of non-bridging dimers. This strongly indicates that the bridging motif (one imine binds to two CPAs) is favored over the bidentate binding. For the bridged dimers, four different arrangements are generally possible. In all cases two CPA molecules are interconnected by four hydrogen bonds over two imine molecules nested in between the CPAs (see Figure 3 top). Their differences originate in the orientation of the second imine molecule. Both PO⁻--H--N⁺ hydrogen bonds can be directed to one CPA, while both PO⁻--H--O hydrogen bonds point to the second CPA molecule (Dimer 0 and III) or each CPA forms one PO⁻--H--N⁺ and one PO⁻--H--O hydrogen bond (I and II). In addition, the second imine can be orientated parallel (0 and I) or antiparallel (II and III). Thermodynamic Integration Free Energy simulations revealed that motifs 0, I and II are similarly thermally accessible, while motif III is 13-14 kJ/mol higher in free energy and thermally not accessible (see SI Table S8). While in dimers 0-II the two imines are stacked in a shifted face-to-face arrangement (see Figure 3 bottom), this is not the case for motif III (compared to the other motif 0 with similar hydrogen bond orientation, the interaction is much weaker). Thus, we assume that the three dimer species observed in the ¹H NMR spectrum for **1a/2a** (see Figure 2B) correspond to dimer motifs 0, I and II.

6. Bidentate Substrate Binding in Brønsted Acid Catalysis: Structural Space, Hydrogen Bonding and Dimerization



MD snapshot of dimer motif 0

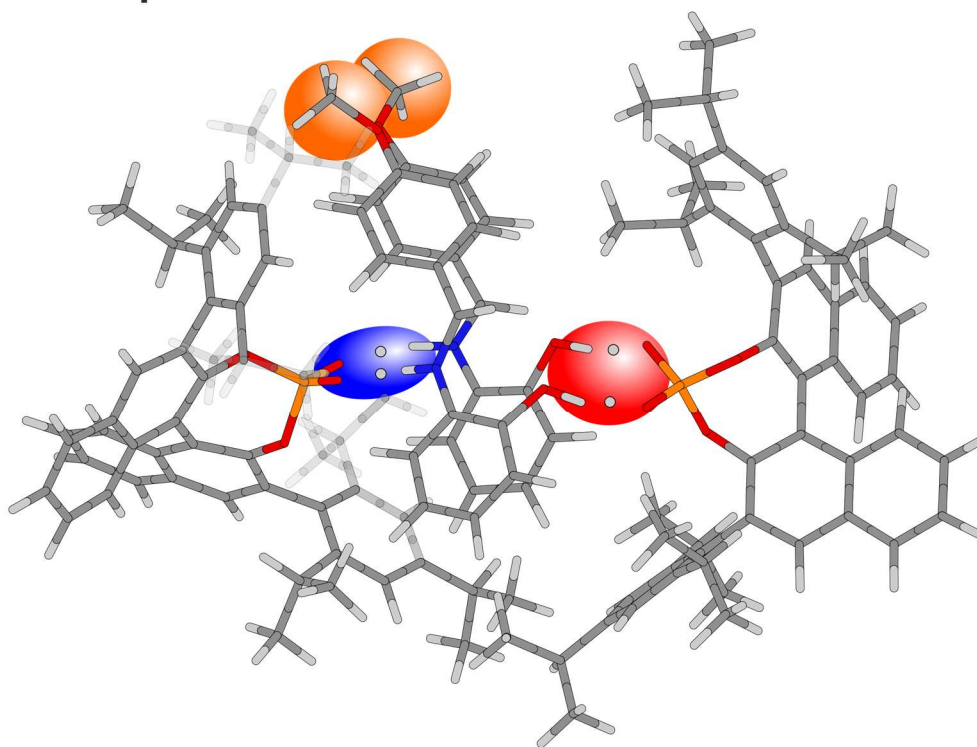


Figure 3: Top: sketch of the four different bridging H-bond dimer motifs 0-III investigated in the MD simulations for **1a/2a**, featuring two CPA and two imine molecules. In all motifs, two different CPA molecules are bridged by two imines via hydrogen bonding. Both $\text{PO}^{\ominus}\text{--H--N}^{\oplus}$ hydrogen bonds (blue) can point towards one CPA, while the two $\text{PO}^{\ominus}\text{--H--O}$ hydrogen bonds (red) are directed to the other CPA (motifs 0 and III) or each CPA can form one $\text{PO}^{\ominus}\text{--H--N}^{\oplus}$ and one $\text{PO}^{\ominus}\text{--H--O}$ hydrogen bond (motifs I and II). The imine can be stacked parallel (motifs 0 and I) or antiparallel (motifs II and III). Bottom: MD snapshot for dimer motif 0, highlighting the bridging of two CPA molecules by two imines. Colour code: red: oxygen; blue: nitrogen; dark grey: carbon; light grey: hydrogen.

Additionally, the MD simulations of motif 0 suggest that even for one specific bridging motif a high degree of flexibility exists, so that transitions between different conformations arising from a rotation of the BINOL backbone (on the side given by the iminium OH groups) of one CPA occur on a timescale below 100 ns (see SI Figure S19). We explain the presence of two different conformations by a shift in

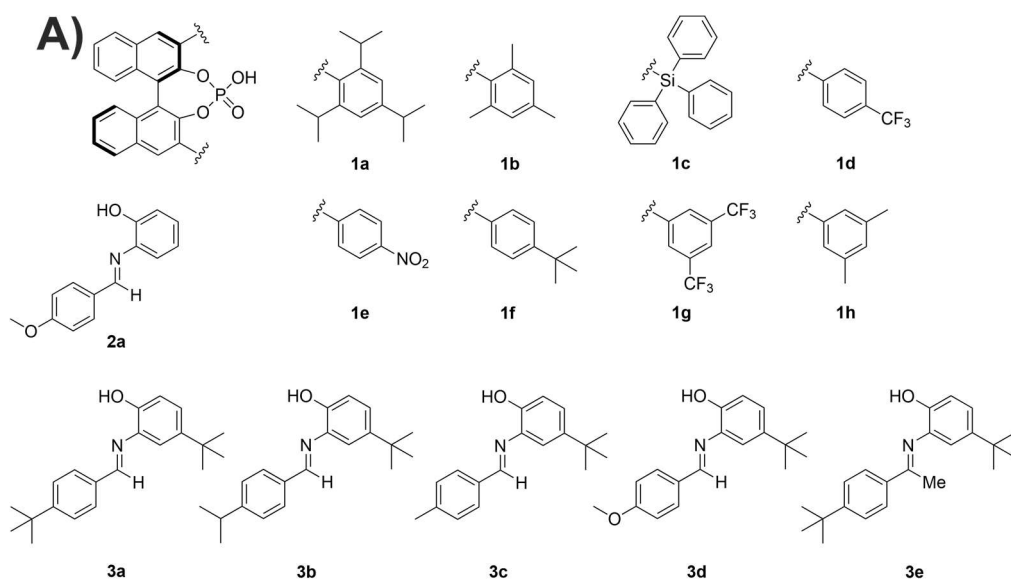
6. Bidentate Substrate Binding in Brønsted Acid Catalysis: Structural Space, Hydrogen Bonding and Dimerization

Van der Waals stabilisation from imine-imine to imine-CPA. In our previous studies with imines without *ortho*-hydroxy substituents (only one hydrogen bond between CPA and imine), we identified [CPA/imine]₂ dimer complexes, in which two stacked imines are nested in between two CPA molecules. These dimers are proposed not to play a role in catalysis and resemble an off-cycle equilibrium with the catalytic relevant monomeric CPA/imine complexes, especially as additional binding of a nucleophile by a second hydrogen bond (see Figure 1, left) is assumed to prevent formation of these dimers.²² However, it was also shown that CPA molecules can form PO--H--OP hydrogen bond bridged dimers which then can act as an alternative active catalyst, opening a concentration dependent dimeric reaction channel.²⁵ For CPA catalysed transformations of imines bearing an *ortho*-hydroxy substituent, originally a bidentate binding to the catalyst was proposed.¹ Typical third reaction partners^{1,15,16,20} for imines with *ortho*-hydroxy substituent feature no hydrogen bond donor. Thus, only a weak preorganisation can be envisioned within the CPA/imine/nucleophile complex. However, these transformations could in principle also proceed over the observed dimer motifs, in which the imine bridges two CPA molecules. This leads to a broad variety of potential transition states, featuring distinct dimer motifs combined with different attack pathways for the nucleophile and potentially also contributions of the respective monomeric reaction pathways. However, the potential dimeric pathway implies that an application of catalyst mixtures (e.g. R and S enantiomers or two catalysts with different 3,3'-substituents) might prove beneficial for optimizing stereoselectivities.

6.3.3. Accessing CPA/imine monomers

The strong tendency of **1/2** complexes towards dimerization opens up a multitude of different potential transition states. Thus, we were intrigued to study, which molecular features suppress dimer formation and force the system towards CPA/imine monomers for an easier selection of optimal catalysts. Since the MD simulations showed stacking of the imines in between the catalysts for all accessible dimers (see Figure 3 bottom), we aimed to hinder dimerization by introducing electronic or steric repulsion. After screening of 13 CPA/imine combinations (**1c-f/2a**; **1a-c,g,h/3a**; **1b/3a-e**; see Figure 4A for selected CPAs and imines and SI Figures S9-11 for respective ¹H NMR spectra and further discussion) we were able to obtain the well resolved system **1b/3a**, showing only two proton signals in the hydrogen bond region of the ¹H NMR spectrum (see Figure 4B). DOSY measurements gave a hydrodynamic radius of 10.9 ± 0.15 Å for **1b/3a** and a value of 10.2 ± 0.16 Å was determined for a monomeric reference system (see SI Table S3 and S4), clearly demonstrating that the observed species is a monomer. Using a combination of ¹H ¹H COSY, ¹H NOESY, ¹H ¹³C HSQC, ¹H ¹³C HMBC and ¹H ³¹P HMBC spectra allowed for a complete chemical shift assignment of the complex (see SI Figure S2).

6. Bidentate Substrate Binding in Brønsted Acid Catalysis: Structural Space, Hydrogen Bonding and Dimerization



Screened combinations; Well resolved monomer spectra for **1b/3a-b**
1c-f with **2a** : steric and electrostatic repulsion by catalyst
1a/b/c/g/h with **3a** and **1b** with **3a-e** : steric repulsion of stacked imines

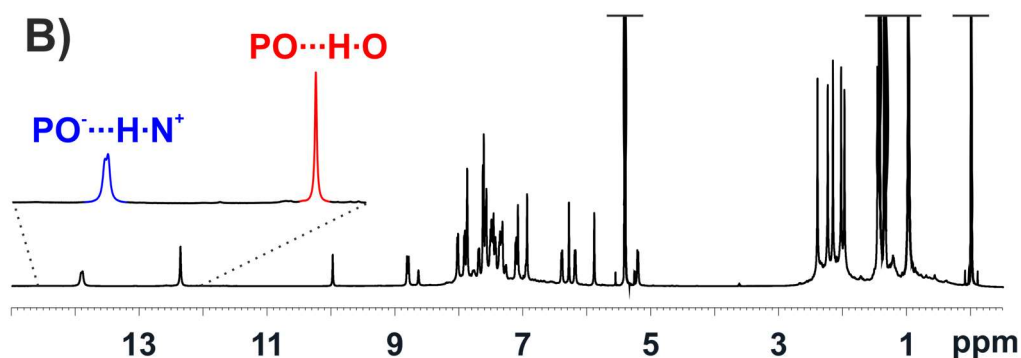


Figure 4: **A)** CPAs and imines which were tested in order to suppress dimer formation. CPAs **1c-f** were employed with substrate **2a** but no well resolved CPA/imine monomers were obtained (see SI Figure S9 for spectra and discussion). For imines **3a-e** well resolved CPA/imine monomers were only found for **1b/3a** and **1b/3b** (see SI Figure S10 and S11 for spectra and discussion). **B)** ^1H NMR spectrum of **1b/3a** at a 1 : 1 ratio and a concentration of 25 mM at 180 K and 600 MHz in CD_2Cl_2 showing two hydrogen bonded proton signals respecting one single complex.

The proton signals at 13.91 ppm (Figure 4B, blue signal) and 12.37 ppm (Figure 4B, red signal) could unambiguously be characterized as the $\text{PO}^- \cdots \text{H}\text{-N}^+$ and $\text{PO} \cdots \text{H}\text{-O}$ hydrogen bonded proton respectively by detection of *trans*-hydrogen bond scalar coupling via ^1H ^1H COSY and ^1H ^{31}P HMBC spectra (see SI Figure S12 for spectra and further discussion). In comparison to our previously investigated monodentate **1b/imine** systems,²⁷ the $\text{PO}^- \cdots \text{H}\text{-N}^+$ hydrogen bond proton signal of **1b/3a** is significantly highfield shifted (~ 2 ppm), which correlates to a weaker H-bond and a stronger proton transfer onto the substrate caused by the cooperativity effect of the second $\text{PO} \cdots \text{H}\text{-O}$ hydrogen bond.²⁵

To shed light onto the structure of **1b/3a** in solution, an analysis of the NOE pattern was done and corroborated by calculations. Hence, **1b/3a** was optimized in CH_2Cl_2 (SMD) at the DFT level of theory

6. Bidentate Substrate Binding in Brønsted Acid Catalysis: Structural Space, Hydrogen Bonding and Dimerization

employing Grimme's D3 empirical dispersion correction (TPSS-D3/dev2-SVP; see SI for details). The resulting most stable complex (see Figure 5) was found to be analogous to the previously reported simplified structure model for CPAs and N-(*ortho*-hydroxyaryl) imines by Akiyama.¹⁴

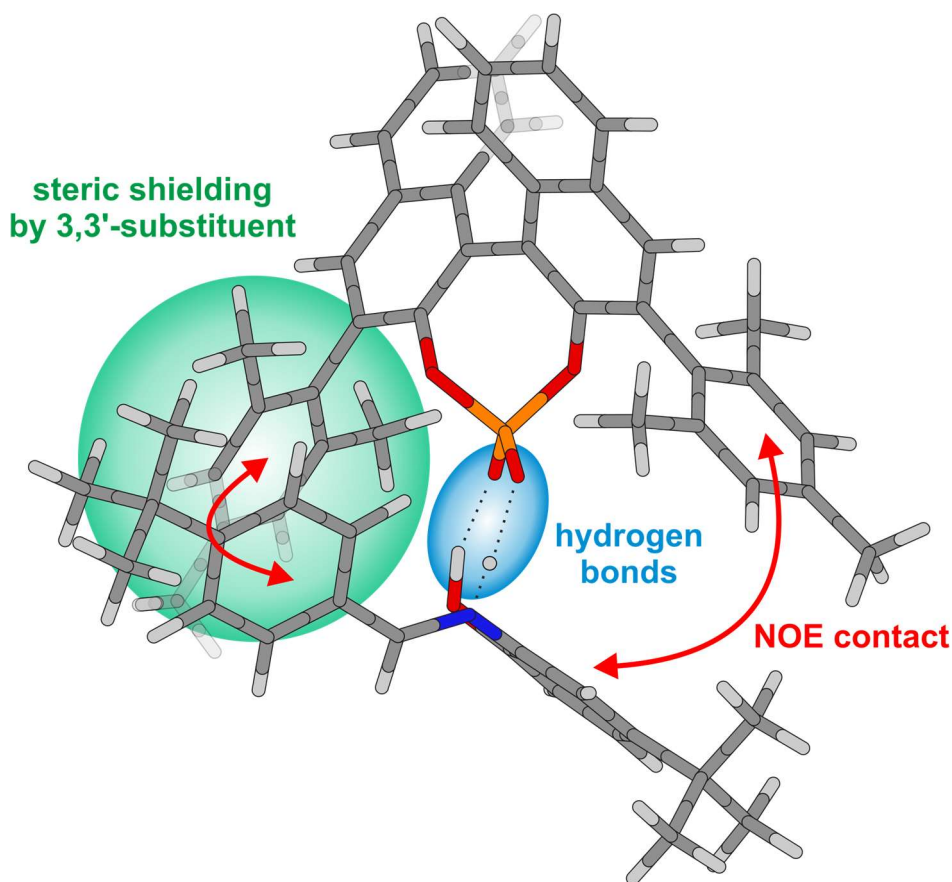


Figure 5: DFT structure model of **1b/3a**. The two hydrogen bonds (highlighted in blue) anchor the substrate in between the two 3,3'-substituents of the catalyst. One side of the substrate is effectively shielded by the 3,3'-substituent, which causes the stereoiduction.

In this complex, the imine is located in between the two 3,3'-substituents of the catalyst and anchored by two hydrogen bonds (see Figure 5, blue area). One side of the substrate is sterically shielded by the 3,3'-substituent, effectively blocking this side for nucleophilic attacks. The computed structure model agrees with the performed NOESY NMR studies, which revealed contacts between the N-aryl moiety of the imine and one 3,3'-substituent of the CPA as well as between the *para*-*t*-butyl phenyl entity of the imine and the other 3,3'-substituent (Figure 5, indicated by red arrows; see SI Figure S13 for NOESY spectrum). Additionally, no NOE contacts have been detected between the imine and the BINOL backbone as it is the case for the respective CPA/imine systems featuring only one hydrogen bond.^{22,23} Remarkably, the two halves of the BINOL backbone, the two 3,3'-substituents and especially the two *ortho* as well as *para* protons of the *para*-*t*-butyl phenyl entity of the imine possess different chemical shifts. Signal splitting of the *ortho* and *para* protons clearly shows that rotation of the *para*-*t*-butyl phenyl ring is slow on the NMR timescale, which is in stark contrast to our previous investigations on

6. Bidentate Substrate Binding in Brønsted Acid Catalysis: Structural Space, Hydrogen Bonding and Dimerization

CPA/imine systems with one hydrogen bond where such splitting was never monitored.^{22,23} The observation that even the rotation of the phenyl group is hindered clearly indicates that the bidentate binding by two hydrogen bonds enforces a rigid and well defined preorganization of catalyst and imine. This is further corroborated by the signal splitting of the CPA, which was not present in our previous studies for many CPA/imine systems with one hydrogen bond due to signal averaging by fast interconversion of different conformers.^{22,28}

Additionally, in the molecular dynamic simulations for monomeric aggregates of **1a/2a**, two different hydrogen bonding motifs were found. One features a bidentate binding of the imine towards both oxygen atoms of **1a**, while the other shows bifurcated binding towards only one oxygen atom (see Figure 6A).

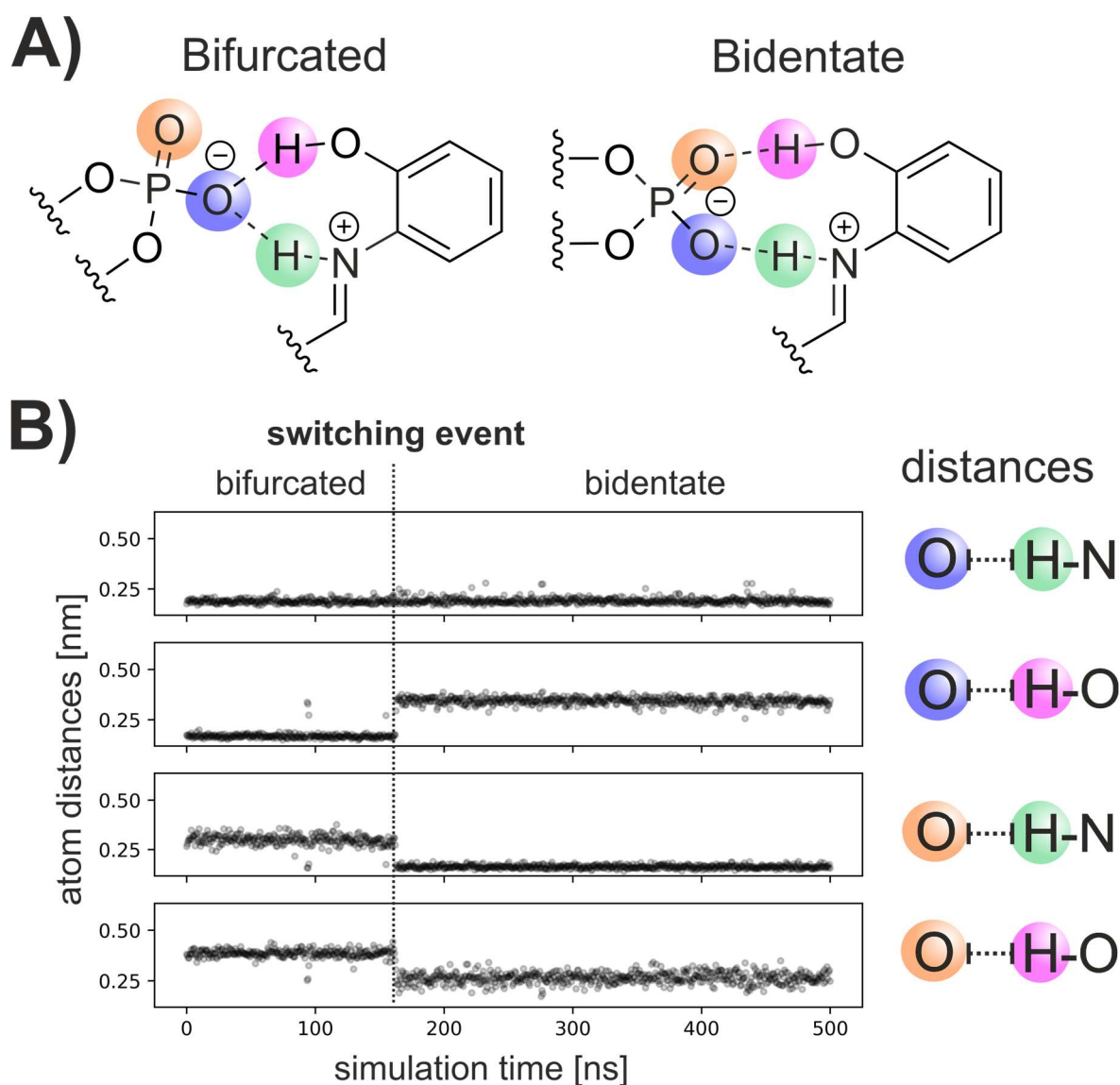


Figure 6: A) Bidentate and bifurcated hydrogen bonding motifs. B) Plot of atom distances of the Brønsted acidic and basic oxygen atom (blue and orange) and hydrogen bond protons (green and magenta) during the MD simulations reveals the rare switching event (dashed line) between two different binding motifs.

6. Bidentate Substrate Binding in Brønsted Acid Catalysis: Structural Space, Hydrogen Bonding and Dimerization

The two binding motifs can interconvert (rare event on the 100 ns timescale), indicating an equilibrium between these two binding states (the switching process occurs in both directions and thus is no equilibration artefact; see SI Figure S15-17). This hints that the Brønsted basic site of the CPA (see Figure 1) might not be blocked entirely by the bidentate binding of a substrate featuring both a hydrogen bond donor and acceptor. Thus, for monomeric CPA/2 complexes, a bifurcated binding of the imine substrate and additional binding of a nucleophile with H-bond donor (see Figure 1 left) could be surmised for certain catalyst/substrate/nucleophile combinations.

Noteworthy, only the combination of **1b/3a** and **1b/3b** (see SI Figure S11) gave a well resolved NMR spectrum of the monomer complex. Slight changes in the catalyst or the substrate led to a variety of species or dimerization of CPA and imine (see SI Figures S9-11 for full overview of systems, spectra, and detailed discussion), indicating a broad structural space featuring different dimeric [CPA/imine]₂ complexes, hydrogen binding motifs and potentially other monomeric CPA/imine conformers. This is surprising, as a bidentate binding motif was expected to confine the structural space and minimize the number and variety of potential species. However, it remains elusive if and how this structural diversity might affect the catalysis or reflects off-cycle equilibria.

6.4. Conclusion

A selection of BINOL derived chiral phosphoric acid catalysts and N-(*ortho*-hydroxyaryl) imines (19 CPA/imine combinations) was studied via NMR spectroscopy to shed light onto the structural space and hydrogen bonding of the respective CPA/imine complexes and to pinpoint the origin of stereoselectivity for related transformations of the imine substrates. Introducing an additional hydrogen bond donor into the substrate (*ortho*-hydroxy group) led to bidentate binding of catalyst and substrate via the formation of two hydrogen bonds. The resulting CPA/imine complexes showed a broad structural space with a variety of different species and a preference for the formation of [CPA/imine]₂ dimers, contradicting the general assumption, that bidentate binding of CPA and substrate results in a highly confined structural space, thus yielding high enantioselectivities. MD simulations showed, that in these dimers, the imines may form each one hydrogen bond to two CPA molecules, effectively bridging them. This indicates that respective transformation might proceed via [CPA/imine]₂ dimers instead of bidentate bound CPA/imine complexes, implying that catalyst mixtures (either R and S enantiomer or two catalysts with different 3,3'-substituents) might prove beneficial for optimizing stereoselectivities. Modulating steric repulsion and noncovalent interactions allowed to access rigid and well-defined monomer structures. NOESY NMR studies corroborated by theoretical calculations showed, that the imine is located in between the two 3,3'-substituents of the catalyst. One side of the substrate is thereby shielded by the catalyst, which creates the stereoinductive environment for asymmetric downstream transformations.

6. Bidentate Substrate Binding in Brønsted Acid Catalysis: Structural Space, Hydrogen Bonding and Dimerization

6.5. References

- 1 T. Akiyama, J. Itoh, K. Yokota and K. Fuchibe, *Angew. Chem. Int. Ed.*, 2004, **43**, 1566–1568.
- 2 D. Uraguchi and M. Terada, *J. Am. Chem. Soc.*, 2004, **126**, 5356–5357.
- 3 D. Parmar, E. Sugiono, S. Raja and M. Rueping, *Chem. Rev.*, 2014, **114**, 9047–9153.
- 4 T. Akiyama, *Chem. Rev.*, 2007, **107**, 5744–5758.
- 5 M. Terada, *Synthesis*, 2010, 1929–1982.
- 6 R. I. Storer, D. E. Carrera, Y. Ni and D. W. C. MacMillan, *J. Am. Chem. Soc.*, 2006, **128**, 84–86.
- 7 M. Rueping, E. Sugiono and C. Azap, *Angew. Chem. Int. Ed.*, 2006, **45**, 2617–2619.
- 8 Q. Kang, Z. A. Zhao and S. L. You, *J. Am. Chem. Soc.*, 2007, **129**, 1484–1485.
- 9 C. Zhu and T. Akiyama, *Org. Lett.*, 2009, **11**, 4180–4183.
- 10 X. Cheng, R. Goddard, G. Buth and B. List, *Angew. Chem. Int. Ed.*, 2008, **47**, 5079–5081.
- 11 L. Simón and J. M. Goodman, *J. Am. Chem. Soc.*, 2008, **130**, 8741–8747.
- 12 L. Simón and J. M. Goodman, *J. Am. Chem. Soc.*, 2009, **131**, 4070–4077.
- 13 L. Simón and J. M. Goodman, *J. Org. Chem.*, 2010, **75**, 589–597.
- 14 M. Yamanaka, J. Itoh, K. Fuchibe and T. Akiyama, *J. Am. Chem. Soc.*, 2007, **129**, 6756–64.
- 15 T. Akiyama, H. Morita and K. Fuchibe, *J. Am. Chem. Soc.*, 2006, **128**, 13070–13071.
- 16 T. Akiyama, Y. Honma, J. Itoh and K. Fuchibe, *Adv. Synth. Catal.*, 2008, **350**, 399–402.
- 17 F. Zhou and H. Yamamoto, *Angew. Chem. Int. Ed.*, 2016, **55**, 8970–8974.
- 18 F. Pecho, Y. Q. Zou, J. Gramüller, T. Mori, S. M. Huber, A. Bauer, R. M. Gschwind and T. Bach, *Chem. Eur. J.*, 2020, **26**, 5190–5194.
- 19 F. Pecho, Y. Sempere, J. Gramüller, F. M. Hörmann, R. M. Gschwind and T. Bach, *J. Am. Chem. Soc.*, 2021, **143**, 9350–9354.
- 20 T. Akiyama, Y. Tamura, J. Itoh, H. Morita and K. Fuchibe, *Synlett*, 2006, 141–143.
- 21 T. Marcelli, P. Hammar and F. Himo, *Chem. Eur. J.*, 2008, **14**, 8562–8571.
- 22 M. Melikian, J. Gramüller, J. Hioe, J. Greindl and R. M. Gschwind, *Chem. Sci.*, 2019, **10**, 5226–5234.
- 23 J. Greindl, J. Hioe, N. Sorgenfrei, F. D. Morana and R. M. Gschwind, *J. Am. Chem. Soc.*, 2016, **49**, 15965–15971.
- 24 N. Sorgenfrei, J. Hioe, J. Greindl, K. Rothermel, F. Morana, N. Lokesh and R. M. Gschwind, *J. Am. Chem. Soc.*, 2016, **138**, 16345–16354.
- 25 D. Jansen, J. Gramüller, F. Niemeyer, T. Schaller, M. C. Letzel, S. Grimme, H. Zhu, R. M. Gschwind and J. Niemeyer, *Chem. Sci.*, 2020, **11**, 4381–4390.
- 26 J. P. Reid and J. M. Goodman, *J. Am. Chem. Soc.*, 2016, **138**, 7910–7917.
- 27 K. Rothermel, M. Melikian, J. Hioe, J. Greindl, J. Gramüller, Matej Žabka, N. Sorgenfrei, T. Hausler, F. Morana and R. M. Gschwind, *Chem. Sci.*
- 28 N. Lokesh, J. Hioe, J. Gramüller and R. M. Gschwind, *J. Am. Chem. Soc.*, 2019, **141**, 16398–16407.

6.6. Supporting Information

6.6.1. General information

Chemicals

Deuterated solvents were purchased from Deutero or Sigma Aldrich. Where dry solvents were essential, CD_2Cl_2 was freshly distilled over CaH_2 and Toluene- d_8 was refluxed over Na/Benzophenone under argon atmosphere. Non-deuterated toluene was refluxed over Na/Benzophenone under Argon atmosphere or purchased by Sigma Aldrich (dry, stored over molecular sieve). All commercially available chemicals were purchased by Sigma Aldrich or abcr and used without further purification.

Sample preparation

The chiral phosphoric acid was weighed into a 5 mm NMR tube and dried at 150 °C for at least 20 min under reduced pressure. After the tube came to room temperature, the respective imine was weighed directly into the NMR tube. The tube was evacuated and flushed with Argon three times. Dry CD_2Cl_2 (0.6 mL) was added under Argon flow and TMS atmosphere (0.5 mL) was added. The tube was closed and sealed with parafilm. The samples were stored in the fridge at -80 °C.

For the preparation of the “*E*-only sample”, prior to adding the solvent the tube was cooled to -80 °C in an acetone/liquid nitrogen bath. Under Argon flow, cooled CD_2Cl_2 (0.6 mL) was added to the CPA and imine. TMS atmosphere (0.5 mL) was added and the tube was closed and sealed with parafilm. The samples were stored in the fridge at -80 °C. *E*-only samples were transported at -80 °C in an acetone/liquid nitrogen cooling bath and only inserted in a precooled spectrometer at 180 K.

For the *in situ* UV VIS illumination experiments, a glass fiber based illumination setup developed by our group was employed.^{1,2} The sample preparation was analogous, except only 0.35 mL of solvent were used. After solvation, the glass fiber was inserted into the ambered tube and fixated with parafilm.

NMR spectrometer, data procession and referencing

All NMR spectroscopic investigations on model systems were performed on a Bruker Avance DRX 600 MHz spectrometer with TBI (Triple resonance broadband inverse) 5 mm CPPBBO $^1\text{H}/^{19}\text{F}$ -BB probe head with Z-gradient and BVT unit. Temperature was controlled in the VT-experiments by a BVT 3000 and BVT 3900 unit and liquid nitrogen. Further NMR experiments were performed on Bruker Avance III HD 400 MHz spectrometer equipped with 5 mm BBO BB-1H/D probe head with Z-Gradients. Spectrometer control and spectra processing was performed with Bruker Software TopSpin (Version 3.2 PL 1). Further plotting of the spectra was performed with Corel Draw 2020 software. ^1H , ^{13}C chemical shifts were referenced to TMS or the respective solvent signals. The heteronucleus ^{31}P was referenced, employing

6. Bidentate Substrate Binding in Brønsted Acid Catalysis: Structural Space, Hydrogen Bonding and Dimerization

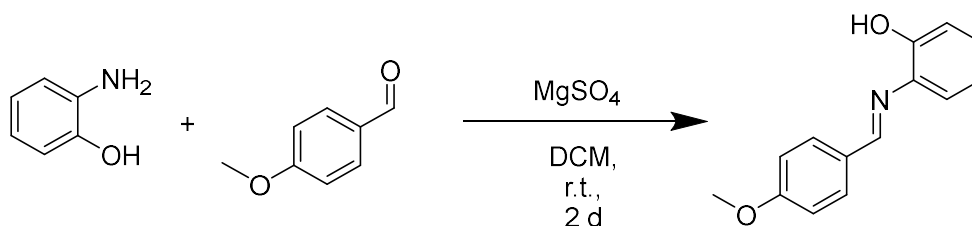
$\nu(X) = \nu(\text{TMS}) \cdot \Xi_{\text{reference}} / 100\%$ according to Harris et al.³ The following frequency ratios and reference compounds was used: $\Xi(^{31}\text{P}) = 40.480742$ (H_3PO_4). For all NMR measurements, 5 mm NMR tubes were used.

Pulse sequences and acquisition parameters

^1H -NMR: Pulse program zg30, Relaxation delay = 2.00 s, Acquisition time = 2.54 s, SW = 22 – 24 ppm, TD = 66 K, ns = 16 – 256; ^{13}C NMR: Pulse program: zgpg30, Relaxation delay = 2.00 s, Acquisition time = 0.80 s, TD = 66 K; SW = 270.0 ppm, TD = 64k, NS = 1k – 4k; ^{31}P -NMR: Pulse program: zgpg30; Relaxation delay = 1.00 s, Acquisition time = 2.25 s, SW = 20 - 60.0 ppm, TD = 65k, NS = 256 - 512; $2\text{D-}^1\text{H}, ^1\text{H}$ NO-ESY: Pulse program: noesygpph; Relaxation delay = 5.00 s, NS = 8-16, mixing time (D8) = 300.00 ms; TD = 4096; increments = 512 - 1k; $2\text{D-}^1\text{H}, ^1\text{H}$ ROESY: Pulse program: roesyphpr.2; Relaxation delay = 5.00 s, NS = 8, mixing time (D8) = 100.00 ms; TD = 4096; increments = 1k; $2\text{D-}^1\text{H}, ^1\text{H}$ COSY: Pulse program: cosygppqf; Relaxation delay = 5.00 s, NS = 4-16, TD = 4096; increments = 512; $2\text{D-}^1\text{H}, ^{13}\text{C}$ HSQC: Pulse program: hsqcedetgppsisp2.3; Relaxation delay = 4 - 8 s, NS = 8-32, $^1J_{\text{XH}} = 145$ Hz; TD = 4096; increments = 512 - 1k; $2\text{D-}^1\text{H}, ^{13}\text{C}$ HMBC: Pulse program: hmbcgplpndqf; Relaxation delay = 4.00 s, NS = 8-16, $^1J_{\text{XH}} = 145$ Hz, $J_{\text{XH}}(\text{long range}) = 10$ Hz; TD = 4096; increments = 512 - 1k; $2\text{D-}^1\text{H}, ^{31}\text{P}$ HMBC: Pulse program: inv4gplrndqf; Relaxation delay = 6.00 s, NS = 4-32, TD = 4096; increments = 256 – 512.

6.6.2. Imine synthesis

(E)-2-((4-methoxybenzylidene)amino)phenol (2a)



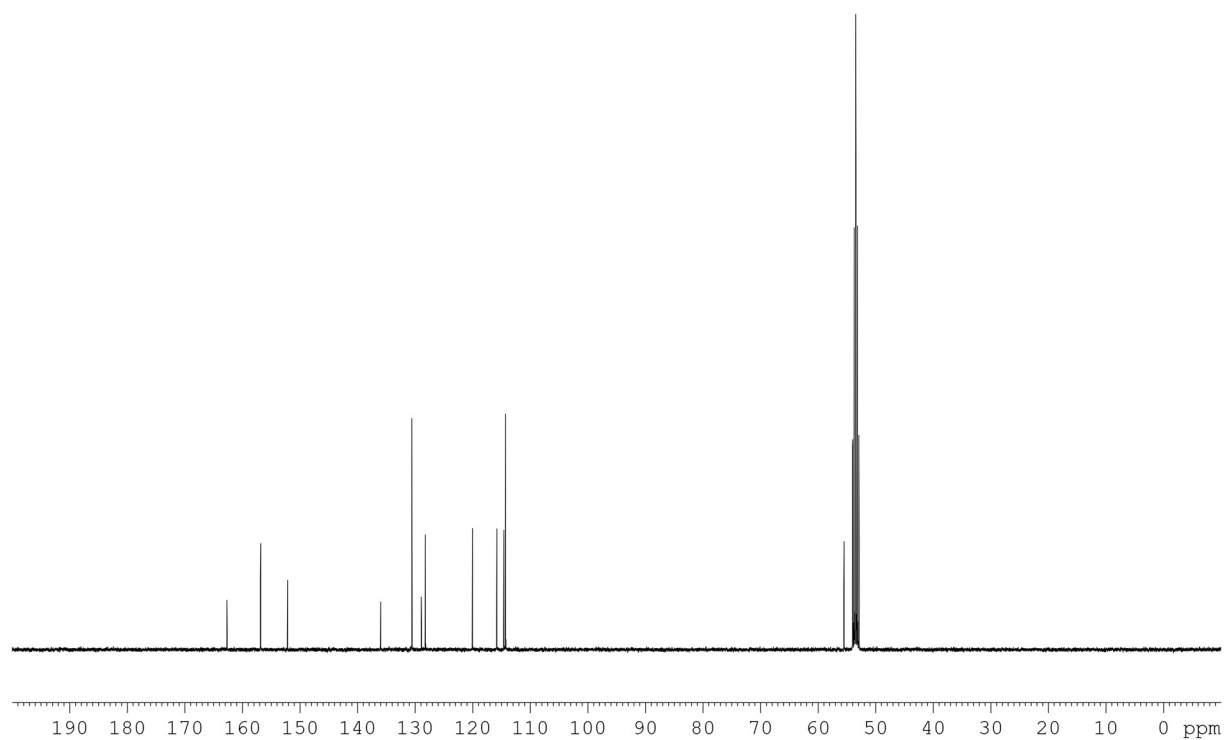
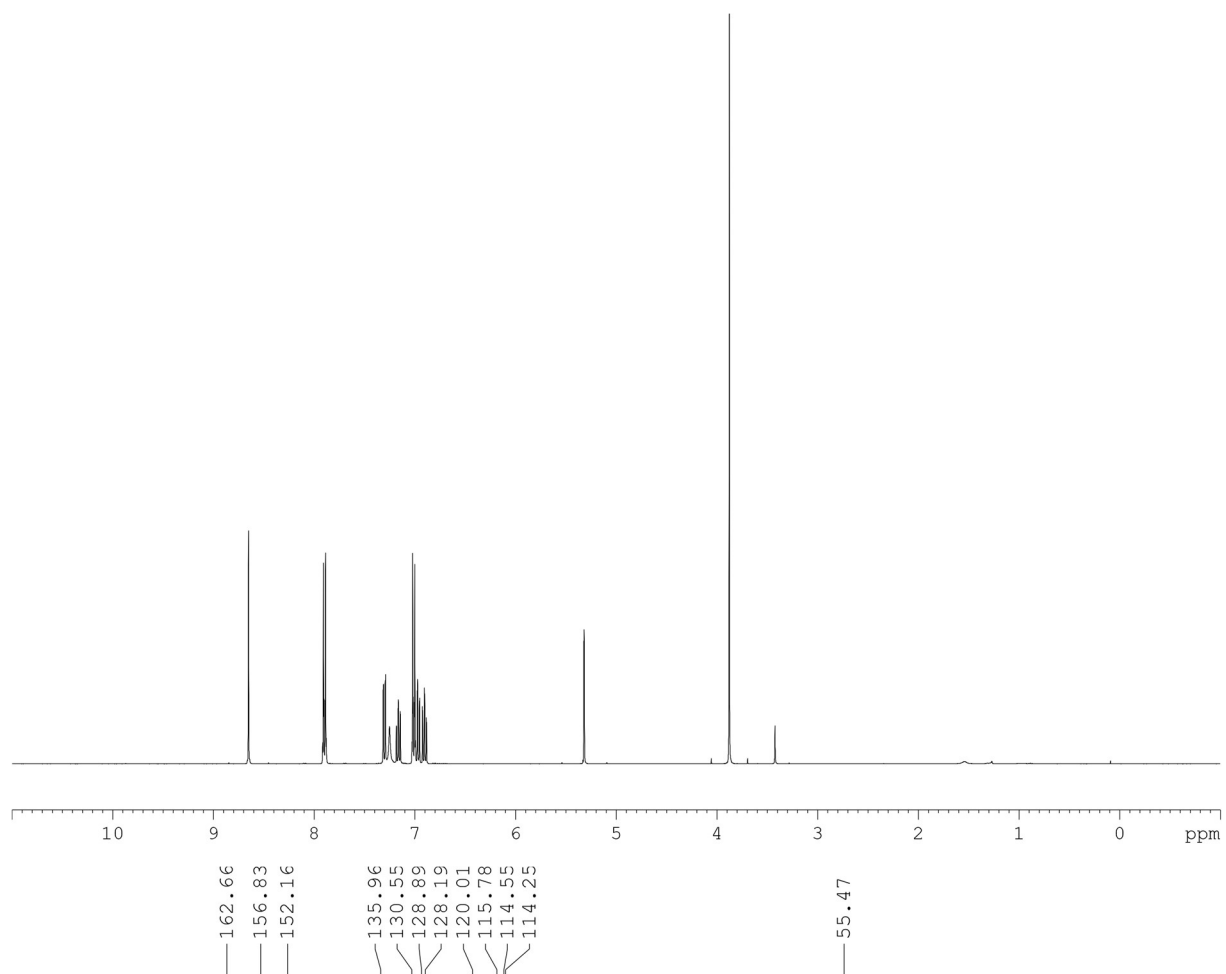
2-Aminophenol (7.00 mmol, 0.65 g, 0.55 mL, 1.7 eq), 4-Methoxybenzaldehyde (4.05 mmol, 0.55 g, 1.0 eq) and MgSO₄ (4.70 g) were weighed into a 50 mL Schlenk flask and dissolved in 20 mL DCM. The solution was stirred for two days at room temperature. Afterwards, the solvent was removed under reduced pressure to give a yellow solid. The crude product was recrystallized in methanol two times to give the product as yellow crystals. (0.55 g, 2.60 mmol, 37%).

¹H-NMR: (400.1 MHz, CD₂Cl₂): δ_H = 8.65 (s, 1H), 7.90 (m, 2H), 7.30 (dd, 1H, ³J = 8.0 Hz, ⁴J = 1.5 Hz), 7.25 (s, 1H), 7.16 (m, 1H), 7.01 (m, 2H), 6.97 (dd, 1H, ³J = 8.1 Hz, ⁴J = 1.4 Hz), 6.90 (m, 1H), 3.88 (s, 1H).

¹³C-NMR: (100.6 MHz, CD₂Cl₂): δ_C = 162.7, 156.8, 152.2, 135.9, 130.5, 128.9, 128.2, 120.0, 115.8, 114.6, 114.3, 55.5.

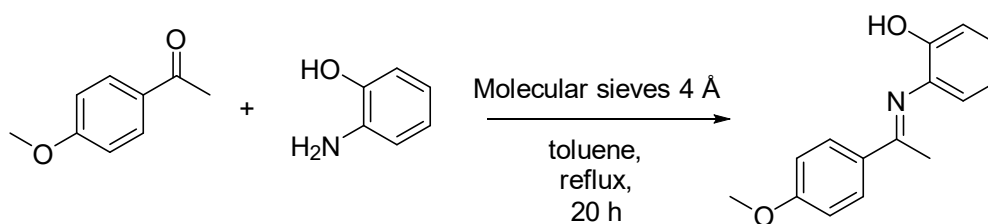
HR-MS (EI, *m/z*): found 226.08607 (M-H)⁺ (calculated 226.08626 for C₁₄H₁₂NO₂); Diff(ppm) = -0.81.

6. Bidentate Substrate Binding in Brønsted Acid Catalysis: Structural Space, Hydrogen Bonding and Dimerization



6. Bidentate Substrate Binding in Brønsted Acid Catalysis: Structural Space, Hydrogen Bonding and Dimerization

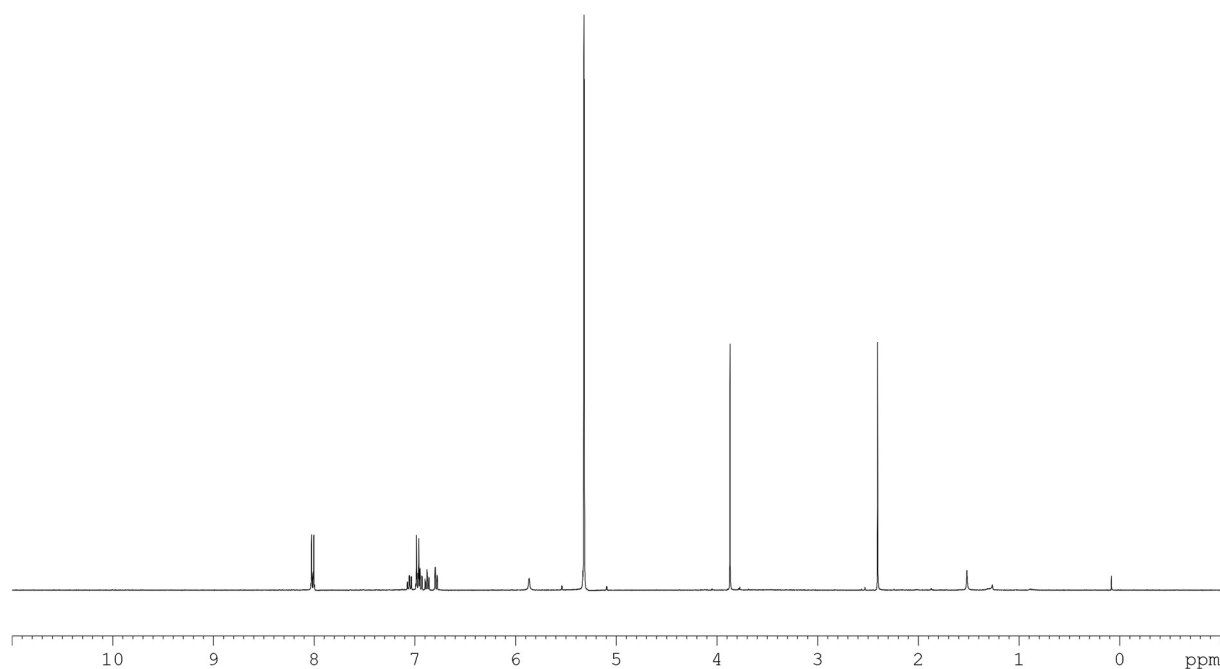
(E)-2-((1-(4-methoxyphenyl)ethylidene)amino)phenol (**2b**)



The molecular sieves 4 Å (approx. 4 g) were weighed into a 50 mL Schlenk flask and dried with a heat gun at 350 °C for 30 min under reduced pressure. 2-Aminophenol (30.0 mmol, 3.27 g, 3.0 eq) and 1-(4-methoxyphenyl)ethan-1-one (10 mmol, 1.50 g, 1.0 eq.) were added under argon flow and dissolved in 20 mL anhydrous toluene. Under argon flow, a reflux condenser was added to the setup. After flushing it for 3 min with argon, a drying tube containing CaCl₂ was added to the setup and the solution was refluxed for 20 h. The reaction mixture was allowed to cool down and the solvent was removed under reduced pressure. The crude product was obtained as an orange solid and was purified two times using a bulb-to-bulb distillation (0.01 mbar, 170 °C) to give the imine **2b** as an orange solid (0.313 g, 1.30 mmol, 13 %).

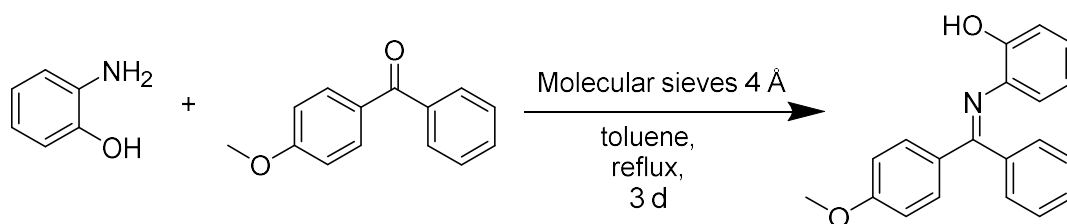
¹H-NMR: (400.1 MHz, CD₂Cl₂): δ_H = 8.02 (m, 2H), 7.06 (m, 1H), 6.97 (m, 2H), 6.94 (m, 1H, ³J = 8.1 Hz, ⁴J = 1.3 Hz), 6.88 (td, 1H, ³J = 7.6 Hz, ⁴J = 1.5 Hz), 6.79 (dd, 1H, ³J = 7.8 Hz, ⁴J = 1.5 Hz), 5.86 (s, 1H), 3.87 (s, 3H), 2.40 (s, 3H).

HR-MS (EI, *m/z*): found 240.10166 (M-H)⁺ (calculated 240.10191 for C₁₅H₁₄NO₂); Diff(ppm) = -1.04.



6. Bidentate Substrate Binding in Brønsted Acid Catalysis: Structural Space, Hydrogen Bonding and Dimerization

(E)-2-(((4-methoxyphenyl)(phenyl)methylene)amino)phenol (**2c**)



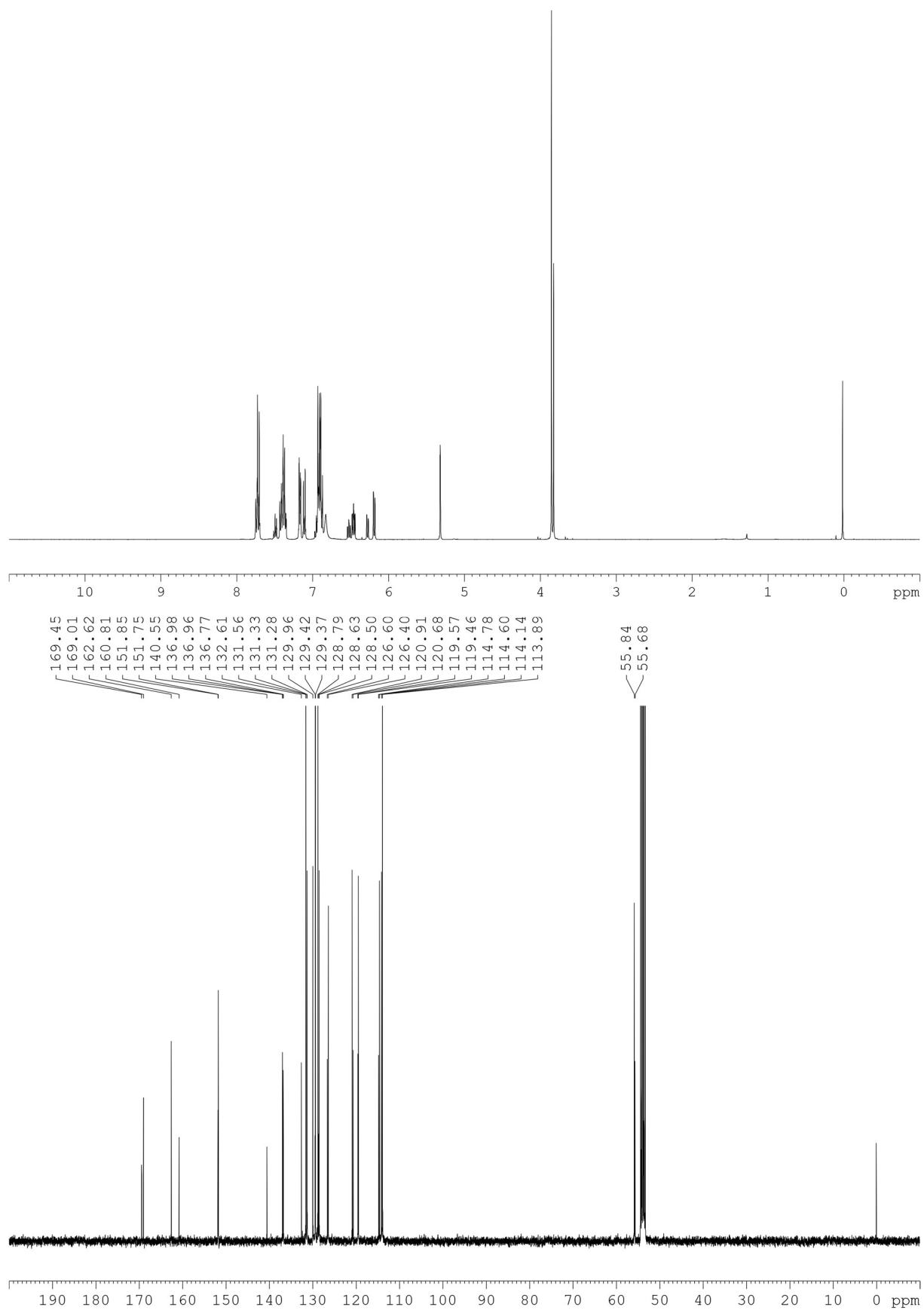
The molecular sieves 4 Å (approx. 4 g) were weighed into a 50 mL Schlenk flask and dried at 350 °C under reduced pressure for 30 min. 2-Aminophenol (30.0 mmol, 3.27 g, 3.0 eq) and (4-methoxyphenyl)(phenyl)methanone (10 mmol, 2.12 g, 1.0 eq.) were added under argon flow and dissolved in 20 mL anhydrous toluene. Under argon flow, a reflux condenser was added to the setup and flushed with argon for 3 min. A drying tube filled with CaCl₂ was added to the setup and the solution was refluxed for 3 d. After cooling down, the mixture was filtrated, and the solvent was removed under reduced pressure to give an orange solid. The crude product was purified two times using a bulb-to-bulb distillation (0.01 mbar, 190 °C) to give the imine **2c** as an orange solid (0.516 g, 1.7 mmol, 17 %) as a mixture of *E* and *Z*-isomer (ratio major/minor = 1.9 : 1).

¹H-NMR: (400.1 MHz, CD₂Cl₂): δ_H = 7.74 (m, 2H, minor), 7.72 (m, 2H, major), 7.49 (m, 1H, minor), 7.44 – 7.33 (m, both), 7.17 (m, 2H, major), 7.11 (m, 2H, minor), 6.99 - 6.86 (m, both), 6.83 (s, 1H, broad, both, OH group), 6.52 (m, 1H, minor), 6.45 (m, 1H, major), 6.26 (dd, 1H, ³J = 8.0 Hz, ⁴J = 1.4 Hz minor), 6.17 (dd, 1H, ³J = 8.0 Hz, ⁴J = 1.4 Hz, major), 3.84 (s, 3H, major), 3.81 (s, 3H, minor).

¹³C-NMR: (100.6 MHz, CD₂Cl₂): δ_C = 169.4 (minor), 169.0 (major), 162.6 (major), 160.8 (minor), 151.9 (minor), 151.7 (major), 140.6, 140.0, 136.9, 136.8, 132.6, 131.6, 131.3, 131.3, 130.0, 129.4 (minor), 129.4 (major), 128.8 (major), 128.6, 128.5 (minor), 126.6 (minor), 126.4 (major), 120.9 (major), 120.7 (minor), 119.6 (minor), 119.5 (major), 114.8 (minor), 114.6 (major), 114.1 (minor), 113.9 (major), 55.8 (major), 55.7 (minor).

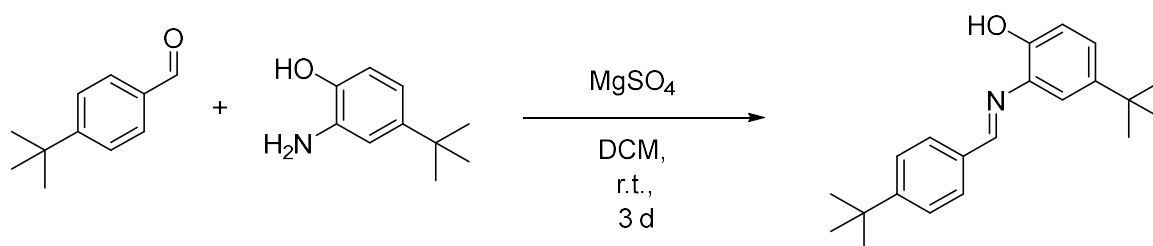
HR-MS (EI, *m/z*): found 302.11714 (M-H)⁺ (calculated 302.11756 for C₂₀H₁₆NO₂); Diff(ppm) = -1.36.

6. Bidentate Substrate Binding in Brønsted Acid Catalysis: Structural Space, Hydrogen Bonding and Dimerization



6. Bidentate Substrate Binding in Brønsted Acid Catalysis: Structural Space, Hydrogen Bonding and Dimerization

(E)-4-(tert-butyl)-2-((4-(tert-butyl)benzylidene)amino)phenol (**3a**)



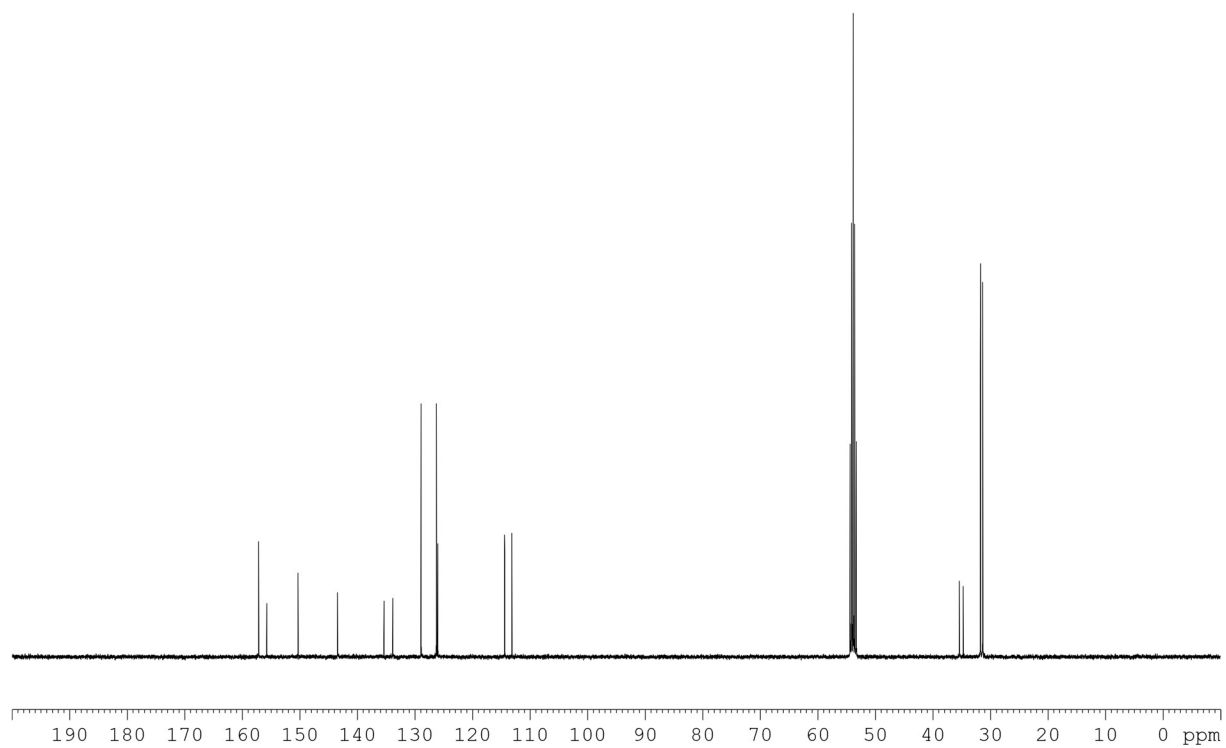
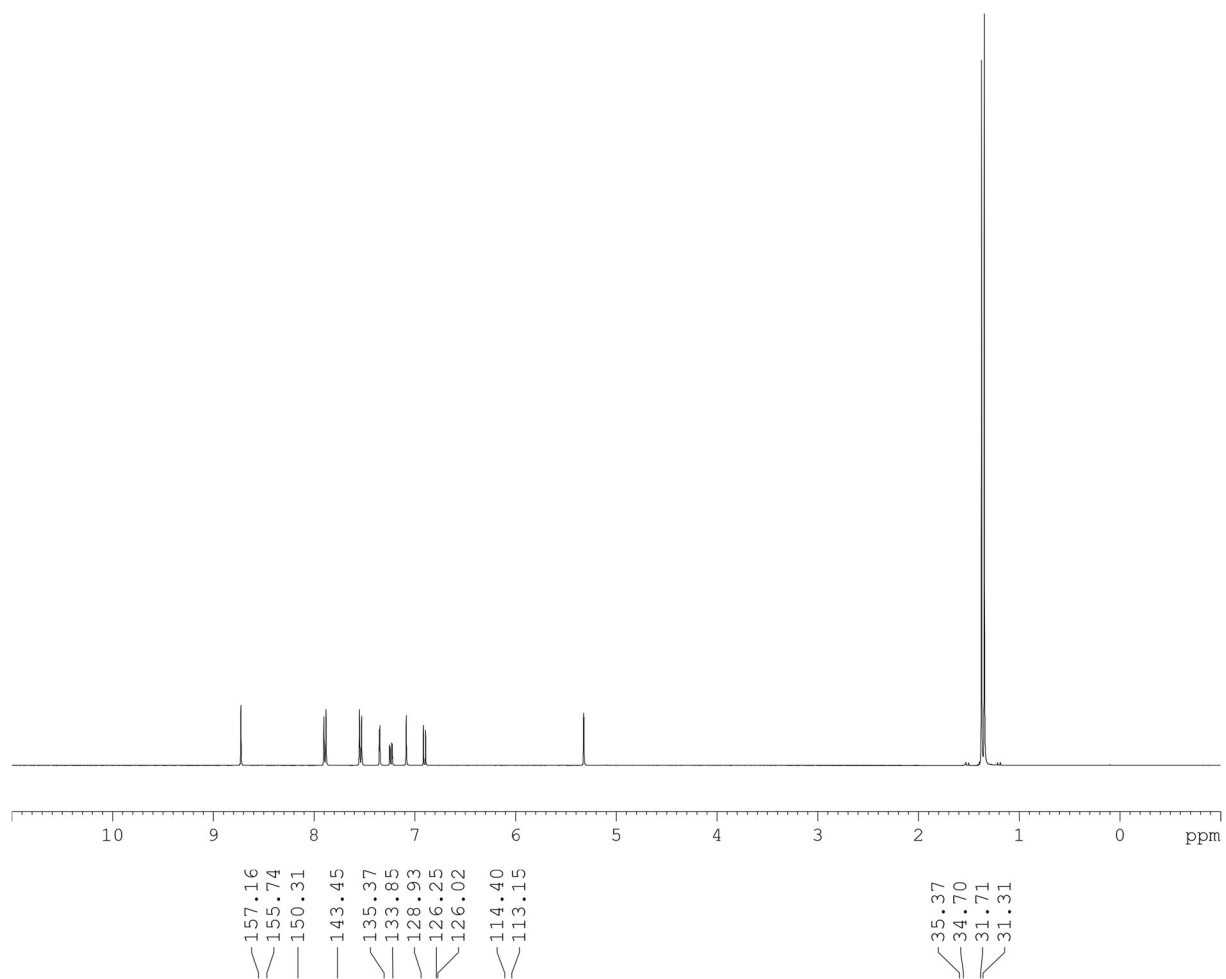
The aldehyde (0.811 g, 0.836 mL, 5.0 mmol, 1.0 eq.) and the hydroxy aniline (0.826 g, 5.0 mmol, 1.0 eq.) and MgSO₄ (5 g) were dissolved in 20 mL DCM and stirred for 3 days at room temperature. Afterwards, MgSO₄ was filtrated off and the solvent was removed under reduced pressure. The crude product was purified by bulb-to-bulb distillation (160 °C, 0.1 mbar) to give imine **3a** (0.883 mg, 2.85 mmol, 57%) as yellow oil which solidified as yellow to white solid after several days/weeks.

¹H-NMR: (400.1 MHz, CD₂Cl₂): δ_H = 8.72 (s, 1H), 7.89 (m, 2H), 7.54 (m, 2H), 7.35 (d, 1H, ⁴J = 2.3 Hz), 7.23 (dd, 1H, ³J = 8.5 Hz, ⁴J = 2.3 Hz), 7.08 (s, 1H), 6.9 (d, 1H, ³J = 8.5 Hz), 1.37 (s, 9H), 1.34 (s, 9H).

¹³C-NMR: (100.6 MHz, CD₂Cl₂): δ_C = 157.2, 155.7, 150.3, 143.5, 135.4, 133.8, 128.9, 126.3, 126.0, 114.4, 113.1, 35.4, 34.7, 31.7, 31.3.

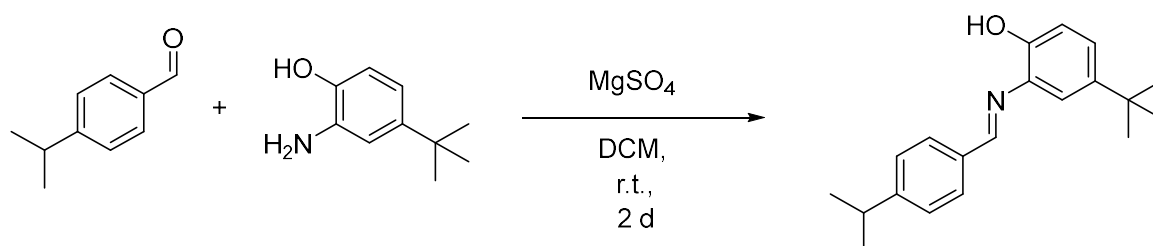
HR-MS (EI, *m/z*): found 308.20058 (M-H)⁺ (calculated 308.20089 for C₂₁H₁₆NO); Diff(ppm) = - 1.02.

6. Bidentate Substrate Binding in Brønsted Acid Catalysis: Structural Space, Hydrogen Bonding and Dimerization



6. Bidentate Substrate Binding in Brønsted Acid Catalysis: Structural Space, Hydrogen Bonding and Dimerization

(E)-4-(tert-butyl)-2-((4-isopropylbenzylidene)amino)phenol (**3b**)



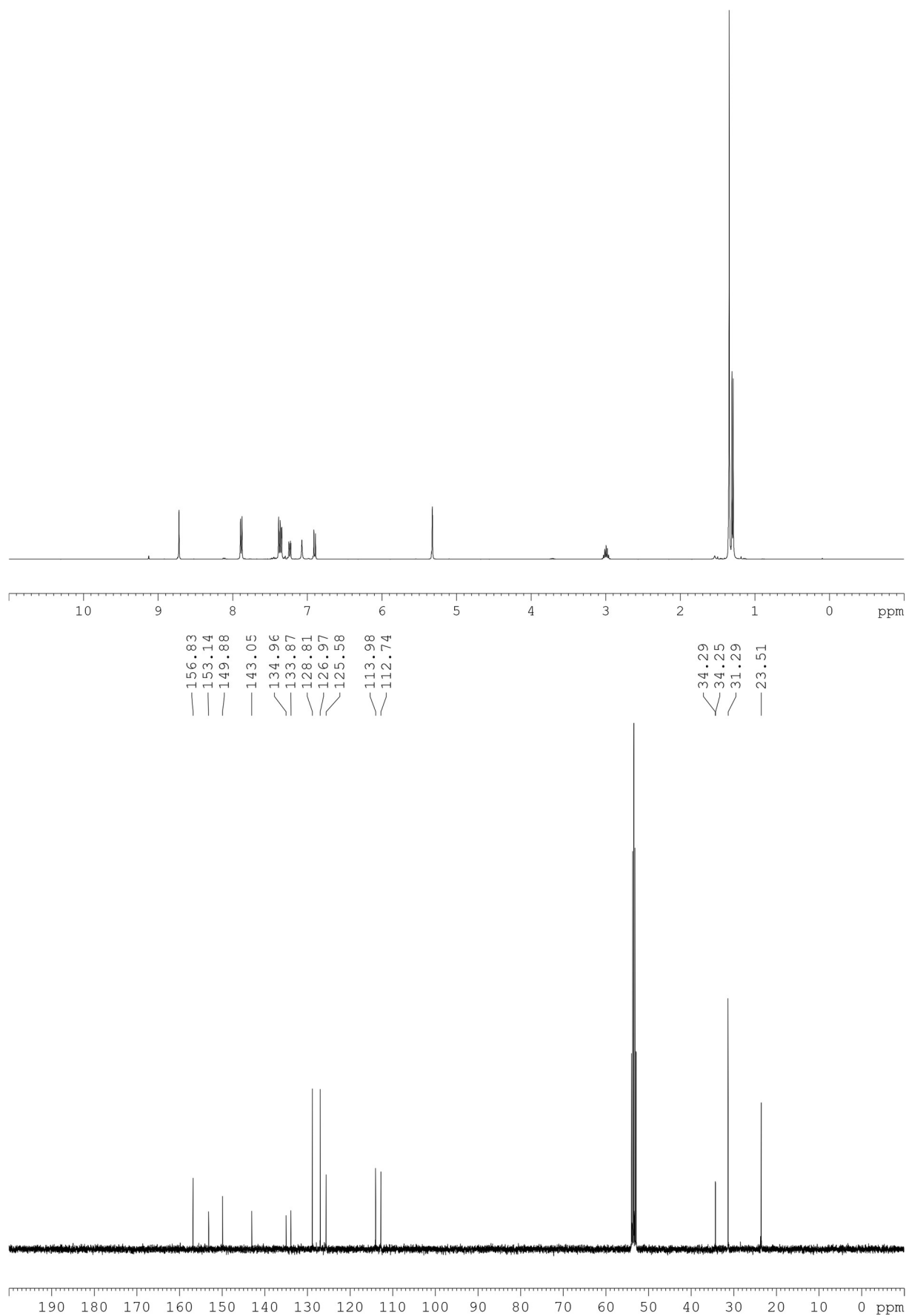
The aldehyde (1.48 g, 1.52 mL, 10.0 mmol, 1.0 eq.) and the hydroxy aniline (1.65 g, 10.0 mmol, 1.0 eq.) and MgSO_4 (6 g) were dissolved in 20 mL dry DCM and stirred for 2 days at room temperature. Afterwards, MgSO_4 was filtrated off and the solvent was removed under reduced pressure. The crude product was purified by bulb-to-bulb distillation (180 °C, 0.1 mbar) to give imine **3b** (0.93 g, 3.2 mmol, 32 %) as a yellow oil.

$^1\text{H-NMR}$: (400.1 MHz, CD_2Cl_2): δ_{H} = 8.72 (s, 1H), 7.89 (m, 2H), 7.37 (m, 2H), 7.35 (d, 4J = 2.3 Hz), 7.23 (dd, 1H, 3J = 8.4 Hz, 4J = 2.3 Hz), 7.07 (s, 1H), 6.90 (d, 1H, 3J = 8.4 Hz), 3.00 (sept, 1H, 3J = 6.9 Hz), 1.34 (s, 9H), 1.30 (d, 6H, 3J = 6.9 Hz).

$^{13}\text{C-NMR}$: (100.6 MHz, CD_2Cl_2): δ_{C} = 156.8, 153.1, 149.9, 143.0, 135.0, 133.9, 128.8, 127.0, 125.6, 114.0, 112.7, 34.3, 34.2, 31.3, 23.5.

HR-MS (EI, m/z): found 295.19322 (M)⁺ (calculated 295.19307 for $\text{C}_{20}\text{H}_{25}\text{NO}$); Diff(ppm) = + 0.53.

6. Bidentate Substrate Binding in Brønsted Acid Catalysis: Structural Space, Hydrogen Bonding and Dimerization



6. Bidentate Substrate Binding in Brønsted Acid Catalysis: Structural Space, Hydrogen Bonding and Dimerization

(E)-4-(tert-butyl)-2-((4-methylbenzylidene)amino)phenol (**3c**)



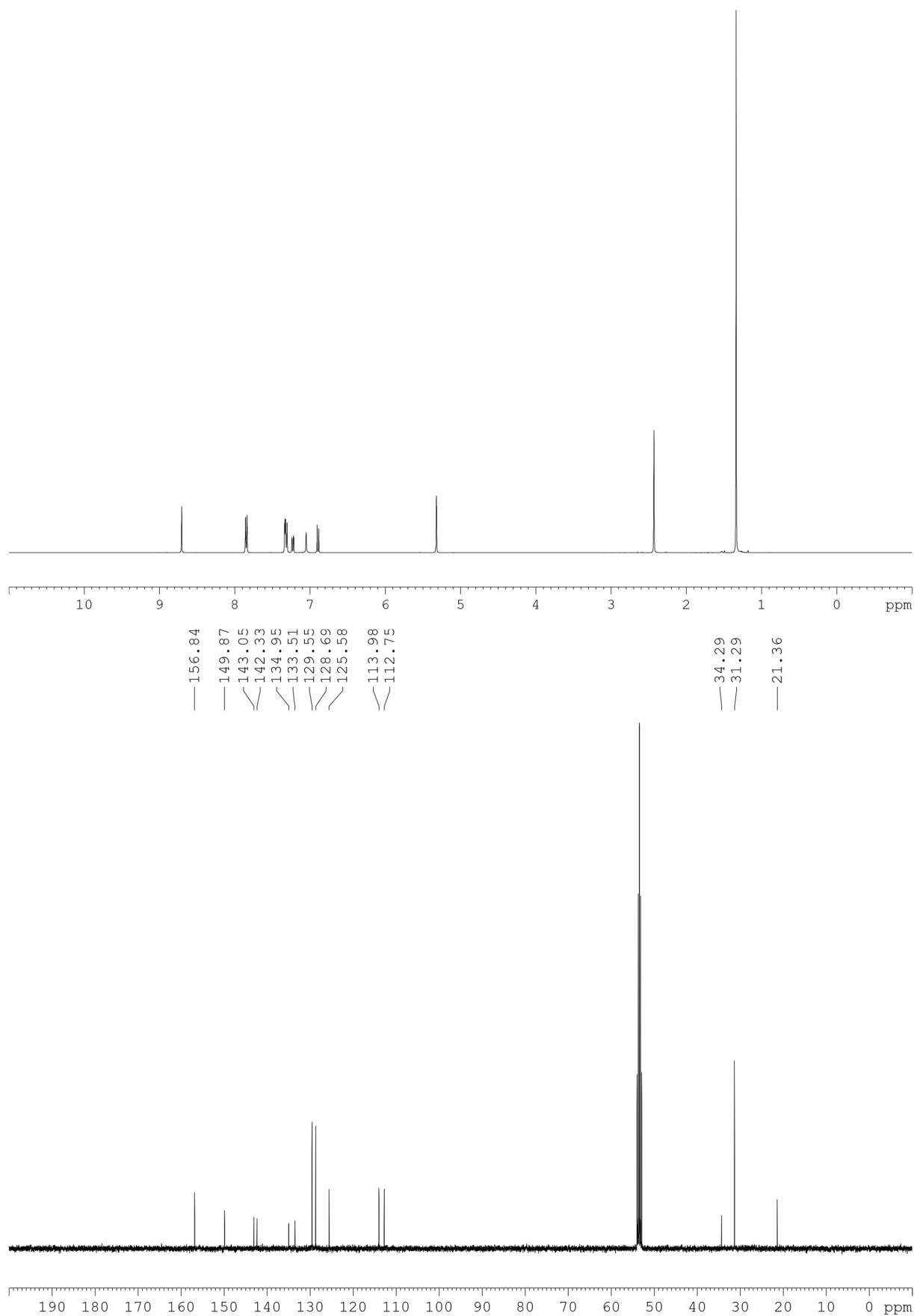
The aldehyde (1.20 g, 1.02 mL, 10.0 mmol, 1.0 eq.) and the hydroxy aniline (1.65 g, 10.0 mmol, 1.0 eq.) and MgSO₄ (7 g) were dissolved in 20 mL dry DCM and stirred for 2 days at room temperature. Afterwards, MgSO₄ was filtrated off and the solvent was removed under reduced pressure. The crude product was purified by bulb-to-bulb distillation (175 °C, 0.1 mbar) to give imine **3c** (1.76 g, 6.0 mmol, 60 %) as a yellow oil.

¹H-NMR: (400.1 MHz, CD₂Cl₂): δ_H = 8.71 (s, 1H), 7.85 (m, 2H), 7.34 (d, 1H, ⁴J = 2.3 Hz), 7.32 (d, 2H, ³J = 7.9 Hz), 7.23 (dd, ³J = 8.4 Hz, ⁴J = 2.3 Hz), 7.05 (s, 1H), 6.90 (d, 1H, ³J = 8.4 Hz), 2.43 (s, 3H), 1.34 (s, 9H).

¹³C-NMR: (100.6 MHz, CD₂Cl₂): δ_C = 156.8, 149.9, 143.1, 142.3, 134.9, 133.5, 129.5, 128.7, 125.6, 114.0, 112.8, 34.3, 31.3, 21.4.

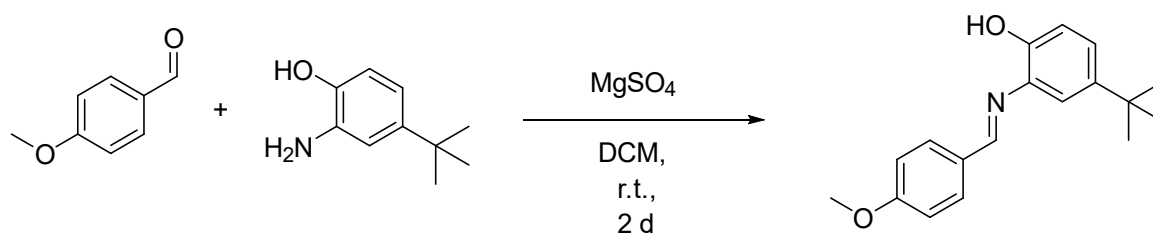
HR-MS (EI, *m/z*): found 266.15369 (M-H)⁺ (calculated 266.15394 for C₁₈H₂₀NO); Diff(ppm) = -0.95.

6. Bidentate Substrate Binding in Brønsted Acid Catalysis: Structural Space, Hydrogen Bonding and Dimerization



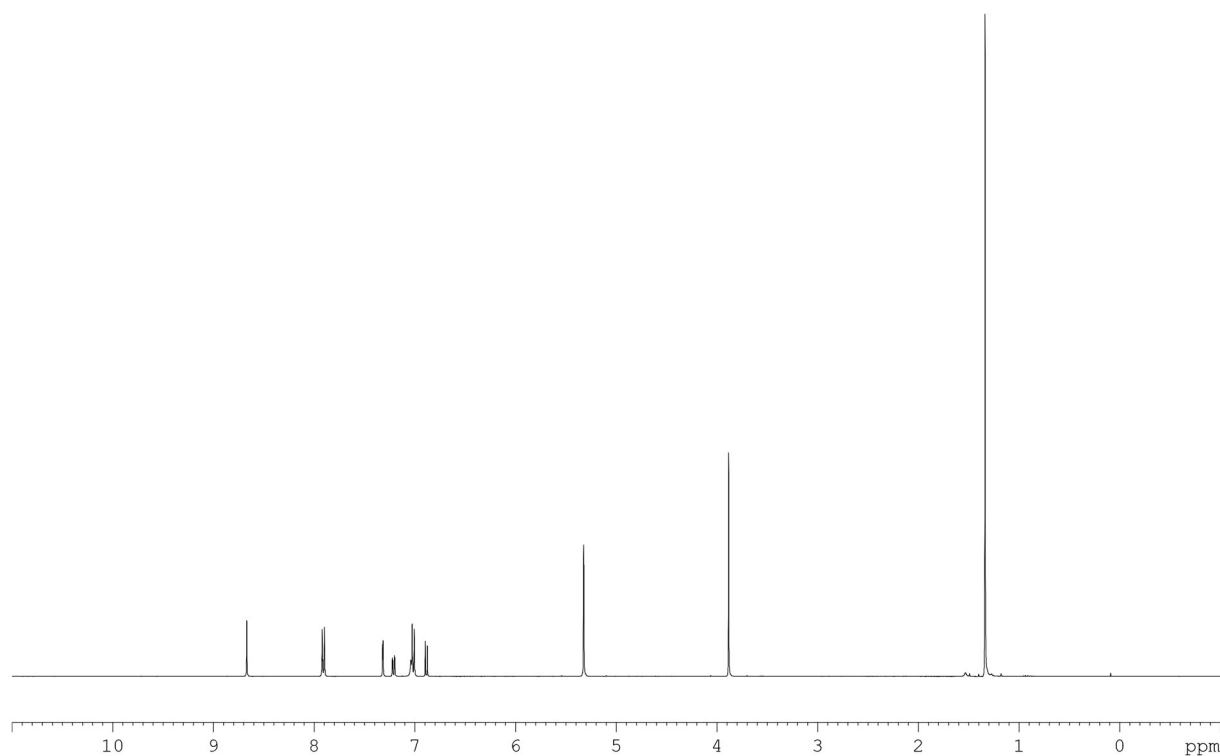
6. Bidentate Substrate Binding in Brønsted Acid Catalysis: Structural Space, Hydrogen Bonding and Dimerization

(E)-4-(tert-butyl)-2-((4-methoxybenzylidene)amino)phenol (**3d**)



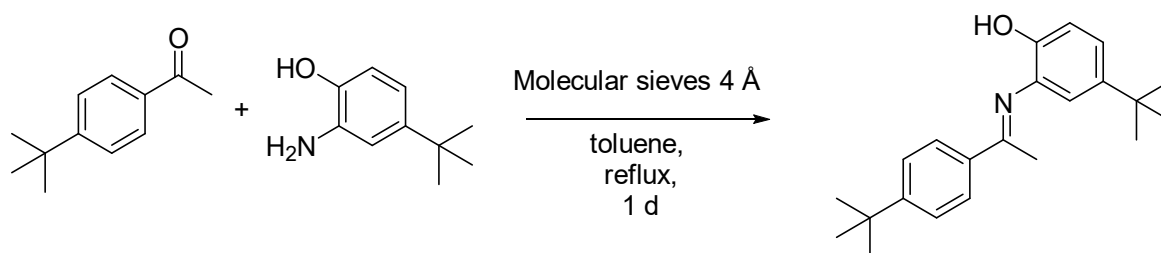
The aldehyde (0.68 g, 0.55 mL, 5.0 mmol, 1.0 eq.) and the hydroxy aniline (0.83 g, 5.0 mmol, 1.0 eq.) and MgSO_4 (7 g) were dissolved in 20 mL dry DCM and stirred for 2 days at room temperature. Afterwards, MgSO_4 was filtrated off and the solvent was removed under reduced pressure. The crude product was recrystallized in methanol to give imine **3d** (0.55 g, 2.4 mmol, 48 %) as a pale orange solid.

$^1\text{H-NMR}$: (400.1 MHz, CD_2Cl_2): δ_{H} = 8.71 (s, 1H), 7.85 (m, 2H), 7.34 (d, 1H, 4J = 2.3 Hz), 7.32 (d, 2H, 4J = 7.9 Hz), 7.23 (dd, 1H, 3J = 8.6 Hz, 4J = 2.3 Hz), 7.05 (s, 1H), 6.90 (d, 1H, 3J = 8.6 Hz), 2.43 (s, 3H), 1.34 (s, 9H).



6. Bidentate Substrate Binding in Brønsted Acid Catalysis: Structural Space, Hydrogen Bonding and Dimerization

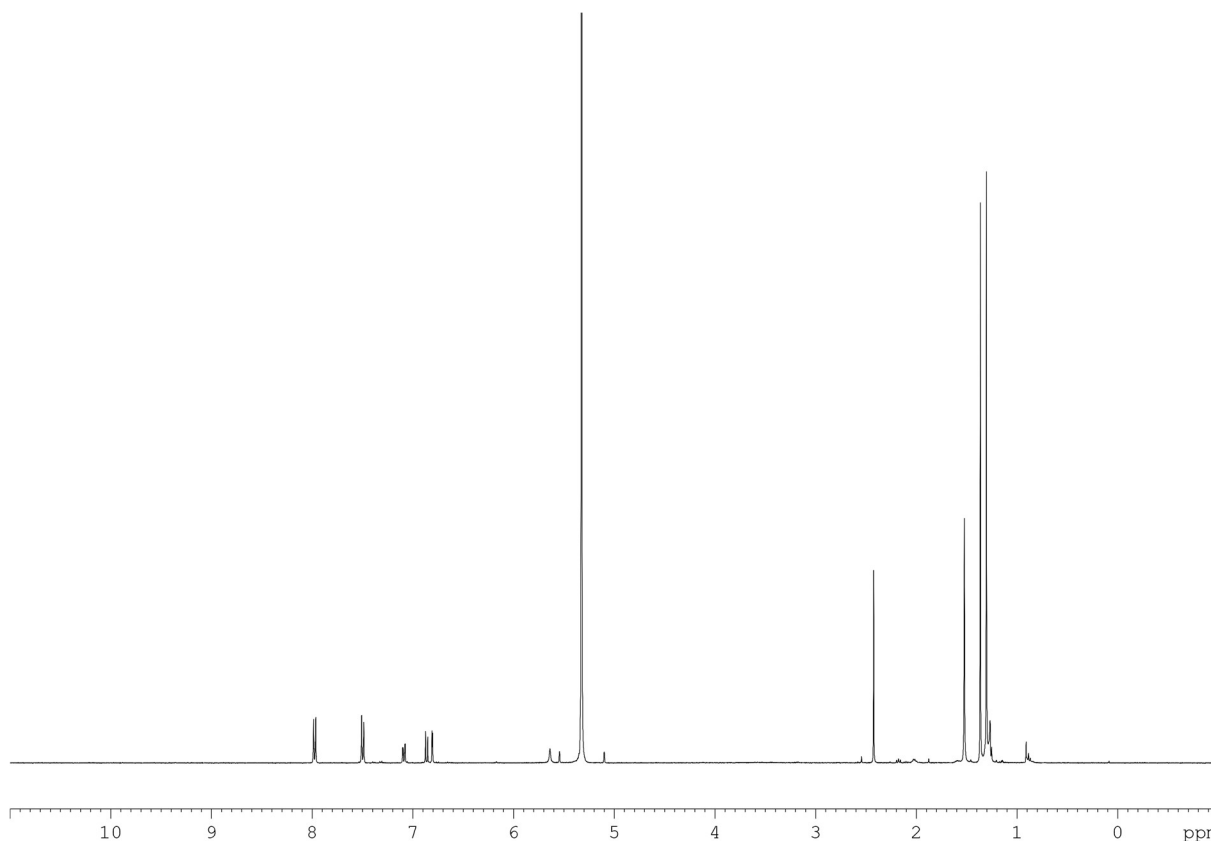
(E)-4-(tert-butyl)-2-((1-(4-(tert-butyl)phenyl)ethylidene)amino)phenol (**3e**)



The molecular sieves 4 Å (approx. 4 g) were weighed into a 50 mL Schlenk flask and dried with a heat gun at 350 °C for 30 min under reduced pressure. The aminophenol (1.65 g, 10.0 mmol, 3.0 eq.) and the ketone (0.881 g, 5 mmol, 1.0 eq.) were added under argon flow and dissolved in 20 mL anhydrous toluene. Under argon flow, a reflux condenser was added to the setup. After flushing it for 3 min with argon, a drying tube containing CaCl₂ was added to the setup and the solution was refluxed for 1 d. The reaction mixture was allowed to cool down and the solvent was removed under reduced pressure. The crude product was obtained as a dark brown solution and purified by recrystallization in Et₂O/MeOH (4:1) to give the imine **3e** (0.108 g, 0.33 mmol, 6.5%) as a colorless powder.

¹H-NMR: (400.1 MHz, CD₂Cl₂): δ_H = 7.98 (m, 2H), 7.50 (m, 2H), 7.09 (dd, 1H, ³J = 8.4 Hz, ⁴J = 2.3 Hz), 6.86 (d, 1H, ³J = 8.4 Hz), 6.87 (d, 1H, ⁴J = 2.3 Hz), 5.64 (s, 1H), 2.43 (s, 3H), 1.36 (s, 9H), 1.30 (s, 9H).

HR-MS (EI, *m/z*): found 322.21654 (M-H)⁺ (calculated 322.21654 for C₁₈H₂₀NO); Diff(ppm) = - 0.01.



6.6.3. Diffusion ordered spectroscopy (DOSY)

DOSY measurements were performed with the convection suppressing DSTE (double stimulated echo) pulse sequence developed by Jerschow and Müller in a pseudo 2D mode.⁴ Smoothed square (SMSQ10.100) gradient shapes and a linear gradient ramp with 20 increments between 5% and 95% of the maximum gradient strength (5.35 G/mm) were used. The diffusion time delay was set to 45 ms. For the homospoil gradient strengths, values of 100, -13.17, 20 and -17.13 % were used. Gradient pulse lengths (p16) were first optimized to obtain a sigmoidal signal decay for increasing gradient strength (3.0 ms for TMS, 6.0 – 6.5 ms for CPA/imine complexes). NMR spectra were processed with Bruker TopSpin 3.2 (T1/T2 relaxation package) and diffusion coefficients were derived according to Jerschow and Müller⁴ Tetramethylsilan was added to the samples to reference chemical shifts and the viscosity of each sample.

The molecular radii were derived by the Stokes-Einstein equation⁵ using Chens correction.⁶

$$D_i = \frac{k_B T}{6\pi\eta r_H} * (1 + 0.695 * \left(\frac{r_{solv}}{r_H}\right)^{2.234})$$

D_i is the self-diffusion coefficient derived by the measurement, η is the viscosity of the solvent, r_H is the hydrodynamic radius of the observed molecule and r_{solv} the radius of the solvent. No form factor correction was applied. The viscosity was determined by measuring the diffusion coefficient of the reference tetramethylsilane (TMS) and solving the equation for η with the literature value⁷ of the radius of 2.96 Å.

To estimate the error, diffusion coefficients for different signals of the same complex were averaged and the standard deviation was determined. The molecular radii were calculated based on the averaged diffusion coefficient, the averaged diffusion coefficient plus the standard deviation and the averaged diffusion coefficient minus the standard deviation. The resulting radii are given as the radius derived from the averaged diffusion coefficient and the error range is given by:

$$Error\ range = \frac{1}{2} * [(r_i^{aver} - r_i^{aver+StDev}) + (r_i^{aver-StDev} - r_i^{aver})]$$

Where r_i^{aver} is the radius derived from the averaged diffusion coefficient, $r_i^{aver+StDev}$ is the minimum radius derived from the averaged diffusion coefficient plus the standard deviation and $r_i^{aver-StDev}$ is the maximum radius derived from the averaged diffusion coefficient minus the standard deviation.

6. Bidentate Substrate Binding in Brønsted Acid Catalysis: Structural Space, Hydrogen Bonding and Dimerization

Table S1: Measured self diffusion coefficients of **1a/2a** at a concentration of 50 mM at 180 K in CD₂Cl₂ for signals 1-5 which were unambiguously assigned to one of the three different species A, B or C (see chemical shift assignment Figure S1). The determined coefficients are similar for all three species within the precision of the measurement (signal intensities were low).

Entry	Chem. Shift [ppm]	Assignment	Self diffusion coefficient [m ² /s]
1	9.58	Species C	3.21E-11
2	8.63	Species A	3.72E-11
3	8.57	Species B	3.55E-11
4	6.69	Species B	3.10E-11
5	3.55	Species C	3.09E-11
6	0.00	TMS	1.90E-10

The self diffusion coefficients determined for signals 1-5 are similar within the error of the experiment, considering the low signal intensities. This clearly shows, that all three species are similar in size, i.e. [CPA/imine]₂ dimers. An average hydrodynamic radius of 11.8 ± 0.87 Å was derived based on the averaged self diffusion coefficient of entries 1-5.

As a reference for monomeric CPA/imine systems, the system depicted below was used. The chemical shift assignment and structural investigations on this system were done in our previous research.⁸ As probe signals, one signal of the CPA for the CPA/E and CPA/Z complex, as well as one signal of the imine for the CPA/E and CPA/Z complex was selected. All signals were similar and based on the averaged self diffusion coefficient, the average hydrodynamic radius of 8.8 ± 0.15 Å was determined.

6. Bidentate Substrate Binding in Brønsted Acid Catalysis: Structural Space, Hydrogen Bonding and Dimerization

Table S2: Measured self diffusion coefficients of the monomeric reference system (see below) at a concentration of 50 mM at 180 K in CD₂Cl₂.

Entry	Chem. Shift [ppm]	Assignment	Self diffusion coefficient [m ² /s]
1	7.88	CPA/E (CPA)	4.76E-11
2	7.75	CPA/Z (CPA)	4.93E-11
3	3.80	CPA/Z (Imin)	4.98E-11
4	2.54	CPA/E (Imin)	4.81E-11
5	0.00	TMS	2.02E-10

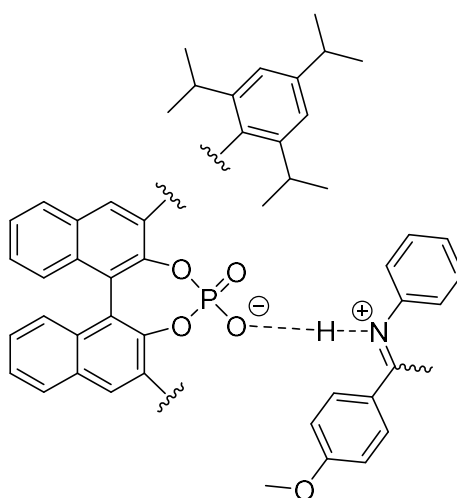


Table S3: Measured self diffusion coefficients of **1b/3a** at a concentration of 25 mM at 180 K in CD₂Cl₂.

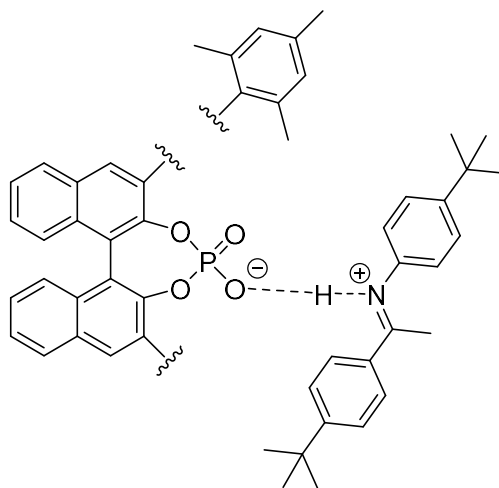
Entry	Chem. Shift [ppm]	Assignment	Self diffusion coefficient [m ² /s]
1	8.81	Imine	4.08E-11
2	8.03	CPA	3.90E-11
3	7.92	CPA	3.96E-11
4	6.29	CPA	3.86E-11
5	5.90	CPA	3.87E-11
6	1.44	Imine	3.88E-11
7	0.98	Imine	3.90E-11
8	0.00	TMS	2.06E-10

The self diffusion coefficients of entries 1, 6 and 7 (imine) are identical to the ones of the CPA (2-5), showing that both molecules are part of the same complex. Hence, the self diffusion coefficients were averaged and a hydrodynamic radius of $10.93 \pm 0.15 \text{ \AA}$ was determined.

6. Bidentate Substrate Binding in Brønsted Acid Catalysis: Structural Space, Hydrogen Bonding and Dimerization

Table S4: Measured self diffusion coefficients of the monomeric reference system depicted below at a concentration of 100 mM and a 1:1 ratio at 180 K in CD₂Cl₂.

Entry	Chem. Shift [ppm]	Assignment	Self diffusion coefficient [m ² /s]
1	7.77	CPA/E (CPA)	4.00E-11
2	2.64	CPA/E (Imin)	4.16E-11
3	1.16	CPA/E (Imin)	4.12E-11
4	0.00	TMS	1.99E-10



To put the found hydrodynamic radius of **1b/3a** (see Table S3) into relation, the reference system depicted above was selected to mimic the steric properties and hydrodynamic radius of a monomeric CPA/imine complex. The chemical shift analysis for this system was done previously⁹ and it was also clarified that the CPA/imine complex is monomeric. Based on the averaged self-diffusion coefficients, a hydrodynamic radius of 10.2 ± 0.16 Å was derived. The obtained radius of the monomeric reference system is close to the one of **1b/3a**, validating that **1b/3a** is indeed a monomeric CPA/imine complex.

Table S5: Measured self diffusion coefficients of **1c/2a** at a 1:1 ratio and a concentration of 10 mM at 180 K in CD₂Cl₂.

Entry	Chem. Shift [ppm]	Assignment	Self diffusion coefficient [m ² /s]
1	4.02	Imine	3.56E-11
2	0.00	TMS	2.13E-10

As a probe signal for the **1c/2a** complex, the methoxy group of **2a** was selected. Based on the self diffusion coefficient, a hydrodynamic radius of ~ 12.36 Å was determined.

6.6.4. Chemical Shift assignments

Chemical shifts of CPA/imine complexes were assigned using ^1H -, ^{13}C -, ^{31}P -NMR, ^1H ^{13}C HSQC, ^1H ^{13}C HMBC, ^1H ^{31}P HMBC, ^1H COSY, ^1H TOCSY and ^1H NOESY spectra. ^1H chemical shifts are given in black, ^{13}C chemical shifts are given in green, ^{31}P chemical shifts are given in red, multiplicities and coupling constants are given in blue.

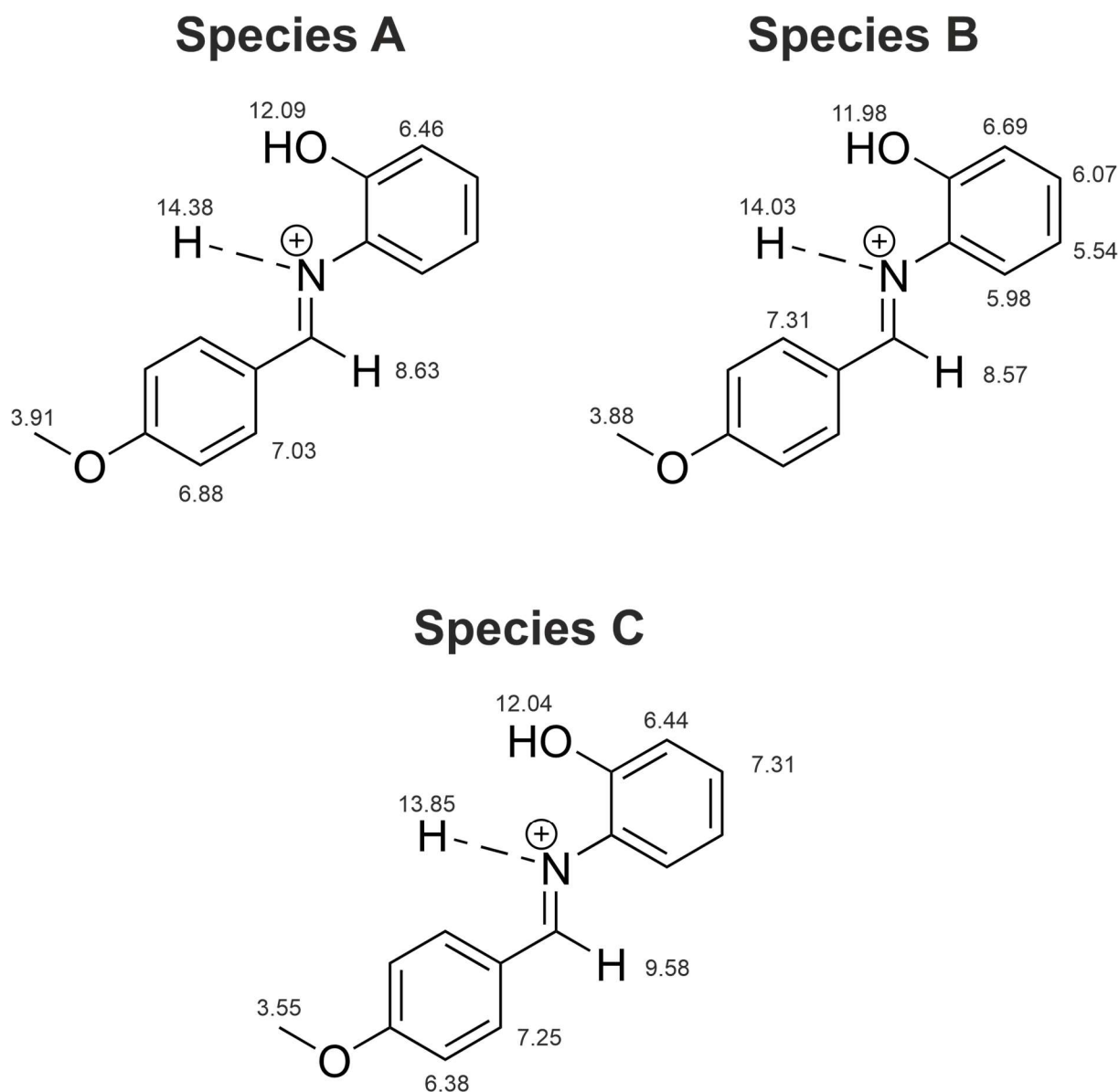


Figure S1: Proton chemical shift assignment of **1a/2a** at a concentration of 50 mM in CD_2Cl_2 at 180 K and 600 MHz.

6. Bidentate Substrate Binding in Brønsted Acid Catalysis: Structural Space, Hydrogen Bonding and Dimerization

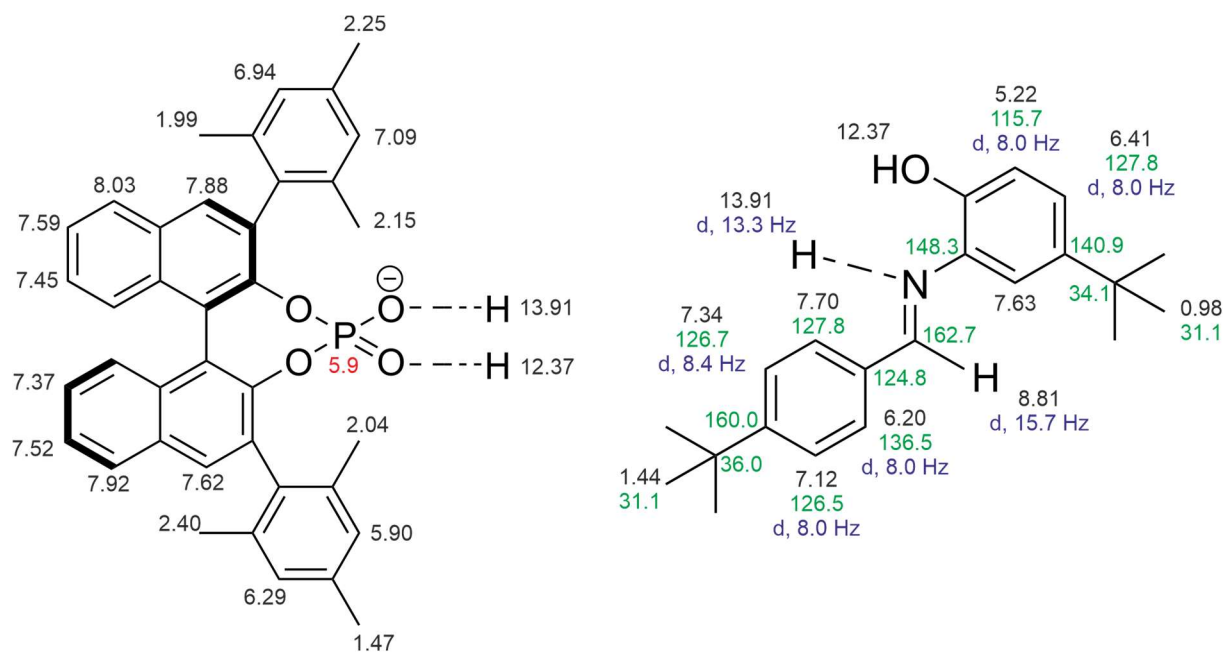


Figure S2: Proton chemical shift assignment of **1b/3a** at a concentration of 25 mM in CD_2Cl_2 at 180 K and 600 MHz.

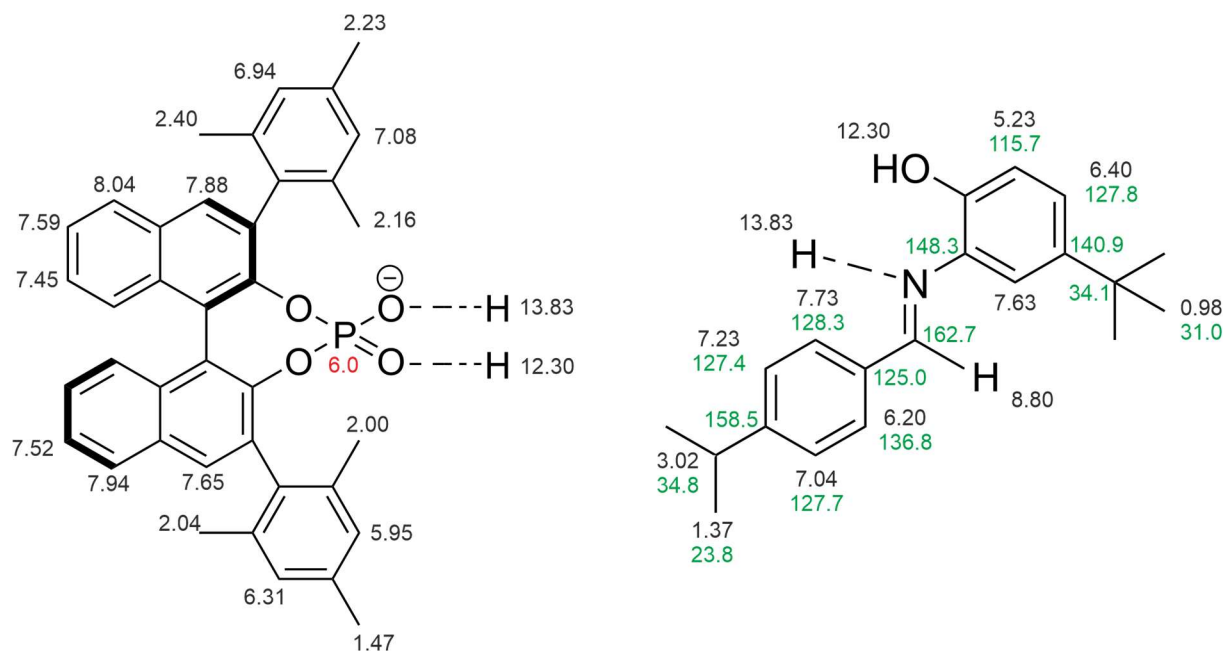


Figure S3: Proton chemical shift assignment of **1b/3b** at a concentration of 25 mM in CD_2Cl_2 at 180 K and 600 MHz.

6.6.5. Initial system screening

Solvent screening

Initially, toluene- d_8 was tried as solvent to investigate the CPA/imine complexes, because in this solvent the best stereoselectivities were obtained in the optimization screening by Akiyama.¹⁰ However, the measured spectra showed severe line broadening and signal overlap. This is similar to our previous NMR investigations, where toluene was not suitable as a solvent.¹¹ We assume, that changing the solvent from toluene to dichloromethane does not drastically change the structural space of the investigated CPA/imine systems. However, it should be noted that during the reaction optimization by Akiyama on the example of one N-(*ortho*-hydroxyphenyl) imine and one CPA, the enantioselectivity in toluene (87% *ee*) was significantly higher than in dichloromethane (13% *ee*).

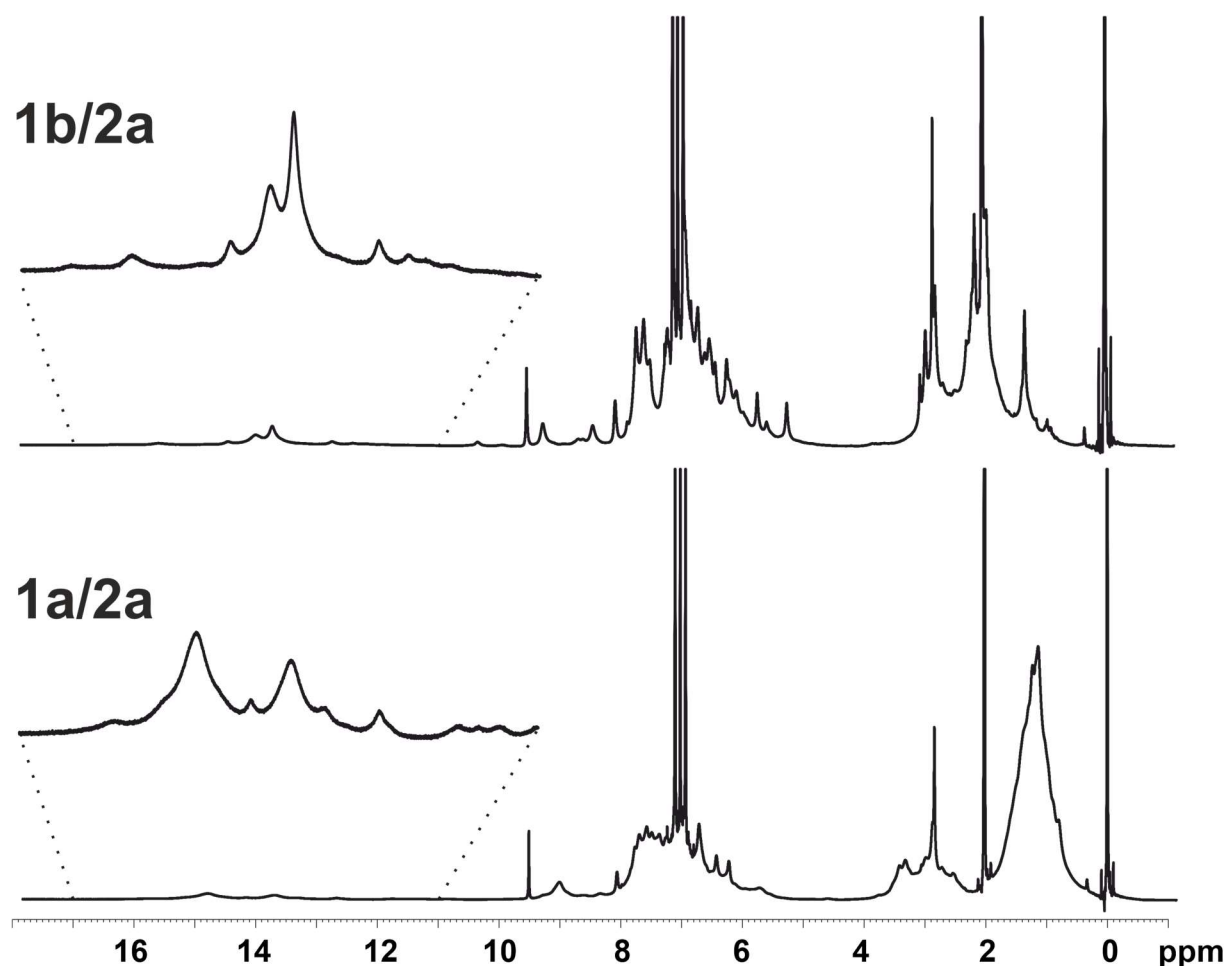


Figure S4: ^1H NMR spectra of **1a/2a** and **1b/2a** in toluene- d_8 at a temperature of 180 K and 600 MHz.

Intramolecular hydrogen bonding

As imines **2a-c** have both a hydrogen bond donor (-OH) and acceptor (C=N), the formation of intra- and intermolecular hydrogen bonds is possible. To confirm, that all observed hydrogen bonded proton signals (see Figure 2 and Figure S6) stem from CPA/imine hydrogen bonds, the proton spectra of imines **2a-c** (see Figure S5) were recorded under analogous conditions (temperature, concentration, sample, sample preparation) as the CPA/imine samples. The resulting spectra clearly show, that none of the monitored hydrogen bonded proton signals for systems **1a-b/2a-c** originate from the imines alone.

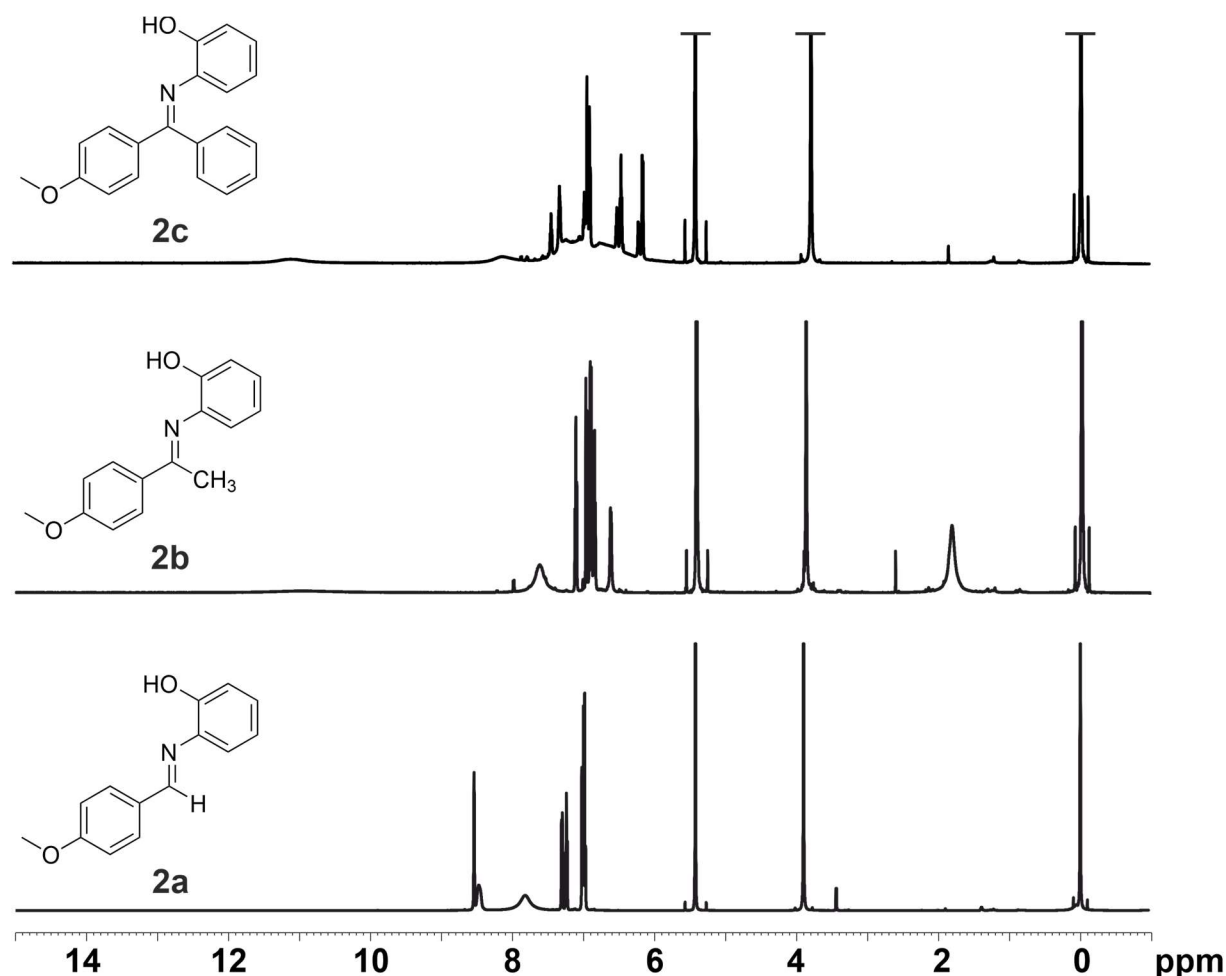


Figure S5: ^1H NMR spectra of imines **2a** (25 mM), **2b** (10 mM) and **2c** (10 mM) in CD_2Cl_2 at 180 K and 600 MHz (concentrations are analogous to the samples of **1a-b/2a-c**). For **2b** and **2c**, broad peaks at 11 ppm are observed which indicate the presence of inter- and/or intramolecular hydrogen bonds. However, these signals were not observed in the samples with the catalysts.

6. Bidentate Substrate Binding in Brønsted Acid Catalysis: Structural Space, Hydrogen Bonding and Dimerization

¹H NMR spectra for systems **1b/2a-c**

For samples containing catalyst **1b** and imines **2a-c**, the recorded ¹H NMR spectra (see Figure S6) were similar to the ones with catalyst **1a** (see Figure 2). For imines **2b** and **2c** many hydrogen bonded proton signals were monitored, reflecting a broad structural space of the complexes. For imine **2a** however, 8 hydrogen bonded proton signal, reflecting 4 different complexes were observed. In contrast to **1a/2a** (see Figure 2), the set of PO⁻---H-N⁺ hydrogen bonds as well as the set of PO---H-O hydrogen bonds have different chemical shifts within the set (2 H-bonds at 14-14.5 ppm, 2 H-bonds at 13 ppm for PO⁻---H-N⁺; 2 H-bonds at 12.4 ppm, 2 H-bonds at 11.5 ppm for PO---H-O), which indicates a structural difference.

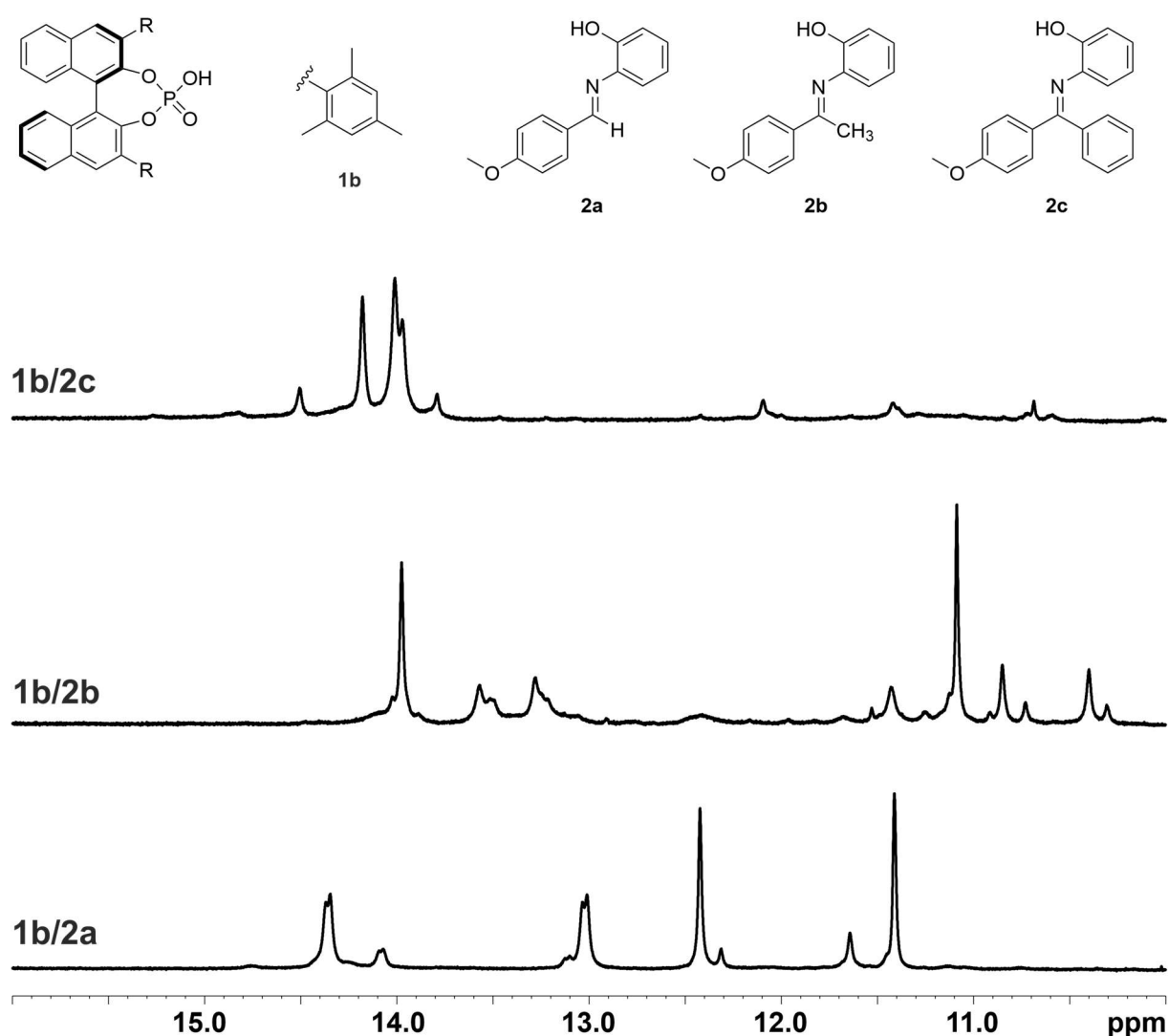


Figure S6: Section of the ¹H NMR spectra of **1b/2a** (bottom), **1b/2b** (middle) and **1b/2c** (top) at a 1:1 ratio and a concentration of 10 mM in CD₂Cl₂ at 600 MHz and 180 K. For **1b/2a**, 8 hydrogen bonds reflecting 4 different CPA/imine species were observed, while for **2b** and **2c** a multitude of different species was found.

E/Z isomerization experiments

For the system **1a/2a** (see Figure 2), a second sample was prepared at low temperature (see Sample Preparation). In our previous work,⁹ this method was applied to exclusively populate CPA/*E*-imine species. In our previous work,^{8,12} the employed imines were predominantly present as the *E*-isomer, but in presence of a chiral phosphoric acid, CPA/*Z*-imine complexes were significantly populated (*E*:*Z* ratios up to approx. 50:50) due to a reduced steric repulsion within the binding pocket of the catalyst. However, at temperatures < -80 °C, the *E*-imine cannot isomerize. Hence, if the sample is prepared at low temperatures, it becomes possible to suppress CPA/*Z*-imine complexes. For **1a/2a**, the population of hydrogen bonded proton signals A, B and C (see Figure S7) are similar for the low-temperature (“*E*-only”) and room-temperature sample (“*E/Z*”). This indicates, that all 3 species feature an *E*-imine. The slight offset most likely originates in an insufficient equilibration of the “*E*-only” sample prior to the measurement.

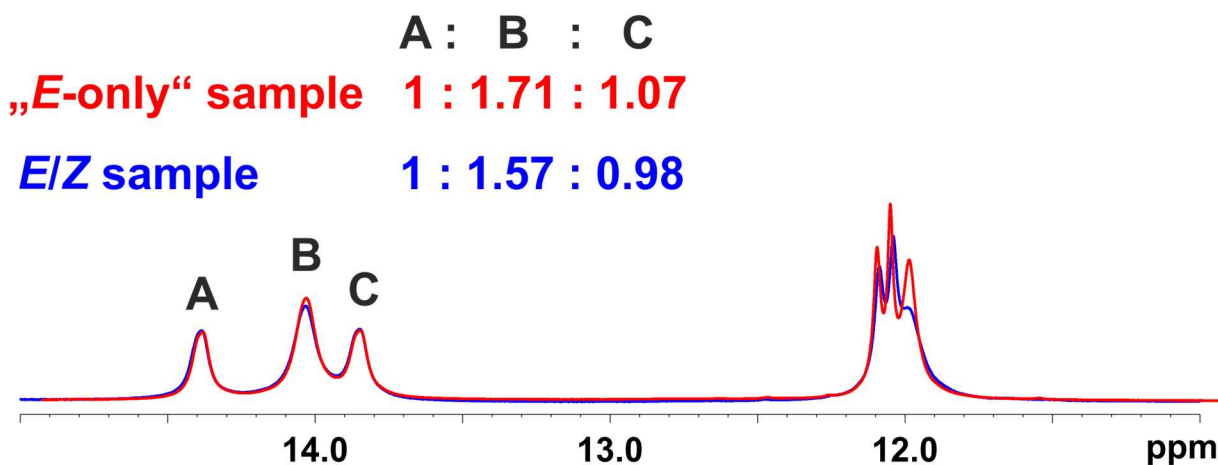


Figure S7: Comparison of the ¹H NMR spectra of 2 samples of **1a/2a** which were prepared at low temperature (red) and at room temperature (blue) in CD₂Cl₂ at 180 K and 600 MHz. No significant differences were observed, indicating that all 3 species feature an *E*-imine.

To further corroborate the assignment of all species as *E*-imine, photoisomerization experiments were carried out. In our previous work it was shown, that it is possible to increase the population of the CPA/*Z*-imine *via* illuminating the sample with an appropriate wavelength to induce a photoisomerization process.¹³ Hence, **1a/2a** (1 : 1 ratio, 50 mM) was illuminated at 180 K first at a wavelength of 13.5 h and afterwards additionally for 3 h at 280 nm (see Figure S8). However, only minor changes in the integral ratios of the hydrogen bonded proton signals A, B and C were monitored, which could also originate in a change in relaxation times under illumination. This indicates, that all three species feature the same imine configuration, which is most likely the more stable *E*.

6. Bidentate Substrate Binding in Brønsted Acid Catalysis: Structural Space, Hydrogen Bonding and Dimerization

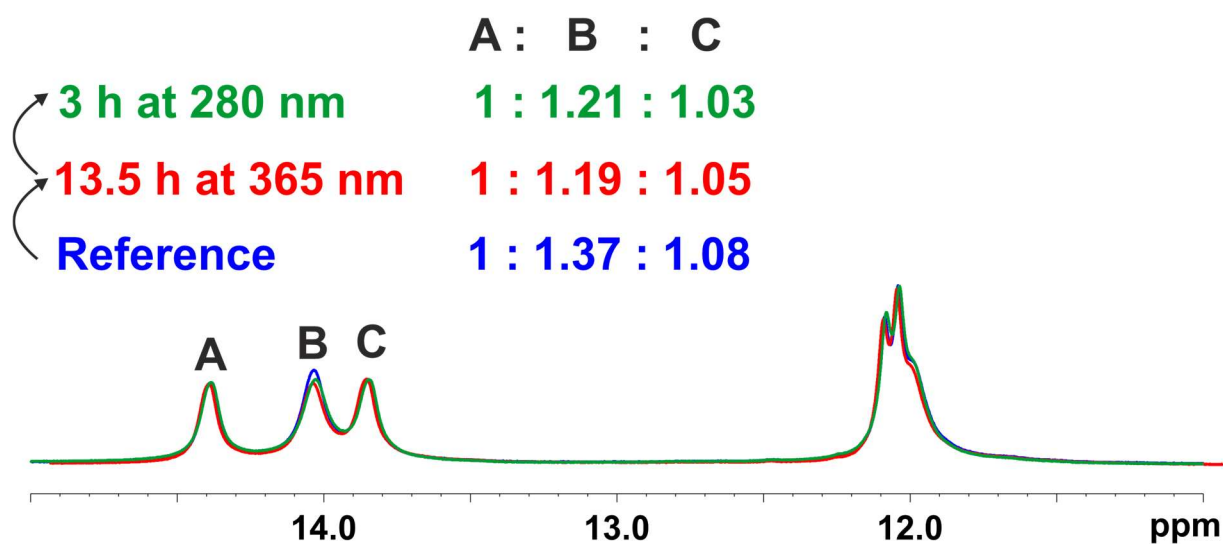


Figure S8: Comparison of the hydrogen bonding section of the ^1H -NMR spectra of **1a/2a** at 180 K and 600 MHz in CD_2Cl_2 . The blue spectrum is the reference spectrum prior to illumination, the red spectra was recorded after 13.5 h of continuous illumination at 365 nm and the green spectrum was recorded after following illumination at 280 nm for 3 h. Minor changes in the populations of species A, B and C were detected but unlikely originate in a change of the imine configuration.

6.6.6. Accessing CPA/imine monomers

In our previous research,¹² we identified the structure of [CPA/imine]₂ complexes featuring CPA **1b** and imines without additional hydrogen bond donor. In these structures, two stacked imines are nested within the binding pocket created by the 3,3'-substituents of the two catalyst molecules in a shifted phase to phase arrangement. Thereby, the 3,3'-substituents of the two catalyst molecules are close to each other. Initially we tried to modify the catalyst to hinder dimerization.

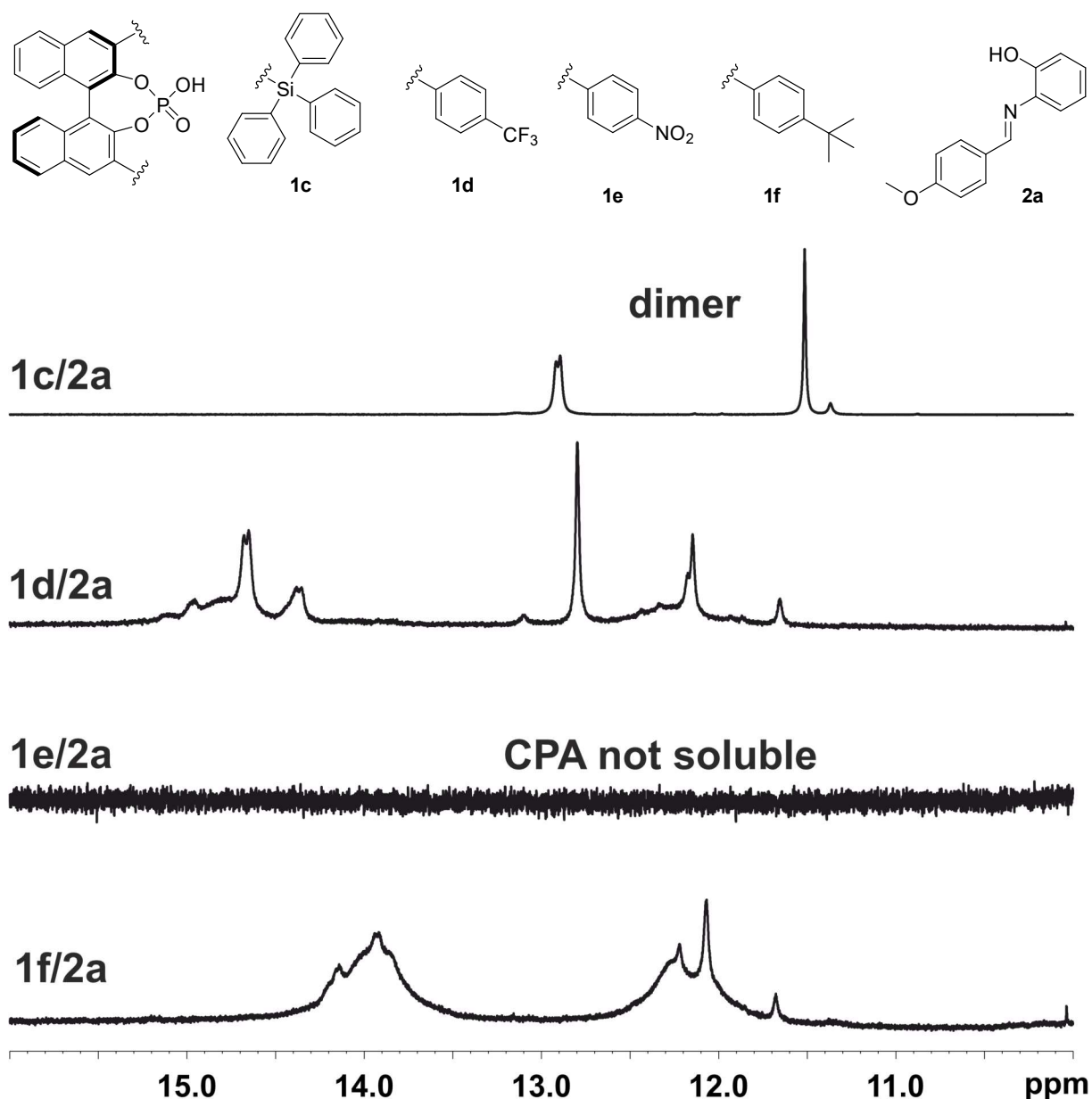


Figure S9: Section of the ¹H NMR spectra of **1c-f/2a** in CD₂Cl₂ at a ratio of 1:1 and a concentration of 10 mM at a temperature of 180 K.

For the combination of **1c/2a** (see Figure S9, top), the steric bulk of the catalyst was increased to minimize the available space inside the binding pocket, so that two stacked imines would not fit in. The

6. Bidentate Substrate Binding in Brønsted Acid Catalysis: Structural Space, Hydrogen Bonding and Dimerization

measured ^1H NMR spectrum showed only two hydrogen bonds, reflecting one distinct species. However, DOSY measurements (see Table S5) showed that the monitored complex is still a dimer, giving a hydrodynamic radius of $\sim 12.36 \text{ \AA}$, which is close to the previously reported hydrodynamic radius of monodentate CPA/imine dimers.¹² For catalysts **1d-f**, the idea was to introduce electronic (**1d** and **1e**) or steric (**1f**) repulsion to the 3,3'-substituents. Catalyst **1e** was not soluble in CD_2Cl_2 at low temperature and hence no hydrogen bonded proton signals are observed. For **1d/2a** and **1f/2a**, no clear and well defined hydrogen bonded proton NMR signals were observed or the spectra could not be analyzed in more detail due to signal overlap and line broadening.

In our previous research, we observed that installing sterically bulky groups such as *tert*-butyl groups on both sides of the imine can efficiently prevent dimerization of CPA/imine complexes.⁹ Hence, imine **3a** was selected and screened with different catalysts. **1b/3a** gave a well defined spectrum with only one monomeric species (see Figure 3), thus showing that this approach can give the intended result. For **1a/3a**, a similar spectrum was recorded but with significantly broadened lines. Additionally, for **1a/3a** spontaneous gel formation – most likely by CPA catalyzed polymerization of **3a** – occurred after some time (the shown spectrum in Figure S10 was measured immediately after sample preparation). For **1c/3a**, **1g/3a** and **1h/3a**, only severely line broadened hydrogen bonded proton signals were found, highlighting the broad possible structural space of bidentate CPA/imine complexes.

After receiving a well resolved spectrum of monomeric **1b/3a**, we slightly changed the *para*-substituent or alpha-substituent to explore if the determined structure for **1b/3a** is retained if the imines are modulated. When changing the *tert*-butyl group to an *iso*-propyl group for **1b/3b** (see Figure S11), again a well resolved spectrum with one defined species was obtained (see Figure S3 for chemical shift assignment). However, when going to a methyl-substituent (**1b/3c**) or methoxy-substituent (**1b/3d**) or if the alpha-substituent is changed from hydrogen to methyl (**1b/3e**), again various broad hydrogen bonded proton signals are detected. This again highlights, that for N-(*ortho*-hydroxyar) substituted imines, a broad structural space is possible and that only for certain CPA/imine combinations, well defined complexes are obtained.

6. Bidentate Substrate Binding in Brønsted Acid Catalysis: Structural Space, Hydrogen Bonding and Dimerization

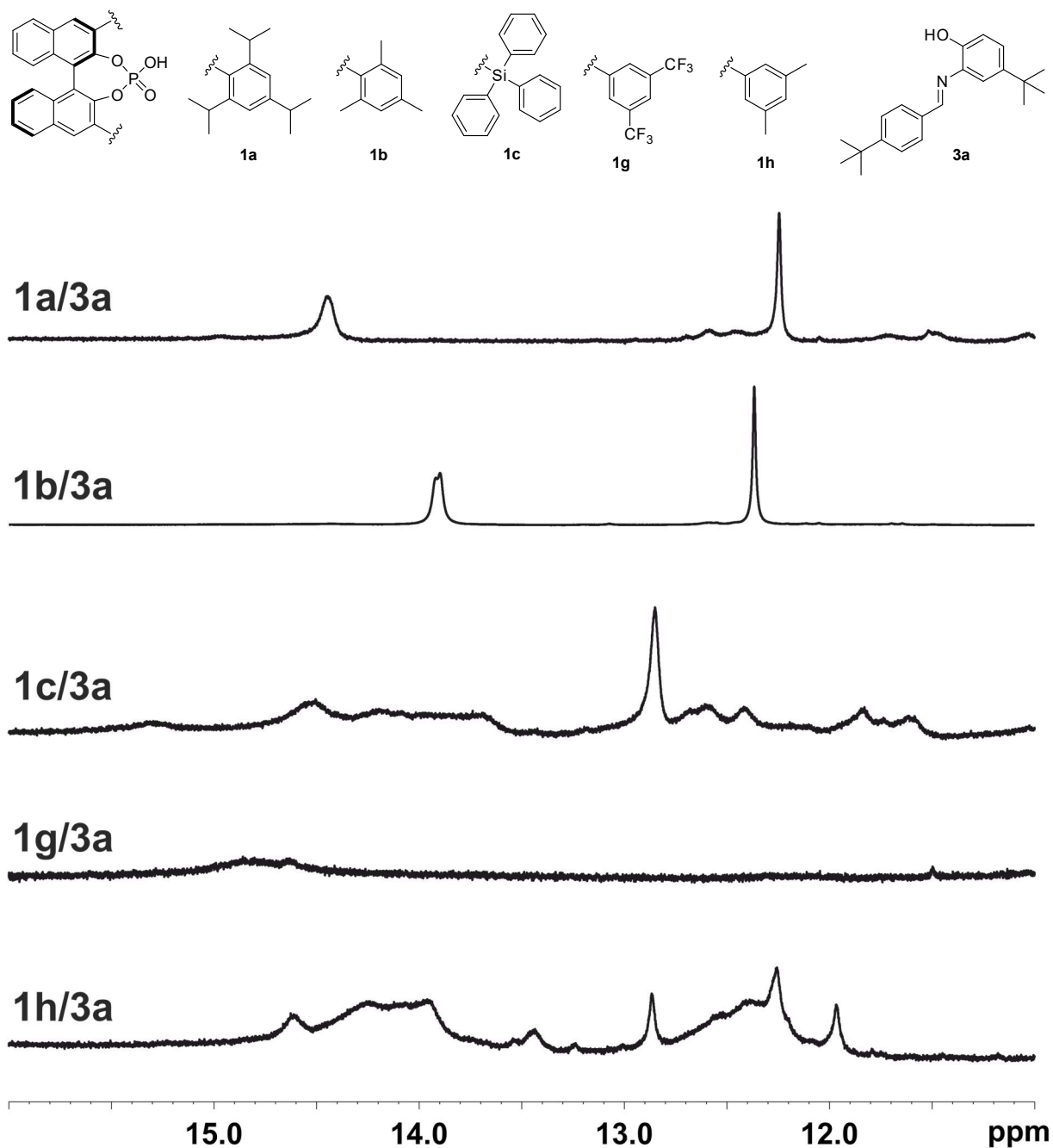


Figure S10: Section of the ¹H NMR spectra of **1a-c,g,h/3a** in CD₂Cl₂ at a ratio of 1:1 and a concentration of 10 mM at a temperature of 180 K.

6. Bidentate Substrate Binding in Brønsted Acid Catalysis: Structural Space, Hydrogen Bonding and Dimerization

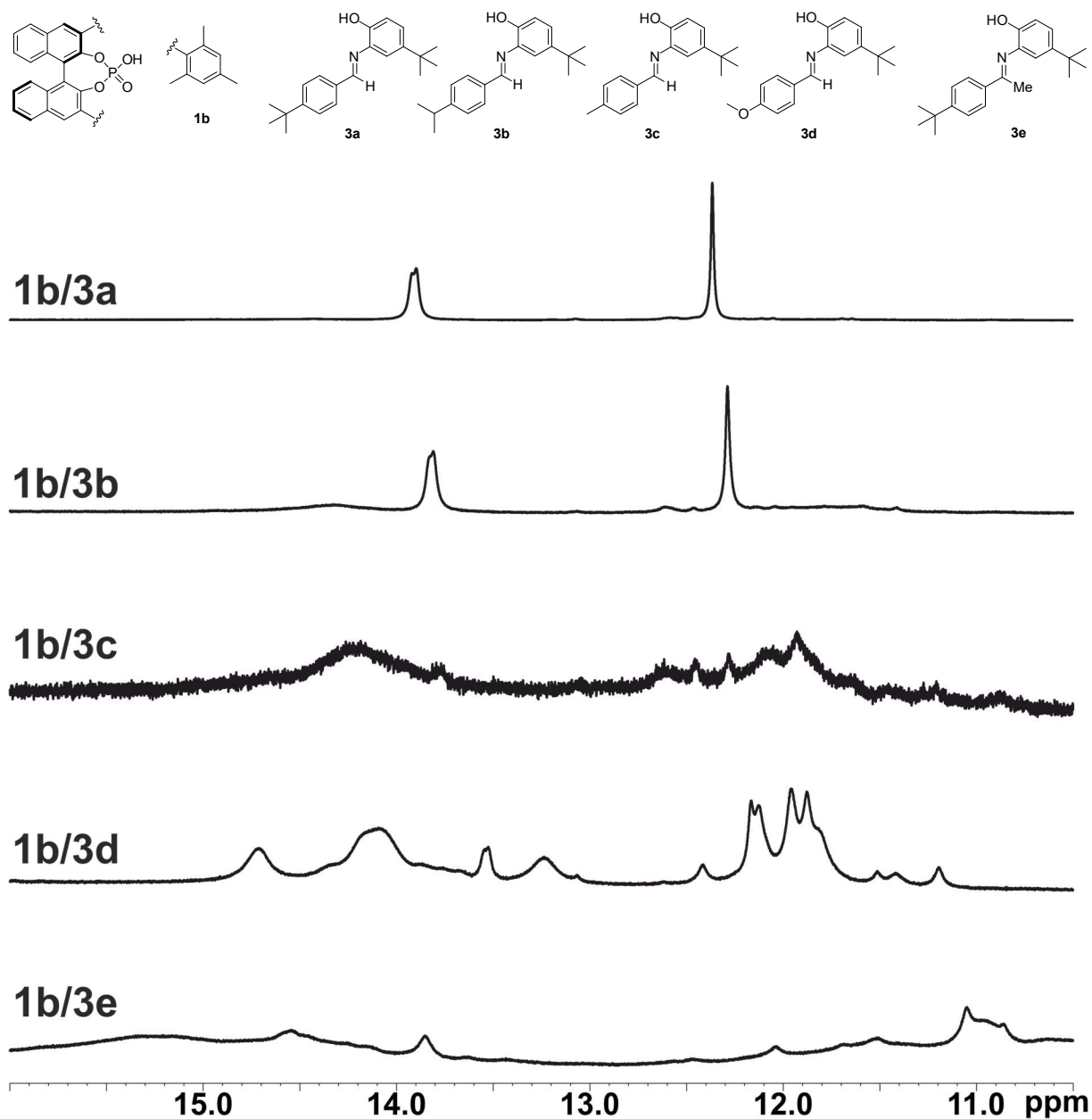


Figure S11: Section of the ¹H NMR spectra of **1b/3a-e** in CD₂Cl₂ at a ratio of 1:1 and a concentration of 25 mM at a temperature of 180 K.

6.6.7. Hydrogen bond analysis

Due to their partial covalent character, hydrogen bonds can be characterized via the detection of scalar coupling between the involved nuclei.^{13,14} For the system **1b/3a**, the full scalar coupling matrix between the two hydrogen bonded protons (PO⁻---H-N⁺ in red and PO⁻---H-O blue; see Figure S12) and the CPA as well as imine was detected *via* ¹H ¹H COSY and ¹H ³¹P HMBC spectra. This clearly validates the assignment as hydrogen bonds and confirms the postulated binding motif featuring two hydrogen bonds as a rigid anchor.

In our previous research with imines featuring no additional hydrogen bond donor, the CPA/imine complexes could be characterized as hydrogen bond assisted ion pairs by analysis of the ¹H and ¹⁵N chemical shifts as well as J_{NH} coupling constants and comparison to reference systems with weak and very strong acids.^{13,14} For CPA/imine complexes with imines **2** and **3**, we assume that the complexes are also present mainly as ion pairs, especially as the cooperativity effect of the second PO⁻---H-O hydrogen bond is expected to better stabilize the resulting phosphate, which suggests an even stronger proton transfer on the imine substrate, resulting in a stronger ion pair character. This would be reflected by the $^1J_{\text{NH}}$ coupling constant, which could not be accessed as imines **2** and **3** could not be ¹⁵N labelled. However, the $^3J_{\text{HH}}$ coupling between the hydrogen bonded proton and the α -H of the imine (see e.g. Figure 12; doublet splitting was observed for all systems with α -H imines) can only be present if the NH binding order is relatively close to 1, clearly indicating that the proton is strongly transferred on the imine, which results in an ion pair character. However, as there is still detectable magnetization transfer by scalar coupling to the CPA (see Figure 12 signal C), the proton transfer is not complete and the complex is best described as hydrogen bond assisted ion pair.

6. Bidentate Substrate Binding in Brønsted Acid Catalysis: Structural Space, Hydrogen Bonding and Dimerization

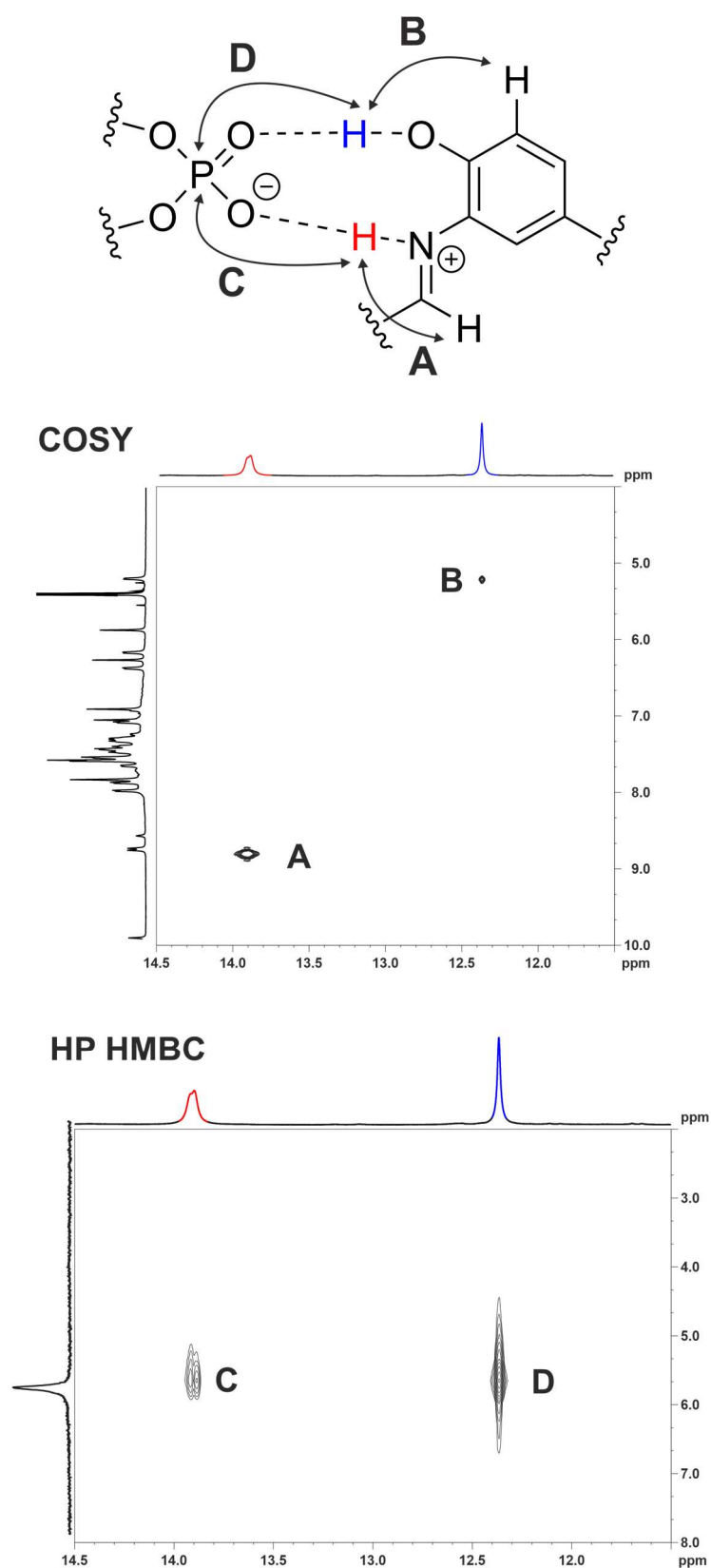


Figure S12: Excerpts of the ^1H ^1H COSY and ^1H ^{31}P HMBC spectra of **1b/3a** at a 1:1 ratio and a concentration of 25 mM at 180 K in CD_2Cl_2 . The cross peaks A-D clearly show the full scalar coupling matrix of the hydrogen bonded protons.

6.6.8. NOE studies

In the computed structure model for the bidentate complex **1b/3a** (see Figure 4) the imine is located in between the two 3,3'-substituents of the catalyst. The performed NOESY study (see Figure S13) validated this structure model, as only NOE contacts between the imine and the two 3,3'-substituents were found and none to the BINOL backbone, which would be typical for monodentate CPA/imine complexes.^{8,12} One site of the imine has only contact to one 3,3'-substituent (NOE cross peaks A and B or C-E), which could be resolved due to the signal splitting of the C₂-symmetric catalyst in the CPA/imine complex.

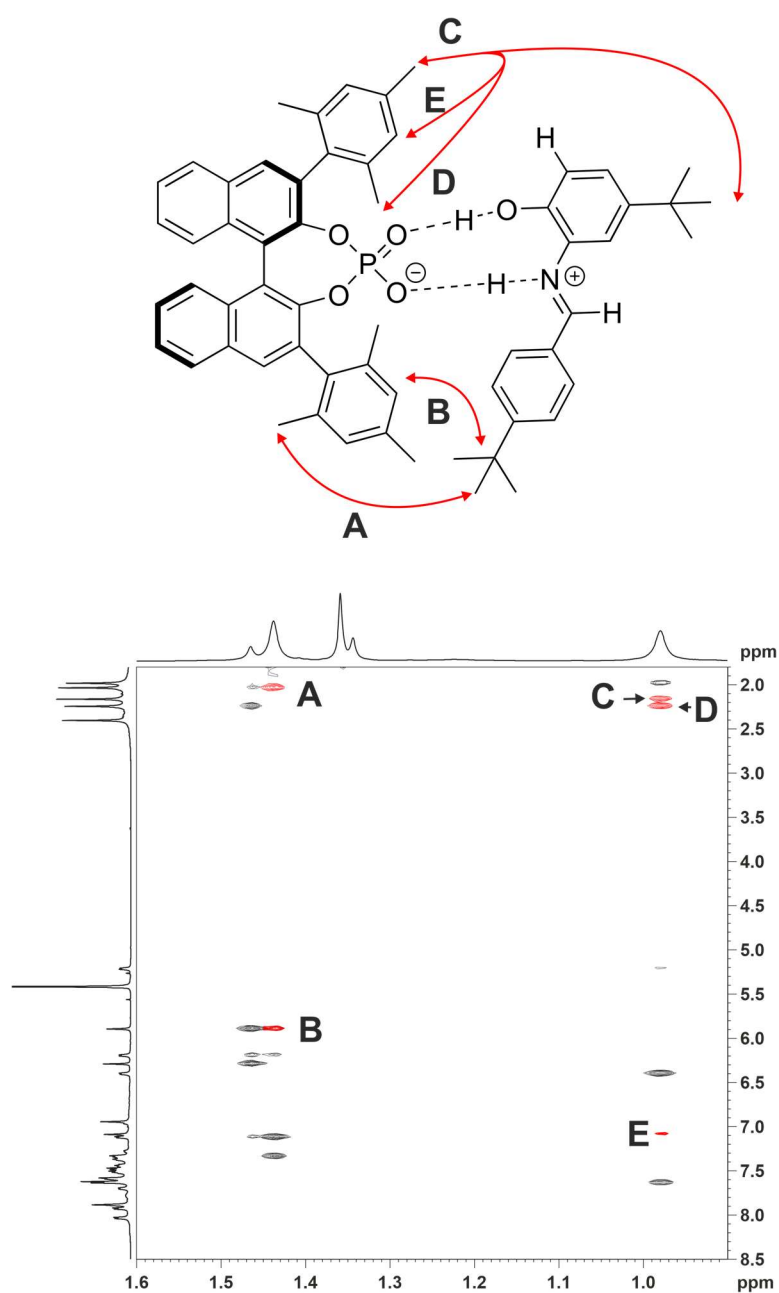


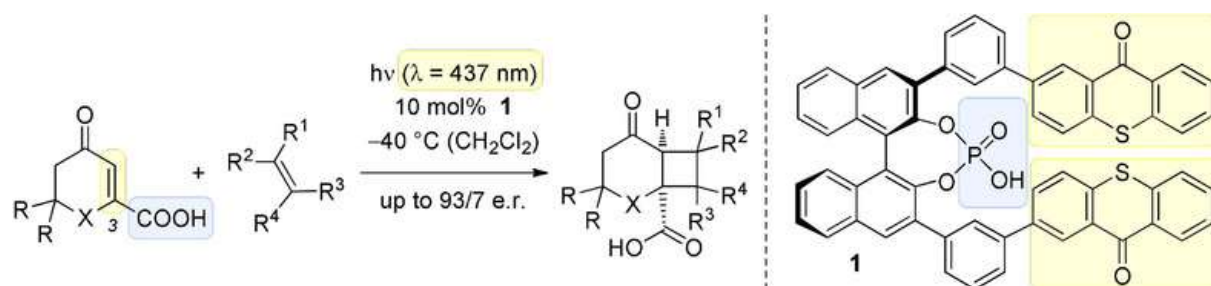
Figure S13: Excerpt of the NOESY spectrum of **1b/3a** at a 1:1 ratio and a concentration of 25 mM at 180 K in CD₂Cl₂. The cross peaks A-E shown in red validate the theoretically computed structure model.

6. Bidentate Substrate Binding in Brønsted Acid Catalysis: Structural Space, Hydrogen Bonding and Dimerization

6.6.9. References

- 1 C. Feldmeier, H. Bartling, E. Riedle and R. M. Gschwind, *J. Magn. Reson.*, 2013, **232**, 39–44.
- 2 A. Seegerer, P. Nitschke and R. M. Gschwind, *Angew. Chem. Int. Ed.*, 2018, **57**, 7493–7497.
- 3 R. K. Harris, E. D. Becker, S. M. Cabral De Menezes, R. Goodfellow and P. Granger, *Concepts Magn. Reson. Part A Bridg. Educ. Res.*, 2002, **14**, 326–346.
- 4 A. Jerschow and N. Müller, *J. Magn. Reson.*, 1997, **125**, 372–375.
- 5 A. MacChioni, G. Ciancaleoni, C. Zuccaccia and D. Zuccaccia, *Chem. Soc. Rev.*, 2008, **37**, 479–489.
- 6 H. C. Chen and S. H. Chen, *J. Phys. Chem.*, 1984, **88**, 5118–5121.
- 7 D. Ben-amotz and K. G. Willis, *J. Phys. Chem.*, 1993, **1**, 7736–7742.
- 8 J. Greindl, J. Hioe, N. Sorgenfrei, F. D. Morana and R. M. Gschwind, *J. Am. Chem. Soc.*, 2016, **49**, 15965–15971.
- 9 N. Lokesh, J. Hioe, J. Gramüller and R. M. Gschwind, *J. Am. Chem. Soc.*, 2019, **141**, 16398–16407.
- 10 T. Akiyama, J. Itoh, K. Yokota and K. Fuchibe, *Angew. Chem. Int. Ed.*, 2004, **43**, 1566–1568.
- 11 J. Greindl, J. Hioe, N. Sorgenfrei, F. Morana and R. M. Gschwind, *J. Am. Chem. Soc.*, 2016, **138**, 15965–15971.
- 12 M. Melikian, J. Gramüller, J. Hioe, J. Greindl and R. M. Gschwind, *Chem. Sci.*, 2019, **10**, 5226–5234.
- 13 K. Rothermel, M. Melikian, J. Hioe, J. Greindl, J. Gramüller, Matej Žabka, N. Sorgenfrei, T. Hausler, F. Morana and R. M. Gschwind, *Chem. Sci.*
- 14 N. Sorgenfrei, J. Hioe, J. Greindl, K. Rothermel, F. Morana, N. Lokesh and R. M. Gschwind, *J. Am. Chem. Soc.*, 2016, **138**, 16345–16354.

7. A Thioxanthone Sensitizer with a Chiral Phosphoric Acid Binding Site: Properties and Applications in Visible Light-Mediated Cycloadditions



Franziska Pecho, You-Quan Zou, Johannes Gramüller, Tadashi Mori, Stefan M. Huber, Andreas Bauer, Ruth M. Gschwind and Thorsten Bach

Chem. Eur. J. **2020**, *26*, 5190-5194. DOI: 10.1002/chem.202000720

A) Franziska Pecho, You-Quan Zhou, Tadashi Mori, Stefan M. Huber, Andreas Bauer and Thorsten Bach conceptualized, performed and analysed all experiments and computations and wrote the manuscript excluding the detailed NMR studies. B) Johannes Gramüller² conceptualized, performed and analysed the detailed NMR studies, including preparation of the samples (chemicals were synthesised and pre-dried by Franziska Pecho) and wrote the respective part of the manuscript. C) For the NMR part, Ruth M. Gschwind contributed to design of experiments, interpretation of data, writing and proof-reading of the manuscript part and provided funding.

Source of this chapter: ECS Publishing, <https://chemistry-europe.onlinelibrary.wiley.com/doi/full/10.1002/chem.202000720>.

Reproduced with permission. Text and figures may differ from the published version. The complete corresponding Supporting Information is provided free of charge at <https://chemistry-europe.onlinelibrary.wiley.com/doi/full/10.1002/chem.202000720>.

7.1. Abstract

A chiral phosphoric acid with a 2,2'-binaphthol core was prepared which displays two thioxanthone moieties at the 3,3'-position as light-harvesting antennas. Despite its relatively low triplet energy, the phosphoric acid was found to be an efficient catalyst for the enantioselective intermolecular [2+2] photocycloaddition of β -carboxyl-substituted cyclic enones (e.r. up to 93/7). Binding of the carboxylic acid to the sensitizer is suggested by NMR studies and by DFT calculations to occur via two hydrogen bonds. The binding event not only enables an enantioface differentiation but also modulates the triplet energy of the substrates.

7.2. Introduction

Recent interest in visible light-mediated reactions has triggered a large number of studies towards the synthesis of new chromophores and chiral catalysts.^[1] The long known thioxanthone chromophore^[2] has been revisited in the context of triplet sensitization^[3] and it has been attached to chiral scaffolds for applications in enantioselective photochemistry.^[4] The most frequently used chiral modification is represented by compound **1** (Figure 1)^[4a] in which a thioxanthone is attached via an oxazole to position C7 of 1,5,7-trimethyl-3-azabicyclo[3.3.1]nonan-2-one. The latter device serves as a hydrogen bonding site^[5] and allows to process lactams in [2+2] photocycloaddition^[4a,6] and deracemization^[7] reactions. By attachment to a chiral bisoxazoline, thioxanthone can be part of a bifunctional chiral metal catalyst and ligand **2** has been successfully employed in the Ni-catalyzed oxygenation of β -ketoesters.^[4b] Chiral imidazolinone-based organocatalysts have recently been reported for enamine catalysis in which the thioxanthone acts via single electron transfer.^[4d] However, not any binding motif known from thermal reactions will automatically lead to a successful chiral catalyst. Thiourea-linked thioxanthenes such as **3**, for example, did not display the expected enantioselectivity in photochemical reactions.^[4c]

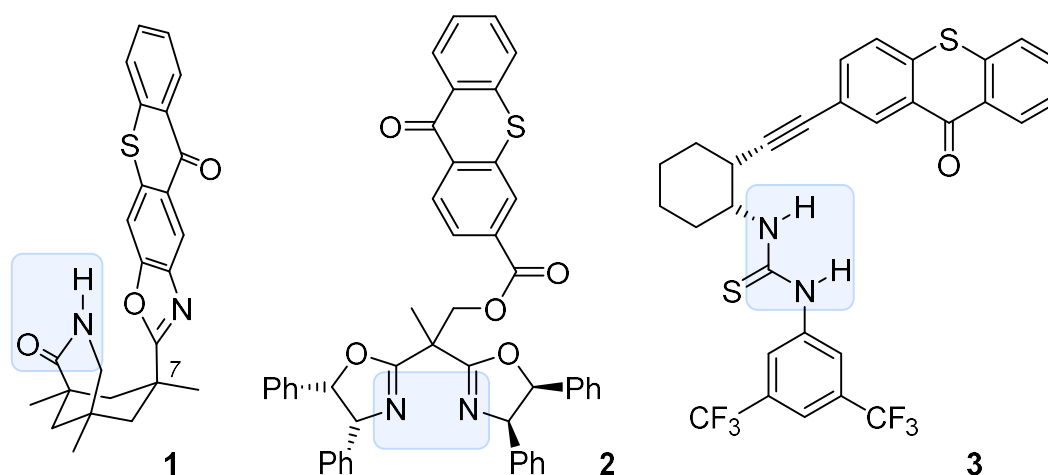
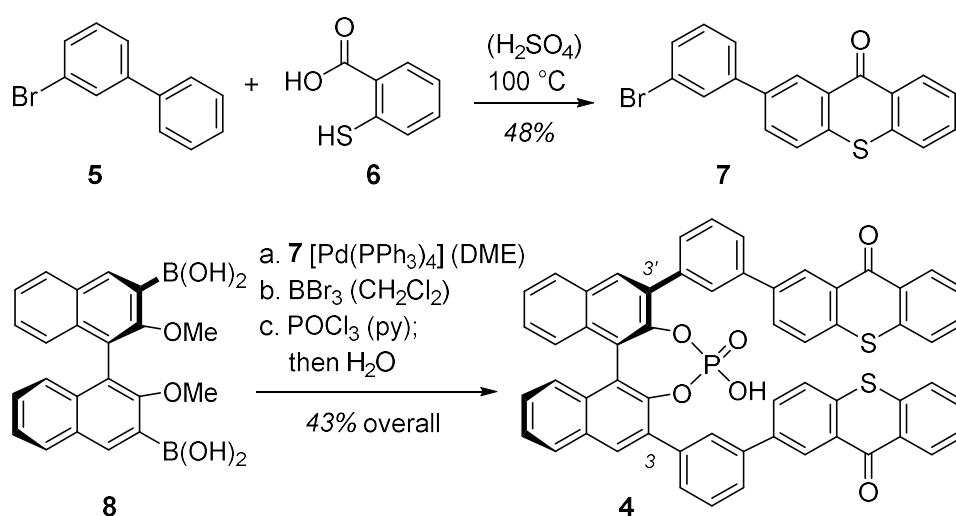


Figure 1. Structure of chiral thioxanthenes **1-3** with a substrate or metal binding site (in gray).

Nonetheless, given the limited number of substrates that can yet be processed by chiral thioxanthenes, it seems desirable to further investigate possible binding motifs to which a thioxanthone entity can be attached. In this communication, we describe the synthesis of a C_2 -symmetric chiral phosphoric acid with two thioxanthone units and report on preliminary studies as to its mode of action in photochemical [2+2] cycloaddition reactions.

7.3. Results and Discussion

Since their initial use in organocatalysis,^[8] chiral phosphoric acids have emerged as a highly efficient class of compounds for a plethora of applications.^[9] Most phosphoric acids display aryl groups in positions C3 and C3' of the 2,2'-binaphthol core and we envisaged that these positions would serve as suitable points of attachment for a thioxanthone unit. However, the direct linkage of a 9-oxo-9*H*-thioxanthen-3-yl group to positions C3 and C3' led to a phosphoric acid which did not induce any enantioselectivity in photochemical test reactions (see SI for further details). Upon further screening, a more promising catalyst **4** (Scheme 1) was discovered which was prepared by Suzuki cross-coupling of aryl bromide **7** and known diboronic acid **8**.^[10]



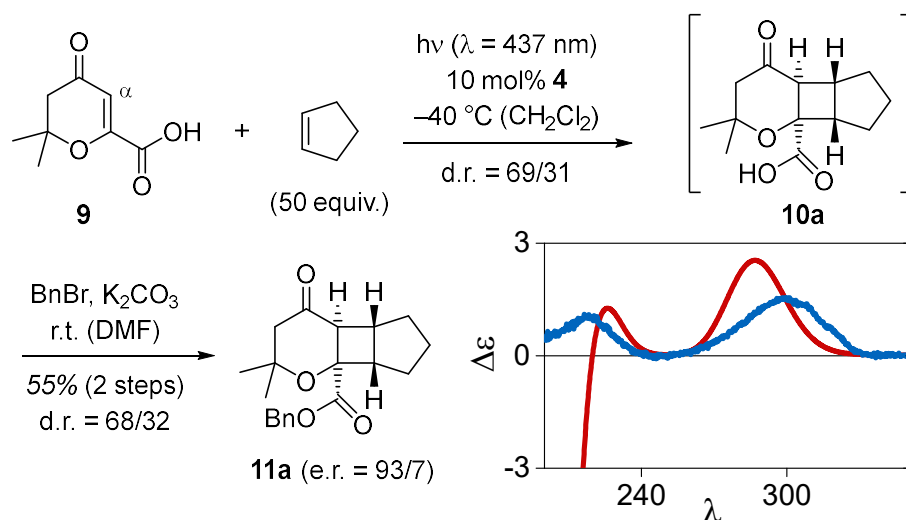
Scheme 1. Synthesis of phosphoric acid **4** from boronic acid **8** and aryl bromide **7**. Conditions and yields for the individual steps a-c: (a) 2.5 equiv. **7**, 10 mol% $\text{Pd}(\text{PPh}_3)_4$, 10 equiv. 2 M Na_2CO_3 (aq), $85\text{ }^\circ\text{C}$, 16 h (DME), 96%; (b) 6.0 equiv. BBr_3 , $0\text{ }^\circ\text{C} \rightarrow \text{rt}$, 2 h (CH_2Cl_2), 83%; (c) 2.0 equiv. POCl_3 , $95\text{ }^\circ\text{C}$, 12 h (py), then H_2O , $95\text{ }^\circ\text{C}$, 54%.

The former component was obtained by a dehydrogenative condensation^[11] of 3-bromobiphenyl (**5**) and thiosalicylic acid (**6**). After demethylation and phosphorylation the free acid was liberated by treatment with water. A major asset of phosphoric acid **4** as compared to thioxanthenes **1** and **3** is its C_2 symmetry which invites the coordination of substrates with a symmetric binding motif. In this context, carboxylic acids RCOOH seemed particularly interesting to us because studies by List and co-workers had established that they can be activated in thermal reactions by coordination to chiral phosphoric acids.^[12]

Preliminary experiments commenced with 3,4-dihydro-2,2-dimethyl-4-oxo-2*H*-pyran-6-carboxylic acid (**9**, Scheme 2) which had been previously employed in intermolecular [2+2] photocycloaddition reactions upon UV irradiation ($\lambda = 366\text{ nm}$).^[13] To our delight, we found that the previously reported reaction with cyclopentene to racemic products *rac*-**10** could be conducted with visible light in the

7. A Thioxanthone Sensitizer with a Chiral Phosphoric Acid Binding Site: Properties and Applications in Visible Light-Mediated Cycloadditions

presence of parent thioxanthone (thioxanthen-9-one, see SI for further details). With catalytic quantities of acid **4**, the reaction proceeded at $\lambda = 437$ nm with improved chemoselectivity (vide infra) and the desired product was isolated as a mixture of two diastereoisomers with the *cis-anti-cis* diastereoisomer **10a** prevailing over the *cis-syn-cis* diastereoisomer (d.r. = 69/31).

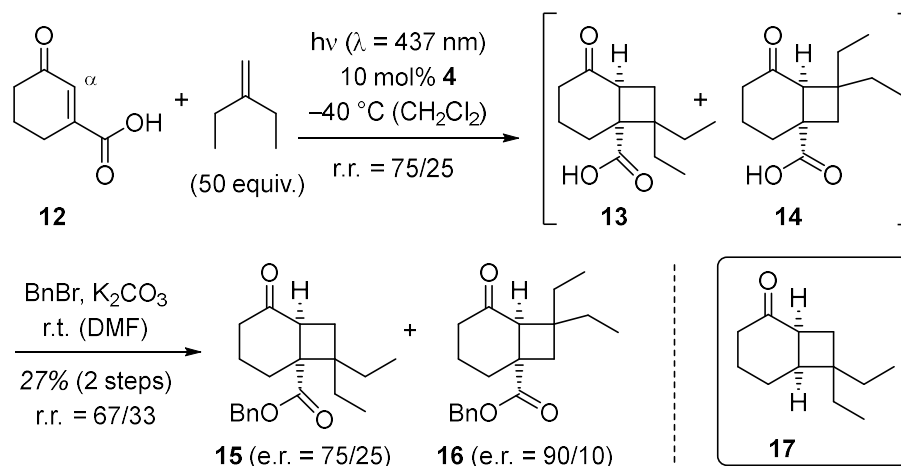


Scheme 2. [2+2] Photocycloaddition of cyclopentene to acid **9** catalyzed by thioxanthone **4** and subsequent benzylation; schematic CD spectrum (calculated in red, vs. measured in blue) of acid **10** (for full details, see SI).

Although isolation of products **10** was possible (61% yield), the enantiomeric ratio (e.r.) could not be determined by chiral HPLC analysis. Derivatization to the UV active benzyl ester was feasible and esters **11** were formed in 55% yield over two steps. Benzyl ester **11a** displayed a remarkable e.r. of 93/7 which suggests a high enantioface differentiation in the [2+2] photocycloaddition to product **10a**. The absolute configuration of the major enantiomer was determined by comparison of the measured and calculated CD spectra of compound **10a**. Formally, the absolute configuration corresponds to a *Si* face approach onto the α -carbon atom in the α,β -unsaturated carbonyl compound **9**.

Cyclohex-2-enone-3-carboxylic acid (**12**) had been previously involved in an enantioselective [2+2] photocycloaddition^[14,15] employing a chiral amine as chiral template. Enantioselectivities of up to 24% *ee* (e.r. = 62/38) had been achieved employing five equivalents of the template ($\lambda > 320$ nm). Products had not been isolated and the enantioselectivity had been determined by GLC upon derivatization. In our case, it was possible to perform the reaction with visible light ($\lambda = 437$ nm) employing only 10 mol% of catalyst **4** but the separation of the polar regioisomeric products **13** and **14** was not feasible. The benzylation turned out to be sluggish and yields of products **15** and **16** were low (Scheme 3).

7. A Thioxanthone Sensitizer with a Chiral Phosphoric Acid Binding Site: Properties and Applications in Visible Light-Mediated Cycloadditions



Scheme 3. Catalyzed enantioselective [2+2] photocycloaddition of 2-cyclohexenone-3-carboxylic acid (**12**) and 2-ethylbutene and subsequent benzylation; inset: structure of the decarboxylation product **17** obtained from intermediate **13**.

Like for product **11a** a significant enantioface differentiation was recorded with the higher e.r. (89/11) being found for the minor regioisomer **16**. The absolute configuration of chiral product **13** was assessed by decarboxylation^[16] to known cyclobutane **17**.^[17] The direction of attack at the α -carbon atom of enone **12** is identical to the direction of attack for compound **9** (*Si* face). The assignment of the absolute configuration for all other major enantiomers in the [2+2] photocycloaddition of **9** and **12** was based on analogy. Indeed, it was established that other olefins also react successfully under sensitized conditions in the presence of chiral phosphoric acid **4**. After benzylation, products **18-21** were isolated with high to moderate enantioselectivities (Figure 2). However, the yield for the two-step protocol remained relatively low, presumably due to the non-optimized benzylation protocol (26-42%, see SI for further details).

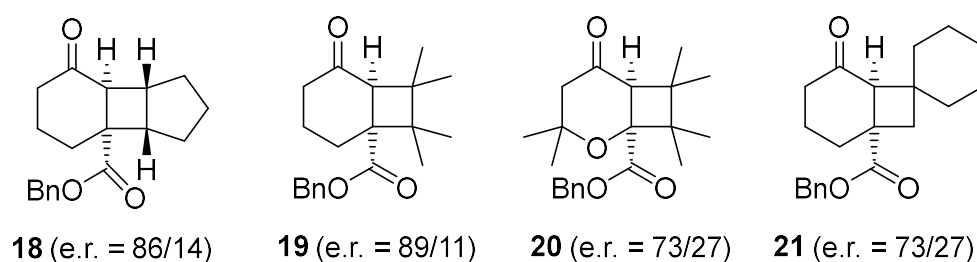


Figure 2. Structure and enantiomeric ratio of [2+2] photocycloaddition products **18-21** obtained from acids **9** and **12** via energy transfer from chiral phosphoric acid **4**.

A notable feature of thioxanthone **4** as compared to the parent compound (thioxanthen-9-one) was the fact that undesired decarboxylation reactions were suppressed and that the photocycloaddition reaction was more efficient (see SI for further details). Luminescence measurements in dichloromethane (Figure 3) revealed that the triplet energy (E_T) of compound **4** is surprisingly low. From the phosphorescence emission (77 K, dichloromethane) at the long wavelength shoulder the energy was

7. A Thioxanthone Sensitizer with a Chiral Phosphoric Acid Binding Site: Properties and Applications in Visible Light-Mediated Cycloadditions

calculated as $E_T = 235 \pm 2 \text{ kJ mol}^{-1}$ which is much lower than the reported triplet energy of thioxanthen-9-one ($E_T = 272 \text{ kJ mol}^{-1}$).^[18] Luminescence spectra of the two carboxylic acids showed the typical signature of α,β -unsaturated enones^[19] with a readily detectable 0-0 transition. The triplet energy calculated from this transition was $E_T = 288 \pm 2 \text{ kJ mol}^{-1}$ for compound **9** and $E_T = 287 \pm 2 \text{ kJ mol}^{-1}$ for compound **12** (77 K, pentane/isopentane). Combined with the results obtained from the thioxanthen-9-one irradiation experiments, the data suggest a preferred energy transfer within a complex between the carboxylic acids and compound **4** while thioxanthen-9-one leads to partial oxidation of the acid. Given the high energy difference of the triplet energies in a non-complexed situation it is also likely that the phosphoric acid lowers the triplet energy of the carboxylic acids upon association. Although it is known that coordination of Lewis acids to carbonyl groups alters the triplet state energy^[1,20] we are not aware of this phenomenon having been observed for phosphoric acid/carboxylic acid combinations.

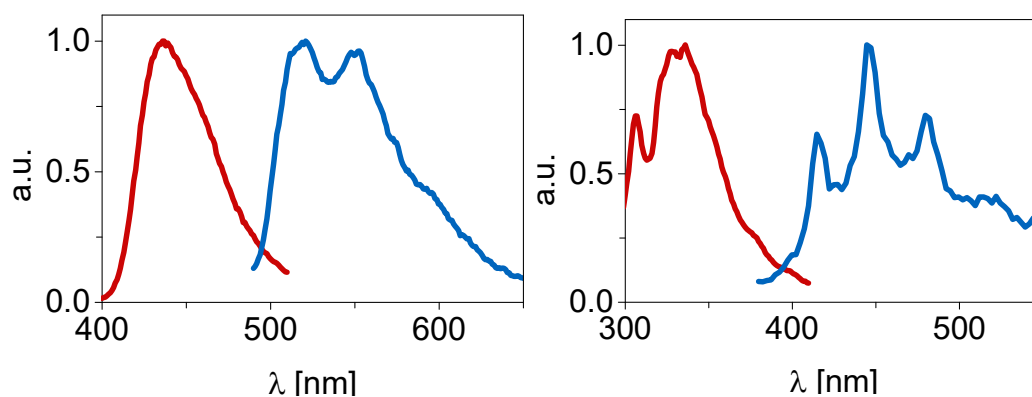


Figure 3. Fluorescence (red) and phosphorescence (blue) spectra recorded at r.t. (fluorescence) and 77 K (phosphorescence) for catalyst **4** (left) in a dichloromethane matrix and for acid **9** (right) in a pentane/isopentane matrix (for further details, see the SI).

At the reaction temperature ($-40 \text{ }^\circ\text{C}$) binding of carboxylic acid **9** to phosphoric acid **4** was proven by NMR studies in CD_2Cl_2 . The identification of two NOE contacts between **4** and **9** as well as Diffusion Ordered Spectroscopy (DOSY) experiments validated **4**·**9** complex formation, the latter showing a significant increase ($\approx 1.7 \text{ \AA}$) of the hydrodynamic radius of carboxylic acid **9** in the presence of catalyst **4** (see SI for details and spectra).^[12a] Significant line broadening and a slight highfield shifting ($\approx 0.1 \text{ ppm}$) of the signals of **9** in the presence of **4** demonstrate a fast exchange on the NMR timescale between **4**·**9** complex and the separated molecules **4** and **9** at this temperature (see SI for spectra).

7. A Thioxanthone Sensitizer with a Chiral Phosphoric Acid Binding Site: Properties and Applications in Visible Light-Mediated Cycloadditions

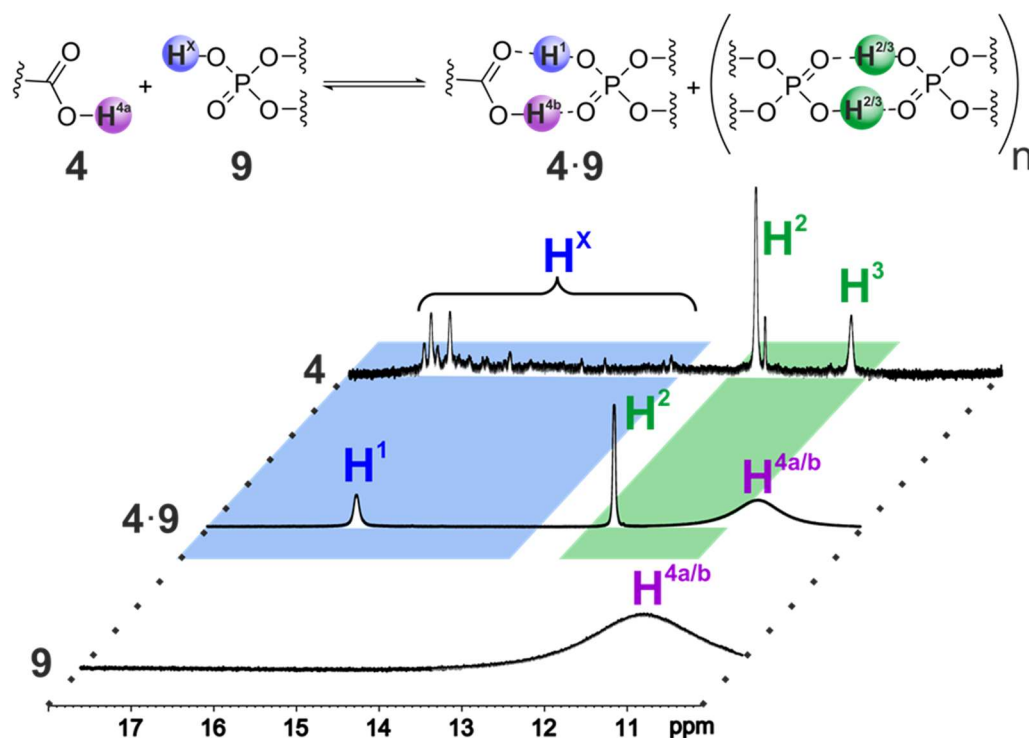


Figure 4: Hydrogen bond region of the ^1H spectra of **4**, **9** and an equimolar solution of **4** and **9** at 600 MHz and -40°C in CD_2Cl_2 , showing the presence of different species of the catalyst.

Next, NMR measurements between -40°C and -93°C were applied to gain information about the hydrogen bond situation in this system. Indeed, specific signals of hydrogen bonds could be detected, which is to our knowledge the first time for complexes between chiral phosphoric acids and carboxylic acids. The hydrogen bond region^[21] of **4** showed various minor populated signals summarized as H^x (blue region in Figure 4) and two distinct signals H^2 and H^3 (green region). The temperature coefficients of H^2 and H^3 are very small (-0.9 ppb/K) indicating that these protons are effectively sequestered from solvent interactions. This is typical for molecules featuring strong internal H-bonds or stable complexes with internal H-bonds, e.g. dimers (or higher aggregates) of **4**.^[22] The minimum temperature coefficient of the signals labelled H^x is significantly higher (-9.6 ppb/K) than that for H^2 and H^3 , but still by far smaller than the one of carboxylic acid **9** (-38.6 ppb/K). This indicates a partial sequestration of the H^x protons from the solvent, which would be rational for different rotational isomers of monomeric **4**. Indeed, signals H^x of the catalyst collapse to one signal H^1 in the presence of **9**, while signals H^2 and H^3 are unaffected.^[23] The respective ^{31}P NMR spectra show a similar behaviour (see SI) and thus support the assignment of H^x and H^1 as monomeric, and H^2 and H^3 as dimeric (or oligomeric) catalyst species. The averaged proton signal H^1 indicates very low rotation barriers of and within the 3,3'-substituent in the **4·9** complex, which is in accordance with the theoretical calculations (vide infra). In contrast, in the absence of **9** the various proton signals H^x indicate higher rotation barriers in monomeric **4** despite

7. A Thioxanthone Sensitizer with a Chiral Phosphoric Acid Binding Site: Properties and Applications in Visible Light-Mediated Cycloadditions

reduced absolute steric hindrance. The combination of a medium temperature coefficient, higher rotation barriers and significant spreading of the chemical shifts of H^X protons over ≈ 3 ppm hints at various internal hydrogen bonds of the phosphoric acid to the aromatic moieties of the 3,3'-substituent (see SI for further discussion), which stabilize different rotational isomers of the free catalyst. To the best of our knowledge, this feature has not yet been observed for chiral phosphoric acids and is potentially useful as a concept for preorganization.

Preliminary DFT calculations revealed a relatively shallow energy hypersurface for the 1:1 complex of catalyst **4** with carboxylic acid **12**. There are several local minima detected upon rotation around the indicated bonds (for more details, see SI). Due to the free rotation around the thioxanthone-phenyl bond (Figure 5, left) the C_2 symmetry of the catalyst is lost in most rotamers which complicates the analysis. The energetically lowest diastereomeric conformation is according to the calculation 3.5 kJ mol⁻¹ more stable than the shown conformation (Figure 5, right). While the former conformation does not account for the correct product configuration, the latter arrangement illustrates the observed preferential approach of the olefin from the *Si* face of the α -carbon atom. The extent of the enantioface differentiation depends on the exact trajectory of the olefin and on the position of initial attack.

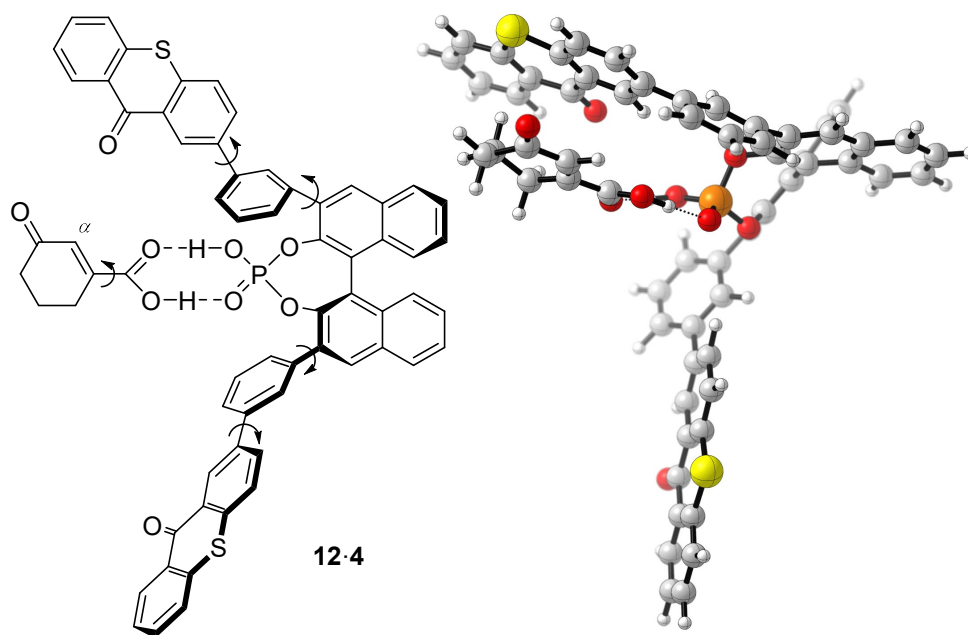


Figure 5. Models for the complex of cyclohex-2-enone-3-carboxylic acid (**12**) with chiral phosphoric acid **4**: Rotatable single bonds influencing the reactive conformation (left), optimized structure of a 1:1 complex in which the *Si* face at the α -carbon atom of acid **12** is accessible (right). DFT calculations were performed using the M06-2X functional^[24] with the def2-TZVP^[25] basis set for all atoms employing Gaussian09^[26] with D3 dispersion^[27] and low-frequency entropy^[28] corrections by Grimme.

7.4. Conclusion

In conclusion, the first member of a new class of bifunctional photocatalysts has been synthesized and screened in [2+2] photocycloaddition reactions. The catalyst appears to lower the triplet energy of the substrates by hydrogen bonding and enables a notable enantioface differentiation. Different catalyst species (monomeric rotational isomers and higher aggregates) were observed by NMR, but only the monomeric catalyst participates in the complexation to the substrate, while higher aggregates are not affected by the substrate. The formation of a catalyst substrate complex was proven by NMR studies and a potential structure of the 1:1 complex was revealed by DFT calculations. A better understanding of the binding mode and of the interaction between the sensitizing unit and the substrate is expected to facilitate the design of modified catalysts.

7.5. References

- [1] Reviews: a) M. Silvi, P. Melchiorre, *Nature* **2018**, *554*, 41-49; b) A. F. Garrido-Castro, M. C. Maestro, J. Alemán, *Tetrahedron Lett.* **2018**, *59*, 1286-1294; c) C. Brenninger, J. D. Jolliffe, T. Bach, *Angew. Chem. Int. Ed.* **2018**, *57*, 14338-14349; *Angew. Chem.* **2018**, *130*, 14536-14547.
- [2] Examples: a) C. D. DeBoer, R. H. Schlessinger, *J. Am. Chem. Soc.* **1972**, *94*, 655-656; b) S. F. Yates, G. B. Schuster, *J. Org. Chem.* **1984**, *49*, 3349-3356; c) K. Meier, H. Zweifel, *J. Photochem.* **1986**, *35*, 353-366.
- [3] Reviews: a) F. Strieth-Kalthoff, M. J. James, M. Teders, L. Pitzer, F. Glorius, *Chem. Soc. Rev.* **2018**, *47*, 7190-7202; b) Q.-Q. Zhou, Y.-Q. Zou, L.-Q. Lu, W.-J. Xiao, *Angew. Chem. Int. Ed.* **2019**, *58*, 1586-1604; *Angew. Chem.* **2019**, *131*, 1600-1619.
- [4] a) R. Alonso, T. Bach, *Angew. Chem. Int. Ed.* **2014**, *53*, 4368-4371; *Angew. Chem.* **2014**, *126*, 4457-4460; b) W. Ding, L.-Q. Lu, Q.-Q. Zhou, Y. Wei, J.-R. Chen, W.-J. Xiao, *J. Am. Chem. Soc.* **2017**, *139*, 63-66; c) F. Mayr, L.-M. Mohr, E. Rodriguez, T. Bach, *Synthesis* **2017**, *49*, 5238-5250; d) T. Rigotti, A. Casado-Sánchez, S. Cabrera, R. Pérez-Ruiz, M. Liras, V. A. de la Peña O'Shea, J. Alemán, *ACS Catal.* **2018**, *8*, 5928-5940.
- [5] F. Burg, T. Bach, *J. Org. Chem.* **2019**, *84*, 8815-8836.
- [6] A. Tröster, R. Alonso, A. Bauer, T. Bach, *J. Am. Chem. Soc.* **2016**, *138*, 7808-7811.
- [7] a) A. Hözl-Hobmeier, A. Bauer, A. V. Silva, S. M. Huber, C. Bannwarth, T. Bach, *Nature* **2018**, *564*, 240-243; b) A. Tröster, A. Bauer, C. Jandl, T. Bach, *Angew. Chem. Int. Ed.* **2019**, *58*, 3538-3541; *Angew. Chem.* **2019**, *131*, 3576-3579.
- [8] Reviews: a) T. Akiyama, *Chem. Rev.* **2007**, *107*, 5744-5758; b) M. Terada, *Synthesis* **2010**, 1929-1962; c) Parmar, E. Sugiono, S. Raja, M. Rueping, *Chem. Rev.* **2014**, *114*, 9047-9153; d) R. Maji, S. C. Mallojjala, S. E. Wheeler, *Chem. Soc. Rev.* **2018**, *47*, 1142-1158.
- [9] Recent examples: a) J. Q. Li, S. Grosslight, S. J. Miller, M. S. Sigman, F. D. Toste, *ACS Cat.* **2019**, *9*, 9794-9799; b) L. Wang, J. L. Zhong, X. F. Li, *Angew. Chem. Int. Ed.* **2019**, *58*, 15824-15828; *Angew. Chem.* **2019**, *131*, 15971-15975; c) M. Sun, C. Ma, S.-J. Zhou, S. F. Lou, J. Xiao, Y. C. Jiao, F. Shi, *Angew. Chem. Int. Ed.* **2019**, *58*, 8703-8708; *Angew. Chem.* **2019**, *131*, 8795-8800; d) J.-S. Lin, T.-T. Li, J.-R. Liu, G.-Y. Jiao, Q.-S. Gu, J.-T. Cheng, Y.-L. Guo, X. Hong, X.-Y. Liu, *J. Am. Chem. Soc.* **2019**, *141*, 1074-1083; e) A. Suneja, C. Schneider, *Org. Lett.* **2018**, *20*, 7576-7580.
- [10] M. Hatano, T. Horibe, K. Ishihara, *J. Am. Chem. Soc.* **2010**, *132*, 56-57.
- [11] E. G. Davis, S. Smiles, *J. Chem. Soc., Trans.* **1910**, *97*, 1290-1299.
- [12] a) M. R. Monaco, B. Poladura, M. Diaz de Los Bernardos, M. Leutzsch, R. Goddard, B. List, *Angew. Chem. Int. Ed.* **2014**, *53*, 7063-7067; *Angew. Chem.* **2014**, *126*, 7183-7187; b) M. R. Monaco, S. Prévost, B. List, *Angew. Chem. Int. Ed.* **2014**, *53*, 8142-8145; *Angew. Chem.* **2014**, *126*, 8280-8283; c) M. R. Monaco, D. Fazzi, N. Tsuji, M. Leutzsch, S. Liao, W. Thiel, B. List, *J. Am. Chem. Soc.* **2016**, *138*, 14740-14749.
- [13] S. Piva-Le Blanc, S. Hénon, O. Piva, *Tetrahedron Lett.* **1998**, *39*, 9683-9684.
- [14] Y. Yanagisawa, Y. Nishiyama, H. Tanimoto, T. Morimoto, K. Kakiuchi, *Tetrahedron Lett.* **2014**, *55*, 2123-2126.

7. A Thioxanthone Sensitizer with a Chiral Phosphoric Acid Binding Site: Properties and Applications in Visible Light-Mediated Cycloadditions

- [15] For racemic photocycloaddition reactions of substrate **12**, see: a) W. C. Agosta, W. W. Lowrance, *Tetrahedron Lett.* **1969**, *10*, 3053-3054; b) W. C. Agosta, W. W. Lowrance, *J. Org. Chem.* **1970**, *35*, 3851-3856; c) G. L. Lange, C. Decicco, S. L. Tan, G. Chamberlain, *Tetrahedron Lett.* **1985**, *26*, 4707-4710; d) F. X. Webster, R. M. Silverstein, *J. Org. Chem.* **1986**, *51*, 5226-5231; e) ref.^[13]; f) K. Tsutsumi, Ken; H. Nakano, A. Furutani, K. Endou, A. Merpuge, T. Shintani, T. Morimoto, K. Kakiuchi, *J. Org. Chem.* **2004**, *69*, 785-789.
- [16] J. D. Griffin, M. A. Zeller, D. A. Nicewicz, *J. Am. Chem. Soc.* **2015**, *137*, 11340-11348.
- [17] S. Poplata, T. Bach, *J. Am. Chem. Soc.* **2018**, *140*, 3228-3231.
- [18] Determined at 77 K in methylcyclohexane: A. Iyer, A. Clay, S. Jockusch, J. Sivaguru, *J. Phys. Org. Chem.* **2017**, *30*, e3738.
- [19] Examples: a) M. Magnifico, E. J. O'Connell, A. V. Fratini, C. M. Shaw, *J. Chem. Soc., Chem. Commun.*, **1972**, 1095-1096; b) P. M. L. Blok, H. P. J. M. Dekkers, *Photochem. Photobiol.* **1991**, *53*, 421-429; c) P. M. L. Blok, H. J. C. Jacobs, H. P. Dekkers, *J. Am. Chem. Soc.* **1991**, *113*, 794-801; d) J. F. D. Kelly, M. E. Doyle, M. Guha, P. V. Kavanagh, J. M. Kelly, T. B. H. McMurry, *J. Chem. Soc., Perkin Trans. 2*, **1998**, 1635-1642; e) S. A. Bagnicha, N. N. Khropika, V. N. Knyukshtoa, A. L. Mikhalchukb, D. B. Rubinovb, *Spectrochim. Acta A* **2005**, *61*, 2161-2167.
- [20] a) T. R. Blum, Z. D. Miller, D. M. Bates, I. A. Guzei, T. P. Yoon, *Science* **2016**, *354*, 1391-1395; b) M. E. Daub, H. Jung, B. J. Lee, J. Won, M.-H. Baik, T. P. Yoon, *J. Am. Chem. Soc.* **2019**, *141*, 9543-9547.
- [21] a) T. Steiner, *Angew. Chem. Int. Ed.* **2002**, *41*, 49-76; *Angew. Chem.* **2002**, *114*, 50-80; b) N. Sorgenfrei, J. Hioe, J. Greindl, K. Rothermel, F. Morana, N. Lokesh, R. M. Gschwind, *J. Am. Chem. Soc.* **2016**, *138*, 16345-16354; c) M. Melikian, J. Gramüller, J. Hioe, J. Greindl, R. M. Gschwind, *Chem. Sci.* **2019**, *10*, 5226-5234.
- [22] N. H. Andersen, J. W. Neidigh, S. M. Harris, G. M. Lee, Z. Liu, T. Tong, *J. Am. Chem. Soc.* **1997**, *119*, 8547-8561.
- [23] In the presence of **9**, proton H³ is overlapped by proton H⁴. However, at 180 K, the detection of H³ is feasible and its chemical shift remains unchanged in presence or absence of **4**. (see SI for spectra).
- [24] Y. Zhao, D. G. Truhlar, *Theor. Chem. Acc.* **2008**, *120*, 215-241.
- [25] F. Weigend, R. Ahlrichs, *Phys. Chem. Chem. Phys.* **2005**, *7*, 3297-3305.
- [26] M. J. Frisch et al. *Gaussian 09, Revision D.01*, Gaussian, Inc., Wallingford CT, **2009**.
- [27] S. Grimme, J. Antony, S. Ehrlich, H. Krieg, *J. Chem. Phys.* **2010**, *132*, 154104-1-154104-19.
- [28] S. Grimme, *Chem. Eur. J.* **2012**, *18*, 9955-9964.

7.6. Supporting Information

Chemicals

Deuterated solvents were purchased from Deutero or Sigma Aldrich. CD₂Cl₂ was freshly distilled over CaH₂ prior to use.

Sample preparation

A 5 mm NMR- tube was dried at 650 °C at vacuum ($< 10^{-3}$ mbar) for 20 minutes. The NMR tube was brought into a glovebox under argon and pre-dried catalyst **4** and/or pre-dried carboxylic acid **9** were directly weighed into the NMR tube. Afterwards, **4** and **9** were dried in the NMR tube at 100 °C at vacuum ($< 10^{-3}$ mbar) for 30 minutes outside of the glovebox. Dry CD₂Cl₂ (0.6 mL, less than 5 ppm H₂O) and 0.5 mL of tetramethylsilane atmosphere were added to the tube under argon flow. The NMR tube was closed and sealed with parafilm. The samples were stored in a -80 °C freezer. In case the sample contains catalyst **4**, brown-glass NMR tubes were used. For the sample with the equimolar solution of **4** and **9**, a concentration of 10 mM was used. For the sample containing only **4** or only **9**, concentrations of 4 mM or 7 mM respectively were used.

To exclude thermal decomposition of the catalyst during the sample preparation, a sample of catalyst **4** was prepared as described above but dissolved in non-dried DMSO. No decomposition products were observed by NMR.

Spectrometer data

Low temperature NMR experiments were performed on Bruker Avance III HD 600 MHz spectrometer, equipped with a 5 mm CPPBBO BB-1H/19F. Temperature was controlled in the VT-experiments by BVT 3000 and BVTE 3900. NMR Data were processed, evaluated and plotted with TopSpin 3.2 software. Further plotting of the spectra was performed with Corel Draw X14 – X17 software. ¹H,¹³C chemical shifts were referenced to TMS. The heteronucleus ³¹P was referenced, employing $\delta(X) = \delta(\text{TMS}) \times \frac{\delta_{\text{reference}}}{100} \%$ according to Harris et al.^[7]

Pulse programs

All pulse programs used are standard Bruker NMR pulse programs. The pulse program for Diffusion Ordered Spectroscopy (DOSY) is described in the respective chapter.

Acquisition Parameters

¹H NMR: Pulse program: zg30; Relaxation delay = 2 – 3 s, Acquisition time = 2.48 s, SW = 22.0 ppm, TD = 64k, NS = 64 – 2048;

7. A Thioxanthone Sensitizer with a Chiral Phosphoric Acid Binding Site: Properties and Applications in Visible Light-Mediated Cycloadditions

³¹P NMR: Pulse program: zgpg30; Relaxation delay = 3 s, Acquisition time = 4.49 s, SW = 30.0 ppm, TD = 64k, NS = 64 – 18k;

2D-¹H,¹H NOESY: Pulse program: noesygpph; Relaxation delay = 5 - 8 s, NS = 12, mixing time (D8) = 300.00 ms; TD = 4096; increments = 1024;

2D-¹H,³¹P HMBC: Pulse program: inv4gplrndqf; Relaxation delay = 4 - 8 s, NS = 8-32, TD = 4096; increments = 256 - 1k;

Content of water

The NMR experiments revealed, that careful exclusion of water is a key prerequisite to observe hydrogen bonded proton signals and complexation of acids **4** and **9**. In case **4** and **9** were not pre-dried and dried a second time prior to solvation, the hydrogen bond region of the spectra showed no signals and complexation of the carboxylic acid could not be shown by DOSY measurements (a similar hydrodynamic radius of **9** in presence and absence of **4** was observed).

Line broadening and chemical shift offsets

Line broadening and a chemical shift offset of the signals of **9** was observed in presence of **4** (see Figure S4). This shows, that **9** is involved in an exchange process fast on the NMR time scale if **4** is present. This occurring fast exchange process is the formation of a **4·9** complex.

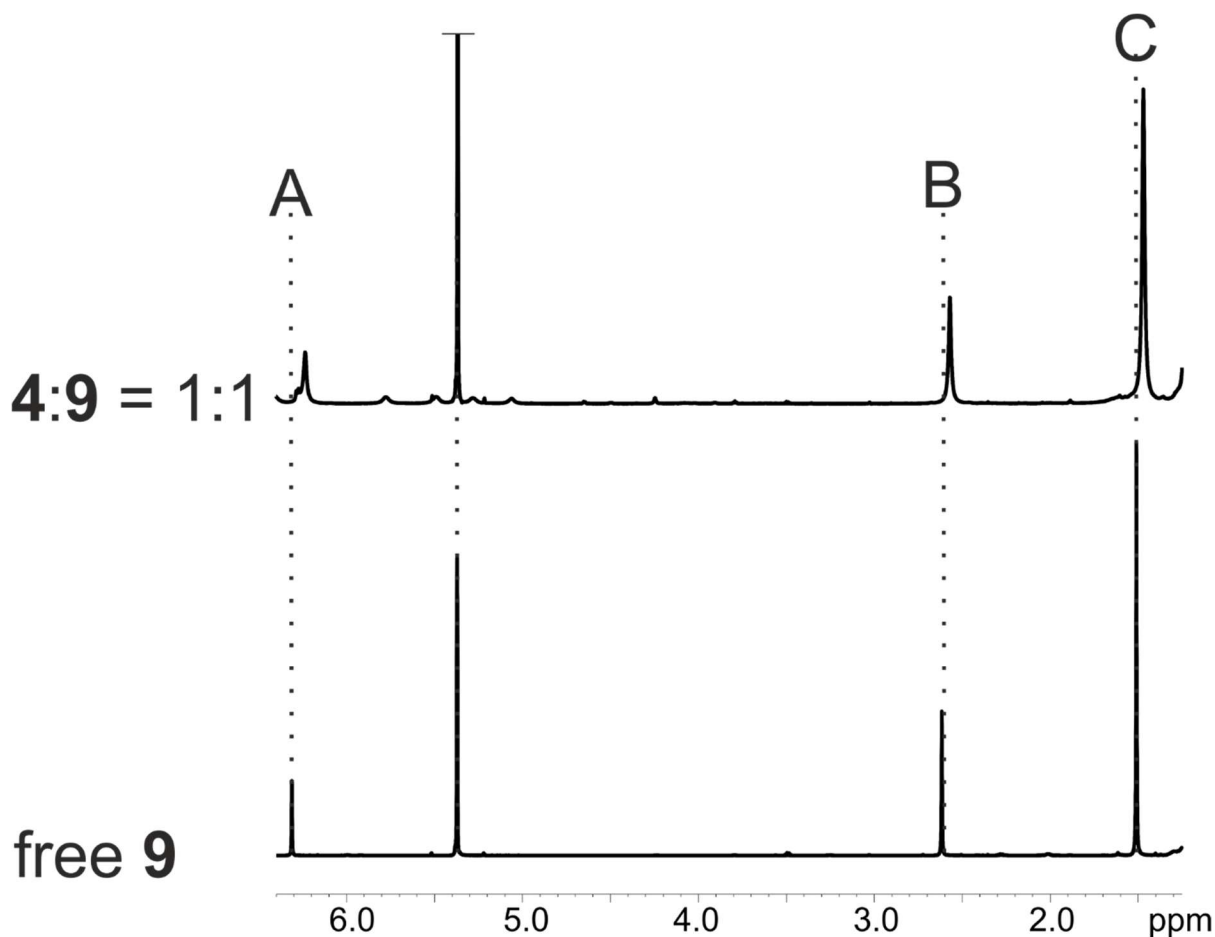


Figure S4: Comparison of the ^1H spectra of **9** in presence (free **9**) or absence of **4** (**4:9** = 1:1) at 233 K and 600 MHz in CD_2Cl_2 . The spectra are referenced on TMS.

Signal A: $\delta(^1\text{H}) = 6.309$ ppm, Halfline width = 2.1 Hz \rightarrow $\delta(^1\text{H}) = 6.234$ ppm, Halfline width = 12.5 Hz

Signal B: $\delta(^1\text{H}) = 2.616$ ppm, Halfline width = 2.3 Hz \rightarrow $\delta(^1\text{H}) = 2.570$ ppm, Halfline width = 9.9 Hz

Signal C: $\delta(^1\text{H}) = 1.510$ ppm, Halfline width = 2.3 Hz \rightarrow $\delta(^1\text{H}) = 1.470$ ppm, Halfline width = 10.2 Hz

Comparison of spectra at 233 K and 180 K

Further cooling of a sample containing an equimolar solution of **4** and **9** lead to additional line broadening of the signals of **9**, indicating that the occurring fast exchange process (**4**-**9** complex formation) is slowed down, but still fast on the NMR time scale (see Figure S5). The offset in chemical shifts can also be caused by the temperature difference.

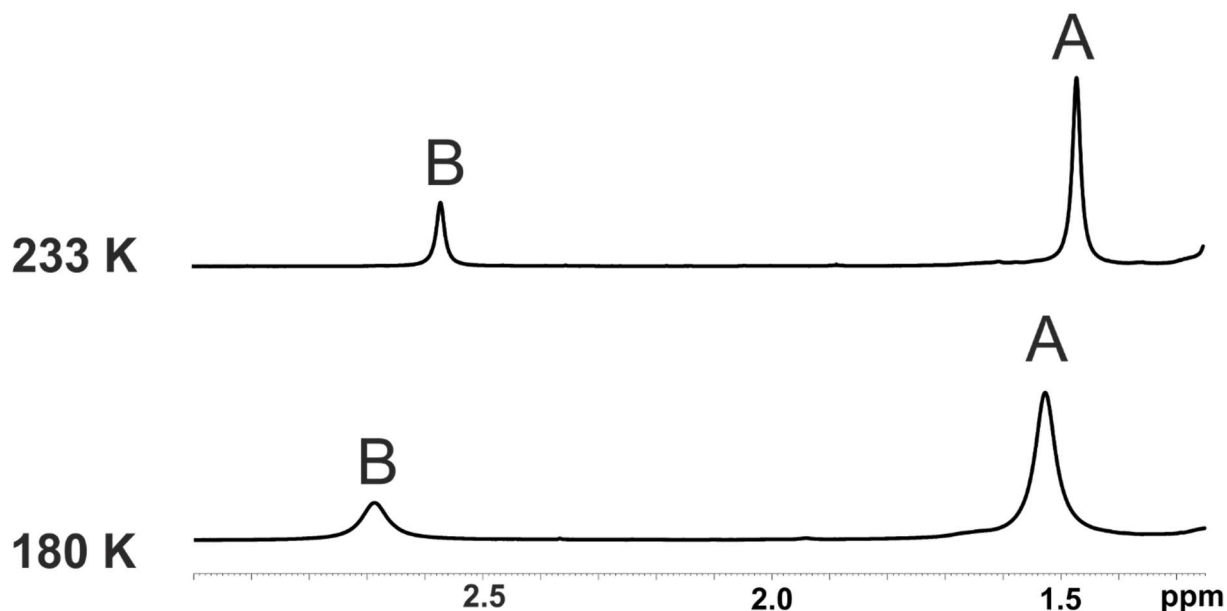


Figure S5: Excerpt of the ^1H spectra of an equimolar solution of **4** and **9** at 233 or 180 K at 600 MHz in CD_2Cl_2 . Signals A and B belong to the carboxylic acid **9**.

Signal A: Halfline width = 10.2 Hz (233 K) \rightarrow 25.9 Hz (180 K)

Signal B: Halfline width = 9.9 Hz (233 K) \rightarrow 31.8 Hz (180 K)

NOE analysis

The presence of a complex of the phosphoric acid **4** and the carboxylic acid **9** was proven by the detection of intermolecular NOE signals between **4** and **9** (see Figure S6). Besides the intramolecular (purple) NOE from protons H^{a} (blue) and H^{b} (red) to proton H^{c} (green) of the carboxylic acid, also two intermolecular (orange) NOE signals from protons H^{a} and H^{b} to two different protons of the phosphoric acid could be detected.

7. A Thioxanthone Sensitizer with a Chiral Phosphoric Acid Binding Site: Properties and Applications in Visible Light-Mediated Cycloadditions

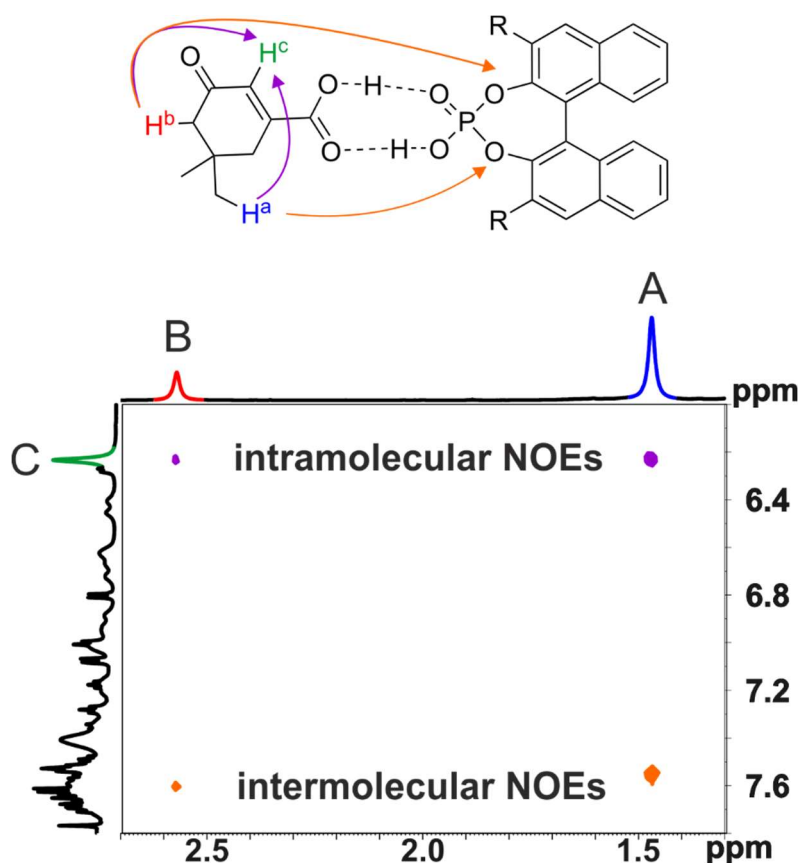


Figure S6: Excerpt of the ^1H - ^1H NOESY spectrum of an equimolar solution of **4** and **9** in CD_2Cl_2 at 233 K and 600 MHz. Intramolecular NOEs within the carboxylic acid are highlighted in purple, while intermolecular NOEs between **4** and **9** are highlighted in orange.

Diffusion Ordered Spectroscopy

The DOSY measurements were performed with the convection suppressing DSTE (double stimulated echo) pulse sequence developed by Jerschow and Müller in a pseudo 2D mode.^[8] TMS was used to reference the viscosity of the solvent. The diffusion time delay was set to 45 ms. The gradient pulse lengths (p16, SINE.100 pulse shape) were optimized for each species to give a sigmoidal signal decay for varying gradient strengths and range between 900 to 2500 μs at 233 K. For each species, twenty spectra with linear varying gradient strength of 5% - 95% have been measured. Suitable probe signals (good base line separation) for the analysis were used. The signal intensities of the respective groups were analyzed as a function of the gradient strength by Bruker TopSpin 3.2 software T1/T2 relaxation package by employing the Stejskal-Tanner equation.^[9] The molecular radii were derived by the Stokes-Einstein equation^[10] using Chens correction.^[11]

$$D_i = \frac{k_B T}{6\pi\eta r_H} * (1 + 0.695 * \left(\frac{r_{solv}}{r_H}\right)^{2.234})$$

7. A Thioxanthone Sensitizer with a Chiral Phosphoric Acid Binding Site: Properties and Applications in Visible Light-Mediated Cycloadditions

D_i is the self-diffusion coefficient derived by the measurement, η is the viscosity of the solvent, r_H is the hydrodynamic radius of the observed molecule and r_{solv} the radius of the solvent. No form factor correction was applied. The viscosity was determined by measuring the diffusion coefficient of the reference tetramethylsilane (TMS) and solving the equation for η with the literature value^[12] of the radius of 2.96 Å. The solvent radius of CD_2Cl_2 (2.46 Å) was taken from the reference.^[13]

Table S6: List of parameters and results for the DOSY measurements.

Sample	Molecule	chem. Shift [ppm]	p16 [ms]	D_i [m^2/s]	D_i [m^2/s] (averaged)	hydrodynamic radius [Å]
4:9 = 1:1	TMS	0.00	1.3	1.059E-09	1.059E-09	---
	9	6.32	1.6	5.934E-10	5.939E-10	6.058
	9	2.62	1.6	6.046E-10		
	9	1.51	1.6	5.837E-10		
4	TMS	0.00	1.6	1.040E-09	1.040E-09	---
	9	2.57	2.5	4.069E-10	3.805E-10	4.329
	9	1.47	2.5	3.541E-10		

Hydrogen bond region at 180 K and 233 K

At 233 K in the spectrum of the equimolar solution of **4** and **9**, proton H^3 of the catalyst is overlapped by proton H^4 of the carboxylic acid (see Figure 4 in the manuscript or Figure S7 in the SI). Further cooling to 180 K lead to a significant shift of proton H^4 and not the detection of proton H^3 is feasible (see Figure S7).

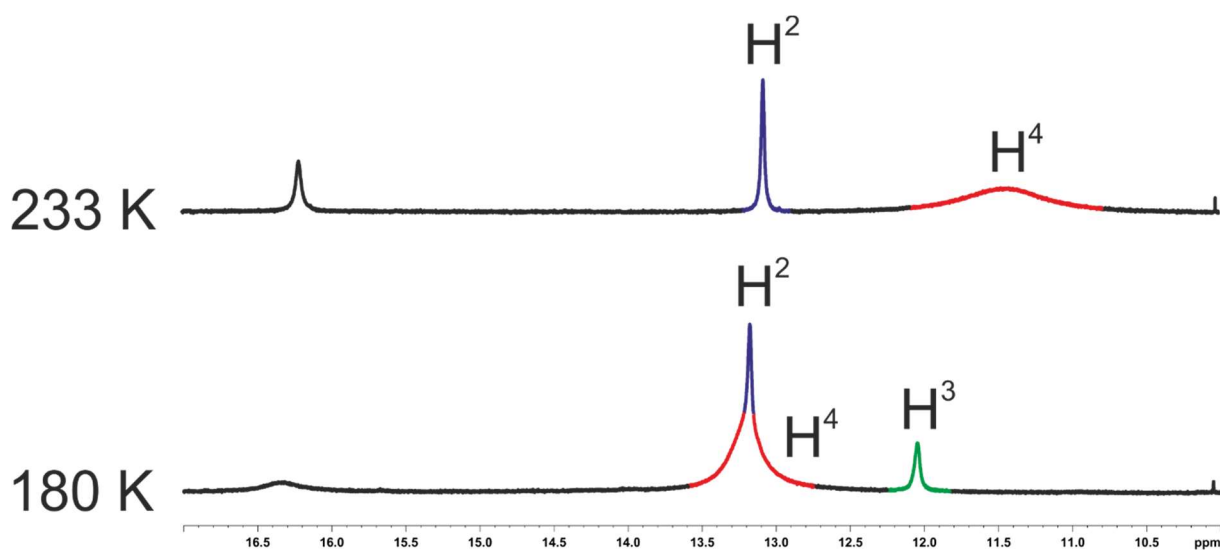


Figure S7: Hydrogen bond region of an equimolar solution of **4** and **9** at 233 K or 180 K. At lower temperatures, the detection of proton H^3 of the catalyst is again feasible.

^1H and ^{31}P spectra of **4** and **4-9**

The ^1H spectra of **4** at 180 K shows various signals in the H-bond region of the ^1H spectrum, as well as in the ^{31}P spectrum, corresponding to different species of the catalyst (see Manuscript). In the presence of **9**, several signals in the ^1H and ^{31}P spectra collapse (named H^{X} in the manuscript). However, two signals (protons H^2 and H^3 in figure 4 of the manuscript) and their respective ^{31}P signals remain unchanged (see Figure S8 and S9). This indicates, that the species corresponding to these ^1H and ^{31}P signals are dimers (or higher aggregates) of **4** and thus unaffected by the complex formation with **9**.

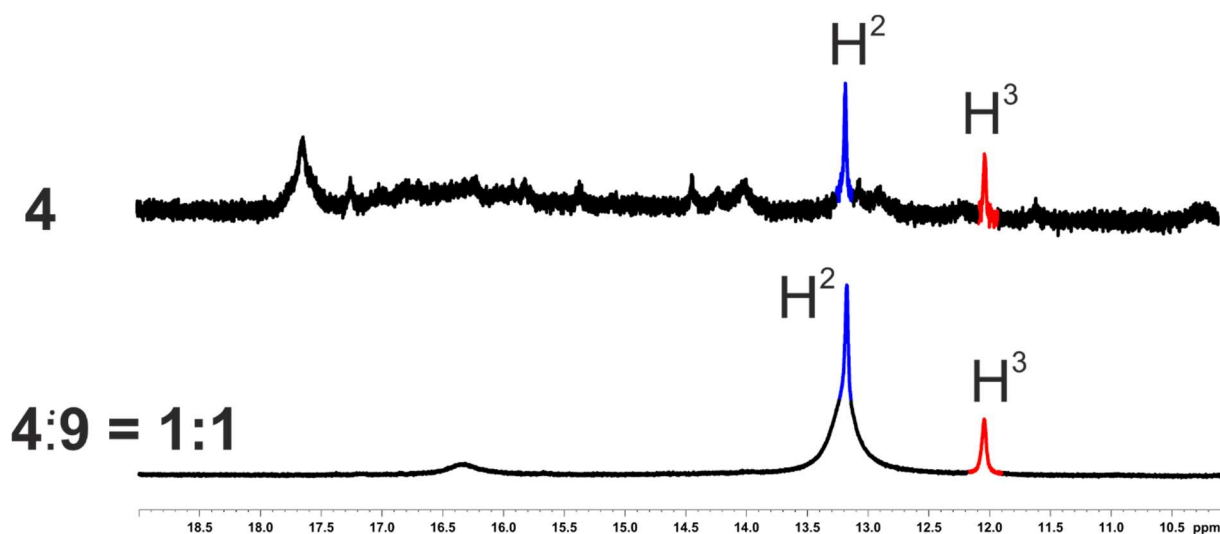


Figure S8: Section of the ^1H spectrum of **4** in presence or absence of **9** at 180 K and 600 MHz in CD_2Cl_2 . Protons H^2 and H^3 are not affected by the presence of **9**, indicating that they correspond to dimers (or higher aggregates) of the catalyst.

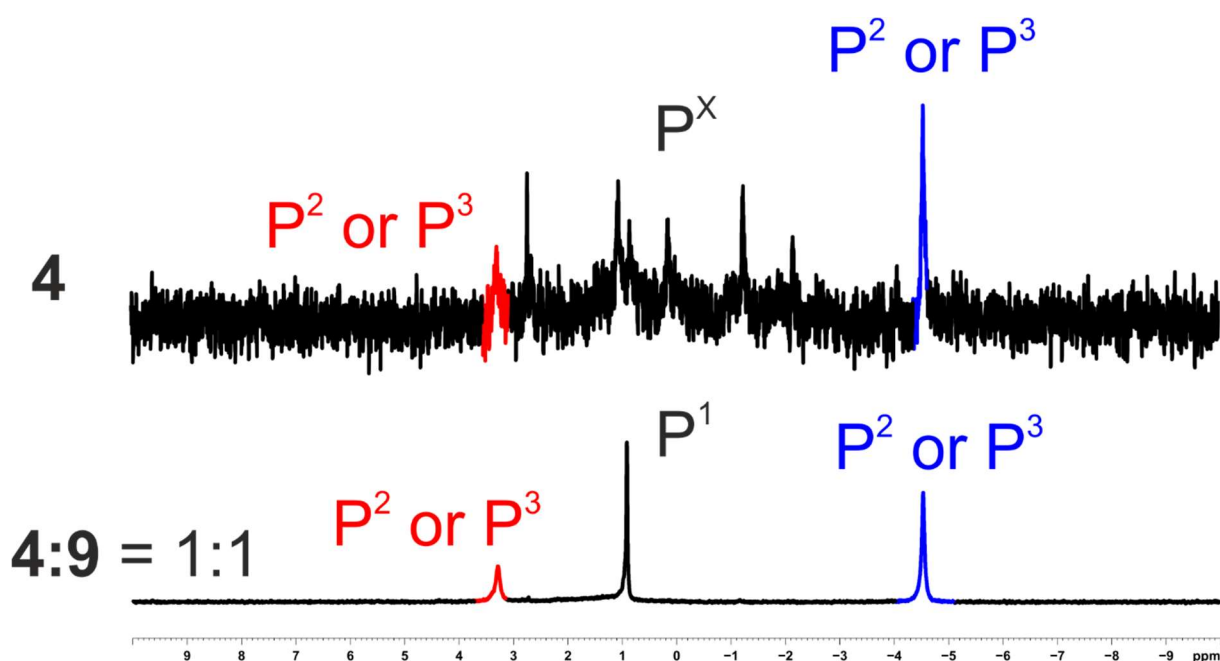


Figure S9: ^{31}P spectrum of **4** in presence or absence of **9** at 180 K and 600 MHz in CD_2Cl_2 . Signals P^2 and P^3 (corresponding to protons H^2 and H^3 in Figure S8) are not affected by the presence of **9**, indicating that they correspond to dimers (or higher aggregates) of the catalyst.

7. A Thioxanthone Sensitizer with a Chiral Phosphoric Acid Binding Site: Properties and Applications in Visible Light-Mediated Cycloadditions

Temperature coefficients

For determination of the temperature coefficients, all spectra were referenced on the solvent signal, which was calibrated to 5.32 ppm. The following chemical shifts for protons H^x and H¹-H⁴ were observed between 180 K and 233 K:

In an equimolar solution of **4** and **9**:

Proton H¹: 16.23 ppm at 180 K → 16.16 at 233 K → -1.32 ppb/K

Proton H²: 13.08 ppm at 180 K → 13.03 at 233 K → -0.94 ppb/K

Proton H⁴: 12.93 ppm at 190 K → 11.27 at 233 K → -38.6 ppb/K

In the spectra of **4**:

Proton H^x: 17.55 ppm at 180 K → 17.04 at 233 K → -9.62 ppb/K

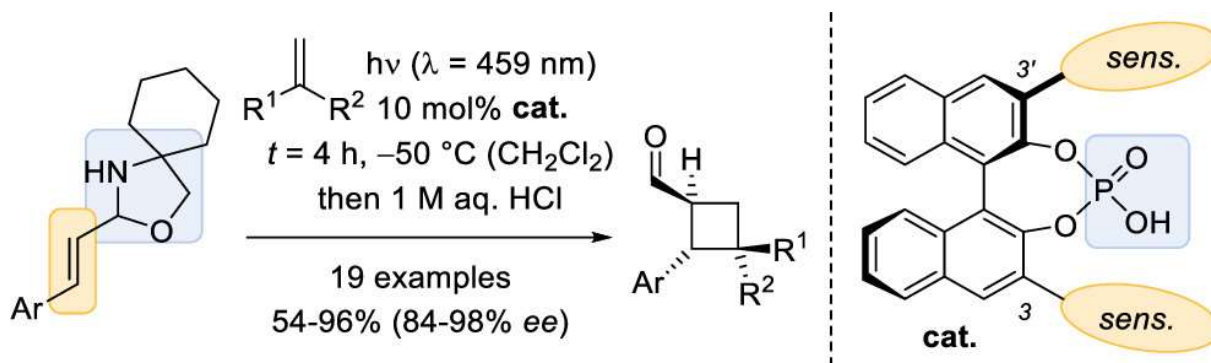
Due to differences in the occurring signals, only the minimum temperature coefficient was determined.

Proton H³: 11.92 ppm at 180 K → 11.87 at 233 K → -0.94 ppb/K

References

- [7] R. K. Harris, E. D. Becker, S. M. Cabral de Menezes, R. Goodfellow, P. Granger, *Magn. Reson. Chem.* **2002**, *40*, 489-505.
- [8] A. Jerschow, N. Müller, *J. Magn. Reson.* **1997**, *125*, 372-375.
- [9] E. O. Stejskal, J. E. Tanner, *J. Chem. Phys.* **1965**, *42*, 288-292.
- [10] A. Macchioni, G. Ciancaleoni, C. Zuccaccia, D. Zuccaccia, *Chem. Soc. Rev.* **2008**, *37*, 479-489.
- [11] H. C. Chen, S. H. Chen, *J. Phys. Chem.* **1984**, *88*, 5118-5121.
- [12] D. Ben-Amotz, K. G. Willis, *J. Phys. Chem.* **1993**, *97*, 7736-7742.
- [13] D. Zuccaccia, A. Macchioni, *Organometallics* **2005**, *24*, 3476-3486.

8. Enantioselective [2+2] Photocycloaddition *via* Iminium Ions: Catalysis by a Sensitizing Chiral Brønsted Acid



Franziska Pecho, Yeshua Sempere, Johannes Gramüller, Fabian M. Hörmann, Ruth M. Gschwind, and Thorsten Bach

J. Am. Chem. Soc. **2021**, 143, 25, 9350–9354. DOI: 10.1021/jacs.1c05240

A) Franziska Pecho, Yeshua Sempere, Fabian M. Hörmann and Thorsten Bach conceptualized, performed and analysed all experiments and computations and wrote the manuscript excluding the detailed NMR studies. B) Johannes Gramüller conceptualized, performed and analysed the detailed NMR studies, including preparation of the samples (chemicals were synthesised and pre-dried by Franziska Pecho) and wrote the respective part of the manuscript. C) For the NMR part, Ruth M. Gschwind contributed to design of experiments, interpretation of data, writing and proof-reading of the manuscript part and provided funding.

Source of this chapter: ACS Publications, <https://pubs.acs.org/doi/10.1021/jacs.1c05240>.

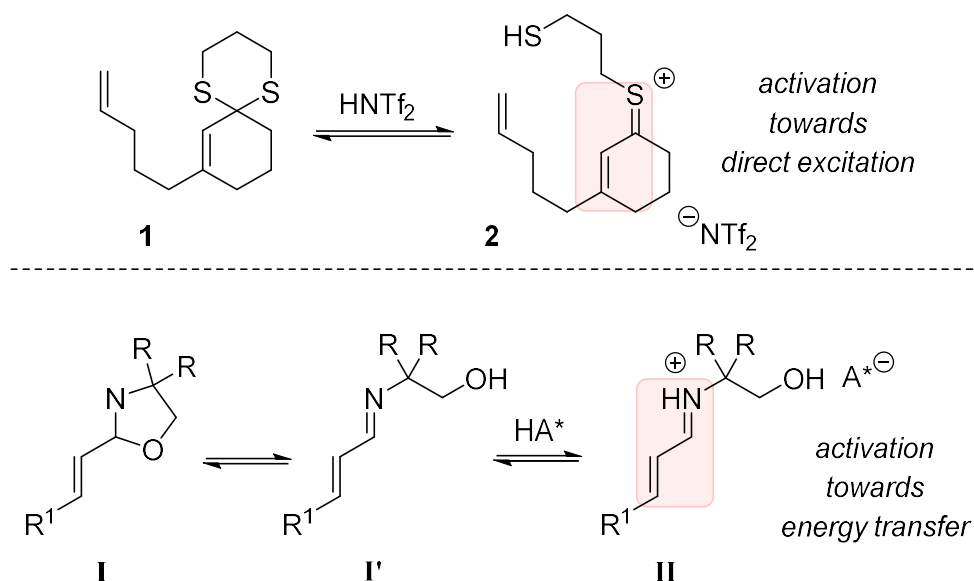
Reproduced with permission. Text and figures may differ from the published version. The complete corresponding Supporting Information is provided free of charge at <https://pubs.acs.org/doi/10.1021/jacs.1c05240>.

8.1. Abstract

N,O-Acetals derived from α,β -unsaturated β -aryl substituted aldehydes and (1-aminocyclohexyl)methanol were found to undergo a catalytic enantioselective [2+2] photocycloaddition to a variety of olefins (19 examples, 54-96% yield, 84-98% *ee*). The reaction was performed by visible light irradiation ($\lambda = 459$ nm). A chiral phosphoric acid (10 mol%) with an (*R*)-1,1'-bi-2-naphthol (binol) backbone served as the catalyst. The acid displays two thioxanthone groups attached to position 3 and 3' of the binol core via a *meta*-substituted phenyl linker. NMR studies confirmed the formation of an iminium ion which is attached to the acid counterion in a hydrogen-bond assisted ion pair. The catalytic activity of the acid rests on the presence of the thioxanthone moieties which enable a facile triplet energy transfer and an efficient enantioface differentiation.

8.2. Introduction

Apart from their occurrence in nature,¹ cyclobutanes represent useful building blocks for synthetic applications² and serve as valuable scaffolds for the precise spatial location of functional groups, e.g. in drug design.³ The intermolecular [2+2] photocycloaddition reaction between two different olefins represents one of the most straightforward methods to access this compound class.⁴ Each carbon atom of the cyclobutane core can be stereogenic, which in turn requires control of the configuration within the ring system. Enantioface differentiation⁵ arguably poses the most complex challenge in this context. Research efforts towards an enantioselective photochemical synthesis of cyclobutanes have increased in recent years and the number of contributions is growing rapidly.^{6,7} A key question that needs to be addressed in catalytic enantioselective [2+2] photocycloaddition chemistry relates to the selective excitation of a given substrate in a chiral environment. Since photochemical reactions occur rapidly after excitation it is of pivotal importance that the substrate is bound to the catalyst once it is promoted to the reactive singlet or triplet state. A possible means to achieve this goal relies on the use of chiral Brønsted acids. If the acid catalyzes reversible formation of a species, that invites a selective excitation, the chiral counterion potentially controls the ensuing carbon-carbon bond forming process. The concept of chiral Brønsted acid catalysis is well established in thermal chemistry⁸ and there are also several elegant applications in photoredox catalysis.^{5c,9} However, chiral Brønsted acids have so far not been successfully exploited to allow for an enantioselective intermolecular [2+2] photocycloaddition reaction.¹⁰ We have now found that iminium ions, which are reversibly formed upon protonation of chiral *N,O*-acetals, serve as useful intermediates to promote an enantioselective reaction on the triplet hypersurface.



Scheme 1. Previous Work on the Activation of Thioacetals by a Brønsted Acid and Current Study towards an Enantioselective [2+2] Photocycloaddition via Iminium Ions II (A*⁻: chiral anion).

8. Enantioselective [2+2] Photocycloaddition via Iminium Ions: Catalysis by a Sensitizing Chiral Brønsted Acid

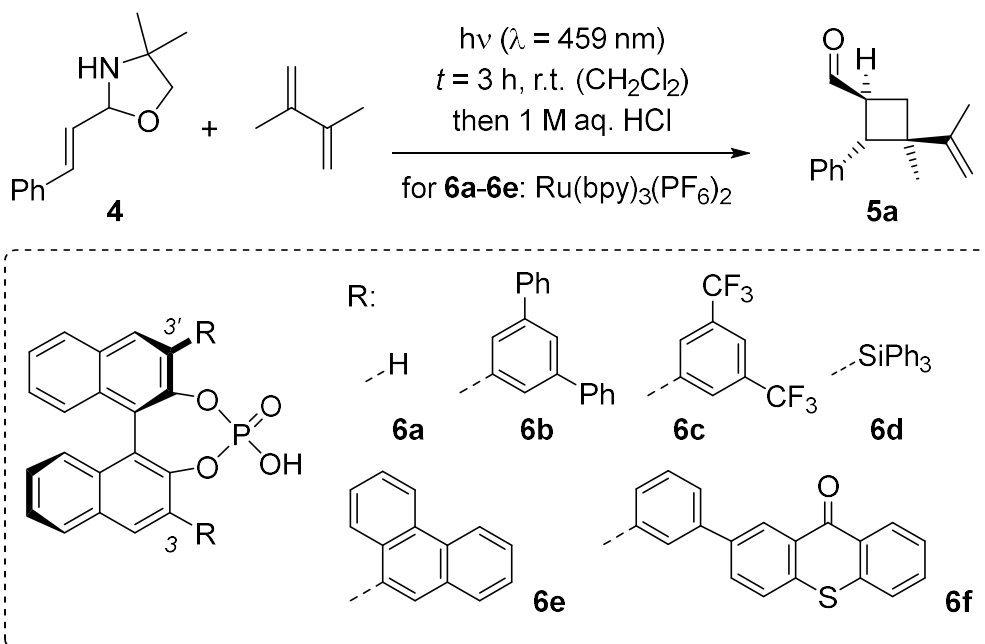
Previously, it was shown that thioacetals, such as compound **1**, are activated towards an intramolecular [2+2] photocycloaddition by protonation with strong acids (Tf = trifluoromethylsulfonyl) and by formation of thoniumions, such as **2** (Scheme 1).^{10a} Unfortunately, the search for chiral acids that allow for a protonation of dithianes remained unsuccessful which is why other acetals were considered as potential precursors for a [2+2] photocycloaddition reaction. Pioneering work by Akiyama and co-workers on the Mannich reaction of aldimines derived from *ortho*-hydroxyaniline¹¹ inspired us to study *N,O*-acetals for this purpose. It was hypothesized that they deliver upon protonation a similar binding element as the aldimines. In addition, the propensity of iminium ions to undergo [2+2] photocycloaddition reactions via triplet energy transfer has been established recently.¹² Taken together, we considered *N,O*-acetals of the general structure **I** to be ideally suited to form iminium ions **II** which are activated towards energy transfer and display a suitable binding element to coordinate to a chiral counterion A^{*-}. The formation of the open-chain form **I'** was considered inconsequential because the triplet energy of imines¹³ is higher than the triplet energy of the respective iminium ion (*vide infra*).

8.3. Results and Discussion

Preliminary work commenced with substrate **4**.¹⁴ A dual catalysis approach was considered according to which the chiral acid would deliver the desired iminium ion pair and excitation would occur by energy transfer from a sensitizer. 2,3-Dimethylbutadiene was employed as the olefin component in the reaction. The intermediate product was hydrolyzed to deliver chiral cyclobutanecarbaldehyde **5a** displaying three contiguous stereogenic centers. Irradiation at $\lambda = 459$ nm was performed for a limited time period (3 hours) to test the efficacy of the catalysts. Under these conditions, there was no background reaction in the absence of a catalyst. Ru(bpy)₃(PF₆)₂ (bpy = 2,2'-bipyridine) was used as the sensitizer (3 mol%) in combination with chiral phosphoric acids (20 mol%) **6a-6e** derived from (*R*)-1,1'-bi-2-naphthol (binol) (Scheme 2). Although a catalytic reaction was observed, the enantioselectivity did not exceed 34% *ee* (see the SI for details). A major breakthrough was achieved when phosphoric acid **6f** was employed as a *single* catalyst.

The acid displays two C₂-symmetrically positioned thioxanthone chromophores which capture long wavelength light ($\lambda_{\text{max}} = 394$ nm) and promote an energy transfer (triplet energy E_T = 235 kJ mol⁻¹, 77 K, CH₂Cl₂).^{15,16} With this acid (10 mol%), the enantioselectivity of the [2+2] photocycloaddition rose to 66% *ee*. Further experiments addressed the role of the substituents in the 2-position of the used 2-aminoalcohol. A bridging cyclohexane unit was found to further improve the performance (52%, 70% *ee*). Gratifyingly, a decrease in the reaction temperature to -50 °C significantly improved the enantioselectivity.

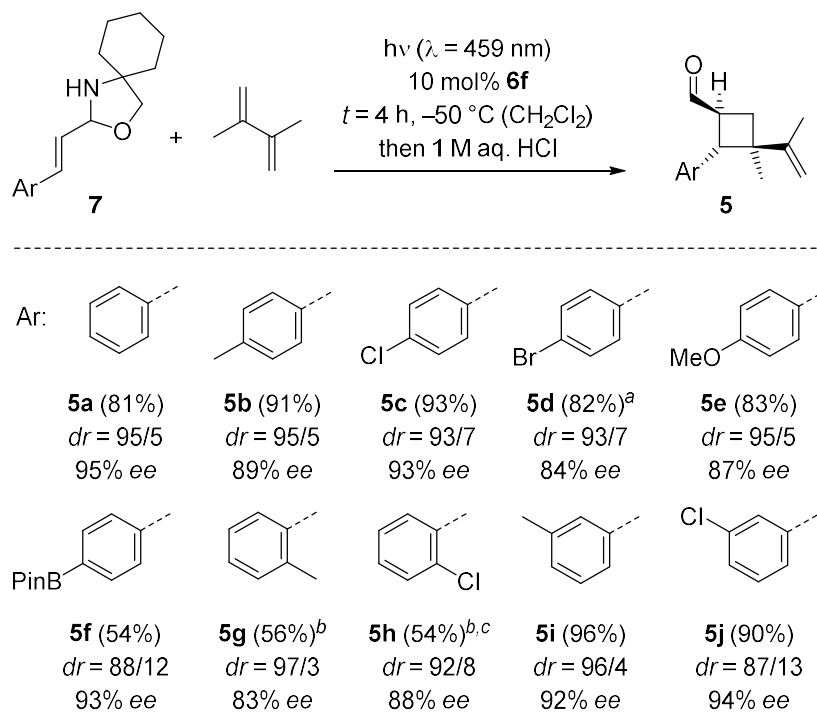
8. Enantioselective [2+2] Photocycloaddition via Iminium Ions: Catalysis by a Sensitizing Chiral Brønsted Acid



Scheme 2. Search for a Chiral Phosphoric Acid that Promotes the Enantioselective Intermolecular [2+2] Photocycloaddition of Substrate **4**.

Under optimized conditions (Table 1), the *N,O*-acetal derived from cinnamic aldehyde and (1-aminocyclohexyl)methanol (**7a**, Ar = phenyl) produced in the presence of 10 mol% **6f** the desired cyclobutane **5a** in 81% yield and with 95% *ee*. A single diastereoisomer prevailed and only traces of a second diastereoisomer were detectable (*dr* = diastereomeric ratio).

Table 1. Variation of the Aryl Group in the Catalytic Enantioselective [2+2] Photocycloaddition of *N,O*-Acetals Derived from the Substituted Cinnamic Aldehydes.



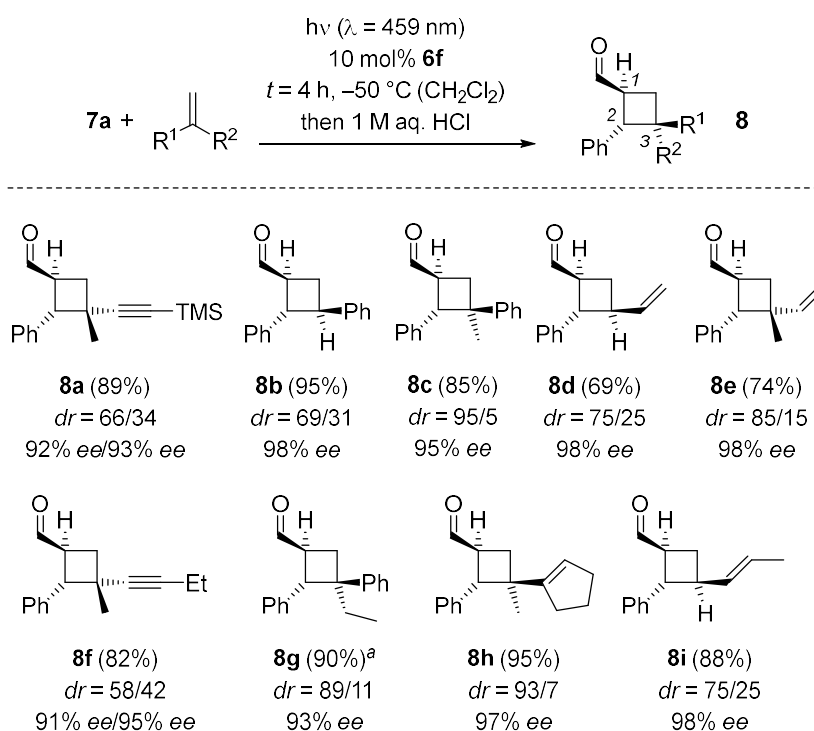
^a Irradiation time $t = 9 \text{ h}$. ^b Incomplete Conversion. ^c Irradiation time $t = 16 \text{ h}$.

8. Enantioselective [2+2] Photocycloaddition via Iminium Ions: Catalysis by a Sensitizing Chiral Brønsted Acid

A variation of the *para*-substituent at the phenyl ring revealed that several useful functional groups were tolerated (products **5b-5f**). Of particular note is the boronate **5f** (pin = pinacolate) which opens several possibilities for further synthetic transformations¹⁷ and which was generated in 93% *ee*. Yields and selectivities remained high without adaptation of the conditions except for the bromo-substituted product **5d** which required an extended irradiation time. A substituent in *ortho*-position also retarded the reaction rate and product yields were moderate (products **5g, 5h**). The same substituents (methyl, chloro) in the *meta*-position, however, turned out to be fully compatible with the optimized conditions. Both products **5i** and **5j** were obtained in excellent yields and with high enantioselectivity. A limitation relates to substrates with acid sensitive hetaryl groups (2-furyl, 2-thiophenyl) which gave only low product yields. The absolute configuration of the products was assigned based on the known absolute configuration of compound **5a**.¹²

The acid catalyzed transformation allows to access cyclobutanecarbaldehydes by an enantioselective catalytic [2+2] photocycloaddition reaction and its synthetic utility relies on the relative wide variety of olefin components which were successfully applied (Table 2). In all reactions of representative *N,O*-acetal **7a**, enantioselectivities exceeded 90% *ee*. Apart from styrenes (products **8b, 8c, 8g**) 1,3-enynes (products **8a** and **8f**) and 1,3-dienes (products **8d, 8e, 8h, 8i**) underwent the [2+2] photocycloaddition cleanly and delivered 1,2,3-trisubstituted cyclobutanes with exquisite enantiocontrol.

Table 2. Variation of the Olefin Component in the Intermolecular Enantioselective [2+2] Photocycloaddition of *N,O*-Acetal **7a**.



^a Irradiation time $t = 15 \text{ h}$.

8. Enantioselective [2+2] Photocycloaddition via Iminium Ions: Catalysis by a Sensitizing Chiral Brønsted Acid

While the relative configuration between the phenyl group in 2-position and the formyl group at C1 is consistently *trans* in cyclobutanes **5** and **8**, the relative configuration between the stereogenic centers C2 and C3 is variable. NOESY experiments were employed to assign the relative configuration of the major and minor diastereoisomer.

NMR studies revealed that all *N,O*-acetals **7** existed as a mixture of the closed (**I**, scheme 1) and the open (**I'**) form with a preference for the closed form (ca. 2/1). Upon protonation, the formation of the open protonated form **II** was indicated by a strong bathochromically shifted UV/vis absorption. However, the species is not competent¹⁸ to undergo a [2+2] photocycloaddition upon irradiation at $\lambda = 459$ nm. Also in the presence of a chiral Brønsted acid, like compound **6e**, there was no reaction of substrate **7a** in the absence of a sensitizer.

In order to assess the triplet energy of the iminium ion, the imine of *para*-bromocinnamic aldehyde and (1-aminocyclohexyl)methyl methyl ether was prepared. Due to the heavy-atom effect¹⁹ we hoped that a phosphorescence signal was detectable upon direct excitation under cryogenic conditions. Indeed, iminium ion **9** obtained from the imine by protonation with HBF_4 emitted a signal at 77 K (Figure 1) which differed clearly from the respective fluorescence. From the emission in the short-wavelength regime, the triplet energy E_T was determined as 213 kJ mol^{-1} . The value is lower than E_T of compound **6f** (235 kJ mol^{-1}) enabling an exothermic energy transfer to the iminium ion. Interestingly, the imine from which the iminium ion **9** derived did not exhibit any phosphorescence despite the heavy atom present.

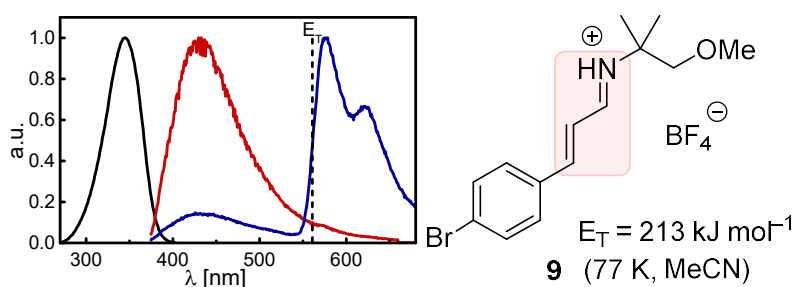


Figure 1. Absorption and luminescence spectra ($\lambda_{\text{exc}} = 360$ nm) of iminium ion **9** in MeCN. Colors: Absorption – black; fluorescence (rt) – red; phosphorescence (77 K) – blue. The energy of the (0,0) transition was calculated from the point of inflection at $\lambda = 562$ nm.

The enantioselectivity of the [2+2] photocycloaddition can be tentatively explained in analogy to a model proposed by Akiyama and co-workers for the addition to related prochiral iminium ions. They suggested a 1:1 complex **10** with the chiral phosphoric acid in which the aryl groups of the acid invite an attack from the *Re* face (Figure 2a).¹¹ If we assume a similar coordination of the iminium ions derived from compounds **7** and an extended *s-trans* conformation, the same enantioface differentiation should apply and it should account for a *Si* face attack in complex **11** (Figure 2b).

8. Enantioselective [2+2] Photocycloaddition via Iminium Ions: Catalysis by a Sensitizing Chiral Brønsted Acid

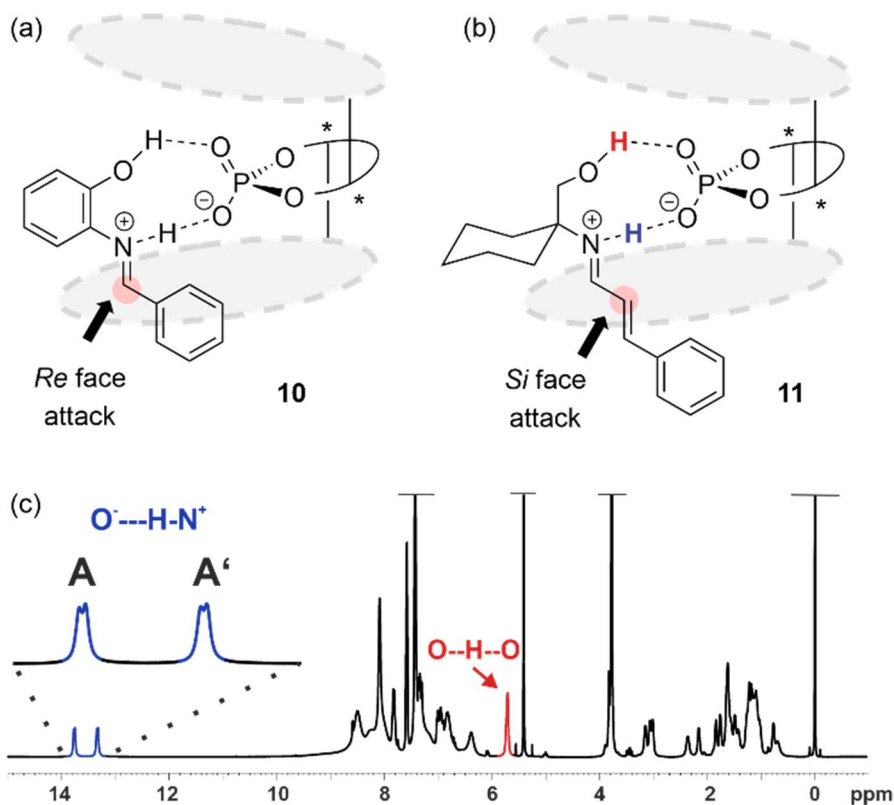


Figure 2. (a) Previously established model for the enantioselective addition to *N*-(*ortho*-hydroxyphenyl) substituted imines in their complex **10** with a chiral phosphoric acid (* = stereogenic center).¹¹ (b) Analogy-based model for the enantioface differentiation in complex **12** of phosphoric acid **6f** and the iminium ion derived from *N,O*-acetal **7a**. (c) ¹H-NMR spectrum of a 1:1 mixture of **6c** and **7e** (1:1, 10 mM, CD₂Cl₂) at -93 °C and 600 MHz. Three different hydrogen bond signals with an integral ratio of ca. 1 : 1.1 : 2.1, corresponding to two conformational isomers of **11** were observed.

Extensive low temperature NMR studies on the complexes between acids **6c**, **6f** and substrates **7a**, **7b**, and **7e** validated the existence of a 1:1 complex as hydrogen-bond assisted ion pair. For **6c/7e**, two distinct species **A** and **A'** were observed (see Figure 2c), differing in the conformation of the cyclohexane ring. For both species, the O⁻---H-N⁺ and O--H--O proton signals could be identified and unambiguously assigned as hydrogen bonded protons by the detection of *trans*-hydrogen bond scalar coupling via ¹H,¹⁵N/³¹P-HMBC and ¹H,¹H-COSY spectra.²⁰ Thus, the bidentate binding motif is clearly confirmed by the complete network of magnetization transfers. Moreover, the assigned ¹⁵N, ¹H_α and ¹³C_α chemical shifts of **A** and **A'** precisely match the expected values for a protonated iminium ion²¹ and thus validate, that the open protonated form **II** of the *N,O*-acetals is bound to the catalyst. Additionally, diffusion ordered spectroscopy (DOSY) NMR experiments confirmed, that the observed species are monomeric and not higher aggregates. For complexes with catalyst **6f**, the identical O⁻---H-N⁺ hydrogen bond patterns were detected. In this case, additional hydrogen bonded species were observed, but the significant line broadening induced by rotational isomers of the catalyst and the flexibility of the substrate-backbone have so far prevented a further assignment. Decreasing the basicity of the substrate (**7e** > **7b** > **7a**) led to a downfield shift of the O⁻---H-N⁺ proton signal, which reflects an increasing

8. Enantioselective [2+2] Photocycloaddition via Iminium Ions: Catalysis by a Sensitizing Chiral Brønsted Acid

hydrogen bond strength. In accordance with our previous results on the analysis of hydrogen bonding in chiral phosphoric acid/imine systems,²⁰ the observation confirms that the observed species are hydrogen-bond assisted ion pairs.

Phosphoric acid **6f** thus provides not only the required energy to promote the substrates to the triplet state but also guarantees the required enantioface differentiation. Remarkably, the enantioselective reactions display a higher degree of diastereoselectivity²² than related reactions with achiral iminium ions which were used to prepare racemic cyclobutanes¹² for comparison. For example, the d.r. for the formation of product **8c** was 67/33 in the racemic case but 95/5 in the catalytic reaction. In the case of product **8e**, the relative configuration at C2/C3 was opposite (d.r. = 85/15) to the racemic series (d.r. = 30/70). It is therefore conceivable that the iminium ion remains bound to the phosphoric acid after initial C–C bond formation and that the acid influences the simple diastereoselectivity.

8.4. Conclusion

In summary, an enantioselective [2+2] photocycloaddition reaction has been accomplished which delivers cyclobutanecarbaldehydes **5** and **8** in high yields and with excellent *ee*. Key to the success of the reaction is the use of a chiral phosphoric acid **6f** that displays two *C*₂-symmetrically arranged thioxanthone substituents for energy transfer. The association of the iminium ion to the phosphoric acid warrants further study to shed light on the enantioface differentiation and to elucidate its potential role in the second carbon-carbon forming step.

8.5. References

- (1) (a) Antonsen, S.; Østby, R. B.; Stenstrøm, Y., Chapter 1 - Naturally Occurring Cyclobutanes: Their Biological Significance and Synthesis. In *Studies in Natural Products Chemistry*, Atta ur, R., Ed. Elsevier: 2018; Vol. 57, pp 1-40. (b) Hansen, T. V.; Stenstrøm, Y., Naturally occurring cyclobutanes. In *Organic Synthesis: Theory and Applications*. Hudlicky, T., Ed. Elsevier: 2001, Vol. 5, pp 1-38.
- (2) (a) Namyslo, J. C.; Kaufmann, D. E., The Application of Cyclobutane Derivatives in Organic Synthesis. *Chem. Rev.* **2003**, *103*, 1485-1537. (b) Lee-Ruff, E.; Mladenova, G., Enantiomerically Pure Cyclobutane Derivatives and their Use in Organic Synthesis. *Chem. Rev.* **2003**, *103*, 1449-1483.
- (3) For some recent examples, see: (a) Cox, B.; Booker-Milburn, K. I.; Elliott, L. D.; Robertson-Ralph, M.; Zdorichenko, V., Escaping from Flatland: [2 + 2] Photocycloaddition; Conformationally Constrained sp³-rich Scaffolds for Lead Generation. *ACS Med. Chem. Lett.* **2019**, *10*, 1512-1517. (b) Chang, Z.; Guillot, R.; Boddaert, T.; Aitken, D. J., Stereocontrolled Preparation of Diversely Trifunctionalized Cyclobutanes. *J. Org. Chem.* **2019**, *84*, 10518-10525. (c) Denisenko, A.; Garbuz, P.; Shishkina, S. V.; Voloshchuk, N. M.; Mykhailiuk, P. K., Saturated Bioisosteres of ortho-Substituted Benzenes. *Angew. Chem. Int. Ed.* **2020**, *59*, 20515-20521.
- (4) Poplata, S.; Tröster, A.; Zou, Y.-Q.; Bach, T. Recent Advances in the Synthesis of Cyclobutanes by Olefin [2 + 2] Photocycloaddition Reactions. *Chem. Rev.* **2016**, *116*, 9748-9815.
- (5) (a) Wang, M.; Lu, P., Catalytic approaches to assemble cyclobutane motifs in natural product synthesis. *Org. Chem. Front.* **2018**, *5*, 254-259. (b) Xu, Y.; Conner, M. L.; Brown, M. K., Cyclobutane and Cyclobutene Synthesis: Catalytic Enantioselective [2+2] Cycloadditions. *Angew. Chem.*

8. Enantioselective [2+2] Photocycloaddition via Iminium Ions: Catalysis by a Sensitizing Chiral Brønsted Acid

Int. Ed. **2015**, *54*, 11918-11928. (c) For a general review on the topic, see: Prentice, C.; Morrisson, J.; Smith, A. D.; Zysman-Colman, E., Recent developments in enantioselective photocatalysis. *Beilstein J. Org. Chem.* **2020**, *16*, 2363-2441.

(6) (a) Du, J.; Skubi, K. L.; Schultz, D. M.; Yoon, T. P. A Dual-Catalysis Approach to Enantioselective [2+2] Photocycloadditions Using Visible Light. *Science* **2014**, *344*, 392-396. (b) Vallavoju, N.; Selvakumar, S.; Jockusch, S.; Sibi, M. P.; Sivaguru, J. Enantioselective Organo-Photocatalysis Mediated by Atropisomeric Thiourea Derivatives. *Angew. Chem. Int. Ed.* **2014**, *53*, 5604-5608. (c) Blum, T. R.; Miller, Z. D.; Bates, D. M.; Guzei, I. A.; Yoon, T. P. Enantioselective photochemistry through Lewis acid-catalyzed triplet energy transfer. *Science* **2016**, *354*, 1391-1395. (d) Huang, X.; Quinn, T. R.; Harms, K.; Webster, R. D.; Zhang, L.; Wiest, O.; Meggers, E. Direct Visible-Light-Excited Asymmetric Lewis Acid Catalysis of Intermolecular [2+2] Photocycloadditions. *J. Am. Chem. Soc.* **2017**, *139*, 9120-9123. (e) Yu, H.; Dong, S.; Yao, Q.; Chen, L.; Zhang, D.; Liu, X.; Feng, X. Enantioselective [2+2] Photocycloaddition Reactions of Enones and Olefins with Visible Light Mediated by N,N'-Dioxide-Metal Complexes. *Chem. Eur. J.* **2018**, *24*, 19361-19367. (f) Daub, M. E.; Jung, H.; Lee, B. J.; Won, J.; Baik, M.-H.; Yoon, T. P. Enantioselective [2+2] Cycloadditions of Cinnamate Esters: Generalizing Lewis Acid Catalysis of Triplet Energy Transfer. *J. Am. Chem. Soc.* **2019**, *141*, 9543-9547. (g) Zheng, J.; Swords, W. B.; Jung, H.; Skubi, K. L.; Kidd, J. B.; Meyer, G. J.; Baik, M.-H.; Yoon, T. P. Enantioselective Intermolecular Excited-State Photoreactions Using a Chiral Ir Triplet Sensitizer: Separating Association from Energy Transfer in Asymmetric Photocatalysis. *J. Am. Chem. Soc.* **2019**, *141*, 13625-13634. (h) Guo, J.; Fan, Y.-Z.; Lu, Y.-L.; Zheng, S.-P.; Su, C.-Y. Visible-Light Photocatalysis of Asymmetric [2+2] Cycloaddition in Cage-Confining Nanospace Merging Chirality with Triplet-State Photosensitization. *Angew. Chem. Int. Ed.* **2020**, *59*, 8661-8669. (i) Rigotti, T.; Mas-Ballesté, R.; Alemán, J., Enantioselective Aminocatalytic [2+2] Cycloaddition through Visible Light Excitation. *ACS Catal.* **2020**, *10*, 5335-5346.

(7) Selected contributions by our group: (a) Müller, C.; Bauer, A.; Maturi, M. M.; Cuquerella, M. C.; Miranda, M. A.; Bach, T. Enantioselective Intramolecular [2+2]-Photocycloaddition Reactions of 4-Substituted Quinolones Catalyzed by a Chiral Sensitizer with a Hydrogen-Bonding Motif. *J. Am. Chem. Soc.* **2011**, *133*, 16689-16697. (b) Brimiouille, R.; Bach, T. Enantioselective Lewis Acid Catalysis of Intramolecular Enone [2+2] Photocycloaddition Reactions. *Science* **2013**, *342*, 840-843. (c) Maturi, M. M.; Bach, T. Enantioselective Catalysis of the Intermolecular [2+2] Photocycloaddition between 2-Pyridones and Acetylenedicarboxylates. *Angew. Chem. Int. Ed.* **2014**, *53*, 7661-7664. (d) Tröster, A.; Alonso, R.; Bauer, A.; Bach, T. Enantioselective Intermolecular [2+2] Photocycloaddition Reactions of 2(1H)-Quinolones Induced by Visible Light Irradiation. *J. Am. Chem. Soc.* **2016**, *138*, 7808-7811. (e) Poplata, S.; Bach, T., Enantioselective Intermolecular [2+2] Photocycloaddition Reaction of Cyclic Enones and Its Application in a Synthesis of (-)-Grandisol. *J. Am. Chem. Soc.* **2018**, *140*, 3228-3231.

(8) (a) Akiyama, T.; Itoh, J.; Fuchibe, K., Recent Progress in Chiral Brønsted Acid Catalysis. *Adv. Synth. Catal.* **2006**, *348*, 999-1010. (b) Terada, M., Chiral Phosphoric Acids as Versatile Catalysts for Enantioselective Transformations. *Synthesis* **2010**, 1929-1962. (c) Parmar, D.; Sugiono, E.; Raja, S.; Rueping, M., Complete Field Guide to Asymmetric BINOL-Phosphate Derived Brønsted Acid and Metal Catalysis: History and Classification by Mode of Activation; Brønsted Acidity, Hydrogen Bonding, Ion Pairing, and Metal Phosphates. *Chem. Rev.* **2014**, *114*, 9047-9153.

(9) Examples: (a) Rono, L. J.; Yayla, H. G.; Wang, D. Y.; Armstrong, M. F.; Knowles, R. R., Enantioselective Photoredox Catalysis Enabled by Proton-Coupled Electron Transfer: Development of an Asymmetric Aza-Pinacol Cyclization. *J. Am. Chem. Soc.* **2013**, *135*, 17735-17738. (b) Proctor, R. S. J.; Davis, H. J.; Phipps, R. J., Catalytic enantioselective Minisci-type addition to heteroarenes. *Science* **2018**, *360*, 419-422. (c) Cao, K.; Tan, S. M.; Lee, R.; Yang, S.; Jia, H.; Zhao, X.; Qiao, B.; Jiang, Z., Catalytic Enantioselective Addition of Prochiral Radicals to Vinylpyridines. *J. Am. Chem. Soc.* **2019**, *141*, 5437-5443.

(10) For racemic [2+2] photocycloaddition reactions, catalyzed by a Brønsted acid, see: (a) Brenninger, C.; Pöthig, A.; Bach, T., Brønsted Acid Catalysis in Visible-Light-Induced [2+2] Photocycloaddition Reactions of Enone Dithianes. *Angew. Chem. Int. Ed.* **2017**, *56*, 4337-4341 (b) Sherbrook, E. M.; Jung, H.; Cho, D.; Baik, M.-H.; Yoon, T. P. Brønsted acid catalysis of photosensitized cycloadditions. *Chem. Sci.* **2020**, *11*, 856-861.

(11) (a) Akiyama, T.; Itoh, J.; Yokota, K.; Fuchibe, K., Enantioselective Mannich-Type Reaction Catalyzed by a Chiral Brønsted Acid. *Angew. Chem. Int. Ed.* **2004**, *43*, 1566-1568. (b) Yamanaka, M.; Itoh, J.; Fuchibe, K.; Akiyama, T. Chiral Brønsted Acid Catalyzed Enantioselective Mannich-Type Reaction. *J. Am. Chem. Soc.* **2007**, *129*, 6756-6764.

(12) Hörmann, F. M.; Kerzig, C.; Chung, T. S.; Bauer, A.; Wenger, O. S.; Bach, T. Triplet Energy Transfer from Ruthenium Complexes to Chiral Eniminium Ions: Enantioselective Synthesis of Cyclobutanecarbaldehydes by [2+2] Photocycloaddition. *Angew. Chem. Int. Ed.* **2020**, *59*, 9659-9668.

8. Enantioselective [2+2] Photocycloaddition via Iminium Ions: Catalysis by a Sensitizing Chiral Brønsted Acid

- (13) Kandappa, S. K.; Valloli, L. K.; Ahuja, S.; Parthiban, J.; Sivaguru, J., Taming the excited state reactivity of imines – from non-radiative decay to aza Paternò–Büchi reaction. *Chem. Soc. Rev.* **2021**, *50*, 1617-1641.
- (14) Compound **4** was found to exist in solution mainly as the respective imine (imine/*N,O*-acetal = 85/15), see: (a) Monleón, L. M.; Grande, M.; Anaya, J. Radical cyclisation of epoxynitrile-2-azetidiones mediated by Cp_2TiCl . *Tetrahedron* **2007**, *63*, 3017-3025. (b) Karade, N. N.; Tiwari, G. B.; Gampawar, S. V. Efficient Oxidative Conversion of Aldehydes to 2-Substituted Oxazolines and Oxazines. Using (Diacetoxyiodo)benzene. *Synthesis* **2007**, 1921-1924.
- (15) Pecho, F.; Zou, Y.-Q.; Gramüller, J.; Mori, T.; Huber, S. M.; Bauer, A.; Gschwind, R. M.; Bach, T. A Thioxanthone Sensitizer with a Chiral Phosphoric Acid Binding Site: Properties and Applications in Visible Light-Mediated Cycloadditions. *Chem. Eur. J.* **2020**, *26*, 5190-5194.
- (16) For related work, see: (a) Takagi, R.; Tabuchi, C., Enantioselective intramolecular [2 + 2] photocycloaddition using phosphoric acid as a chiral template. *Org. Biomol. Chem.* **2020**, *18*, 9261-9267. (b) Lyu, J.; Claraz, A.; Vitale, M. R.; Allain, C.; Masson, G., Preparation of Chiral Photosensitive Organocatalysts and Their Application for the Enantioselective Synthesis of 1,2-Diamines. *J. Org. Chem.* **2020**, *85*, 12843-12855.
- (17) (a) Fyfe, J. W. B.; Watson, A. J. B. Recent Developments in Organoboron Chemistry: Old Dogs, New Tricks. *Chem.* **2017**, *3*, 31–55. (b) Lennox, A. J. J.; Lloyd-Jones, G. C. Selection of Boron Reagents for Suzuki–Miyaura Coupling. *Chem. Soc. Rev.* **2014**, *43*, 412–443.
- (18) For recent applications of chiral iminium ions in photocatalytic reactions on the singlet hypersurface, see: Mazzarella, D.; Crisenza, G. E. M.; Melchiorre, P., Asymmetric Photocatalytic C–H Functionalization of Toluene and Derivatives. *J. Am. Chem. Soc.* **2018**, *140*, 8439-8443 and refs. cited therein.
- (19) Koziar, J. C.; Cowan, D. O. Photochemical heavy-atom effects. *Acc. Chem. Res.* **1978**, *11*, 334-341.
- (20) (a) Sorgenfrei, N.; Hioe, J.; Greindl, J.; Rothermel, K.; Morana, F.; Lokesh, N.; Gschwind, R. M., NMR Spectroscopic Characterization of Charge Assisted Strong Hydrogen Bonds in Brønsted Acid Catalysis. *J. Am. Chem. Soc.* **2016**, *138*, 16345–16354. (b) Rothermel, K.; Melikian, M.; Hioe, J.; Greindl, J.; Gramüller, J.; Žabka, M.; Sorgenfrei, N.; Hausler, T.; Morana, F.; Gschwind, R. M., Internal acidity scale and reactivity evaluation of chiral phosphoric acids with different 3,3'-substituents in Brønsted acid catalysis. *Chem. Sci.* **2019**, *10*, 10025-10034.
- (21) (a) Greindl, J.; Hioe, J.; Sorgenfrei, N.; Morana, F.; Gschwind, R. M., Brønsted Acid Catalysis—Structural Preferences and Mobility in Imine/Phosphoric Acid Complexes. *J. Am. Chem. Soc.* **2016**, *138*, 15965–15971. (b) Melikian, M.; Gramüller, J.; Hioe, J.; Greindl, J.; Gschwind, R. M., Brønsted acid catalysis – the effect of 3,3'-substituents on the structural space and the stabilization of imine/phosphoric acid complexes. *Chem. Sci.* **2019**, *10*, 5226-5234.
- (22) The simple diastereoselectivity can be governed by the orientation of the two spin center in the ISC step. For a discussion, see: Griesbeck, A. G., Spin-Selectivity in Photochemistry: A Tool for Organic Synthesis. *Synlett* **2003**, 451-472.

8.6. Supporting Information

8.6.1. General information

Chemicals

Deuterated CD₂Cl₂ was purchased from Deutero or Sigma Aldrich. CD₂Cl₂ was freshly distilled over CaH₂ and stored over molecular sieves (3 Å) under argon atmosphere.

Spectrometer data

Low temperature NMR experiments were performed on Bruker Avance III HD 600 MHz spectrometer, equipped with a 5 mm CPPBBO BB-1H/19F. Temperature was controlled in the VT-experiments by BVT 3000 and BVTE 3900. NMR Data were processed, evaluated and plotted with TopSpin 3.2 software. Further plotting of the spectra was performed with Corel Draw 2020 software. ¹H and ¹³C chemical shifts were referenced to TMS.

Pulse programs

All pulse programs used are standard Bruker NMR pulse programs. The pulse program for Diffusion Ordered Spectroscopy (DOSY) is described in the respective chapter.

Acquisition Parameters

¹H NMR: Pulse program: zg30; Relaxation delay = 2 – 3 s, Acquisition time = 2.48 s, SW = 18-30 ppm, TD = 64k, NS = 16 – 512;

³¹P NMR: Pulse program: zgpg30; Relaxation delay = 3 s, Acquisition time = 0.66 s, SW = 30.0-200 ppm, TD = 64k, NS = 64 – 512;

2D-¹H,¹H NOESY: Pulse program: noesygpph; Relaxation delay = 5 - 8 s, NS = 8, mixing time (D8) = 300.00 ms; TD = 4096; increments = 512;

2D-¹H,³¹P HMBC: Pulse program: inv4gplrndqf; Relaxation delay = 4 - 8 s, NS = 8-32, TD = 4096; increments = 256;

2D-¹H,¹H COSY: Pulse program: cosygpqf; Relaxation delay = 5.00 s, NS = 8, TD = 4096; increments = 512;

2D-¹H,¹³C HSQC: Pulse program: hsqcedetgpsisp2.3; Relaxation delay = 4 - 8 s, NS = 8, ¹J_{XH} = 145 Hz; TD = 4096; increments = 512;

2D-¹H,¹³C HMBC: Pulse program: hmbcgpplndqf; Relaxation delay = 4.00 s, NS = 8, ¹J_{XH} = 145 Hz, J_{XH}(long range) = 10 Hz; TD = 4096; increments = 512;

8. Enantioselective [2+2] Photocycloaddition via Iminium Ions: Catalysis by a Sensitizing Chiral Brønsted Acid

2D-¹H,¹⁵N HMBC: Pulse program: inv4gplrndqf; Relaxation delay = 4.00 s, NS = 64, delay for evolution of long range couplings (D6) = 20.00 ms; TD = 4096; increments = 256;

8.6.2. Sample preparation

Catalyst and substrate were weighed directly into a 5 mm NMR tube (for all samples containing catalyst **6f**, brown-glass NMR tubes were used; For samples containing other catalysts as **6f**, the chiral phosphoric acid was first weighed in and dried at 130 °C under vacuum for 30 min). The NMR tube was evacuated and flushed with argon three times and dry CD₂Cl₂ (0.6 mL) and TMS atmosphere (1.0 mL) were added under argon flow. The tube was closed and sealed with parafilm. For the *E*-only sample, the NMR tube and CD₂Cl₂ Schlenk flask were precooled to < -80 °C in an acetone/liquid nitrogen cooling bath and the sample was kept at < -80 °C at all times.

8.6.3. Variable temperature NMR

Temperatures as low as 180 K were necessary to sufficiently slow down exchange processes and to detect separated hydrogen bond signals (see Figure S7). At the reaction temperature of -50°C/223.2 K, the signals corresponding to species A and A' (differing in the orientation of the N-(Cyclohexylmethanol) residue; see below) coalescence and hence a temperature of 180 K was chosen for the structural investigations to obtain better insights. For a detailed discussion about the difference in the monitored species see below.

8. Enantioselective [2+2] Photocycloaddition via Iminium Ions: Catalysis by a Sensitizing Chiral Brønsted Acid

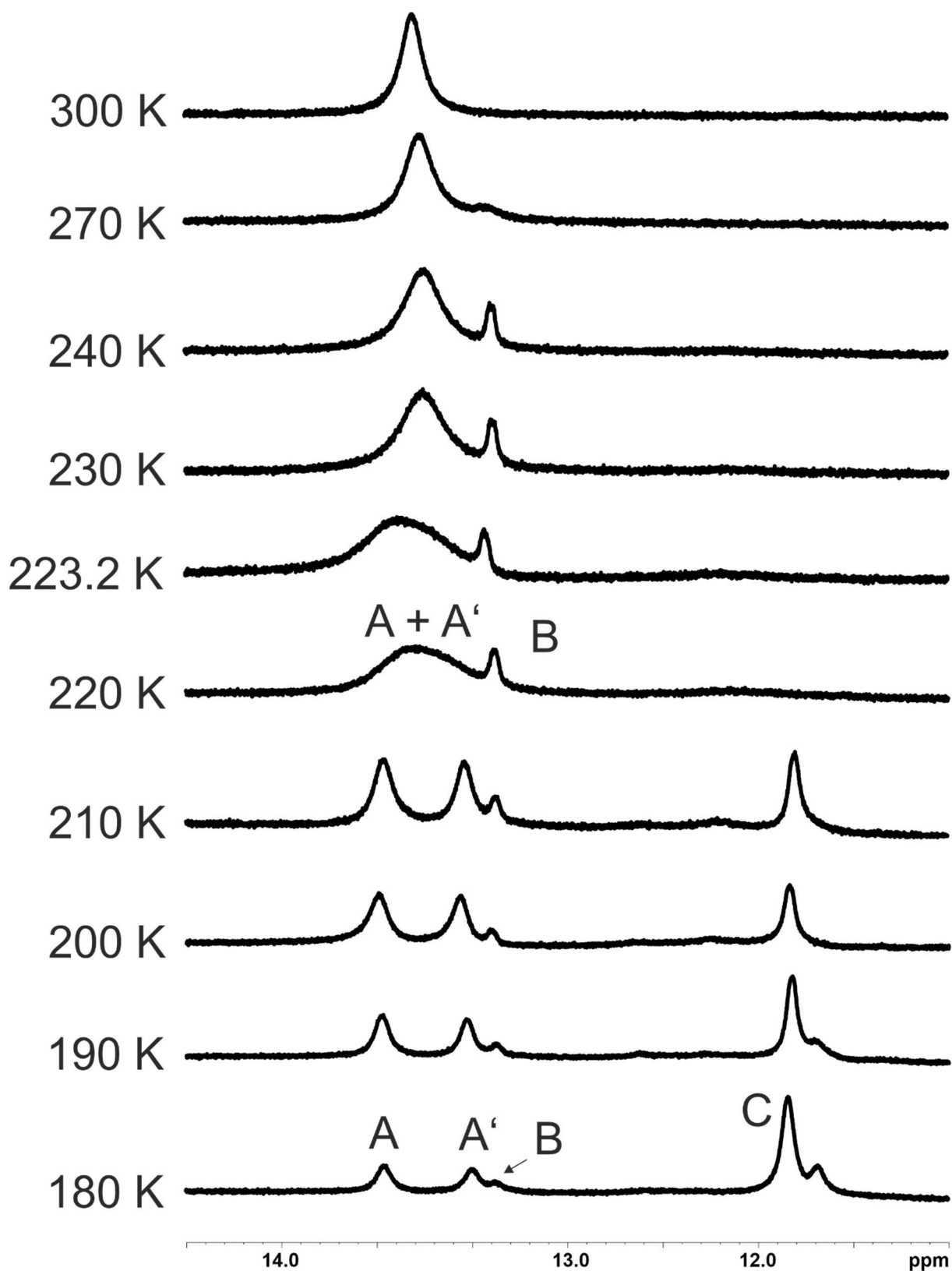


Figure S7: Hydrogen bond region of 6f/7e (1:1, 10 mM) in CD₂Cl₂ at 600 MHz at variable temperatures. For a detailed discussion about the structures of species A, A', B and C see chapter below.

8.6.4. Chemical shift assignment and structural analysis of 6c/7e

For the system 6c/7e a partial chemical shift assignment was accomplished by a combination of ^1H , ^{13}C , ^{31}P , ^1H , ^1H COSY, ^1H , ^1H NOESY, ^1H , ^{13}C HSQC, ^1H , ^{13}C HMBC, ^1H , ^{15}N HMBC and ^1H , ^{31}P HMBC. However, not all chemical shifts, especially of the catalyst could be assigned due to the line broadening and signal overlap induced by the flexibility of the N-(Cyclohexylmethanol) backbone.

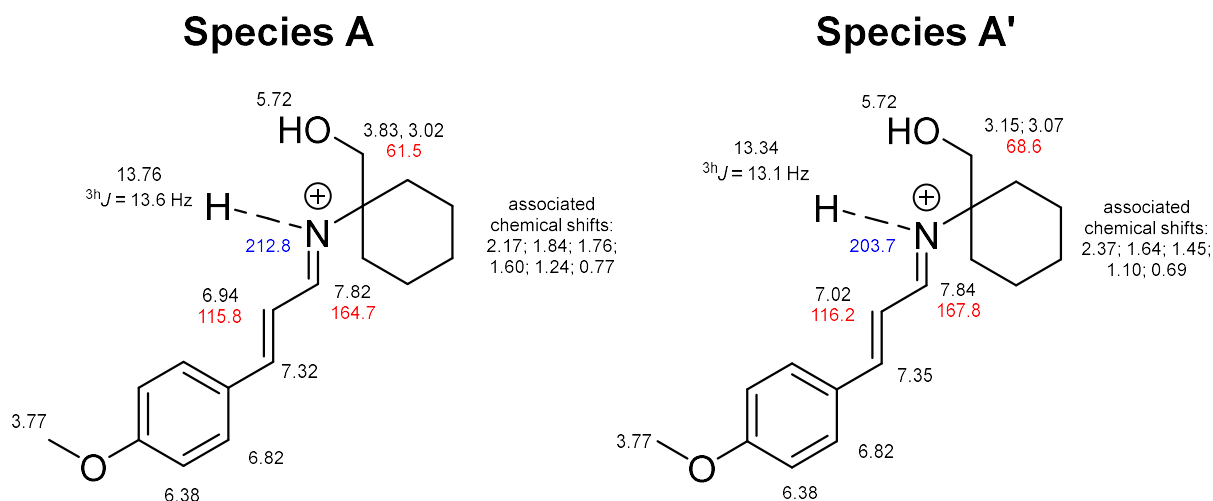


Figure S8: Partial chemical shift assignment of species A (left) and A' (right) 6c/7e (1:1, 50 mM) in CD_2Cl_2 at 180 K and 600 MHz. Black: ^1H ; Red: ^{13}C ; Blue: ^{15}N .

Most importantly, the $^1\text{H}_{\alpha}$ and $^{13}\text{C}_{\alpha}$ chemical shifts (7.82; 164.7 / 7.84; 167.8) match precisely the expected values^[13] and differ strongly from the values expected for *N,O*-acetals (~5.00 ppm; ~90 ppm; see chapter 4.1).

For both species, the chemical shifts of the cinnamaldehyde part of the imine are almost identical. Additionally, the NOE patterns of the O---H-N hydrogen bonded protons (13.76 ppm or 13.34 ppm) to the cinnamaldehyde part are identical (see Figure S9), corroborating an *E*-trans conformation and an *EE* configuration of the CN and CC double bonds, as the NOE cross peak to the β -hydrogen atom is the most intense. The only significant offset in proton chemical shifts is observed for the N-(Cyclohexylmethanol) residue. The diastereotopic CH_2 group next to the OH group was identified *via* COSY and the associated chemical shifts of the cyclohexyl substituent were identified *via* NOESY spectrum. In conclusion, this shows that the difference between both species is based on a different conformation of the nitrogen substituent. However, the exact structural difference could not be identified due to the severe line broadening and signal overlap in the spectra. In the spectra of the respective complex with a dimethyl backbone, only one species is detected (see Figure S10).

8. Enantioselective [2+2] Photocycloaddition via Iminium Ions: Catalysis by a Sensitizing Chiral Brønsted Acid

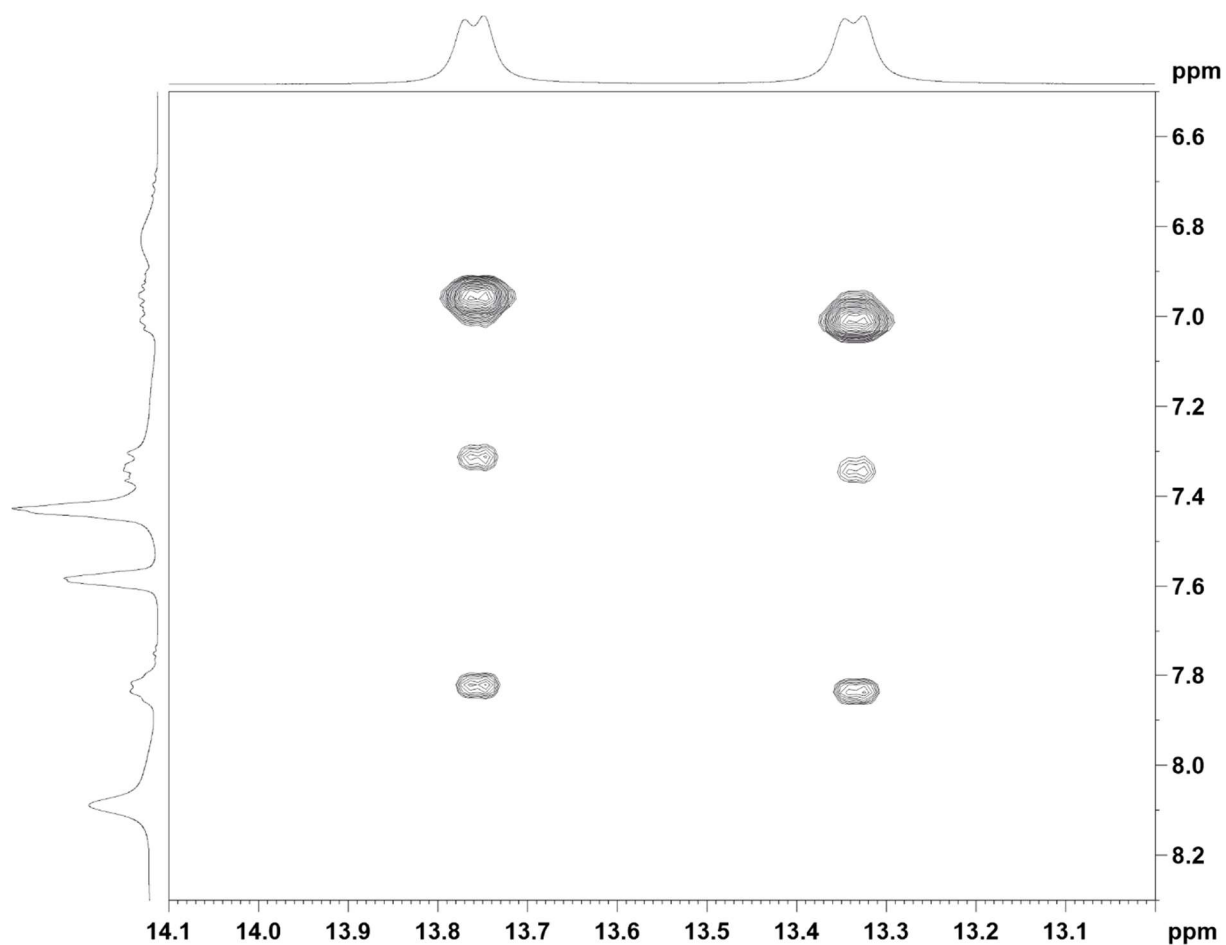


Figure S9: NOE pattern of the O---H-N hydrogen bond proton signals to the cinnamaldehyde part of the substrate of the complex **6c/7e** at 180 K and 600 MHz in CD₂Cl₂. For both species, an identical NOE pattern is observed, demonstrating that they do not differ in the CN or CC double bond configuration.

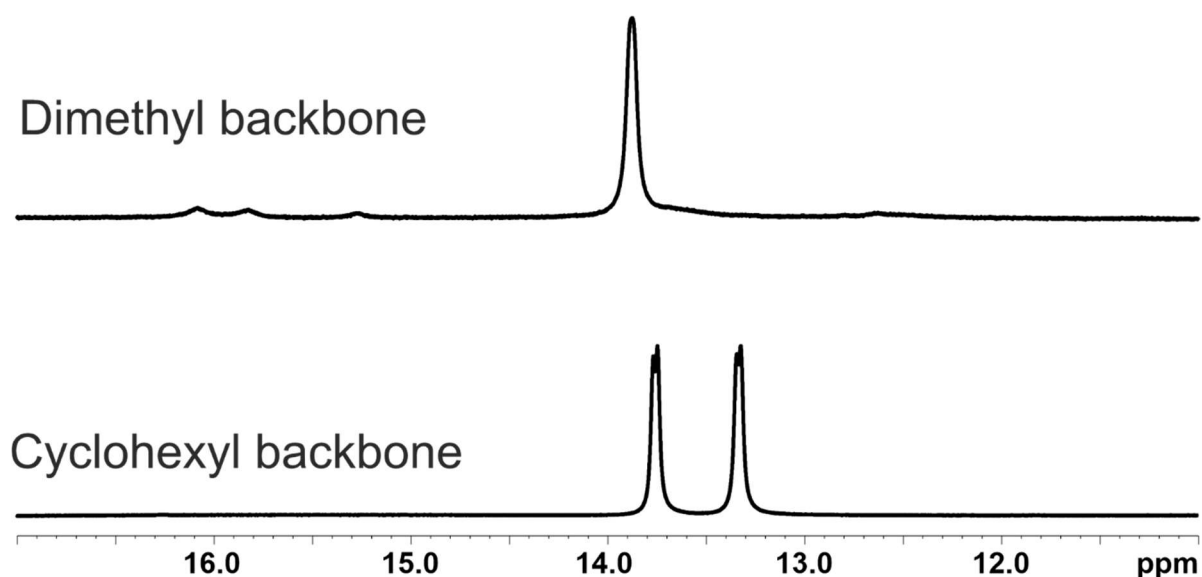


Figure S10: Hydrogen bond region of the ¹H spectra of **6c/S28** (top) and **6c/7e** (bottom) at a 1:1 ratio and a concentration of 10 mM in CD₂Cl₂ and 600 MHz. While for the complex with the cyclohexyl backbone two species are observed, only one is observed for the respective complex bearing a dimethyl backbone.

8.6.5 Hydrogen bonding analysis in **6c/7e**

Hydrogen bonds are often described as beginning proton transfer reactions and hence can be experimentally proven by detecting their covalent nature *via* magnetization transfer by scalar couplings. For **6c/7e**, the O---H-N hydrogen bond proton signals belonging to A and A' showed cross peaks in the $^1\text{H},^{15}\text{N}$ - and $^1\text{H},^{31}\text{P}$ -HMBC spectra (see Figure S12 and S13). For the O--H--O hydrogen bond proton signals belonging to A and A', cross signals in the $^1\text{H},^{31}\text{P}$ -HMBC and COSY (Figure S14) spectra were observed. The magnetization transfer by scalar couplings of the O---H-N and O--H--O hydrogen bonds to the imine **7e** as well as to the chiral phosphoric acid **6c** clearly show, that these signals are part of a hydrogen bond. Hence, the bidentate binding of catalyst and substrate is clearly proven by the detection of the above described network of magnetization transfers (see Figure S11).

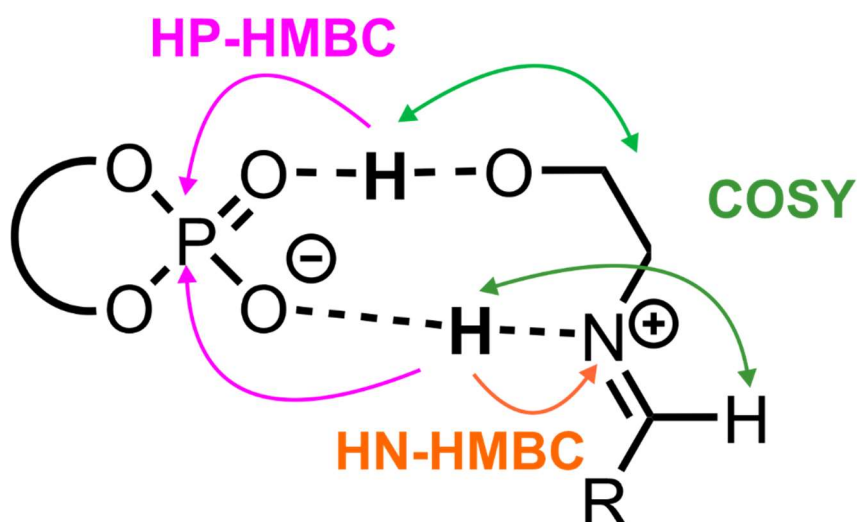


Figure S11: Bidentate binding motive and detected scalar couplings for both species A and A' of the complex **6c/7e**.

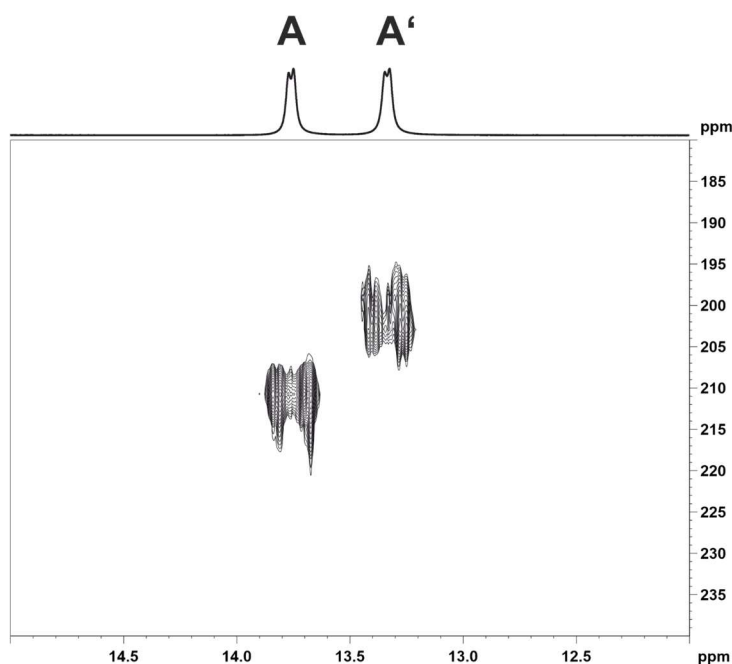


Figure S12: Cross section of the $^1\text{H},^{15}\text{N}$ -HMBC spectrum of **6c/7e** at 180 K and 600 MHz in CD_2Cl_2 .

8. Enantioselective [2+2] Photocycloaddition via Iminium Ions: Catalysis by a Sensitizing Chiral Brønsted Acid

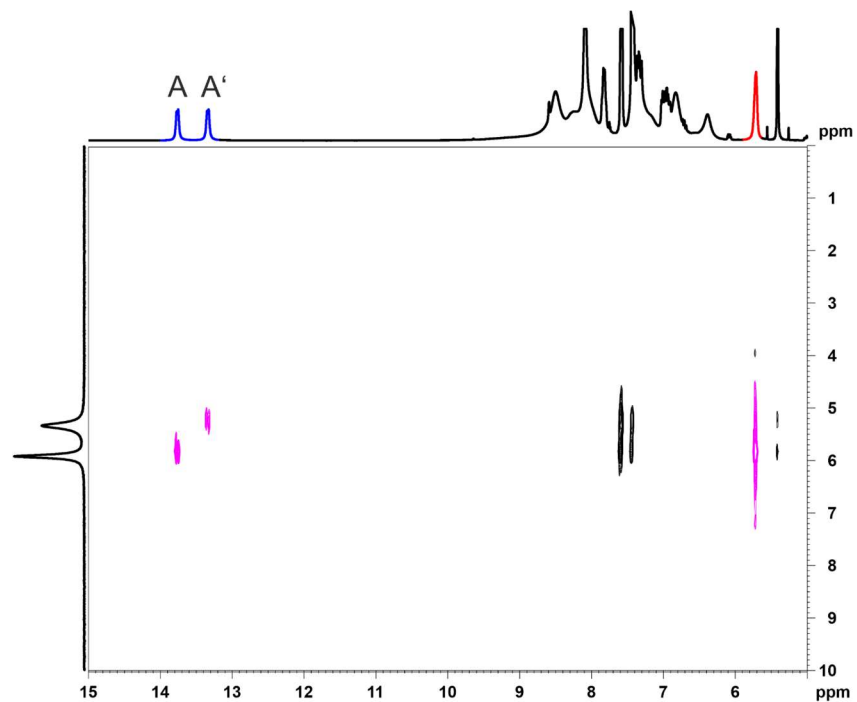


Figure S13: Cross section of the $^1\text{H},^{31}\text{P}$ -HMBC spectrum of **6c/7e** at 180 K and 600 MHz in CD_2Cl_2 . Both, the O---H-N hydrogen bonded protons (blue) and the O—H--O hydrogen bond protons (red) show cross peaks and hence scalar couplings to the respective ^{31}P signals of species A and A'.

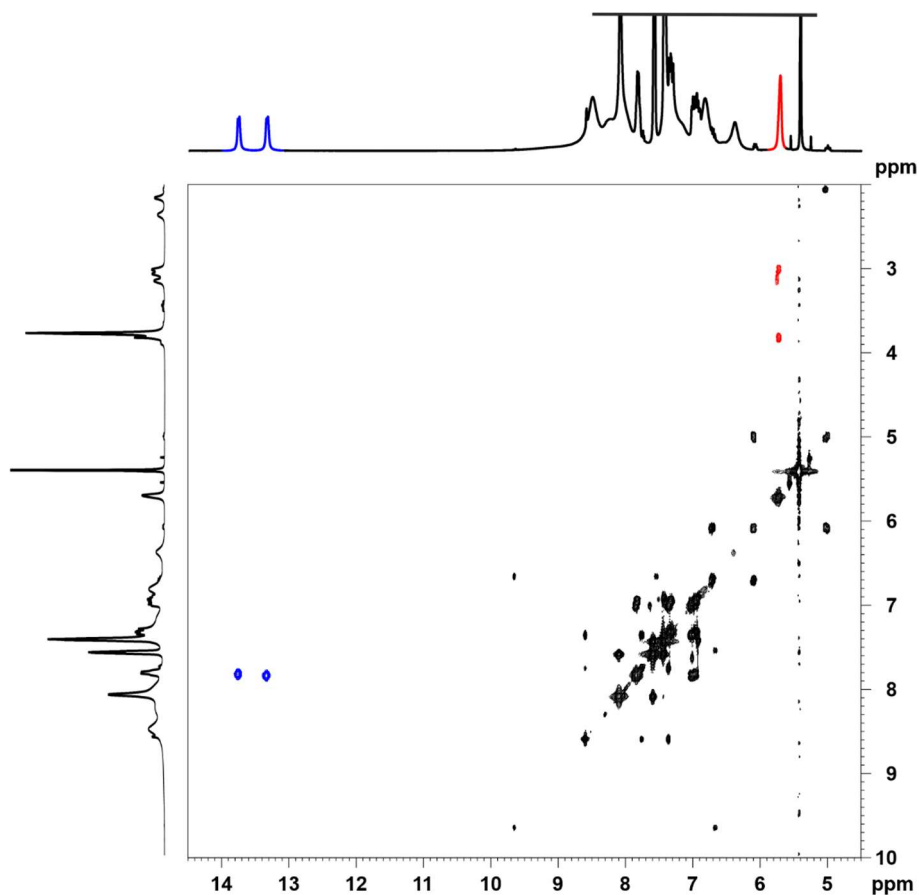


Figure S14: Cross section of the ^1H -COSY spectrum of **6c/7e** at 180 K and 600 MHz in CD_2Cl_2 . Both, the O---H-N hydrogen bonded protons (blue) and the O—H--O hydrogen bond protons (red) show cross peaks to the imine.

8.6.6. Diffusion ordered spectroscopy (DOSY)

The DOSY measurements were performed with the convection suppressing DSTE (double stimulated echo) pulse sequence developed by Jerschow and Müller in a pseudo 2D mode.^[14] Smoothed square (SMSQ10.100) gradient shapes and a linear gradient ramp with 20 increments between 5% and 95% of the maximum gradient strength (5.35 G/mm) were used. The diffusion time delay was set to 45 ms. For the homospoil gradient strengths, values of 100, -13.17, 20 and -17.13 % were used. Gradient pulse lengths (p16) were first optimized to obtain a sigmoidal signal decay for increasing gradient strength (3.0 ms for TMS, 6.0 ms for **6c/7e**). NMR spectra were processed with Bruker TopSpin 3.2 (T1/T2 relaxation package) and diffusion coefficients were derived according to Jerschow and Müller^[14] Tetramethylsilane was added to the samples to reference chemical shifts and the viscosity of each sample.

The molecular radii were derived by the Stokes-Einstein equation^[15] using Chens correction.^[16]

$$D_i = \frac{k_B T}{6\pi\eta r_H} * (1 + 0.695 * \left(\frac{r_{solv}}{r_H}\right)^{2.234})$$

D_i is the self-diffusion coefficient derived by the measurement, η is the viscosity of the solvent, r_H is the hydrodynamic radius of the observed molecule and r_{solv} the radius of the solvent. No form factor correction was applied. The viscosity was determined by measuring the diffusion coefficient of the reference tetramethylsilane (TMS) and solving the equation for η with the literature value^[17] of the radius of 2.96 Å. The solvent radius of C_6D_6 (2.655 Å) was calculated according to the increment system by Bond.^[18]

Table S7: Measured self diffusion coefficients of various signals in the spectrum of **6c/7e**. For signals 1-3, the chemical shift of A and A' overlap and hence the averaged self diffusion coefficient is measured. Signal 4 belongs to species A' and signal 5 to species A (see Figure S8). Both signals 4 and 5 are similar in the error range of the experiment, hence indicating that both species are similar in size (and that therefore the diffusion coefficient for both species can be averaged for signals 1-3 without falsifying the result).

Signal	δ [ppm]	D_i [m ² /s]
1	7.83	4.42E-11
2	5.72	4.31E-11
3	3.77	4.23E-11
4	3.07	4.77E-11
5	3.02	4.51E-11

Based on the averaged self diffusion coefficient of signals 1-5 and the measured value for TMS (1.73E-10 m²/s), a hydrodynamic radius of ~8.3 Å was determined, which is in line with values previously reported for monomeric complexes of chiral phosphoric acids and imine substrates.^[13b]

8.6.7. Low temperature NMR studies with catalyst **6f**

¹H NMR spectra of complexes with catalyst **6f** and substrates **7a**, **7b**, **7e**, **4**, **S28** and **S29** with a ratio of catalyst:substrate = 1:1 and a concentration of 10 mM were measured at 180 K and 600 MHz (see Figure S15). Similar to the systems of catalyst **6c** and substrates **7e** and **S28**, two species A and A' were observed for the substrates bearing a cyclohexyl backbone, while only one species A is observed for the respective systems with dimethyl backbone. The O---H-N hydrogen bond pattern for all six complexes matches the observed pattern for the investigated system with catalyst **6c**, demonstrating that the same binding motive as described in chapter 10.3 is present for catalyst **6f**. However, some additional signals corresponding to the new species B and C are monitored and discussed below. For the system **6f/S28** (Figure S9, bottom right), a partial chemical shift analysis for species A could be achieved (see Figure S16) and the assigned chemical shifts are similar to the ones determined for **6c/7e** (see Figure S8). Especially the ones for H_α and C_α (7.68; 159.2 ppm), clearly show that species A is the open protonated form of the imine. For all species, severe line broadening and signal overlap was observed, originating in the flexibility of the nitrogen substituent and the degree of rotational freedom of the 3,3'-substituent of catalyst **6f**, preventing any clear and detailed structural analysis.

Decreasing the basicity of the substrate by modulating the phenyl substituent from methoxy to methyl to hydrogen led to a downfield shift of the O---H-N hydrogen bond proton signals. In accordance with our previous analysis about the hydrogen bonding in chiral phosphoric acid/substrate complexes, this reflects an increasing hydrogen bond strength (i.e. the proton is moved more towards the PO hydrogen bond donor).^[19] Hence, according to the previously established Steiner-Limbach correlation for these systems,^[19] the O---H-N proton is almost completely transferred onto the substrate (which is also corroborated by the detection of scalar coupling to the nitrogen or α-hydrogen atom as shown in Figures S12 and S14). Hence, the complex is best described as a hydrogen bond assisted ion pair.

8. Enantioselective [2+2] Photocycloaddition via Iminium Ions: Catalysis by a Sensitizing Chiral Brønsted Acid

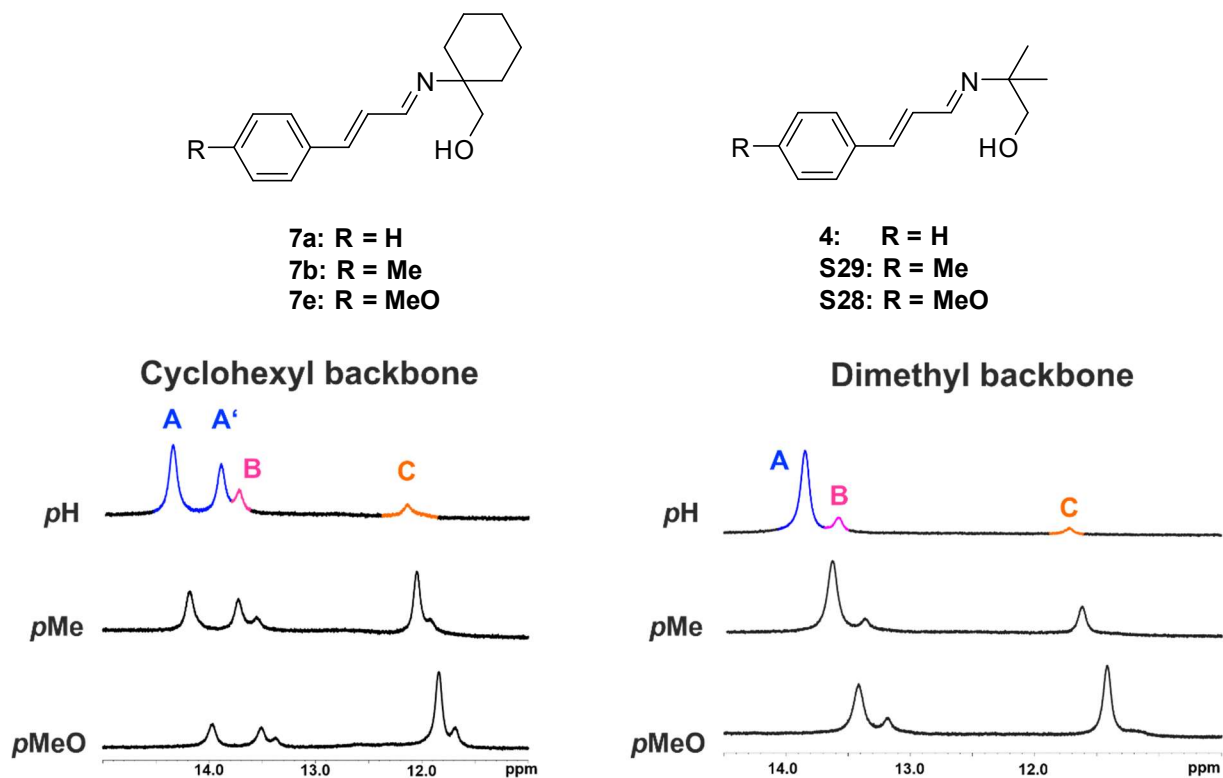


Figure S15: Excerpt of the ^1H spectra of catalyst **6f** with substrates **7a**, **7b** and **7e** bearing a cyclohexyl backbone (left) and the respective complexes with **4**, **S28** and **S29** bearing a dimethyl backbone.

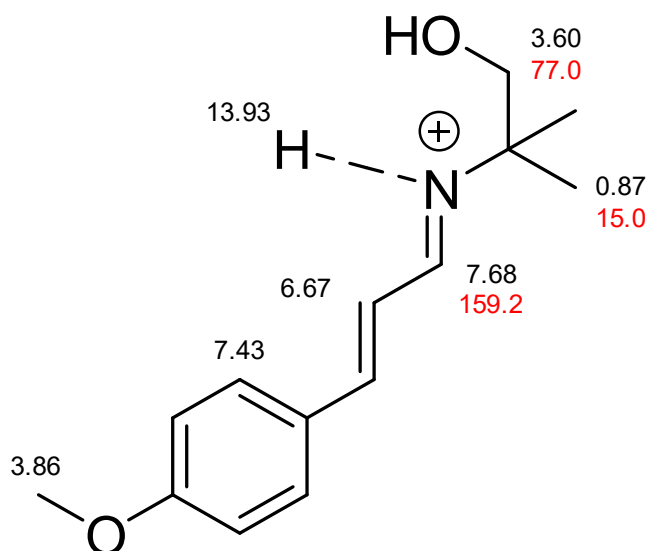


Figure S16: Partial chemical shift assignment of **6f/S28** at 180 K and 600 MHz in CD_2Cl_2 . Due to the severe line broadening and signal overlap, only some chemical shifts could be assigned via various 2D NMR experiments.

Species B and C, which are only present in the systems with catalyst **6f** and not in the respective systems with catalyst **6c**, could not unambiguously be assigned. For species B we tentatively propose a complex similar to A or A' but with a Z-configured C=N double bond, as previously reported for chiral phosphoric acid/imine systems.^[13] While the free substrate is only present as the E-isomer of the open imine or N,O-acetal, upon protonation and complexation by the acid, the Z-isomer of the C=N double

8. Enantioselective [2+2] Photocycloaddition via Iminium Ions: Catalysis by a Sensitizing Chiral Brønsted Acid

bond could be stabilized. If the sample of **6f/7a** is prepared at $< -80\text{ }^{\circ}\text{C}$ with addition of precooled solvent and constant cooling in an acetone/liquid nitrogen bath and measured at the spectrometer precooled to 180 K, the signal corresponding to species B is not detected (see Figure S17). Analogous experiments have been carried out before on chiral phosphoric acid/imine systems and revealed, that by this approach isomerization of the C=N double is effectively prevented (in these systems, the Z-isomer of the imine was unambiguously identified *via* NOESY spectra).^[17] After heating the sample up to the reaction temperature of $-50\text{ }^{\circ}\text{C}/223.2\text{ K}$ inside the spectrometer, species B was detected (see Figure S17) as the increased temperature now allowed for $E\rightarrow Z$ isomerization of the C=N double bond.^[19b] Additionally, the population of species B relative to A and A' increases with increasing temperature up to 270 K (see Figure S7), showing that the suggested C=N Z-isomer is less thermodynamically favored compared to A and A'. These observations are in line with our previous investigations regarding the E/Z isomerization of imines and thus suggest, that species B is indeed the C=N Z-isomer of either A or A'. However, an unambiguous assignment was not achievable due to the low population, line broadening and signal overlap in the spectra.

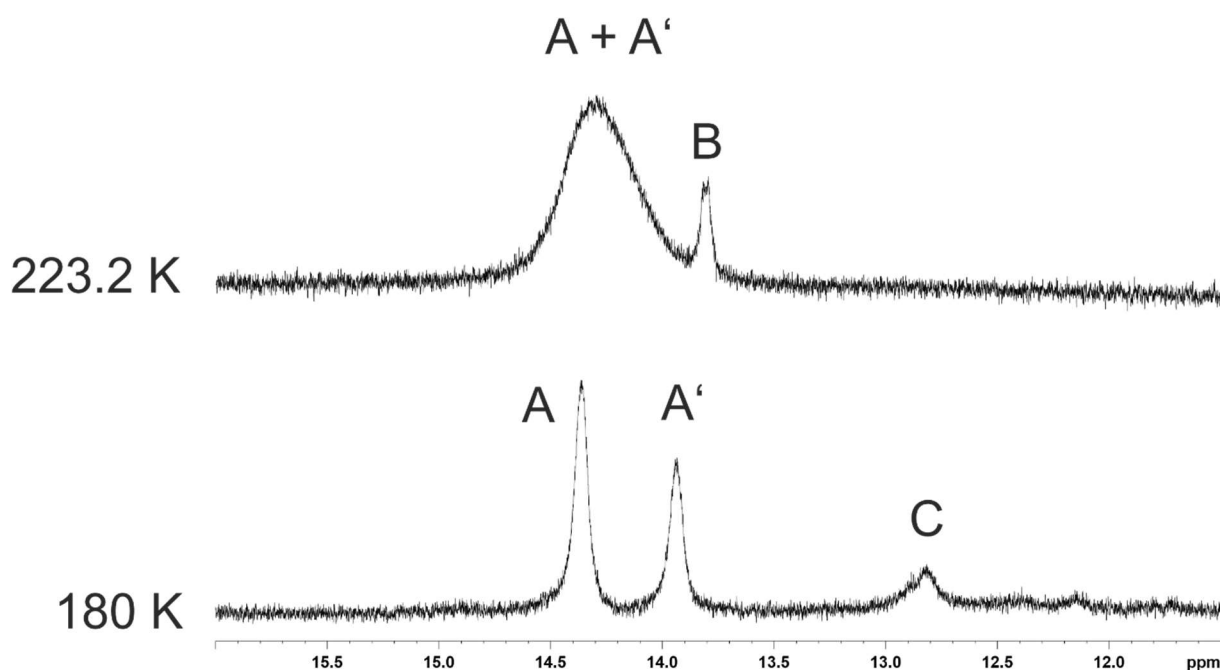


Figure S17: Excerpt of the ^1H spectra of **6f/7a** at a 1:1 ratio in CD_2Cl_2 at 600 MHz. The sample was prepared at temperatures below $-80\text{ }^{\circ}\text{C}$ and continuously cooled in an acetone/liquid nitrogen bath. Afterwards the spectrometer was heated up to 223.2 K and the upper spectrum was recorded. While at low temperatures species B was not observed, it was monitored at higher temperatures.

The nature of species C remained elusive. One possible assignment is a dimeric structure (catalyst/substrate)₂ of the identified complexes described above. In our previous investigations, this type of dimer was observed at significantly highfield shifted chemical shifts, i.e. with weakened, more ionic hydrogen bonds.^[13b] Additionally, in these dimers the imine occupies a position in between the two 3,3'-substit-

8. Enantioselective [2+2] Photocycloaddition via Iminium Ions: Catalysis by a Sensitizing Chiral Brønsted Acid

uents similar to the theoretically calculated structures of chiral phosphoric acids and N-(ortho-hydroxyphenyl) substituted imines,^[21] which also bind to the catalyst by two hydrogen bonds. Hence, the position of the imine in between the two 3,3'-substituents might already be preformed due to the bidentate binding, thus facilitating dimerization. However, it was not achievable to validate this by DOSY measurements carried out for the system **6f/S28**, as the assigned chemical shifts for species C were too severely line broadened to allow appropriate DOSY curves.

8.6.8. References

- [13] (a) Greindl, J.; Hioe, J.; Sorgenfrei, N.; Morana, F.; Gschwind, R. M., Brønsted Acid Catalysis—Structural Preferences and Mobility in Imine/Phosphoric Acid Complexes, *J. Am. Chem. Soc.* 2016, *138*, 15965–15971. (b) Melikian, M.; Gramüller, J.; Hioe, J.; Greindl, J.; Gschwind, R. M., Brønsted acid catalysis – the effect of 3,3'-substituents on the structural space and the stabilization of imine/phosphoric acid complexes, *Chem. Sci.*, **2019**, *10*, 5226-5234.
- [14] Jerschow A.; Müller N., Suppression of Convection Artifacts in Stimulated-Echo Diffusion Experiments. Double-Stimulated-Echo Experiments, *J. Magn. Reson.* **1997**, *125*, 372–375.
- [15] Macchioni A.; Ciancaleoni G.; Zuccaccia C.; Zuccaccia D., Determining accurate molecular sizes in solution through NMR diffusion spectroscopy, *Chem. Soc. Rev.* **2008**, *37*, 479–489.
- [16] Chen H. C.; Chen S. H., Diffusion of Crown Ethers in Alcohols, *J. Phys. Chem.* **1984**, *88*, 5118–5121.
- [17] Ben-Amotz D.; Willis K. G., Molecular Hard-Sphere Volume Increments, *J. Phys. Chem.* **1993**, *97*, 7736–7742.
- [18] Bondi A., van der Waals Volumes and Radii, *J. Phys. Chem.* **1964**, *68*, 441–451.
- [19] (a) Sorgenfrei, N.; Hioe, J.; Greindl, J.; Rothermel, K.; Morana, F.; Lokesh, N.; Gschwind, R. M., NMR Spectroscopic Characterization of Charge Assisted Strong Hydrogen Bonds in Brønsted Acid Catalysis, *J. Am. Chem. Soc.* 2016, *138*, 16345–16354. (b) Rothermel, K.; Melikian, M.; Hioe, J.; Greindl, J.; Gramüller, J.; Žabka, M.; Sorgenfrei, N.; Hausler, T.; Morana, F.; Gschwind, R.M., Internal acidity scale and reactivity evaluation of chiral phosphoric acids with different 3,3'-substituents in Brønsted acid catalysis, *Chem. Sci.*, **2019**, *10*, 10025-10034.
- [20] Lokesh N.; Hioe J.; Gramüller J.; Gschwind R. M., Relaxation Dispersion NMR to Reveal Fast Dynamics in Brønsted Acid Catalysis: Influence of Sterics and H-Bond Strength on Conformations and Substrate Hopping, *J. Am. Chem. Soc.* 2019, *141*, 16398–16407.
- [21] Yamanaka, M.; Itoh, J.; Fuchibe, K.; Akiyama, T. Chiral Brønsted Acid Catalyzed Enantioselective Mannich-Type Reaction. *J. Am. Chem. Soc.* **2007**, *129*, 6756-6764.

8.7. Additional Findings

8.7.1. Structural studies at 298 K

In the low temperature NMR measurements for **6c** and **6f** with substrates **4a/b/e** and **7a/b/e** (see figure 3), no detailed structural insights could be obtained due to signal overlap and line broadening. Therefore, measurements were performed for **6c/4e** and **6f/4a** at 298 K. Due to the higher temperature exchange processes are faster, which leads to fewer and narrower signals. The downside to this approach is that different catalyst/substrate aggregates cannot be distinguished anymore. However, this allows to obtain at least some qualitative insights into the arrangement of the complexes.

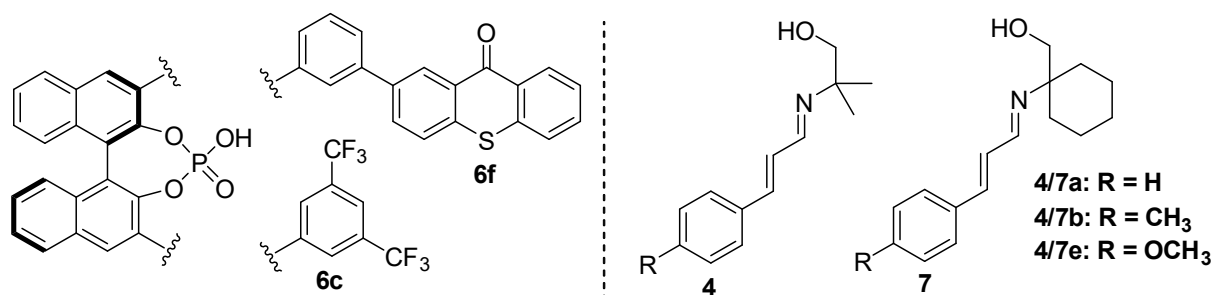


Figure 3: Catalysts and substrates used for the structural investigations.

For **6c/7e**, the spectra at 298 K were adequately resolved and a chemical shift assignment could be achieved based on a series of homo- and heteronuclear 2D NMR experiments. In the NOESY spectrum, cross peaks between the nitrogen substituent (see figure 4, green) and the aryl entity (figure 4, blue) of the imine to the 3,3'-substituents of the CPA were observed (red arrows). Additionally, no NOE contacts to the BINOL backbone could be observed.

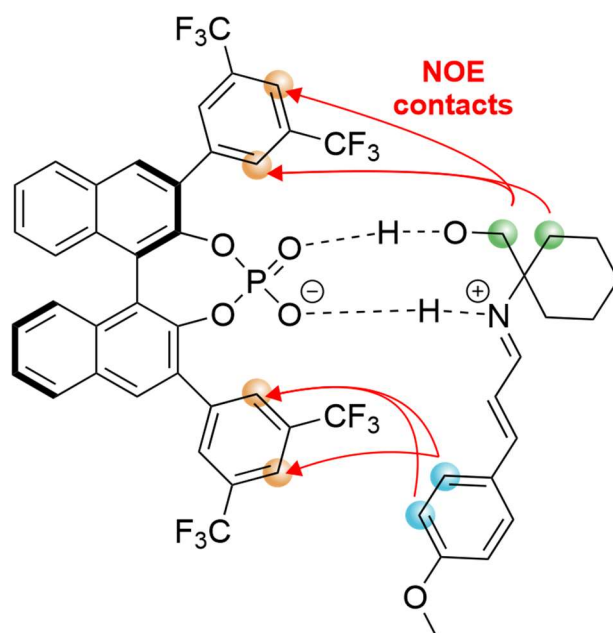


Figure 4: Observed NOE pattern for **6c/7e** showing NOE contacts between the imine and the 3,3'-substituent of the catalyst. No NOE contacts to the BINOL backbone were observed.

8. Enantioselective [2+2] Photocycloaddition via Iminium Ions: Catalysis by a Sensitizing Chiral Brønsted Acid

This NOE pattern suggests, that the imine is located in between the two 3,3'-substituents of the catalyst. This arrangement is analogous to binary CPA/imine complexes with imines bearing an N-(*ortho*)-hydroxyaryl substituent, which also feature bidentate binding of CPA and catalyst by two hydrogen bonds (see chapter 6). However, for **6c/4a** which gave the best resolution and fewest species at low temperature, such an analysis could not be performed. Even at 298 K, the signals for the imine were significantly line broadened and no chemical shift analysis could be achieved. In the NOESY and ROESY spectra, no NOE contacts for the signals which are suggested to stem from the imine could be observed.

8.7.2. Illumination experiments

To elucidate, if isomerization processes of the substrates are possible at synthetic conditions, NMR kinetic measurements under illumination were performed using the *in situ* glass fiber LED NMR tube insert.^[1] First, the reference system **6c/7a** was investigated. As the 3,5-di-(trifluoromethyl)phenyl substituent of **6c** is not a photosensitizer in contrast to the thioxanthone unit of **6f**, [Ru(bpy)₃](PF₆)₂ was added as photocatalyst in analogy to the screening reactions for suitable CPA catalysts (see chapter 8.3, scheme 2). The measurements were done at a ratio of **6c** : **7a** : [Ru(bpy)₃](PF₆)₂ of 0.5 : 1 : 0.2 at an imine concentration of 10 mM in CD₂Cl₂ at 180 K under continuous illumination at 455 nm. Before illumination the hydrogen bond region showed two signals (see figure 5) belonging to the species A and A', which correspond to two conformers of the binary **6c/7a** complex differing in the cyclohexyl backbone (see chapter 8.3. figure 2). Illumination at 455 K led to the population of two new minor species (figure 5, orange signals), which are slightly lowfield shifted. Changing the illumination wavelength to 375 nm led to a strong population increase of these two species (figure 5, left).

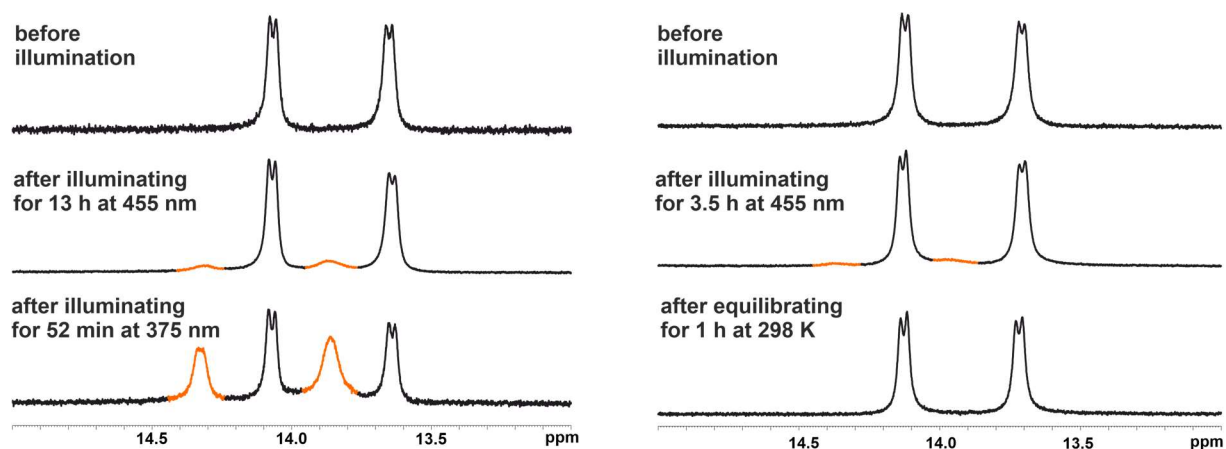


Figure 5: NMR kinetic measurements of **6c** : **7a** : [Ru(bpy)₃](PF₆)₂ at a ratio of 0.5 : 1 : 0.2 at an imine concentration of 10 mM in CD₂Cl₂ at 180 K under continuous illumination at 455 nm.

8. Enantioselective [2+2] Photocycloaddition via Iminium Ions: Catalysis by a Sensitizing Chiral Brønsted Acid

The formation of these two new species was shown to be thermally reversible (see figure 5 right). Heating the sample (without illumination) from 180 K to 298 K, equilibrating it at this temperature for 1 hour and cooling it down to 180 K again caused the two new signals to disappear. Due to this reversibility, most likely these two new species are the respective C=N Z-isomers of the A and A' complexes. In the previous studies on CPA/imine systems, it was shown that imines can undergo C=N isomerization upon illumination and that the population of CPA/Z-imine complexes can be increased by that at low temperature, where thermal back-isomerization is prevented.^[2,3] It is assumed, that this isomerization process is enabled by direct absorption and is possible in absence of the [Ru(bpy)₃](PF₆)₂ catalyst.

Next, **6f/4a** was investigated. Prior to illumination, the hydrogen bond region of the spectrum showed one major species A, as well as one minor species B (see figure 6 top). It is assumed, that A and B correspond to the CPA/imine complex featuring either an *E*- or *Z*-configuration of the C=N double bond, respectively (see figure S15). Illumination at 455 K for 130 min led to the formation of an additional signal corresponding to species D (for species C see figure S15). Equilibrating the sample at 300 K without illumination and cooling back down to 180 K did not significantly change the integral ratio of D : A+B (1 : 2.82 before and 1 : 2.94 after equilibration) within the error of the measurement. This shows that in contrast to **6c/7a** the formation of species D is not thermally reversible. This strongly suggests that species D features a C=C Z-double bond, which is only accessible by light driven photo-sensitized isomerization. However, due to severe line broadening and signal overlap, this could not be confirmed by analysis of the NOESY spectrum. Additionally, for species D the configuration of the C=N double bond remained elusive.

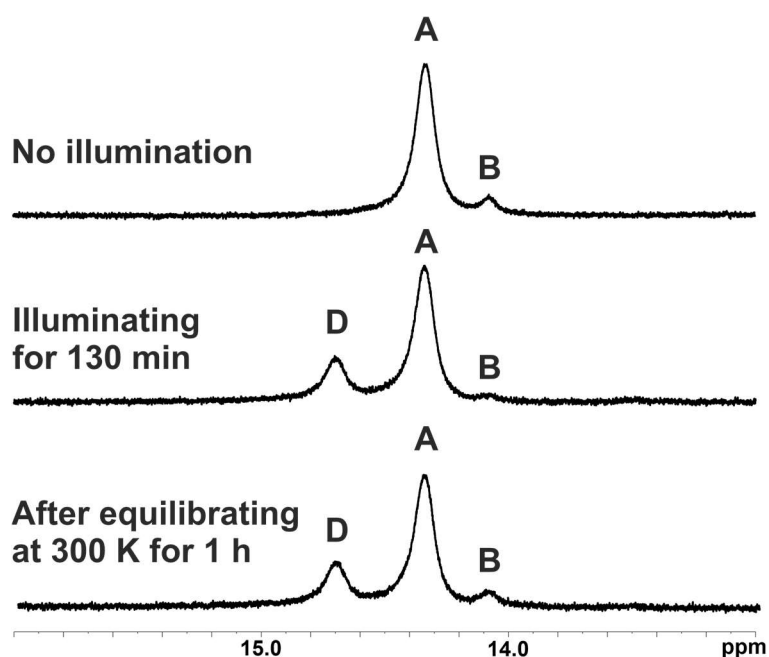


Figure 6: NMR kinetic measurements of **6f** : **4a** at a 1 : 1 ratio at an imine concentration of 10 mM in CD₂Cl₂ at 180 K before (top) and after (middle) continuous illumination at 455 K, as well as after equilibrating the sample at 300 K for 1 hour and cooling back to 180 K (bottom).

8. Enantioselective [2+2] Photocycloaddition via Iminium Ions: Catalysis by a Sensitizing Chiral Brønsted Acid

After elucidating the isomerization processes in these two simplified reference systems, kinetic measurements close to reaction conditions were performed. Therefore, a sample with catalyst **6f**, imine **7a** and olefin 2,3-dimethylbutadiene at a ratio of 1 : 1 : 20 respectively was studied. Prior to illumination, in the hydrogen bond region of the ^1H NMR spectrum the species A and A' are observable, which feature an *E*-configuration of the C=N and C=C double bond and differ in the conformation of the cyclohexyl backbone. At 180 K, illumination at 455 nm led to the continuous build-up of two new species D and D', as well as the continuous decrease of the species A and A', resulting in an exclusive population of D and D' after approximately 100 min (see figure 7).

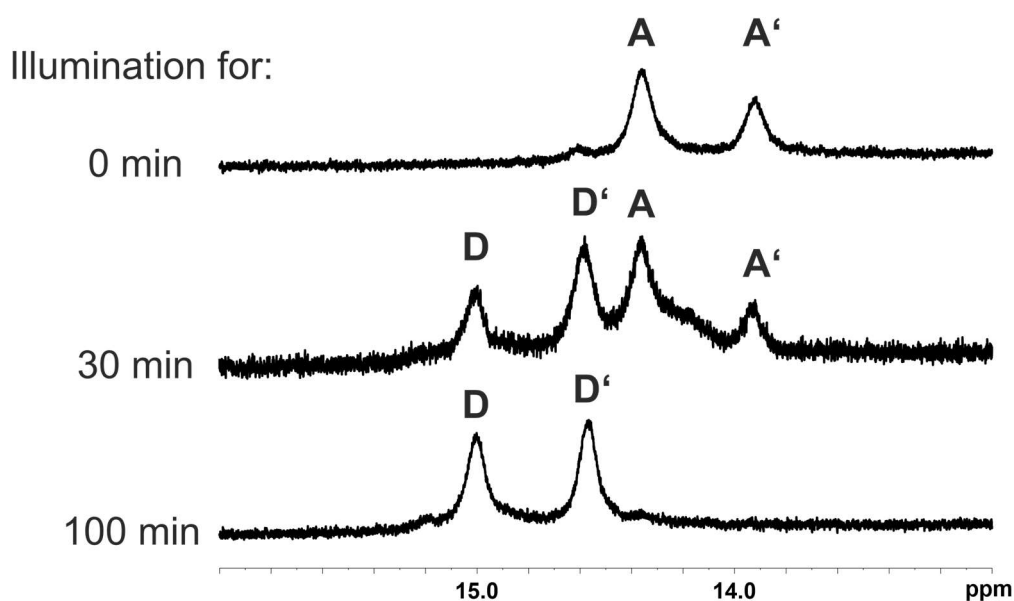


Figure 7: NMR kinetic measurements of **6f** : **7a** : 2,3-dimethylbutadiene at a ratio of 1 : 1 : 20 at an imine concentration of 10 mM in CD_2Cl_2 at 180 K under continuous illumination at 455 K.

In analogy to the measurements for **6f/4a** it is assumed that species D and D' correspond to the CPA/imine complexes featuring a *Z*-configured C=C double bond. Again, the C=N double bond configuration remained elusive. At 180 K, no [2+2] photocycloaddition with the olefin could be observed. Therefore, the temperature was increased to 198 K, where the reaction is still possible (see table S5 of reference^[4]). After heating the sample to 198 K and illuminating it for 30 min, signals for the major species D and D', as well as signals for the minor species A and A' were detectable (see figure 8). Illuminating the sample for 15 hours led to a decrease of these signals, as well as to the build-up of signals E and F. Most likely, these signals correspond to the PO---H-N and PO---H-O hydrogen bonded protons of the complex of catalyst **6f** and the cycloaddition product. Additional formation of new species, especially the **6f/7a** complexes with a C=N *Z*-configured double bond were not observable. However, it was not possible to identify, which of the species D, D', A or A' is primarily converted to the product.

8. Enantioselective [2+2] Photocycloaddition via Iminium Ions: Catalysis by a Sensitizing Chiral Brønsted Acid

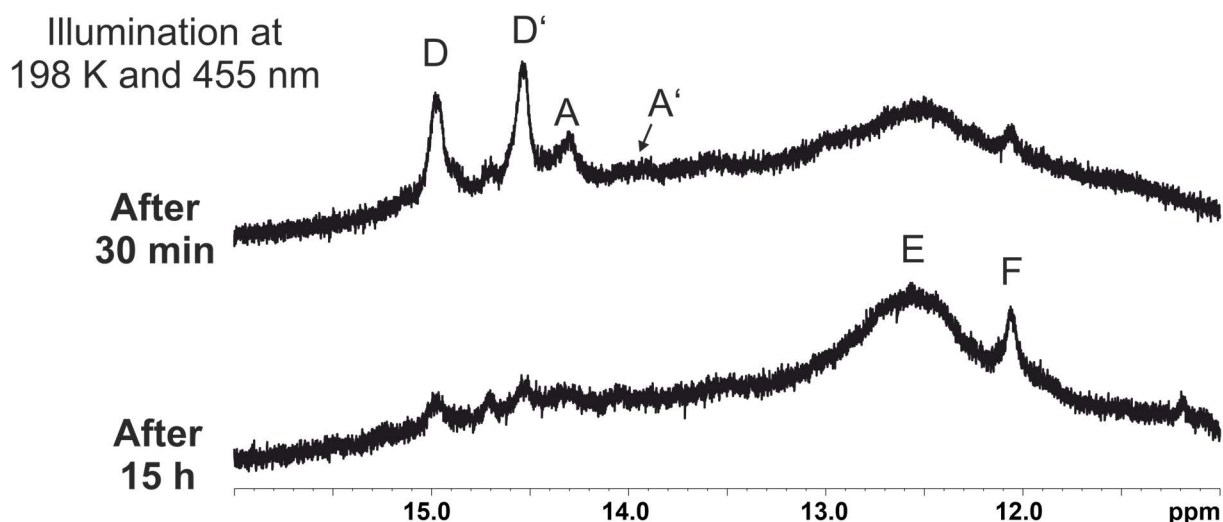


Figure 7: NMR kinetic measurements of **6f** : **7a** : 2,3-dimethylbutadiene at a ratio of 1 : 1 : 20 at an imine concentration of 10 mM in CD₂Cl₂ at 198 K under continuous illumination at 455 K. Before the measurement, the sample was illuminated at 180 K for 100 min (see figure 7).

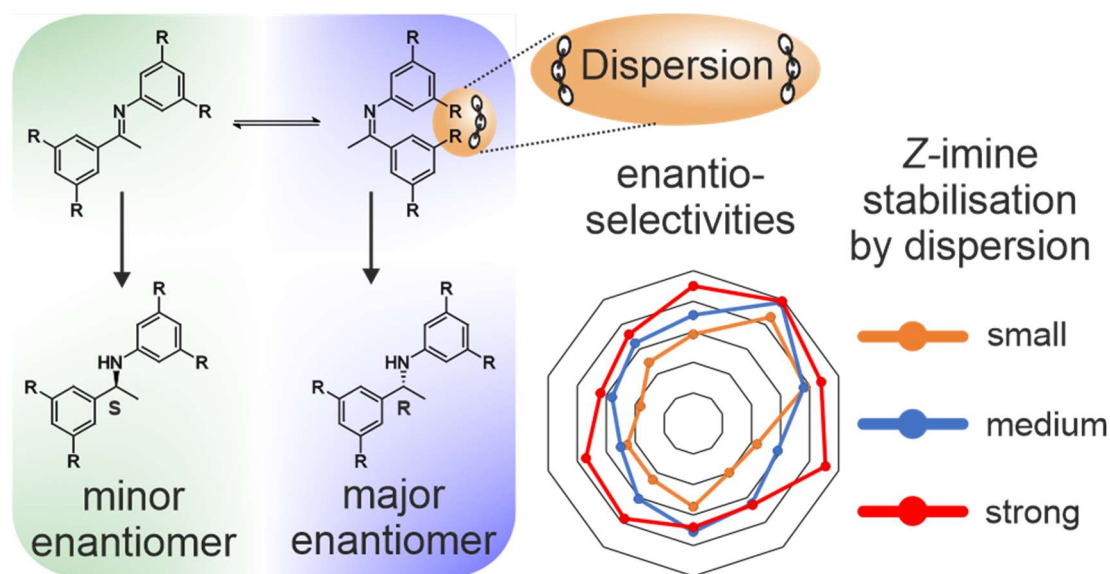
In conclusion, the low temperature illumination NMR studies indicated that for catalyst **6c** isomerization of the C=N double bond is possible. Direct absorption by the substrate allows to form the C=N Z-configured isomer and it was shown, that this process is thermally reversible. In contrast, for catalyst **6f** bearing the thioxanthone photosensitizer unit as 3,3'-substituent, no isomerization of the C=N double bond is observed. Most likely, this is because the light is mainly absorbed by the catalyst and not by the imine, which prevents this direct photoisomerization. However, for catalyst **6f** most likely isomerization of the C=C double bond occurs upon illumination and was found not to be thermally reversible. *E*- and *Z*-isomers of the C=C double bond translate to different diastereoisomers of the product, having either a *trans* or *cis* orientation of the aryl and nitrogen residues respectively. In the reaction, the *trans*-isomer is obtained as the main product, showing that although C=C double bond isomerization can occur under catalytic conditions, it is not significant for the reaction outcome. It can have a minor influence on the reaction yield as it would give a side-product. On the other hand, isomerization of the C=N double bond will not have a direct influence on the stereoconfiguration of the products (the imine is hydrolyzed in the reaction workup). However, C=N double bond isomerization will lead to a different orientation of the imine inside the binding pocket of the catalyst, which will affect the enantiodiscrimination upon cycloaddition with the olefin. Hence, light-driven C=N double bond isomerization of the imine during the reaction will enable more reaction pathways and respective transition states. If these additional C=N Z-imine transition states are close in energy to the *E*-imine ones, lower enantioselectivities are expected. This can explain the significantly lower enantioselectivities obtained for CPAs **6a-e** in combination with a photocatalyst in comparison to only using catalyst **6f**, where no C=N double bond isomerization is possible.

8. Enantioselective [2+2] Photocycloaddition via Iminium Ions: Catalysis by a Sensitizing Chiral Brønsted Acid

8.7.3. References

- [1] C. Feldmeier, H. Bartling, E. Riedle, R. M. Gschwind, *J. Magn. Reson.* **2013**, *232*, 39–44.
- [2] P. Renzi, J. Hioe, R. M. Gschwind, *J. Am. Chem. Soc.* **2017**, *139*, 6752–6760.
- [3] K. Rothermel, M. Melikian, J. Hioe, J. Greindl, J. Gramüller, Matej Žabka, N. Sorgenfrei, T. Hausler, F. Morana, R. M. Gschwind, *Chem. Sci.* **2019**.
- [4] F. Pecho, Y. Sempere, J. Gramüller, F. M. Hörmann, R. M. Gschwind, T. Bach, *J. Am. Chem. Soc.* **2021**, *143*, 9350–9354.

9. Tilting the Balance: London Dispersion Systematically Enhances Enantioselectivities in Brønsted Acid Catalyzed Transfer Hydrogenation of Imines



Johannes Gramüller, Maximilian Franta and Ruth M. Gschwind

J. Am. Chem. Soc. **2022**, *144*, 19861-19871. DOI: 10.1021/jacs.2c07563

A) Johannes Gramüller planned, performed and analyzed all experiments, especially synthesis of all imines, all NMR experiments and all catalytic reactions. He wrote the manuscript with input from Ruth M. Gschwind. B) Maximilian Franta laid the foundation for accessing the ternary complexes and assisted in interpreting the experimental data related to the ternary complex measurements. These experiments were performed by Johannes Gramüller based on the parallel studies of Maximilian Franta on ternary complexes. C) Ruth M. Gschwind contributed to design of experiments, interpretation of data, writing and proof-reading of the manuscript part and provided funding.

Source of this chapter: ACS Publications, <https://doi.org/10.1021/jacs.2c07563>.

Reprinted with permission from [J. Gramüller, M. Franta, R. M. Gschwind, *J. Am. Chem. Soc.* **2022**, DOI: 10.1021/jacs.2c07563]. Copyright [2022] American Chemical Society. Text and figures may differ from the published version. The complete corresponding Supporting Information is provided free of charge online.

9.1. Abstract

London dispersion (LD) is attracting more and more attention in catalysis since LD is ubiquitously present and cumulative. Since dispersion is hard to grasp recent research concentrated mainly on the effect of LD in individual catalytic complexes or on the impact of dispersion energy donors (DED) on balance systems. The systematic transfer of LD effects onto confined and more complex systems in catalysis is still in its infancy and no general approach for using DED residues in catalysis has emerged so far. Thus, on the example of asymmetric Brønsted acid catalyzed transfer hydrogenation of imines we translated the findings of previously isolated balance systems onto confined catalytic intermediates, resulting in a systematic enhancement of stereoselectivity when employing DED substituted substrates. As the imine substrate is present as *Z* and *E* isomer, which can respectively be converted to the *R*- and *S*-product enantiomers, implementing *tert*-butyl groups as DED residues led to an additional stabilization of the *Z*-imine by up to 4.5 kJ/mol. NMR studies revealed that this effect is transferred onto catalyst/imine and catalyst/imine/nucleophile intermediates and that the underlying reaction mechanism is not affected. A clear correlation between *ee* and LD stabilization was demonstrated for 3 substrates and 10 catalysts, allowing to convert moderate-good to good-excellent enantioselectivities. Our findings conceptualize a general approach on how to beneficially employ DED residues in catalysis: They clearly showcase that bulky alkyl residues such as *tert*-butyl groups must not only be considered regarding their repulsive steric, but also their attractive properties even in catalytic complexes.

9.2. Introduction

Although the first examples of Organocatalysis date back to the 19th century,^{1,2} it only manifested itself within the last two decades as the third pillar of asymmetric catalysis besides bio- and metal catalysis. It is now an essential part of an organic chemists toolbox,³ as recently highlighted by awarding the Nobel Prize 2021 to two pioneers in this field. To promote reactivity and shape a stereoinductive environment, organocatalysts often rely on a framework of intermolecular interactions. These feature e.g. Coulomb-, hydrogen bonding-, π - π -, CH- π and van der Waals interactions. London Dispersion (LD), the attractive part of van der Waals interactions originates in spontaneous polarization and induced dipoles. LD is ubiquitously present but frequently neglected due to its hard to pinpoint nature.^{4,5} However, London Dispersion is cumulative over the number of involved atoms and thus can significantly stabilize conformations relevant for catalysis. In recent years, the impact of London Dispersion on structure,^{6–10} bonding,^{11–15} aggregation^{16–21} and reactivity^{22–30} has been more and more explored *in silico* and experimentally. Several molecular balance systems have been employed to quantify London dispersion and to probe solvent effects on it.^{5,31–36} Exemplarily, Wegner *et al.* used *meta*-substituted azobenzenes to probe the balance between steric repulsion and London dispersion attraction for various alkyl substituents (see Figure 1A).³¹ While in the *E*-isomer the substituents of the two fragments are directed away from each other, they come close to each other in the *Z*-isomer. Counterintuitive to purely steric considerations, it was shown that big alkyl substituents such as *tert*-butyl and adamantyl, typically considered only regarding their bulkiness can significantly stabilize the *Z*-azobenzene by London dispersion, effectively overwriting steric repulsion.³¹ Due to the ongoing paradigm shift that London dispersion is not in general negligible, there is an increasing number of studies highlighting the presence and impact of London dispersion interactions in catalysis. Employing a combination of computational analysis/non-covalent interaction analysis and spectroscopic methods, it becomes possible to track down dispersion interactions and elucidate their impact on e.g. stereoselectivities.^{24,25,30} Additionally, these insights allow to further optimize reactions by modulating the respective moieties decisive for dispersion interactions.^{28,37}

However, there are only very few examples where dispersion effects are used in a systematic approach to enhance stereoselectivities in catalysis so far, e.g. given by Schreiner *et al.* for the Corey-Bakshi-Shibata reduction.²⁸ A general approach can be applied to reactions in which the substrate is present as two isomers, whose relative populations can be modulated via dispersion energy donor (DED^{38,39}) substituents. In case one of these isomers is converted into the major, and the other into the minor product stereoisomer via a robust and conserved mechanistic pathway, it should be possible to influence the stereoselective outcome of the reaction by implementing DED residues.

9. Tilting the Balance: London Dispersion Systematically Enhances Enantioselectivities in Brønsted Acid Catalyzed Transfer Hydrogenation of Imines

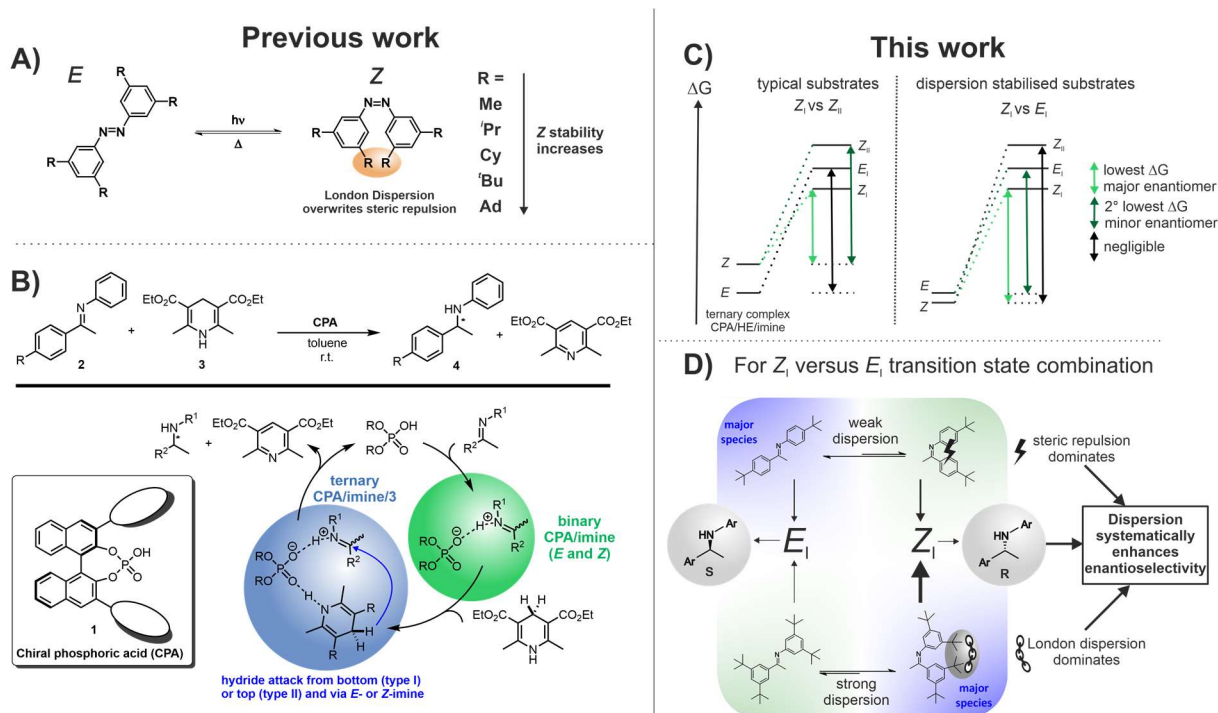


Figure 1: **A)** $E \rightleftharpoons Z$ isomerization of azobenzenes by Wegner *et al.* demonstrated that bigger alkyl substituents significantly stabilize the Z-isomer by London dispersion (adamantyl > ^tBu > cyclohexyl > ⁱPr > Me).³¹ **B)** Transfer hydrogenation of N-aryl imines **2** with Hantzsch Ester **3** catalyzed by chiral phosphoric acids **1** (CPA). Upon complexation by the catalyst, CPA/*E*- and *Z*-imine complexes can be formed and were characterized as hydrogen bond assisted ion pairs. After binding of the Hantzsch ester by an additional hydrogen bond, a ternary CPA/imine/HE complex is formed, in which a hydride and proton are transferred onto the substrate. Four possible transition states E_I , E_{II} , Z_I and Z_{II} were found, where either the *E*- or *Z*-isomer is attacked from bottom (type I) or top (type II) by the nucleophile.^{40–42} **C)** Qualitative representation of transition state energies and activation barrier for the hydride transfer step. For previous substrates **2**, Z_I was found to be the lowest lying transition state, followed by E_I , Z_I and E_{II} (not shown). Through the higher ground state energy for the *Z*-pathway, the Z_I and Z_{II} pathways had the lowest activation barriers (dark green and bright green arrows). Stabilizing the *Z*-imine ground state by London dispersion might lead to a shift of operating transition states to Z_I versus E_I (right side) by increasing the activation barrier for the *Z*-pathway in case the effect of London dispersion is lesser in the transition states. **D)** Exemplarily, for a Z_I versus E_I transition state combination, stabilization of the *Z*-imine *via* dispersion analogously to Wegners *et al.* azobenzene systems³¹ leads to a population increase of the *Z*-intermediates. As the reaction rates of $E \rightleftharpoons Z$ -imine isomerization and hydride transfer were shown to be similar in magnitude, a higher *Z*-imine population will lead to a faster overall reaction rate of the *Z*-pathway, potentially resulting in a systemic enhancement of stereoselectivity.

Analogously, the idea that light driven isomerization can be used to shift the population of systems featuring *E/Z*-double bonds for enhancement of stereoselectivity (and/or reactivity) was previously established by our group in the concept “Decrypting Transition States by Light” (DTS- $h\nu$)⁴⁰ and proved beneficial in catalysis e.g. by Gilmour *et al.*^{43–46} The beauty of light as isomerization stimulus is that the general mechanistic pathway is not affected at all in these light independent reactions. However, the general drawbacks of this approach are fast thermal back-isomerization, relative kinetics of isomerization versus stereoselective reaction step and potential light-induced side reactions. In contrast, using London dispersion energy donor (DED) substituents offers the opportunity to thermodynamically increase the *Z*-isomer population versus *E*-isomer population in a controlled and directed way. This pre-

9. Tilting the Balance: London Dispersion Systematically Enhances Enantioselectivities in Brønsted Acid Catalyzed Transfer Hydrogenation of Imines

vents potential problems with back-isomerization, relative kinetics and induced side reactions. However, typically bulky DED residues such as *tert*-butyl groups can change the relative energy levels within the mechanistic pathway or in extreme cases the mechanistic pathway itself. Therefore, the successful application of DED substituents to enhance stereoselectivities via population changes of e.g. *E/Z*-isomers requires ideally i) a highly conserved structural space of reaction intermediates and transition states independent of the substrate structure, ii) similar energetic effects of the DED substituents on the relevant intermediates and iii) conserved transition state combinations (in case more than two transition states are accessible).

The chiral phosphoric acid **1** (CPA) catalyzed transfer hydrogenation of *N*-aryl substituted imines **2**, which we extensively studied in our previous research^{40,47–51} is promising in meeting these criteria (see Figure 1B for reaction mechanism). For the binary CPA/imine complexes, composed of catalyst **1** and imine **2** we showed an extremely stable structural space independent of the substituent pattern of CPA or imine,^{48,50} due to the strong hydrogen bond acting as a structural anchor.⁴⁷ In the subsequent ternary CPA/imine/Hantzsch ester complexes and following transition states of the hydride transfer an additional hydrogen bond to the Hantzsch ester **3** was proposed and calculated. This supports the assumption of stable structural spaces also in these stages of the mechanism.^{40–42} The existence of this second hydrogen bond was experimentally confirmed on the example of analogous disulfonimide Brønsted acid catalysts.⁵² Within this confined ternary CPA/imine/Hantzsch ester complex, the hydride is transferred onto the imine substrate. This stereo determining step can proceed via four different transition states (Z_I , Z_{II} , E_I and E_{II}), featuring either the *E*- or *Z*-imine or transfer from the bottom (type I) or top (type II). Goodman *et al.* proposed in his seminal calculations a Z_I vs. E_I transition state combination for obtaining the major and minor product enantiomer respectively. Thus, ideal conditions should be given for the enhancement of enantioselectivities via *Z*-isomer stabilization using dispersion energy donors. Theoretical calculations of the relative transition state energies by our group confirmed the Z_I vs. E_I combination to be the lowest energy transition states (see Figure 1C).⁴⁰ However, this analysis only accounted for the relative transition state energies and not the respective activation barriers for the hydride transfer steps. Thus, an experimental analysis of the transition state combinations using “Decrypting Transition States by Light” (DTS-hv) revealed a Z_I versus Z_{II} pathway.⁴⁰ Theoretical calculations revealed that the high energy difference between the *E*- and *Z*-configuration in combination with a high isomerization barrier can explain this offset (see Figure 1C).

Dispersion energy donors as substituents now offer in principle the potential to modulate these *E/Z*-imine energy differences. In case a *Z* versus *E* transition state combination can be reached (e.g. via similar energies of *E* and *Z* isomers; see Figure 1C) an enhancement of the enantioselectivities by in-

9. Tilting the Balance: London Dispersion Systematically Enhances Enantioselectivities in Brønsted Acid Catalyzed Transfer Hydrogenation of Imines

creasing the *Z*-imine population should be possible (see Figure 1D). The reaction rates for imine isomerization and hydride transfer are assumed to be in a similar order of magnitude. Hence, an increased *Z*-imine population could lead to a faster overall reaction rate of the *Z*-pathway compared to the *E*-pathway, resulting in higher enantioselectivities. In this work, an experimental approach was preferred to validate this hypothesis, since there are severe difficulties to theoretically reproduce the energetics of the experimental *E:Z* ratios of CPA/imine complexes as mechanistic intermediates.⁵⁰

Thus, in this work *tert*-butyl groups are used as dispersion energy donor substituents to boost the relative population of *Z*-imines in a CPA catalyzed transfer hydrogenation in order to enhance enantioselectivities. The effect of *tert*-butyl groups on the *E/Z* ratios of the free imines and the subsequent binary and ternary complex intermediates is investigated. Finally, the effect of DED substituents on the enantioselectivities for three imines and twelve catalysts is elucidated, showing a systematic increase of enantioselectivity with increasing dispersion effects.

9.3. Results and Discussion

9.3.1. Accessing *Z*-imine populations via CEST

Initially, it was necessary to stabilize the *Z*-imines by London dispersion and quantify the effect by comparing it to imines without such intramolecular London dispersion interactions. However, in our previous work we found that imines such as **2a** (see Figure 2) are predominantly present as their *E*-isomer and no additional set of signals was identified by ¹H-NMR for the *Z*-imine.⁴⁸ Low sensitivity is one major limitation of NMR-spectroscopy but certain methods can enhance the detection limit. If two different molecules (e.g. *E*-imine and *Z*-imine) are exchanging slow on the NMR-timescale (i.e. there are two different sets of NMR signals), a signal of the low populated exchange partner can be selectively saturated. This leads to a decrease in signal intensity of the respective signal of the major exchange partner as the saturation is transferred by chemical exchange. This approach is called chemical exchange saturation transfer (CEST)^{53,54} and can increase sensitivity by a factor of $\sim 10^{55,56}$ as now not the build-up of a small signal is monitored, but the decrease of a signal with good signal/noise ratio.

9. Tilting the Balance: London Dispersion Systematically Enhances Enantioselectivities in Brønsted Acid Catalyzed Transfer Hydrogenation of Imines

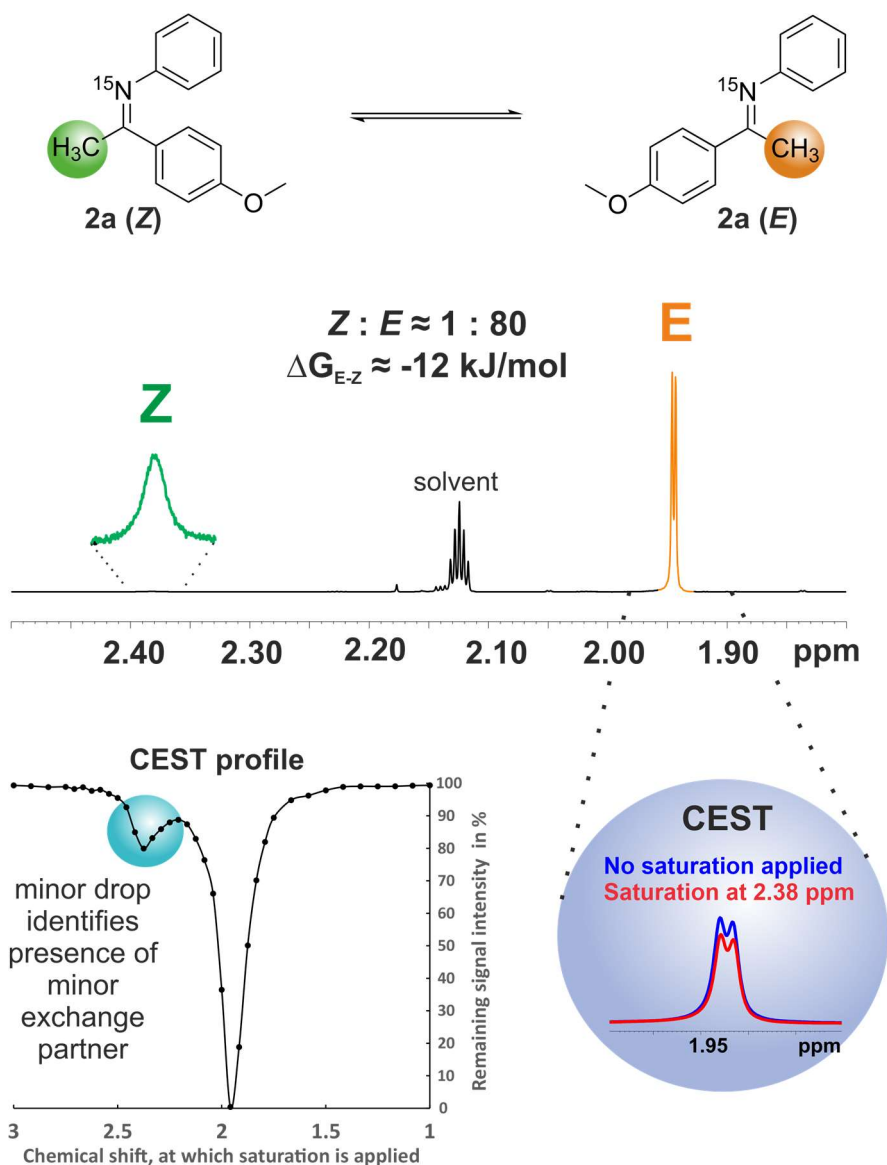


Figure 2: $E \rightleftharpoons Z$ equilibrium of imine **2a** and section of the ^1H NMR spectrum of **2a** at 330 K in toluene- d_8 . If a selective saturation is applied on the $\alpha\text{-CH}_3$ signal of $Z\text{-2a}$ at 2.38 ppm, a decrease in signal intensity of the $\alpha\text{-CH}_3$ signal of $E\text{-2a}$ at 1.94 ppm is observed due to chemical exchange saturation transfer (bottom right). Sweeping the saturation offset in 50 Hz increments allows to identify the chemical shift of the minor exchange partner (bottom left).

As a proof of concept, we applied CEST NMR to the $\alpha\text{-CH}_3$ group of ^{15}N labelled imine **2a**. Due to the $^3J_{\text{HN}}$ coupling, the $\alpha\text{-CH}_3$ shows doublet splitting and thus can be easily recognized. The saturation offset was swept in 25 and 50 Hz steps between 1.00 and 3.00 ppm and the decrease in signal intensity of the E -imine $\alpha\text{-CH}_3$ compared to a reference spectrum was monitored. Thus, a CEST profile (see Figure 2) could be obtained showing two distinct drops in intensity. The main decrease of signal intensity is observed if the saturation is applied close to the monitored signal of the E -imine $\alpha\text{-CH}_3$ group. The second, minor drop is observed if the saturation is applied at the chemical shift of the minor exchange partner ($Z\text{-2a}$). This identifies the signal belonging to the Z -imine $\alpha\text{-CH}_3$ group and is further corroborated by a $^3J_{\text{NH}}$ doublet splitting observed at lower temperatures. Based on the $Z : E$ integral ratio of \approx

9. Tilting the Balance: London Dispersion Systematically Enhances Enantioselectivities in Brønsted Acid Catalyzed Transfer Hydrogenation of Imines

1:80, an energetic difference ΔG_{E-Z} of $\approx -12.0 \pm 0.3$ kJ/mol favoring the *E*-imine was determined (see SI for error estimation). Modulating the electronic properties of the imine by replacing the $-\text{OCH}_3$ group of **2a** with $-\text{CH}_3$, $-\text{CF}_3$ or $-\text{NO}_2$ did not show any significant change on the *Z* : *E* integral ratios (*Z* : *E* \approx 1:60 / 1:78 / 1:66 respectively; see SI Figure S1 for CEST profiles).

After this proof of principle we focused on elucidating if the *Z*-imine can be significantly stabilized via intramolecular dispersion interaction similar to Wegners *et al.*³¹ azobenzene systems or if steric repulsion between the bulky dispersion energy donor (DED) groups would be dominant. Hence, imines **2b-d** with ^tBu-groups in *para*- and/or *meta*- position were selected to increase the putative dispersion interactions in the *Z*-imine while retaining steric and electrostatic properties as closely as possible. For all imines, the *E*-imine was the major populated species and the *Z*-imine was identified by ¹H CEST NMR as the minor exchange partner (see Figure 3). *Z* : *E* ratios in toluene at 330 K of 1 : 70, 1 : 46 and 1 : 14 were determined for imines **2b-d**, reflecting an energetic difference ΔG_{E-Z} of $\approx -11.7 \pm 0.3$ / -10.5 ± 0.2 / -7.2 ± 0.1 kJ/mol respectively.

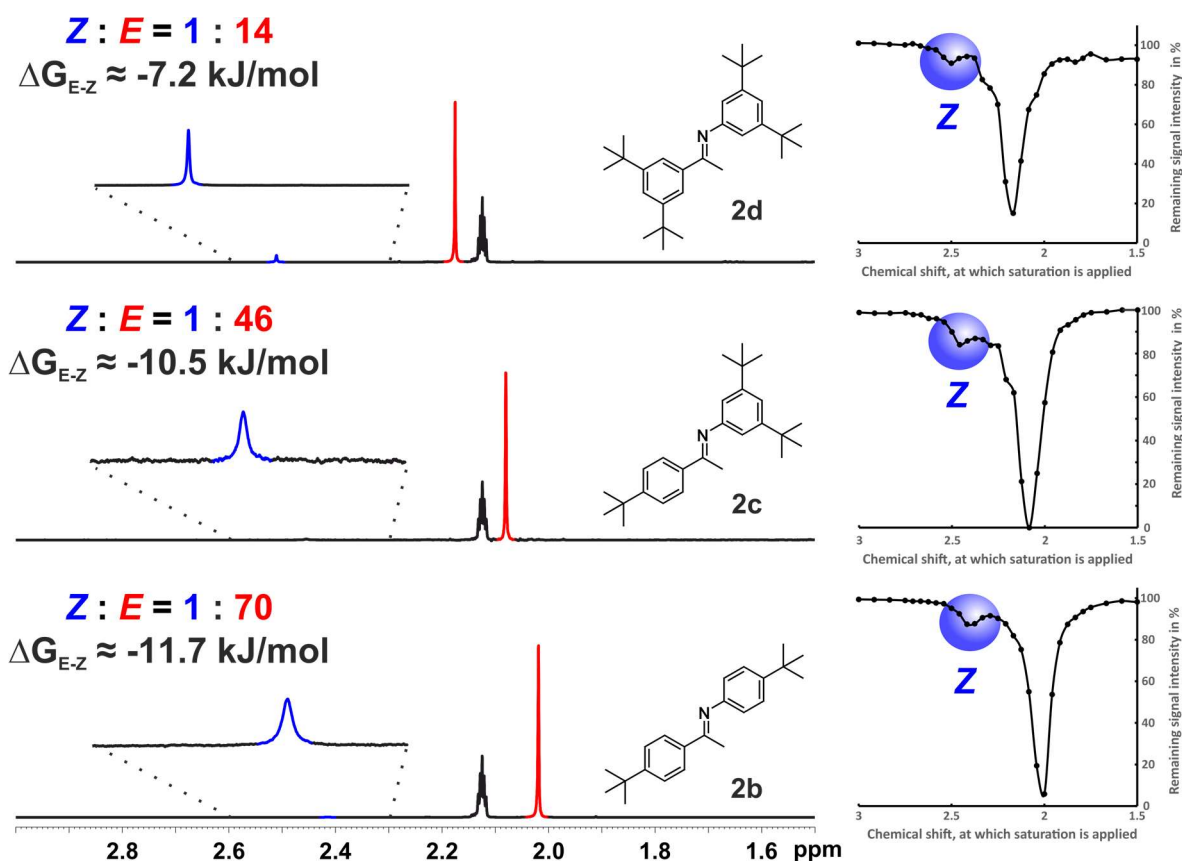


Figure 3: Excerpts of the ¹H spectra of imines **2b-d** in toluene-*d*₈ at 330 K and 600 MHz, showing an increasing population of the *Z*-imine with an increasing number of ^tBu-residues. The *Z*-imine was identified via CEST NMR plots (right), elucidating the minor exchange partner (blue circle) of the *E*-imine.

Imine **2b** shows a similar *Z*/*E* ratio to **2a** (and to the $-\text{CH}_3$, $-\text{CF}_3$ or $-\text{NO}_2$ substituted analogues depicted in the SI Figure S1), highlighting that for *para*-substitution the putative effect of the DED groups is

9. Tilting the Balance: London Dispersion Systematically Enhances Enantioselectivities in Brønsted Acid Catalyzed Transfer Hydrogenation of Imines

negligible as the substituents are too far away in the *Z*-isomer to interact. For imine **2c**, a slightly higher *Z/E* ratio was observed, reflecting a stabilization of $\Delta\Delta G_{2c-2b} = 1.2\pm 0.3$ kJ/mol introduced by the *meta*-substitution pattern. For imine **2d**, the highest *Z/E* ratio was monitored, accounting for a $\Delta\Delta G_{2d-2b} = 4.5\pm 0.4$ kJ/mol, if DED groups are placed in all *meta* positions. This clearly shows that the attractive dispersion interactions introduced by the ^tBu groups is overwriting the steric repulsion between these groups in the *Z*-imine, corroborating the findings by Wegner *et al.*³¹ on *meta*-substituted azobenzene systems. Additionally, the stabilization by the all-*meta* substitution pattern is similar in magnitude, but slightly smaller as for a diarylthiourea balance systems ($\Delta\Delta G = 4.5$ kJ/mol for the imine balance and 7.1 kJ/mol for the thiourea balance when comparing *tert*-butyl groups to hydrogen atoms in all *meta*-positions).⁵⁷

Replacing the α -CH₃ group of imine **2d** with α -H led to an exclusive population of the *E*-imine, as the steric size of the α -substituent is the main driving force towards the *Z*-imine (see SI Figure S2 for ratios and CEST profile). Replacing the *N*-phenyl with a *N*-benzyl residue resulted in an even higher stabilization of the *Z*-imine for both α -CH₃ and α -H (1 : 13 and 1 : 28 respectively), presumably due to less steric hindrance and a better interaction pattern in the *Z*-imine (see SI Figure S2 for systems, spectra and further discussion). These findings suggest that the beneficial effect of DED substituents on stereoselectivities as described below can be transferred onto analogous *N*-benzyl systems, frequently used in synthesis.

9.3.2. London dispersion in CPA/*N*-aryl imine complexes

In our previous work, we observed that although imines such as **2a** are present predominantly as their *E*-isomer (*Z:E* ratio ~ 1 : 80), the population of the *Z* imine is significantly enhanced in hydrogen bonded CPA/imine complexes. These are formed in presence of a chiral phosphoric acid and *Z:E* ratios up to ~ 55 : 45 are reached.^{48,50} This is caused by a more compact structure of the *Z*-imine, allowing it to fit into the binding pocket of the CPA with reduced steric repulsion between CPA and imine compared to the *E*-imine. Hence, we needed to control whether the stabilization of *Z*-imines by intramolecular London dispersion is transferred on the binary CPA/imine complexes (and subsequently on the ternary CPA/imine/nucleophile complexes and transition states). To validate this, detailed low temperature (180 K) NMR studies were performed. Such low temperatures are necessary to slow down exchange processes between different species (e.g. the isomerization of *E*- and *Z*-imine in presence of a CPA) and to monitor the proton signals corresponding to the hydrogen bonds anchoring the binary complex. Dichloromethane (CD₂Cl₂) was selected as solvent for all measurements, as it provided superior line widths and solubility in our previous investigations.⁴⁸ No significant changes of the stabilization of *Z*-

9. Tilting the Balance: London Dispersion Systematically Enhances Enantioselectivities in Brønsted Acid Catalyzed Transfer Hydrogenation of Imines

2b-d were observed when changing the solvent from toluene to dichloromethane (see SI Figure S5). For all samples, a ratio of catalyst to imine of 1 : 1 was used and the concentration typically ranged from 10 to 50 mM.

Binary complex samples of CPAs **1a-c** and imines **2b-d** were prepared and analyzed (see Figure 4 and SI Figure S6). The assignment of *Z*- and *E*-complex was achieved via NOESY NMR and the typically observed slight highfield shift of the hydrogen bond signal of CPA/*E*-imine compared to the CPA/*Z*-imine.^{47,48} Exemplarily for **1a/2b-d**, *Z*:*E* ratios of 55:45, 70:30 and 90:10 were determined. This reveals an increasing stabilization of the *Z*-complexes with increasing number of ^tBu groups and reflects the general trend for free imines **2b-d**. Similar trends were observed for CPAs **1b** and **1c** (see Table 1), reaching an almost *Z*-exclusive ratio of 99:1 for **1c/2d**. For the systems **1a/2d** and **1b/2d** a set of 2D spectra was measured to achieve a chemical shift assignment for **1a/Z-2d** and **1b/Z-2d**. Based on an analysis of the NOESY spectra, the characteristic NOE contacts between BINOL backbone and imine fragments were detected, ensuring that the core structures of CPA/*Z*-imine complexes elucidated in our previous work are conserved (for structures see references^{48,50}).

9. Tilting the Balance: London Dispersion Systematically Enhances Enantioselectivities in Brønsted Acid Catalyzed Transfer Hydrogenation of Imines

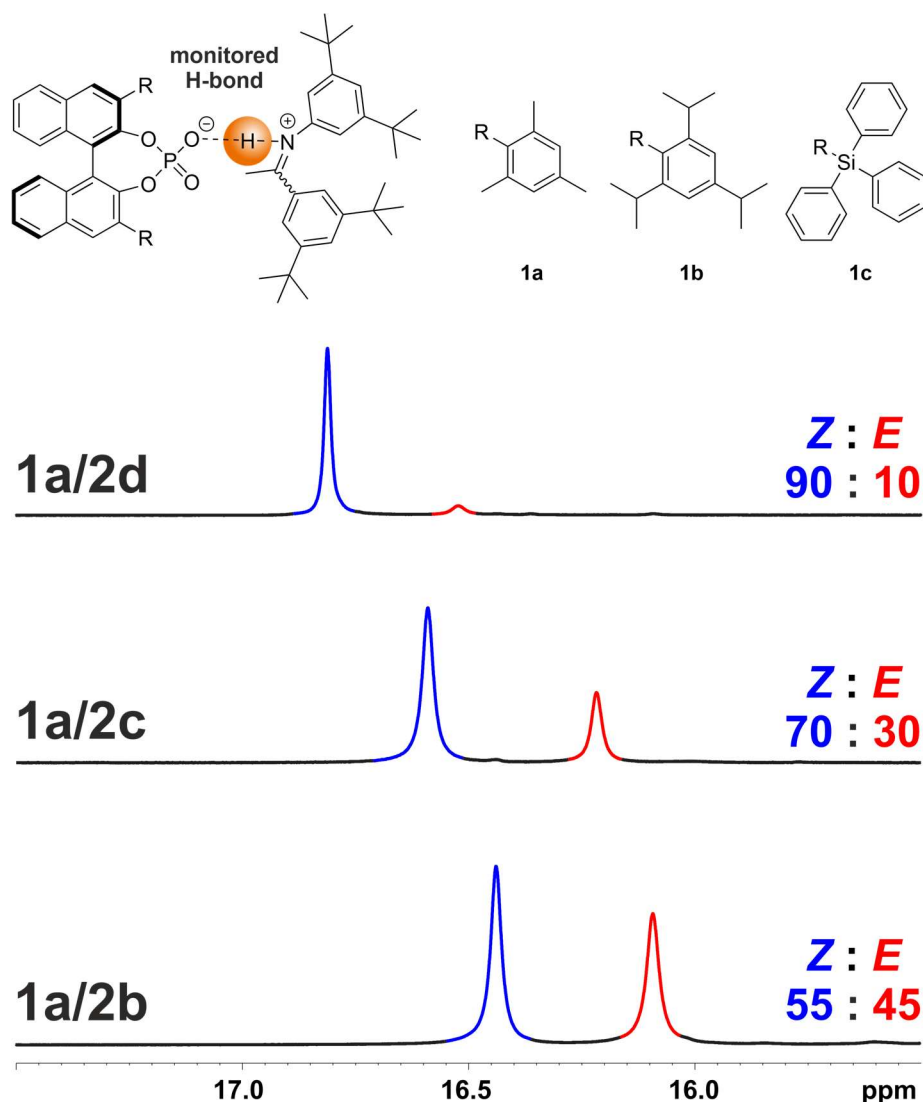


Figure 4 Excerpt of the ^1H NMR spectra of **1a/2b-d** in CD_2Cl_2 at 180 K and 600 MHz depicting the hydrogen bonding region, highlighting the H-bond signal of **1a/Z-2b-d** (blue) and **1a/E-2b-d** (red). When increasing the number of ^tBu groups from **2b** to **2c** to **2d**, an increasing stabilization of the **1a/Z-imine** complex is observed, reflecting the trend of free imines **2b-d** (for spectra with **1b** and **1c** see SI Figure S6).

Based on the determined Z/E ratios, the energetic differences ΔG_{E-Z} for free imines **2b-d** at 330 K in toluene (values in dichloromethane at 298 K are similar; see SI Figure S5) and **1a-c/2b-d** at 180 K in dichloromethane were determined. To shed light onto the contribution of intramolecular London dispersion on the stabilization of the CPA/ Z -imine complex, $\Delta\Delta G_{2d-2c}$ and $\Delta\Delta G_{2d-2b}$ were derived (see Table 1). Assuming similar structures for **1a-c/2b-d**,⁵⁰ these $\Delta\Delta G$ values to some extent account for the effect of intramolecular London dispersion. However, these are modulated by the different interaction patterns of imines **2b-d** with the respective catalyst and the steric repulsion introduced by additional ^tBu groups.

Comparing the $\Delta\Delta G$ values of the binary complexes to the free imines (see Table 1) shows an identical trend (Z -stability: **2d** > **2c** > **2b**) and similar magnitude, giving slightly lower $\Delta\Delta G$ values for catalysts **1a**

9. Tilting the Balance: London Dispersion Systematically Enhances Enantioselectivities in Brønsted Acid Catalyzed Transfer Hydrogenation of Imines

and **1b** and slightly higher $\Delta\Delta G$ values for catalyst **1c**. These small offsets reflect the different intermolecular interaction pattern between CPA and imine for the CPA/*Z*-imine and CPA/*E*-imine complexes including intermolecular dispersion and steric. Additionally, the imine inside the binding pocket is partially sequestered from the solvent, while the free imine is solvent-exposed. This change in solvent-solute interaction pattern might modulate the *Z/E* ratios, but the difference is expected to be by far smaller than between vacuum and solution as shown for H-bond complexes by Chen *et al.*³⁶ However, the $\Delta\Delta G$ values for free imines and CPA/imine complexes are very similar, clearly indicating that the stabilization of the *Z*-imine via intramolecular London dispersion is transferred on the binary catalyst/substrate complexes. This is further corroborated by the detection of NOE contacts between the *tert*-butyl groups of the two aryl moieties in the NOESY spectrum of **1a/Z-2d** (see SI figure S6). This validates a spacial proximity of the *tert*-butyl groups and thus strongly suggests the presence of intramolecular dispersion interactions between these groups even inside the CPAs binding pocket.

Table 1: Comparison of *Z/E* ratios of **2b-d** at 330 K in toluene and **1a-c/2b-d** at 180 K in CD₂Cl₂.

	<i>Z/E</i> ratio for CPA/imine			$\Delta\Delta G$ [kJ/mol]	
	2b	2c	2d	2d-2b	2d-2c
no CPA	1:70	1:46	1:14	4.5±0.4	3.3±0.3
1a	55:45	70:30	90:10	3.0±0.2	2.0±0.2
1b	n.d.	75:25	89:11	n.d.	1.5±0.2
1c	48:52	73:27	99:1	5.9±0.3	4.3±0.3

For **1b/2b**, the *Z/E* ratio could not be determined precisely due to signal overlap, but a preference for the **1b/Z-2b** complex is assumed. Based on the ratios, the energetic differences ΔG_{E-Z} between *E* and *Z* were determined and the difference $\Delta\Delta G_{2d-2b} = (\Delta G_{E-Z}(\mathbf{2d}) - \Delta G_{E-Z}(\mathbf{2b}))$ and $\Delta\Delta G_{2d-2c} = (\Delta G_{E-Z}(\mathbf{2d}) - \Delta G_{E-Z}(\mathbf{2c}))$ was determined. Assuming similar structures for **1a-c/2b-d**, the $\Delta\Delta G$ values give qualitative insights about the contribution of intramolecular London dispersion towards the stabilization of the CPA/*Z*-imine complex, showing that the contribution in the free imine (no CPA) is in the same range as for the binary complexes with CPAs **1a-c**.

Noteworthy, for an analogous system to **2d** featuring an N-benzyl instead of N-phenyl substituent, similar results were obtained, leading to an inversion of *Z/E* preference by London dispersion (see SI Figure S4 and Table S1 for spectra, ratios and further discussion). This further corroborates the assumption that the beneficial effect of DED residues on stereoselectivities as described below can be transferred onto analogous N-benzyl systems, hinting a broader applicability for different substrates.

9.3.3. London dispersion in CPA/imine/nucleophile complexes

After demonstrating that London dispersion significantly affects the *Z/E* ratios in binary CPA/imine complexes, next we aimed to ensure that the same applies for ternary CPA/imine/nucleophile complexes. The ternary complexes are spectroscopically accessible precursors to the transition states for the hydride transfer. More importantly, it is necessary to ensure that the ternary complex can still be

9. Tilting the Balance: London Dispersion Systematically Enhances Enantioselectivities in Brønsted Acid Catalyzed Transfer Hydrogenation of Imines

formed despite the bulky substrate occupying the binding pocket of the catalyst., This ensures that the underlying reaction mechanism proceeding via the “three-point-interaction model” is still available.⁴¹ Exemplarily, Hantzsch ester **3a** was selected as a model nucleophile, as the CPA catalyzed transfer hydrogenation is well optimized and deeply investigated *in silico*.^{40–42} Computational studies showed that the transition states feature a ternary complex in which both the imine and Hantzsch ester are bound to the catalyst via hydrogen bonding. However, accessing ternary CPA/imine/**3a** complexes by NMR spectroscopy is not achievable due to the reactivity of this mixture and mainly due to the low solubility of **3a** in the necessary solvents like toluene or dichloromethane, especially at lower temperatures (-93 °C) needed for detailed investigations. This can be overcome by employing the phenyl-substituted Hantzsch ester **3b** as an unreactive and well soluble mimic of **3a**.⁵² Additional ¹⁵N labelling allows to access the PO---H-¹⁵N(**3b**) hydrogen bond via ¹H_{NH} coupling.

Addition of one equivalent of **3b** to **1a-b/2d** led to line broadening (half widths increase by ~10 Hz for **1a**, ~15 Hz for **1b**) and a significant highfield shift (~0.2 ppm) of the hydrogen bonded proton signal (see Figure 5A). No new additional set of signals for the ternary CPA/**2d/3b** complex was observed. This indicates that the binary CPA/**2d** and ternary CPA/**2d/3b** complex are exchanging fast on the NMR time scale and one averaged signal set is observed for both species. This is further corroborated by severe line broadening of the signals of **3b** in presence of **1a** or **1b** and **2d**. Noteworthy, the strong preference for Z-intermediates observed for the binary complexes is also present for the ternary complexes leading to an almost exclusive population of the Z-species (see Figure 5A). This further highlights the transfer of dispersion interactions within the imine onto the highly confined ternary intermediates. To further corroborate the formation of the ternary complex, system **1d/2d/3b** was selected and investigated in detail as the spectra with this catalyst were better resolved, giving narrower line widths and less signal overlap (see Figure 5B). Only one species was observed, corresponding to the binary **1d/Z-2d** and ternary **1d/Z-2d/3b** complex which are fast exchanging on the NMR time scale. Based on a set of homo- and heteronuclear spectra featuring ¹H, ¹³C, ¹⁹F, ³¹P, ¹H ¹H COSY, ¹H NOESY, ¹H ¹³C HSQC, ¹H ¹³C HMBC, ¹H ³¹P HMBC and ¹H ¹⁹F HOESY, a chemical shift assignment could be achieved. The Z-imine configuration was determined via the NOE pattern of the hydrogen bonded proton and α-CH₃ group. Analysis of the ¹H NOESY (see SI Figure S7) and ¹H ¹⁹F HOESY spectra showed NOE contacts between **3b** and **1d** and especially between **3b** and **2d**, which only can originate from the ternary complex (see Figure 5C),⁵² thus validating that indeed the ternary **1d/2d/3b** complex is formed.

9. Tilting the Balance: London Dispersion Systematically Enhances Enantioselectivities in Brønsted Acid Catalyzed Transfer Hydrogenation of Imines

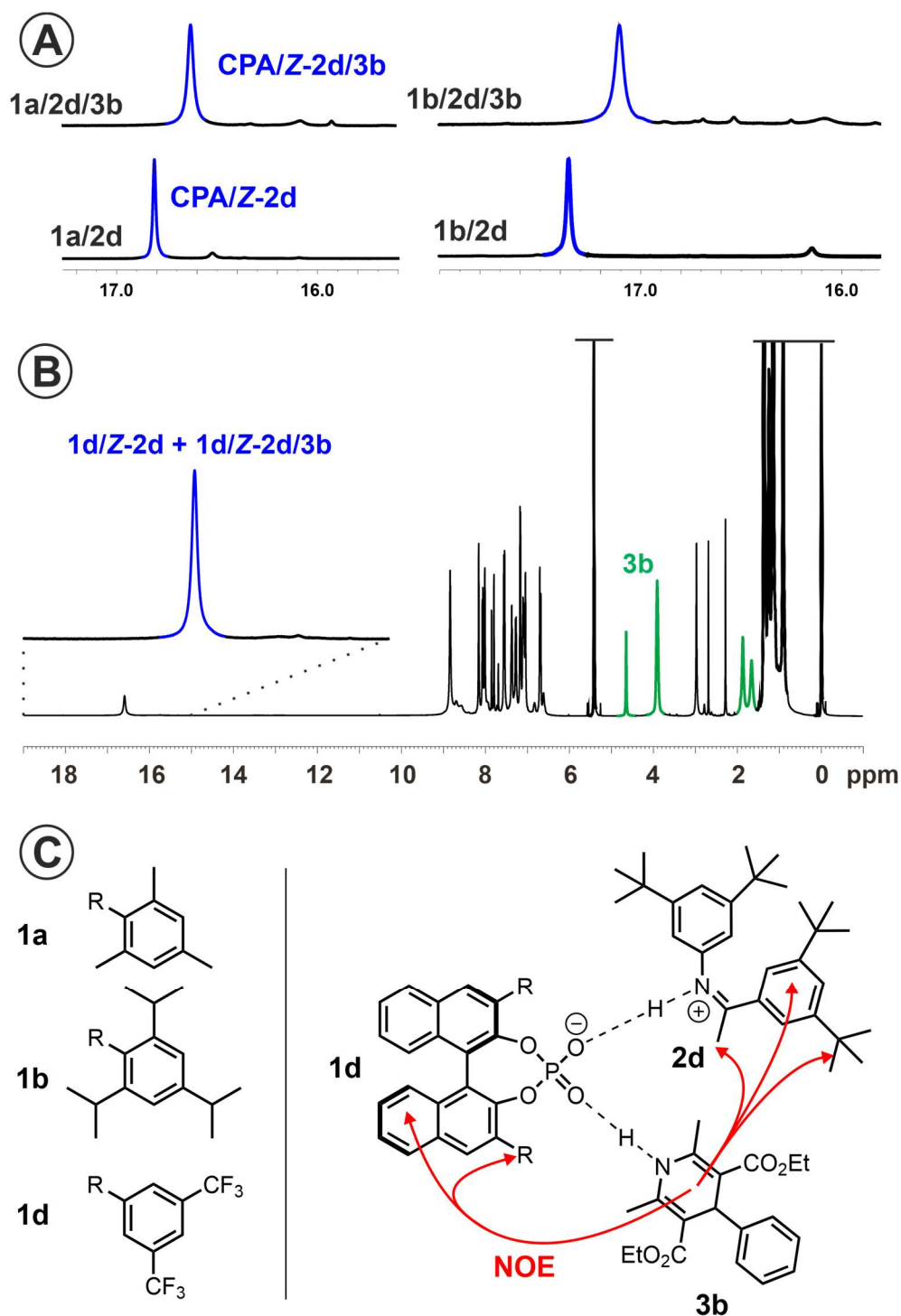


Figure 5: A) Excerpt of the ^1H NMR spectra of **1a-b/2d** and **1a-b/2d/3b** at a 1:1 or 1:1:1 ratio in CD_2Cl_2 at 180 K and 600 MHz depicting the hydrogen bonding region. Addition of **3b** causes line broadening and a highfield shift of the hydrogen bonded proton signal, indicating a fast exchange process of the binary CPA/**2d** and ternary CPA/**2d/3b** complex. B) ^1H spectrum of **1d/2d/3b** at a 1:1:1 ratio in CD_2Cl_2 at 180 K and 600 MHz. One set of signals is observed for the fast exchanging binary **1d/2d** and ternary **1d/2d/3b** complex. C) Observed NOE pattern for **1d/2d/3b** demonstrating the presence of the ternary complex.

To estimate, whether the system is present mainly as binary complex and free **3b** or mainly as ternary complex, diffusion ordered spectroscopy (DOSY) measurements were carried out to determine self-diffusion coefficients D_i for **1a/b/d**, **2d** and **3b**. If DOSY measurements are performed on a signal which

9. Tilting the Balance: London Dispersion Systematically Enhances Enantioselectivities in Brønsted Acid Catalyzed Transfer Hydrogenation of Imines

reflects two fast exchanging species, the resulting self-diffusion coefficient is the sum of the self-diffusion coefficients of each species weighed by their population.⁵⁸ Hence, if the two exchanging species have a significant offset in size (e.g. free Hantzsch ester and complexed one), the derived self-diffusion coefficient gives qualitative insights about the dominant species. For all systems, CPA and imine showed identical self-diffusion coefficients, while for **3b** slightly higher values (smaller aggregate) were determined (see SI Table S2 for values and further discussion). However, D_i for free **3b** (in absence of CPA and imine) was significantly higher. In combination with the observed line broadening and NOE pattern this clearly shows that despite the increased steric bulk of the imine **2d**, the ternary complex can still be formed in a significant amount. Thus, the general reaction mechanism is conserved and the clear preference for *Z*-intermediates for imines with dispersion energy donor substituents is present in the ternary complexes as precursors to the transition states for the hydride transfer. Noteworthy, by employing Hantzsch ester **3b** it was to our knowledge for the first time possible to access by NMR-spectroscopy ternary complexes with CPA catalysts despite the use of a bulky substrate **2d**.

9.3.4. Impact of London dispersion on enantioselectivity

We demonstrated the impact of London dispersion on the stabilization of *Z*-imines and ensured the transfer on catalyst/substrate and catalyst/substrate/nucleophile reaction intermediates. Based on these findings we aimed to showcase that this additional stabilization can affect the stereoselective outcome of CPA catalyzed transformations on the example of transfer hydrogenations with Hantzsch ester **3a**. Theoretical calculations of Goodman⁴¹ and our group⁴⁰ showed that the lowest energy transition state is Z_i (attack from bottom; *Z*-imine) followed by E_i (attack from bottom; *E*-imine). In case the *Z*-imines and their intermediates are equal in energy or lower than the *E*-imines, this Z_i/E_i transition state combination should be operative (see Fig. 1C). Thus, stabilizing the *Z*-imine via dispersion and increasing the populations of the *Z*-imine and all subsequent *Z*-imine intermediates (binary CPA/*Z*-imine and ternary CPA/*Z*-imine/Hantzsch ester complex) can have a beneficial effect on the stereoselectivity. Previously, it was shown that the imine isomerization is not fast compared to the hydride transfer,⁴⁹ meaning that an increased population of CPA/*Z*-imine/Hantzsch ester will result in an increased overall reaction rate of the hydride transfer for the *Z*-pathway compared to the *E*-pathway. Additionally, the effect of London dispersion on stabilizing the *Z*-imine could also contribute in a beneficial way to the relative transition state energies of the hydride transfer. Dispersion could reduce the activation barrier for the *Z*-pathway compared to the *E*-pathway without changing the transition state combination. Thus, stabilizing the *Z*-imine via London dispersion could lead to a systematic increase in enantioselectivities by kinetically and potentially also thermodynamically favoring the *Z*-pathway for the hydride transfer step. Given the previous offsets between experimental and computed ground

9. Tilting the Balance: London Dispersion Systematically Enhances Enantioselectivities in Brønsted Acid Catalyzed Transfer Hydrogenation of Imines

state energies for binary complexes⁵⁰ and inadequate description of dispersion attenuation in solution by current implicit solvent models,³⁶ we preferred an experimental approach to ensure the necessary *Z* versus *E* transition state competition. If a clear correlation between stereoselectivity and dispersion stabilization is observed over a broad set of catalysts, a *Z* versus *E* transition state competition can be assumed. This is because the increase in enantioselectivity should be rather independent of the catalysts 3,3'-substituents and mainly be enforced by the dispersion energy donor residues. Hence, to pinpoint the applicability of utilizing dispersion interactions to enhance stereoselectivities, transfer hydrogenations of substrates **2b-d** with a series of 12 different catalysts were performed (see Figure 6). Imines **2b-d** were selected to modulate the contribution of intramolecular London dispersion on the *Z*-imine stability while conserving the steric and electrostatic properties of the imine as much as possible. CPAs **1a-k** were selected as examples typically used in synthesis and disulfonimide (DSI) catalyst **1l** was selected to account for modulations of the acidic functionality.

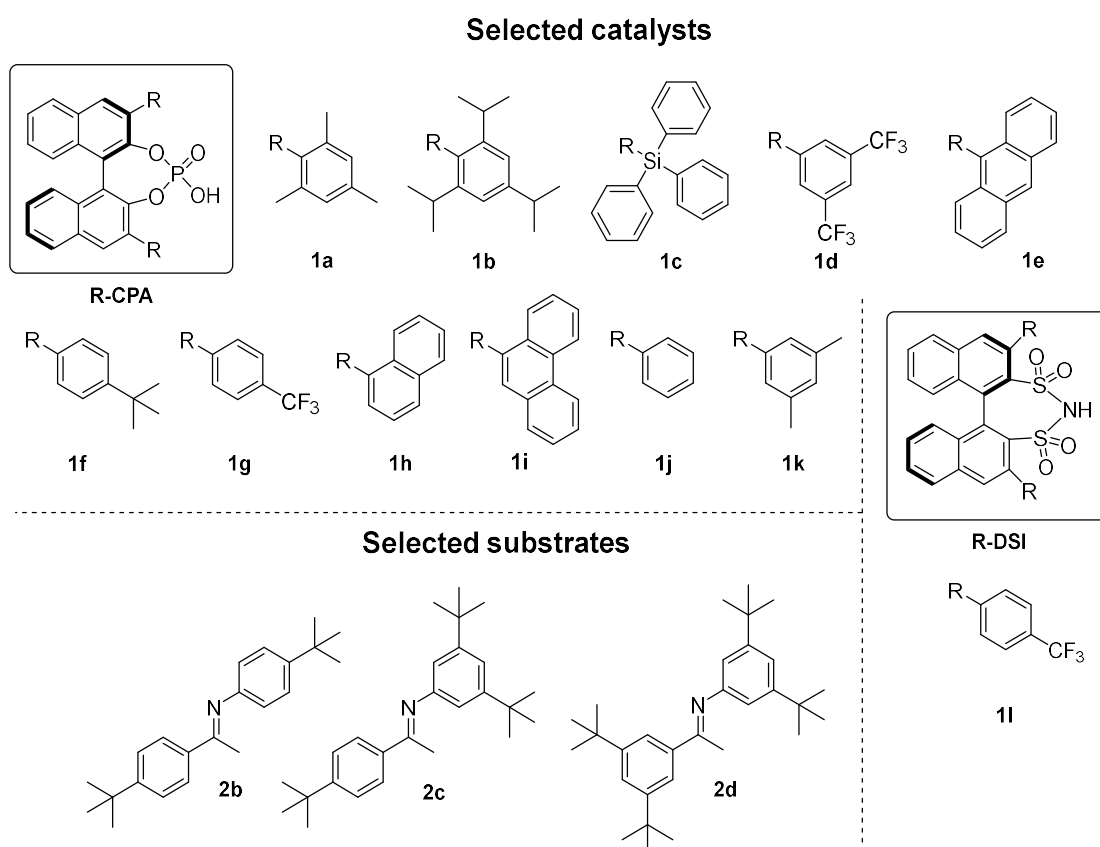


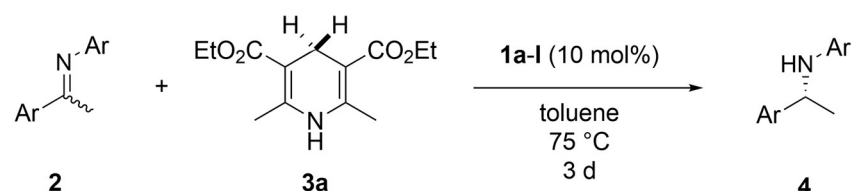
Figure 6: Selected catalysts for the screening of enantiomeric excess for the CPA catalyzed transfer hydrogenation of imines **2-d**. For the disulfonimide (DSI) catalyst **1l**, the R- or S-enantiomer was used, while for CPAs **1a-k**, the R-enantiomer was used. Imine **2b** and **2c** were selected as steric mimics with reduced (**2c**) or negligible (**2b**) intramolecular dispersion interactions.

The reaction conditions were taken over from previous optimization studies.⁵⁹⁻⁶¹ However, as the reaction proceeded rather slowly compared to the transfer hydrogenation of imines such as **2a**, a catalyst loading of 10 mol% and a reaction temperature of 75 °C was necessary to achieve sufficient conversion

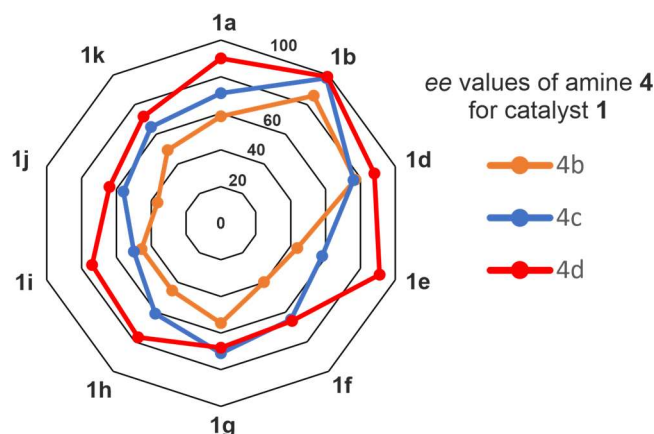
9. Tilting the Balance: London Dispersion Systematically Enhances Enantioselectivities in Brønsted Acid Catalyzed Transfer Hydrogenation of Imines

within a reaction times of 3 days. Control experiments were performed to ensure that these conditions do not affect the enantioselective outcome. Although an uncatalyzed reaction is possible at 75 °C, it is negligible in presence of the catalyst. Additionally, hydrogen-bond bridged dimers of the catalyst as previously reported as active catalyst species for the transfer hydrogenation of quinolines are not affecting the enantioselectivities (see SI Table S3 for experimental data and full discussion).⁶²

Table 2: enantioselectivities for the transfer hydrogenation of imines **2b-d** for a variety of catalysts **1a-l**.



Entry	Catalyst 3,3'	ee (4d)	ee (4c)	ee (4b)
1	2,4,6-(Me) ₃ C ₆ H ₂ (1a)	90	71	58
2	2,4,6-(<i>i</i> Pr) ₃ C ₆ H ₂ (1b)	99	98	86
3	3,5-(CF ₃) ₂ C ₆ H ₃ (1d)	88	76	77
4	9-anthryl (1e)	91	58	44
5	4-(<i>t</i> Bu)C ₆ H ₄ (1f)	66	65	40
6	4-(CF ₃)C ₆ H ₄ (1g)	68	71	55
7	1-naphthyl (1h)	77	61	45
8	9-phenanthryl (1i)	74	50	46
9	C ₆ H ₅ (1j)	64	56	36
10	3,5-(CH ₃) ₂ C ₆ H ₃ (1k)	72	65	49
11	SiPh ₃ (1c)	58	68	80
12	DSI-4-(CF ₃)C ₆ H ₄ (1l) ^a	-66	58	64



In general, the highest ee values were obtained for **4d**, followed by **4c** and **4b**, reflecting the trend of Z-imine stabilization by London dispersion of substrates **2b-d** as highlighted in the graphic on the top right (note that catalyst **1c** and **1l** are excluded in the graphic).^a For substrate **2d** and **2c**, the S enantiomer of **1l** was employed, resulting in ee values of +66 and -58 respectively. To avoid confusion, the inverted ee values for the R enantiomer are given in the table.

9. Tilting the Balance: London Dispersion Systematically Enhances Enantioselectivities in Brønsted Acid Catalyzed Transfer Hydrogenation of Imines

Enantioselectivities up to 99% were received, with **4d** yielding in general the highest *ee*, followed by **4c** and **4b** (see Table 2). For **4d**, the absolute (R)-stereo configuration was determined via X-ray crystallography after tosyl-protection of the amine received from entry 2 (99% *ee*) and is coherent with previous reports.^{59–61} For **4b** and **4c**, an identical stereo configuration of the major enantiomer was assumed based on analogy. Excluding catalysts **1c** and **1l** where we assume a change in transition state combination (see discussion below), the catalyst independent trend of enantioselectivity (**4d** > **4c** > **4b**) clearly correlates with the *Z*-imine stabilization of the substrate (**2d** > **2c** > **2b**) by London dispersion (see Table 2 bottom graphic). This validates the *Z* versus *E* transition state competition (see above) and showcases a systematic approach to enhance stereoselectivities with DED residues. Noteworthy, when comparing the same catalyst similar *ee* values are reported for substrate **2a** (and analogous imines with a *para*-CH₃ or -CF₃) as determined for substrate **2b** and **2c**, all featuring no or weak dispersion stabilization. On the other hand, for the same catalyst the *ee* values of substrate **2d** in general exceed the reported values for imines without DED residues (see SI Table S4).^{50,59,61} This highlights the potential benefit of DED residues on stereoselectivity if assuming the same transition state competition.

Catalysts **1c** and **1l** however deviate from the correlation of dispersion stabilization (**2d** > **2c** > **2b**) and enantioselectivity (*ee* **4d** < **4c** < **4b**) due to presumable changes from the *Z_i* versus *E_i* transition state combination. Previously, it was shown that DSI catalysts (**1l**) can adapt a broader structural space due to the additional S=O hydrogen bond acceptor functionalities. Most likely the observed inversion of *ee* originates in a different hydrogen bonding pattern of substrate and Hantzsch ester, resulting in a different transition state combination.^{52,63} For catalyst **1c**, it was shown that the *Z*-imine stabilization in the binary complex exceeds the amount observed in the free imine (see Table 1), which likely originates in the extremely small binding pocket of **1c**, which is additionally favoring the *Z*-complexes.⁶⁴ We assume that therefore a competition of Type I *Z* versus Type II *Z* (attack of the hydride over bottom or top) instead of *Z* versus *E* is operating and thus the dispersion effects are not reflected in the enantioselectivities. However, the clear correlation between *ee* and *Z*-imine stabilization by London dispersion observed for the vast majority of systems demonstrates the potential impact of London dispersion in catalysis, allowing to convert moderate-good to good-excellent enantioselectivities. Additionally, it highlights that dispersion can have a crucial impact even in a highly confined structural space. It showcases that substituents such as *tert*-butyl must not only be considered regarding their steric bulk, but also regarding their dispersion energy donor properties.

9.4. Conclusions

London dispersion (LD) is frequently neglected in designing catalytic systems despite its ubiquitous presence and cumulative property. On the example of Brønsted acid catalyzed transfer hydrogenation of imines we could conceptualize a systematic approach on beneficially using dispersion energy donor (DED) residues for catalysis. The imine substrate is present as *Z* and *E* isomer, which can be transformed to the *R*- and *S*-product enantiomer respectively. Employing *tert*-butyl DED groups led to a stabilization of the *Z*-imine by up to 4.5 kJ/mol, corroborating previous findings on azobenzene dispersion balances. Due to the strong offset in populations of the *E*-imine (major species; ~99% without LD) and *Z*-imine (minor species; ~1% without LD), chemical exchange saturation transfer (CEST) NMR was used for sensitivity enhancement and identification of the low populated *Z*-imine. Low temperature NMR measurements allowed to analyze the transfer onto confined catalyst/imine and catalyst/imine/nucleophile complexes, resembling the catalytic intermediates. It was shown that the intrinsic stabilization of the *Z*-imine by LD is conserved in these binary and ternary catalytic intermediates. Counterintuitively and despite the intrinsic steric bulkiness of the DEDs the stabilization is added on top of the reduced steric repulsion (compared to the *E*-imine) between catalyst and *Z*-imine in the binding pocket of the catalyst, leading potentially to an almost exclusive population of the *Z*-intermediates. Furthermore, this study shows that the general reaction mechanism and involved intermediate structures are not affected by the increased steric bulk of the substrate when decorated with *tert*-butyl groups. As the reaction presumably proceeds over a *Z*-imine transition state leading to the major enantiomer and *E*-imine transition state leading to the minor enantiomer, the effect of stabilizing the *Z*-intermediates via LD could be read out on the enantioselectivities. A clear correlation between *ee* and LD stabilization was demonstrated for 3 substrates and 10 catalysts. Our results showcase the potential impact of LD in catalysis, allowing to convert in a systematic way moderate-good to good-excellent enantioselectivities by dispersion control. This highlights that substituents such as *tert*-butyl must not only be considered regarding their steric bulk, but also regarding their dispersion energy donor properties even in confined spaces such as crowded catalytic intermediates and transition states.

9. Tilting the Balance: London Dispersion Systematically Enhances Enantioselectivities in Brønsted Acid Catalyzed Transfer Hydrogenation of Imines

9.5. References

- (1) Wöhler, F.; von Liebig, J. Untersuchungen Über Das Radikal Der Benzoesäure. *Ann. der Pharm.* **1832**, *3*, 249–282.
- (2) von Liebig, J. Ueber Die Bildung Des Oxamids Aus Cyan. *Justus Liebigs Ann. Chem.* **1860**, *113*, 246–247.
- (3) *Comprehensive Enantioselective Organocatalysis*; Dalko, P. I., Ed.; Wiley-VCH Verlag GmbH & Co. KGaA: Weinheim, Germany, 2013.
- (4) Wagner, J. P.; Schreiner, P. R. London Dispersion in Molecular Chemistry — Reconsidering Steric Effects. *Angew. Chem. Int. Ed.* **2015**, *54*, 12274–12296.
- (5) Strauss, M. A.; Wegner, H. A. Molecular Systems for the Quantification of London Dispersion Interactions. *Eur. J. Org. Chem.* **2019**, No. 2, 295–302.
- (6) Carter, R. E.; Nilsson, B.; Olsson, K. Barriers to Internal Rotation in 1,3,5-Trineopentylbenzenes. Evidence for Attractive Steric Effects. *J. Am. Chem. Soc.* **1975**, *6155*–6159.
- (7) Lyttle, M. H.; Streitwieser, A.; Kluttz, R. Q. Unusual Equilibrium between 1,4- and 1.6- Di-Tert-Butylcyclooctatetraenes. *J. Am. Chem. Soc.* **1981**, *103*, 3232–3233.
- (8) Oki, M. 1,9-Disubstituted Triptycenes: An Excellent Probe for Weak Molecular Interactions. *Acc. Chem. Res.* **1990**, *23*, 351–356.
- (9) Paul, M.; Breugst, M.; Neudörfl, J. M.; Sunoj, R. B.; Berkessel, A. Keto-Enol Thermodynamics of Breslow Intermediates. *J. Am. Chem. Soc.* **2016**, *138*, 5044–5051.
- (10) Lu, Q.; Neese, F.; Bistoni, G. Formation of Agostic Structures Driven by London Dispersion. *Angew. Chem. Int. Ed.* **2018**, *57*, 4760–4764.
- (11) Schreiner, P. R.; Chernish, L. V.; Gunchenko, P. A.; Tikhonchuk, E. Y.; Hausmann, H.; Serafin, M.; Schlecht, S.; Dahl, J. E. P.; Carlson, R. M. K.; Fokin, A. A. Overcoming Lability of Extremely Long Alkane Carbon-Carbon Bonds through Dispersion Forces. *Nature* **2011**, *477*, 308–311.
- (12) Wagner, J. P.; Schreiner, P. R. London Dispersion Decisively Contributes to the Thermodynamic Stability of Bulky NHC-Coordinated Main Group Compounds. *J. Chem. Theory Comput.* **2016**, *12*, 231–237.
- (13) Rösel, S.; Balestrieri, C.; Schreiner, P. R. Sizing the Role of London Dispersion in the Dissociation of All-Meta Tert-Butyl Hexaphenylethane. *Chem. Sci.* **2016**, *8*, 405–410.
- (14) Fokin, A. A.; Zhuk, T. S.; Blomeyer, S.; Pérez, C.; Chernish, L. V.; Pashenko, A. E.; Antony, J.; Vishnevskiy, Y. V.; Berger, R. J. F.; Grimme, S.; Logemann, C.; Schnell, M.; Mitzel, N. W.; Schreiner, P. R. Intramolecular London Dispersion Interaction Effects on Gas-Phase and Solid-State Structures of Diamondoid Dimers. *J. Am. Chem. Soc.* **2017**, *139*, 16696–16707.
- (15) Jung, J.; Löffler, S. T.; Langmann, J.; Heinemann, F. W.; Bill, E.; Bistoni, G.; Scherer, W.; Atanasov, M.; Meyer, K.; Neese, F. Dispersion Forces Drive the Formation of Uranium-Alkane Adducts. *J. Am. Chem. Soc.* **2020**, *142*, 1864–1870.
- (16) Rösel, S.; Quanz, H.; Logemann, C.; Becker, J.; Mossou, E.; Cañadillas-Delgado, L.; Caldeweyher, E.; Grimme, S.; Schreiner, P. R. London Dispersion Enables the Shortest Intermolecular Hydrocarbon H···H Contact. *J. Am. Chem. Soc.* **2017**, *139*, 7428–7431.
- (17) Löffler, S.; Wuttke, A.; Zhang, B.; Holstein, J. J.; Mata, R. A.; Clever, G. H. Influence of Size, Shape, Heteroatom Content and Dispersive Contributions on Guest Binding in a Coordination Cage. *Chem. Commun.* **2017**, *53*, 11933–11936.
- (18) Dietrich, F.; Bernhard, D.; Fatima, M.; Pérez, C.; Schnell, M.; Gerhards, M. The Effect of Dispersion on the Structure of Diphenyl Ether Aggregates. *Angew. Chem. Int. Ed.* **2018**, *57*, 9534–9537.
- (19) Rösel, S.; Becker, J.; Allen, W. D.; Schreiner, P. R. Probing the Delicate Balance between Pauli Repulsion and London Dispersion with Triphenylmethyl Derivatives. *J. Am. Chem. Soc.* **2018**, *140*, 14421–14432.
- (20) Fatima, M.; Steber, A. L.; Poblitzki, A.; Pérez, C.; Zinn, S.; Schnell, M. Rotational Signatures of Dispersive Stacking in the Formation of Aromatic Dimers. *Angew. Chem. Int. Ed.* **2019**, *58*, 3108–3113.
- (21) Pollice, R.; Chen, P. Origin of the Immiscibility of Alkanes and Perfluoroalkanes. *J. Am. Chem. Soc.* **2019**, *141*, 3489–3506.
- (22) Zhang, Z.; Rooshenas, P.; Hausmann, H.; Schreiner, P. R. Asymmetric Transfer Hydrogenation of Ketimines with Trichlorosilane: Structural Studies. *Synthesis* **2009**, No. 9, 1531–1544.

9. Tilting the Balance: London Dispersion Systematically Enhances Enantioselectivities in Brønsted Acid Catalyzed Transfer Hydrogenation of Imines

- (23) Kötznér, L.; Webber, M. J.; Martínez, A.; Defusco, C.; List, B. Asymmetric Catalysis on the Nanoscale: The Organocatalytic Approach to Helicenes. *Angew. Chem. Int. Ed.* **2014**, *53*, 5202–5205.
- (24) Wende, R. C.; Seitz, A.; Niedeck, D.; Schuler, S. M. M.; Hofmann, C.; Becker, J.; Schreiner, P. R. The Enantioselective Dakin-West Reaction. *Angew. Chem. Int. Ed.* **2016**, *55*, 2719–2723.
- (25) Procházková, E.; Kolmer, A.; Ilgen, J.; Schwab, M.; Kaltschnee, L.; Fredersdorf, M.; Schmidts, V.; Wende, R. C.; Schreiner, P. R.; Thiele, C. M. Uncovering Key Structural Features of an Enantioselective Peptide-Catalyzed Acylation Utilizing Advanced NMR Techniques. *Angew. Chem. Int. Ed.* **2016**, *55*, 15754–15759.
- (26) Yatham, V. R.; Harnying, W.; Kootz, D.; Neudörfel, J. M.; Schlörner, N. E.; Berkessel, A. 1,4-Bis-Dipp/Mes-1,2,4-Triazolylidenes: Carbene Catalysts That Efficiently Overcome Steric Hindrance in the Redox Esterification of α - And β -Substituted α,β -Enals. *J. Am. Chem. Soc.* **2016**, *138*, 2670–2677.
- (27) Meyer, T. H.; Liu, W.; Feldt, M.; Wuttke, A.; Mata, R. A.; Ackermann, L. Manganese(I)-Catalyzed Dispersion-Enabled C–H/C–C Activation. *Chem. Eur. J.* **2017**, *23*, 5443–5447.
- (28) Eschmann, C.; Song, L.; Schreiner, P. R. London Dispersion Interactions Rather than Steric Hindrance Determine the Enantioselectivity of the Corey–Bakshi–Shibata Reduction. *Angew. Chem. Int. Ed.* **2021**, *60*, 4823–4832.
- (29) Pöllöth, B.; Sibi, M. P.; Zipse, H. The Size-Accelerated Kinetic Resolution of Secondary Alcohols. *Angew. Chem. Int. Ed.* **2021**, *60*, 774–778.
- (30) Yepes, D.; Neese, F.; List, B.; Bistoni, G. Unveiling the Delicate Balance of Steric and Dispersion Interactions in Organocatalysis Using High-Level Computational Methods. *J. Am. Chem. Soc.* **2020**, *142*, 3613–3625.
- (31) Schweighauser, L.; Strauss, M. A.; Bellotto, S.; Wegner, H. A. Attraction or Repulsion? London Dispersion Forces Control Azobenzene Switches. *Angew. Chem. Int. Ed.* **2015**, *54*, 13436–13439.
- (32) Strauss, M. A.; Wegner, H. A. Exploring London Dispersion and Solvent Interactions at Alkyl–Alkyl Interfaces Using Azobenzene Switches. *Angew. Chem. Int. Ed.* **2019**, *58*, 18552–18556.
- (33) Strauss, M. A.; Wegner, H. A. London Dispersion in Alkane Solvents. *Angew. Chem. Int. Ed.* **2021**, *60*, 779–786.
- (34) Schümann, J. M.; Wagner, J. P.; Eckhardt, A. K.; Quanz, H.; Schreiner, P. R. Intramolecular London Dispersion Interactions Do Not Cancel in Solution. *J. Am. Chem. Soc.* **2021**, *143*, 41–45.
- (35) König, H. F.; Rummel, L.; Hausmann, H.; Becker, J.; Schümann, J. M.; Schreiner, P. R. Gauging the Steric Effects of Silyl Groups with a Molecular Balance. *J. Org. Chem.* **2022**, *87*, 4670–4679.
- (36) Pollice, R.; Bot, M.; Kobylanski, I. J.; Shenderovich, I.; Chen, P. Attenuation of London Dispersion in Dichloromethane Solutions. *J. Am. Chem. Soc.* **2017**, *139*, 13126–13140.
- (37) Singha, S.; Buchsteiner, M.; Bistoni, G.; Goddard, R.; Fürstner, A. A New Ligand Design Based on London Dispersion Empowers Chiral Bismuth-Rhodium Paddlewheel Catalysts. *J. Am. Chem. Soc.* **2021**, *143*, 5666–5673.
- (38) Grimme, S.; Huenerbein, R.; Ehrlich, S. On the Importance of the Dispersion Energy for the Thermodynamic Stability of Molecules. *ChemPhysChem* **2011**, *12*, 1258–1261.
- (39) Solel, E.; Ruth, M.; Schreiner, P. R. London Dispersion Helps Refine Steric A-Values: Dispersion Energy Donor Scales. *J. Am. Chem. Soc.* **2021**, *143*, 20837–20848.
- (40) Renzi, P.; Hioe, J.; Gschwind, R. M. Decrypting Transition States by Light: Photoisomerization as a Mechanistic Tool in Brønsted Acid Catalysis. *J. Am. Chem. Soc.* **2017**, *139*, 6752–6760.
- (41) Simón, L.; Goodman, J. M. Theoretical Study of the Mechanism of Hantzsch Ester Hydrogenation of Imines Catalyzed by Chiral BINOL-Phosphoric Acids. *J. Am. Chem. Soc.* **2008**, *130*, 8741–8747.
- (42) Marcelli, T.; Hammar, P.; Himo, F. Phosphoric Acid Catalyzed Enantioselective Transfer Hydrogenation of Imines: A Density Functional Theory Study of Reaction Mechanism and the Origins of Enantioselectivity. *Chem. Eur. J.* **2008**, *14*, 8562–8571.
- (43) Livingstone, K.; Tenberge, M.; Pape, F.; Daniliuc, C. G.; Jamieson, C.; Gilmour, R. Photocatalytic $e^- \rightarrow Z$ Isomerization of β -Ionyl Derivatives. *Org. Lett.* **2019**, *21*, 9677–9680.

9. Tilting the Balance: London Dispersion Systematically Enhances Enantioselectivities in Brønsted Acid Catalyzed Transfer Hydrogenation of Imines

- (44) Hostmann, T.; Molloy, J. J.; Bussmann, K.; Gilmour, R. Light-Enabled Enantiodivergence: Stereospecific Reduction of Activated Alkenes Using a Single Organocatalyst Enantiomer. *Org. Lett.* **2019**, *21*, 10164–10168.
- (45) Onneken, C.; Bussmann, K.; Gilmour, R. Inverting External Asymmetric Induction via Selective Energy Transfer Catalysis: A Strategy to β -Chiral Phosphonate Antipodes. *Angew. Chem. Int. Ed.* **2020**, *59*, 330–334.
- (46) Molloy, J. J.; Morack, T.; Gilmour, R. Positional and Geometrical Isomerisation of Alkenes: The Pinnacle of Atom Economy. *Angew. Chem. Int. Ed.* **2019**, *58*, 13654–13664.
- (47) Sorgenfrei, N.; Hioe, J.; Greindl, J.; Rothermel, K.; Morana, F.; Lokesh, N.; Gschwind, R. M. NMR Spectroscopic Characterization of Charge Assisted Strong Hydrogen Bonds in Brønsted Acid Catalysis. *J. Am. Chem. Soc.* **2016**, *138*, 16345–16354.
- (48) Greindl, J.; Hioe, J.; Sorgenfrei, N.; Morana, F.; Gschwind, R. M. Brønsted Acid Catalysis-Structural Preferences and Mobility in Imine/Phosphoric Acid Complexes. *J. Am. Chem. Soc.* **2016**, *138*, 15965–15971.
- (49) Rothermel, K.; Melikian, M.; Hioe, J.; Greindl, J.; Gramüller, J.; Žabka, M.; Sorgenfrei, N.; Hausler, T.; Morana, F.; Gschwind, R. M. Internal Acidity Scale and Reactivity Evaluation of Chiral Phosphoric Acids with Different 3,3'-Substituents in Brønsted Acid Catalysis. *Chem. Sci.* **2019**, *10*, 10025–10034.
- (50) Melikian, M.; Gramüller, J.; Hioe, J.; Greindl, J.; Gschwind, R. M. Brønsted Acid Catalysis-the Effect of 3,3'-Substituents on the Structural Space and the Stabilization of Imine/Phosphoric Acid Complexes. *Chem. Sci.* **2019**, *10*, 5226–5234.
- (51) Lokesh, N.; Hioe, J.; Gramüller, J.; Gschwind, R. M. Relaxation Dispersion NMR to Reveal Fast Dynamics in Brønsted Acid Catalysis: Influence of Sterics and H-Bond Strength on Conformations and Substrate Hopping. *J. Am. Chem. Soc.* **2019**, *141*, 16398–16407.
- (52) Žabka, M.; Gschwind, R. M. Ternary Complexes of Chiral Disulfonimides in Transfer-Hydrogenation of Imines: The Relevance of Late Intermediates in Ion Pair Catalysis. *Chem. Sci.* **2021**, 15263–15272.
- (53) Liu, G.; Song, X.; Chan, K. W. Y.; McMahon, M. T. Nuts and Bolts of Chemical Exchange Saturation Transfer MRI. *NMR Biomed.* **2013**, *26*, 810–828.
- (54) Lokesh, N.; Seegerer, A.; Hioe, J.; Gschwind, R. M. Chemical Exchange Saturation Transfer in Chemical Reactions: A Mechanistic Tool for NMR Detection and Characterization of Transient Intermediates. *J. Am. Chem. Soc.* **2018**, *140*, 1855–1862.
- (55) Ward, K. M.; Aletras, A. H.; Balaban, R. S. A New Class of Contrast Agents for MRI Based on Proton Chemical Exchange Dependent Saturation Transfer (CEST). *J. Magn. Reson.* **2000**, *143*, 79–87.
- (56) Guivel-Scharen, V.; Sinnwell, T.; Wolff, S. D.; Balaban, R. S. Detection of Proton Chemical Exchange between Metabolites and Water in Biological Tissues. *J. Magn. Reson.* **1998**, *133*, 36–45.
- (57) Rummel, L.; Domanski, M. H. J.; Hausmann, H.; Becker, J.; Schreiner, P. R. London Dispersion Favors Sterically Hindered Diarylthiourea Conformers in Solution. *Angew. Chem. Int. Ed.* **2022**, 202204393.
- (58) Cabrita, E. J.; Berger, S. HR-DOSY as a New Tool for the Study of Chemical Exchange Phenomena. *Magn. Reson. Chem.* **2002**, *40*, 122–127.
- (59) Hoffmann, S.; Seayad, A. M.; List, B. A Powerful Brønsted Acid Catalyst for the Organocatalytic Asymmetric Transfer Hydrogenation of Imines. *Angew. Chem. Int. Ed.* **2005**, *44*, 7424–7427.
- (60) Storer, R. I.; Carrera, D. E.; Ni, Y.; MacMillan, D. W. C. Enantioselective Organocatalytic Reductive Amination. *J. Am. Chem. Soc.* **2006**, *128*, 84–86.
- (61) Rueping, M.; Sugiono, E.; Azap, C.; Theissmann, T.; Bolte, M. Enantioselective Brønsted Acid Catalyzed Transfer Hydrogenation: Organocatalytic Reduction of Imines. *Org. Lett.* **2005**, *7*, 3781–3783.
- (62) Jansen, D.; Gramüller, J.; Niemeyer, F.; Schaller, T.; Letzel, M. C.; Grimme, S.; Zhu, H.; Gschwind, R. M.; Niemeyer, J. What Is the Role of Acid-Acid Interactions in Asymmetric Phosphoric Acid Organocatalysis? A Detailed Mechanistic Study Using Interlocked and Non-Interlocked Catalysts. *Chem. Sci.* **2020**, *11*, 4381–4390.
- (63) Rothermel, K.; Žabka, M.; Hioe, J.; Gschwind, R. M. Disulfonimides versus Phosphoric Acids in Brønsted Acid Catalysis: The Effect of Weak Hydrogen Bonds and Multiple Acceptors on Complex Structures and Reactivity. *J. Org. Chem.* **2019**, *84*, 13221–13231.

9. Tilting the Balance: London Dispersion Systematically Enhances Enantioselectivities in Brønsted Acid Catalyzed Transfer Hydrogenation of Imines

(64) Reid, J. P.; Goodman, J. M. Goldilocks Catalysts: Computational Insights into the Role of the 3,3' Substituents on the Selectivity of BINOL-Derived Phosphoric Acid Catalysts. *J. Am. Chem. Soc.* **2016**, *138*, 7910–7917.

9.6. Supporting Information

9.6.1. General information

Chemicals

Deuterated solvents were purchased from Deutero or Sigma Aldrich. Where dry solvents were essential, CD₂Cl₂ was freshly distilled over CaH₂ and Toluene-d₈ was refluxed over Na/Benzophenone under argon atmosphere. Non-deuterated toluene was refluxed over Na/Benzophenone under Argon atmosphere or purchased by Sigma Aldrich (dry, stored over molecular sieve). All commercially available chemicals were purchased by Sigma Aldrich or abcr and used without further purification. Hantzsch ester **3b** was prepared according to literature.¹

Sample preparation

The chiral phosphoric acid was weighed into a 5 mm NMR tube and dried at 150 °C for at least 20 min under reduced pressure. After the tube came to room temperature, the respective imine was weighed directly into the NMR tube. The tube was evacuated and flushed with Argon three times. Dry CD₂Cl₂ (0.6 mL) was added under Argon flow and TMS atmosphere (0.5 mL) was added. The tube was closed and sealed with parafilm. The samples were stored in the fridge at -80 °C.

For the preparation of the “*E*-only sample”, prior to adding the solvent the tube was cooled to -80 °C in an acetone/liquid nitrogen bath. Under Argon flow, cooled CD₂Cl₂ (0.6 mL) was added to the CPA and imine. TMS atmosphere (0.5 mL) was added and the tube was closed and sealed with parafilm. The samples were stored in the fridge at -80 °C. *E*-only samples were transported at -80 °C in an acetone/liquid nitrogen cooling bath and only inserted in a precooled spectrometer at 180 K.

NMR spectrometer, data procession and referencing

All NMR spectroscopic investigations on model systems were performed on a Bruker Avance DRX 600 MHz spectrometer with TBI (Triple resonance broadband inverse) 5 mm CPPBBO ¹H/¹⁹F-BB probe head with Z-gradient and BVT unit. Temperature was controlled in the VT-experiments by a BVT 3000 and BVT 3900 unit and liquid nitrogen. Further NMR experiments were performed on Bruker Avance III HD 400 MHz spectrometer equipped with 5 mm BBO BB-1H/D probe head with Z-Gradients. Spectrometer

9. Tilting the Balance: London Dispersion Systematically Enhances Enantioselectivities in Brønsted Acid Catalyzed Transfer Hydrogenation of Imines

control and spectra processing was performed with Bruker Software TopSpin (Version 3.2 PL 1). Further plotting of the spectra was performed with Corel Draw 2020 software. ^1H , ^{13}C chemical shifts were referenced to TMS or the respective solvent signals. The heteronucleus ^{31}P was referenced, employing $\nu(\text{X}) = \nu(\text{TMS}) \cdot \Xi_{\text{reference}} / 100\%$ according to Harris et al.² The following frequency ratios and reference compounds was used: $\Xi(^{31}\text{P}) = 40.480742$ (H_3PO_4). For all NMR measurements, 5 mm NMR tubes were used.

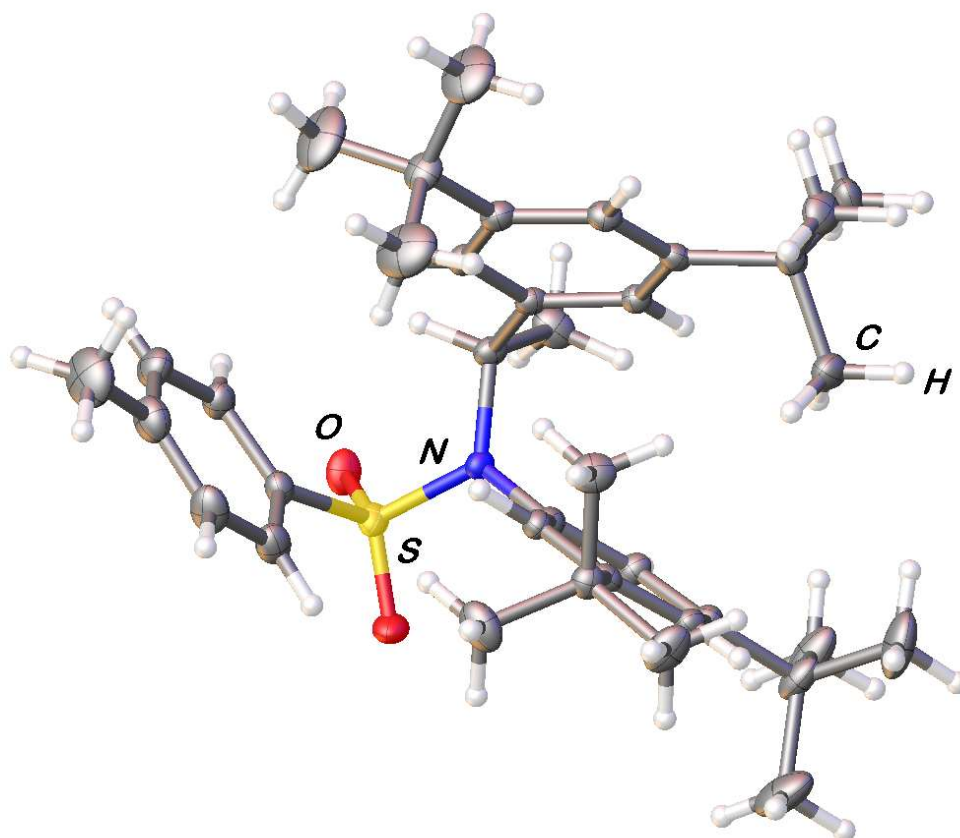
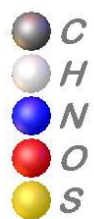
Pulse sequences and acquisition parameters

^1H -NMR: Pulse program zg30, Relaxation delay = 2.00 s, Acquisition time = 2.54 s, SW = 20 – 24 ppm, TD = 66 K, ns = 16 – 256; ^{13}C NMR: Pulse program: zgpg30, Relaxation delay = 2.00 s, Acquisition time = 0.80 s, TD = 66 K; SW = 270.0 ppm, TD = 64k, NS = 1k – 4k; ^{31}P -NMR: Pulse program: zgpg30; Relaxation delay = 1.00 s, Acquisition time = 2.25 s, SW = 20 - 60.0 ppm, TD = 65k, NS = 256 - 512; $2\text{D-}^1\text{H}, ^1\text{H}$ NOESY: Pulse program: noesygpph; Relaxation delay = 5.00 s, NS = 8-16, mixing time (D8) = 300.00 ms; TD = 4096; increments = 512 - 1k; $2\text{D-}^1\text{H}, ^1\text{H}$ ROESY: Pulse program: roesyphpr.2; Relaxation delay = 5.00 s, NS = 8, mixing time (D8) = 100.00 ms; TD = 4096; increments = 1k; $2\text{D-}^1\text{H}, ^1\text{H}$ COSY: Pulse program: cosygpqf; Relaxation delay = 5.00 s, NS = 4-16, TD = 4096; increments = 512; $2\text{D-}^1\text{H}, ^{13}\text{C}$ HSQC: Pulse program: hsqcedetgpsisp2.3; Relaxation delay = 4 - 8 s, NS = 8-32, $^1J_{\text{XH}} = 145$ Hz; TD = 4096; increments = 512 - 1k; $2\text{D-}^1\text{H}, ^{13}\text{C}$ HMBC: Pulse program: hmbcgplpndqf; Relaxation delay = 4.00 s, NS = 8-16, $^1J_{\text{XH}} = 145$ Hz, $J_{\text{XH}}(\text{long range}) = 10$ Hz; TD = 4096; increments = 512 - 1k; $2\text{D-}^1\text{H}, ^{31}\text{P}$ HMBC: Pulse program: inv4gplrndqf; Relaxation delay = 6.00 s, NS = 4-32, TD = 4096; increments = 256 – 512. $2\text{D-}^1\text{H}, ^{15}\text{N}$ HMBC: Pulse program: inv4gplrndqf; Relaxation delay = 4.00 s, NS = 4-16, delay for evolution of long range couplings (D6) = 20.00 ms; TD = 4096; increments = 256; $2\text{D-}^1\text{H}, ^{19}\text{F}$ HOESY: Pulse program: hoesyph; Relaxation delay = 5.00 s, NS = 8, mixing time (D8) = 350.00 ms; TD = 4096; increments = 512 - 1024;

9. Tilting the Balance: London Dispersion Systematically Enhances Enantioselectivities in Brønsted Acid Catalyzed Transfer Hydrogenation of Imines

Crystallographic details

Dull colorless prism-shaped crystals of **5** were obtained after recrystallization in methanol.



9. Tilting the Balance: London Dispersion Systematically Enhances Enantioselectivities in Brønsted Acid Catalyzed Transfer Hydrogenation of Imines

Compound	5
Formula	C ₃₇ H ₅₃ NO ₂ S
$D_{calc.}/g\ cm^{-3}$	1.120
μ/mm^{-1}	1.067
Formula Weight	575.86
Colour	dull colorless
Shape	prism-shaped
Size/mm ³	0.32×0.17×0.13
T/K	123.01(10)
Crystal System	orthorhombic
Flack Parameter	-0.008(7)
Hooft Parameter	-0.017(6)
Space Group	<i>P</i> 2 ₁ 2 ₁ 2 ₁
$a/\text{Å}$	10.14400(10)
$b/\text{Å}$	10.89390(10)
$c/\text{Å}$	30.9176(4)
$\alpha/^\circ$	90
$\beta/^\circ$	90
$\gamma/^\circ$	90
$V/\text{Å}^3$	3416.63(6)
Z	4
Z'	1
Wavelength/Å	1.54184
Radiation type	Cu K α
$\theta_{min}/^\circ$	4.303
$\theta_{max}/^\circ$	66.657
Measured Refl's.	23950
Indep't Refl's	6006
Refl's $I \geq 2\ \sigma(I)$	5837
R_{int}	0.0457
Parameters	415
Restraints	45
Largest Peak	0.378
Deepest Hole	-0.339
GooF	1.047
wR_2 (all data)	0.0953
wR_2	0.0938
R_1 (all data)	0.0391
R_1	0.0378

9.6.2. Imine synthesis and transfer hydrogenations

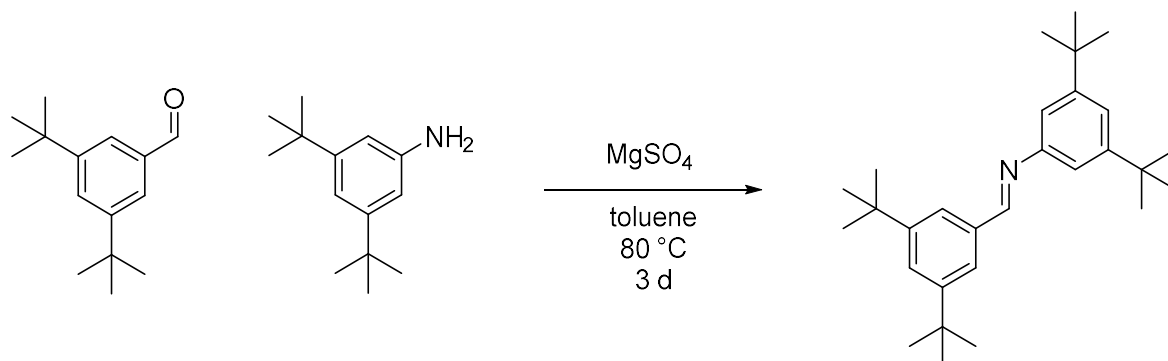
General procedure for imine synthesis (GP I)

Molecular sieves 4 Å (approx. 3 - 5 g) was weighed into a 50 mL Schlenk flask and dried with a heat gun at 450 °C for at least 30 min under reduced pressure. Under Argon flow, the respective amine (1.0 equiv) and respective ketone (1.0 equiv.) were added and dissolved in 25 mL anhydrous toluene. Under Argon flow, a reflux condenser was added to the setup and flushed with argon for 3 min and afterwards the setup was closed with a septum and balloon insert. The solution was refluxed for 3 d. Afterwards, the heating bath was removed, and the reaction mixture allowed to cool down. The mixture was filtrated, and the solvent was removed under reduced pressure. The crude product was either recrystallized in methanol or distilled *via* a bulb-to-bulb distill to give the respective imine.

Imines **2a-b**, **2e-g** were synthesized following GP I. The spectral data matched the previous literature reports.^{3,4}

9. Tilting the Balance: London Dispersion Systematically Enhances Enantioselectivities in Brønsted Acid Catalyzed Transfer Hydrogenation of Imines

(E)-N,1-bis(3,5-di-tert-butylphenyl)methanimine (2h)



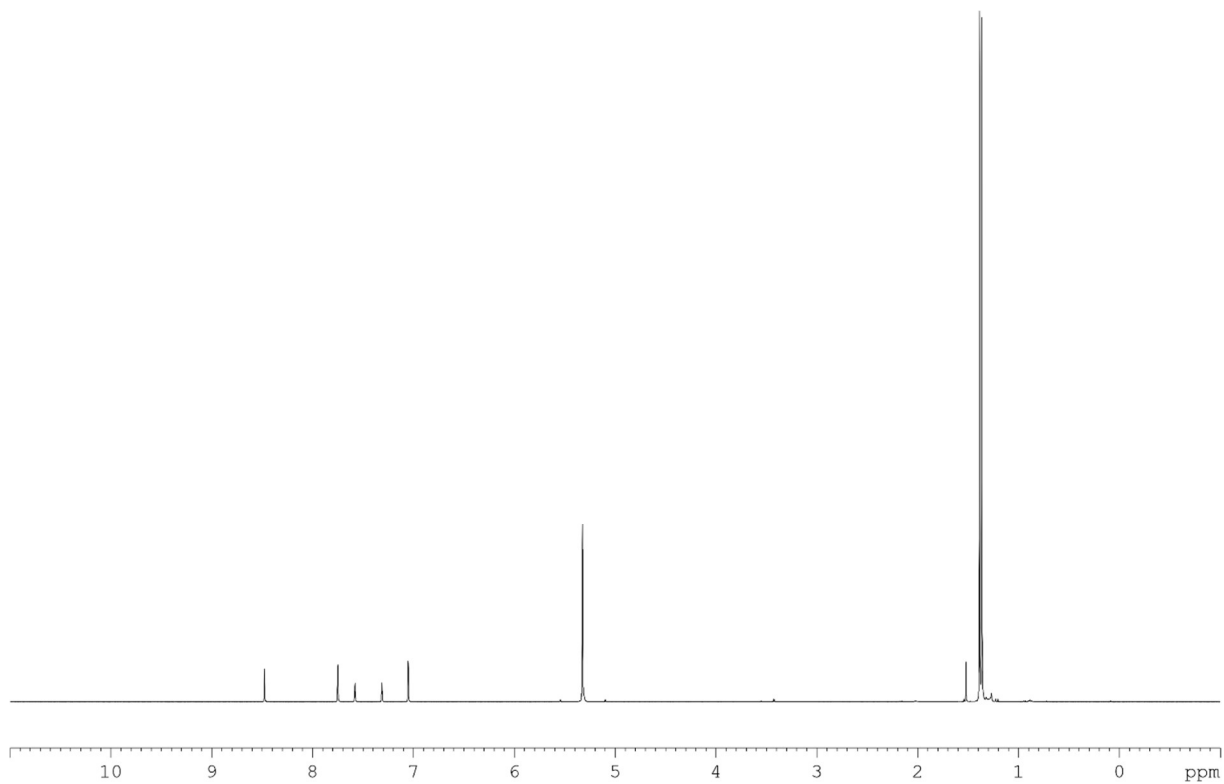
MgSO₄ (500 mg) was given into a Schlenk flask and dried at 350°C for 30 min. 3,5-di-tert-butylbenzaldehyde (1.00 mmol, 218 mg, 1.0 eq.) and 3,5-di-tert-butylaniline (1.00 mmol, 205 mg, 1.0 eq.) and dry toluene (5 mL) were added under argon flow and the mixture was stirred at 80°C for 3 d. Afterwards, the mixture was filtrated and the solvent was removed under reduced pressure. The crude product was purified by recrystallization from MeOH to yield the product as colorless needles (264 mg, 0.65 mmol, 65%) exclusively as the *E*-isomer (*Z* : *E* < 1 : 99 in CD₂Cl₂ at 298 K).

¹H-NMR: (400.1 MHz, CD₂Cl₂): δ_H = 8.48 (s, 1H), 7.75 (d, 2H, ⁴*J* = 1.8 Hz), 7.58 (t, 1H, ⁴*J* = 1.8 Hz), 7.31 (t, 1H, ⁴*J* = 1.7 Hz), 7.05 (d, 2H, ⁴*J* = 1.8 Hz), 1.39 (s, 18H), 1.36 (s, 18H).

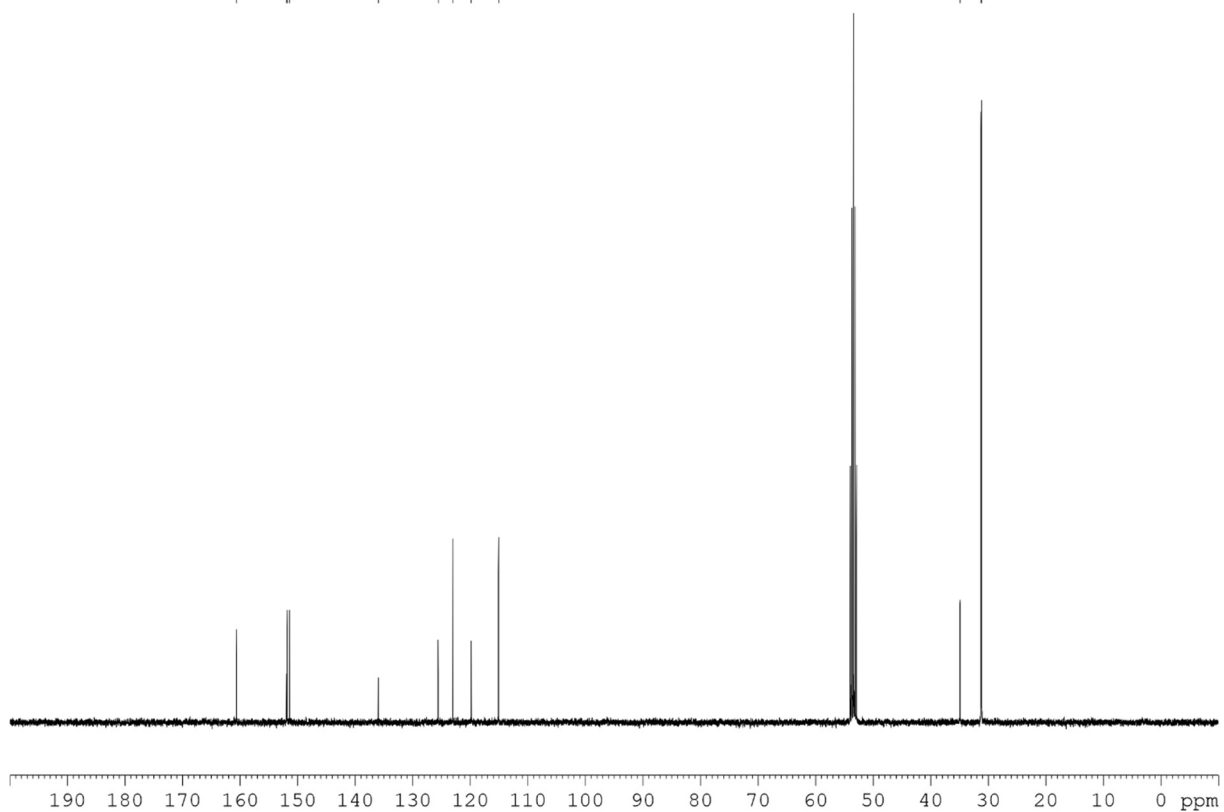
¹³C-NMR: (100.6 MHz, CD₂Cl₂): δ_C = 160.6, 151.9, 151.8, 151.4, 135.9, 125.6, 123.0, 119.8, 115.1, 34.9, 34.8, 31.2, 31.1.

HR-MS (EI, *m/z*): found 406.3472 (M+H)⁺ (calculated 405.3399 for C₂₉H₄₃N); Diff(ppm) = 0.92.

9. Tilting the Balance: London Dispersion Systematically Enhances Enantioselectivities in Brønsted Acid Catalyzed Transfer Hydrogenation of Imines

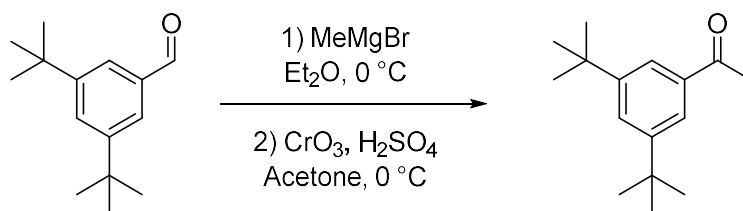


160.60
151.89
151.80
151.39
135.96
125.56
122.99
119.82
115.06
34.88
34.84
31.22
31.15



9. Tilting the Balance: London Dispersion Systematically Enhances Enantioselectivities in Brønsted Acid Catalyzed Transfer Hydrogenation of Imines

3,5-di-*tert*-butylacetophenone



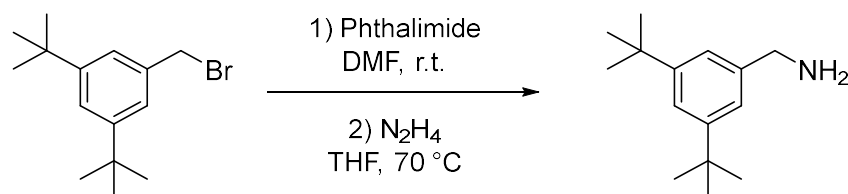
3,5-di-*tert*-butylbenzaldehyde (2.18 g, 10.0 mmol, 1.0 equiv.) was dissolved in Et₂O (25 mL), cooled to 0 °C and a solution of methylmagnesium bromide (3.0 M in Et₂O, 5.0 mL, 15.0 mmol, 1.5 equiv.) was added dropwise over 15 minutes. Afterwards, the reaction mixture was quenched by slow addition of a saturated NH₄Cl solution and extracted with EtOAc (3x 30 mL). The organic phase was dried over MgSO₄, filtered and the solvent was removed under reduced pressure to receive a white solid, which was dissolved in acetone (30 mL) and cooled to 0 °C. Jones reagent (CrO₃ in H₂SO₄, 2.67 M, 7.5 mL, 20.0 mmol, 2.0 equiv.) was added dropwise and the reaction was stirred at room temperature for 2 h. The reaction mixture was quenched by addition of a saturated NaHCO₃ solution and extracted with CH₂Cl₂ (3x 50 mL). The organic layers were combined, dried over MgSO₄, filtered and the solvent was removed under reduced pressure to receive the product 3,5-di-*tert*-butylacetophenone as a yellowish oil (2.30 g, 99%).

¹H NMR (400 MHz, CDCl₃): δ = 7.81 (d, ⁴J = 1.8 Hz, 2H), 7.65 (t, ⁴J = 1.8 Hz, 1H), 2.62 (s, 3H), 1.36 (s, 18H).

The spectral data matches the literature report.⁵

9. Tilting the Balance: London Dispersion Systematically Enhances Enantioselectivities in Brønsted Acid Catalyzed Transfer Hydrogenation of Imines

3,5-di-*tert*-butylphenyl)methanamine



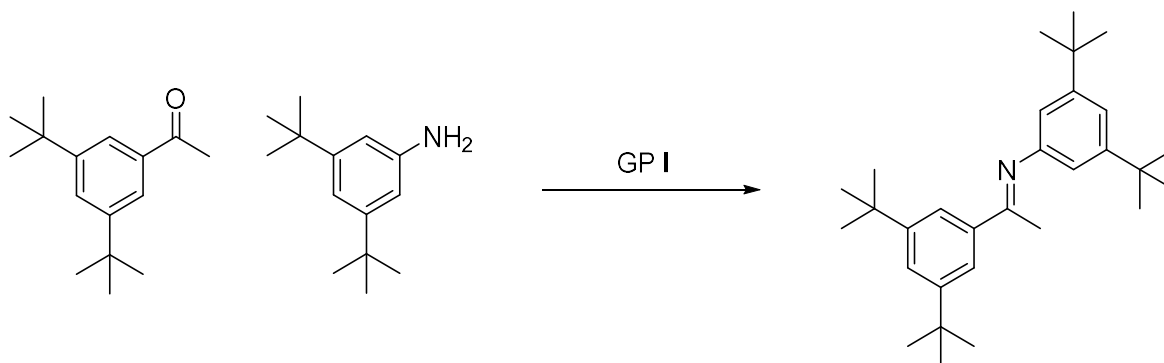
3,5-di-*tert*-butylbenzylbromide (5.67 g, 20.0 mmol, 1.0 equiv.), K_2CO_3 (4.15 g, 30.0 mmol, 1.5 equiv.) and phthalimide (3.83 g, 26.0 mmol, 1.3 equiv.) were stirred for 24 h at room temperature in THF (25 mL). The reaction mixture was diluted with Et_2O (75 mL) and the organic layer was washed with water (4x 250 mL). The organic phase was dried over $MgSO_4$, filtered and the solvent was removed under reduced pressure to receive a colorless solid, which was dissolved in THF (50 mL). Hydrazine monohydrate (5.89 g, 5.71 mL, 120.0 mmol, 6.0 equiv.) was added dropwise to that stirred solution. Afterwards the reaction mixture was heated at reflux (70 °C) for 3 h, whereby a colorless solid precipitated. After cooling to room temperature, the precipitate was dissolved by addition of water and the mixture was extracted with *tert*butylmethylether (2x 70 mL). The combined organic layers were washed with brine, dried over $MgSO_4$, filtered and the solvent was removed under reduced pressure to give the product as a yellow oil (2.20 g, 10.0 mmol, 50%).

1H NMR (400 MHz, $CDCl_3$): δ = 7.34 (t, 4J = 1.8 Hz, 1H), 7.20 (d, 4J = 1.8 Hz, 2H), 3.91 (s, 2H), 3.24 (br s, 2H), 1.32 (s, 18H).

The spectral data matches the literature report.⁶

9. Tilting the Balance: London Dispersion Systematically Enhances Enantioselectivities in Brønsted Acid Catalyzed Transfer Hydrogenation of Imines

(E)-N,1-bis(3,5-di-tert-butylphenyl)ethan-1-imine (2d)



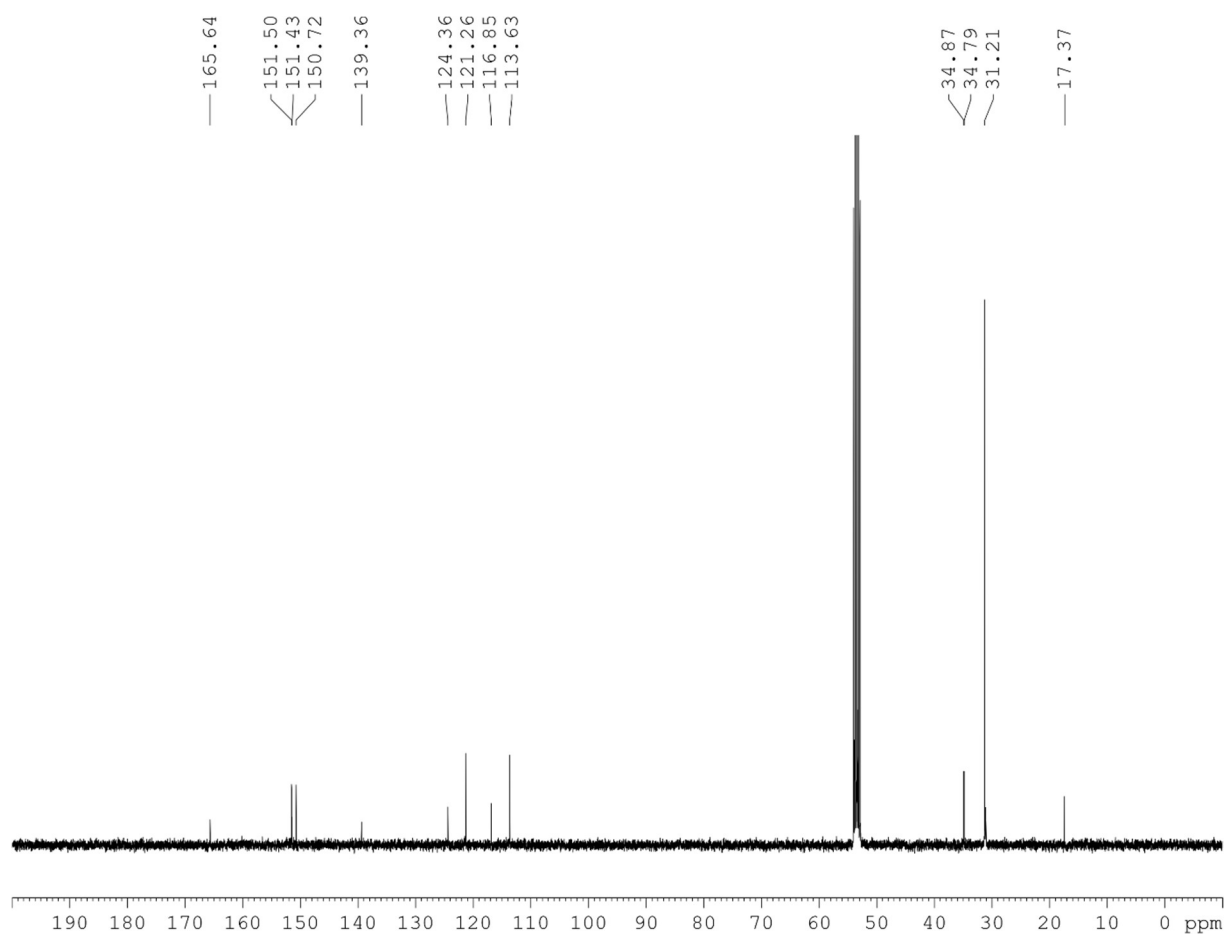
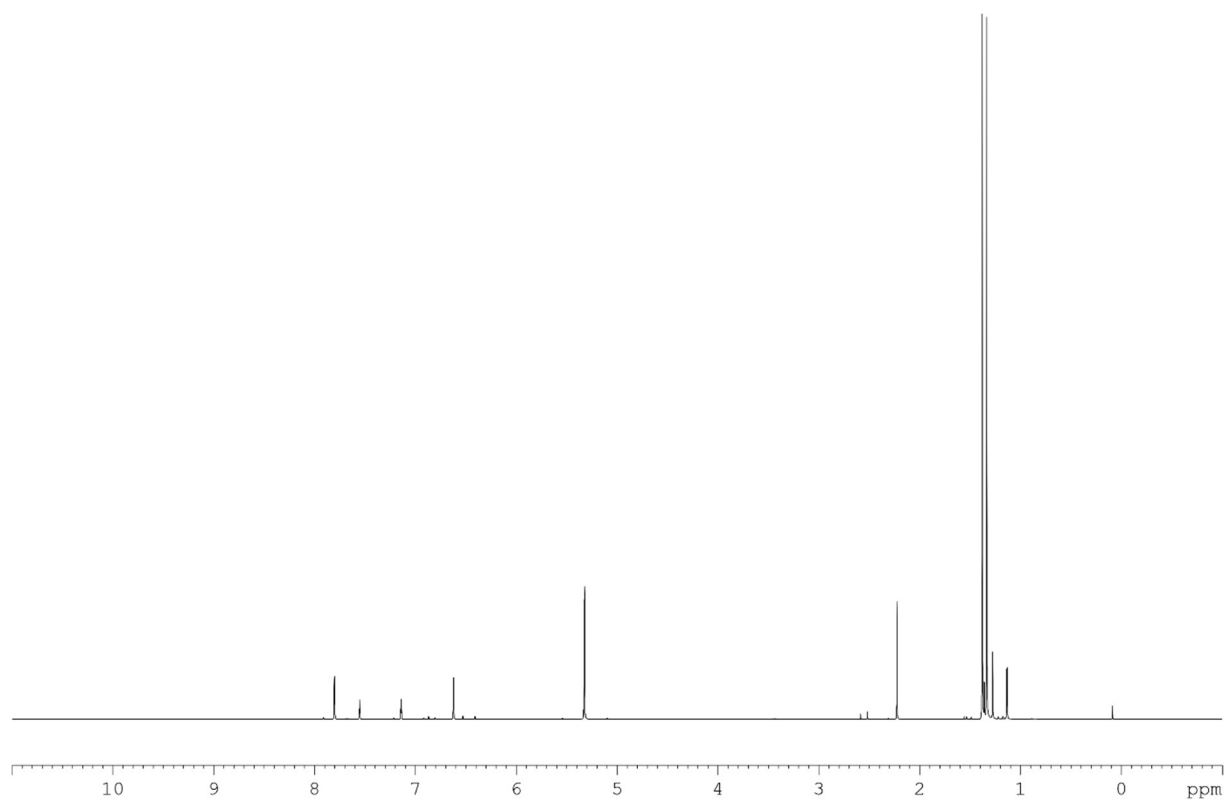
Following GPI, 3,5-di-tert-butylacetophenone (4.65 g, 20 mmol, 1.0 equiv.) and 3,5-di-tert-butylaniline (4.11 g, 20.0 mmol, 1.0 equiv.) were reacted. The crude product was distilled *via* a bulb-to-bulb distillation (0.1 mbar, 140-180 °C) and the product was received as a highly viscous, yellow oil (4.70 g, 11.2 mmol, 56%). The product was received as a mixture of *E* and *Z* isomer (*Z* : *E* \approx 1 : 14 in CD₂Cl₂ at 298 K).

¹H NMR (*E*-imine; 400 MHz, CD₂Cl₂): δ = 7.34 (t, *J* = 1.8 Hz, 1H), 7.20 (d, *J* = 1.8 Hz, 2H), 3.91 (s, 2H), 3.24 (br s, 2H), 1.32 (s, 18H).

¹³C NMR (*E*-imine; 100 MHz, CD₂Cl₂): δ = 165.6, 151.5, 151.4, 150.7, 139.4, 124.4, 121.3, 116.8, 113.6, 34.9, 34.7, 31.2 (2C), 17.4.

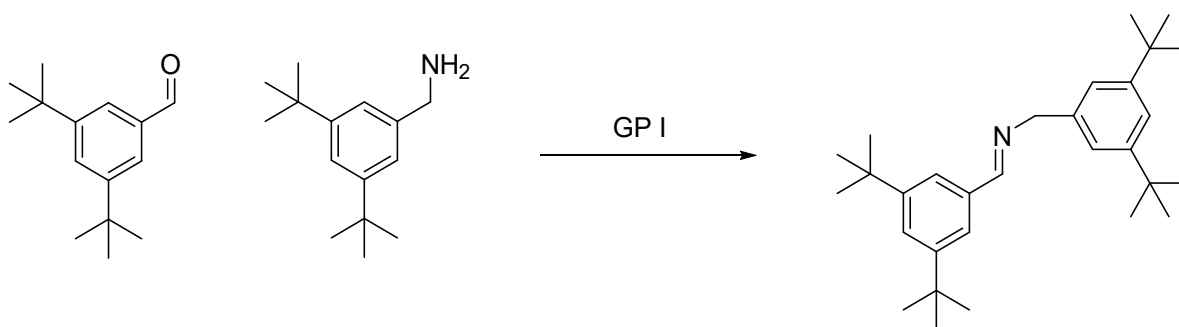
HR-MS (EI, *m/z*): found 419.35389 (M)⁺ (calculated 419.35465 for C₃₀H₄₅N); Diff(ppm) = -0.76.

9. Tilting the Balance: London Dispersion Systematically Enhances Enantioselectivities in Brønsted Acid Catalyzed Transfer Hydrogenation of Imines



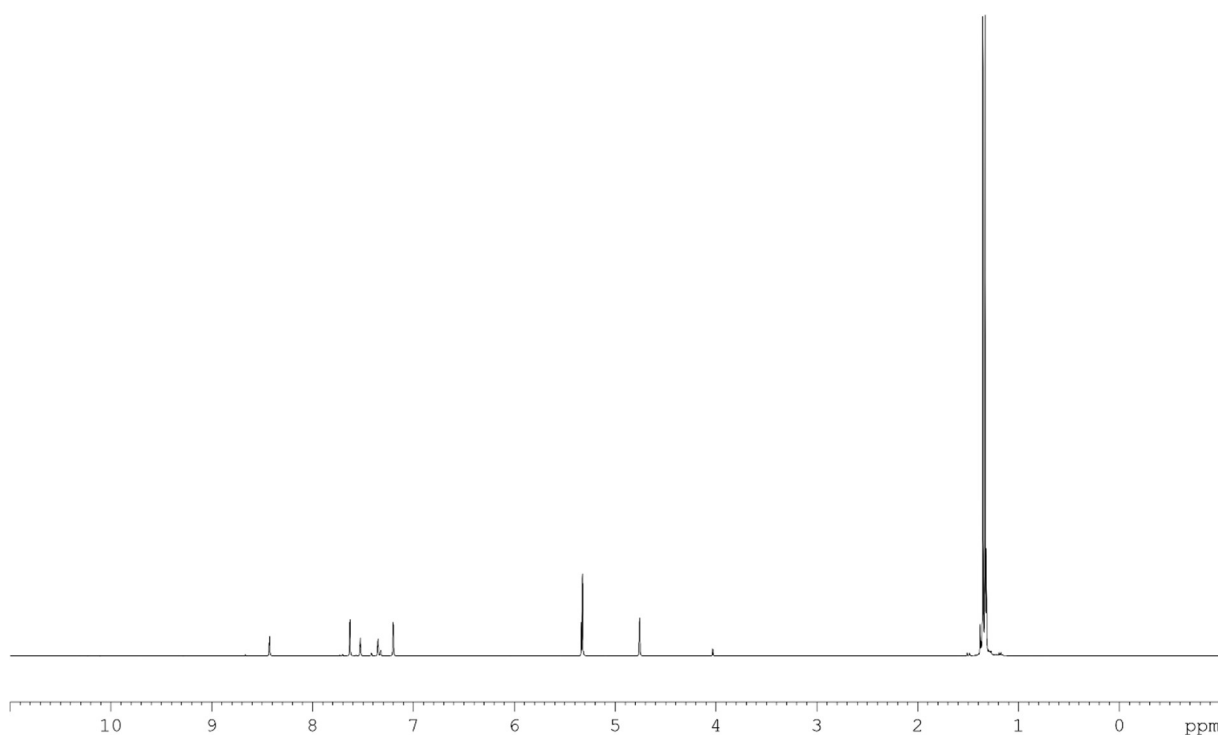
9. Tilting the Balance: London Dispersion Systematically Enhances Enantioselectivities in Brønsted Acid Catalyzed Transfer Hydrogenation of Imines

(E)-N-(3,5-di-tert-butylbenzyl)-(3,5-di-tert-butylphenyl)methanimine (2i)



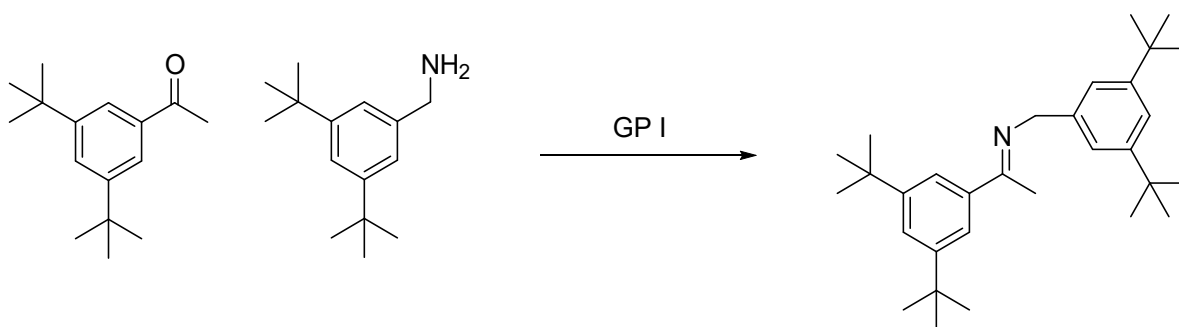
Following GP I, 3,5-di-*tert*-butylbenzaldehyde (218.34 mg, 1.00 mmol, 1.0 eq.) and (3,5-di-*tert*-butylphenyl)methanamine (219.37 mg, 1.00 mmol, 1.0 eq.) were dissolved in toluene (5 mL) and stirred at 120 °C for 3 d. The reaction mixture was filtered and the solvent was removed under reduced pressure. The crude product was distilled twice *via* a bulb-to-bulb distillation (0.1 mbar, 180-210 °C) and the product was received as a highly viscous, yellow oil (130 mg, 0.31 mmol, 31%). The product was received as a mixture of *E* and *Z* isomer (*Z* : *E* \approx 1 : 22 in CD₂Cl₂ at 298 K).

¹H NMR (*E*-imine; 400 MHz, CD₂Cl₂): δ = 8.43 (s, 1H), 7.63 (d, ⁴*J* = 1.8 Hz, 2H), 7.53 (t, ⁴*J* = 1.8 Hz, 1H), 7.35 (t, ⁴*J* = 1.8 Hz, 1H), 7.20 (d, ⁴*J* = 1.8 Hz, 2H), 4.76 (s, 2H), 1.35 (s, 18H), 1.33 (s, 18H).



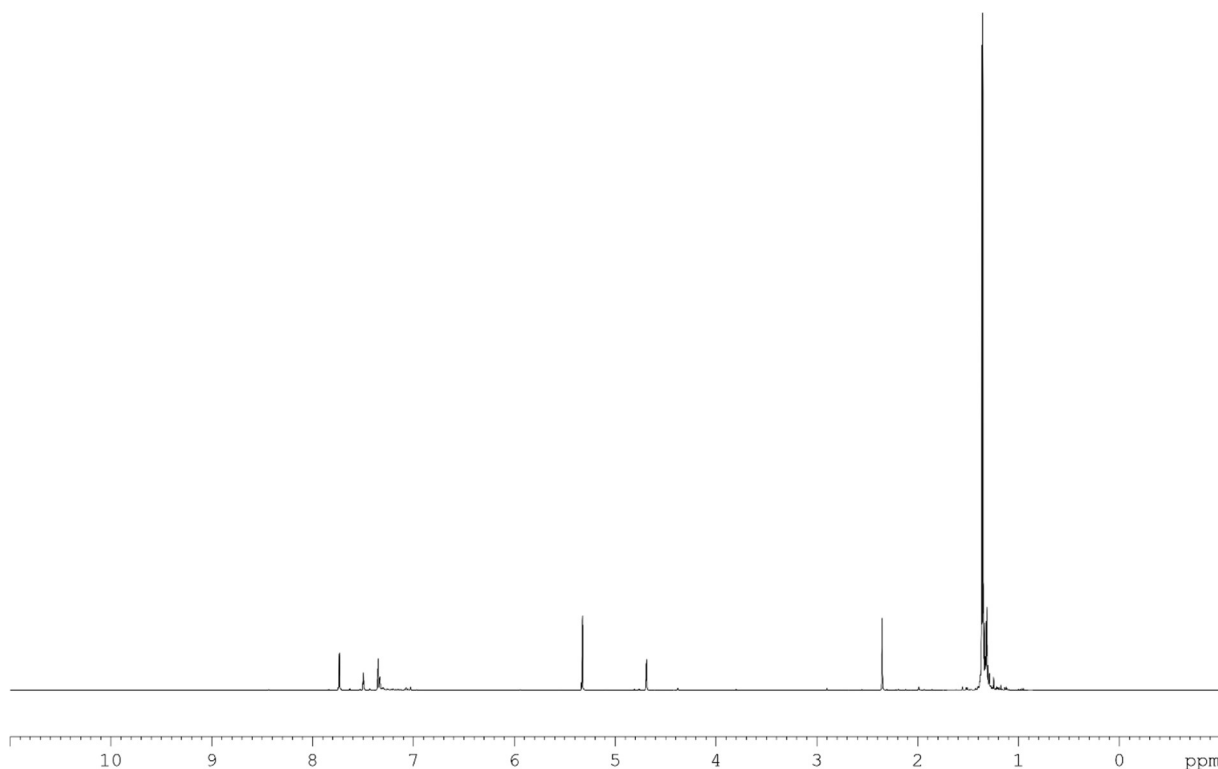
9. Tilting the Balance: London Dispersion Systematically Enhances Enantioselectivities in Brønsted Acid Catalyzed Transfer Hydrogenation of Imines

(E)-N-(3,5-di-tert-butylbenzyl)-1-(3,5-di-tert-butylphenyl)ethan-1-imine (2j)



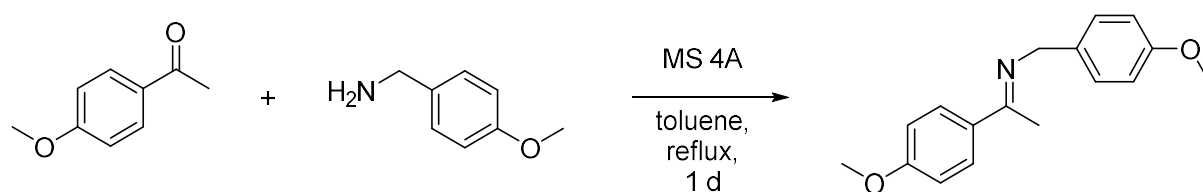
Following GP I, (3,5-di-*tert*-butylphenyl)methanamine (1.05 g, 4.8 mmol, 1.0 equiv.) and 3,5-di-*tert*-butylacetophenone (1.16 g, 5.0 mmol, 1.05 equiv.) were reacted. The crude product was distilled *via* a bulb-to-bulb distillation (0.1 mbar, 170-195 °C) and the was product received as a highly viscous, yellow oil (0.69 g, 1.6 mmol, 33%).

^1H NMR (400 MHz, CD_2Cl_2): δ = 7.74 (d, 4J = 1.8 Hz, 2H), 7.50 (t, 4J = 1.8 Hz, 1H), 7.35 (m, 2H), 7.33 (m, 1H), 4.69 (s, 2H), 2.35 (s, 3H), 1.37 (s, 18H), 1.35 (s, 18H).



9. Tilting the Balance: London Dispersion Systematically Enhances Enantioselectivities in Brønsted Acid Catalyzed Transfer Hydrogenation of Imines

N-(4-methoxybenzyl)-1-(4-methoxyphenyl)ethan-1-imine (2k)

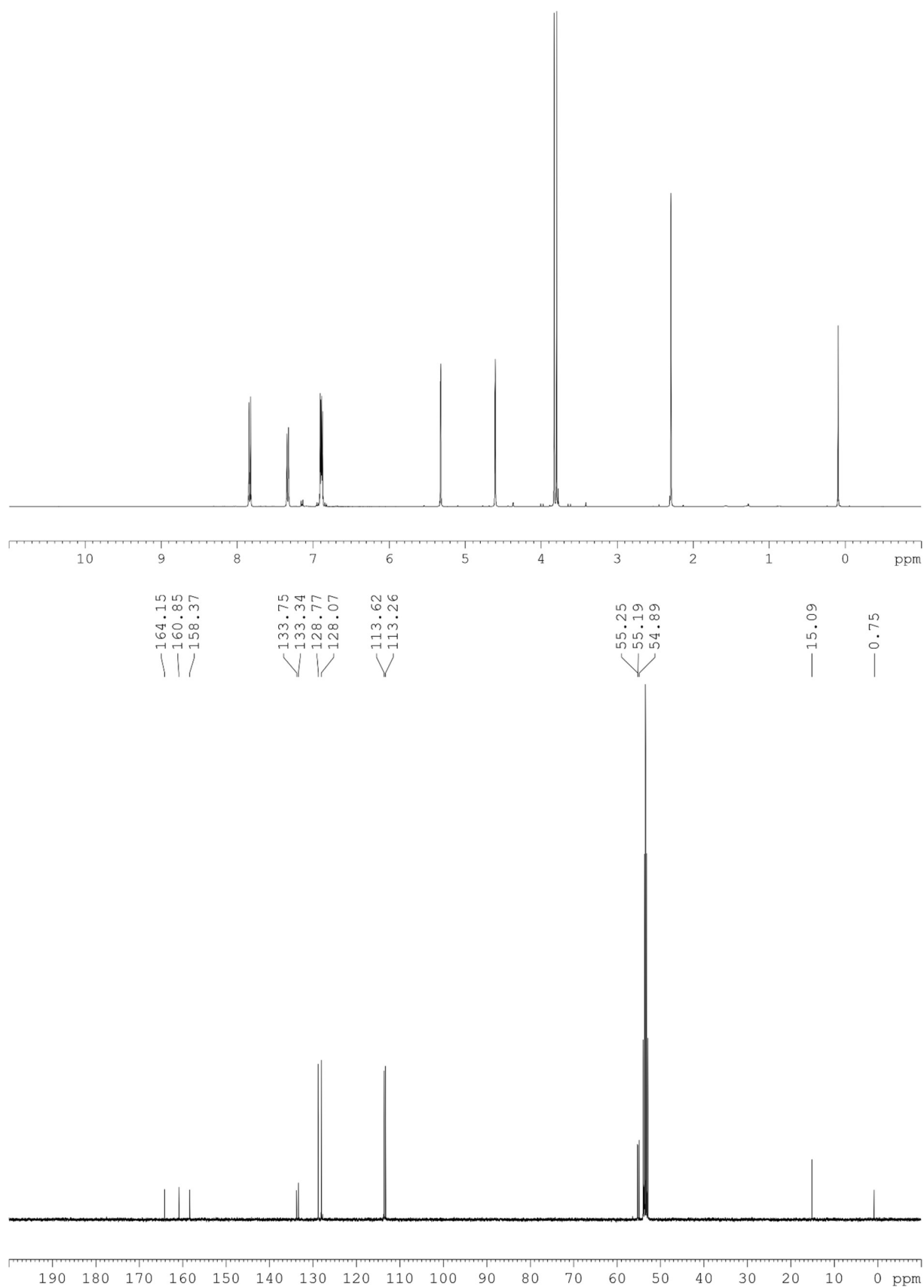


Following GP I, ketone (3.75 g, 25 mmol, 1.0 equiv.) and amine (4.46 g, 5.25 mL, 32.5 mmol, 1.3 equiv.) were refluxed for 1 d. The yellow crude product was recrystallized in methanol to give imine **3e** (3.53 g, 13.8 mmol, 55%) was received as colorless needles and stored at -35 °C in the glovebox (at air atmosphere, the product turns slightly yellowish due to decomposition).

^1H NMR (400 MHz, CD_2Cl_2): δ = 7.84 (m, 2H), 7.33 (m, 2H), 6.90 (m, 4H), 4.60 (s, 2H), 3.83 (s, 3H), 3.79 (s, 3H), 2.30 (s, 3H).

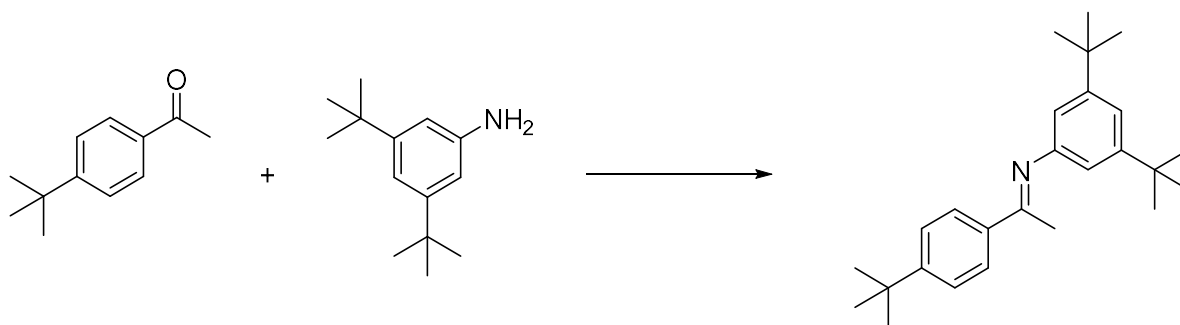
^{13}C NMR (*E*-imine; 100 MHz, CD_2Cl_2): δ = 164.1, 160.9, 158.4, 133.7, 128.8, 113.6, 113.3, 55.3, 55.2, 54.9, 15.1.

9. Tilting the Balance: London Dispersion Systematically Enhances Enantioselectivities in Brønsted Acid Catalyzed Transfer Hydrogenation of Imines



9. Tilting the Balance: London Dispersion Systematically Enhances Enantioselectivities in Brønsted Acid Catalyzed Transfer Hydrogenation of Imines

1-(4-(tert-butyl)phenyl)-N-(3,5-di-tert-butylphenyl)ethan-1-imine (2c)



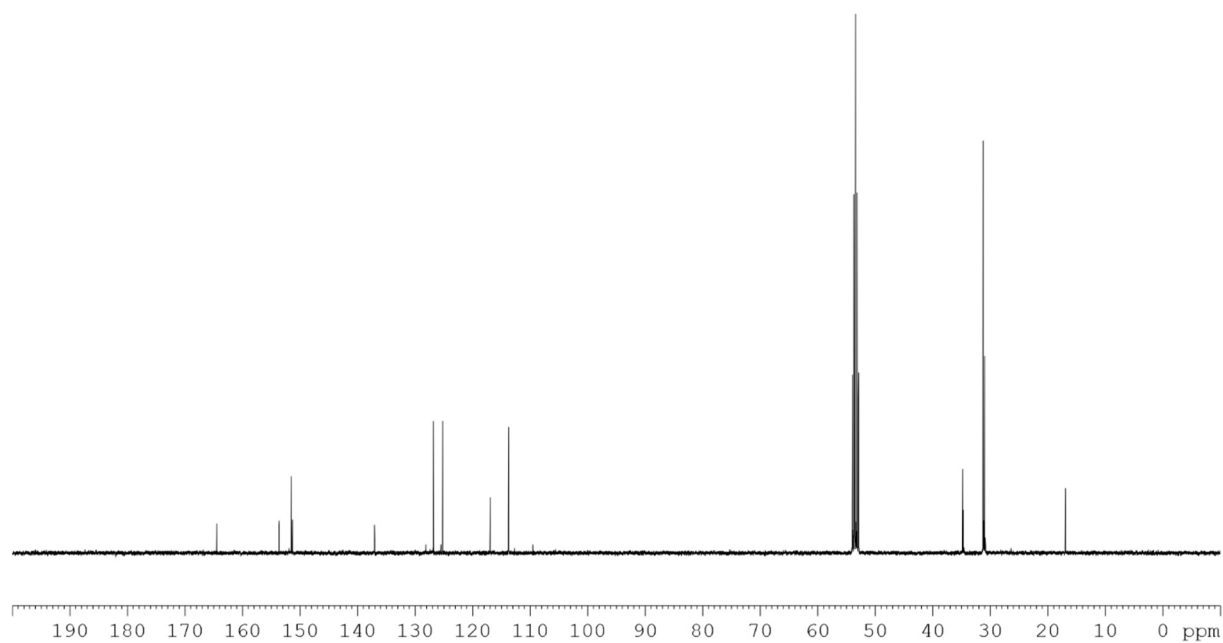
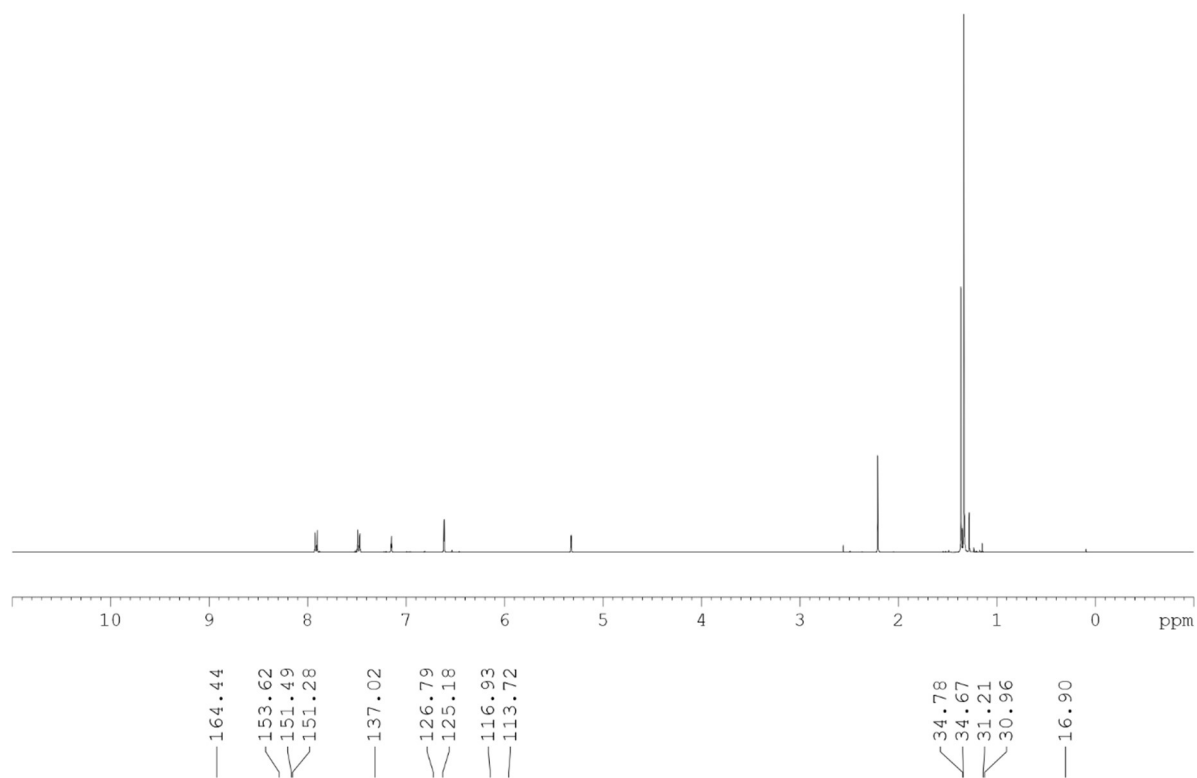
Ketone (1.76 g, 10 mmol, 1.0 equiv.) and amine (2.05 g, 10.0 mmol, 1.0 equiv.) were reacted following GP I. The crude product was purified *via* recrystallization from methanol and the product was received as colorless to beige needles (2.07 g, 5.7 mmol, 57%) predominantly as the *E*-isomer (*Z* : *E* \approx 1 : 64 in CD_2Cl_2 at 298 K).

^1H NMR (400 MHz, CD_2Cl_2): δ = 7.91 (m, 2H), 7.84 (m, 2H), 7.15 (t, J = 1.8 Hz, 1H), 6.61 (d, J = 1.8 Hz, 2H), 2.21 (s, 3H), 1.37 (s, 9H), 1.33 (s, 18H).

^{13}C NMR (100 MHz, CD_2Cl_2): δ = 164.4, 153.6, 151.5, 151.3, 137.0, 126.8, 125.2, 116.9, 113.7, 34.8, 34.7, 31.2, 31.0, 16.9.

HR-MS (EI, m/z): found 364.2999 ($\text{M}+\text{H}$)⁺ (calculated 364.2999 for $\text{C}_{26}\text{H}_{37}\text{N}$); Diff(ppm) = 0.2.

9. Tilting the Balance: London Dispersion Systematically Enhances Enantioselectivities in Brønsted Acid Catalyzed Transfer Hydrogenation of Imines



9. Tilting the Balance: London Dispersion Systematically Enhances Enantioselectivities in Brønsted Acid Catalyzed Transfer Hydrogenation of Imines

General procedure for the asymmetric transfer hydrogenation of imines (GP II)

Imine (0.2 mmol, 1.0 eq.), hydride source (0.28 mmol, 1.4 equiv.) and catalyst (0.02 mmol, 0.1 equiv.) were weighed into a flame dried Schlenk tube. The Schlenk tube was evacuated and flushed with argon three times. Afterwards, toluene (2 mL) was added under argon flow and the reaction was stirred for 1-5 days at the given temperature. The solvent was removed under reduced pressure. Either the crude product was subjugated to HPLC or the mixture was first purified by column chromatography (flash silica gel, petrolether/EtOAc = 9:1) before subjugating it to HPLC. No yields were determined.

For the transfer hydrogenation of imine **2d** at 75 °C (for both hydride sources), the reaction time was 3 d and the crude mixture was subjugated directly to HPLC.

For the transfer hydrogenation of imine **2d** at room temperature, the reaction time was 5 d and the crude mixture was first purified by column chromatography and then subjugated to HPLC.

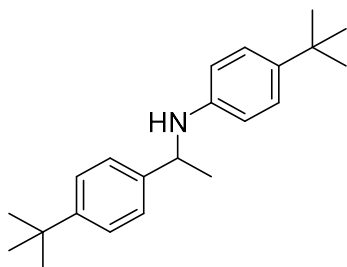
For the transfer hydrogenation of imine **2b** and **2c** at 75 °C, the reaction time was 1 d and the crude mixture was subjugated directly to HPLC.

General procedure for the racemic transfer hydrogenation of imines (GP III)

Imine (0.6 mmol, 1.0 equiv.) and NaBH₄ (227.0 mg, 6.0 mmol, 10 equiv.) were dissolved in CH₂Cl₂ (5 mL) and MeOH (1 mL) was added and the mixture was stirred at room temperature for 3 days. Afterwards, the mixture was quenched by addition of a saturated NaHCO₃ solution and extracted three times with Et₂O. The organic layers were combined and dried with MgSO₄, filtrated and the solvent was removed under reduced pressure. The crude mixture was purified via flash silica gel column chromatography.

9. Tilting the Balance: London Dispersion Systematically Enhances Enantioselectivities in Brønsted Acid Catalyzed Transfer Hydrogenation of Imines

(R)-4-(tert-butyl)-N-(1-(4-(tert-butyl)phenyl)ethyl)aniline (4b)



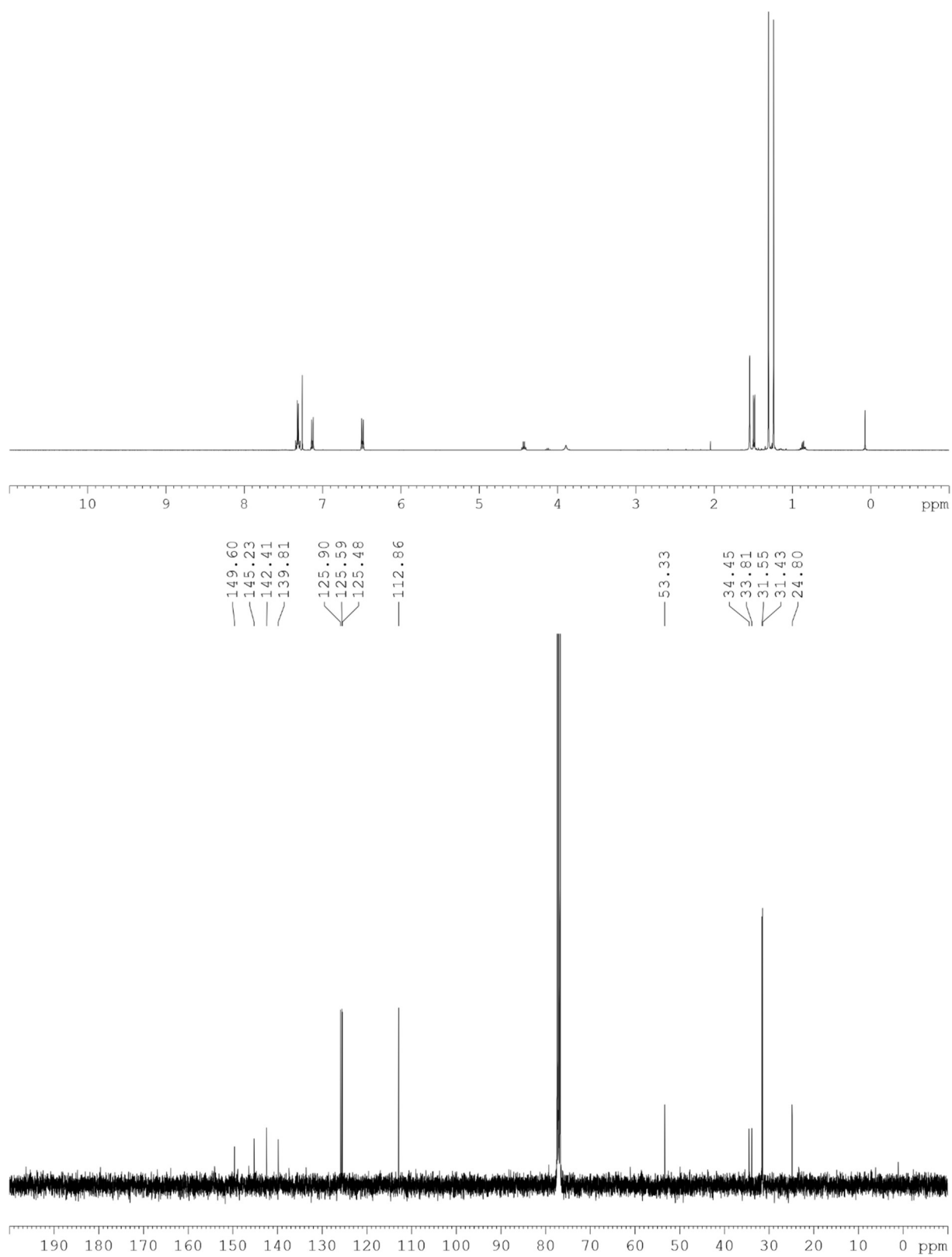
Racemic amine **4b** was synthesised following GP III, eluting with PE/EtOAc 10:1 during column chromatography and received as yellowish solid (117 mg, 0.38 mmol, 63%). The racemate could be separated by CSP-HPLC, CHIRALCEL OD-H column, eluent n-hexane, flow 0.7 mL/min, retention times: τ_1 = 24.38 min, τ_2 = 33.68 min, column compartment temperature 25 °C, λ = 254 nm.

^1H NMR (400 MHz, CDCl_3): δ = 7.32(m, 4H), 7.13 (m, 2H), 6.49 (m, 2H), 4.43 (q, J = 6.7 Hz, 1H), 3.90 (s, 1H), 1.49 (d, J = 6.7 Hz, 3H), 1.30 (s, 9H), 1.24 (s, 9H).

^{13}C NMR (100 MHz, CD_2Cl_2): δ = 149.6, 145.2, 142.4, 139.8, 125.9, 125.6, 125.5, 112.9, 53.3, 34.4, 33.8, 31.5, 31.4, 24.8.

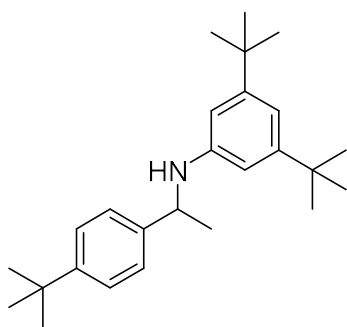
HR-MS (EI, m/z): found 310.2528 (M+H)⁺ (calculated 309.2456 for $\text{C}_{30}\text{H}_{45}\text{N}$); Diff(ppm) = -0.26.

9. Tilting the Balance: London Dispersion Systematically Enhances Enantioselectivities in Brønsted Acid Catalyzed Transfer Hydrogenation of Imines



9. Tilting the Balance: London Dispersion Systematically Enhances Enantioselectivities in Brønsted Acid Catalyzed Transfer Hydrogenation of Imines

3,5-di-tert-butyl-N-(1-(4-(tert-butyl)phenyl)ethyl)aniline (4c)



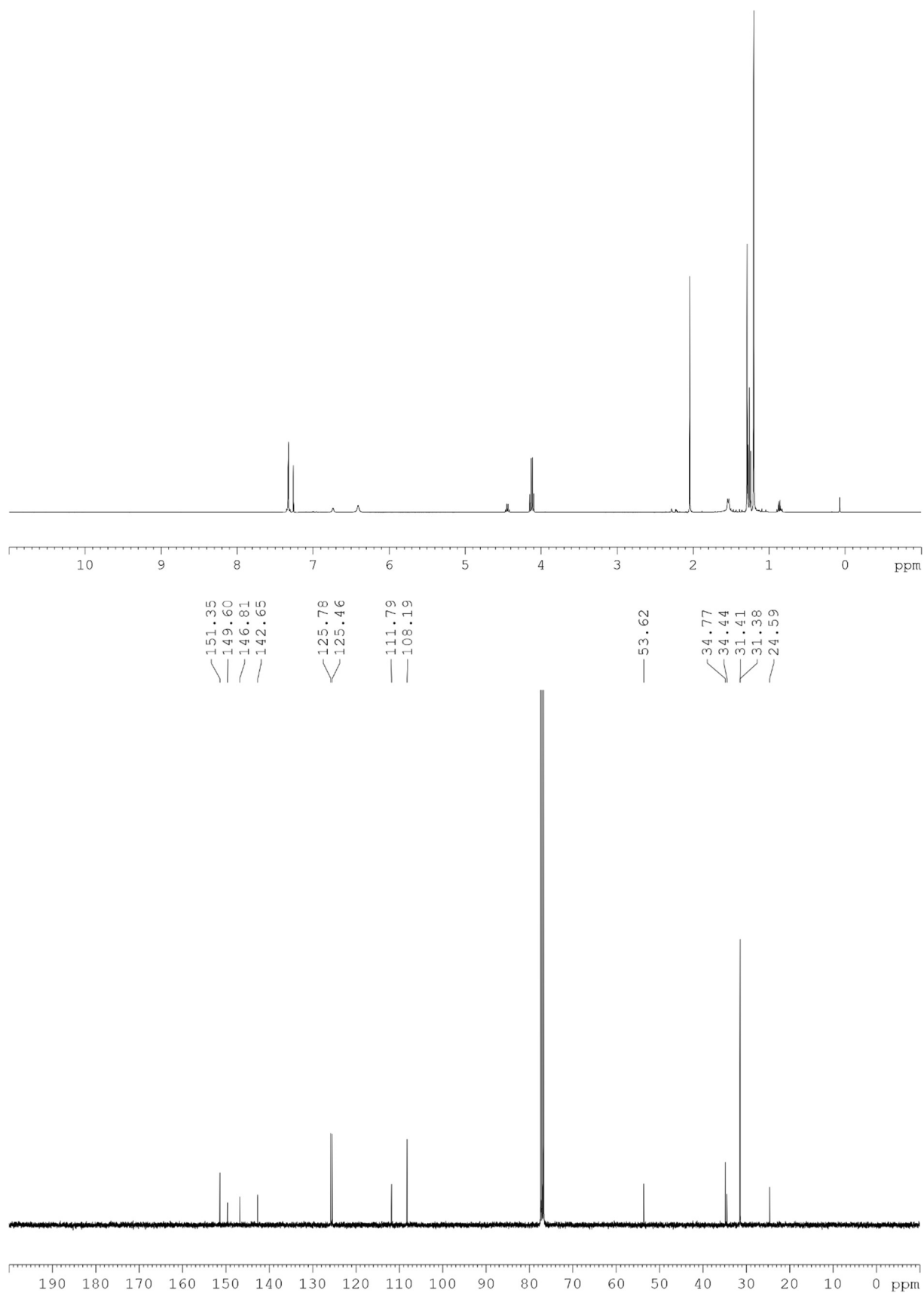
Racemic amine **5f** was synthesised following GP III, eluting with PE/EtOAc 10:1 during column chromatography and received as colourless oil (117 mg, 0.32 mmol, 54%). The racemate could be separated by CSP-HPLC, CHIRALCEL OD-H column, eluent n-hexane, flow 0.2 mL/min, retention times: τ_1 = 45.93 min, τ_2 = 49.66 min, column compartment temperature 20 °C, λ = 254 nm.

^1H NMR (400 MHz, CDCl_3): δ = 7.33 (m, 4H), 6.74 (s, 1H), 6.41 (s, 2H), 4.45 (q, J = 6.6 Hz, 1H), 1.54 (d, J = 6.6 Hz, 3H), 1.29 (s, 9H), 1.20 (s, 18H).

^{13}C NMR (100 MHz, CDCl_3): δ = 151.4, 149.6, 146.8, 142.7, 125.8, 125.5, 111.8, 108.2, 53.6, 34.8, 34.4, 31.4, 31.4, 24.6.

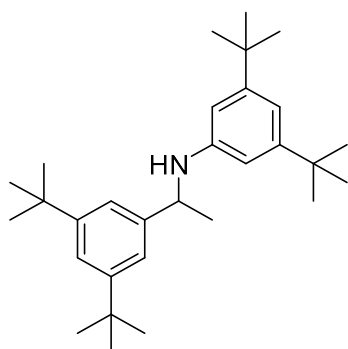
HR-MS (EI, m/z): found 366.3162 ($\text{M}+\text{H}$)⁺ (calculated 365.309 for $\text{C}_{26}\text{H}_{39}\text{N}$); Diff(ppm) = 2.07.

9. Tilting the Balance: London Dispersion Systematically Enhances Enantioselectivities in Brønsted Acid Catalyzed Transfer Hydrogenation of Imines



9. Tilting the Balance: London Dispersion Systematically Enhances Enantioselectivities in Brønsted Acid Catalyzed Transfer Hydrogenation of Imines

3,5-di-tert-butyl-N-(1-(3,5-di-tert-butylphenyl)ethyl)aniline (4d)



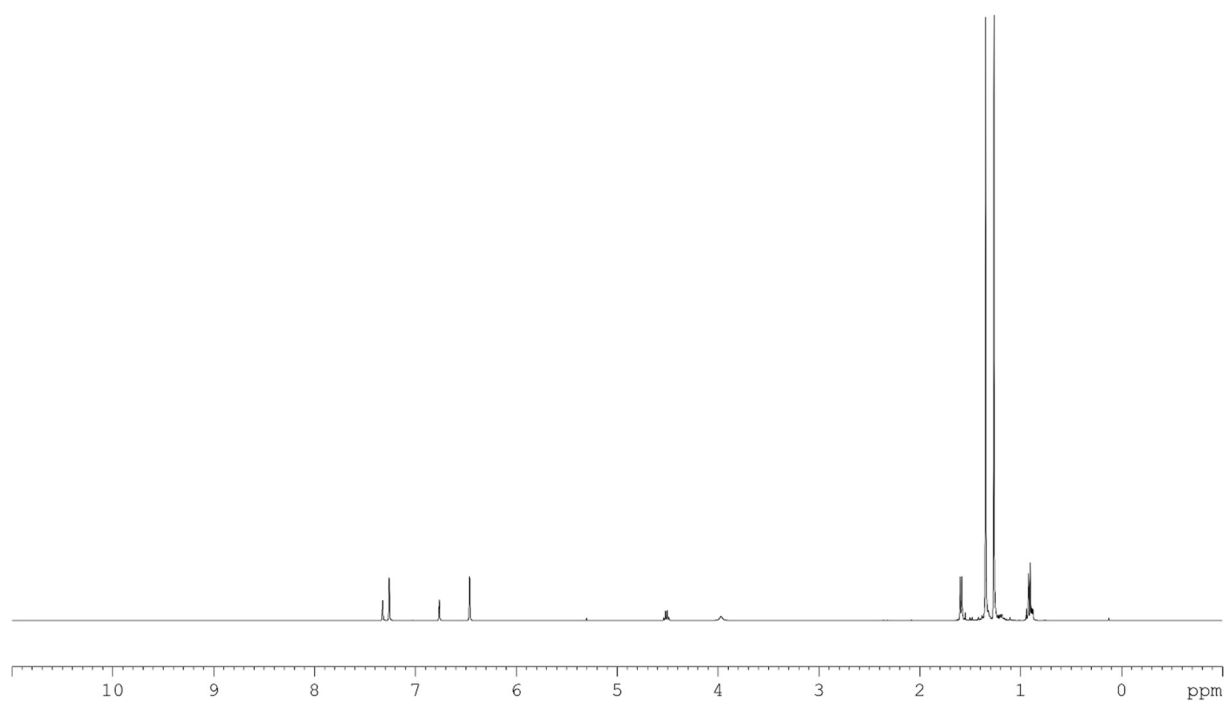
Racemic amine **4d** was synthesised following GP III, eluting with PE/EtOAc 9:1 during column chromatography and received as colourless oil (168 mg, 0.4 mmol, 66%). The racemate could be separated by CSP-HPLC, CHIRALCEL OD-H column, eluent n-hexane, flow 0.2 mL/min, retention times: τ_1 = 13.15 min, τ_2 = 14.86 min, column compartment temperature 20 °C, λ = 254 nm.

^1H NMR (400 MHz, CDCl_3): δ = 7.28 (t, 4J = 1.5 Hz, 1H), 7.22 (d, 4J = 1.6 Hz, 2H), 6.72 (d, 4J = 1.5 Hz, 1H), 6.42 (d, 4J = 1.5 Hz, 2H), 4.47 (q, 3J = 6.7 Hz, 1H), 3.93 (broad s, 1H), 1.55 (d, 3J = 6.7 Hz, 3H), 1.30 (s, 18H), 1.22 (s, 18H).

^{13}C NMR (100 MHz, CDCl_3): δ = 151.3, 150.8, 147.1, 144.7, 120.5, 111.8, 108.4, 54.8, 34.9, 34.8, 31.6, 31.4, 24.4.

HR-MS (EI, m/z): found 422.3783 (M+H)⁺ (calculated 422.371 for $\text{C}_{30}\text{H}_{48}\text{N}$); Diff(ppm) = 0.46.

9. Tilting the Balance: London Dispersion Systematically Enhances Enantioselectivities in Brønsted Acid Catalyzed Transfer Hydrogenation of Imines



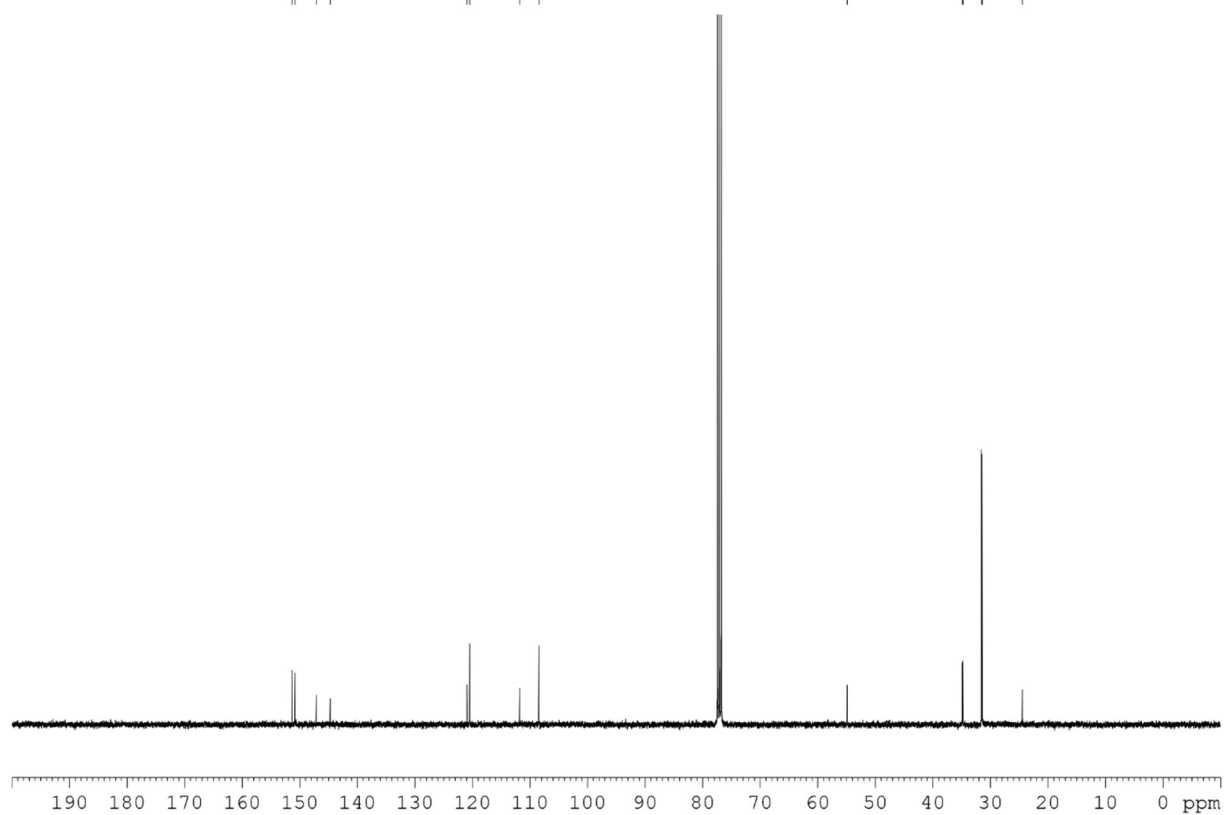
151.29
150.83
147.11
144.70

120.90
120.45

111.77
108.44

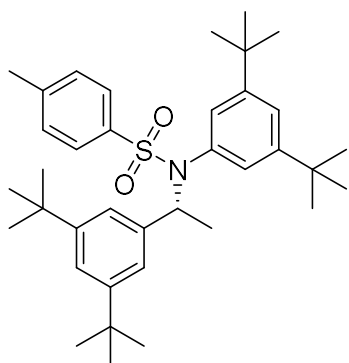
54.84

34.89
34.76
31.55
31.42
24.42



9. Tilting the Balance: London Dispersion Systematically Enhances Enantioselectivities in Brønsted Acid Catalyzed Transfer Hydrogenation of Imines

**(R)-N-(3,5-di-tert-butylphenyl)-N-(1-(3,5-di-tert-butylphenyl)ethyl)-4-methylbenzenesulfonamide
(5)**



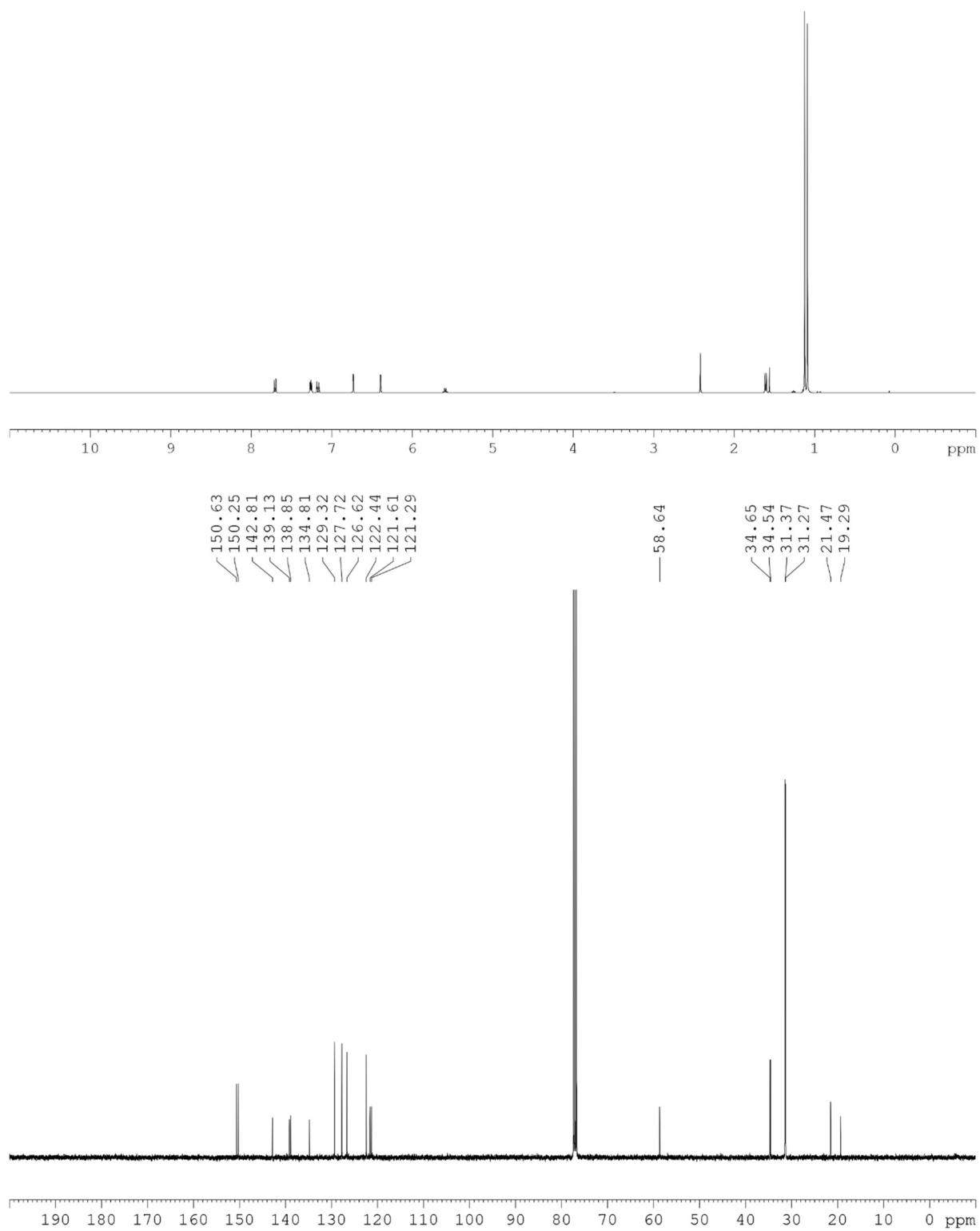
Amine **4d** (253.0 mg, 0.6 mmol, ee >98%, 1.0 equiv.) and tosyl chloride (148.7 mg, 0.78 mmol, 1.3 equiv.) were weighed in a round bottom flask and pyridine (6 mL) was added. The reaction was stirred at 100 °C for 3 days giving a red-brownish mixture. Water (15 mL) was added and the mixture was extracted with EtOAc (3x 25 mL). The organic layers were combined, dried over MgSO₄, filtrated and the solvent was removed under reduced pressure. The crude product was recrystallized from methanol to yield the product as colorless needles (187 mg, 0.32 mmol, 54%), which were sufficient for single crystal X-Ray analysis.

¹H NMR (400 MHz, CDCl₃): δ = 7.70 (m, 2H), 7.26 (m, 2H), 7.18 (t, *J* = 1.7 Hz, 1H), 7.16 (t, *J* = 1.7 Hz, 1H), 6.73 (d, *J* = 1.7 Hz, 2H), 6.39 (d, *J* = 1.7 Hz, 2H), 5.59 (q, *J* = 7.0 Hz, 1H), 2.42 (s, 3H), 1.61 (d, *J* = 7.0 Hz, 3H), 1.12 (s, 18H), 1.09 (s, 18H).

¹³C NMR (100 MHz, CDCl₃): δ = 150.6, 150.3, 142.8, 139.1, 138.8, 134.8, 129.3, 127.7, 126.6, 122.4, 121.6, 58.6, 34.6, 34.5, 31.4, 31.3, 21.5, 19.3

HR-MS (EI, *m/z*): found 576.3871 (M+H)⁺ (calculated 575.3799 for C₃₇H₅₃NO₂S); Diff(ppm) = 0.33.

9. Tilting the Balance: London Dispersion Systematically Enhances Enantioselectivities in Brønsted Acid Catalyzed Transfer Hydrogenation of Imines



9.6.3. Chemical exchange saturation transfer (CEST) experiments

Qualitative CEST measurements were done using an adapted pulse sequence previously introduced in our group.⁷ For the selective saturation, a power (PLW10) of 40-50 -dBW (hard pulse: 12 [W], -10.79 [-dBW]) and a saturation length (D6) of 0.5-1.0 s was applied. The saturation power was optimized to achieve a maximum signal reduction of the observed signal of the major exchange partner (saturation applied on respective signal of minor exchange partner), while still not affecting the signal of the major exchange partner directly. Therefore, the saturation was applied on the same chemical shift difference $\delta_{\text{minor}} - \delta_{\text{major}}$ on the other side of the observed peak. For the reference spectrum, the saturation power was set to 0 W. The saturation length was optimized to obtain a significant drop in signal intensity while still being the shortest length possible. To obtain the CEST profiles, the saturation offset was swept through the part of the spectrum in 25 or 50 Hz increment steps and referenced to the reference spectrum to obtain the signal reduction.

Additional CEST measurements

In addition to imine **2a**, CEST profiles of imines **2e-g** were recorded to reveal, if the *Z/E* ratio is affected by the electrostatic properties of the substituent. For all three imines, similar CEST profiles were recorded, revealing the presence of the *Z*-imine. *Z/E* integral ratios of 1:60, 1:78 and 1:66 were determined, which is similar to the *Z/E* ratios of imines **2a** and **2b**, considering the error range of integration for two peaks with a strong difference in intensity. The population difference reflects an energetic difference ΔG_{E-Z} of $\approx -11.2 / -11.5 / -12.0$ kJ/mol, which is close to the one determined for imines **2a** and **2b**. Hence, modulating the electrostatic properties of the substrate does not significantly influence the *Z/E* ratios.

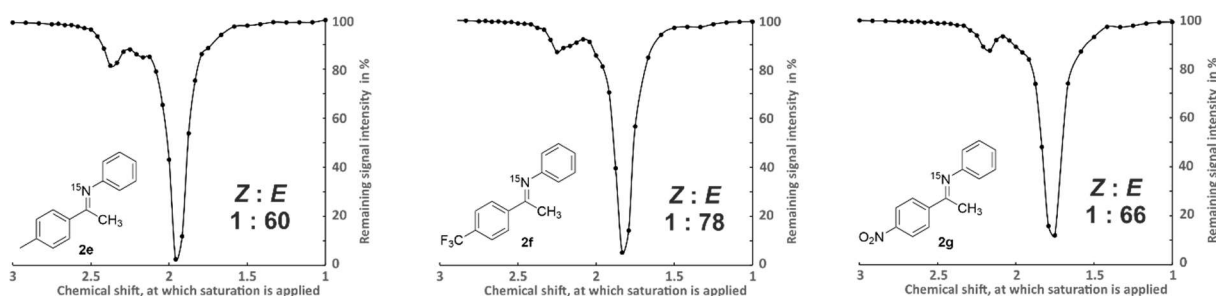


Figure S1: CEST plot of imines **2e-g** in toluene at 330 K.

Next, imines **2h-j** (see Figure S2) were employed to elucidate the impact of London dispersion on the *Z/E* equilibrium. Hence, *tert*-butyl groups in all *meta*-positions were selected as suitable London dispersion energy donors as the respective starting materials were readily available and an observable impact was expected if – similar to the azobenzene systems investigated by Wegner *et al.*⁸ – London

9. *Tilting the Balance: London Dispersion Systematically Enhances Enantioselectivities in Brønsted Acid Catalyzed Transfer Hydrogenation of Imines*

dispersion overwrites steric repulsion. Additionally, the α -substituent as one key factor affecting the *Z/E* ratio was modulated (α -H and α -CH₃) to see, whether *Z*-aldimines can be populated as aldimines are a suitable target for various nucleophiles whereas ketimines are usually only targeted in asymmetric transfer hydrogenations. Moreover, the *N*-aryl moiety was modulated to a *N*-benzyl moiety to add more flexibility and to include the *N*-benzyl protected imine framework which is frequently used in synthesis.

For 2h, no *Z*-imine was detectable. Given that an increased size of the α -substituent is the main driving force to populate the *Z*-imine, it is not surprising that the potential London dispersion interactions between the *tert*-butyl groups in *Z*-2h cannot overcome this. Due to the significant offset in chemical shifts of the α -H signal observed e.g. for *Z*-2j (8.72 ppm) and *E*-2j (8.31 ppm), it is unlikely that the signals of *Z*-2h and *E*-2h overlap. A fast exchange on the NMR time scale between *Z*-2h and *E*-2h is also unlikely due to the expected similar activation barrier compared to e.g. imine 2a-d.

For 2d, both imine isomers were unambiguously identified *via* the CEST profile (see Figure S2, B, highlighted area) and an *Z/E* integral ratio of 1 : 14 was determined, reflecting an energetic difference ΔG_{E-Z} of = -7.2 kJ/mol. Comparison to the London dispersion free reference systems 2b ($\Delta G_{E-Z} \approx -11.7$ kJ/mol) clearly shows, that the attractive interactions caused by the *tert*-butyl groups overwrite their steric repulsion and account to ~ 4 -5 kJ/mol stabilizing the *Z*-imine.

9. Tilting the Balance: London Dispersion Systematically Enhances Enantioselectivities in Brønsted Acid Catalyzed Transfer Hydrogenation of Imines

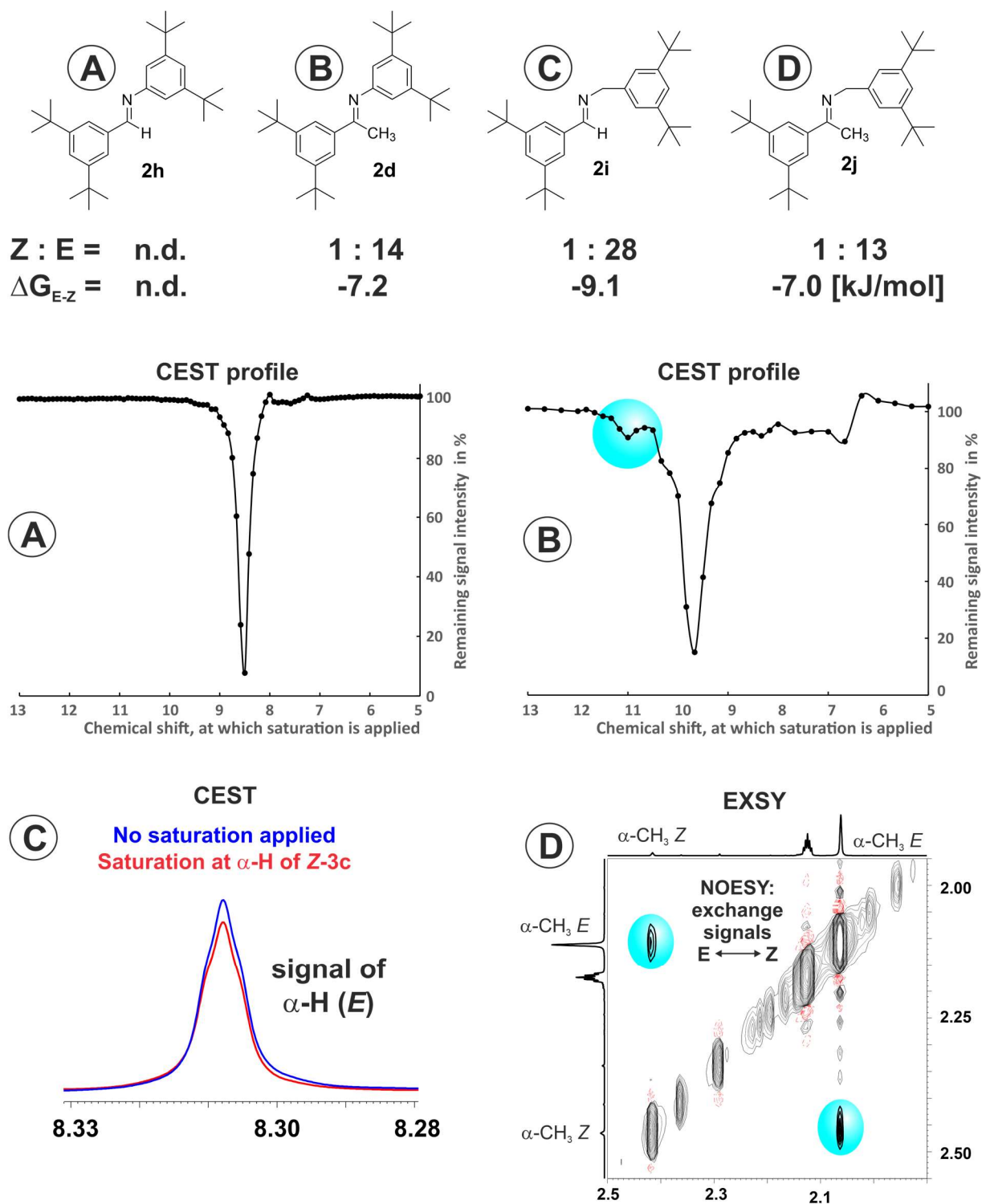


Figure S2: Z/E ratios of imines **2d** and **2h-j** determined by integration at 330 K in C₆D₆ and energetic difference derived by the Boltzmann equilibrium. For imine **2h**, no Z-imine was detectable (see CEST profile A). For imine **2d**, the Z-imine was unambiguously identified *via* the CEST profile (see highlighted part of B). For imine **2i**, the Z-imine could be identified *via* qualitative CEST at 360 K and was validated by ¹H ¹³C HSQC spectrum. For imine **2j**, CEST measurements were not fruitful, but the minor exchange partner could be identified *via* the exchange signals observed in the phase-sensitive NOESY spectrum.

9. Tilting the Balance: London Dispersion Systematically Enhances Enantioselectivities in Brønsted Acid Catalyzed Transfer Hydrogenation of Imines

For aldimine **2i**, the presence of Z-**2i** could be shown by qualitative CEST measurements at 360 K (see Figure S2C) and was validated by ^1H ^{13}C HSQC and an integral ratio of Z/E of 1 : 28 (at 330 K) was obtained, reflecting an energetic difference of ΔG_{E-Z} of = -9.1 kJ/mol. We assume, that for **2i** – in contrast to **2h** – now the Z-imine is energetically more stable because the N-benzyl group acts as a flexible spacer, reducing the steric repulsion between the two aryl moieties in the Z-imine and allowing for an optimised interaction pattern.

For imine **2j**, CEST measurements were not fruitful in identifying the Z-imine most likely due to selectivity issues. However, the exchange signals monitored in a ^1H NOESY spectrum (see Figure S2D highlighted area) clearly pinpointed the presence of the Z-imine and an integral ratio of Z/E of 1 : 13 was obtained, reflecting an energetic difference of ΔG_{E-Z} of = -7.0 kJ/mol. For imines **2d** and **2j**, the additional flexibility introduced by the N-benzyl group has close to no effect on the Z/E ratio, indicating that for already in **2d** the London dispersion interaction pattern is optimal.

Error estimation for Z/E ratios

All Z/E ratios which were translated to thermodynamic data were determined by integration in the ^1H NMR spectra. All samples were equilibrated at the temperature of the measurements inside the spectrometer for a sufficient amount of time. No significant changes in the ratios were monitored over the course of the measurements (>1 hour). The signals selected for integration were well baseline separated. A sufficient relaxation time delay was set in between the scans to achieve full relaxation. We assumed a general integration error of 5, 7 or 10% for ratios of < 1:20; 1:20 < ratio < 1:50 and > 1:50 respectively (e.g. at a Z/E ratio of 1:100, the error range would be ratios of 1:90 – 1:110). When estimating the error of ΔG_{E-Z} we calculated the ΔG_{E-Z} values for the lower and upper limit of the ratio range and the error is given as the average by: $(\Delta G_{E-Z}(\text{ratio}+\text{error}) - \Delta G_{E-Z}(\text{ratio}) + \Delta G_{E-Z}(\text{ratio}) - \Delta G_{E-Z}(\text{ratio}-\text{error}))/2$. The values were rounded to the first decimal. For the error for $\Delta\Delta G_{E-Z}$ values we added the rounded errors of the two ΔG_{E-Z} contributions. This was applied to the ratios obtained for the free imines as well as for the ratios of binary CPA/imine complexes.

9.6.4. Additional measurements on CPA/N-aryl complexes

Initially, we investigated complexes of imine **2h** with various catalysts **1** to control, if a CPA/Z-aldimine complex can be sufficiently populated by combining reduced steric repulsion between CPA and imine with the putative stabilization of Z-**2h** by London dispersion (see Figure S3).

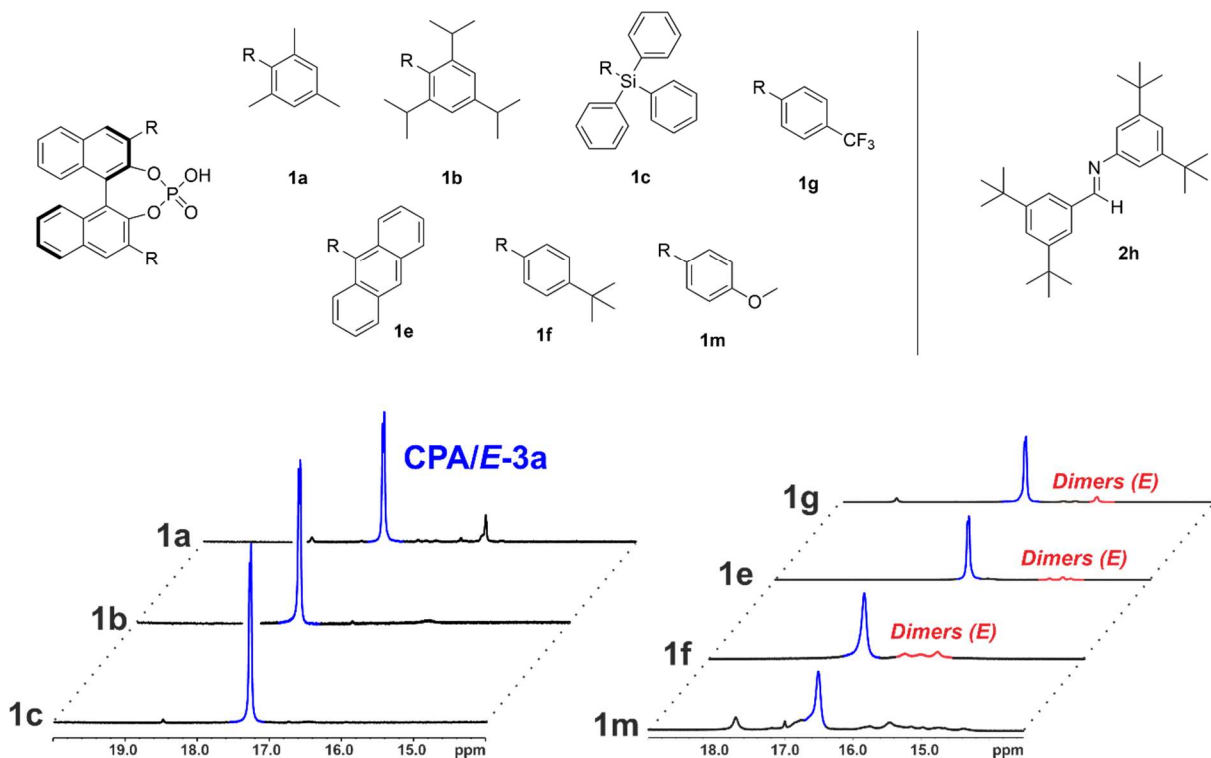


Figure S3: Excerpt of the ¹H NMR spectra of **1/2h** in CD₂Cl₂ at 180 K and 600 MHz depicting the hydrogen bonding region. For all systems, one dominant species highlighted in blue was observed, corresponding to the CPA/E-**2h** complex. No significant signal corresponding to CPA/E-**2h** was monitored. For **1e-g/2h**, additional signals highlighted in red could be assigned as dimers of CPA/E-**2h** based on DOSY NMR measurements.

For all systems, one dominant hydrogen bonded proton signal (see Figure S3, highlighted in blue) was observed, corresponding to the CPA/E-**2h** complex as validated by ¹H NOESY spectra and the preparation of *E*-only samples (samples prepared at low temperature to prevent *E*→*Z* imine isomerization and thus bearing near exclusive *E*-imine population). For **1e-g/2h**, some characteristic additional signals highlighted in red were monitored. For **1g/2h**, a chemical shift assignment for this species was achieved via a series of homo- and heteronuclear 2D spectra and diffusion ordered spectroscopy (DOSY) NMR measurements revealed, that this species likely is a [**1d/2h**]₂ dimer, giving a hydrodynamic volume of ~7800 Å³ compared to a hydrodynamic volume of ~4800 Å³ for the monomeric **1d/E-2h** (red signal). Such dimers were previously characterised for e.g. **1a/2a** and feature two stacked imines inside the binding pocket spanned by two CPA molecules.⁹ However, the presence of such dimers for imine **2h**

9. Tilting the Balance: London Dispersion Systematically Enhances Enantioselectivities in Brønsted Acid Catalyzed Transfer Hydrogenation of Imines

was unexpected as it was previously shown on **1a/2b**, that the steric bulk of *tert*-butyl groups effectively prevents the stacking of the imines inside the binding pocket of the two catalysts in the [CPA/imine]₂ dimer and thus suppresses dimerization.⁴ The formation of [**1g/2h**]₂ dimers might be caused by an extended interaction framework overcoming the steric repulsion between two stacked imines.

9.6.5. Additional measurements on CPA/N-benzyl complexes

In addition to N-aryl substituted imines **2d** and **2h**, also complexes with the N-benzyl substituted imine **2j** were investigated to show the transfer of intramolecular London dispersion on the respective binary CPA/imine complexes bearing a more flexible nitrogen substituent. Catalysts **1a** and **1b** were selected as they are widely applied in synthesis, have good solubility and are symmetric. Imine **2k** was selected as a dispersion free reference, bearing two methoxy-groups as ideal probes for NMR investigations. Noteworthy, for **2k** in absence of an CPA, no *Z*-imine could be detected, corroborating the suitability as reference system. Imine **2j** was selected exemplarily for imines with significant intramolecular London dispersion interactions in the *Z*-imine and a minimum stabilization energy of ~4-5 kJ/mol by London dispersion was assumed based on the results shown previously (see Figure S2).

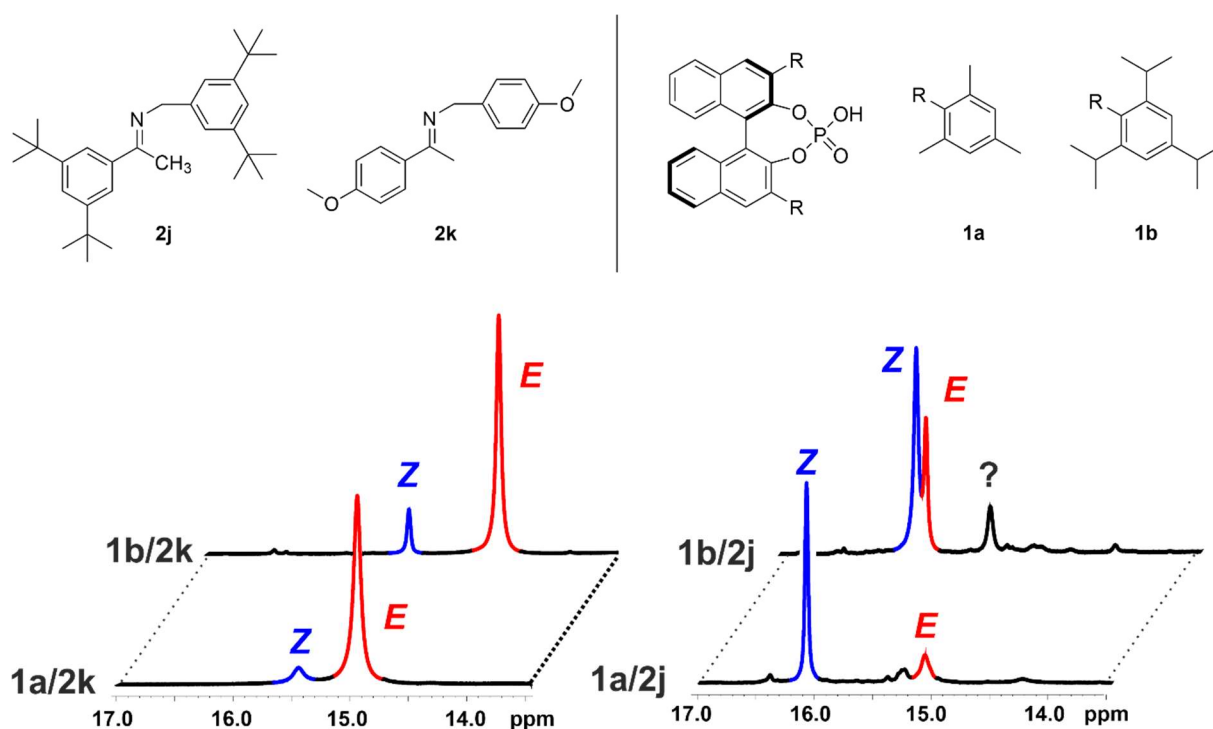


Figure S4: Excerpt of the ¹H NMR spectra of **1a-b/2j-k** in CD₂Cl₂ at 180 K and 600 MHz depicting the hydrogen bonding region. For **1a-b/2k**, two complexes were found, corresponding to the CPA/*Z*-**2k** (blue, minor) and CPA/*E*-**3e** (red, major) complex. For **1a-b/2j**, the CPA/*Z*-**2j** was found as the dominant species (blue) and the CPA/*E*-**2j** was identified (red) as the minor species. However, additional signals were monitored which could not be clearly assigned. For determining the *Z/E* ratios, the additional signals were ignored.

9. Tilting the Balance: London Dispersion Systematically Enhances Enantioselectivities in Brønsted Acid Catalyzed Transfer Hydrogenation of Imines

For **1a/2k** and **1b/2k**, two distinct proton signals were detected in the hydrogen bond region, corresponding to the **1a-b/Z-2k** (see Figure S4, blue signals) and **1a-b/E-2k** complexes (see Figure S4, red signals). Based on a set of 2D spectra, a chemical shift assignment for both systems could be achieved. Analysis of the NOE pattern validated the assignment of the imine configuration and corroborated, that the four core structures Type I and II *E* (fast exchanging, one signal set CPA/*E-2k*), as well as Type I and II *Z* (fast exchanging, one signal set CPA/*Z-2k*) which were found in our previous work on *N*-aryl imines^{9,10} are conserved for *N*-benzyl imines, thus ensuring comparability of the *Z/E* ratios and interaction energies. For both systems, the CPA/*E-2k* complex is significantly favored (see Table S1 for integral ratios) by ~2.9 kJ/mol.

In contrast, for **1a/2j** and **1b/2j**, the CPA/*Z-2j* complex (see Figure S4 right, blue signals) was found to be the dominant species (see Table S1 for integral ratios), favored by 1.0-1.6 kJ/mol. The respective CPA/*E-2j* complexes (see Figure S4 right, red signals) were identified *via* the characteristic highfield shift of the hydrogen bonded proton and lowfield shift of the α -CH₃ group compared to CPA/*Z-2j*, as well as *via* the characteristic NOE pattern of those two groups. However, additional signals in the hydrogen bond region were detected but the corresponding species could not be elucidated due to the too low signal intensities. For comparison of the *Z/E* ratios of **1a-b/2j** to **1a-b/2k**, these species were ignored as they only would have a minor impact on the ratios and would not change the qualitative trend.

Table S1: *Z/E* ratios of complexes **1a-b/2j-k** in CD₂Cl₂ at 180 K and resulting energetic difference between CPA/*E*-imine and CPA/*Z*-imine ΔG_{E-Z} (positive values \rightarrow CPA/*Z*-imine is more stable than CPA/*E*-imine) and London dispersion interaction energy $\Delta\Delta G_{3b-2a}$ ($\Delta G_{E-Z}(\mathbf{2j}) - \Delta G_{E-Z}(\mathbf{2k})$).

Catalyst	<i>Z/E</i> ratio with imine		ΔG_{E-Z} [kJ/mol] for imine		$\Delta\Delta G_{2k-2j}$ [kJ/mol]
	2k	2j	2k	2j	
1a	12 : 88	75 : 25	-3.0	1.6	4.6
1b	13 : 87	66 : 34	-2.8	1.0	3.8

Comparing ΔG_{E-Z} of **1a-b/2j** and **1a-b/2k**, it becomes clear that the *Z/E* preferences gets inverted, if intramolecular London dispersion interactions are present within the *Z*-imine. The $\Delta\Delta G_{3e-3d}$ value, reflecting the energetic contribution of these interactions, accounts to 3.8-4.6 kJ/mol, which is close to the stabilization energy of ~4-5 kJ/mol observed for the free imine **2j**. This suggests, that unlike for **1a-c/2d** (see manuscript Figure 6 and Table 1) where an $\Delta\Delta G$ range of 3.2-7.2 kJ/mol was observed, steric factors affect the *Z/E* ratio much less and London dispersion interaction is the main driving force. This is reasonable, as the additional flexibility of the imine obtained by the introduction of the CH₂-group on the *N*-benzyl fragment allows for a better adjustment of the *E*-imine inside the binding pocket of

9. Tilting the Balance: London Dispersion Systematically Enhances Enantioselectivities in Brønsted Acid Catalyzed Transfer Hydrogenation of Imines

the catalyst. Hence, intramolecular London dispersion interactions can significantly affect the stabilization of CPA/Z-N-benzyl imine complexes and can even invert the favored imine configuration.

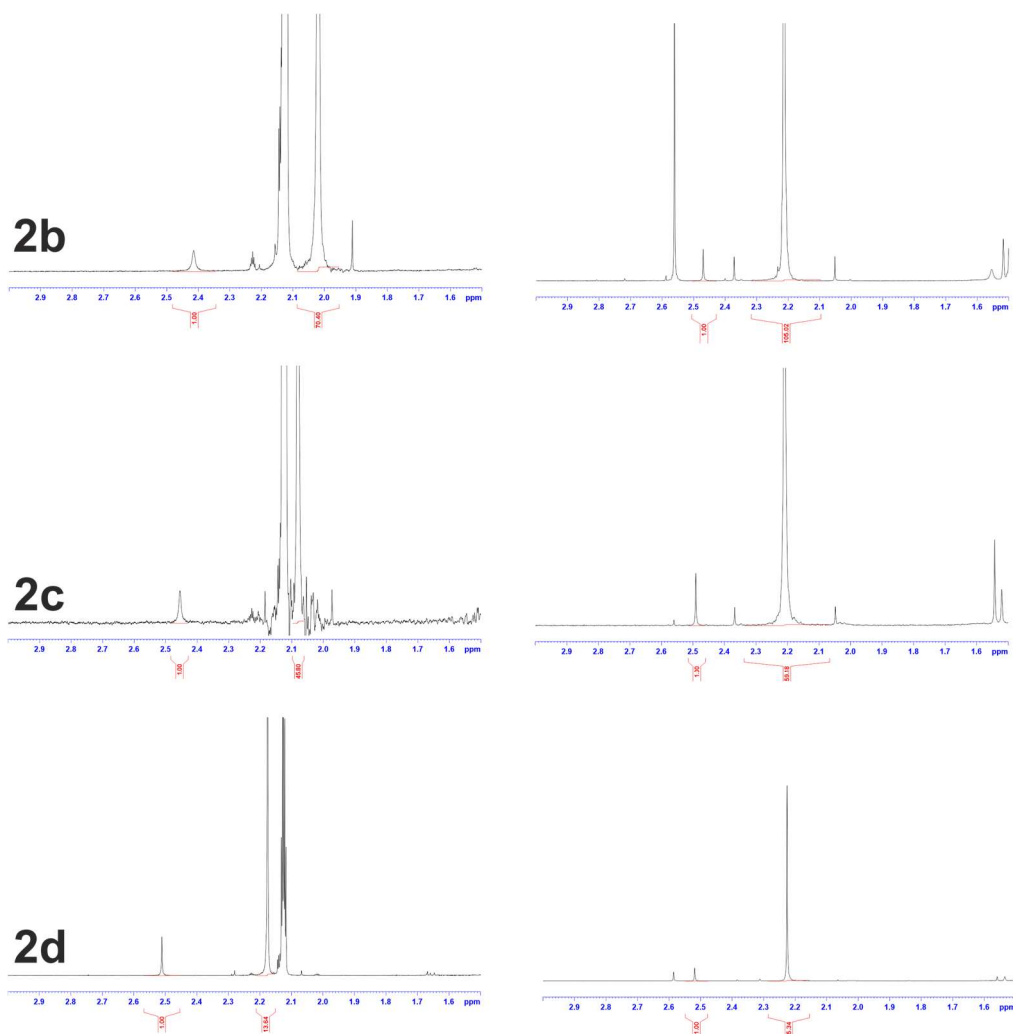
9.6.3. Overview and spectra for Z/E ratios

Figure S5: Z:E ratios and ^1H NMR spectra of imines **2b-d** in toluene at 330K or in dichloromethane at 298 K. In DCM, the Z-imine has a slightly higher stability than in toluene (0.2, 0.4 and 0.2 kJ/mol respectively for **2b**, **2c** and **2d**), but in general the ratios and $\Delta G(\text{E-Z})$ values are similar.

	2b		2c		2d	
Z/E ratios in toluene 330K	1	70	1	46	1	14
$\Delta G(\text{E-Z})$ in toluene 330 K		-11.7		-10.5		-7.2
Z/E ratios in DCM 298K	1	105	1	59	1	16.8
$\Delta G(\text{E-Z})$ in DCM 298K		-11.5		-10.1		-7.0

Toluene, 330K

Dichloromethane, 298K



9. Tilting the Balance: London Dispersion Systematically Enhances Enantioselectivities in Brønsted Acid Catalyzed Transfer Hydrogenation of Imines

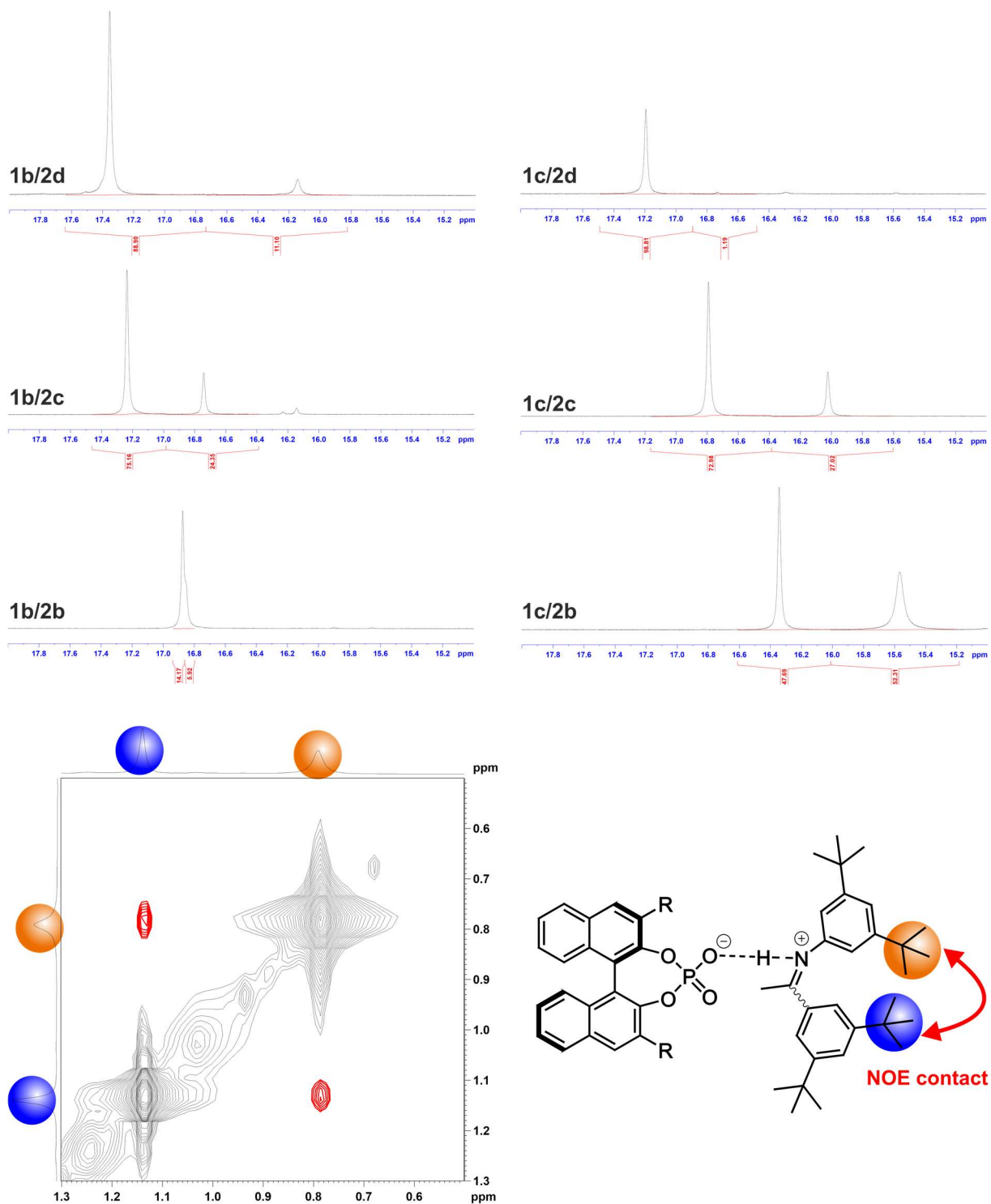


Figure S6: Top: *Z:E* ratios and ^1H NMR spectra of binary complexes **1b-c/2b-d** in dichloromethane at 180 K. Bottom: Excerpt of the NOESY spectrum of **1a/2d** at 180 K showing intramolecular NOE contacts (red) between the *tert*-butyl groups of the two aryl moieties (blue and orange) of the *Z*-imine.

9.6.7. Ternary complex formation

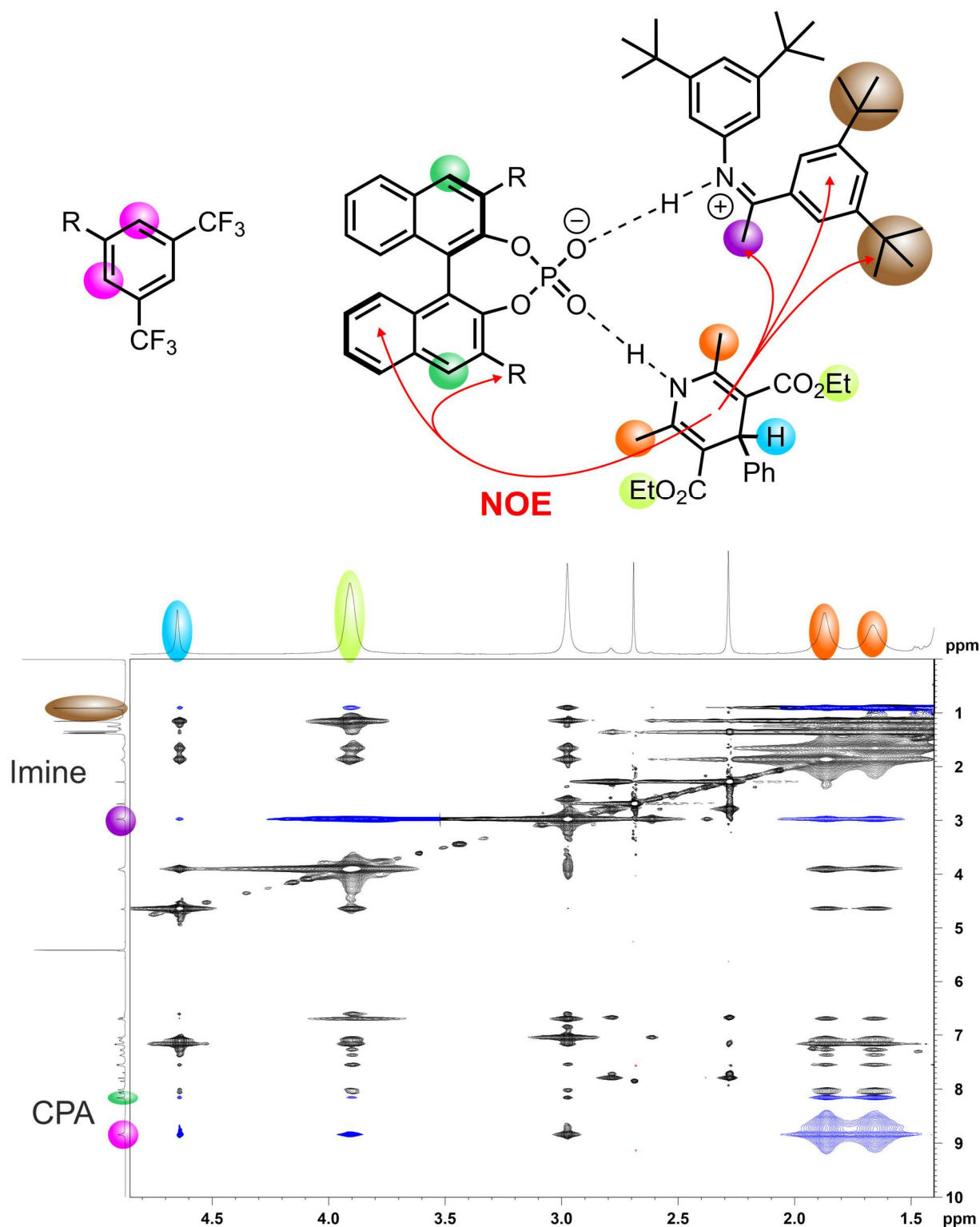


Figure S7: Section of the ^1H NOESY spectrum of **1d/2d/3b** at a 1:1:1 ratio and a concentration of 25 mM in CD_2Cl_2 at 180 K and 600 MHz. NOE cross peaks marked in dark blue between the Hantzsch ester (bright blue, bright green and orange marked signals) and the CPA (3,3'-substituent in magenta, BINOL backbone in dark green) as well as the imine ($\alpha\text{-CH}_3$ group in violet and ^tBu -group in brown) were observed. Especially the NOE contacts between imine and Hantzsch ester were shown to be only possible within the ternary complex, validating the formation of the ternary complex.

9. Tilting the Balance: London Dispersion Systematically Enhances Enantioselectivities in Brønsted Acid Catalyzed Transfer Hydrogenation of Imines

To obtain qualitative insights, whether the equilibrium between binary and ternary complex is mainly on the binary or the ternary side, DOSY experiments were performed. If DOSY measurements are performed on a signal, which reflects two fast exchanging species, the resulting self-diffusion coefficient is the sum of the self-diffusion coefficients of each species weighed by their population. Hence, if the two exchanging species have a significant offset in size (e.g. free Hantzsch ester and complexed one), the derived self-diffusion coefficient gives qualitative insights about the dominant species.

DOSY measurements were performed with the convection suppressing DSTE (double stimulated echo) pulse sequence developed by Jerschow and Müller in a pseudo 2D mode.¹¹ Smoothed square (SMSQ10.100) gradient shapes and a linear gradient ramp with 20 increments between 5% and 95% of the maximum gradient strength (5.35 G/mm) were used. The diffusion time delay was set to 45 ms. For the homospoil gradient strengths, values of 100, -13.17, 20 and -17.13 % were used. Gradient pulse lengths (p16) were first optimized to obtain a sigmoidal signal decay for increasing gradient strength (3.0 ms for TMS, 6.0 – 6.5 ms for CPA/imine complexes). NMR spectra were processed with Bruker TopSpin 3.2 (T1/T2 relaxation package) and diffusion coefficients were derived according to Jerschow and Müller.¹¹ Tetramethylsilan was added to the samples to reference chemical shifts and the viscosity of each sample.

The molecular radii were derived by the Stokes-Einstein equation¹² using Chens correction.¹³

$$D_i = \frac{k_B T}{6\pi\eta r_H} * (1 + 0.695 * \left(\frac{r_{solv}}{r_H}\right)^{2.234})$$

D_i is the self-diffusion coefficient derived by the measurement, η is the viscosity of the solvent, r_H is the hydrodynamic radius of the observed molecule and r_{solv} the radius of the solvent. No form factor correction was applied. The viscosity was determined by measuring the diffusion coefficient of the reference tetramethylsilane (TMS) and solving the equation for η with the literature value¹⁴ of the radius of 2.96 Å.

Table S2: Self-diffusion coefficients D_i referenced on the coefficient of TMS inside the sample to reference the viscosity of the sample. For all three ternary systems, similar diffusion coefficients are obtained for the CPA and **2d**, while the value for **3b** is slightly higher (smaller size), but significantly smaller than free **3b**, indicating the formation of a ternary CPA/**2d**/**3b** complex.

System	D_i referenced to DTMS [m ² /s]		
	CPA	3b	4a
1a/3b/4b	4.02	4.02	4.51
1b/3b/4b	3.73	3.79	4.12
1h/3b/4b	3.88	3.76	3.99
4b	-	-	6.20

9. Tilting the Balance: London Dispersion Systematically Enhances Enantioselectivities in Brønsted Acid Catalyzed Transfer Hydrogenation of Imines

For **1d/2d/3b**, almost identical D_i (referenced) were obtained for catalyst, imine and Hantzsch ester, which in combination with the NOE results (Figure S7) clearly shows, that the system is dominantly present as ternary complex. For **1d**, **2d** and **3b**, an averaged hydrodynamic volume of $\sim 4200 \text{ \AA}^3$ was determined, while for free **3b** an hydrodynamic volume of $\sim 1600 \text{ \AA}^3$ was derived. For the systems with catalysts **1a** and **1b**, CPA and imine showed identical self-diffusion coefficients, while for **3b** a slightly higher value was measured, although significantly smaller than for free **3b**. This shows, that for these two systems, the equilibrium between ternary complex and binary complex plus free Hantzsch ester is shifted towards the binary complex, but still mainly on the ternary side.

Hence, it was demonstrated that the strong preference for CPA/*Z*-imine complexes is conserved in presence of a nucleophile and that the steric bulk of imine **2d** does not completely block the binding site of the catalyst, ensuring conservation of the general reaction mechanism *via* a ternary CPA/imine/nucleophile complex.

9.6.8. Competing transition states

After demonstrating the impact of London dispersion on the stabilization of *Z*-imines, we aimed to explore, if this additional stabilization can affect the stereoselective outcome of CPA catalyzed transformations on the example of transfer hydrogenations with Hantzsch ester **3a** (see Figure S8 top). Computational studies revealed, that the reaction proceeds *via* a ternary CPA/imine/Hantzsch ester complex and that four transition states are possible, featuring either a *Z*- or *E*-imine configuration and hydride attack from top or bottom (see Figure S8).^{3,15,16} Assuming that the hydride transfer is the rate determining step of the transformation, Goodman *et al.* showed, that the transition state Type I *Z* leading to the major enantiomer and the transition state Type I *E* leading to the minor enantiomer are energetically most stable and thus the operating combination.¹⁵ However, Goodman only examined the relative transition state energies and did not account for the ground state energies (ternary complexes) and the respective activation barriers originating from them.

9. Tilting the Balance: London Dispersion Systematically Enhances Enantioselectivities in Brønsted Acid Catalyzed Transfer Hydrogenation of Imines

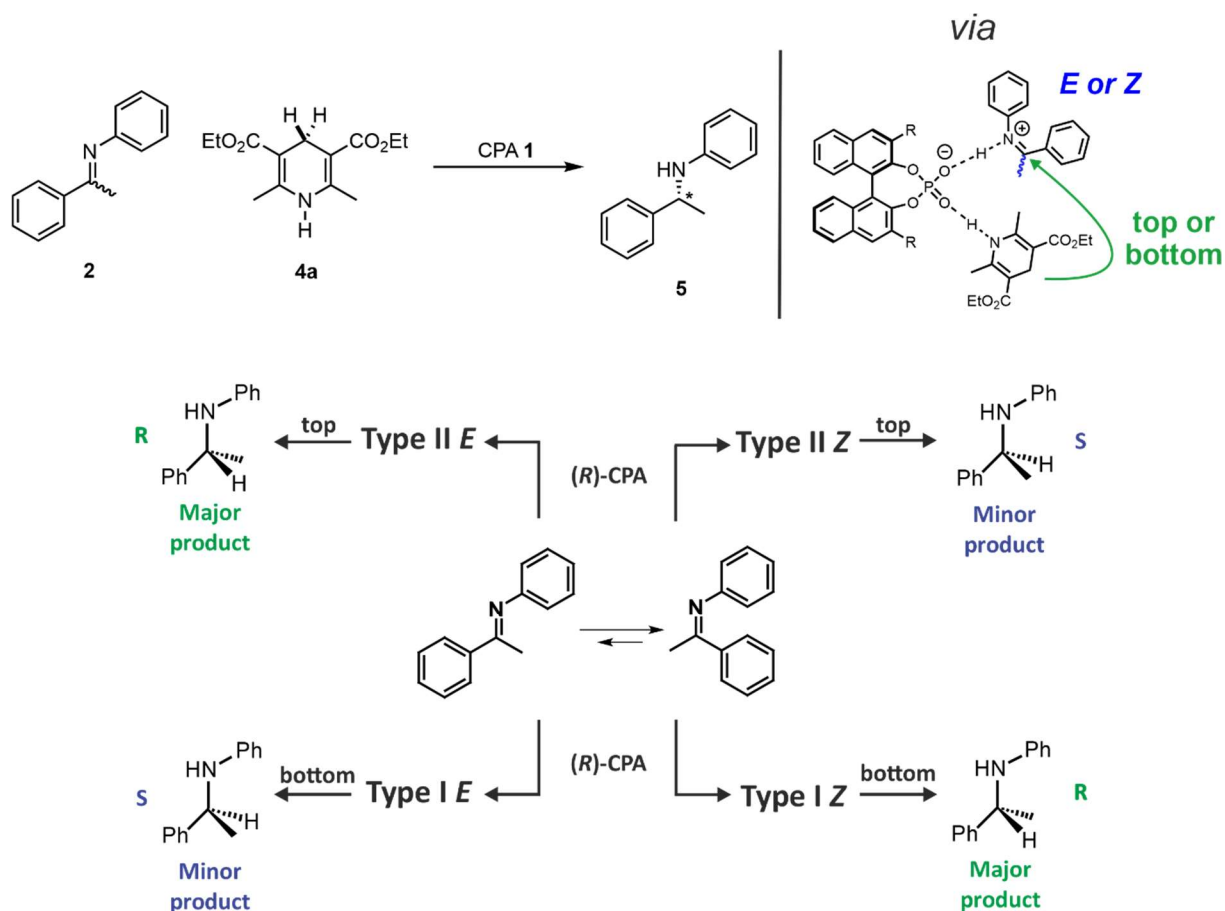


Figure S8: Selected model reaction to study the effect of intramolecular dispersion interactions in the Z-imine, proceeding via a ternary complex featuring CPA, imine and Hantzsch Ester. Four transition states are possible, featuring a Z- or E-imine configuration and attack from bottom or top.

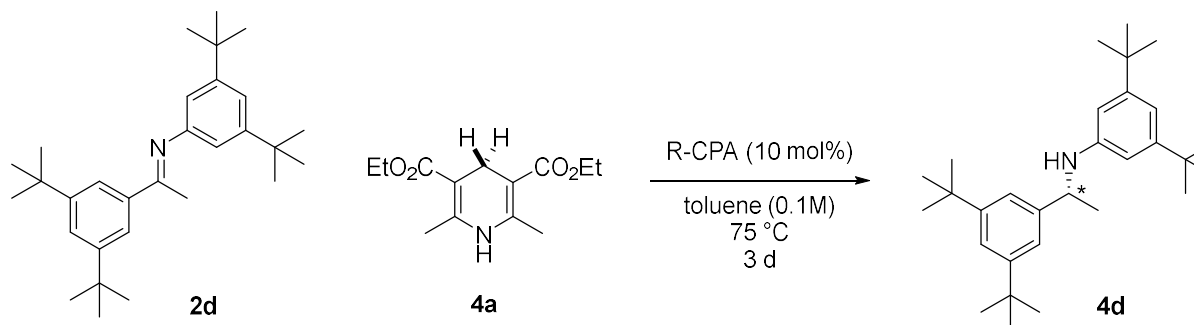
On the other side, our previous research showed, that the $Z \leftrightarrow E$ imine isomerization can be rate determining and thus it becomes necessary to not only account the energy of the ternary transition states, but also of the respective Z/E ground states to derive the energetically smallest barrier for the transformation.³ However, if the imine isomerization is rate determining depends on the exact experimental conditions as a slow formation of the ternary complex, e.g. due to low solubility of Hantzsch ester **3a** can bottleneck the reaction steps following the imine isomerization and thus lead to a delicate balance of the rate determining step between imine isomerization and hydride transfer.¹⁷ For the transfer hydrogenation of substrates **2b-d**, we observed that the reaction proceeds significantly slower than for substrates such as **2a**, which is reflected in the need of high catalyst loadings (10mol%), higher temperature (75 °C) and long reaction times (3 d) to achieve a sufficient conversion (standard conditions are 1 mol% catalyst, room temperature and 1 d). As the introduction of tert-butyl groups should only affect the ground state stability of the Z-imine and consequently the activation barrier for the $Z \rightarrow E$ isomerization, but not of the $E \rightarrow Z$ isomerization,⁸ we strongly assume, that the increase in reaction time reflected by the higher catalyst loading, increased reaction temperature and longer reaction times originates in a higher activation barrier of the hydride transfer due to the increased steric repulsion

9. Tilting the Balance: London Dispersion Systematically Enhances Enantioselectivities in Brønsted Acid Catalyzed Transfer Hydrogenation of Imines

introduced by the tert-butyl substituents. This indicates, that the rate determining step for our systems is the hydride transfer. However, we cannot assume that the $Z \leftrightarrow E$ imine isomerization is fast compared to the hydride transfer and thus the populations of the *Z*- and *E*-imine as well as their catalytic intermediates have to be taken into account when considering the enantioselectivities.

9.6.9. Control experiments

Table S3: Initial control experiments for the CPA catalyzed transfer hydrogenation of imine **2d** with 1.4 equivalents of **3a** as hydride source.



Entry	Catalyst 3,3'	Modification	ee [%]
1	2,4,6-(CH ₃) ₃ C ₆ H ₂ (1a)	0.1 mol%	90
2	2,4,6-(CH ₃) ₃ C ₆ H ₂ (1a)	1 mol%	90
3	2,4,6-(CH ₃) ₃ C ₆ H ₂ (1a)	10 mol%	90
4	3,5-(CF ₃) ₂ C ₆ H ₃ (1d)	1 mol%	84
5	3,5-(CF ₃) ₂ C ₆ H ₃ (1d)	10 mol%	88
6	3,5-(CF ₃) ₂ C ₆ H ₃ (1d)	25 mol%	90
7	2,4,6-(<i>i</i> Pr) ₃ C ₆ H ₂ (1b)	10 mol%	98
8	3,5-(CF ₃) ₂ C ₆ H ₃ (1d)	r.t.	90
9	2,4,6-(CH ₃) ₃ C ₆ H ₂ (1a)	r.t.	90
10	2,4,6-(<i>i</i> Pr) ₃ C ₆ H ₂ (1b)	r.t.	98
11	no catalyst	75 °C	0 ^a
12	no catalyst	r.t.	no rct.

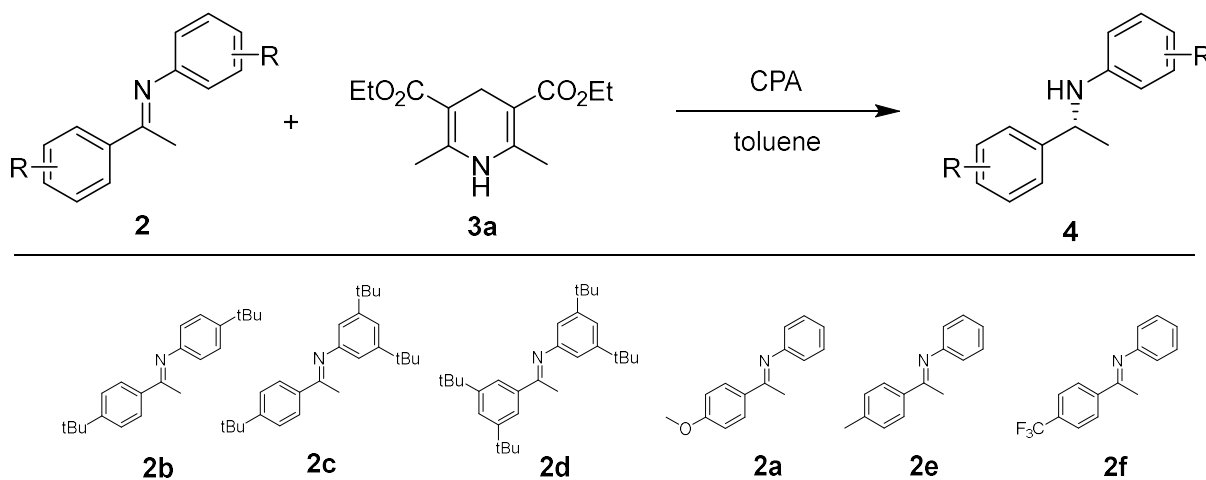
^aminor product formation could be detected on the HPLC.

9. Tilting the Balance: London Dispersion Systematically Enhances Enantioselectivities in Brønsted Acid Catalyzed Transfer Hydrogenation of Imines

As the reaction proceeded rather slowly compared to the transfer hydrogenation of imines such as **2a**, a catalyst loading of 10 mol% and a reaction temperature of 75 °C was necessary to achieve sufficient conversion. Control experiments were performed to evaluate, whether these conditions might affect the enantioselective outcome as our previous research showed, that chiral phosphoric acid catalysts can form dimers as the active catalyst species, leading to a different reaction mechanism and concentration dependent *ee*.¹⁸ Catalyst **1a** and **1d**, which showed a strong tendency for the dimeric pathway in our ongoing research, were employed at different catalyst loadings (Table S3, entries 1-6). While for catalyst **1a**, no changes in *ee* were determined, for catalyst **1d**, the *ee* was slightly smaller at lower catalyst loadings. However, this might originate in a small contribution of racemic uncatalyzed background reaction, which is – unlike to room temperature - possible at 75 °C (Table 4, entries 11-12). Comparing the enantioselectivities at room temperature (entries 8-10) to the respective ones at 75 °C (entry 2, 5, 7) shows, that the uncatalyzed, racemic background reaction is negligible at a catalyst loading of 10 mol%. Hence, the *ee* screening reactions can be performed at these conditions without modulating the *ee* value by changes in the mechanism.

9.6.10. Additional enantioselectivities

Table S4: *ee* values obtained of the CPA catalyzed transfer hydrogenation obtained for various substrates. The values for **4a**, **4e** and **4f** were taken from literature.⁹



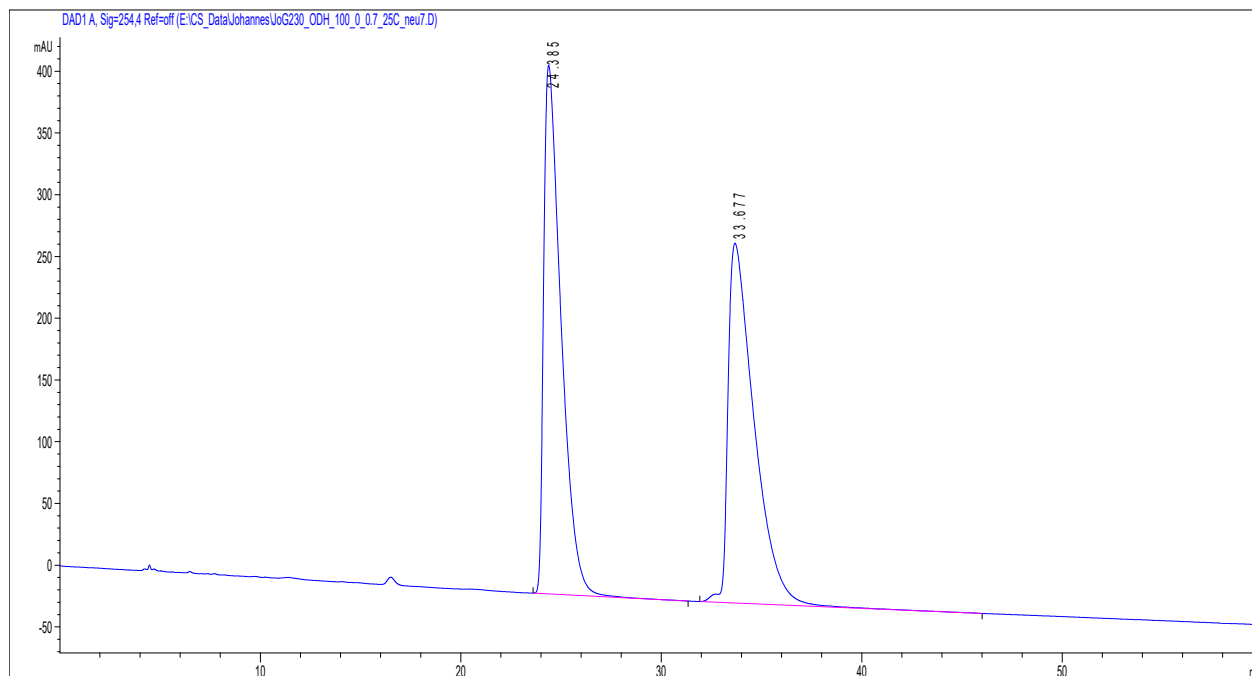
Entry	CPA	enantiomeric excess for substrate					
		4d	4c	4b	4a	4e	4f
1	2,4,6-(Me) ₃ C ₆ H ₂ (1a)	90	71	58	70	71	56
2	2,4,6-(iPr) ₃ C ₆ H ₂ (1b)	99	98	86	86	84	83
3	SiPh ₃ (1c)	58	68	80	92	90	95
4	3,5-(CF ₃) ₂ C ₆ H ₃ (1d)	88	76	77	74	75	91
5	9-anthryl (1e)	91	58	44	39	n.d.	27
8	1-naphthyl (1h)	77	61	45	56	56	46
9	9-phenanthryl (1i)	74	50	46	56	59	47

In general, enantioselectivities obtained for the reduction of imines **2a**, **2e** and **2f** are very similar to the ones obtained for **2b**. All imines feature similar *Z:E* ratios and show no stabilisation of the *Z*-imine by dispersion (see SI chapter 3). This strongly indicates, that boosting the population of the *Z*-imine and its catalytic intermediates by dispersion (**2c** and **2d**) is the main driving force for obtaining higher *ee* values within the investigated systems.

9.6.11. HPLC chromatograms

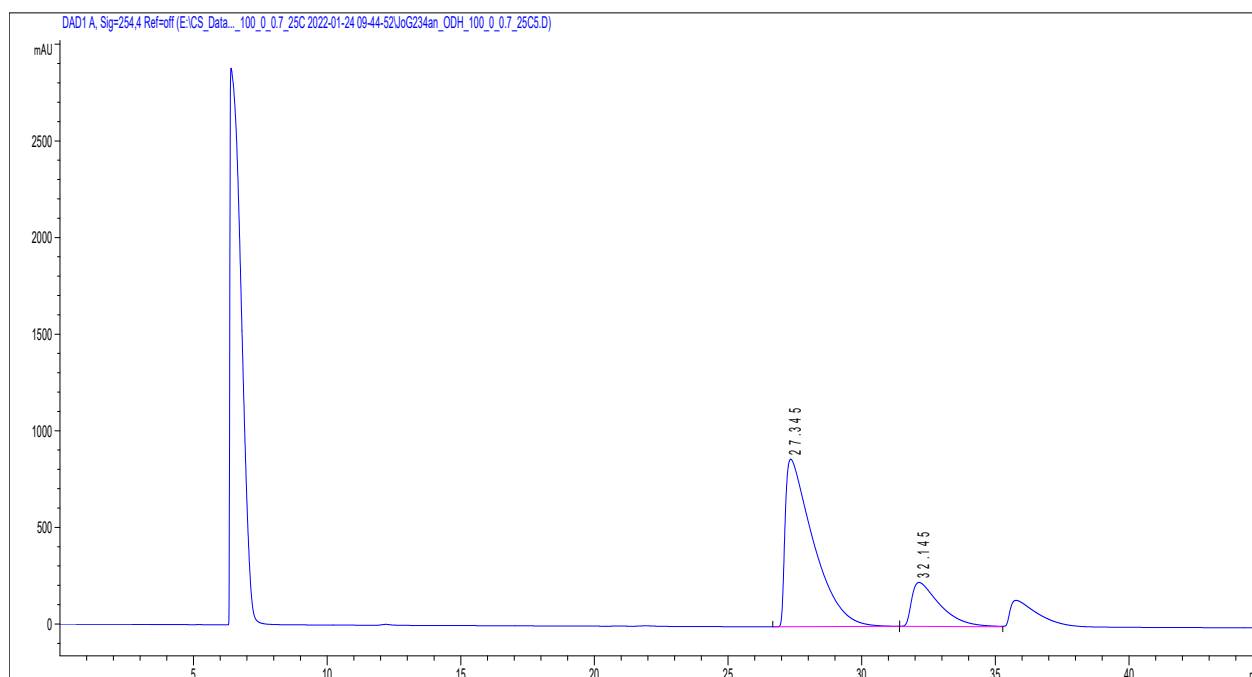
Transfer hydrogenation of imine **2b**; CSP-HPLC ODH, *n*-hexane, 0.7 mL/min, 25 °C; @254 nm

Racemic compound **4a**



#	Time	Area	Height	Width	Area%	Symmetry
1	24.385	25890.1	428	0.8997	49.499	0.371
2	33.677	26414	291.4	1.3177	50.501	0.338

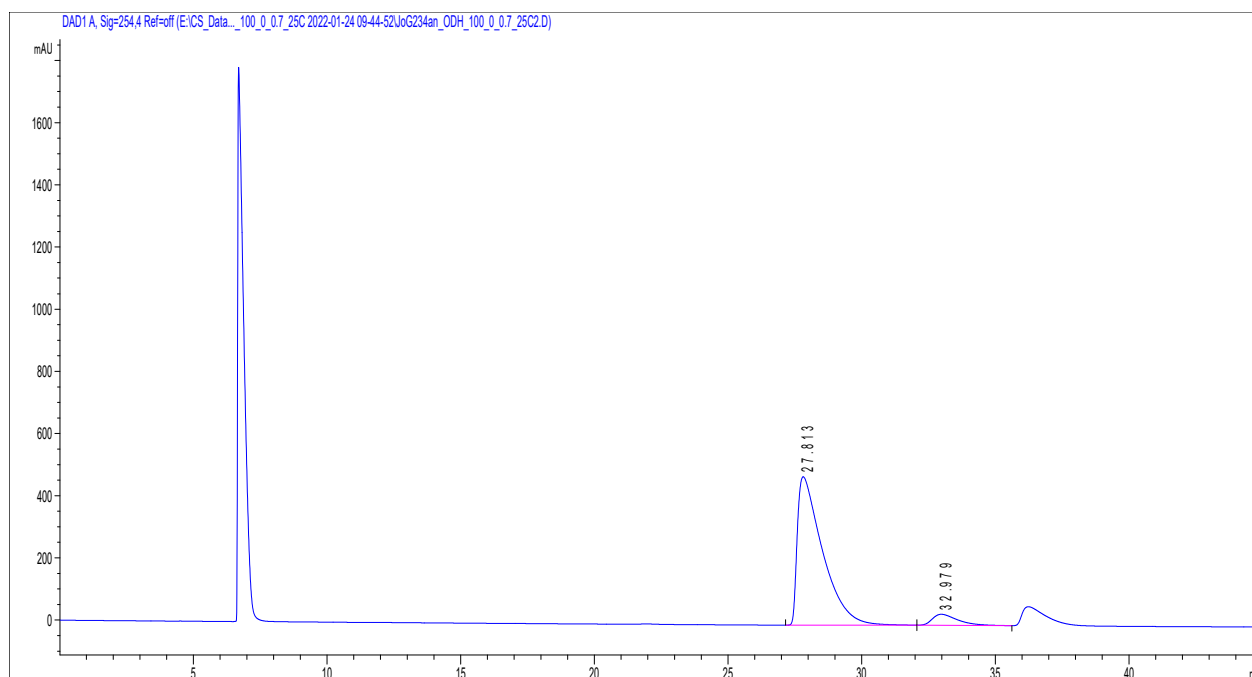
Catalyst 2,4,6-(Me)₃C₆H₂ (**1a**)



#	Time	Area	Height	Width	Area%	Symmetry
1	27.345	63622.7	867.5	1.0517	79.187	0.22
2	32.145	16722.1	227.8	1.0742	20.813	0.32

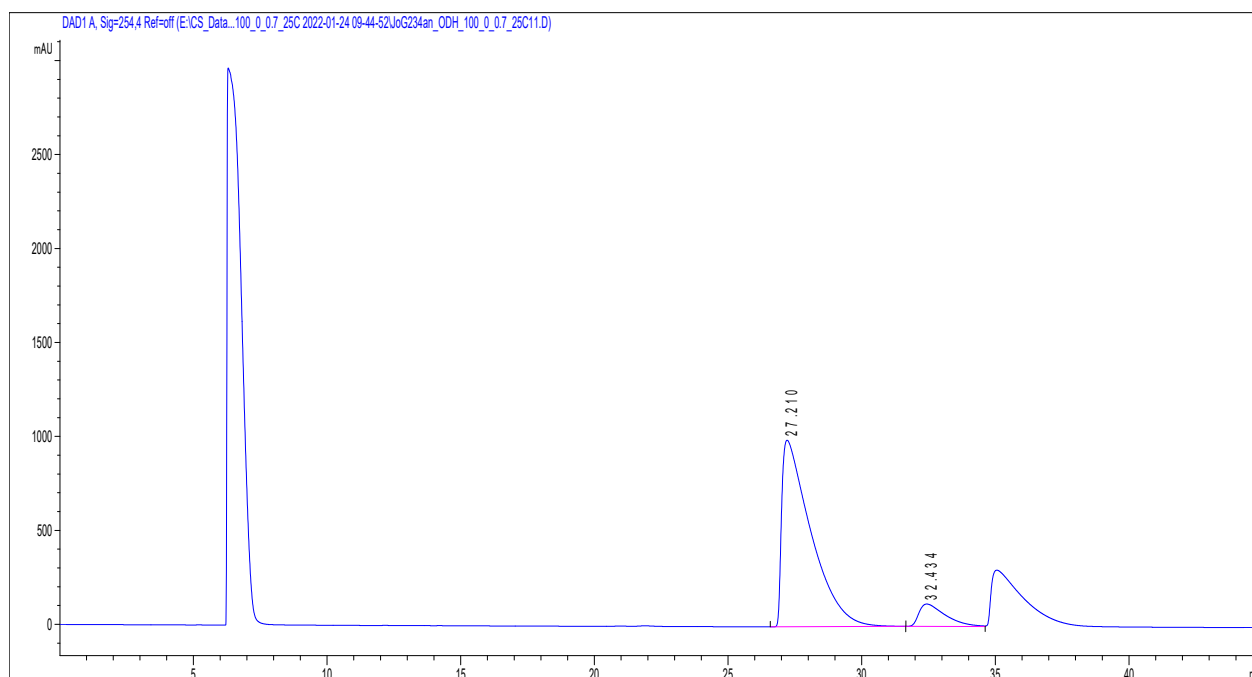
9. Tilting the Balance: London Dispersion Systematically Enhances Enantioselectivities in Brønsted Acid Catalyzed Transfer Hydrogenation of Imines

Catalyst 2,4,6-(*i*Pr)₃C₆H₂ (**1b**)



#	Time	Area	Height	Width	Area%	Symmetry
1	27.813	31276.9	477.6	0.9461	93.089	0.278
2	32.979	2322.1	35.4	0.9835	6.911	0.509

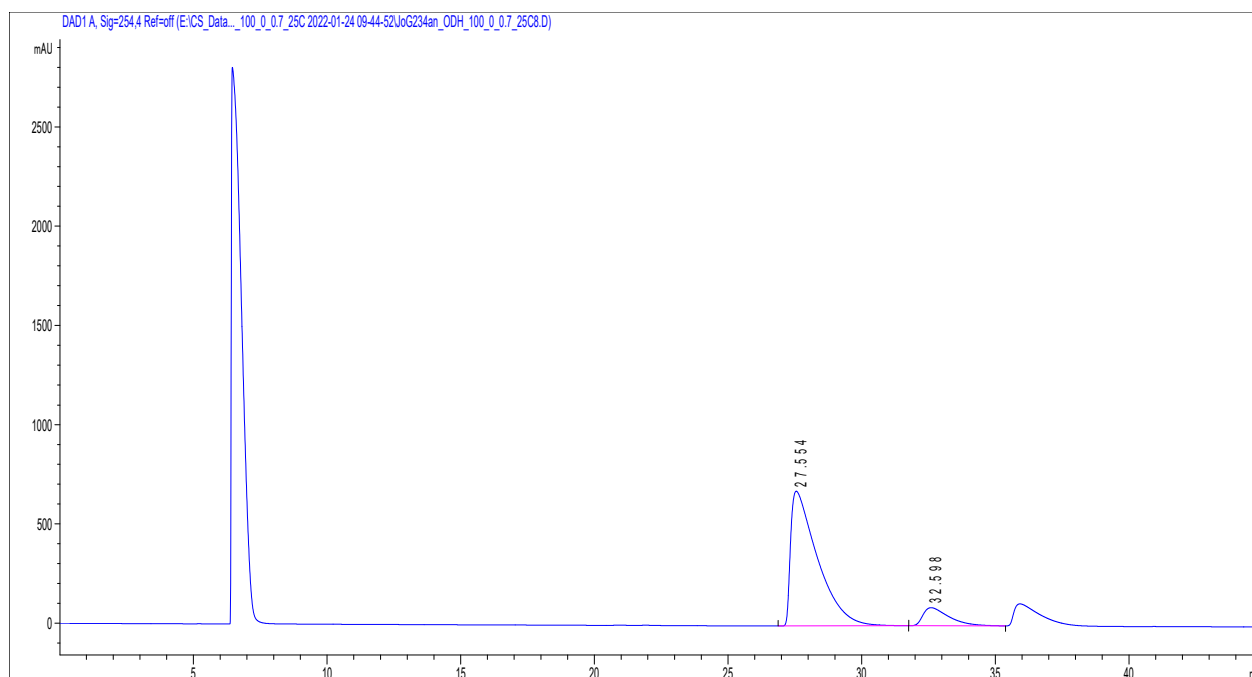
Catalyst SiPh₃ (**1c**)



#	Time	Area	Height	Width	Area%	Symmetry
1	27.21	75400.3	993.1	1.0918	90.167	0.206
2	32.434	8222.4	119.5	1.015	9.833	0.388

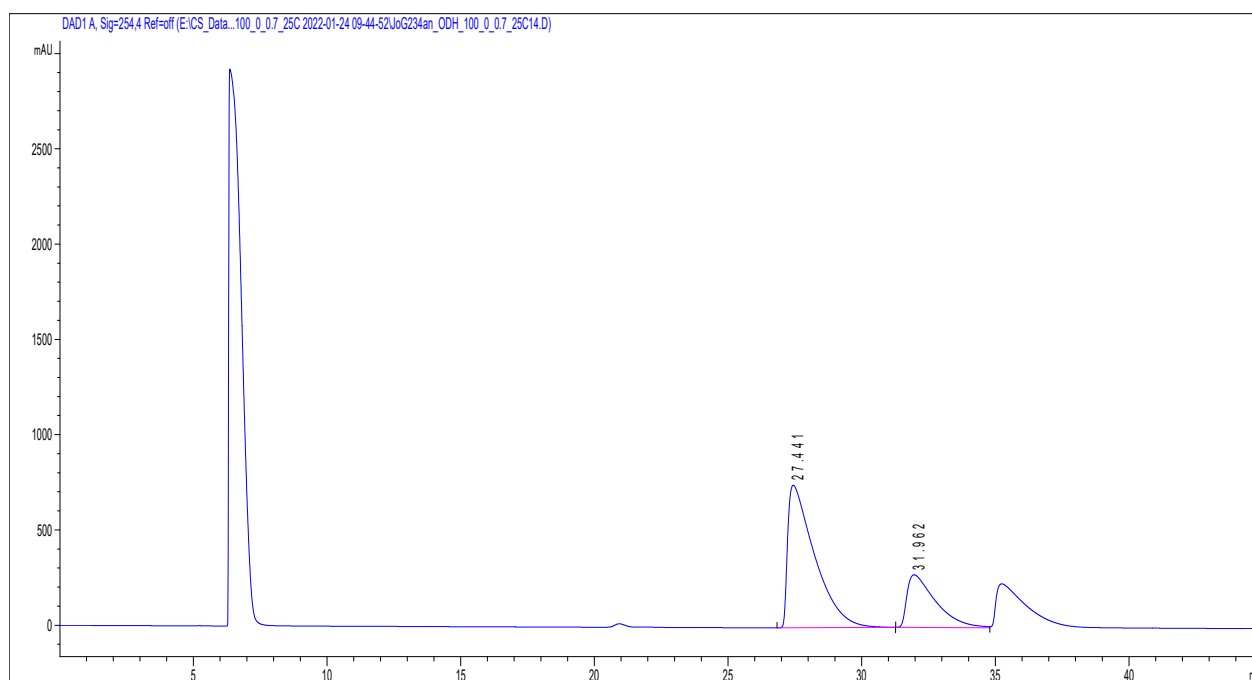
9. Tilting the Balance: London Dispersion Systematically Enhances Enantioselectivities in Brønsted Acid Catalyzed Transfer Hydrogenation of Imines

Catalyst 3,5-(CF₃)₂C₆H₄ (**1d**)



#	Time	Area	Height	Width	Area%	Symmetry
1	27.554	47423.6	679.1	1.0007	88.513	0.243
2	32.598	6154.6	91.2	0.9911	11.487	0.422

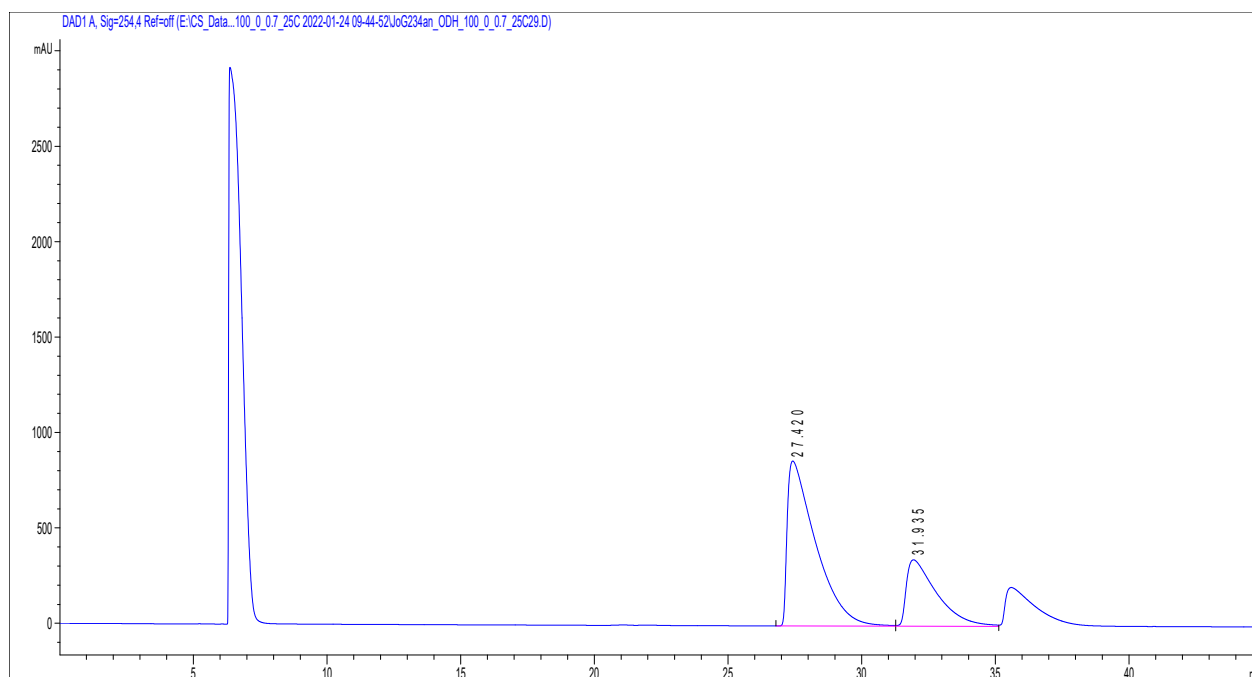
Catalyst 9-anthryl (**1e**)



#	Time	Area	Height	Width	Area%	Symmetry
1	27.441	52338.7	748.5	1.0098	71.858	0.236
2	31.962	20497.5	276.4	1.0751	28.142	0.304

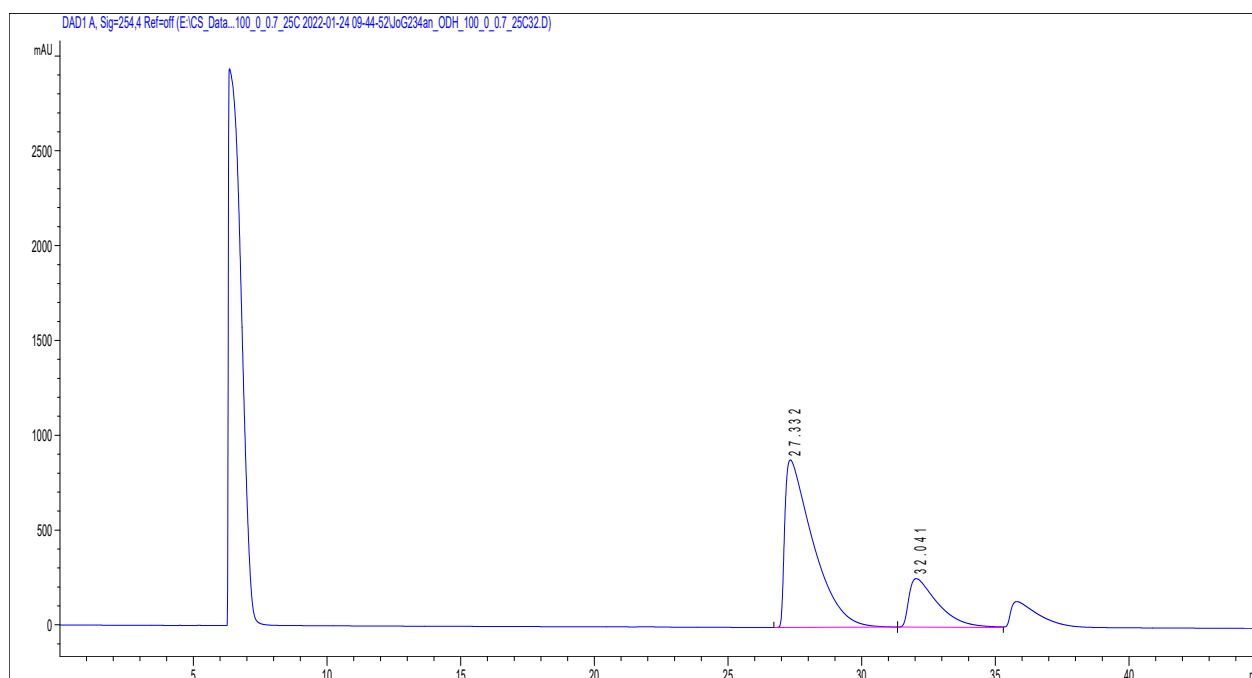
9. Tilting the Balance: London Dispersion Systematically Enhances Enantioselectivities in Brønsted Acid Catalyzed Transfer Hydrogenation of Imines

Catalyst 4-(^tBu)₂C₆H₄ (**1f**)



#	Time	Area	Height	Width	Area%	Symmetry
1	27.42	63738.9	864.6	1.0621	69.850	0.219
2	31.935	27512	348.1	1.1422	30.150	0.277

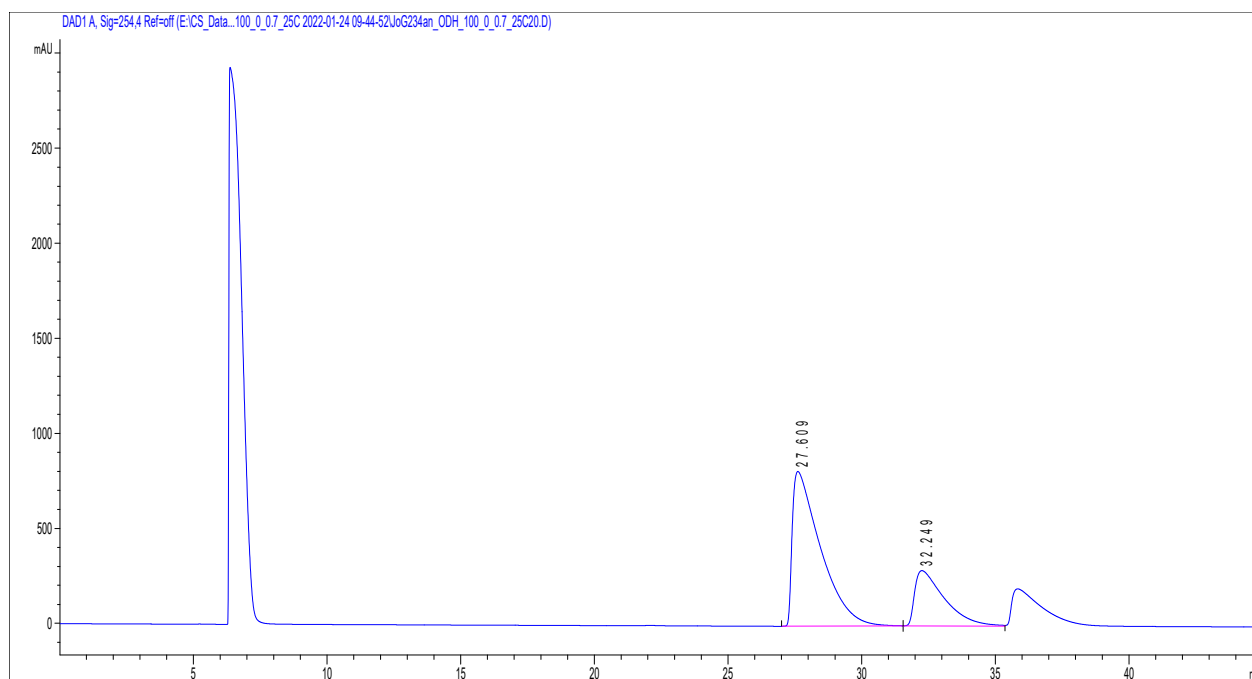
Catalyst 4-(CF₃)₂C₆H₃ (**1g**)



#	Time	Area	Height	Width	Area%	Symmetry
1	27.332	64832.7	883.5	1.0362	77.282	0.219
2	32.041	19057.9	256.1	1.0801	22.718	0.309

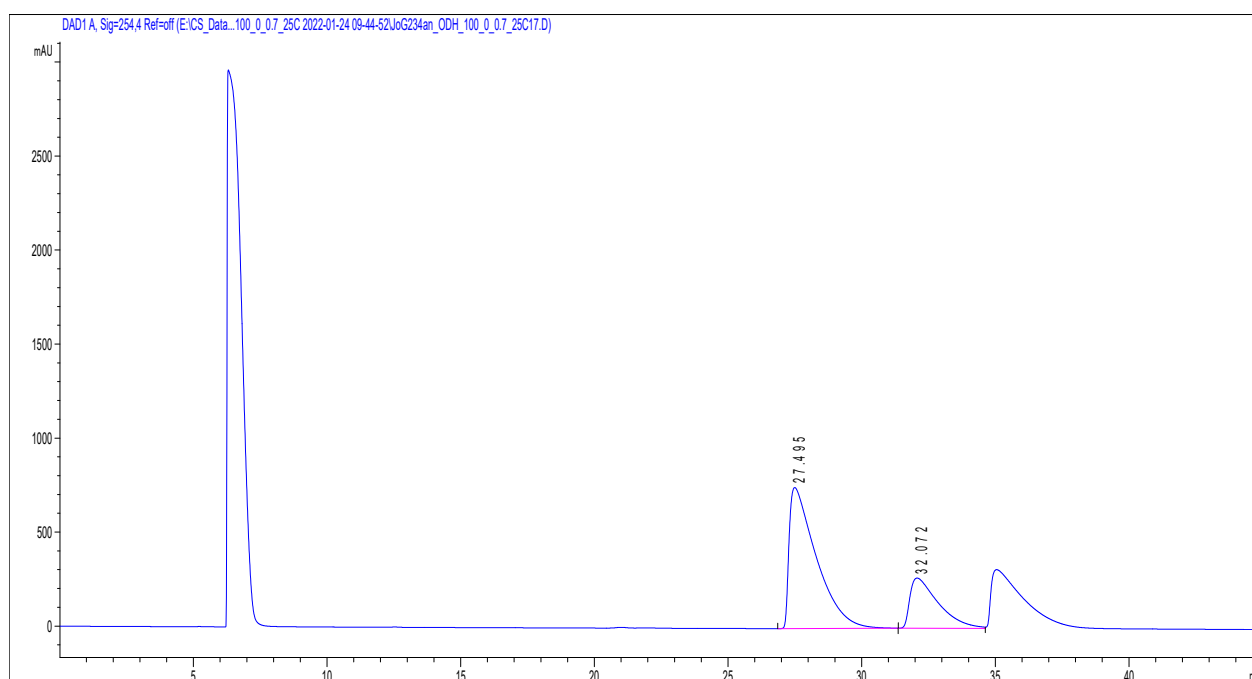
9. Tilting the Balance: London Dispersion Systematically Enhances Enantioselectivities in Brønsted Acid Catalyzed Transfer Hydrogenation of Imines

Catalyst 1-naphthyl (**1h**)



#	Time	Area	Height	Width	Area%	Symmetry
1	27.609	59609.9	813.4	1.035	72.742	0.226
2	32.249	22337.7	290.5	1.1112	27.258	0.294

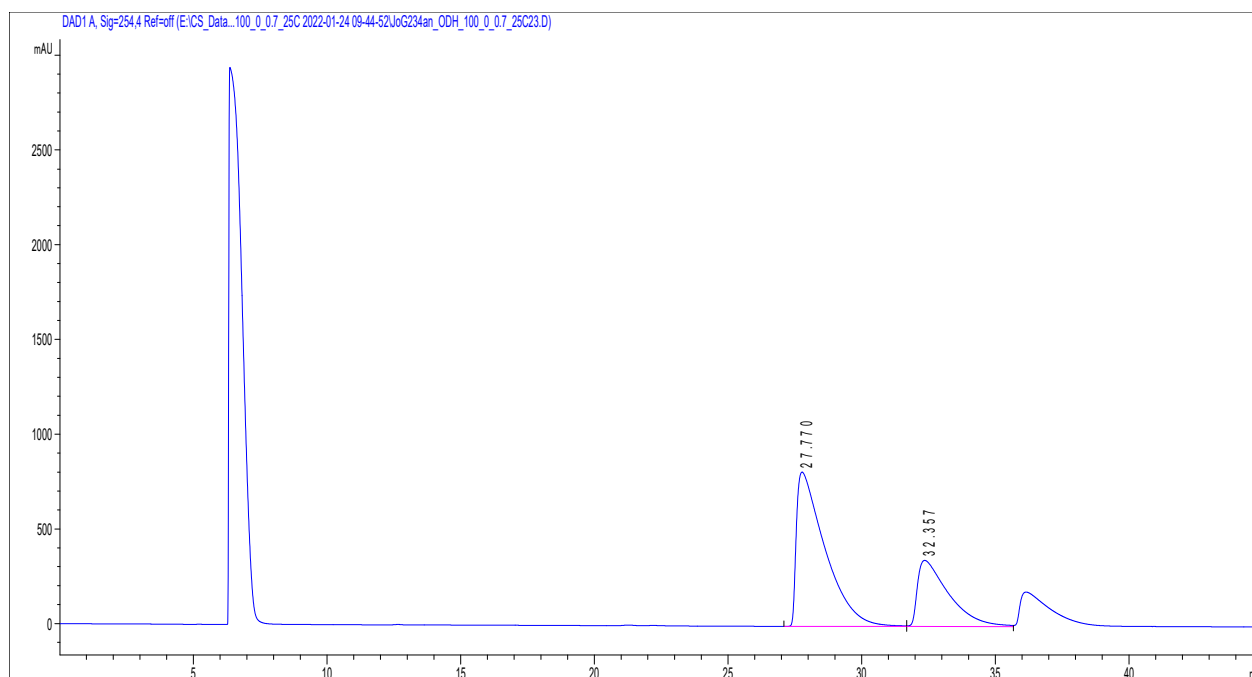
Catalyst 9-phenanthryl (**1i**)



#	Time	Area	Height	Width	Area%	Symmetry
1	27.495	52916.1	750.2	1.0149	72.843	0.234
2	32.072	19728.3	267.2	1.0775	27.157	0.309

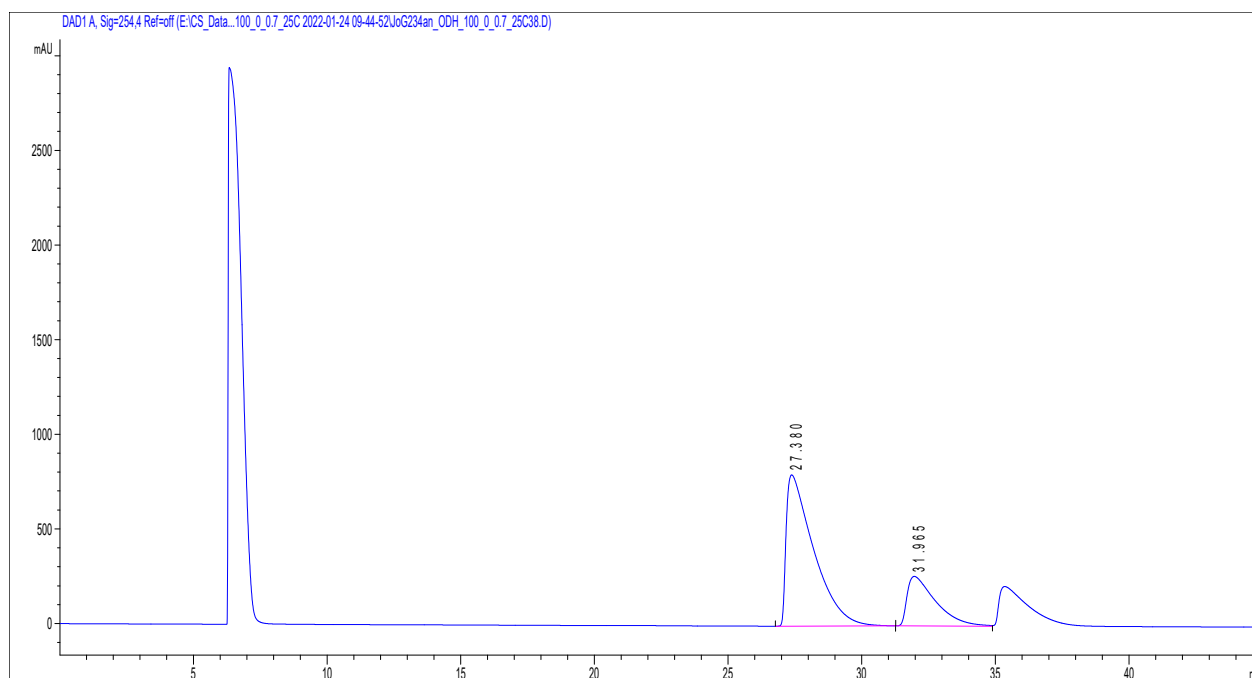
9. Tilting the Balance: London Dispersion Systematically Enhances Enantioselectivities in Brønsted Acid Catalyzed Transfer Hydrogenation of Imines

Catalyst C₆H₅ (**1j**)



#	Time	Area	Height	Width	Area%	Symmetry
1	27.77	60563.2	814.3	1.0557	68.188	0.224
2	32.357	28254.1	349	1.1606	31.812	0.276

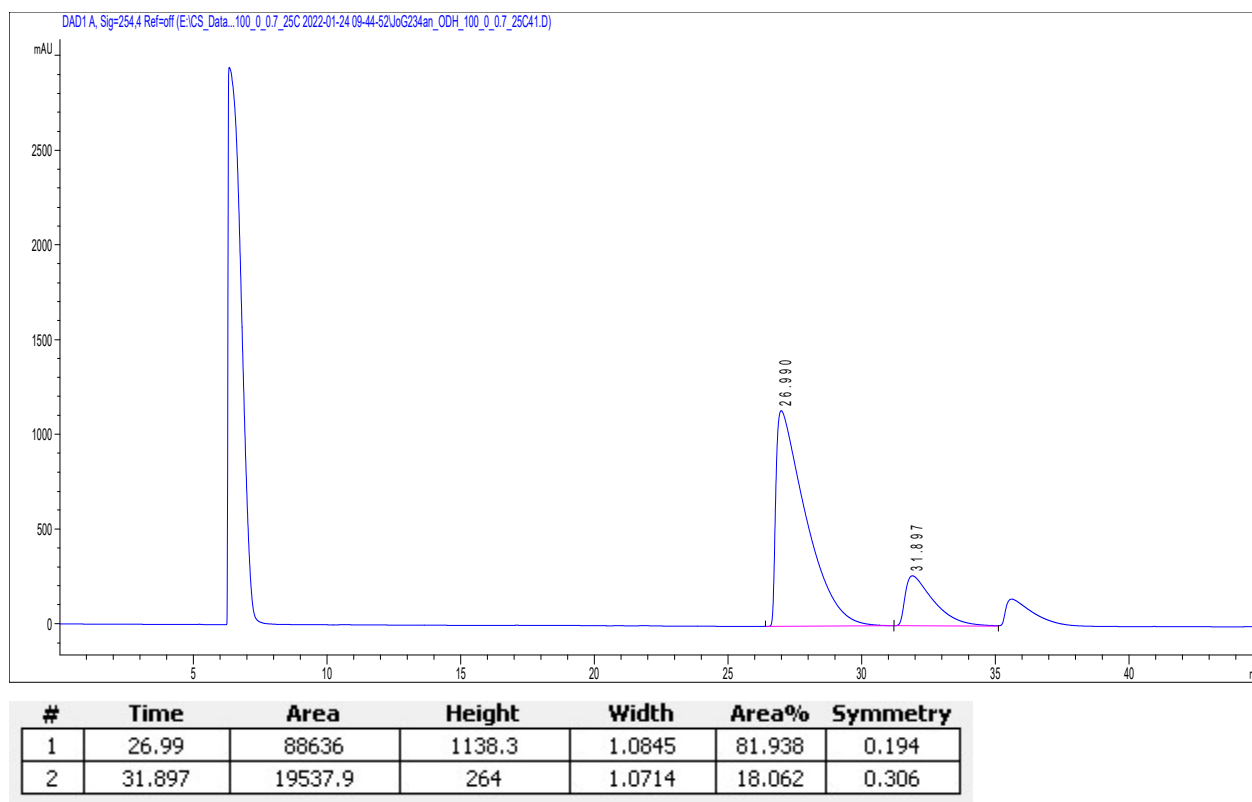
Catalyst 3,5-(CH₃)₂C₆H₂ (**1k**)



#	Time	Area	Height	Width	Area%	Symmetry
1	27.38	57040.3	799.4	1.0124	74.666	0.229
2	31.965	19353.1	261.8	1.0705	25.334	0.307

9. Tilting the Balance: London Dispersion Systematically Enhances Enantioselectivities in Brønsted Acid Catalyzed Transfer Hydrogenation of Imines

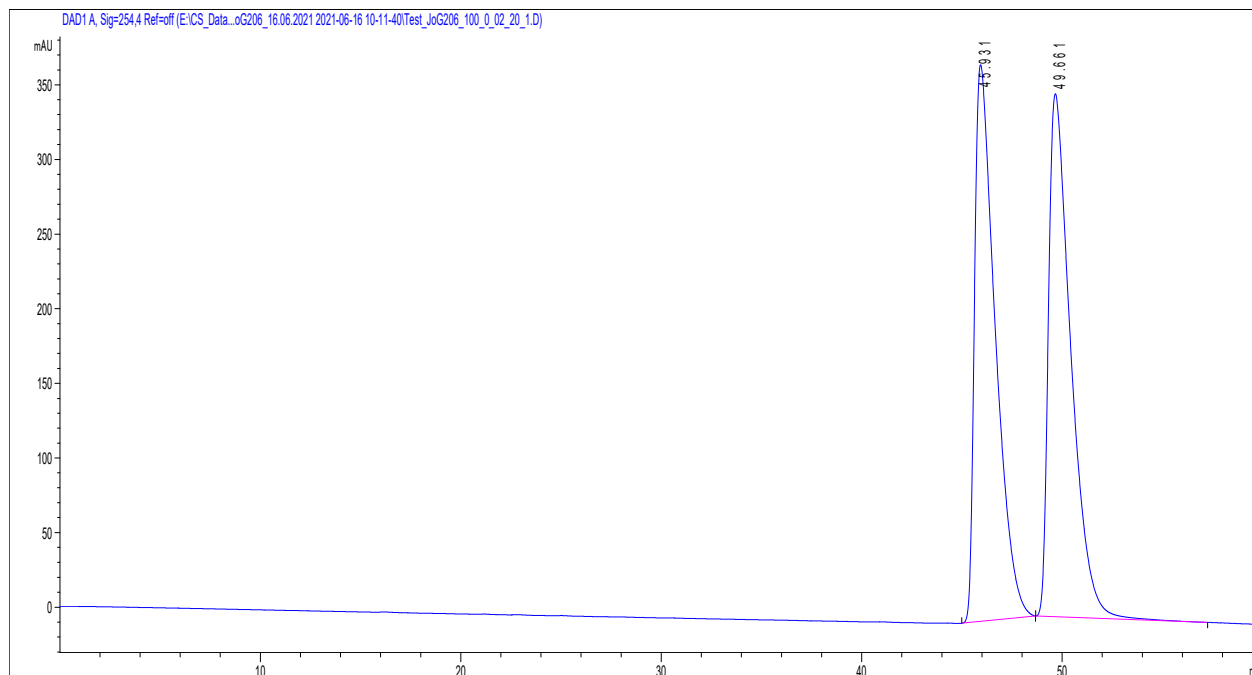
Catalyst (R)-DSI-4-(CF₃)C₆H₄ (**11**)



9. Tilting the Balance: London Dispersion Systematically Enhances Enantioselectivities in Brønsted Acid Catalyzed Transfer Hydrogenation of Imines

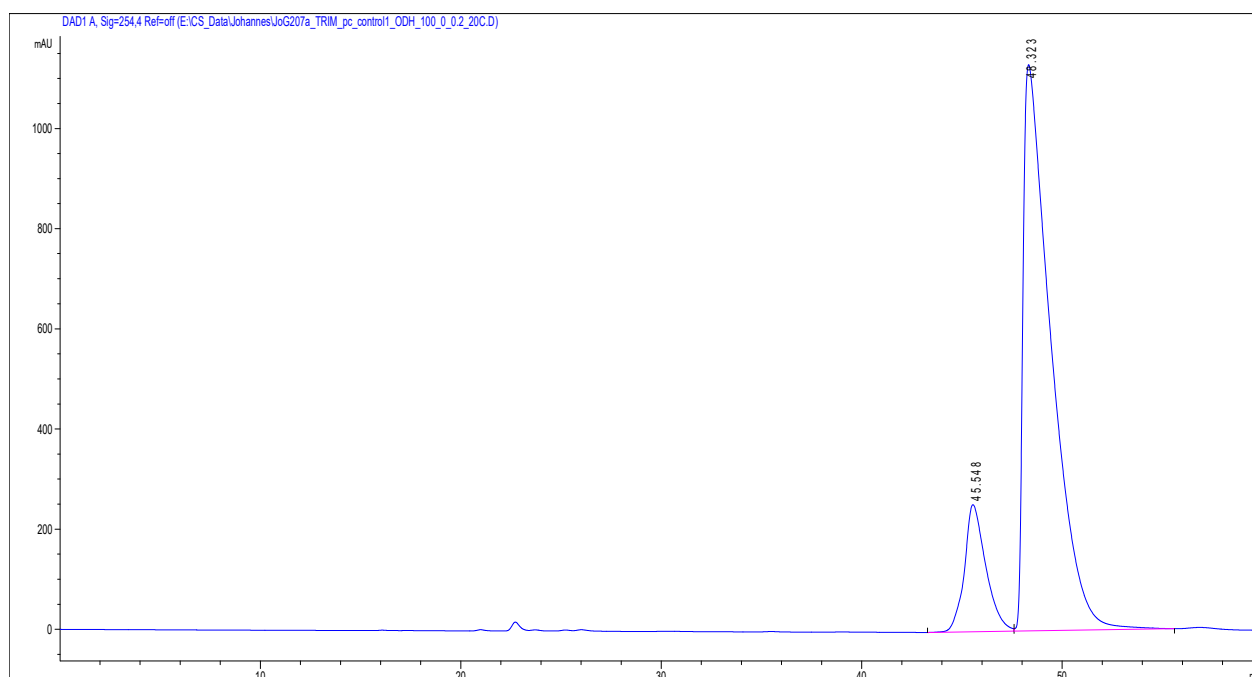
Transfer hydrogenation of imine **2c**; CSP-HPLC ODH, *n*-hexane, 0.2 mL/min, 20 °C; @254 nm

Racemic compound **4c**



#	Time	Area	Height	Width	Area%	Symmetry
1	45.931	26766.9	373	1.0592	49.642	0.38
2	49.661	27153.3	350.5	1.1458	50.358	0.407

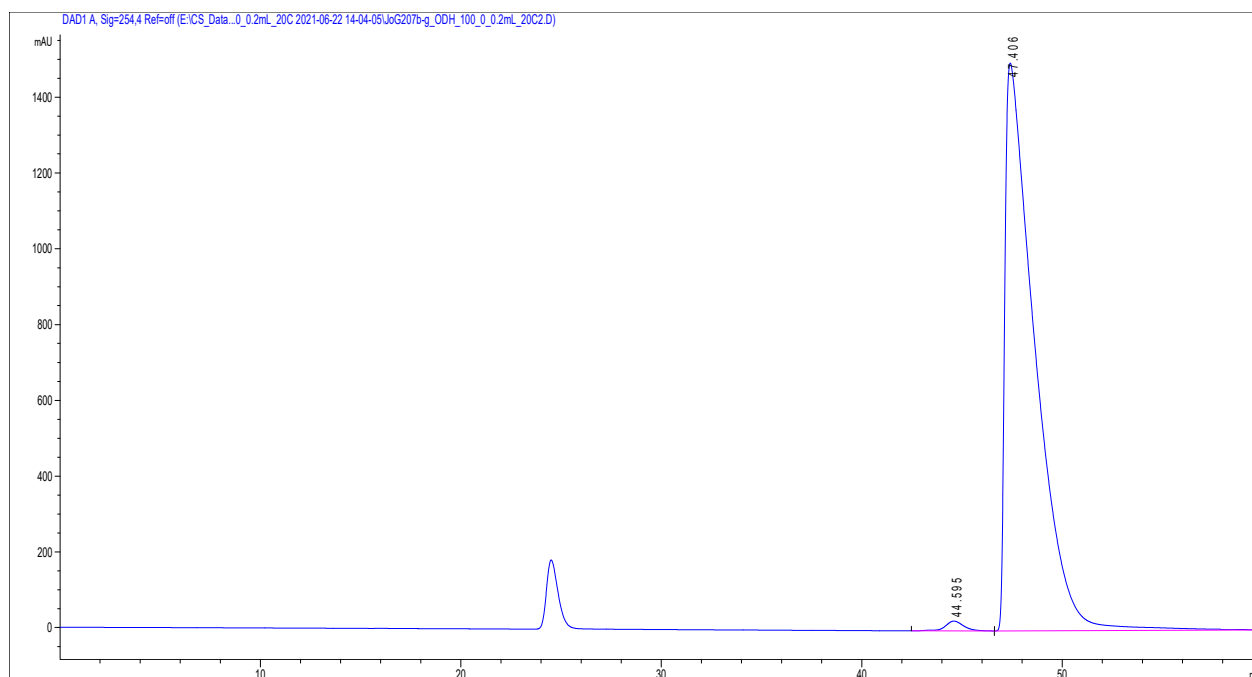
Catalyst 2,4,6-(Me)₃C₆H₂ (**1a**)



#	Time	Area	Height	Width	Area%	Symmetry
1	45.548	18859	253.7	1.0791	14.691	0.655
2	48.323	109515.3	1130.7	1.336	85.309	0.226

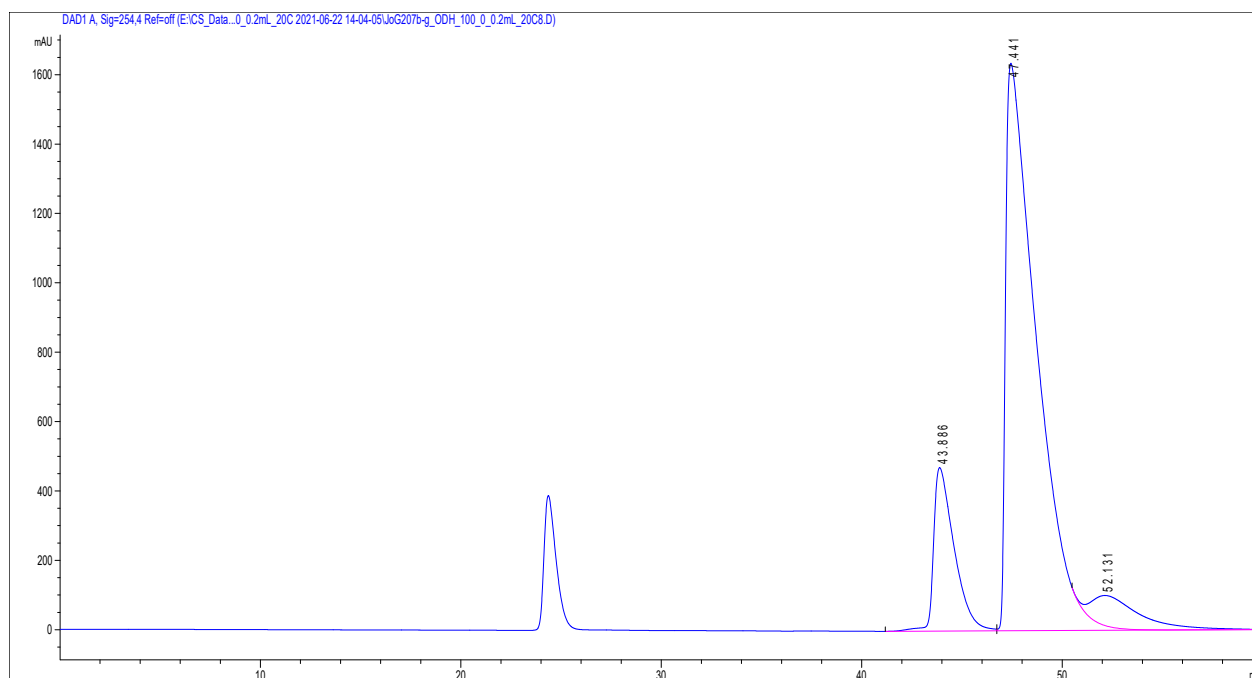
9. Tilting the Balance: London Dispersion Systematically Enhances Enantioselectivities in Brønsted Acid Catalyzed Transfer Hydrogenation of Imines

Catalyst 2,4,6-(*i*Pr)₃C₆H₂ (**1b**)



#	Time	Area	Height	Width	Area%	Symmetry
1	44.595	1650.4	25.9	0.9507	1.053	0.881
2	47.406	155083.2	1498.2	1.3917	98.947	0.196

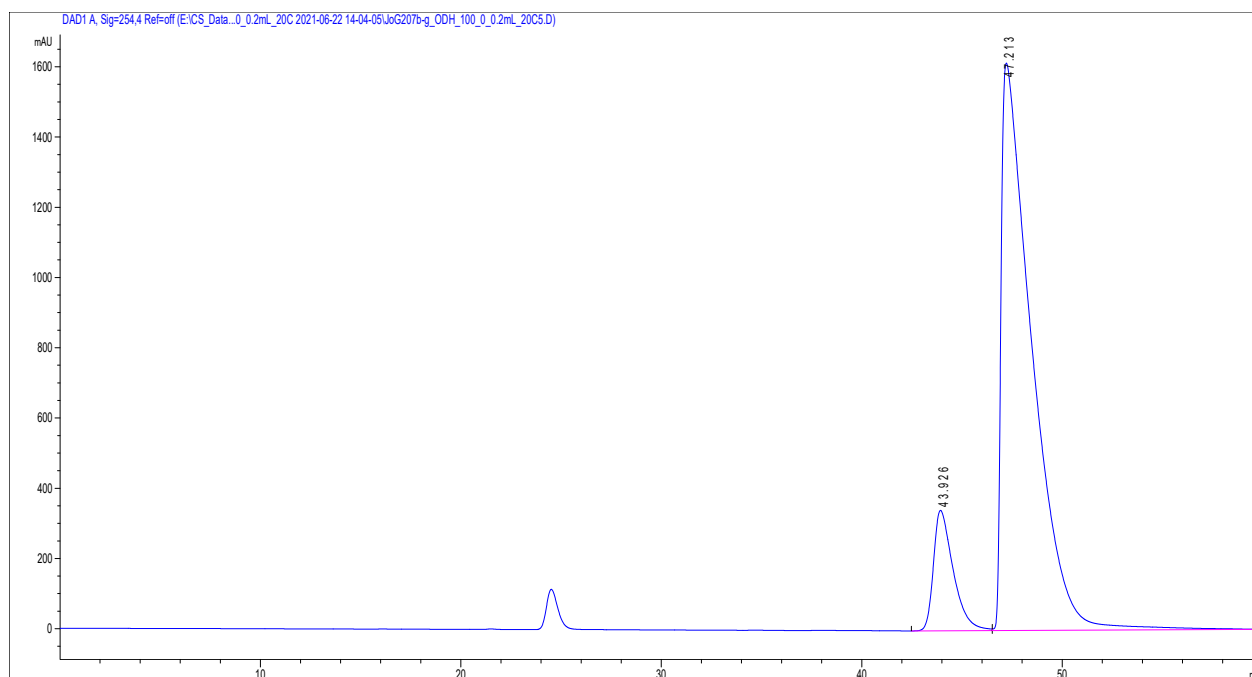
Catalyst SiPh₃ (**1c**)



#	Time	Area	Height	Width	Area%	Symmetry
1	43.886	33566	471.4	1.0546	14.996	0.399
2	47.441	175018.8	1635.9	1.4622	78.191	0.187
3	52.131	15251.5	86.6	2.3657	6.814	0.34

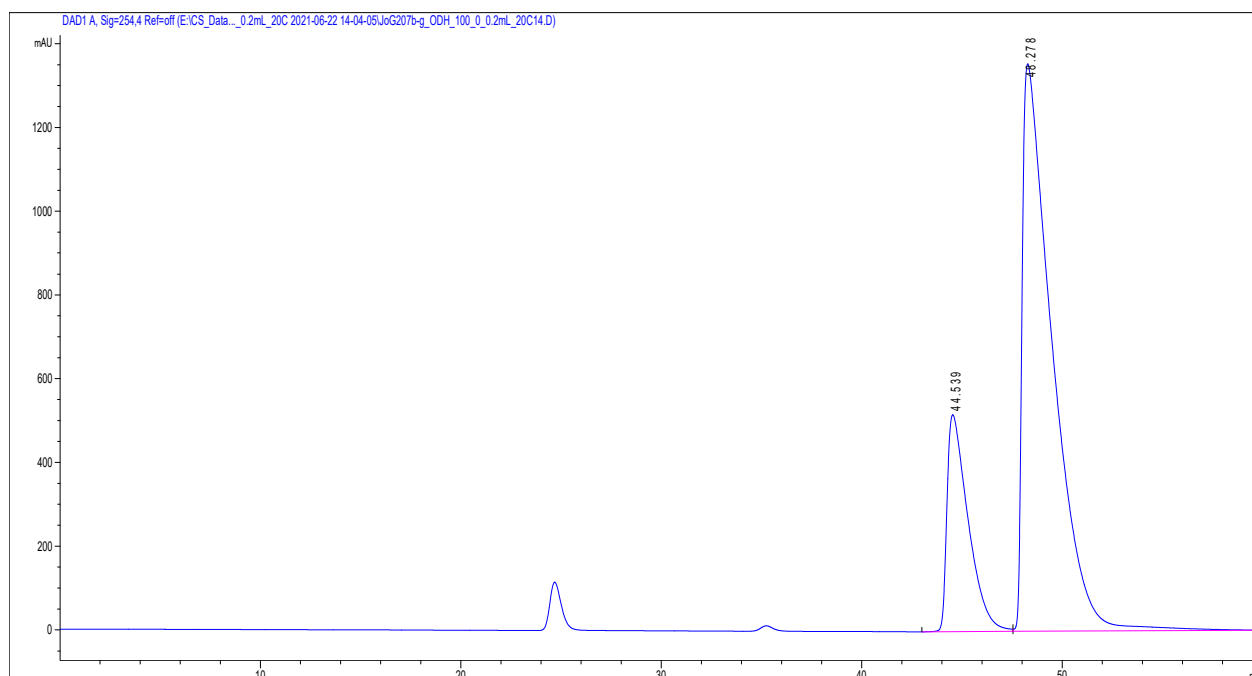
9. Tilting the Balance: London Dispersion Systematically Enhances Enantioselectivities in Brønsted Acid Catalyzed Transfer Hydrogenation of Imines

Catalyst 3,5-(CF₃)₂C₆H₄ (**1d**)



#	Time	Area	Height	Width	Area%	Symmetry
1	43.926	23481.7	342.9	1.023	12.043	0.522
2	47.213	171493.8	1615.3	1.4426	87.957	0.188

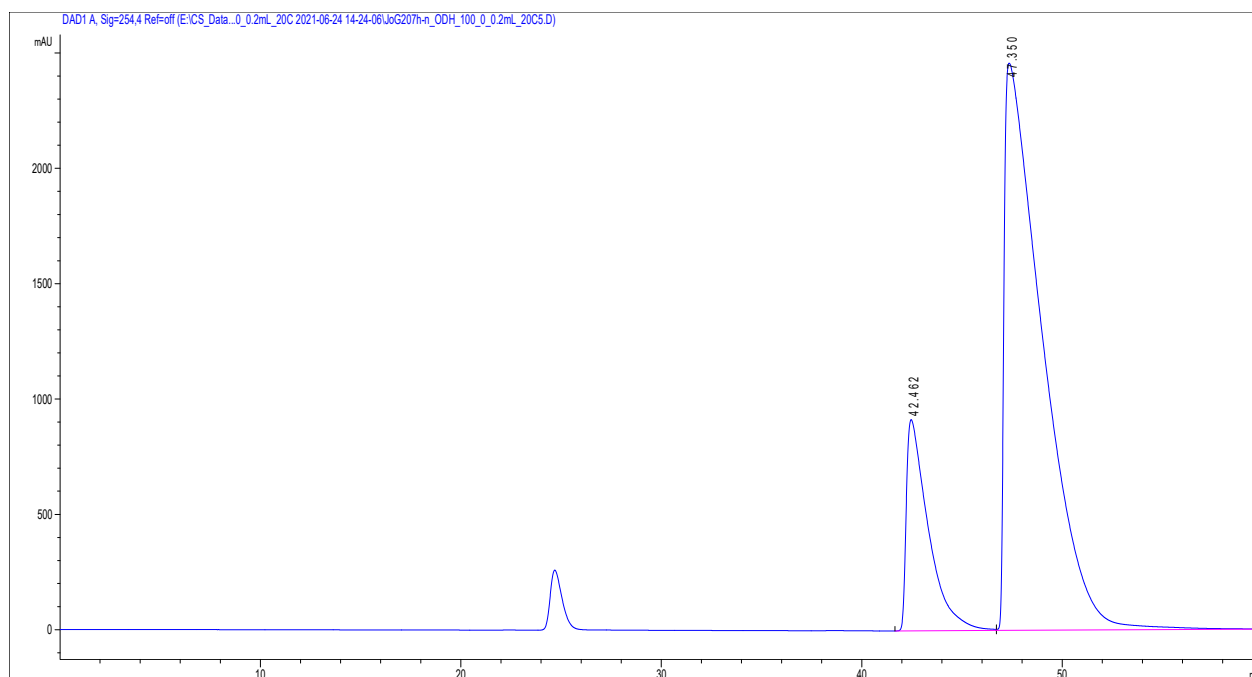
Catalyst 9-anthryl (**1e**)



#	Time	Area	Height	Width	Area%	Symmetry
1	44.539	37937.9	518.4	1.0699	21.199	0.344
2	48.278	141019.8	1355.5	1.3937	78.801	0.203

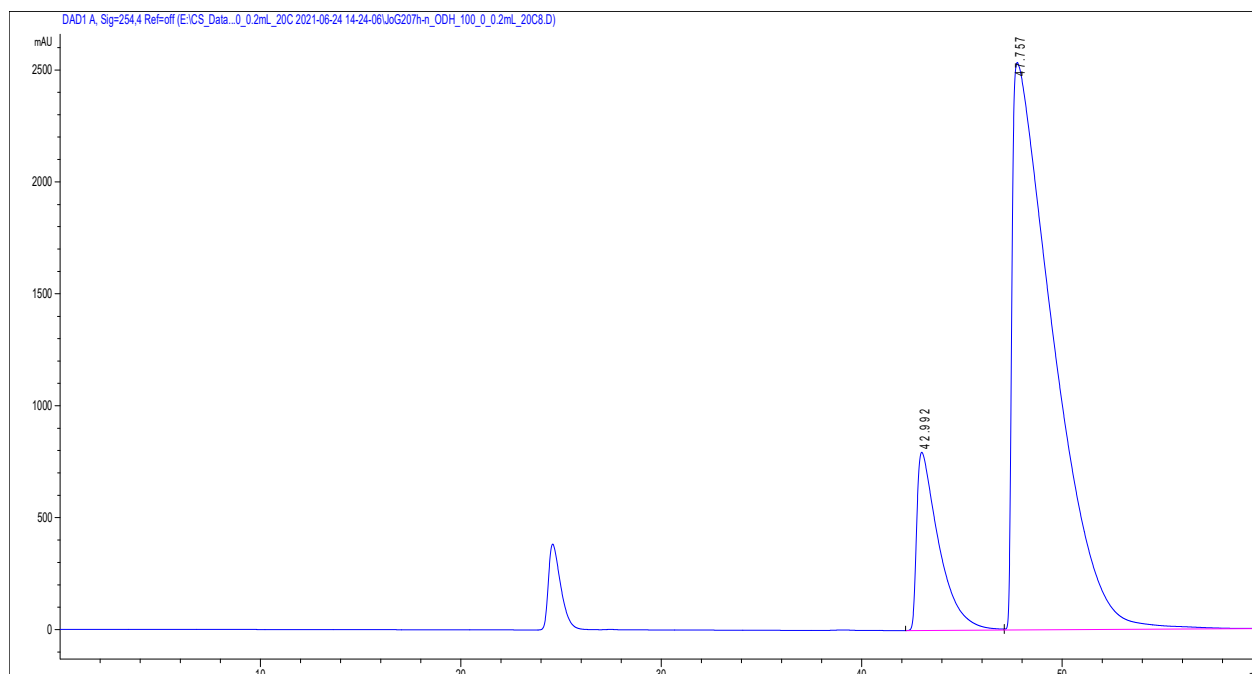
9. Tilting the Balance: London Dispersion Systematically Enhances Enantioselectivities in Brønsted Acid Catalyzed Transfer Hydrogenation of Imines

Catalyst 4-(^tBu)₂C₆H₄ (**1f**)



#	Time	Area	Height	Width	Area%	Symmetry
1	42.462	69779.4	915.7	1.085	17.629	0.254
2	47.35	326032.4	2458.6	1.6691	82.371	0.135

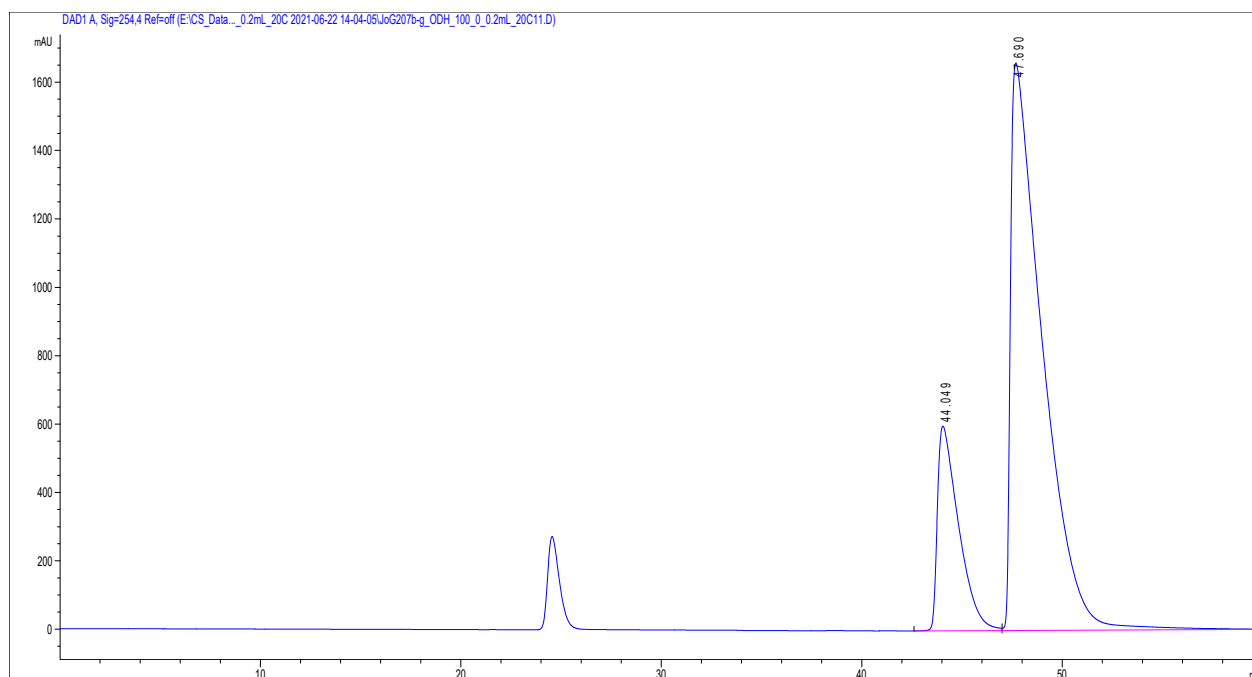
Catalyst 4-(CF₃)₂C₆H₃ (**1g**)



#	Time	Area	Height	Width	Area%	Symmetry
1	42.992	61196.1	796.3	1.0986	14.497	0.265
2	47.757	360927.5	2534.5	1.7654	85.503	0.13

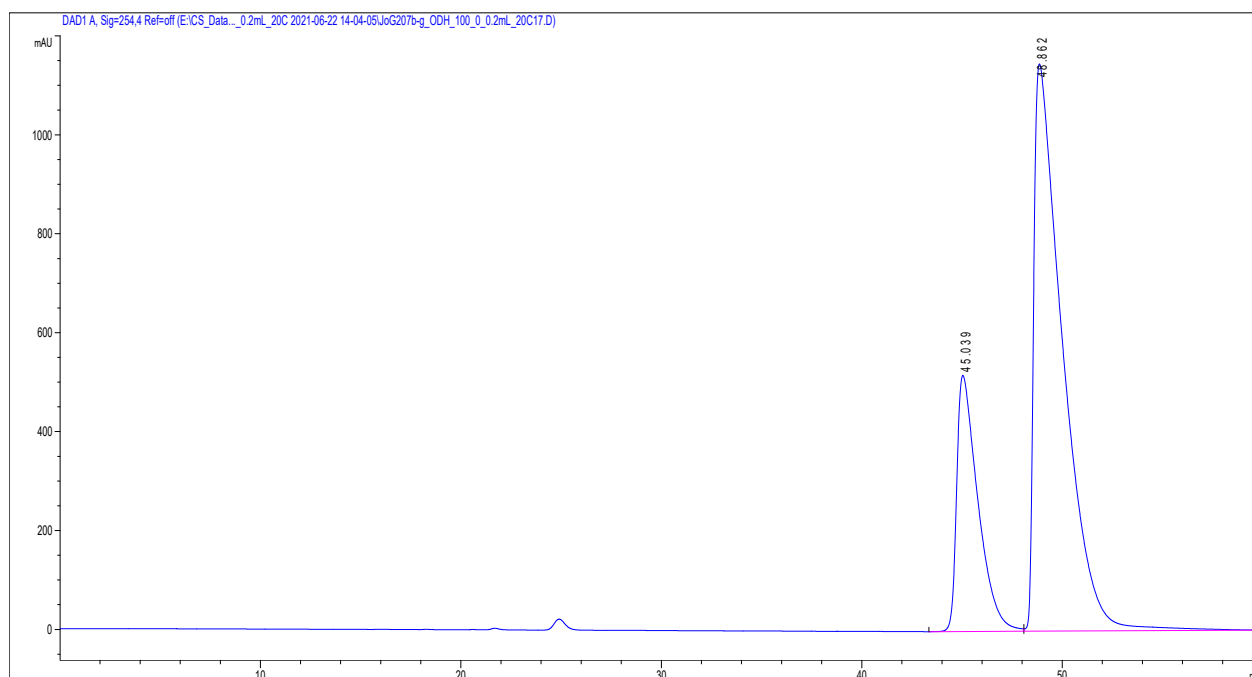
9. Tilting the Balance: London Dispersion Systematically Enhances Enantioselectivities in Brønsted Acid Catalyzed Transfer Hydrogenation of Imines

Catalyst 1-naphthyl (**1h**)



#	Time	Area	Height	Width	Area%	Symmetry
1	44.049	43929.8	598.4	1.0624	19.409	0.322
2	47.69	182404.4	1659.5	1.4703	80.591	0.182

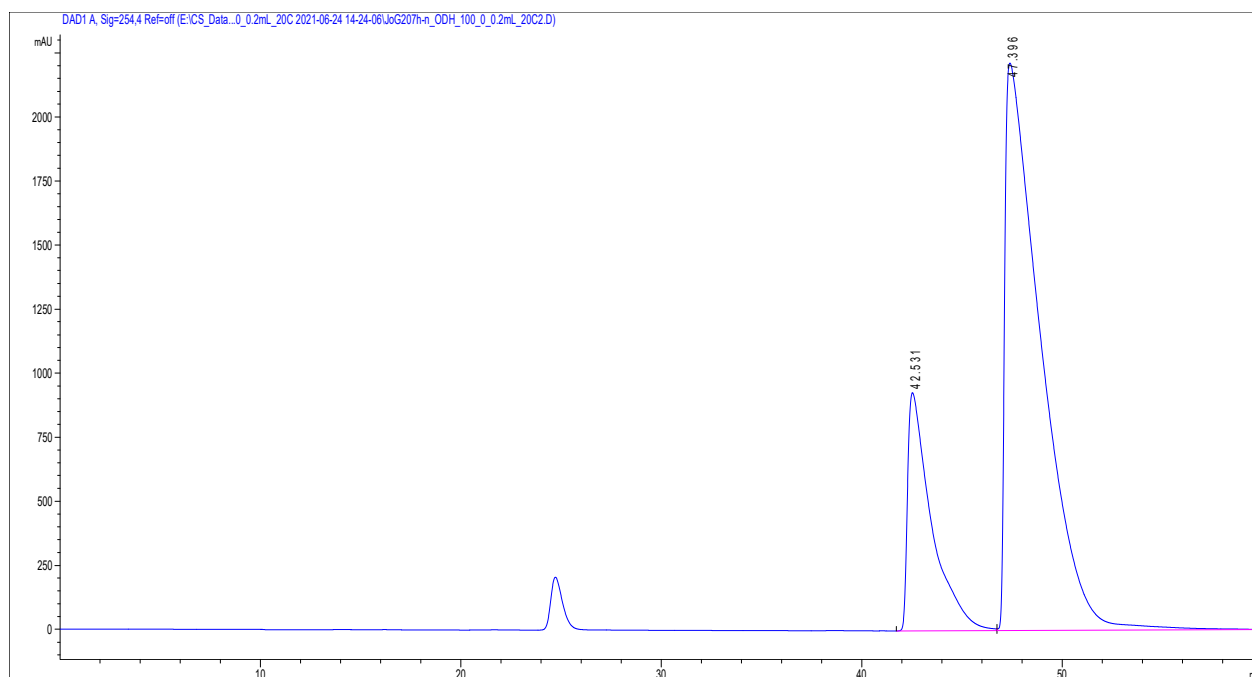
Catalyst 9-phenanthryl (**1i**)



#	Time	Area	Height	Width	Area%	Symmetry
1	45.039	38054.4	518	1.063	24.923	0.378
2	48.862	114631.2	1146.8	1.3942	75.077	0.223

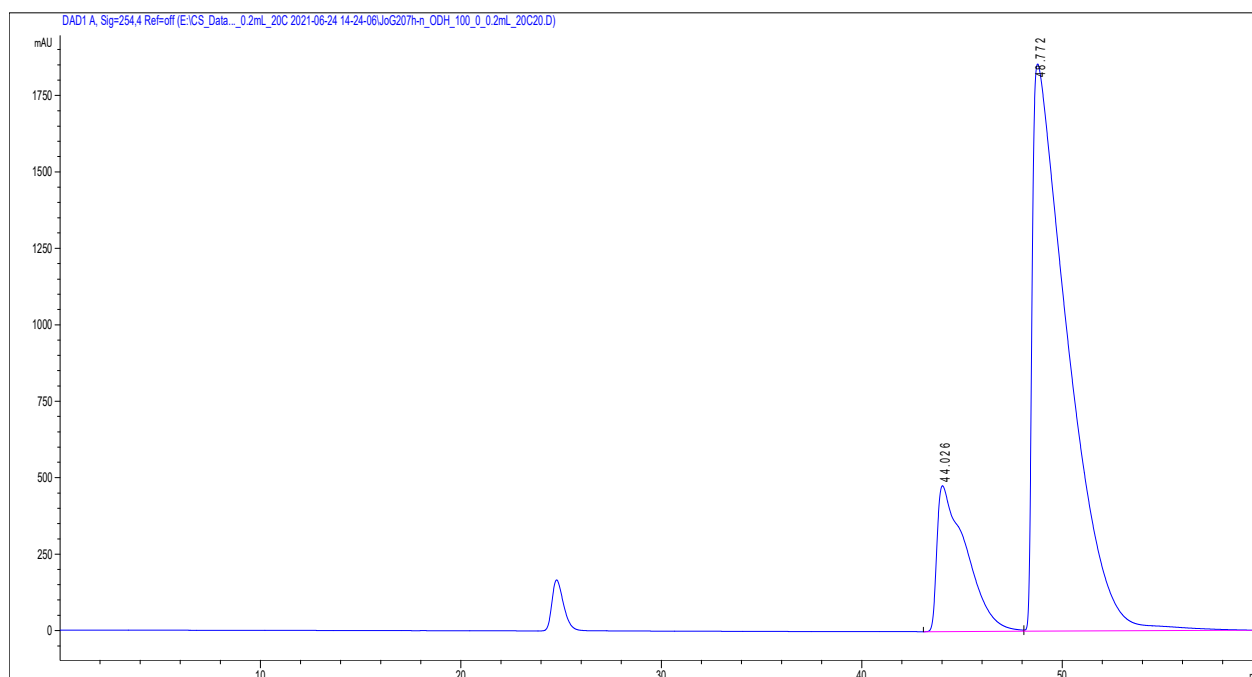
9. Tilting the Balance: London Dispersion Systematically Enhances Enantioselectivities in Brønsted Acid Catalyzed Transfer Hydrogenation of Imines

Catalyst C₆H₅ (**1j**)



#	Time	Area	Height	Width	Area%	Symmetry
1	42.531	76616.2	929.6	1.1555	21.738	0.232
2	47.396	275842	2214.3	1.6153	78.262	0.151

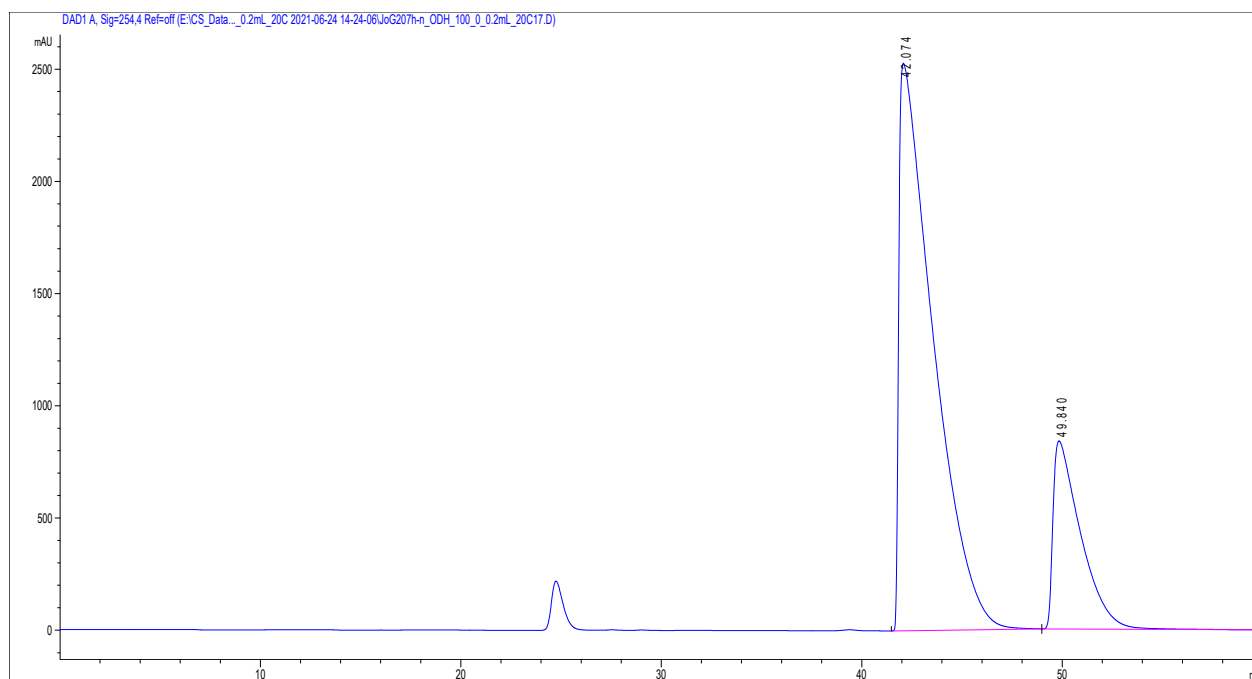
Catalyst 3,5-(CH₃)₂C₆H₂ (**1k**)



#	Time	Area	Height	Width	Area%	Symmetry
1	44.026	48211.2	477.2	1.3386	17.415	0.215
2	48.772	228624.7	1854.8	1.598	82.585	0.161

9. Tilting the Balance: London Dispersion Systematically Enhances Enantioselectivities in Brønsted Acid Catalyzed Transfer Hydrogenation of Imines

Catalyst (S)-DSI-4-(CF₃)C₆H₄ (**11**)

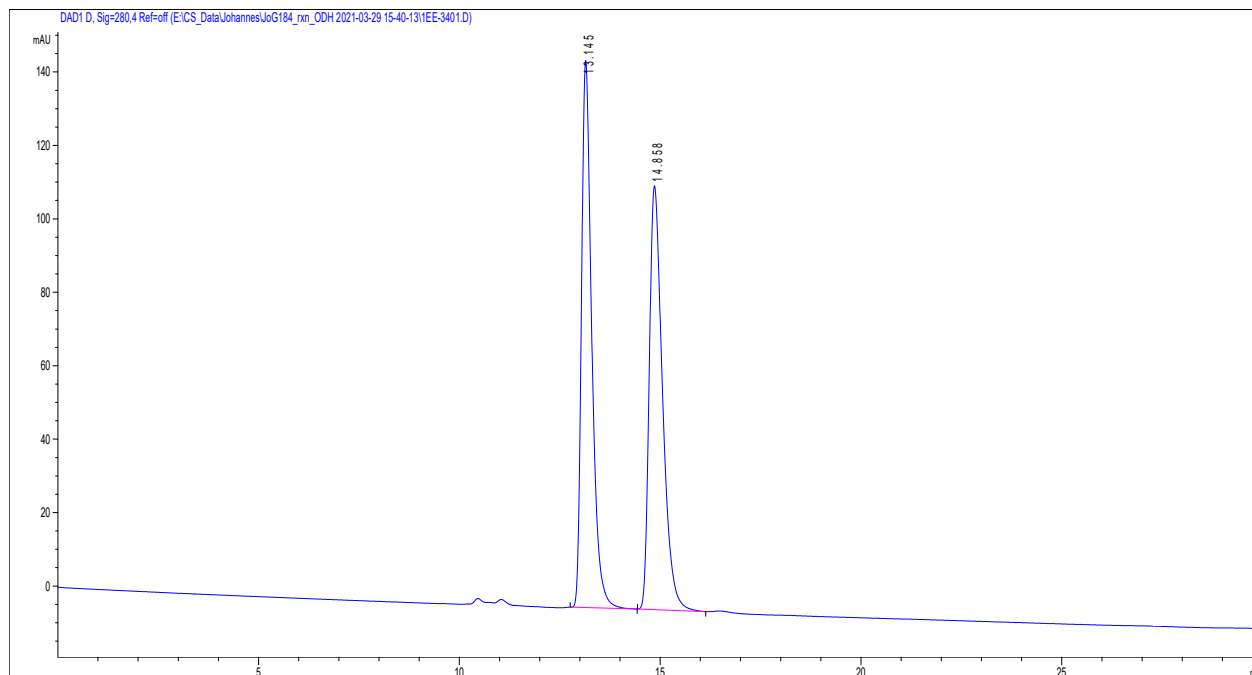


#	Time	Area	Height	Width	Area%	Symmetry
1	42.074	300439.5	2530	1.4874	78.938	0.135
2	49.84	80162.2	838.2	1.3378	21.062	0.253

9. Tilting the Balance: London Dispersion Systematically Enhances Enantioselectivities in Brønsted Acid Catalyzed Transfer Hydrogenation of Imines

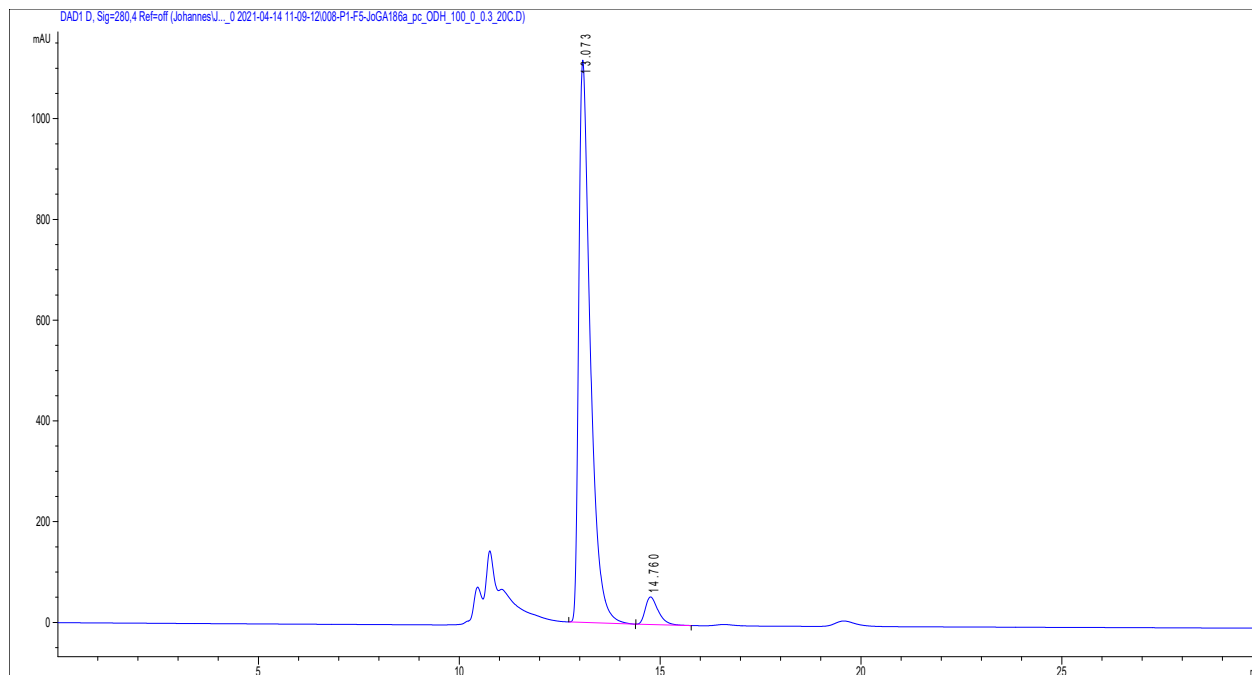
Transfer hydrogenation of imine **2d**; CSP-HPLC ODH, *n*-hexane, 0.2 mL/min, 20 °C; @280 nm

Racemic compound **4d**



#	Time	Area	Height	Width	Area%	Symmetry
1	13.145	2649.8	149	0.2694	50.047	0.631
2	14.858	2644.8	115.5	0.3492	49.953	0.598

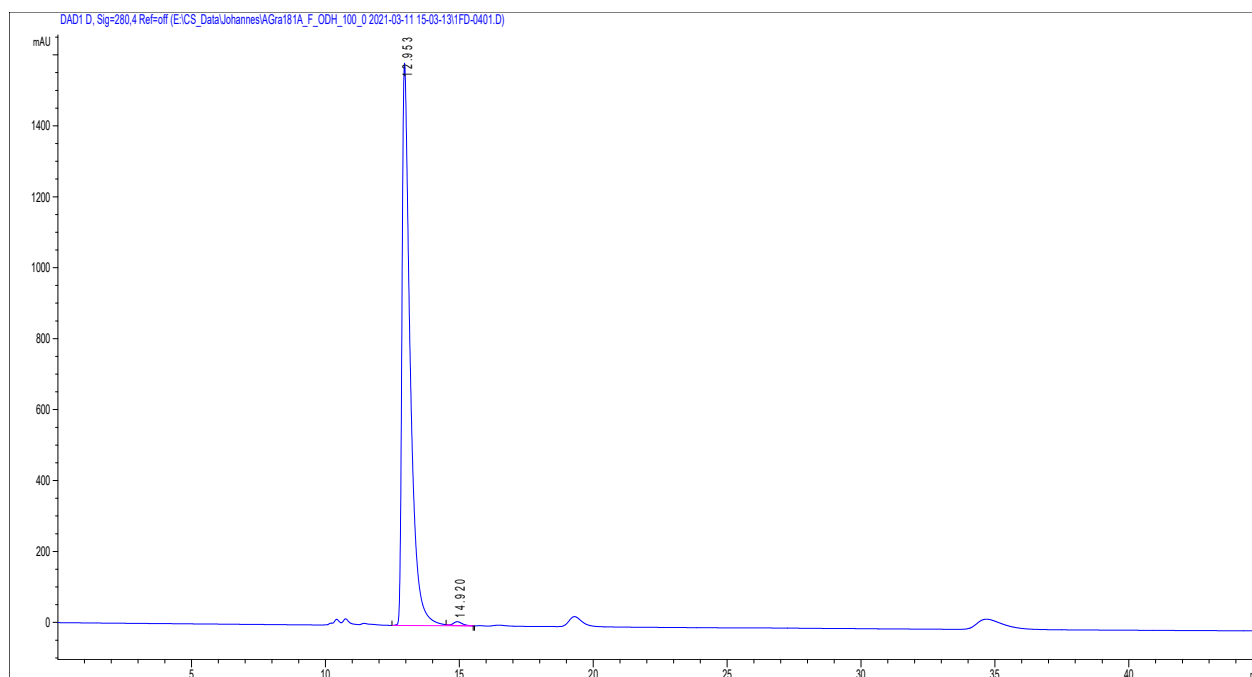
Catalyst 2,4,6-(Me)₃C₆H₂ (**1a**)



#	Time	Area	Height	Width	Area%	Symmetry
1	13.073	22305.9	1115.8	0.2972	94.807	0.475
2	14.76	1221.9	54.8	0.3401	5.193	0.629

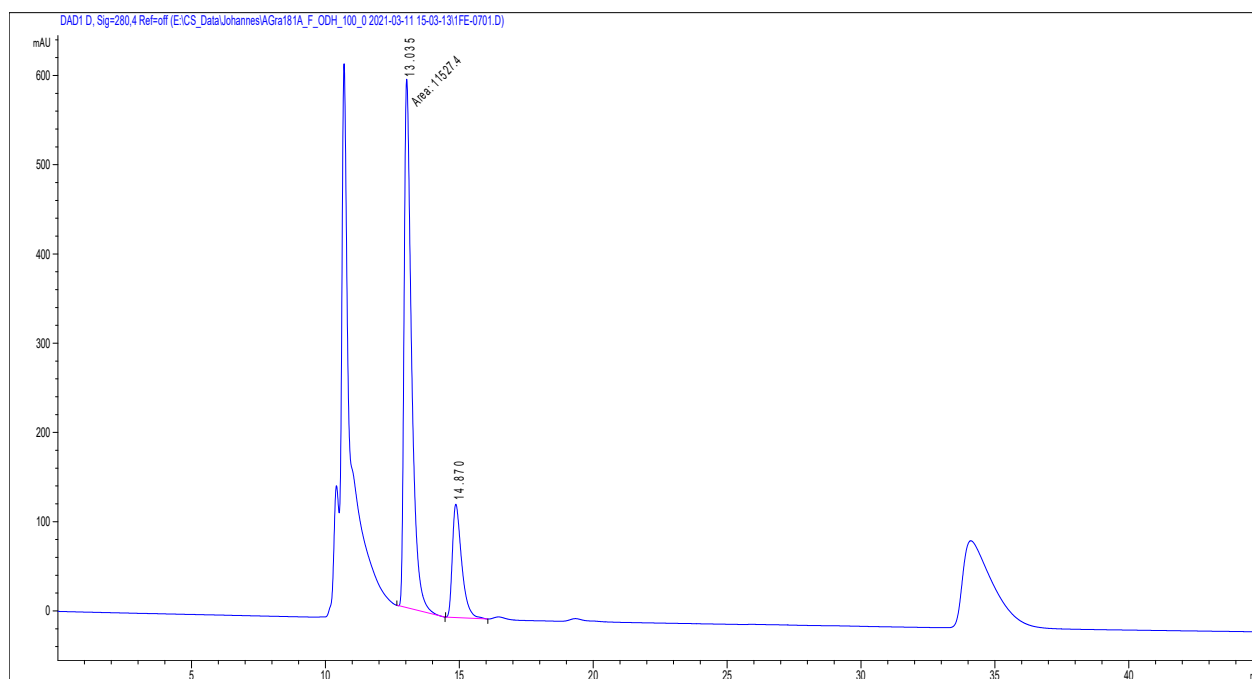
9. Tilting the Balance: London Dispersion Systematically Enhances Enantioselectivities in Brønsted Acid Catalyzed Transfer Hydrogenation of Imines

Catalyst 2,4,6-(*i*Pr)₃C₆H₂ (**1b**)



#	Time	Area	Height	Width	Area%	Symmetry
1	12.953	33959.4	1585.4	0.3119	99.280	0.406
2	14.92	246.3	10.9	0.3408	0.720	0.675

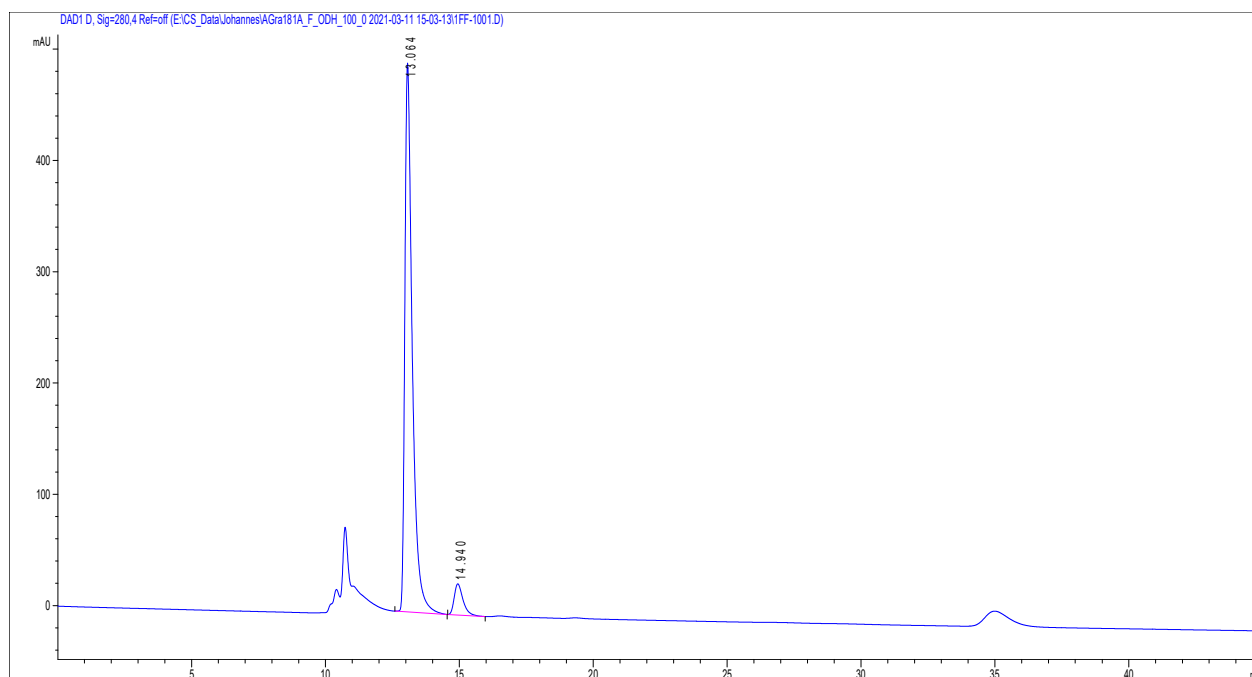
Catalyst SiPh₃ (**1c**)



#	Time	Area	Height	Width	Area%	Symmetry
1	13.035	11527.4	592.2	0.3244	79.004	0.521
2	14.87	3063.6	127.1	0.3632	20.996	0.551

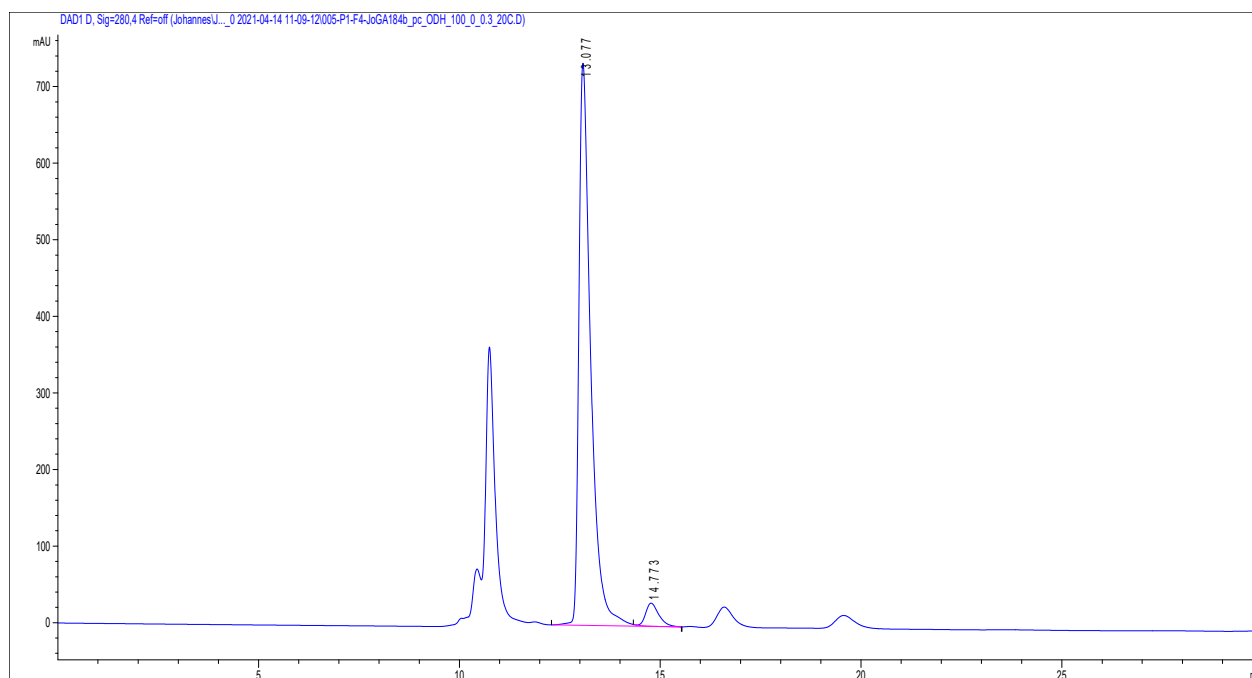
9. Tilting the Balance: London Dispersion Systematically Enhances Enantioselectivities in Brønsted Acid Catalyzed Transfer Hydrogenation of Imines

Catalyst 3,5-(CF₃)₂C₆H₄ (**1d**)



#	Time	Area	Height	Width	Area%	Symmetry
1	13.064	9546	493.1	0.2879	93.717	0.516
2	14.94	640	28	0.3444	6.283	0.636

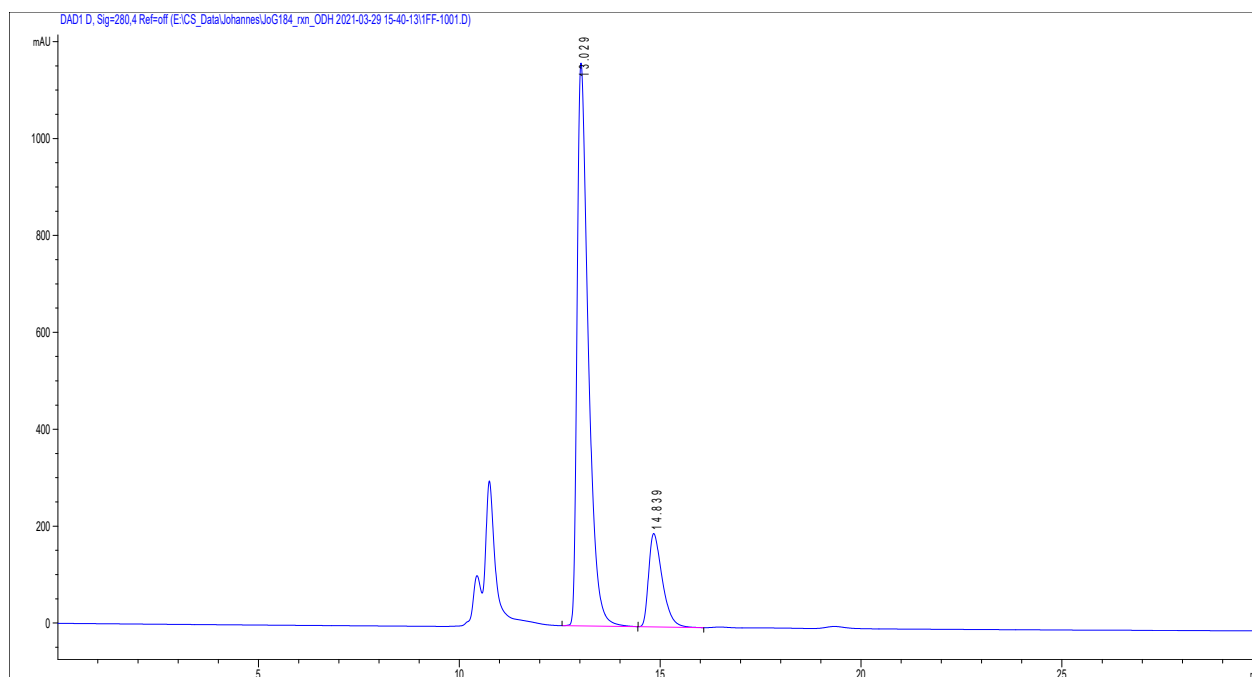
Catalyst 9-anthryl (**1e**)



#	Time	Area	Height	Width	Area%	Symmetry
1	13.077	15007.3	734.1	0.3005	95.669	0.477
2	14.773	679.4	30.1	0.3416	4.331	0.652

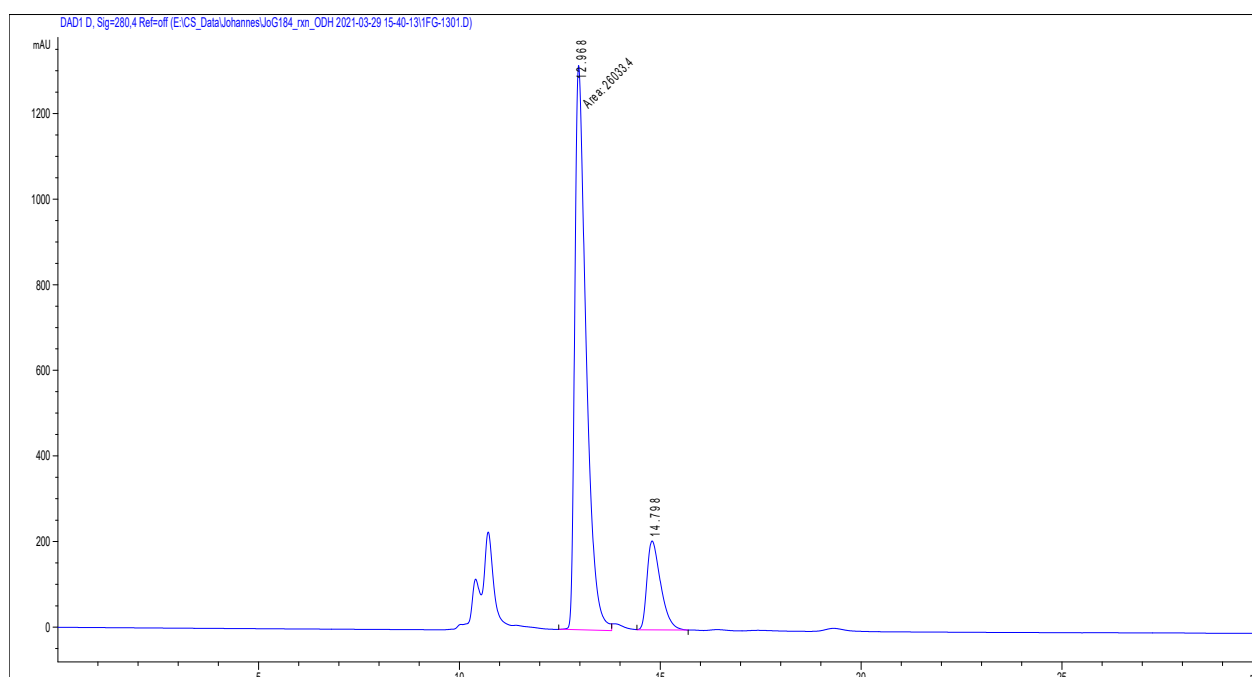
9. Tilting the Balance: London Dispersion Systematically Enhances Enantioselectivities in Brønsted Acid Catalyzed Transfer Hydrogenation of Imines

Catalyst 4-(^tBu)₂C₆H₄ (**1f**)



#	Time	Area	Height	Width	Area%	Symmetry
1	13.029	22450.2	1161.8	0.2894	83.150	0.494
2	14.839	4549.6	192.7	0.3574	16.850	0.554

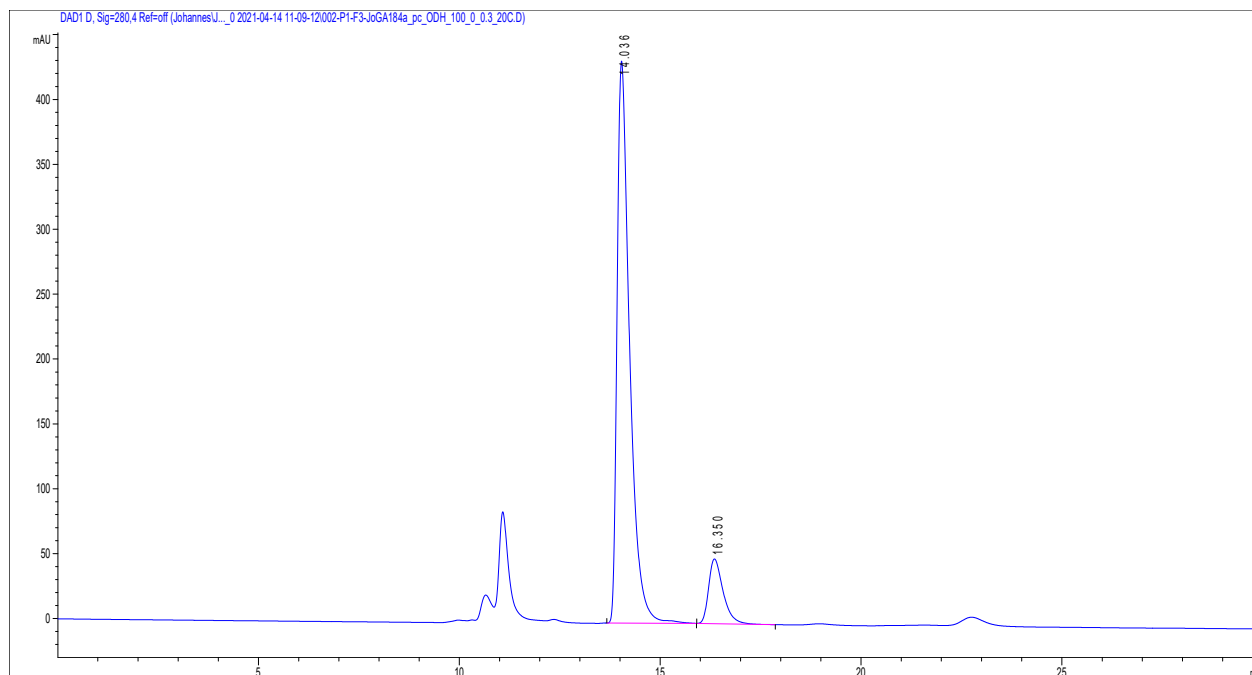
Catalyst 4-(CF₃)₂C₆H₃ (**1g**)



#	Time	Area	Height	Width	Area%	Symmetry
1	12.968	26033.4	1318.7	0.329	84.124	0.489
2	14.798	4913	207.6	0.3601	15.876	0.555

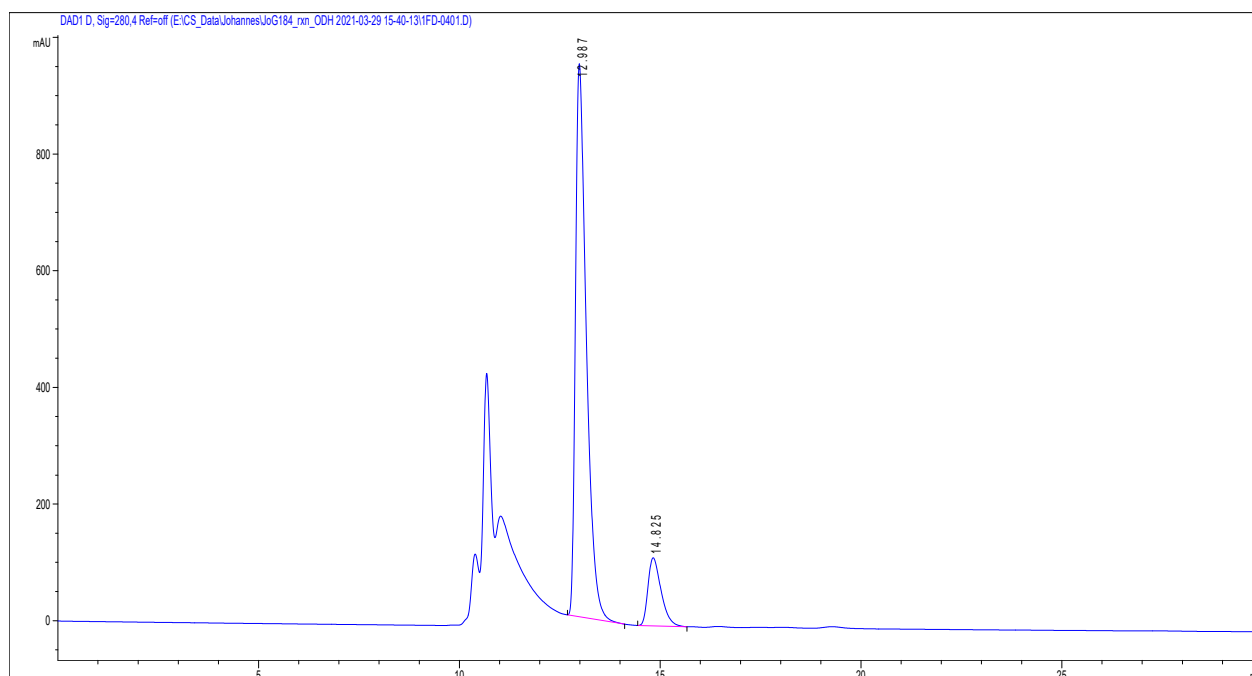
9. Tilting the Balance: London Dispersion Systematically Enhances Enantioselectivities in Brønsted Acid Catalyzed Transfer Hydrogenation of Imines

Catalyst 1-naphthyl (**1h**)



#	Time	Area	Height	Width	Area%	Symmetry
1	14.036	9384.6	433	0.3248	88.267	0.494
2	16.35	1247.5	49.8	0.3801	11.733	0.622

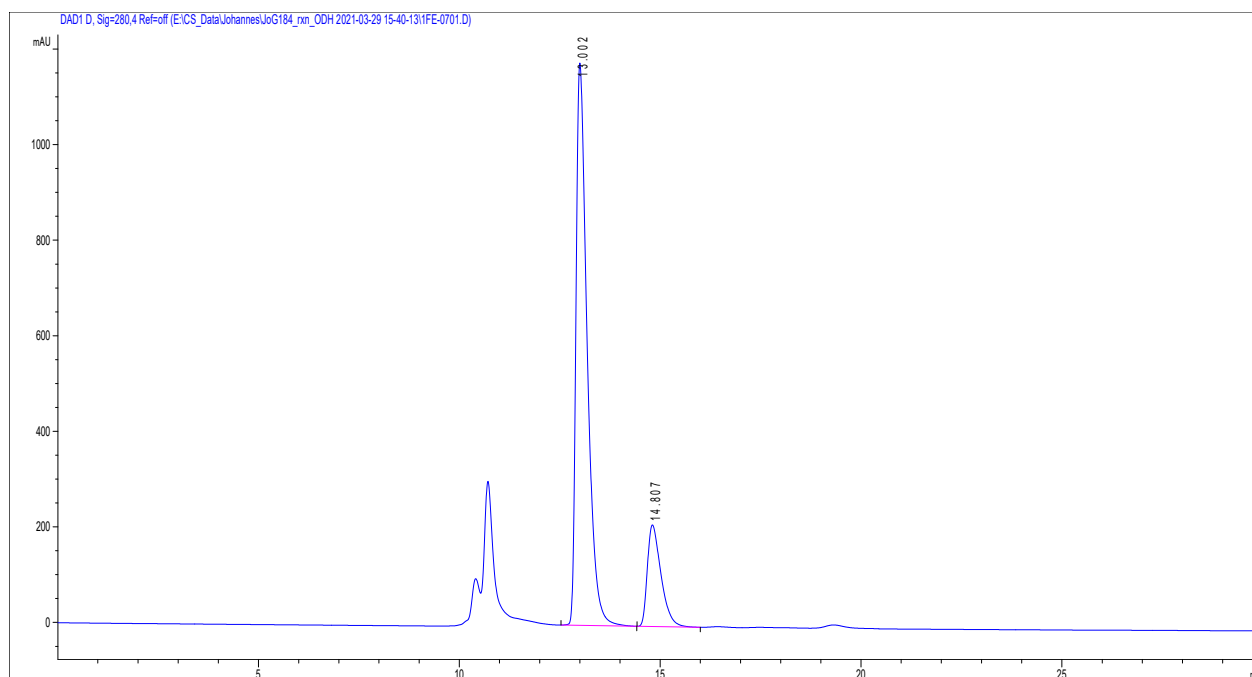
Catalyst 9-phenanthryl (**1i**)



#	Time	Area	Height	Width	Area%	Symmetry
1	12.987	17832.9	948	0.2835	87.071	0.509
2	14.825	2647.9	116.7	0.3466	12.929	0.611

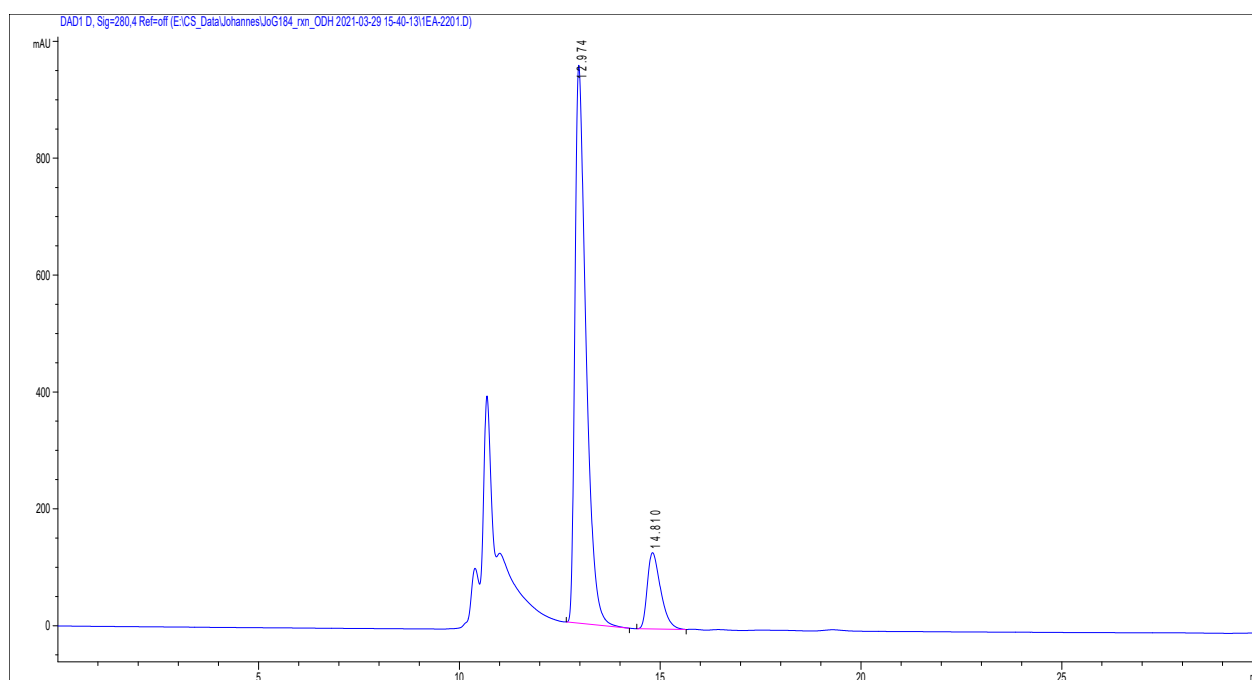
9. Tilting the Balance: London Dispersion Systematically Enhances Enantioselectivities in Brønsted Acid Catalyzed Transfer Hydrogenation of Imines

Catalyst C₆H₅ (**1j**)



#	Time	Area	Height	Width	Area%	Symmetry
1	13.002	22673.9	1177.1	0.2887	81.865	0.497
2	14.807	5022.7	212.8	0.3574	18.135	0.545

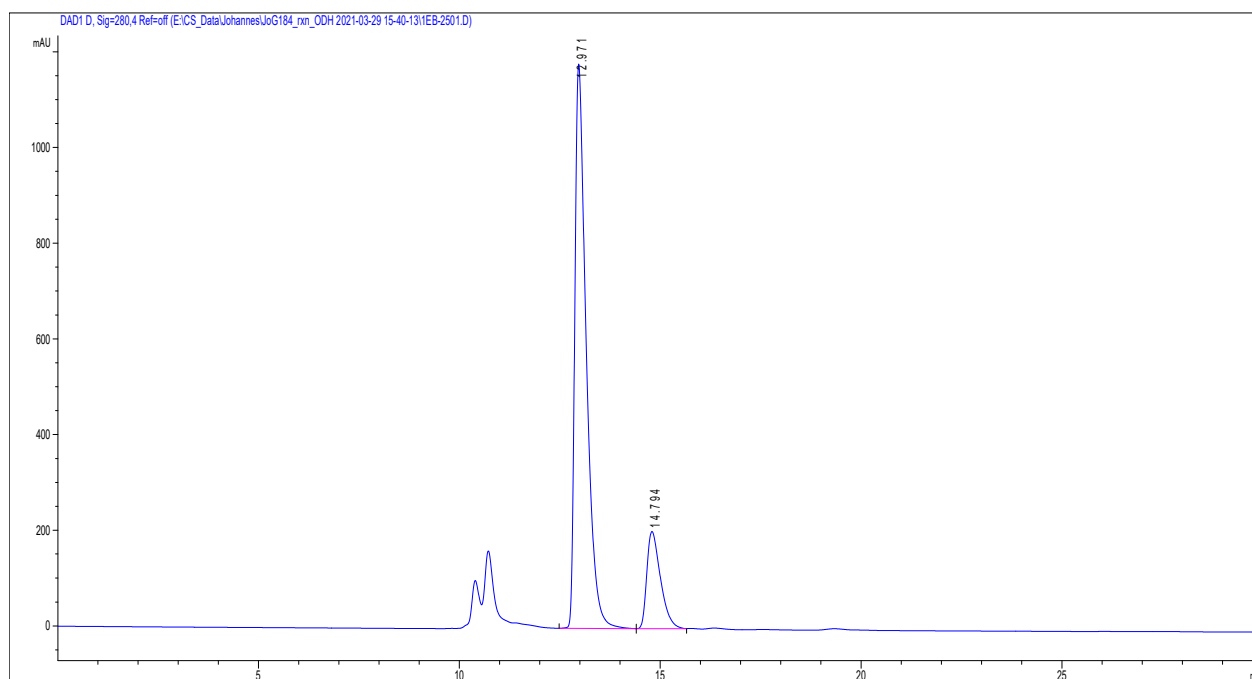
Catalyst 3,5-(CH₃)₂C₆H₂ (**1k**)



#	Time	Area	Height	Width	Area%	Symmetry
1	12.974	18371.7	954.6	0.2885	85.925	0.497
2	14.81	3009.4	130.6	0.3508	14.075	0.599

9. Tilting the Balance: London Dispersion Systematically Enhances Enantioselectivities in Brønsted Acid Catalyzed Transfer Hydrogenation of Imines

Catalyst (S)-DSI-4-(CF₃)C₆H₄ (**1**)



#	Time	Area	Height	Width	Area%	Symmetry
1	12.971	23222.3	1179.3	0.2937	82.891	0.474
2	14.794	4793.2	203	0.3595	17.109	0.559

9. Tilting the Balance: London Dispersion Systematically Enhances Enantioselectivities in Brønsted Acid Catalyzed Transfer Hydrogenation of Imines

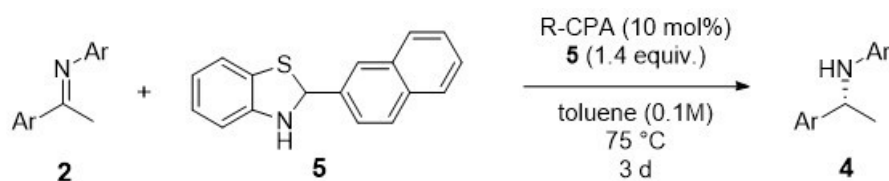
9.6.12. References

- (1) Žabka, M.; Gschwind, R. M. Ternary Complexes of Chiral Disulfonimides in Transfer-Hydrogenation of Imines: The Relevance of Late Intermediates in Ion Pair Catalysis. *Chem. Sci.* **2021**, 15263–15272.
- (2) Harris, R. K.; Becker, E. D.; Cabral De Menezes, S. M.; Goodfellow, R.; Granger, P. NMR Nomenclature: Nuclear Spin Properties and Conventions for Chemical Shifts (IUPAC Recommendations 2001). *Concepts Magn. Reson. Part A Bridg. Educ. Res.* **2002**, 14, 326–346.
- (3) Renzi, P.; Hioe, J.; Gschwind, R. M. Decrypting Transition States by Light: Photoisomerization as a Mechanistic Tool in Brønsted Acid Catalysis. *J. Am. Chem. Soc.* **2017**, 139, 6752–6760.
- (4) Lokesh, N.; Hioe, J.; Gramüller, J.; Gschwind, R. M. Relaxation Dispersion NMR to Reveal Fast Dynamics in Brønsted Acid Catalysis: Influence of Sterics and H-Bond Strength on Conformations and Substrate Hopping. *J. Am. Chem. Soc.* **2019**, 141, 16398–16407.
- (5) Schramm, Y.; Barrios-Landeros, F.; Pfaltz, A. Discovery of an Iridacycle Catalyst with Improved Reactivity and Enantioselectivity in the Hydrogenation of Dialkyl Ketimines. *Chem. Sci.* **2013**, 4, 2760–2766.
- (6) Grunder, S.; Muñoz Torres, D.; Marquardt, C.; Bałaszcyk, A.; Krupke, R.; Mayor, M. Synthesis and Optical Properties of Molecular Rods Comprising a Central Core-Substituted Naphthalenediimide Chromophore for Carbon Nanotube Junctions. *Eur. J. Org. Chem.* **2011**, No. 3, 478–496.
- (7) Lokesh, N.; Seegerer, A.; Hioe, J.; Gschwind, R. M. Chemical Exchange Saturation Transfer in Chemical Reactions: A Mechanistic Tool for NMR Detection and Characterization of Transient Intermediates. *J. Am. Chem. Soc.* **2018**, 140, 1855–1862.
- (8) Schweighauser, L.; Strauss, M. A.; Bellotto, S.; Wegner, H. A. Attraction or Repulsion? London Dispersion Forces Control Azobenzene Switches. *Angew. Chem. Int. Ed.* **2015**, 54, 13436–13439.
- (9) Melikian, M.; Gramüller, J.; Hioe, J.; Greindl, J.; Gschwind, R. M. Brønsted Acid Catalysis—the Effect of 3,3'-Substituents on the Structural Space and the Stabilization of Imine/Phosphoric Acid Complexes. *Chem. Sci.* **2019**, 10, 5226–5234.
- (10) Greindl, J.; Hioe, J.; Sorgenfrei, N.; Morana, F.; Gschwind, R. M. Brønsted Acid Catalysis—Structural Preferences and Mobility in Imine/Phosphoric Acid Complexes. *J. Am. Chem. Soc.* **2016**, 138, 15965–15971.
- (11) Jerschow, A.; Müller, N. Suppression of Convection Artifacts in Stimulated-Echo Diffusion Experiments. Double-Stimulated-Echo Experiments. *J. Magn. Reson.* **1997**, 125, 372–375.
- (12) MacChioni, A.; Ciancaleoni, G.; Zuccaccia, C.; Zuccaccia, D. Determining Accurate Molecular Sizes in Solution through NMR Diffusion Spectroscopy. *Chem. Soc. Rev.* **2008**, 37, 479–489.
- (13) Chen, H. C.; Chen, S. H. Diffusion of Crown Ethers in Alcohols. *J. Phys. Chem.* **1984**, 88, 5118–5121.
- (14) Ben-amotz, D.; Willis, K. G. Molecular Hard-Sphere Volume. *J. Phys. Chem.* **1993**, 1, 7736–7742.
- (15) Simón, L.; Goodman, J. M. Theoretical Study of the Mechanism of Hantzsch Ester Hydrogenation of Imines Catalyzed by Chiral BINOL-Phosphoric Acids. *J. Am. Chem. Soc.* **2008**, 130, 8741–8747.
- (16) Marcelli, T.; Hammar, P.; Himo, F. Phosphoric Acid Catalyzed Enantioselective Transfer Hydrogenation of Imines: A Density Functional Theory Study of Reaction Mechanism and the Origins of Enantioselectivity. *Chem. Eur. J.* **2008**, 14, 8562–8571.
- (17) Rothermel, K.; Melikian, M.; Hioe, J.; Greindl, J.; Gramüller, J.; Matej Žabka; Sorgenfrei, N.; Hausler, T.; Morana, F.; Gschwind, R. M. Internal Acidity Scale and Reactivity Evaluation of Chiral Phosphoric Acids with Different 3,3'-Substituents in Brønsted Acid Catalysis. *Chem. Sci.* **2019**.
- (18) Jansen, D.; Gramüller, J.; Niemeyer, F.; Schaller, T.; Letzel, M. C.; Grimme, S.; Zhu, H.; Gschwind, R. M.; Niemeyer, J. What Is the Role of Acid-Acid Interactions in Asymmetric Phosphoric Acid Organocatalysis? A Detailed Mechanistic Study Using Interlocked and Non-Interlocked Catalysts. *Chem. Sci.* **2020**, 11, 4381–4390.

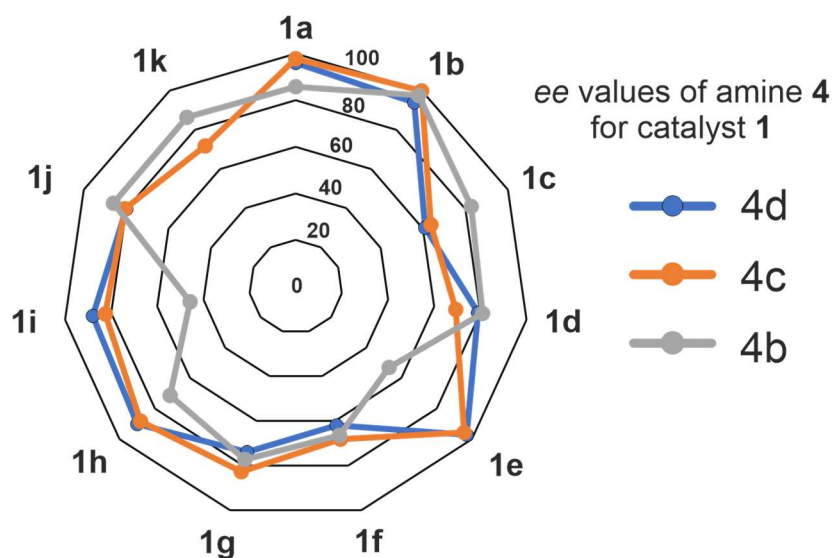
9.7. Additional Findings

After establishing the clear correlation between dispersion stabilization of the Z-imine and increase in enantioselectivity in the CPA catalyzed transfer hydrogenation of N-aryl imines with Hantzsch ester as hydride source, we explored the general applicability and limitations of this approach. Therefore, the hydride source was changed to benzothiazoline **5** (see table 3).^[1]

Table 3: enantioselectivities for the transfer hydrogenation of imines **2b-d** for a variety of catalysts **1a-l**.



Entry	Catalyst 3,3'	ee (4d) [%]	ee (4c) [%]	ee (4b) [%]
1	2,4,6-(Me) ₃ C ₆ H ₂ (1a)	96	98	86
2	2,4,6-(<i>i</i> Pr) ₃ C ₆ H ₂ (1b)	94	99	98
3	SiPh ₃ (1c)	61	64	83
4	3,5-(CF ₃) ₂ C ₆ H ₃ (1d)	79	69	81
5	9-anthryl (1e)	97	96	53
6	4-(<i>t</i> Bu)C ₆ H ₄ (1f)	62	68	67
7	4-(CF ₃)C ₆ H ₄ (1g)	74	83	77
8	1-naphthyl (1h)	90	88	71
9	9-phenanthryl (1i)	88	83	46
10	C ₆ H ₅ (1j)	80	81	86
11	3,5-(CH ₃) ₂ C ₆ H ₂ (1k)	n.d.	72	86
12	DSI-4-(CF ₃)C ₆ H ₄ (1l)	-76	-71	-62



9. Tilting the Balance: London Dispersion Systematically Enhances Enantioselectivities in Brønsted Acid Catalyzed Transfer Hydrogenation of Imines

In contrast to the transfer hydrogenation with Hantzsch ester **4**, a general clear correlation between dispersion stabilization (**2d** > **2c** > **2b**) was not observed with benzothiazoline **5**. For most catalysts, the enantioselectivities obtained for substrates **2c** and **2d** were nearly identical and the *ee* values for imine **2b** with close to no dispersion stabilization were for most CPAs either close or higher. Only for catalysts bearing an extended aromatic system as 3,3'-substituent (catalyst **1e**, **1h** and **1i**), a correlation between dispersion stabilization and increase in enantioselectivity was observed (entry 5, 8, 9). Most likely, for the transfer hydrogenation with benzothiazoline **5** the competing transition state combination is changed and therefore the dispersion stabilization is not translated to the enantioselectivities. In the CPA catalyzed transfer hydrogenation of similar imines bearing an α -ethyl group it was shown that for some substrates Hantzsch ester **4** and benzothiazoline **5** gave opposite enantiomers.^[2] This strongly indicates a change in transition state combination and corroborates the assumption, that this change is also the reason for the lacking correlation of *ee* and dispersion stabilization in the transfer hydrogenation of imines **2b-d**. Nevertheless, the *ee* values for imine **2d** were not significantly lower as for **2b** which demonstrates, that the introduction of several bulky *tert*-butyl groups has no negative effect on the enantioselectivities due to steric repulsion.

References

- [1] C. Zhu, T. Akiyama, *Org. Lett.* **2009**, *11*, 4180–4183.
[2] K. Saito, K. Horiguchi, Y. Shibata, M. Yamanaka, T. Akiyama, *Chem. Eur. J.* **2014**, *20*, 7616–7620.

General procedure for the asymmetric transfer hydrogenation of imines (GP II)

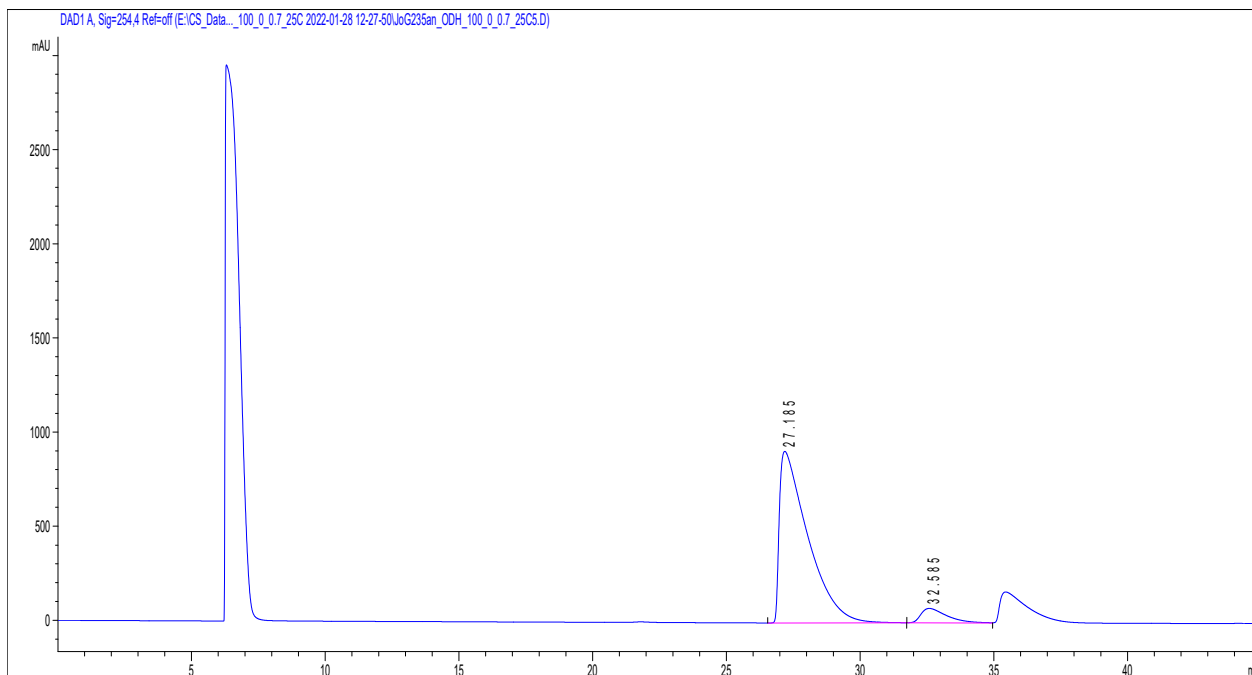
Imine (0.2 mmol, 1.0 eq.), benzothiazoline **5** (0.28 mmol, 73.7 mg, 1.4 equiv.) and catalyst (0.02 mmol, 0.1 equiv.) were weighed into a flame dried Schlenk tube. The Schlenk tube was evacuated and flushed with argon three times. Afterwards, toluene (2 mL) was added under argon flow and the reaction was stirred for 3 days at 75 °C. The solvent was removed under reduced pressure and the crude product was directly subjected to HPLC. No yields were determined.

9. Tilting the Balance: London Dispersion Systematically Enhances Enantioselectivities in Brønsted Acid Catalyzed Transfer Hydrogenation of Imines

HPLC Chromatograms

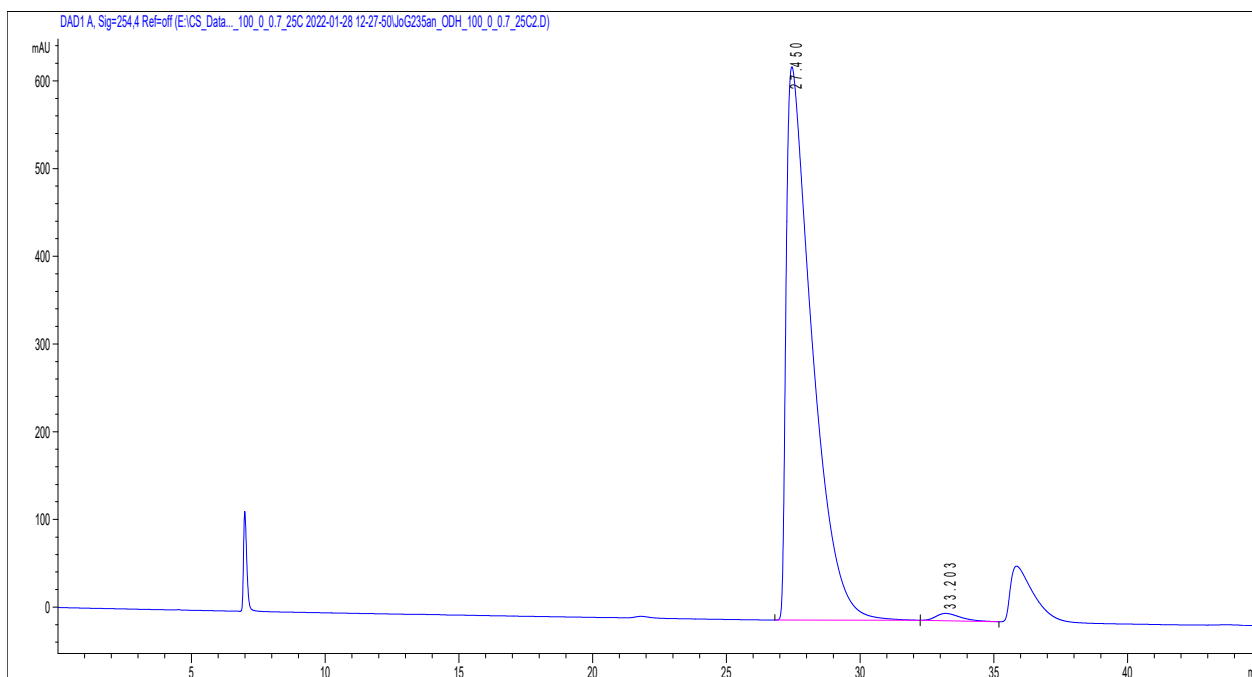
Transfer hydrogenation of imine **2b**; CSP-HPLC ODH, *n*-hexane, 0.7 mL/min, 25 °C; @254 nm

Catalyst 2,4,6-(Me)₃C₆H₂ (**1a**)



#	Time	Area	Height	Width	Area%	Symmetry
1	27.185	67318.1	911.6	1.0516	92.948	0.214
2	32.585	5107.2	76.4	0.9976	7.052	0.438

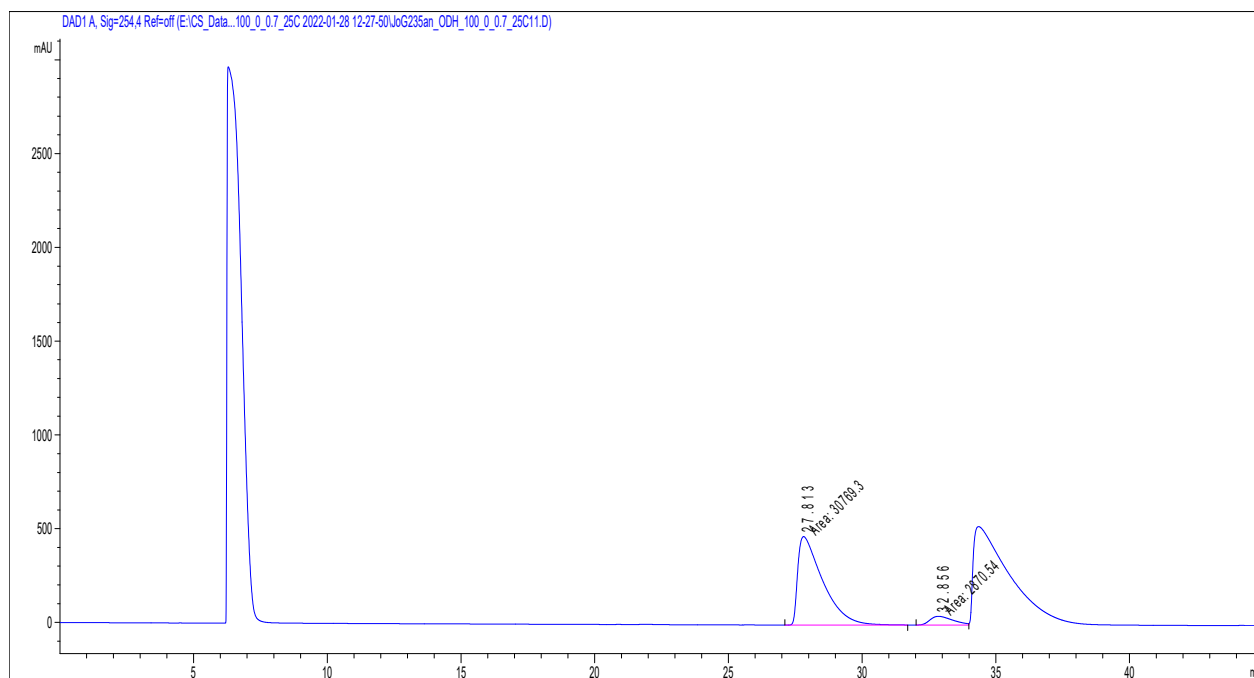
Catalyst 2,4,6-(*i*Pr)₃C₆H₂ (**1b**)



#	Time	Area	Height	Width	Area%	Symmetry
1	27.45	42502.5	630.9	0.974	98.764	0.253
2	33.203	531.9	8.3	0.8957	1.236	0.616

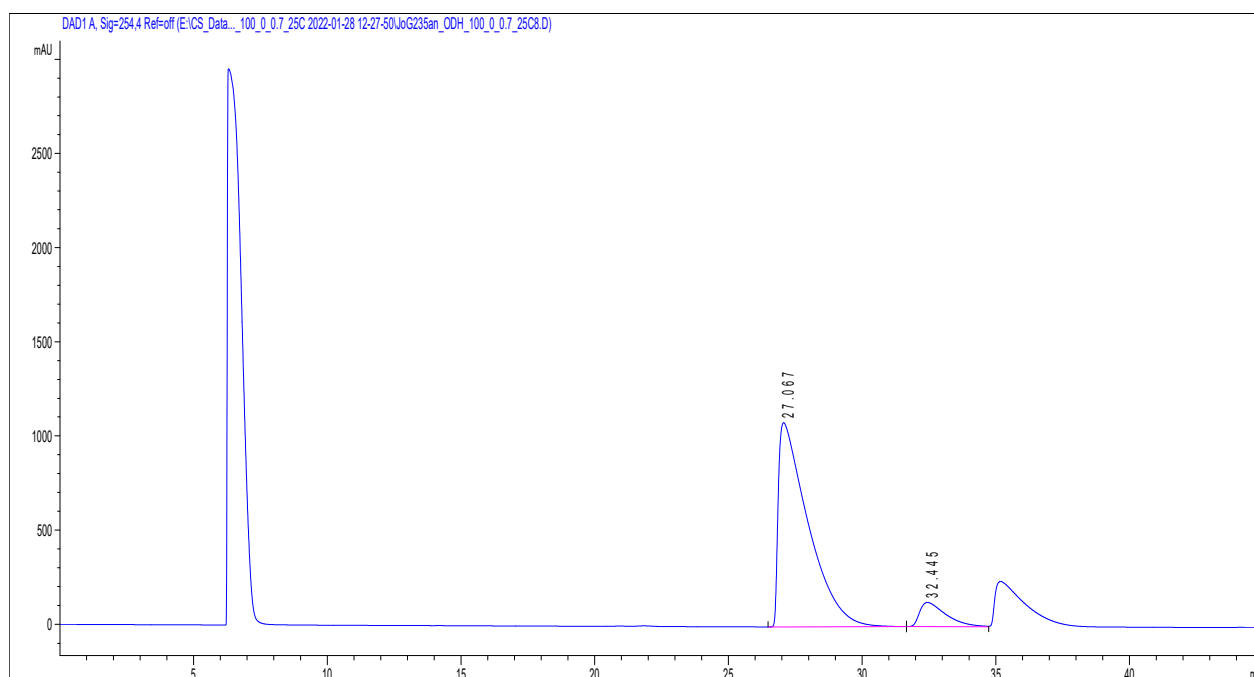
9. Tilting the Balance: London Dispersion Systematically Enhances Enantioselectivities in Brønsted Acid Catalyzed Transfer Hydrogenation of Imines

Catalyst SiPh₃ (**1c**)



#	Time	Area	Height	Width	Area%	Symmetry
1	27.813	30769.3	472.7	1.0848	91.467	0.293
2	32.856	2870.5	47.4	1.0093	8.533	0.575

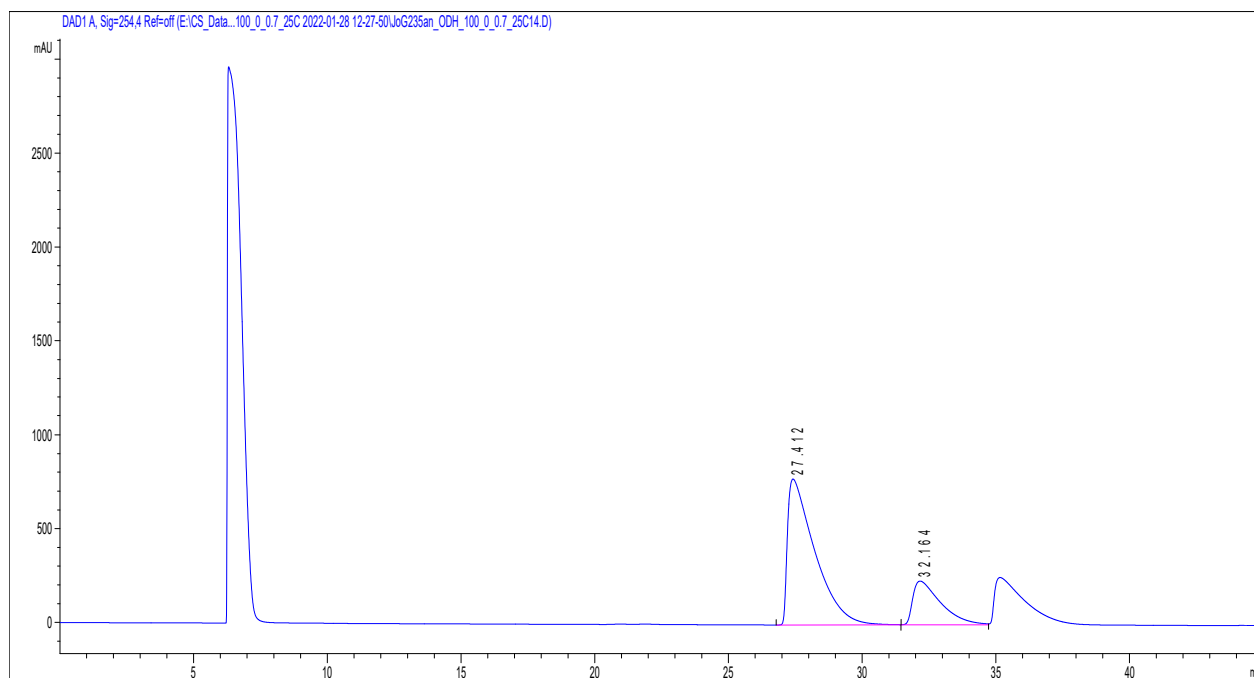
Catalyst 3,5-(CF₃)₂C₆H₄ (**1d**)



#	Time	Area	Height	Width	Area%	Symmetry
1	27.067	84023.5	1084.3	1.1141	90.498	0.198
2	32.445	8822.3	128.6	1.0085	9.502	0.389

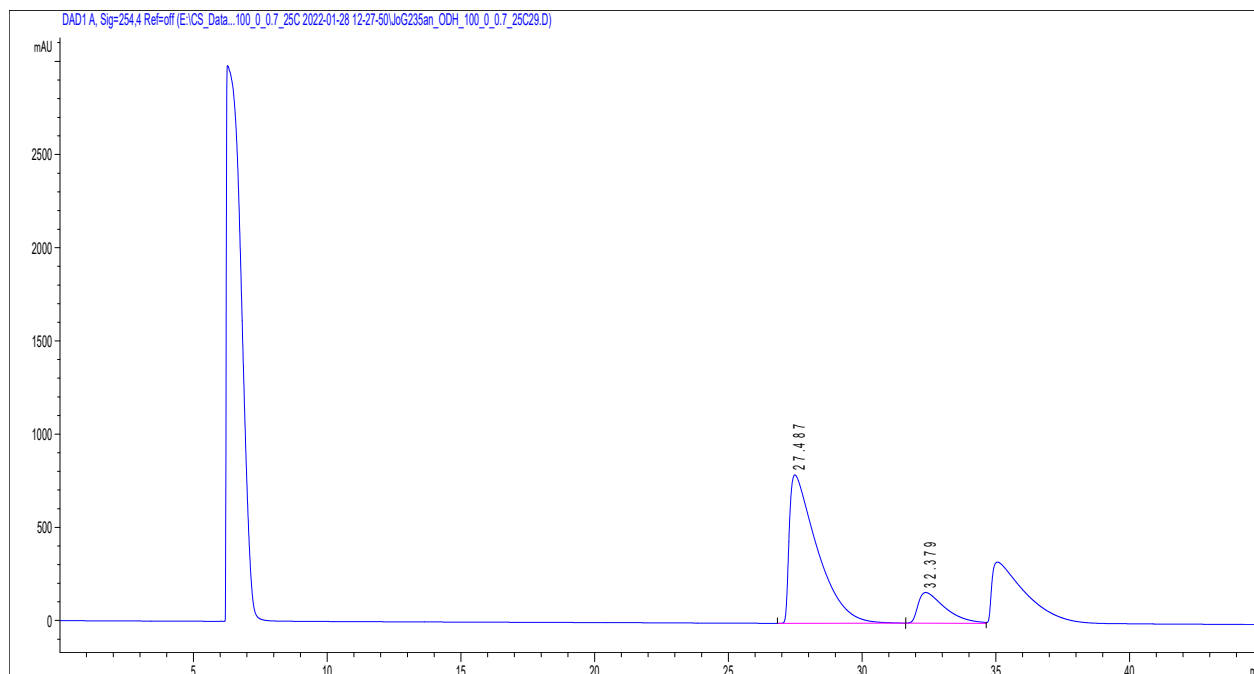
9. Tilting the Balance: London Dispersion Systematically Enhances Enantioselectivities in Brønsted Acid Catalyzed Transfer Hydrogenation of Imines

Catalyst 9-anthryl (**1e**)



#	Time	Area	Height	Width	Area%	Symmetry
1	27.412	55057.2	777.5	1.0062	76.530	0.232
2	32.164	16884.8	232.9	1.056	23.470	0.324

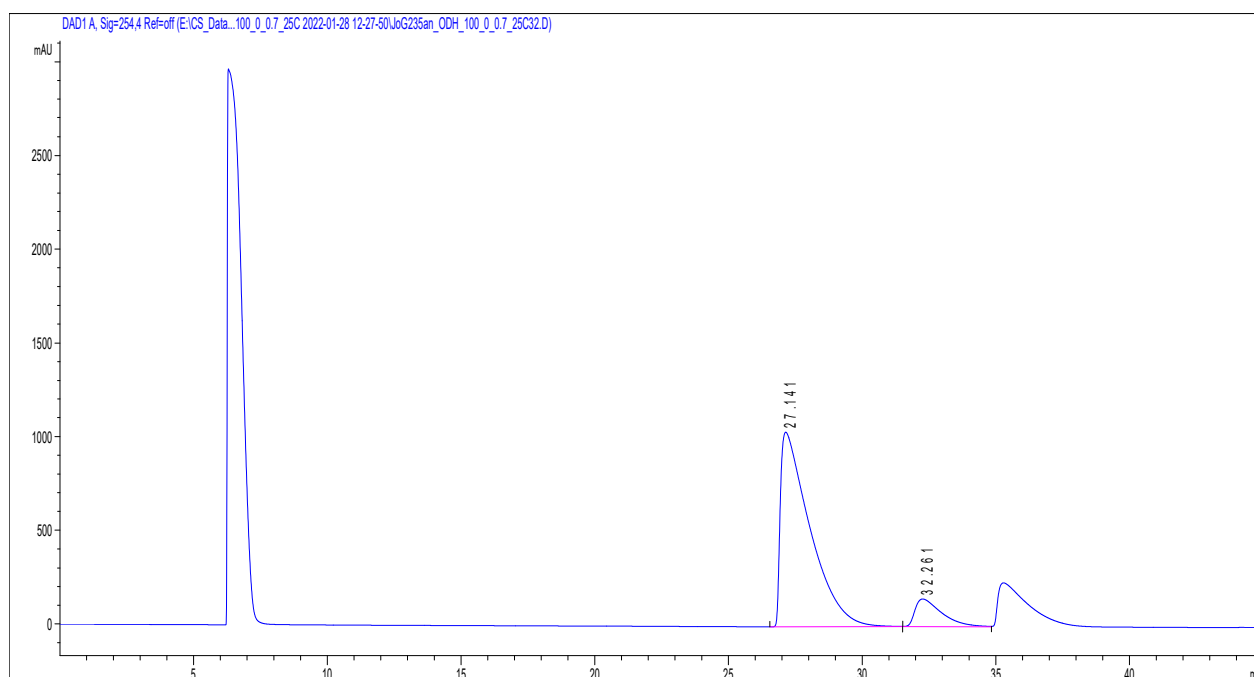
Catalyst 4-(^tBu)₂C₆H₄ (**1f**)



#	Time	Area	Height	Width	Area%	Symmetry
1	27.487	57553.5	795.9	1.0376	83.310	0.227
2	32.379	11530.4	164.6	1.0374	16.690	0.361

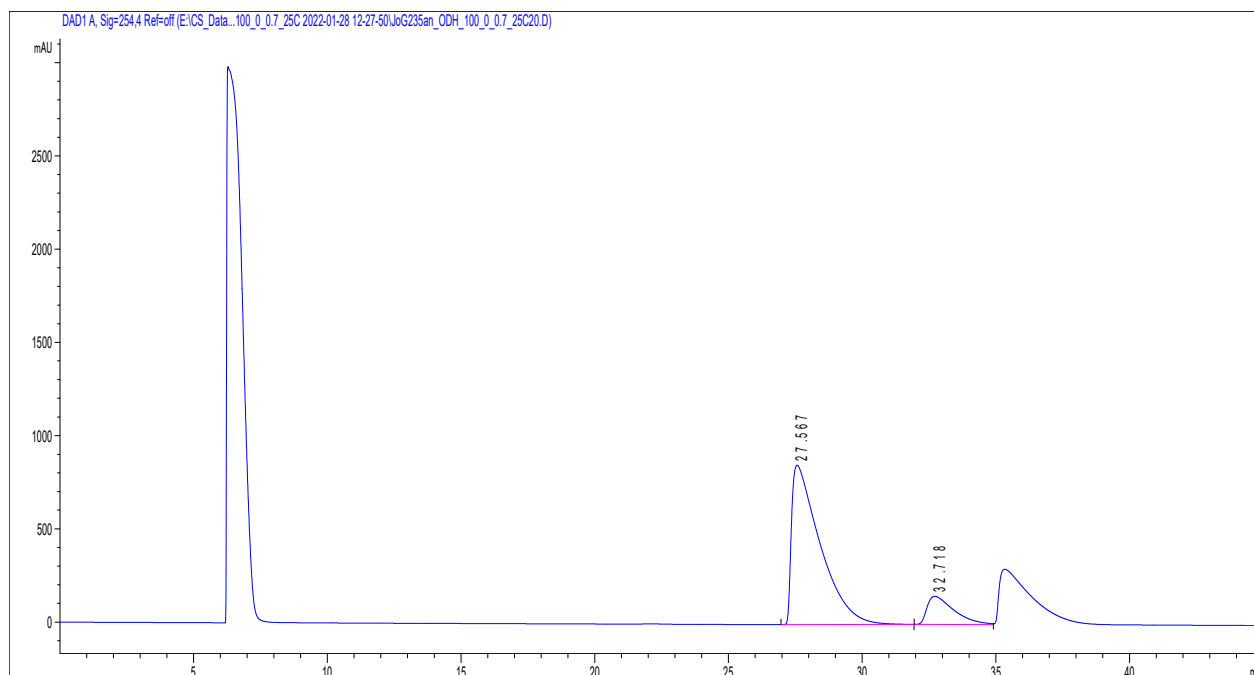
9. Tilting the Balance: London Dispersion Systematically Enhances Enantioselectivities in Brønsted Acid Catalyzed Transfer Hydrogenation of Imines

Catalyst 4-(CF₃)C₆H₃ (**1g**)



#	Time	Area	Height	Width	Area%	Symmetry
1	27.141	79698.8	1038	1.0738	88.721	0.202
2	32.261	10132.2	147	1.0022	11.279	0.372

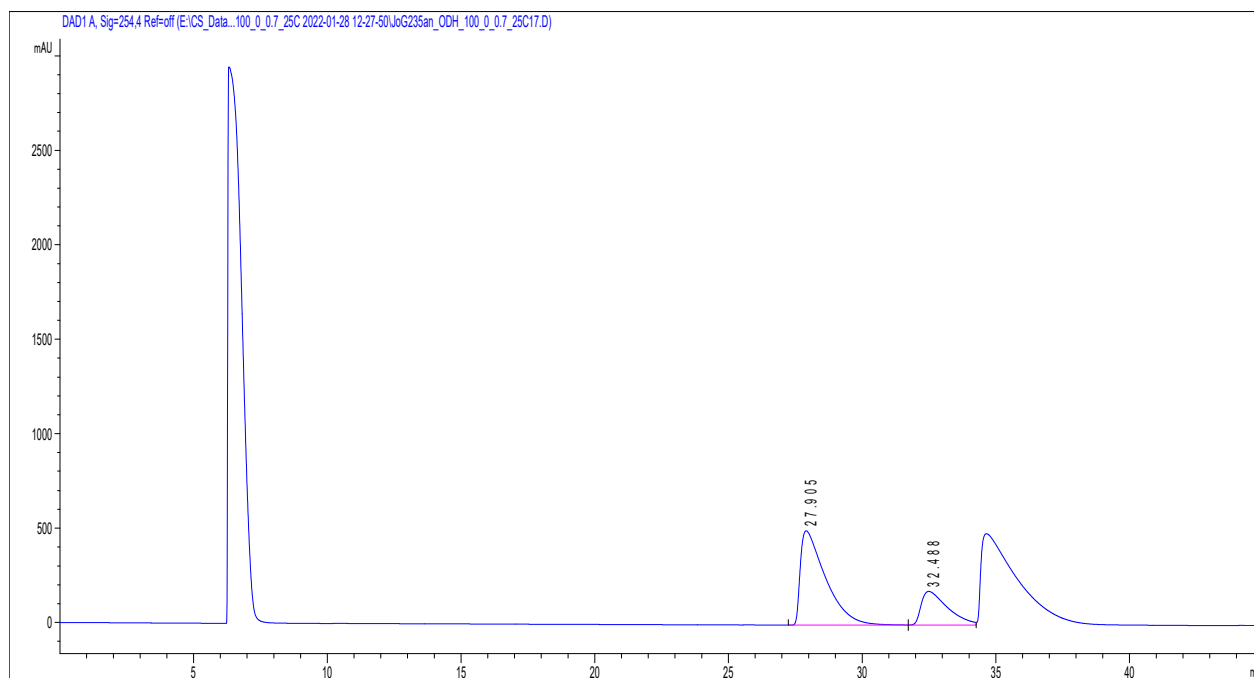
Catalyst 1-naphthyl (**1h**)



#	Time	Area	Height	Width	Area%	Symmetry
1	27.567	63500.3	855.4	1.0701	85.708	0.219
2	32.718	10588.4	151.2	1.0408	14.292	0.371

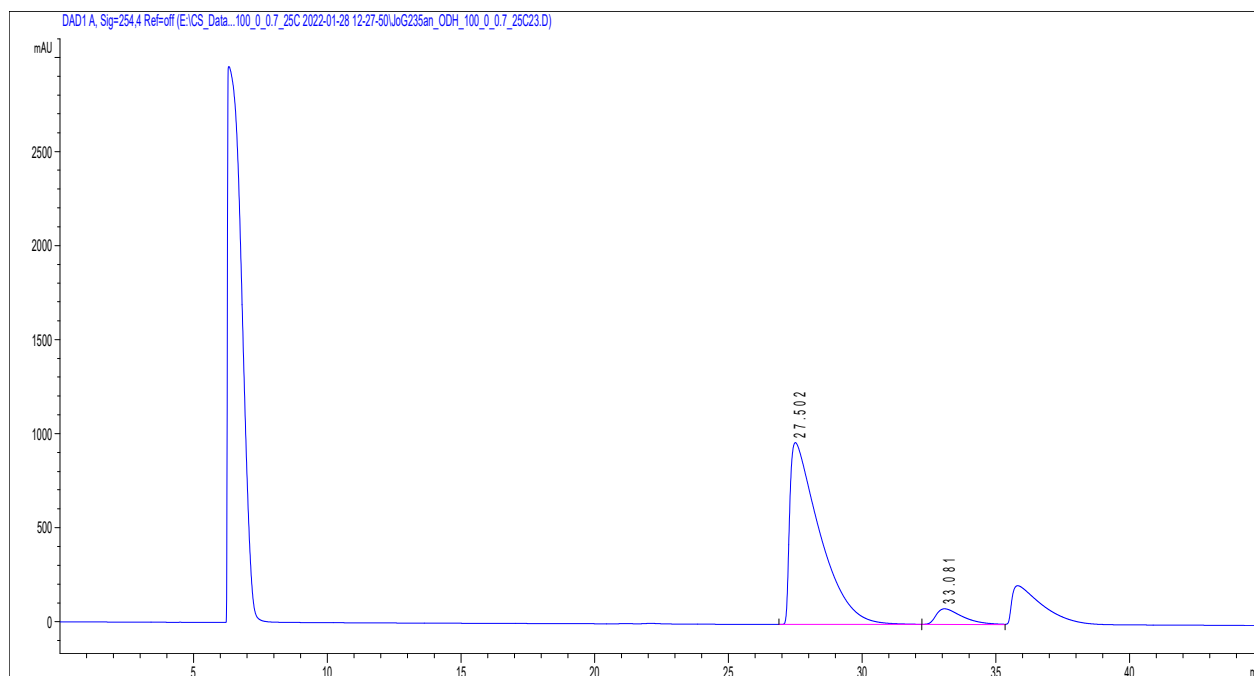
9. Tilting the Balance: London Dispersion Systematically Enhances Enantioselectivities in Brønsted Acid Catalyzed Transfer Hydrogenation of Imines

Catalyst 9-phenanthryl (**1i**)



#	Time	Area	Height	Width	Area%	Symmetry
1	27.905	32713.4	499.7	0.9518	72.922	0.275
2	32.488	12147.3	178.1	1.0197	27.078	0.371

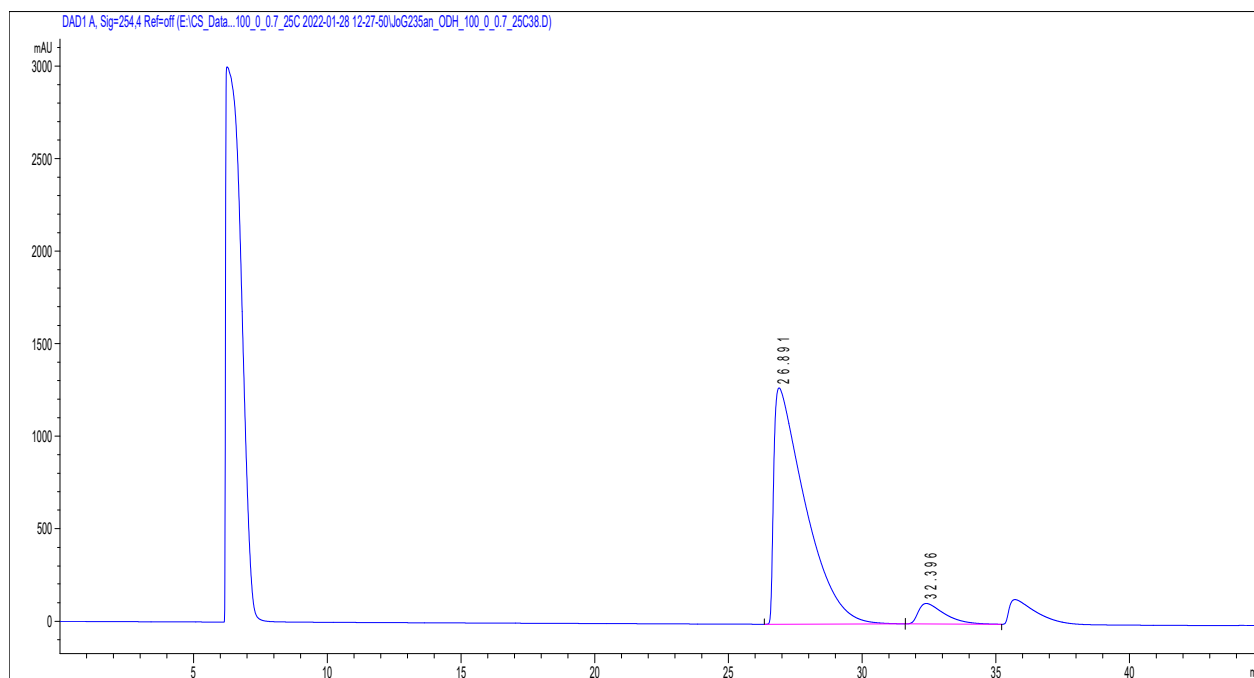
Catalyst C₆H₅ (**1j**)



#	Time	Area	Height	Width	Area%	Symmetry
1	27.502	75174.4	967	1.0949	92.974	0.207
2	33.081	5681.1	83	1.0069	7.026	0.432

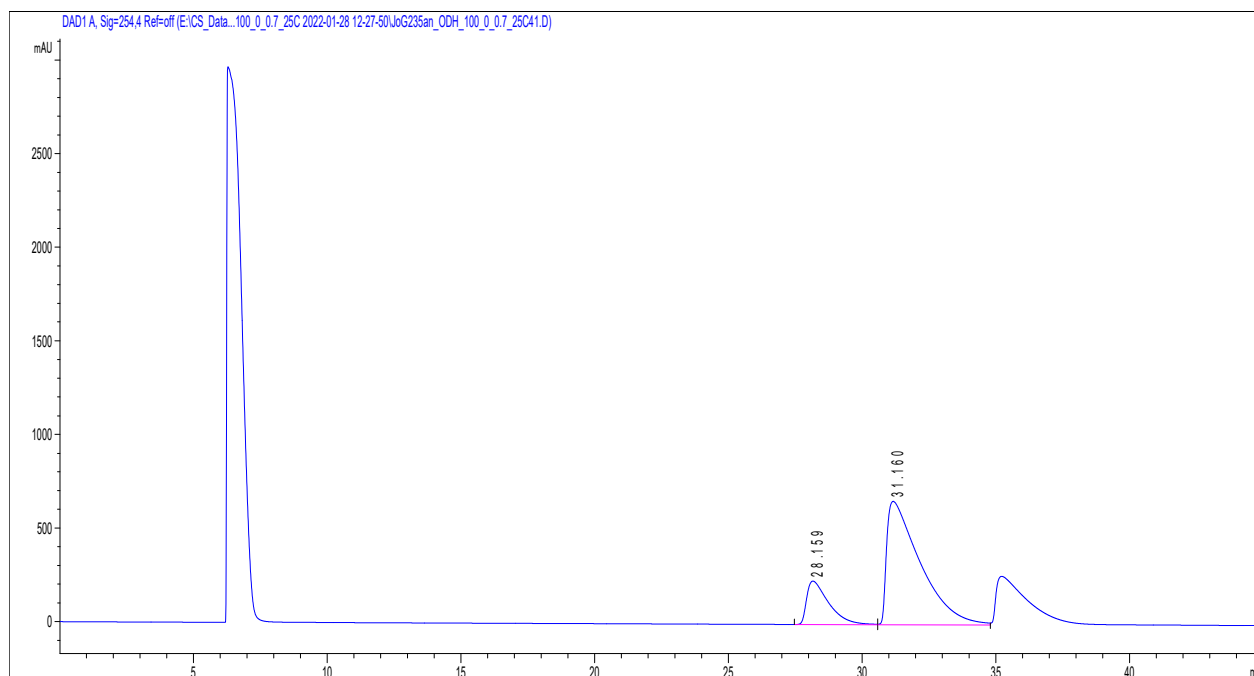
9. Tilting the Balance: London Dispersion Systematically Enhances Enantioselectivities in Brønsted Acid Catalyzed Transfer Hydrogenation of Imines

Catalyst 3,5-(CH₃)₂C₆H₂ (**1k**)



#	Time	Area	Height	Width	Area%	Symmetry
1	26.891	104233.1	1277.1	1.1202	93.199	0.182
2	32.396	7605.6	110.9	0.9978	6.801	0.398

Catalyst (R)-DSI-4-(CF₃)C₆H₄ (**1l**)

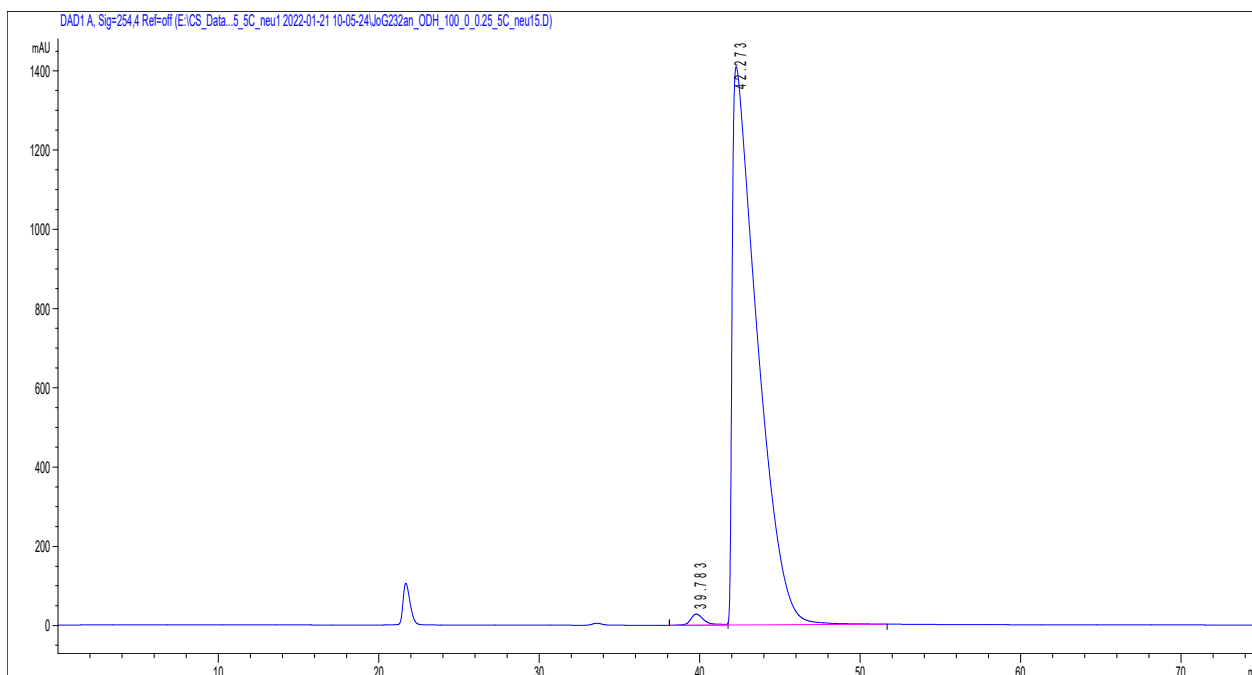


#	Time	Area	Height	Width	Area%	Symmetry
1	28.159	13285.2	232.3	0.8452	18.800	0.359
2	31.16	57379.3	659	1.2458	81.200	0.217

9. Tilting the Balance: London Dispersion Systematically Enhances Enantioselectivities in Brønsted Acid Catalyzed Transfer Hydrogenation of Imines

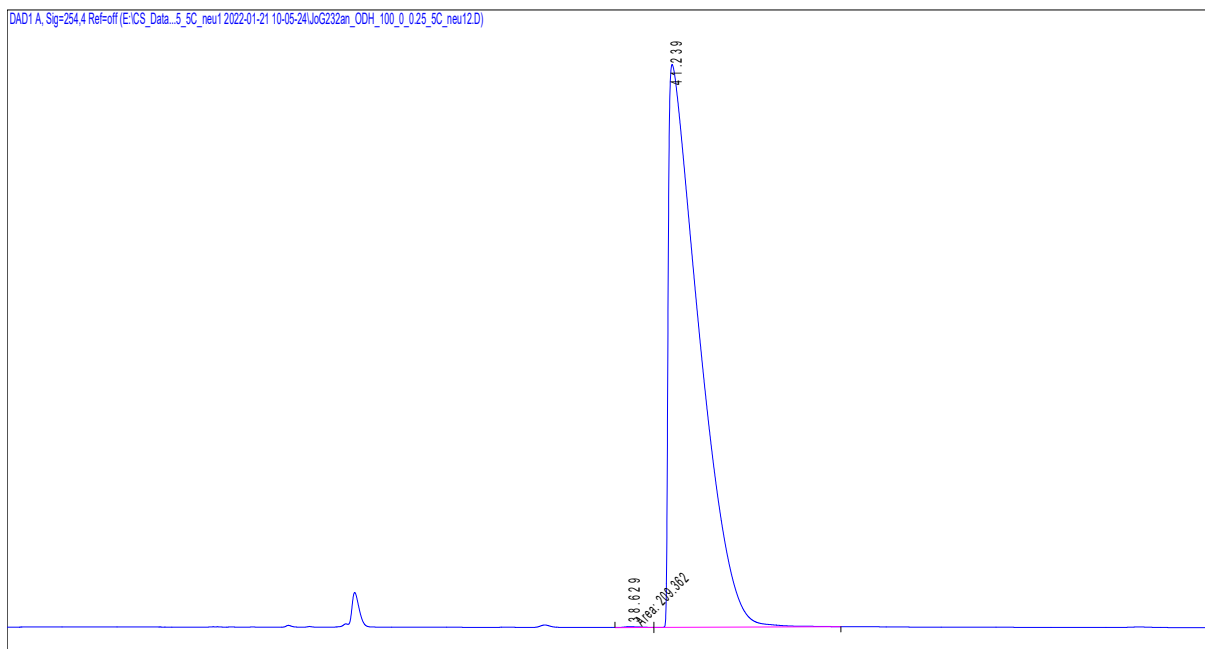
Transfer hydrogenation of imine **2c**; CSP-HPLC ODH, *n*-hexane, 0.2 mL/min, 20 °C; @254 nm

Catalyst 2,4,6-(Me)₃C₆H₂ (**1a**)



#	Time	Area	Height	Width	Area%	Symmetry
1	39.783	1657.8	28.1	0.8633	1.078	0.688
2	42.273	152127.3	1408.5	1.4461	98.922	0.187

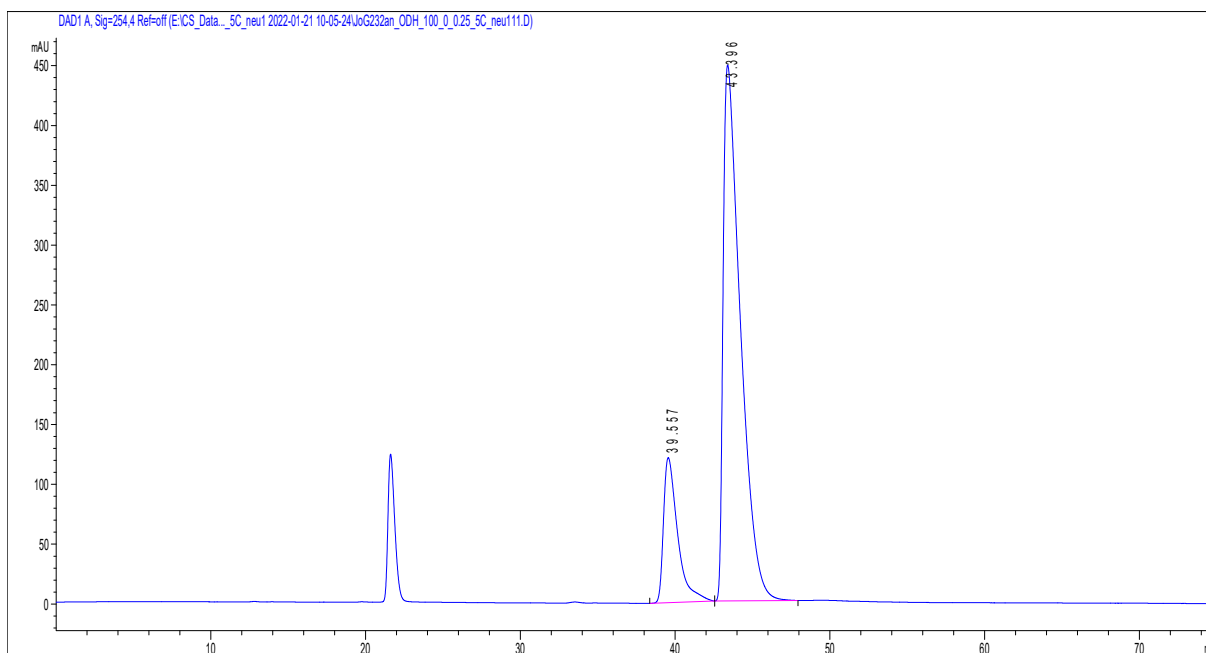
Catalyst 2,4,6-(*i*Pr)₃C₆H₂ (**1b**)



#	Time	Area	Height	Width	Area%	Symmetry
1	38.629	209.4	3.3	1.0631	0.072	0.644
2	41.239	289497.4	2193.4	1.6319	99.928	0.127

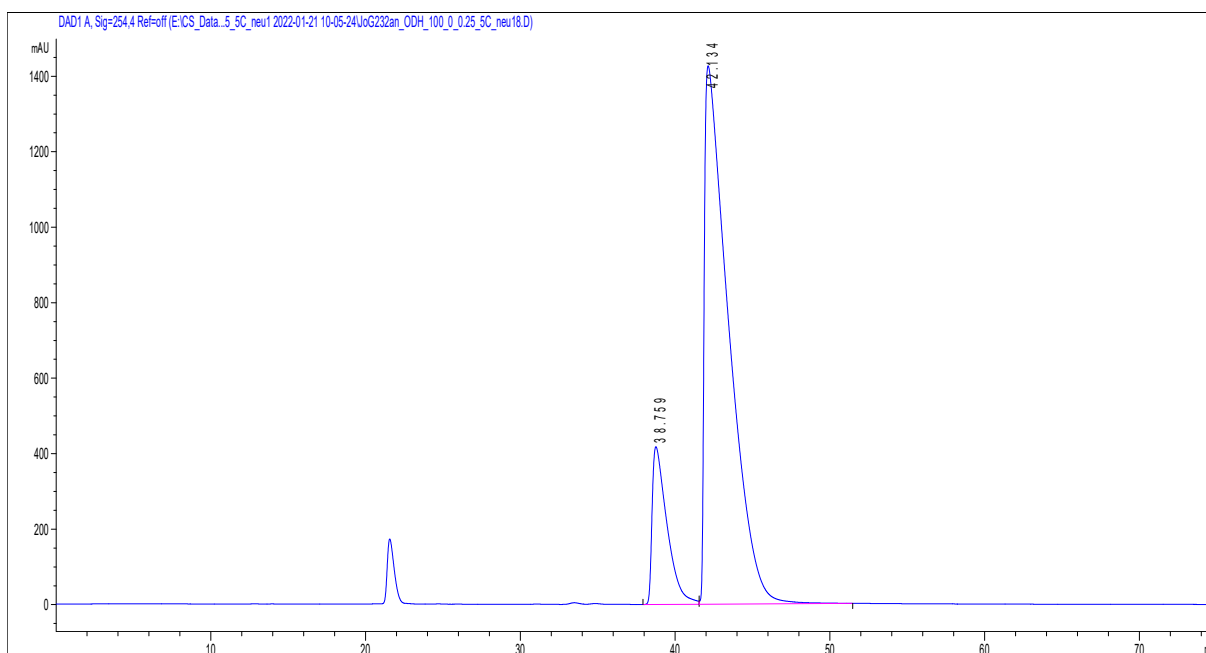
9. Tilting the Balance: London Dispersion Systematically Enhances Enantioselectivities in Brønsted Acid Catalyzed Transfer Hydrogenation of Imines

Catalyst SiPh₃ (**1c**)



#	Time	Area	Height	Width	Area%	Symmetry
1	39.557	7708.3	121.3	0.9432	18.138	0.464
2	43.396	34788.9	448.1	1.1417	81.862	0.323

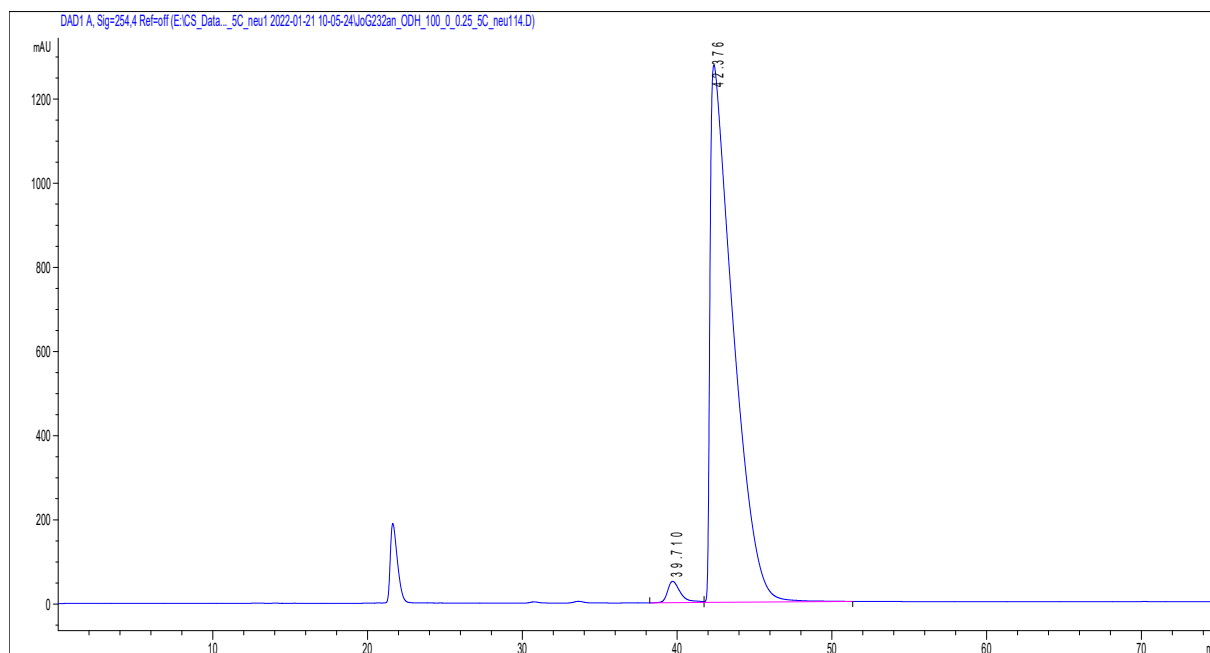
Catalyst 3,5-(CF₃)₂C₆H₄ (**1d**)



#	Time	Area	Height	Width	Area%	Symmetry
1	38.759	28102.8	418.1	0.9763	15.308	0.31
2	42.134	155478.1	1426.4	1.4377	84.692	0.169

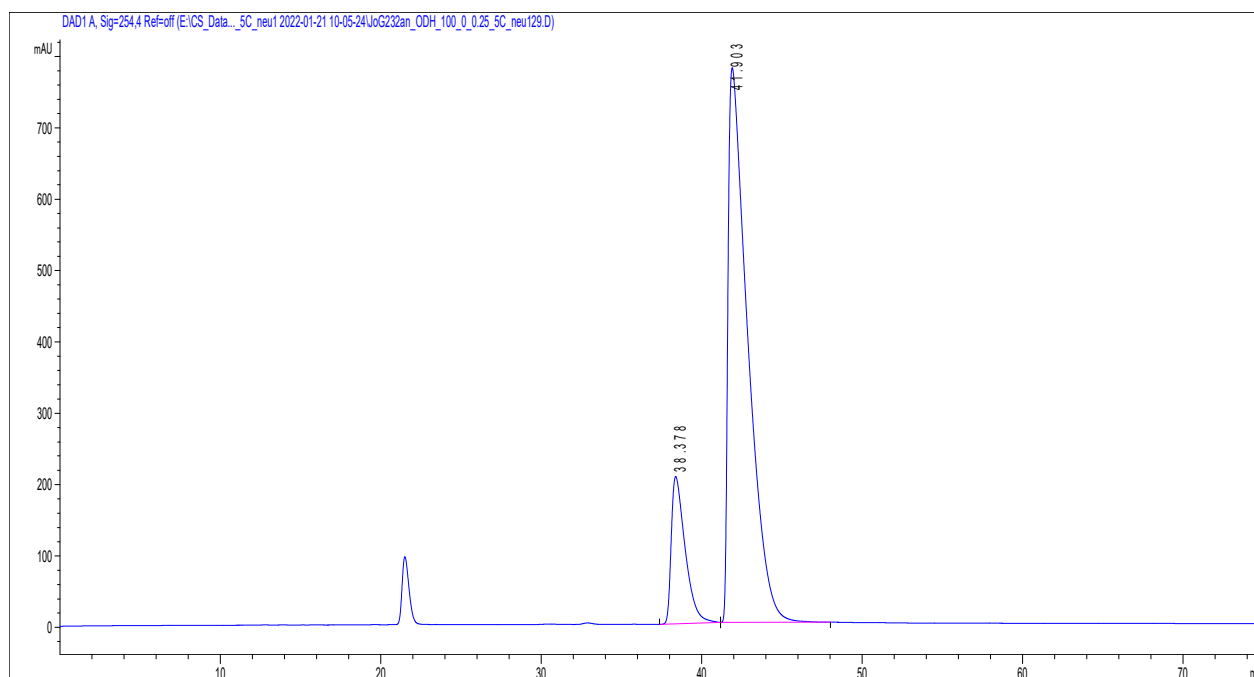
9. Tilting the Balance: London Dispersion Systematically Enhances Enantioselectivities in Brønsted Acid Catalyzed Transfer Hydrogenation of Imines

Catalyst 9-anthryl (**1e**)



#	Time	Area	Height	Width	Area%	Symmetry
1	39.71	3005.5	51.1	0.8716	2.234	0.605
2	42.376	131507.9	1277.1	1.3854	97.766	0.181

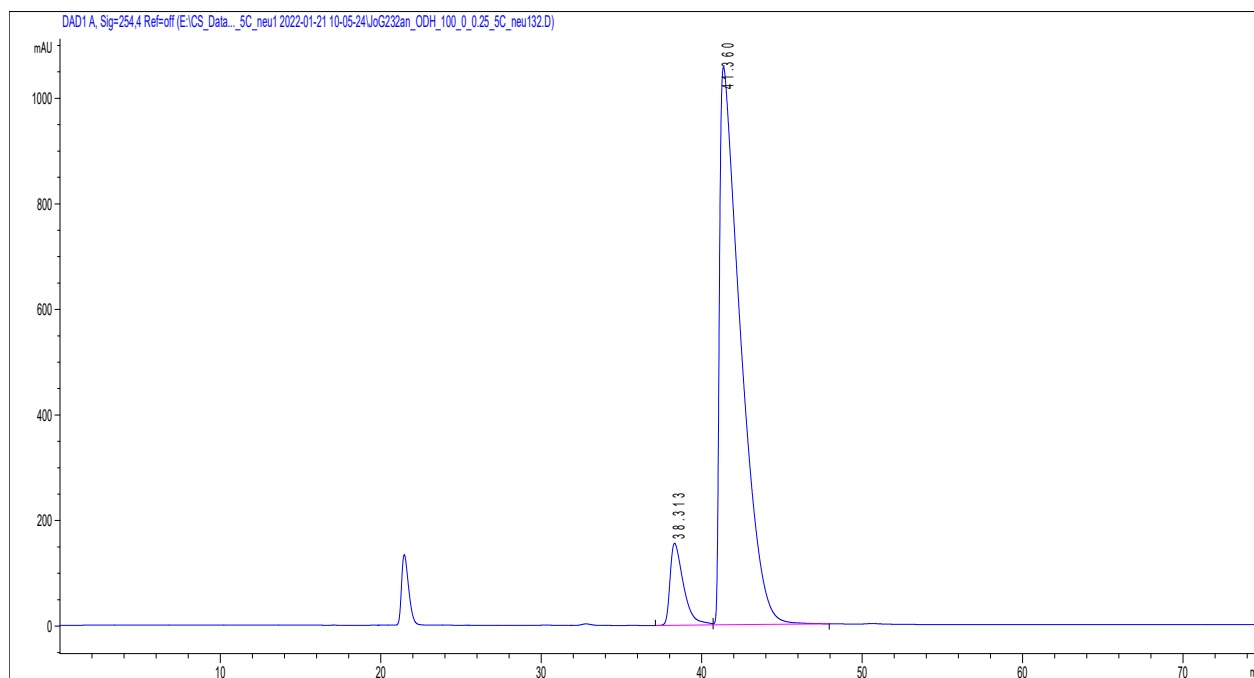
Catalyst 4-(^tBu)₄C₆H₄ (**1f**)



#	Time	Area	Height	Width	Area%	Symmetry
1	38.378	12452.6	206.7	0.8908	15.861	0.429
2	41.903	66058	777.6	1.2131	84.139	0.248

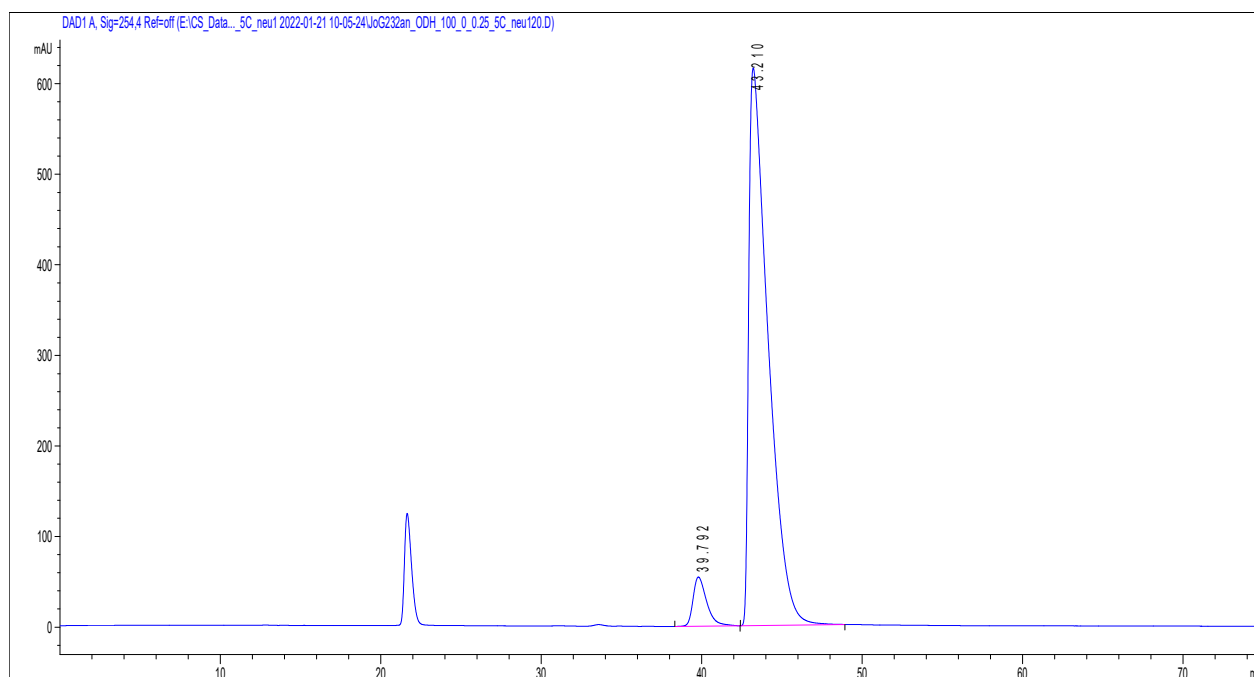
9. Tilting the Balance: London Dispersion Systematically Enhances Enantioselectivities in Brønsted Acid Catalyzed Transfer Hydrogenation of Imines

Catalyst 4-(CF₃)C₆H₃ (**1g**)



#	Time	Area	Height	Width	Area%	Symmetry
1	38.313	9056.6	155.6	0.8692	8.601	0.467
2	41.36	96246.6	1057.2	1.2642	91.399	0.212

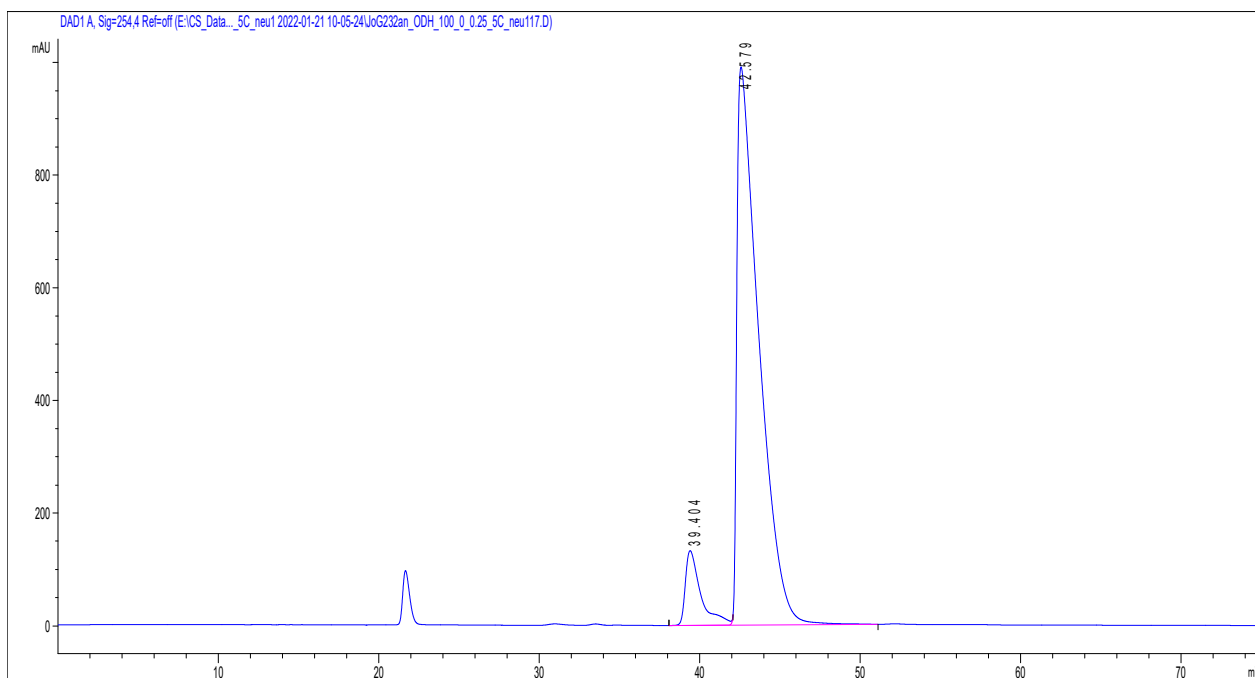
Catalyst 1-naphthyl (**1h**)



#	Time	Area	Height	Width	Area%	Symmetry
1	39.792	3204.2	54.3	0.8682	5.867	0.609
2	43.21	51414.1	615.8	1.1961	94.133	0.275

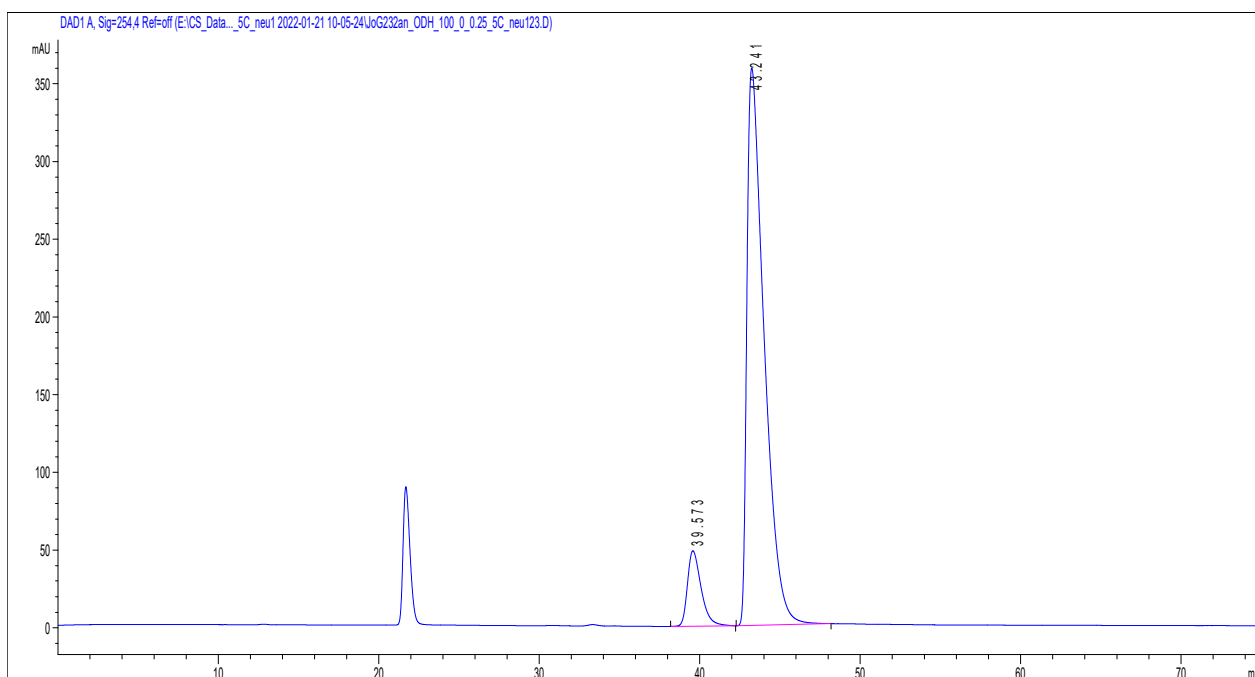
9. Tilting the Balance: London Dispersion Systematically Enhances Enantioselectivities in Brønsted Acid Catalyzed Transfer Hydrogenation of Imines

Catalyst 9-phenanthryl (**1i**)



#	Time	Area	Height	Width	Area%	Symmetry
1	39.404	8905	132.7	0.9748	8.651	0.403
2	42.579	94036.1	990.9	1.3131	91.349	0.405

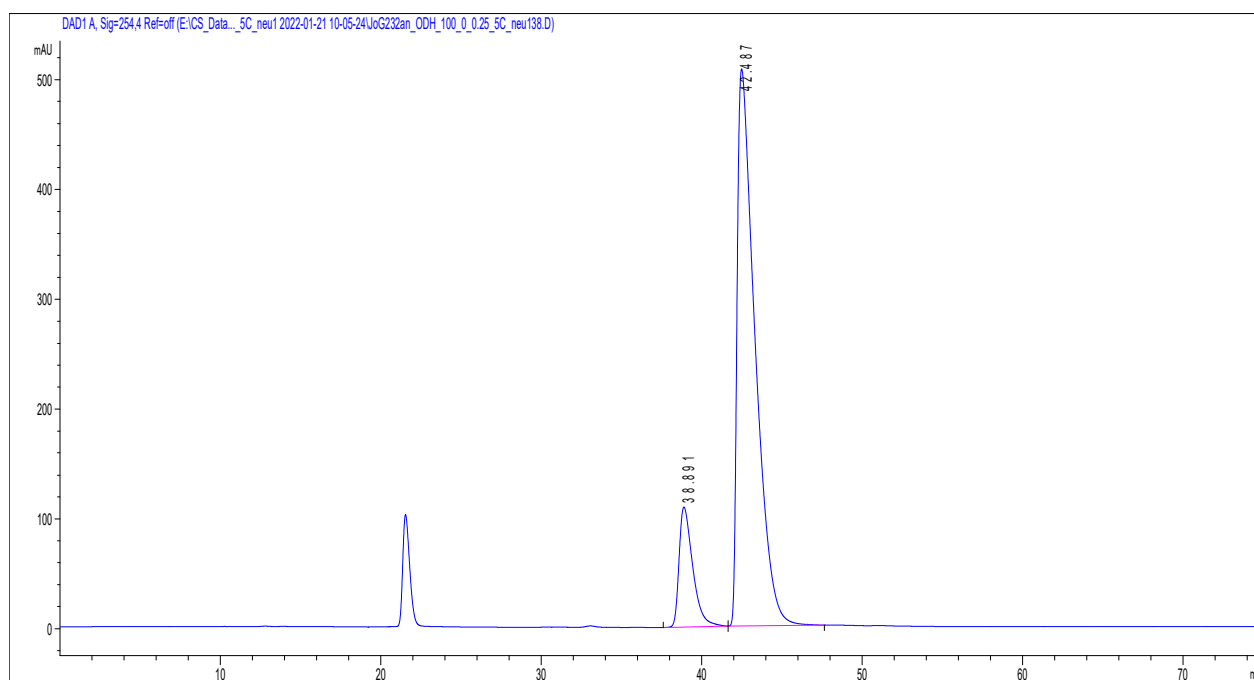
Catalyst C₆H₅ (**1j**)



#	Time	Area	Height	Width	Area%	Symmetry
1	39.573	2871.7	48.6	0.8839	9.685	0.624
2	43.241	26779.9	358.8	1.0948	90.315	0.358

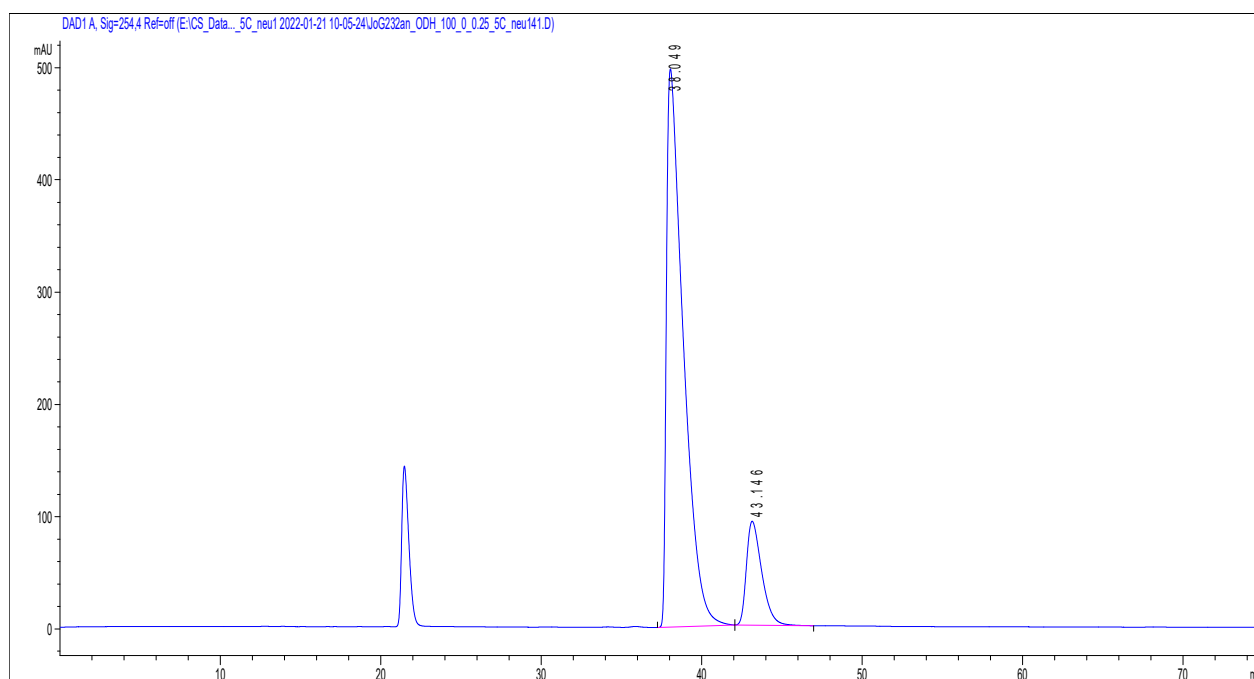
9. Tilting the Balance: London Dispersion Systematically Enhances Enantioselectivities in Brønsted Acid Catalyzed Transfer Hydrogenation of Imines

Catalyst 3,5-(CH₃)₂C₆H₂ (**1k**)



#	Time	Area	Height	Width	Area%	Symmetry
1	38.891	6458.5	109.4	0.883	14.146	0.517
2	42.487	39197.7	507.4	1.1253	85.854	0.31

Catalyst (R)-DSI-4-(CF₃)C₆H₄ (**1l**)

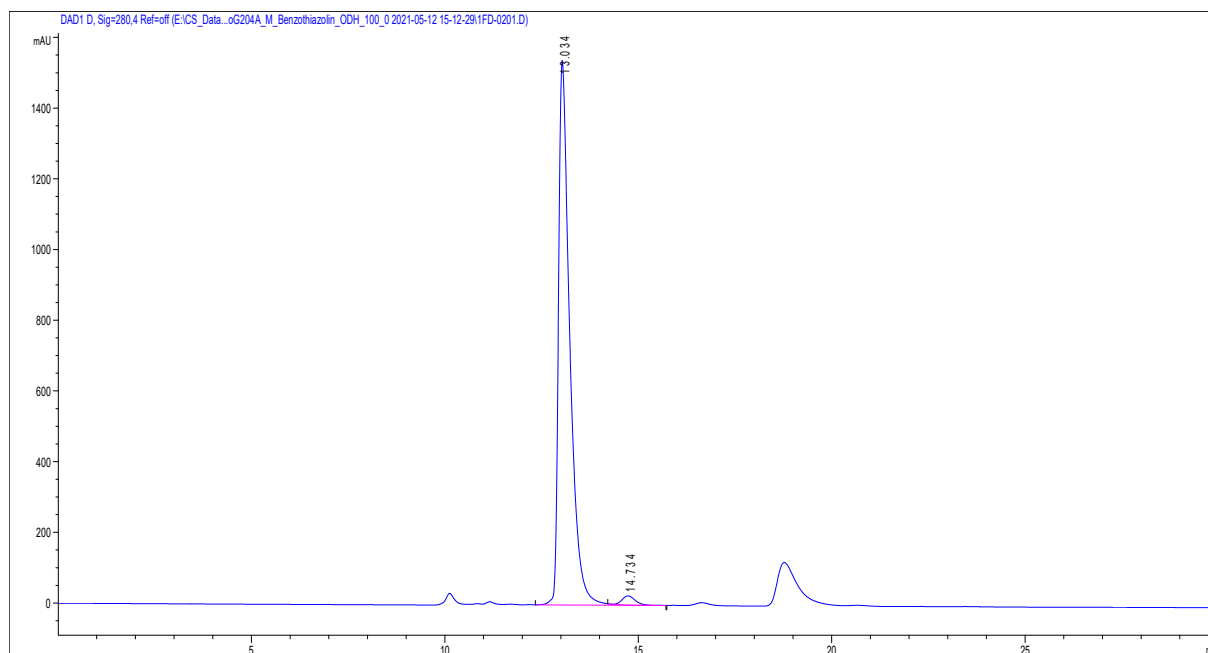


#	Time	Area	Height	Width	Area%	Symmetry
1	38.049	36269.9	497.3	1.0509	85.543	0.279
2	43.146	6129.7	92.6	0.9964	14.457	0.563

9. Tilting the Balance: London Dispersion Systematically Enhances Enantioselectivities in Brønsted Acid Catalyzed Transfer Hydrogenation of Imines

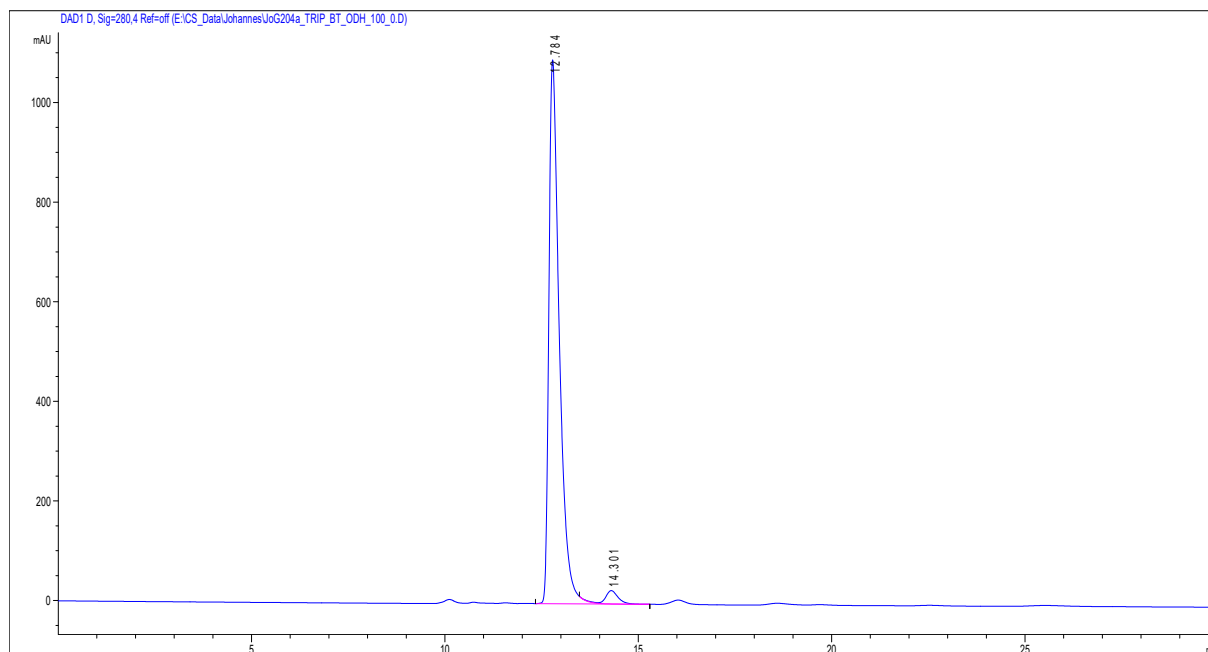
Transfer hydrogenation of imine **2d**; CSP-HPLC ODH, *n*-hexane, 0.2 mL/min, 20 °C; @280 nm

Catalyst 2,4,6-(Me)₃C₆H₂ (**1a**)



#	Time	Area	Height	Width	Area%	Symmetry
1	13.034	31211.3	1540	0.2984	98.037	0.457
2	14.734	625.1	26.1	0.3674	1.963	0.756

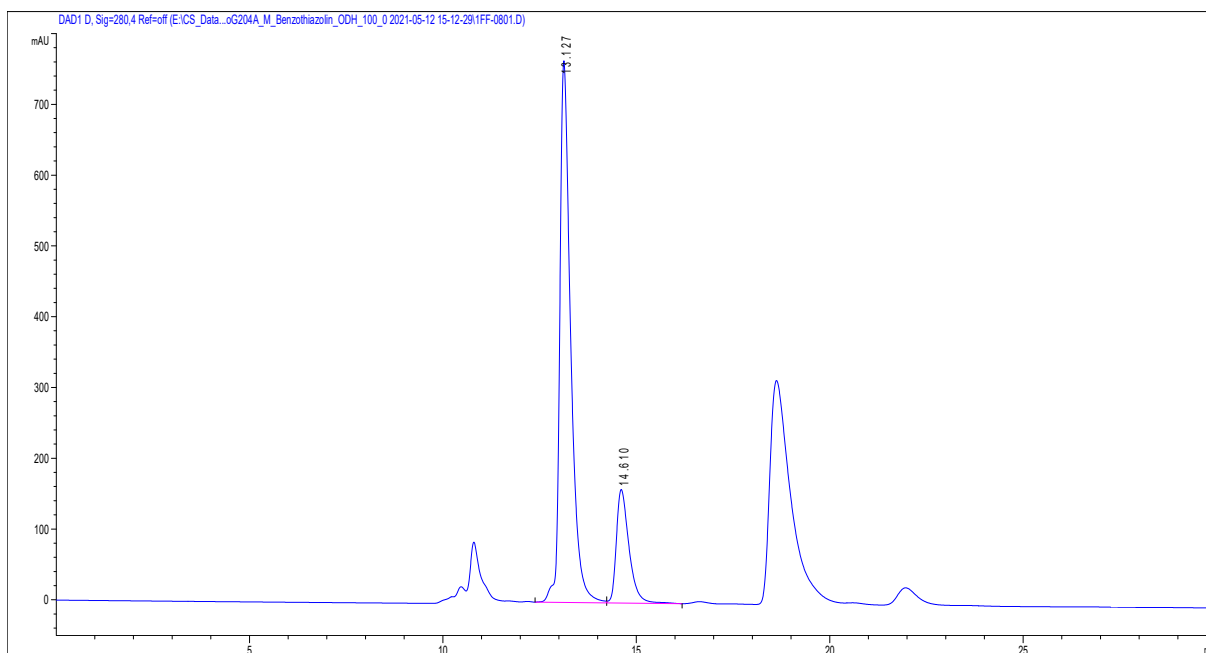
Catalyst 2,4,6-(^tPr)₃C₆H₂ (**1b**)



#	Time	Area	Height	Width	Area%	Symmetry
1	12.784	20508.9	1092.1	0.2811	97.106	0.5
2	14.301	611.3	26.8	0.3396	2.894	0.812

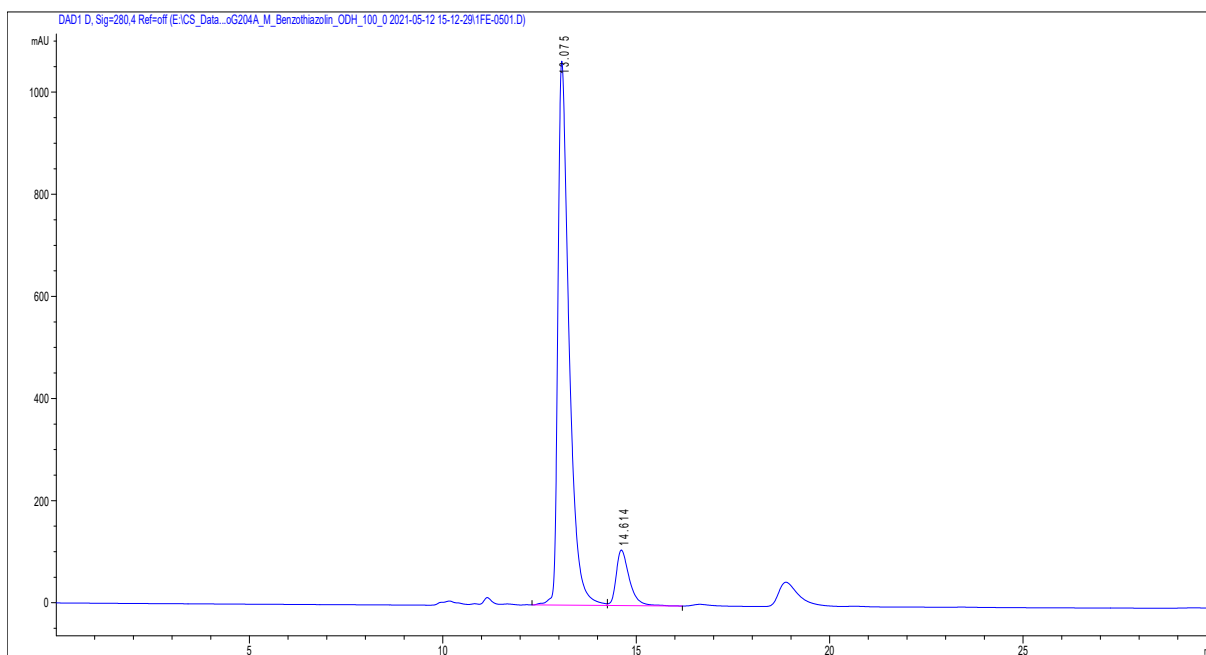
9. Tilting the Balance: London Dispersion Systematically Enhances Enantioselectivities in Brønsted Acid Catalyzed Transfer Hydrogenation of Imines

Catalyst SiPh₃ (**1c**)



#	Time	Area	Height	Width	Area%	Symmetry
1	13.127	14960.3	765.3	0.2901	80.408	0.567
2	14.61	3645.2	160.5	0.343	19.592	0.582

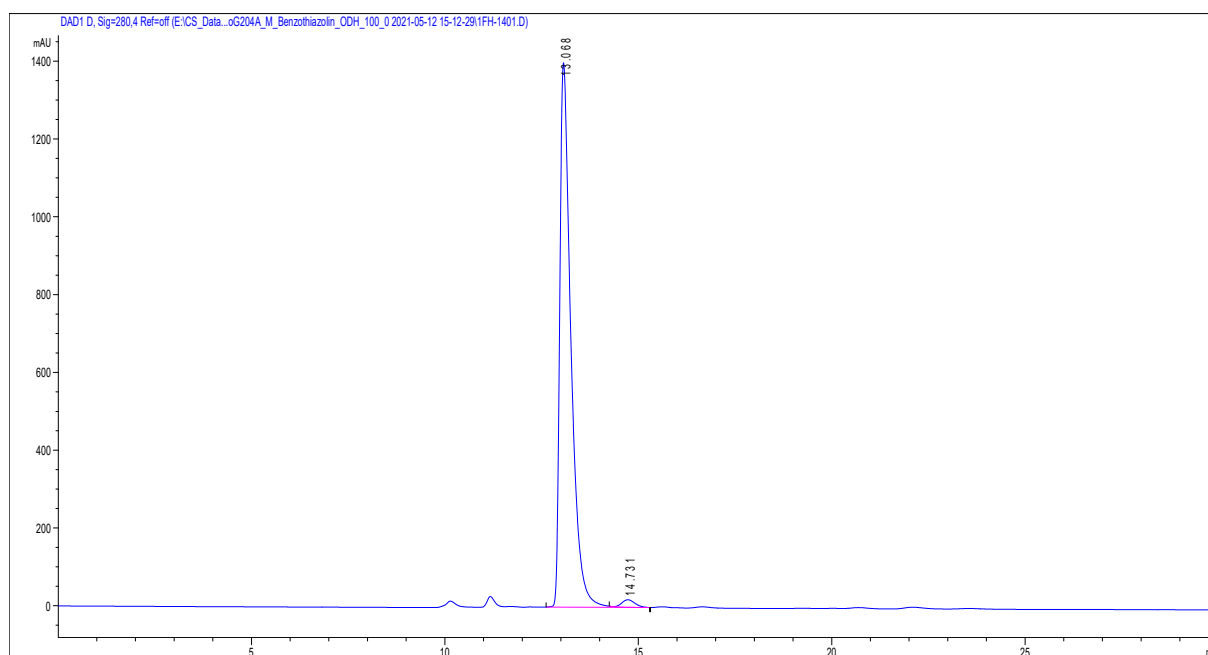
Catalyst 3,5-(CF₃)₂C₆H₄ (**1d**)



#	Time	Area	Height	Width	Area%	Symmetry
1	13.075	21417.1	1065.5	0.2985	89.295	0.499
2	14.614	2567.4	108.9	0.3551	10.705	0.599

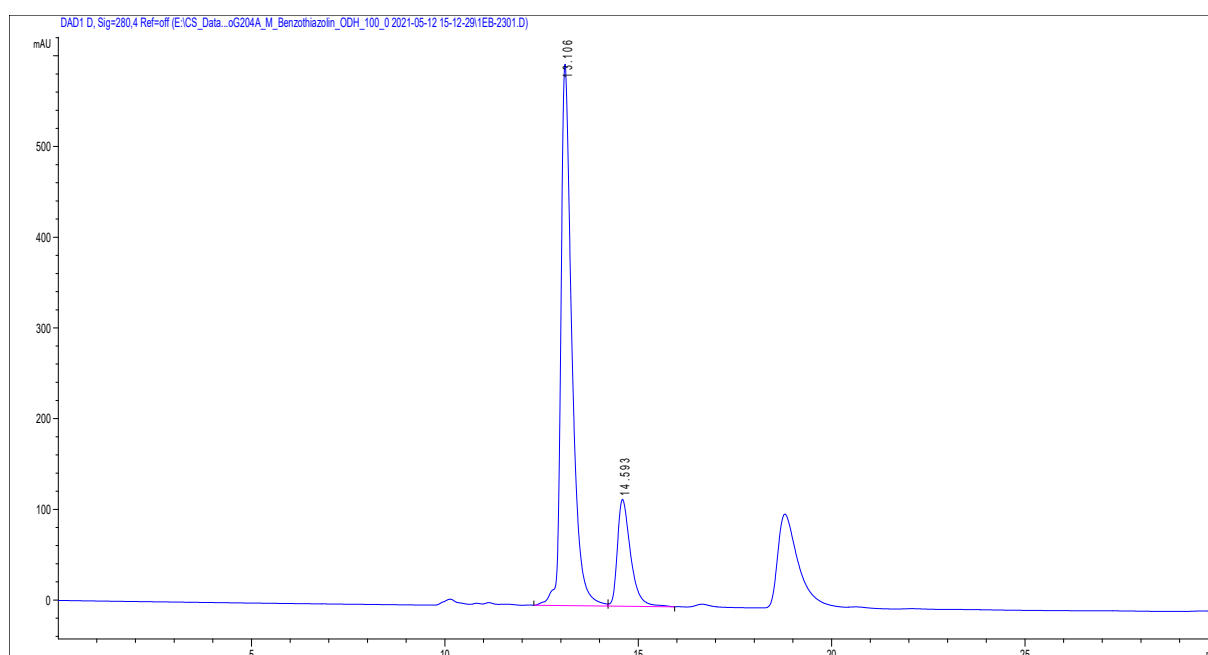
9. Tilting the Balance: London Dispersion Systematically Enhances Enantioselectivities in Brønsted Acid Catalyzed Transfer Hydrogenation of Imines

Catalyst 9-anthryl (**1e**)



#	Time	Area	Height	Width	Area%	Symmetry
1	13.068	27935.3	1399.6	0.2949	98.402	0.46
2	14.731	453.7	19.4	0.3652	1.598	0.794

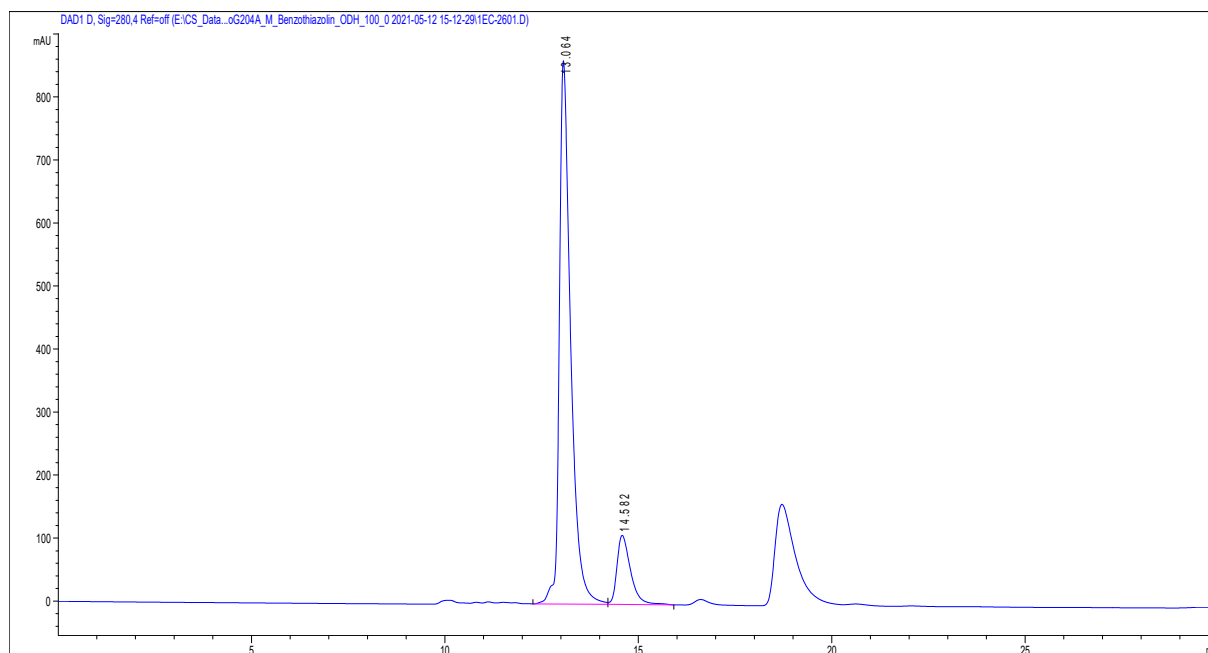
Catalyst 4-(^tBu)₂C₆H₄ (**1f**)



#	Time	Area	Height	Width	Area%	Symmetry
1	13.106	11838.5	596.8	0.2934	80.953	0.568
2	14.593	2785.4	117.8	0.3578	19.047	0.58

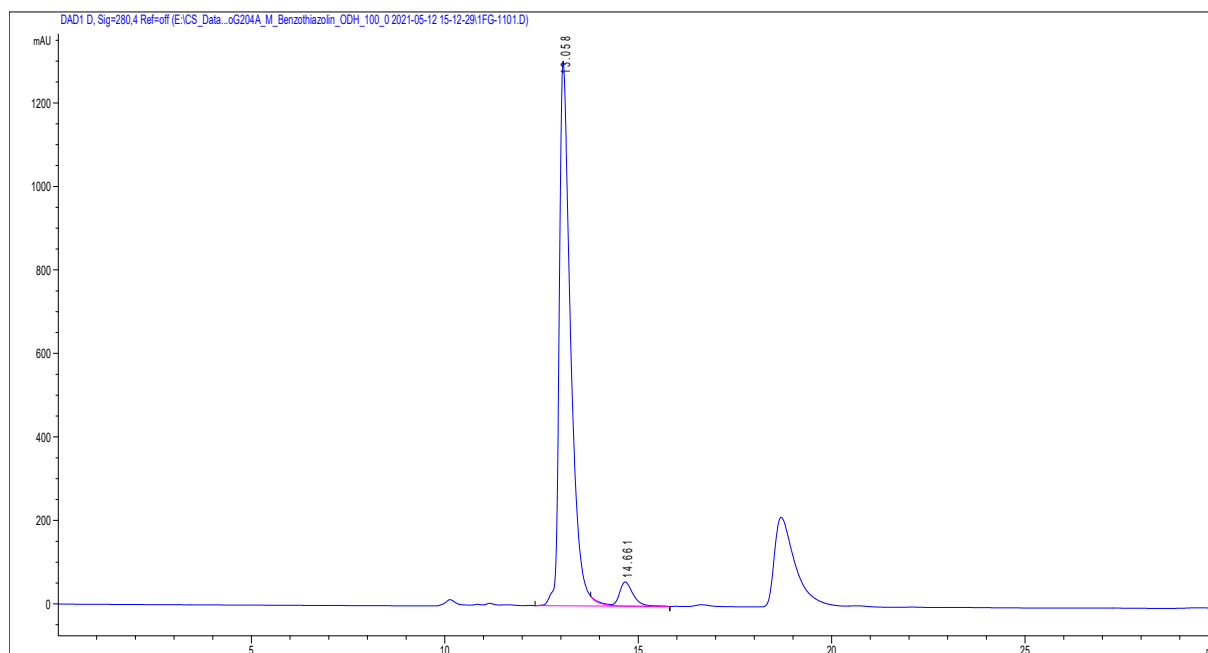
9. Tilting the Balance: London Dispersion Systematically Enhances Enantioselectivities in Brønsted Acid Catalyzed Transfer Hydrogenation of Imines

Catalyst 4-(CF₃)C₆H₃ (**1g**)



#	Time	Area	Height	Width	Area%	Symmetry
1	13.064	17569	862	0.3018	86.745	0.539
2	14.582	2684.6	109.7	0.3695	13.255	0.58

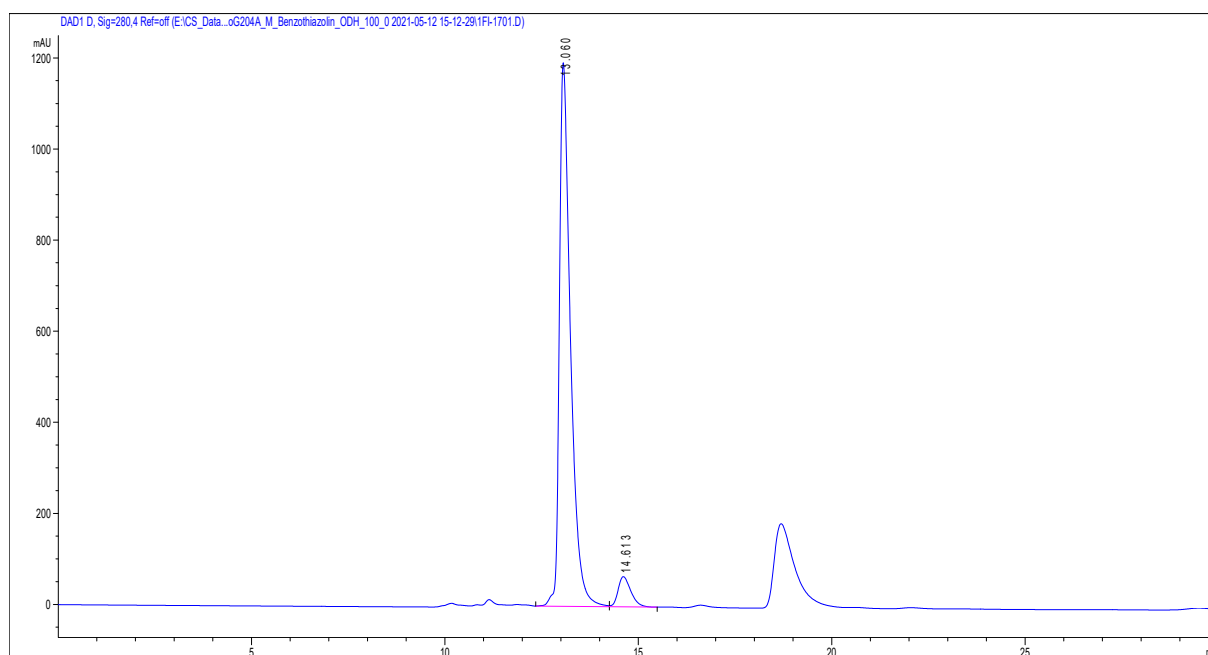
Catalyst 1-naphthyl (**1h**)



#	Time	Area	Height	Width	Area%	Symmetry
1	13.058	26791.5	1304.4	0.3036	94.880	0.488
2	14.661	1445.8	57.7	0.3782	5.120	0.705

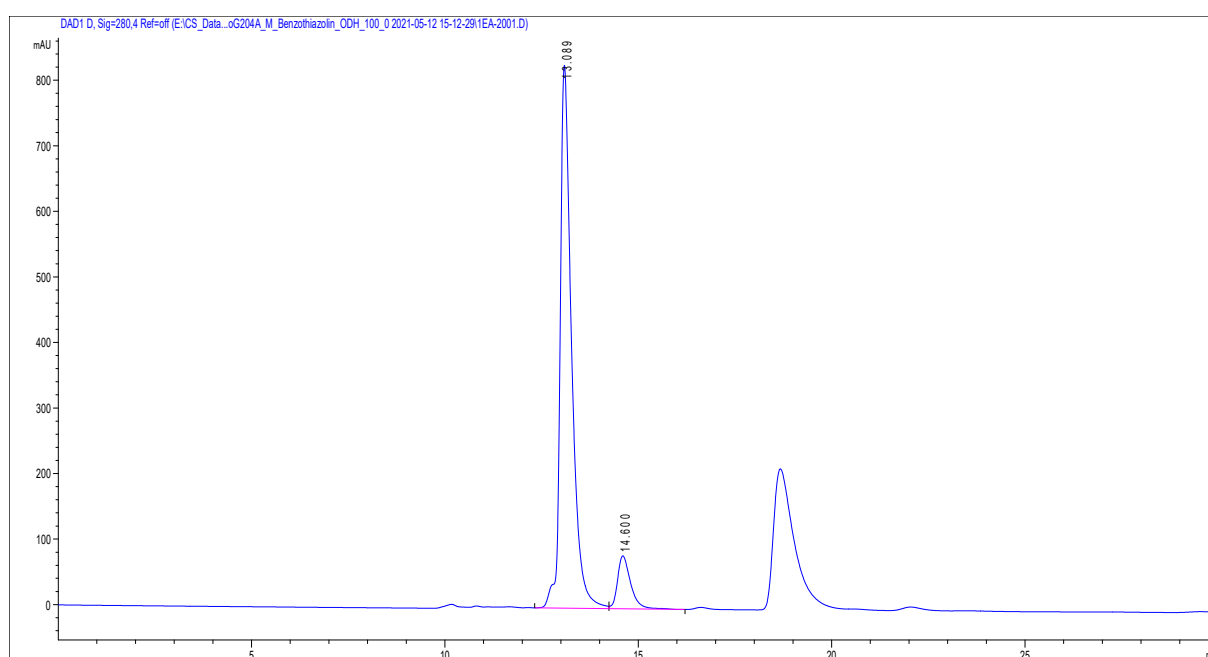
9. Tilting the Balance: London Dispersion Systematically Enhances Enantioselectivities in Brønsted Acid Catalyzed Transfer Hydrogenation of Imines

Catalyst 9-phenanthryl (**1i**)



#	Time	Area	Height	Width	Area%	Symmetry
1	13.06	23853.7	1193.5	0.2972	93.994	0.508
2	14.613	1524.2	66.4	0.3539	6.006	0.662

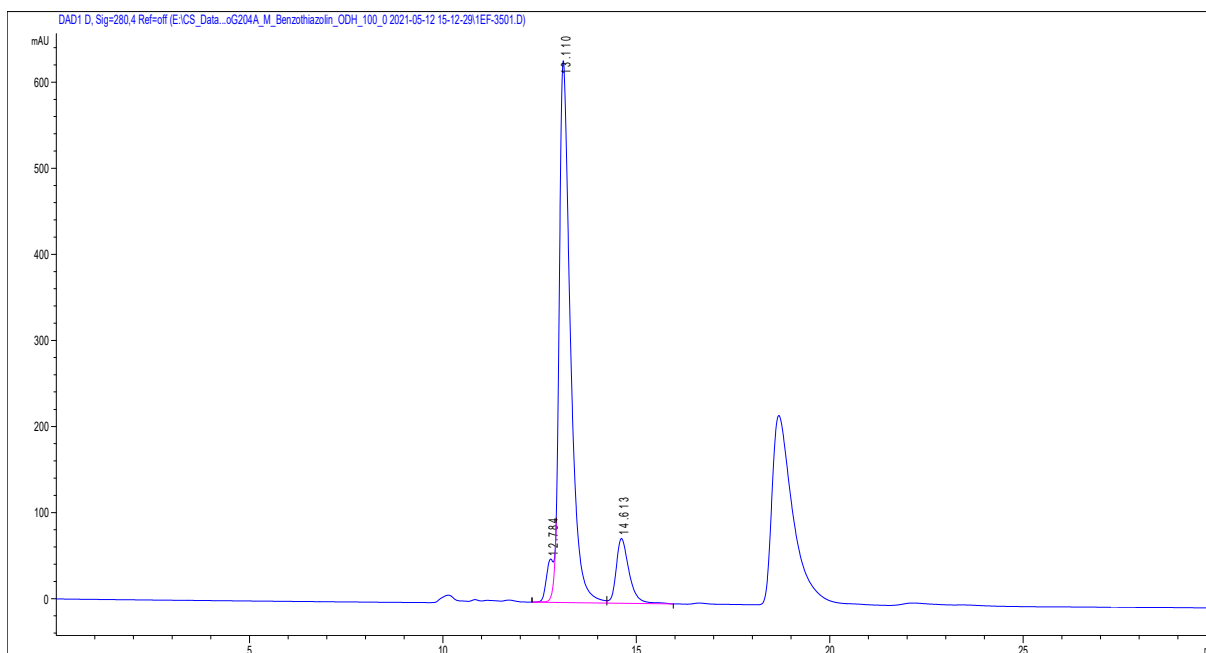
Catalyst C₆H₅ (**1j**)



#	Time	Area	Height	Width	Area%	Symmetry
1	13.089	16951.6	828	0.3028	89.883	0.554
2	14.6	1908.1	80.9	0.3553	10.117	0.616

9. Tilting the Balance: London Dispersion Systematically Enhances Enantioselectivities in Brønsted Acid Catalyzed Transfer Hydrogenation of Imines

Catalyst (S)-DSI-4-(CF₃)C₆H₄ (**11**)



#	Time	Area	Height	Width	Area%	Symmetry
1	12.784	559.3	44.2	0.1915	3.694	1.866
2	13.11	12832.1	629.3	0.3039	84.759	0.674
3	14.613	1748	75.3	0.3509	11.546	0.631

10. Conclusion

Catalysis with Brønsted acids is a long-lasting success story and was realized in the field of (asymmetric) organocatalysis by combining an acidic motif with a chiral organic framework consisting of a backbone as source of chirality and substituents to shape a stereoinductive environment. Modulation of the acidic motif, backbone and substituents allowed to adapt these chiral Brønsted acids to a myriad of different transformations and challenges. However, this adaptability also makes a sophisticated and rational catalyst design crucial. General design principles rely on detailed insights into the reaction mechanism and a good understanding of possible reaction pathways and parameters. Therefore, in this thesis chiral phosphoric acids (CPA) were exemplarily selected as catalyst class and studied regarding their mode and degree of activation, structural space and confinement, secondary non-covalent interactions decisive for stereoselectivity, association and aggregation of catalyst and reactants and different general reaction pathways.

The structural space of CPA/substrate intermediates was elucidated in the third chapter of this thesis on the example of the transfer hydrogenation of imines with Hantzsch ester as hydride source. For the binary CPA/imine complexes, four general core structures (Type I *E*, Type II *E*, Type I *Z* and Type II *Z*) were found which are anchored by a strong hydrogen bond. These complexes feature either the *E*- or *Z*-imine in each two conformations (rotation of the imine by $\sim 180^\circ$). The structures of the complexes are highly conserved over a range of different 3,3'-substituents of the CPA and different substituents of the imine. Additionally, for the first time [CPA/imine]₂ dimers of the binary CPA/imine complexes were observed in solution and identified via characteristic highfield shifts and Diffusion Ordered Spectroscopy (DOSY) NMR measurements. These [CPA/imine]₂ dimers are expected not to affect the reaction as they resemble an off-cycle equilibrium with the monomeric CPA/imine complexes.

The equilibrium between the different imine conformations (Type I and Type II) for the CPA/*E*-imine intermediates was studied in the fourth chapter of this thesis. The exchange between Type I *E* and Type II *E* is fast on the NMR time scale but could be accessed by adapting the Relaxation Dispersion R_{1ρ} NMR method for the first time to an organocatalytic system. This method allowed to extend the time-frame of observable dynamic processes from the millisecond to the microsecond (nanosecond with additional low temperature) time scale. Different exchange pathways were found featuring either switching of the PO⁻---H-N⁺ hydrogen bond from one oxygen atom of the phosphoric acid to the other one or switching and rotation of the imine inside the binding pocket of the CPA. The exchange rate of the switching process was found to depend on the hydrogen bond strength of the CPA/imine intermediate, allowing a faster switching process for weaker hydrogen bonds. Moreover, the rotation of the imine inside the binding pocket was found to be only possible for smaller CPA or imine substituents.

10. Conclusion

Additionally, measurements at different temperatures allowed to not only access the exchange rates but even the populations of the Type I *E* and Type II *E* conformations. Based on this, the equilibrium between these two conformations was investigated as a molecular balance system for quantification of weak London dispersion interactions between CPA and imine. The CPA/imine complex structures were shown to be conserved for imines with bulky dispersion energy donor (DED) substituents such as *iso*-propyl and *tert*-butyl groups and the exchange process between the Type I *E* and Type II *E* conformations could in principle be accessed by the $R_{1\rho}$ NMR method. However, the interaction energy between DED substituent and CPA could not be clearly dissected, as the DED substituent was shown to affect both the Type I *E* and Type II *E* structure either through a direct interaction or its substituent effect even for CPAs with 3,3'-substituents as small as a phenyl group.

An alternative reaction pathway featuring hydrogen bond bridged CPA dimers was studied in the fifth chapter of this thesis on the example of the two-fold transfer hydrogenation of quinolines. A strong dependence of the enantioselectivity on the catalyst loading was observed and kinetic measurements revealed a catalyst order of 1.25 to 1.75 depending on the catalyst concentration. Low temperature NMR measurements at a 2:1 ratio of catalyst and quinoline substrate confirmed the presence of dimeric CPA/CPA/quinoline intermediates and were confirmed by DOSY NMR measurements. Additionally, CPA/CPA/imine complexes were also found, indicating the potential impact of the dimeric reaction channel for this substrate class. Compared to the monomeric CPA/imine complexes, the CPA/CPA/imine dimers feature a stronger proton transfer onto the substrate (weaker $\text{PO}^- \cdots \text{H-N}^+$ hydrogen bond) and their formation was found to be strongly dependent on the 3,3'-substituent of the catalyst and less on the imine substituents. Applying the Relaxation Dispersion $R_{1\rho}$ NMR method, the presence of a fast exchange process was revealed which indicates the presence of at least two fast exchanging CPA/CPA/*E*-imine conformers.

CPA/imine intermediates with imines featuring an additional hydroxy group as hydrogen bond donor were studied in the sixth chapter of this thesis. In contrast to the previous assumption that a bidentate binding of catalyst and imine by two hydrogen bonds results in a well-defined reaction intermediate, a broad structural space was found for these CPA/imine systems. Different dimer species were found as dominant species for most systems and characterized via DOSY NMR. In these dimers, two imine molecules form each one hydrogen bond to two different CPA molecules, effectively bridging them. Molecular dynamic simulations revealed different bridging motifs and it is suggested that these bridged dimers can act as an alternative reaction pathway. Fine-tuning of steric and electrostatic properties of CPA and imine allowed to access monomeric CPA/imine dimers and the bidentate binding motif was clearly validated. NOESY NMR revealed the structure of these intermediates, in which the imine is placed in between the two 3,3'-substituents of the CPA. One 3,3'-substituent is shielding one

10. Conclusion

site of the imine which confirms the postulated origin of stereoselectivity for the following transformations.

The seventh and eighth chapter of this thesis were done in collaboration with Franziska Pecho from the group of Prof. Dr. Thorsten Bach and focused on merging Brønsted acid catalysis with photocatalysis. A chiral phosphoric acid was used as organocatalysts and thioxanthone unites were implemented as 3,3'-substituents which served as light-harvesting photosensitizer. In the asymmetric [2+2] photocycloaddition of β -carboxyl-substituted cyclic enones, binding of the carboxylic acid substrate to the CPA catalyst was proven by low temperature NMR studies via NOESY and DOSY NMR experiments. Temperature coefficients for the chemical shift of the hydrogen bonded proton signals were derived by variable temperature NMR experiments and revealed the presence of monomeric and dimeric/oligomeric CPA/substrate species. In the asymmetric [2+2] photocycloaddition of cyclic N,O-acetals, the generation of an open iminium ion form was validated upon protonation of the cyclic N,O-acetal and bidentate binding by two hydrogen bonds of the resulting imine substrate to the CPA was proven. The CPA/imine intermediate was characterized as hydrogen bond assisted ion pair and two different substrate conformations were identified, differing in the arrangement of the substrate backbone. Additionally, NMR kinetic measurements during illumination with visible light showed that during the reaction isomerization of the C=C or C=N double bond of the substrate is possible. These isomerization processes can in principle affect the reaction, changing the environment for the addition step (if the C=N double bond is isomerized) or lead to a different diastereomer of the product (if the C=C double bond is isomerized).

The secondary non-covalent interactions decisive for the enantioselectivities in CPA catalyzed transformations were studied in the ninth chapter of this thesis, resulting in a conceptual approach on exploiting London dispersion interactions to systematically enhance stereoselectivities. For the CPA catalyzed transfer hydrogenation of (*E*)- or (*Z*)-*N*-phenyl ketimines, *tert*-butyl groups as dispersion energy donors (DED) were placed in all meta-positions of the substrate, which lead to a stabilization of the *Z*-imine by up to 4.5 kJ/mol. For the free imines, the equilibrium between low populated *Z*-imine (~1%) and major populated *E*-imine (~99%) was accessed by Chemical Exchange Saturation Transfer (CEST) NMR. The effect of stabilizing the *Z*-imine by DED residues was proven to be transferred onto the binary CPA/imine and ternary CPA/imine/Hantzsch ester intermediates, leading to a thermodynamic preference of the *Z*-intermediates. For the enantioselectivities, a clear correlation between London dispersion stabilization and enantioselectivity was found, allowing to convert moderate-good to good-excellent enantioselectivities under dispersion control and exceeding the typical enantiomeric ratios for standard imine substrates.

11. Curriculum Vitae

Personal Data

Date of Birth	23.09.1994
Place of Birth	Landshut, Deutschland
Adress	Schmerlenweg 13, 84036 Landshut
E-Mail	johannes.gramueller@chemie.uni-regensburg.de
Languages	German (native), English (fluent), Spanish (basic knowledge)

Education

Since 12/2018	Ph. D. candidate at the University of Regensburg, Deutschland Dissertation: „NMR-Spectroscopic Investigations in Asymmetric Brønsted Acid Catalysis – Structural Space, Hydrogen Bonding and Non-Covalent Interactions “ Thesis Advisor: Professor Dr. Ruth M. Gschwind
10/2016 - 09/2018	Master of Science Chemistry, University of Regensburg, Deutschland Degree : Master of Science (1,1) Master thesis: “NMR Spectroscopic Investigations in Brønsted Acid Catalysis” (1,0) Thesis Advisor: Professor Dr. Ruth M. Gschwind
10/2013 - 11/2016	Bachelor of Science Chemistry, University of Regensburg, Deutschland Degree: Bachelor of Science (1,6) Bachelor thesis: „Synthesis and Derivatization of (±)-Paeonolid“ (1,0) Thesis Advisor: Professor Dr. Oliver Reiser
06/2013	General University Entrance Qualification, Hans-Carossa Gymnasium Landshut (1,3)

Scholarships

08/2019 – 07/2021	Kekulé-Fellowship for PhD candidates; Fonds der Chemischen Industrie
06/2019	Travel scholarship of the GdCh for attending the “Gordon Research Conference on Physical Organic Chemistry” in Holderness, USA

Attended conferences and scientific presentations

06/2022	71 st Lindau Nobel Laureate Meeting in Lindau, Germany.
03/2021; 03/2022	“SPP Winter School” of the Schwerpunktprogramm 1807 Control of London Dispersion Interactions in Molecular Chemistry; Short Talks.
09/2019	“SMASH Small Molecule NMR Conference” in Porto, Portugal; Poster presentation.
06/2019	“Gordon Research Conference on Physical Organic Chemistry” in Holderness, USA; Poster presentation.
02/2019	“691. WE-Heraeus-Seminar on Physical Organic Chemistry” in Bad Honnef, Deutschland; Poster presentation.
07/2018; 07/2019	“SPP Summer School” of the Schwerpunktprogramm 1807 Control of London Dispersion Interactions in Molecular Chemistry; Short Talks.

Publications

- [1] J. Gramüller, M. Franta, R. M. Gschwind, *Journal of the American Chemical Society* **2022**, *accepted*.
- [2] J. Kelly, J. Gramüller, R. M. Gschwind, R. Wolf, *Dalton Transactions*, **2021**, *50*, 13985-13992.
- [3] R. Yadav, M. Weber, A. K. Singh, L. Münzfeld, J. Gramüller, R. M. Gschwind, M. Scheer, P. W. Roesky, *Chemistry – A European Journal*, **2021**, *27*, 14128-14137.
- [4] F. Pecho, Y. Sempere, J. Gramüller, F.M. Hörmann, R.M. Gschwind, T. Bach, *Journal of the American Chemical Society* **2021**, *143*, 9350-9354.
- [5] R. R. Annapureddy, F. Burg, J. Gramüller, T. P. Golub, C. Merten, S. M. Huber, T. Bach, *Angewandte Chemie Int. Ed.* **2021**, *60*, 7920-7926.
- [6] P. Degot, V. Huber, A. E. Maangar, J. Gramüller, L. Rohr, D. Tourad, T. Zemb, R. M. Gschwind, W. Kunz, *Journal of Molecular Liquids* **2021**, *329*, 115538.

11. Curriculum Vitae

- [7] D. Jansen, J. Gramüller, F. Niemeyer, T. Schaller, M.C. Letzel, S. Grimme, H. Zhu, R.M. Gschwind, J. Niemeyer, *Chemical Science* **2020**, *11*, 4381-4390.
- [8] F. Pecho, Y. Zou, J. Gramüller, T. Mori, S.M. Huber, A. Bauer, R.M. Gschwind, T. Bach, *Chemistry – A European Journal* **2020**, *26*, 5190-5194.
- [9] N. Lokesh, J. Hioe, J. Gramüller, R.M. Gschwind, *Journal of the American Chemical Society* **2019**, *141*, 16398-16407.
- [10] M. Melikian, J. Gramüller, J. Hioe, J. Greindl, R.M. Gschwind *Chemical Science* **2019**, *10*, 5226-5234. (shared first author)
- [11] K. Rothermel, M. Melikian, J. Hioe, J. Greindl, J. Gramüller, M. Žabka, N. Sorgenfrei, T. Hausler, F. Morana, R.M. Gschwind, *Chemical Science* **2019**, *10*, 10025-10034.
-

12. Danksagung

Zuallererst möchte ich mich herzlichst bei Frau Prof. Dr. Ruth Gschwind bedanken, besonders für all die hilfreichen Diskussionen, den Freiraum bei der Bearbeitung und Gestaltung meiner Projekte sowie für ihre Unterstützung bei den Anträgen für das Kekulé-Stipendium und der Lindauer Nobelpreisträgertagung. Herrn Prof. Dr. Kremer möchte ich herzlich dafür danken, dass er die Aufgabe des Zweitgutachters übernommen hat. Frau Prof. Dr. Rehbein möchte ich ebenfalls für ihre Bereitschaft als Drittprüferin danken. Herrn Prof. Dr. Müller möchte ich dafür danken, dass er den Vorsitz des Prüfungsausschusses übernommen hat.

Darüber hinaus möchte ich mich herzlich bei der NMR-Abteilung für ihre Unterstützung bedanken, allen voran Fritz Kastner für seine verlässliche Hilfe bei Problemen am Spektrometer und bei Problemen und Unklarheiten mit der IT. Ilya Shenderovich und Tuan Anh Nguyen möchte ich ebenfalls für ihre Unterstützung danken. Nikola Kastner-Pustet möchte ich herzlichst für ihre Hilfe bei allerhand auftretenden Problemen und Unklarheiten danken, ebenso wie Veronica Scheidler und Michelle Brückner für ihre Unterstützung im Laboralltag. Ebenso möchte ich Ulrike Weck herzlichst danken für ihre andauernde Unterstützung bei allerhand bürokratischen Problemen und Unklarheiten.

Besonderer Dank gilt meinen früheren und aktuellen Arbeitskollegen und Kolleginnen am AK Gschwind für ihre Unterstützung und die schöne Zeit während meiner Promotion. Besonderer Dank gilt Julian Greindl für seine Hilfe und Bemühungen mir während meiner Masterarbeit und dem Beginn meiner Promotion die grundlegenden Arbeitsweisen beizubringen. Ebenso möchte ich mich bei Kerstin Rothermel für ihre Hilfe zu Beginn meiner Arbeit bedanken. Lokesh Nanjundappa, Andreas Seegerer, Florian Hastreiter, Johnny Hioe, Philipp Nitschke, Verena Streitferdt, Nele Berg und Matej Žabka möchte ich für ihre Unterstützung, die Zusammenarbeit bei Projekten und die tolle Zeit auf Konferenzen sowie in und außerhalb der Universität danken.

Besonderer Dank gilt Willibald Stockerl für seine praktische und theoretische Unterstützung über die Dauer meiner Promotionszeit hinweg sowie für die gute Zeit. Maximilian Franta möchte ich für seine Unterstützung sowie für alle organisatorischen Tätigkeiten danken, ebenso für die lustige Zeit im Büro und außerhalb der Universität. Johannes Eder möchte ich ebenfalls für die angenehme Zeit im Büro und außerhalb der Arbeitszeit danken. Franz Westermair möchte ich für seine Hilfe und Unterstützung am Spektrometer und bei IT-Problemen danken. Philipp Dullinger möchte ich für die Hilfe bei IT-Problemen, Verständnisfragen zu theoretischer Chemie sowie für die gute Zusammenarbeit bei Projekten danken. Anton Abramov und Maximilian Philipp sei gedankt für die angenehme Zeit sowie die nicht unerhebliche Erweiterung meines Wortschatzes. Darüber hinaus möchte ich Bastian Dauth, Christian Scholtes, Lavakumar Naviri, Lea Müller, Mona Peschik und Markus Hecht für die tolle Zeit während

12. Danksagung

meiner Promotion danken. Kumar Motiram Corral und Wagner Menezes da Silva möchte ich für ihre Hilfe am Spektrometer und der Datenauswertung danken.

Besonderer Dank gilt all meinen Kooperationspartnern und Partnerinnen für die gute und unkomplizierte Zusammenarbeit, besonders Franziska Pecho und Prof. Dr. Thorsten Bach, Pierre Degot, Verena Huber und Prof. Dr. Werner Kunz, Jochen Niemeyer und Dennis Jansen, Martin Weber, John Kelly und Tanja Bauer.

Ganz besonders möchte ich mich bei Stephan Reichl und Nikolai Wurzer bedanken, für ihre durchgängige Hilfe und Unterstützung im Studium und der Promotion, ihre Freundschaft und die unvergessliche gemeinsame Zeit der letzten 9 Jahre sowie die regelmäßigen Donnerstags-Treffen, die immer ein Highlight im Alltag der Promotion waren.

Zuletzt möchte ich mich noch besonders bei meiner Familie, allen voran meinen Eltern Andrea und Wolfgang und meiner Oma Waltraud bedanken, für ihre durchgängige Unterstützung und Hilfe, die mir eine Promotion erst möglich gemacht hat.

Euch allen, vielen Dank.

13. Eidesstattliche Versicherung

(1) Ich erkläre hiermit an Eides statt, dass ich die vorliegende Arbeit ohne unzulässige Hilfe Dritter und ohne Benutzung anderer als der angegebenen Hilfsmittel angefertigt habe; die aus anderen Quellen direkt oder indirekt übernommenen Daten und Konzepte sind unter Angabe des Literaturzitats gekennzeichnet.

(2) Bei der Auswahl und Auswertung folgenden Materials haben mir die zu Beginn des jeweiligen Kapitels aufgeführten Personen in der jeweils beschriebenen Weise unentgeltlich geholfen.

(3) Weitere Personen waren an der inhaltlich-materiellen Herstellung der vorliegenden Arbeit nicht beteiligt. Insbesondere habe ich hierfür nicht die entgeltliche Hilfe eines Promotionsberaters oder anderer Personen in Anspruch genommen. Niemand hat von mir weder unmittelbar noch mittelbar geldwerte Leistungen für Arbeiten erhalten, die im Zusammenhang mit dem Inhalt der vorgelegten Dissertation stehen.

(4) Die Arbeit wurde bisher weder im In- noch im Ausland in gleicher oder ähnlicher Form einer anderen Prüfungsbehörde vorgelegt.

Regensburg, den

Johannes Gramüller